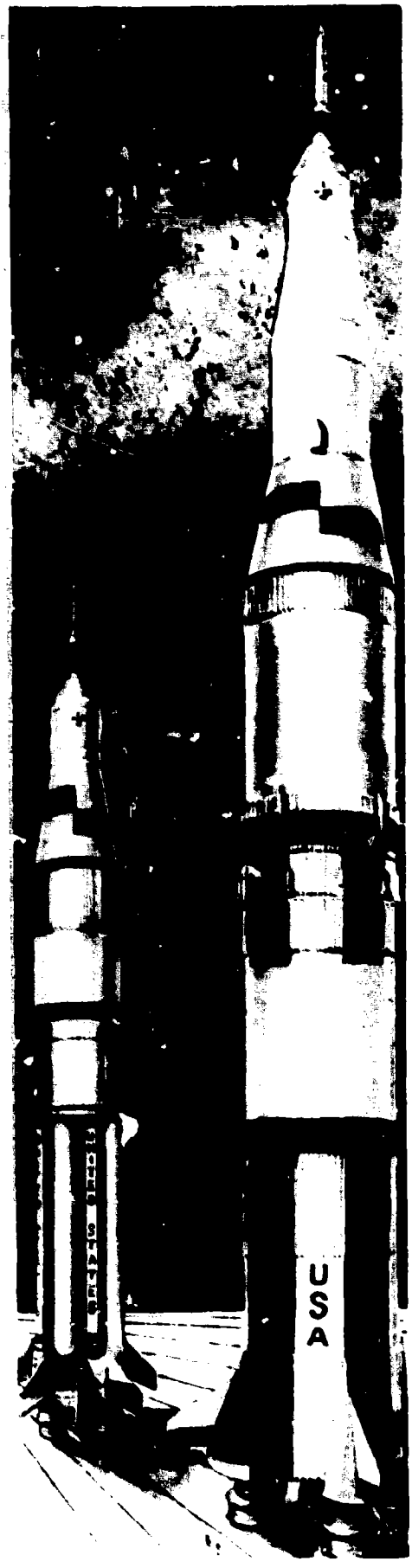

GEORGE C. MARSHALL SPACE FLIGHT CENTER

SATURN

MPR-SAT-FE-69-1

FEBRUARY 20, 1969

SATURN V LAUNCH VEHICLE FLIGHT EVALUATION REPORT-AS-503 APOLLO 8 MISSION

FACILITY FORM 602

N69-24692	
(ACCESSION NUMBER)	(THRU)
560	1
(PAGES)	(CODE)
TMX-61651	31
(NASA CR OR TMX OR AD NUMBER)	(CATEGORY)

PREPARED BY

SATURN V FLIGHT EVALUATION WORKING GROUP

NATIONAL AERONAUTICS AND SPACE ADMINISTRATION

C - Form 774 (Rev October 1967)

GEORGE C. MARSHALL SPACE FLIGHT CENTER

MPR-SAT-FE-69-1

SATURN V LAUNCH VEHICLE
FLIGHT EVALUATION REPORT - AS-503
APOLLO 8 MISSION

PREPARED BY

SATURN V FLIGHT EVALUATION WORKING GROUP

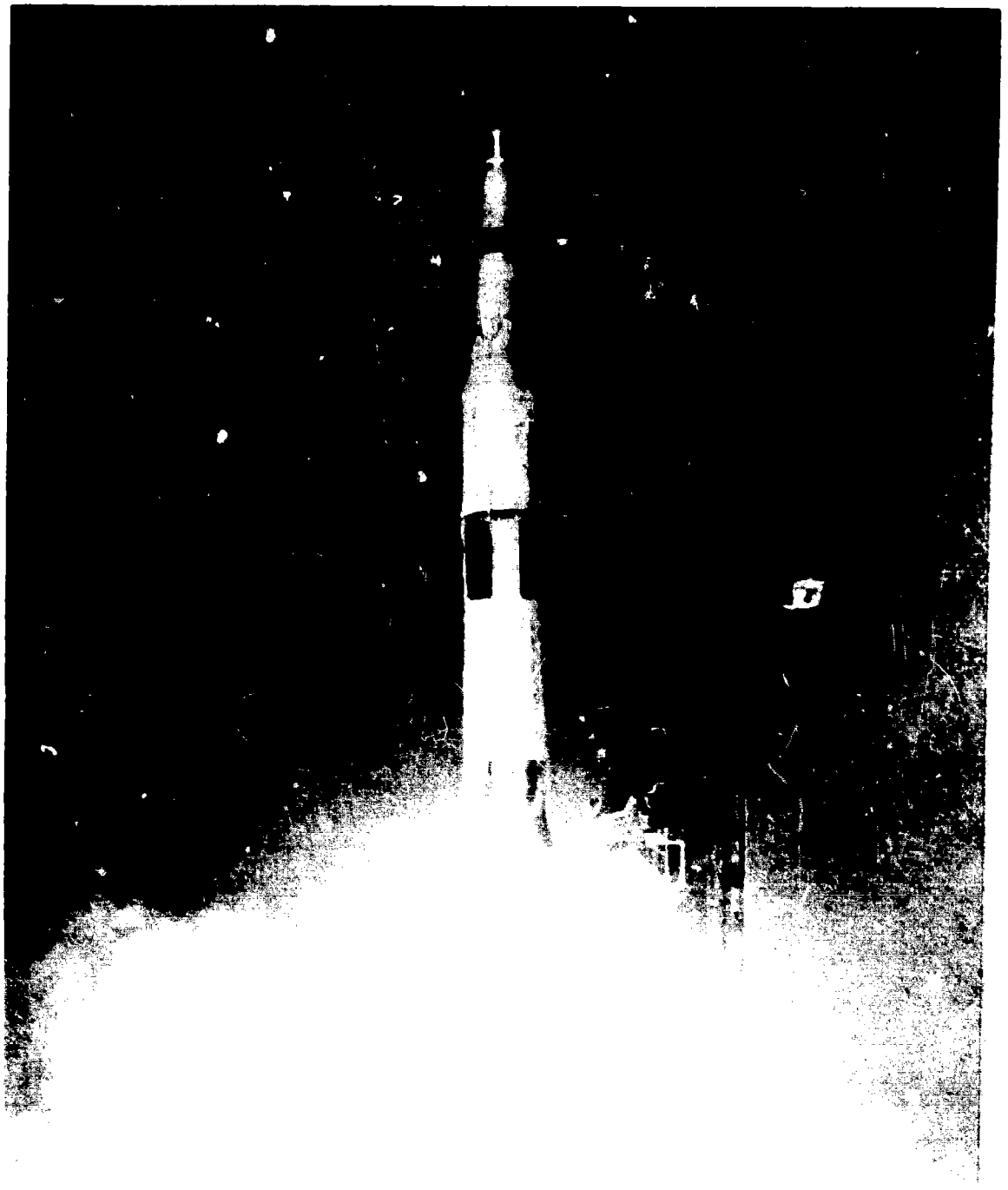

AS-503 Launch Vehicle

TABLE OF CONTENTS

Section			Page
	TABLE OF CONTENTS		iii
	LIST OF ILLUSTRATIONS		xiii
	LIST OF TABLES		xxvii
	ACKNOWLEDGEMENT		xxxii
	ABBREVIATIONS		xxxiii
	MISSION PLAN		xxxvi
	FLIGHT TEST SUMMARY		xxxviii
1	INTRODUCTION		
	1.1	Purpose	1-1
	1.2	Scope	1-1
2	EVENT TIMES		
	2.1	Summary of Events	2-1
	2.2	Sequence of Events	2-2
3	LAUNCH OPERATIONS		
	3.1	Summary	3-1
	3.2	Prelaunch Milestones	3-1
	3.3	Countdown Events	3-4
	3.4	Propellant Loading	3-4
	3.4.1	RP-1 Loading	3-4
	3.4.2	LOX Loading	3-4
	3.4.3	LH_2 Loading	3-5
	3.4.4	Auxiliary Propulsion System Propellant Loading	3-5
	3.4.5	S-IC Stage Propellant Load	3-6
	3.4.6	S-II Stage Propellant Load	3-6
	3.4.7	S-IVB Stage Propellant Load	3-6

TABLE OF CONTENTS (CONTINUED)

Section			Page
	3.5	S-II Insulation Purge and Leak Detection	3-6
	3.6	Ground Support Equipment	3-8
4	TRAJECTORY		
	4.1	Summary	4-1
	4.2	Tracking Data Utilization	4-2
	4.2.1	Tracking During the Ascent Phase of Flight	4-2
	4.2.2	Tracking During Orbital Flight	4-2
	4.2.3	Tracking During the Injection Phase of Flight	4-3
	4.3	Trajectory Evaluation	4-3
	4.3.1	Ascent Trajectory	4-3
	4.3.2	Parking Orbit Trajectory	4-7
	4.3.3	Injection Trajectory	4-8
	4.3.4	Post TLI Trajectory	4-9
	4.3.5	S-IVB/IU Post Separation Trajectory	4-9
5	S-IC PROPULSION		
	5.1	Summary	5-1
	5.2	S-IC Ignition Transient Performance	5-1
	5.3	S-IC Main Stage Performance	5-3
	5.4	S-IC Engine Shutdown Transient Performance	5-6
	5.5	S-IC Stage Propellant Management	5-7
	5.6	S-IC Pressurization Systems	5-7
	5.6.1	S-IC Fuel Pressurization System	5-7
	5.6.2	S-IC LOX Pressurization System	5-10
	5.7	S-IC Pneumatic Control Pressure System	5-13
	5.8	S-IC Purge System	5-13
	5.9	POGO Suppression System	5-15
	5.10	S-IC Camera Purge and Ejection System	5-17

TABLE OF CONTENTS (CONTINUED)

Section			Page
6	S-II PROPULSION		
	6.1	Summary	6-1
	6.2	S-II Chilldown and Buildup Transient Performance	6-2
	6.3	S-II Main Stage Performance	6-6
	6.4	S-II Stage Shutdown Transient Performance	6-15
	6.5	S-II Stage Propellant Management	6-16
	6.6	S-II Pressurization Systems	6-20
	6.6.1	S-II Fuel Pressurization System	6-20
	6.6.2	S-II LOX Pressurization System	6-21
	6.7	S-II Pneumatic Control Pressure System	6-25
	6.8	S-II Helium Injection System	6-27
6A	STRUCTURAL RESPONSE TO S-II ENGINE OSCILLATIONS		
	6A.1	Summary	6A-1
	6A.2	S-II Stage Structural Response	6A-1
	6A.3	Spacecraft Structural Response	6A-4
	6A.4	Response Thrust Calculations	6A-4
7	S-IVB PROPULSION		
	7.1	Summary	7-1
	7.2	S-IVB Chilldown and Buildup Transient Performance for First Burn	7-2
	7.3	S-IVB Main Stage Performance for First Burn	7-2
	7.4	S-IVB Shutdown Transient Performance for First Burn	7-9
	7.5	S-IVB Parking Coast Phase Conditioning	7-10

TABLE OF CONTENTS (CONTINUED)

Section			Page
	7.6	S-IVB Chilldown and Restart for Second Burn	7-17
	7.7	S-IVB Main Stage Performance for Second Burn	7-27
	7.8	S-IVB Shutdown Transient Performance for Second Burn	7-31
	7.9	S-IVB Stage Propellant Utilization	7-31
	7.10	S-IVB Pressurization System	7-36
	7.10.1	S-IVB LH_2 Tank Pressurization System	7-36
	7.10.2	S-IVB LOX Pressurization System	7-38
	7.11	S-IVB Pneumatic Control System	7-41
	7.12	S-IVB Auxiliary Propulsion System	7-44
	7.13	S-IVB Orbital Safing Operation	7-47
	7.13.1	Fuel Tank Safing	7-47
	7.13.2	LOX Tank Dump and Safing	7-48
	7.13.3	Cold Helium Dump	7-50
	7.13.4	Ambient Helium Dump	7-51
	7.13.5	Stage Pneumatic Control Sphere Safing	7-51
	7.13.6	Engine Start Sphere Safing	7-51
	7.13.7	Engine Control Sphere Safing	7-53
8	HYDRAULIC SYSTEMS		
	8.1	Summary	8-1
	8.2	S-IC Hydraulic System	8-1
	8.3	S-II Hydraulic System	8-1
	8.4	S-IVB Hydraulic System (First Burn)	8-4
	8.5	S-IVB Hydraulic System (Coast Phase)	8-6
	8.6	S-IVB Hydraulic System (Second Burn)	8-6
	8.7	Translunar Injection Coast and Propellant Dump	8-6

TABLE OF CONTENTS (CONTINUED)

Section			Page
9	STRUCTURES		
	9.1	Summary	9-1
	9.2	Total Vehicle Structures Evaluation	9-2
	9.2.1	Longitudinal Loads	9-2
	9.2.2	Bending Moments	9-2
	9.2.3	Vehicle Dynamic Characteristics	9-9
	9.2.4	S-IC Fin Dynamics	9-13
	9.3	Vibration Evaluation	9-16
	9.3.1	S-IC Stage and Engine Evaluation	9-16
	9.3.2	S-II Stage and Engine Evaluation	9-18
	9.3.3	S-IVB Stage and Engine Evaluation	9-28
	9.3.4	Instrument Unit Evaluation	9-28
10	GUIDANCE AND NAVIGATION		
	10.1	Summary	10-1
	10.1.1	Flight Program	10-1
	10.1.2	Instrument Unit Components	10-1
	10.2	Guidance and Navigation System Description	10-2
	10.2.1	Flight Program Description	10-2
	10.2.2	Instrument Unit System Description	10-6
	10.3	Guidance Comparisons	10-8
	10.4	Navigation and Guidance Scheme Evaluation	10-16

TABLE OF CONTENTS (CONTINUED)

Section			Page
	10.4.1	Flight Program Performance	10-16
	10.4.2	Attitude Error Computations	10-17
	10.4.3	Program Sequencing	10-17
	10.5	Guidance System Component Evaluation	10-20
	10.5.1	LVDC Performance	10-20
	10.5.2	LVDA Performance	10-20
	10.5.3	Ladder Outputs	10-20
	10.5.4	Telemetry Outputs	10-20
	10.5.5	Discrete Outputs	10-20
	10.5.6	Switch Selector Functions	10-20
	10.5.7	ST-124M-3 Inertial Platform Performance	10-20
11	CONTROL SYSTEM		
	11.1	Summary	11-1
	11.2	Control System Description	11-2
	11.3	S-IC Control System Evaluation	11-3
	11.3.1	Liftoff Clearances	11-3
	11.3.2	S-IC Flight Dynamics	11-4
	11.4	S-II Control System Evaluation	11-16
	11.4.1	Attitude Control Dynamics and Stability	11-16
	11.4.2	Liquid Propellant Dynamics and Their Effects on Flight Control	11-20
	11.5	S-IVB Control System Evaluation	11-22
	11.5.1	Control System Evaluation During First Burn	11-22
	11.5.2	Control System Evaluation During Parking Orbit	11-26
	11.5.3	Control System Evaluation During Second Burn	11-26
	11.5.4	Control System Evaluation After Second Burn	11-33
	11.6	Instrument Unit Control Components Evaluation	11-50
	11.6.1	Control-EDS Rate Gyros/Control Signal Processor Analysis	11-50

TABLE OF CONTENTS (CONTINUED)

Section			Page
	11.6.2	Flight Control Computer Analysis	11-50
12	SEPARATION		
	12.1	Summary	12-1
	12.2	S-IC/S-II Separation Evaluation	12-1
	12.2.1	S-IC Retro Motor Performance	12-1
	12.2.2	S-II Ullage Motor Performance	12-4
	12.2.3	S-IC/S-II Separation Dynamics	12-4
	12.3	S-II Second Plane Separation Evaluation	12-9
	12.4	S-II/S-IVB Separation Evaluation	12-9
	12.4.1	S-II Retro Motor Performance	12-9
	12.4.2	S-IVB Ullage Motor Performance	12-12
	12.4.3	S-II/S-IVB Separation Dynamics	12-12
	12.5	S-IVB-IU-LM Test Article (LTA) Command Service Module (CSM) Separation Evaluation	12-12
13	ELECTRICAL NETWORKS		
	13.1	Summary	13-1
	13.2	S-IC Stage Electrical System	13-1
	13.3	S-II Stage Electrical System	13-2
	13.4	S-IVB Stage Electrical System	13-9
	13.5	Instrument Unit Electrical System	13-15
14	RANGE SAFETY AND COMMAND SYSTEMS		
	14.1	Summary	14-1
	14.2	Range Safety Command Systems	14-1
	14.3	Command and Communications System	14-2

TABLE OF CONTENTS (CONTINUED)

Section			Page
15	EMERGENCY DETECTION SYSTEM		
	15.1	Summary	15-1
	15.2	System Description	15-1
	15.3	System Evaluation	15-2
	15.3.1	General Performance	15-2
	15.3.2	Propulsion System Sensors	15-2
	15.3.3	Angular Overrates	15-2
	15.3.4	Angle-of-Attack	15-2
	15.3.5	Tank Pressures	15-2
	15.3.6	EDS Sequential Events	15-4
16	VEHICLE PRESSURE AND ACOUSTIC ENVIRONMENT		
	16.1	Summary	16-1
	16.2	Surface Pressures and Compartment Venting	16-1
	16.2.1	S-IC Stage	16-1
	16.2.2	S-II Stage	16-3
	16.2.3	S-IVB Stage	16-8
	16.3	Base Pressures	16-8
	16.3.1	S-IC Base Pressures	16-8
	16.3.2	S-II Base Pressures	16-12
	16.4	Acoustic Environment	16-15
	16.4.1	External Acoustics	16-15
	16.4.2	Internal Acoustics	16-18
17	VEHICLE THERMAL ENVIRONMENT		
	17.1	Summary	17-1
	17.2	S-IC Base Heating and Separation Environment	17-1
	17.2.1	S-IC Base Heating	17-1
	17.2.2	S-IC/S-II Separation Environment	17-9

TABLE OF CONTENTS (CONTINUED)

Section			Page
	17.3	S-II Base Heating and Separation Environment	17-10
	17.4	S-IVB Engine Area Thermal Environment	17-15
	17.5	Vehicle Aeroheating Thermal Environment	17-15
	17.5.1	S-IC Stage Aeroheating Environment	17-15
	17.5.2	S-II Stage Aeroheating Environment	17-28
	17.5.3	S-IVB Stage Aeroheating Environment	17-33
	17.5.4	IU Aeroheating Environment	17-36
	17.6	Vehicle Orbital Heating Environment	17-36
18	ENVIRONMENTAL CONTROL SYSTEM		
	18.1	Summary	18-1
	18.2	S-IC Environmental Control	18-1
	18.3	S-II Environmental Control	18-4
	18.4	S-IVB Environmental Control	18-6
	18.5	IU Environmental Control	18-7
	18.5.1	Thermal Conditioning System	18-7
	18.5.2	Gas Bearing Supply System	18-10
19	DATA SYSTEMS		
	19.1	Summary	19-1
	19.2	Vehicle Measurements Evaluation	19-1
	19.2.1	S-IC Stage Measurement Analysis	19-3
	19.2.2	S-II Stage Measurement Analysis	19-4
	19.2.3	S-IVB Stage Measurement Analysis	19-9
	19.2.4	S-IU Stage Measurement Analysis	19-10
	19.3	Airborne Telemetry Systems	19-10
	19.3.1	S-IC Stage Telemetry System	19-10
	19.3.2	S-II Stage Telemetry System	19-11
	19.3.3	S-IVB Stage Telemetry System	19-12
	19.3.4	S-IU Stage Telemetry System	19-12

TABLE OF CONTENTS (CONTINUED)

Section			Page
	19.4	Airborne Tape Recorders	19-13
	19.4.1	S-IC Stage Recorder	19-13
	19.4.2	S-II Stage Recorders	19-13
	19.4.3	S-IU Stage Recorder	19-13
	19.5	RF Systems Evaluation	19-14
	19.5.1	Telemetry Systems RF Propagation Evaluation	19-15
	19.5.2	Tracking Systems RF Propagation Evaluation	19-17
	19.5.3	Command Systems RF Evaluation	19-19
	19.5.4	Television Propagation Evaluation	19-22
	19.6	Optical Instrumentation	19-22
	19.6.1	Onboard Cameras	19-22
	19.6.2	Ground Engineering Cameras	19-24
20	VEHICLE AERODYNAMIC CHARACTERISTICS		
	20.1	Summary	20-1
	20.2	Vehicle Axial Force Characteristics	20-1
	20.3	Vehicle Static Stability	20-3
	20.4	Fin Pressure Loading	20-3
21	MASS CHARACTERISTICS		
	21.1	Summary	21-1
	21.2	Mass Evaluation	21-1
22	MISSION OBJECTIVES ACCOMPLISHMENT		22-1
23	FAILURES, ANOMALIES AND DEVIATIONS		
	23.1	Summary	23-1
	23.2	System Failures and Anomalies	23-1
	23.3	System Deviations	23-1

TABLE OF CONTENTS (CONTINUED)

Section			Page
24	SPACECRAFT SUMMARY		24-1
Appendix			
A	ATMOSPHERE		
	A.1	Summary	A-1
	A.2	General Atmospheric Conditions at Launch Time	A-1
	A.3	Surface Observations at Launch Time	A-1
	A.4	Upper Air Measurements	A-1
	A.4.1	Wind Speed	A-1
	A.4.2	Wind Direction	A-1
	A.4.3	Pitch Wind Component	A-2
	A.4.4	Yaw Wind Component	A-2
	A.4.5	Component Wind Shears	A-2
	A.4.6	Extreme Wind Data in the High Dynamic Pressure Region	A-2
	A.5	Thermodynamic Data	A-2
	A.5.1	Temperature	A-2
	A.5.2	Atmospheric Pressure	A-2
	A.5.3	Atmospheric Density	A-2
	A.5.4	Optical Index of Refraction	A-3
	A.6	Comparison of Selected Atmospheric Data for all Saturn Launches	A-3
B	AS-503 VEHICLE DESCRIPTION		
	B.1	Summary	B-1
	B.2	S-IC Stage	B-1
	B.2.1	S-IC Configuration	B-1
	B.3	S-II Stage	B-6
	B 3.1	S-II Configuration	B-6

TABLE OF CONTENTS (CONTINUED)

Section		Page
B.4	S-IVB Stage	B-9
B.4.1	S-IVB Configuration	B-9
B.5	Instrument Unit (IU)	B-13
B.5.1	IU Configuration	B-13
B.6	Spacecraft	B-16
B.6.1	Spacecraft Configuration	B-16

LIST OF ILLUSTRATIONS

Figure		Page
2-1	AS-503 Transmission Delay Time	2-2
3-1	S-II LH_2 Tank Sidewall Insulation Closeouts	3-9
4-1	Ascent Trajectory Position Comparison	4-7
4-2	Ascent Trajectory Earth-Fixed Velocity Comparison	4-8
4-3	Ascent Trajectory Space-Fixed Velocity Comparison	4-9
4-4	Ascent Trajectory Acceleration Comparison	4-10
4-5	Dynamic Pressure and Mach Number Versus Range Time	4-11
4-6	Acceleration Due to Venting	4-13
4-7	Ground Track	4-13
4-8	Injection Phase Space-Fixed Velocity Comparison	4-15
4-9	Injection Phase Acceleration Comparison	4-15
4-10	Slingshot Maneuver Velocity Increment	4-16
4-11	Resultant Slingshot Maneuver Conditions	4-16
4-12	S-IVB/IU Velocity Relative to Earth Distance	4-18
4-13	Projection of Spacecraft - S-IVB/IU Positions	4-19
5-1	S-IC Start Box Requirements	5-2
5-2	S-IC Engine Buildup Transient	5-4
5-3	S-IC Steady State Operation	5-5
5-4	S-IC Outboard Engine Cutoff Deviations	5-8
5-5	S-IC Engine Shutdown Transient Performance	5-8
5-6	S-IC Fuel Ullage Pressure	5-11
5-7	S-IC Fuel Pump Inlet Pressure, Engine No. 1	5-11
5-8	S-IC Helium Bottle Pressure for Fuel Pressurization	5-12

LIST OF ILLUSTRATIONS (CONTINUED)

Figure		Page
5-9	S-IC LOX Tank Ullage Pressure	5-13
5-10	S-IC LOX Suction Duct Pressure, Engine No. 1	5-14
5-11	S-IC LOX Suction Duct Pressure, Engine No. 5	5-14
5-12	S-IC Control Sphere Pressure	5-15
5-13	S-IC POGO Suppression System	5-16
5-14	S-IC Prevalve Liquid Level, Typical Outboard Engine	5-16
6-1	S-II Thrust Chamber Jacket Temperature	6-3
6-2	S-II Engine Start Tank Performance	6-4
6-3	S-II Engine Pump Start Requirements	6-5
6-4	S-II Engine Buildup Transients	6-7
6-5	S-II Steady State Operation	6-8
6-6	Engine No. 5 Pressure Parameter after EMR Step	6-13
6-7	Engine No. 5 LOX Inlet Pressure	6-14
6-8	LOX NPSP History	6-15
6-9	S-II Engine Shutdown Transient	6-17
6-10	S-II Stage Thrust Decay	6-17
6-11	S-II PU Valve Position	6-19
6-12	S-II Fuel Tank Ullage Pressure	6-21
6-13	S-II Fuel Pump Inlet Conditions	6-22
6-14	S-II LOX Tank Ullage Pressure	6-23
6-15	S-II LOX Pump Inlet Conditions	6-24
6-16	S-II Pneumatic Control Pressure	6-26
6A-1	S-II Stage Engine No. 5 - Longitudinal Oscillation Time Histories	6A-2

LIST OF ILLUSTRATIONS (CONTINUED)

Figure		Page
6A-2	S-II Stage Engine No. 1 - Longitudinal Oscillation Time Histories	6A-3
6A-3	S-II Stage Crossbeam and Center Engine Chamber Pressure Frequency	6A-5
6A-4	S-II-3 and S-II-4 Thrust Structure Comparison	6A-6
6A-5	Command Module Longitudinal Oscillation Time Histories	6A-7
7-1	S-IVB Start Box and Run Requirement - First Burn	7-3
7-2	S-IVB Thrust Chamber Temperature - First Burn	7-4
7-3	S-IVB Start Tank Performance - First Burn	7-5
7-4	J-2 Engine Control and Stage Ambient Bottles Tie-In Schematic	7-6
7-5	S-IVB Buildup Transient - First Burn	7-7
7-6	S-IVB Steady State Performance - First Burn	7-9
7-7	S-IVB Performance Shifts - First Burn and Second Burn	7-12
7-8	Revised J-2 LOX ASI Line	7-13
7-9	Revised J-2 LH_2 ASI Line	7-14
7-10	ASI Line Conditions - First Burn and Second Burn	7-15
7-11	S-IVB Shutdown Transient Performance - First Burn	7-16
7-12	O_2/H_2 Burner Propellant Tanks Pressurization	7-18
7-13	S-IVB Stage O_2/H_2 Burner	7-19
7-14	S-IVB Ullage Conditions During Repressurization Using O_2/H_2 Burner	7-20

LIST OF ILLUSTRATIONS (CONTINUED)

Figure		Page
7-15	O_2/H_2 Burner LOX and LH_2 Pressurant Coil Pressure	7-21
7-16	LOX and LH_2 Pressurant Coil Temperatures and Cold Helium Pressure	7-21
7-17	S-IVB O_2/H_2 Burner Thrust and Pressurant Flowrate	7-22
7-18	S-IVB O_2/H_2 Burner Chamber Pressure and Temperature	7-23
7-19	S-IVB Start Box and Run Requirements - Restart	7-25
7-20	S-IVB J-2 Fuel Lead Restart - Second Burn	7-26
7-21	S-IVB Start Tank Performance - Second Burn	7-27
7-22	S-IVB Buildup Transients - Second Burn	7-28
7-23	S-IVB Steady State Performance - Second Burn	7-29
7-24	S-IVB Shutdown Transient Performance - Second Burn	7-33
7-25	S-IVB PU System Nonlinearities	7-35
7-26	S-IVB LH_2 Ullage Pressure - First Burn and Parking Orbit	7-36
7-27	S-IVB LH_2 Ullage Pressure - Second Burn and Translunar Coast	7-37
7-28	S-IVB Fuel Pump Inlet Conditions - First Burn	7-38
7-29	S-IVB Fuel Pump Inlet Conditions - Second Burn	7-39
7-30	S-IVB LOX Tank Ullage Pressure - First Burn and Parking Orbit	7-40
7-31	S-IVB LOX Tank Ullage Pressure - Second Burn and Translunar Coast	7-41
7-32	S-IVB LOX Pump Inlet Conditions - First Burn	7-42
7-33	S-IVB LOX Pump Inlet Conditions - Second Burn	7-43
7-34	S-IVB Cold Helium Supply History	7-44

LIST OF ILLUSTRATIONS (CONTINUED)

Figure		Page
7-35	S-IVB Pneumatic Control Performance	7-45
7-36	S-IVB APS Mass History - Module No. 2	7-49
7-37	S-IVB APS Mass History - Module No. 1	7-50
7-38	S-IVB Orbital Safing and Propellant Dump Sequence	7-51
7-39	S-IVB LOX Dump Parameter Histories	7-52
7-40	S-IVB Start Bottle and Engine Control Bottle Safing	7-54
8-1	S-IC Hydraulic System Performance	8-2
8-2	S-II Hydraulic System Performance	8-3
8-3	S-IVB Hydraulic System Performance - First Burn	8-5
8-4	S-IVB Hydraulic System Performance - Orbital Coast	8-7
8-5	S-IVB Hydraulic System Performance - Second Burn	8-8
8-6	S-IVB Hydraulic System Performance During Translunar Coast	8-9
8-7	S-IVB Hydraulic System Pressures During LOX Dump	8-10
8-8	S-IVB Hydraulic System Performance During LOX Dump	8-11
9-1	Longitudinal Structural Dynamic Response Due to Thrust Buildup and Release	9-3
9-2	Release Rod Force Displacement Curves	9-4
9-3	Longitudinal Loads at Maximum Bending Moment, Inboard Engine Cutoff, and Outboard Engine Cutoff	9-5
9-4	Longitudinal Structural Dynamic Response Due to Outboard Engine Cutoff	9-6
9-5	Lateral Loads and Structural Dynamic Response During Thrust Buildup and Release	9-7

LIST OF ILLUSTRATIONS (CONTINUED)

Figure		Page
9-6	Maximum Bending Moment Near Max Q	9-8
9-7	First Longitudinal Modal Frequencies and Amplitudes During S-IC Powered Flight	9-10
9-8	Longitudinal Mode Shapes During S-IC Powered Flight	9-11
9-9	Lateral Modal Frequencies and Amplitudes During S-IC Powered Flight	9-14
9-10	S-IC Fin Vibration Response and Bending and Torsional Modal Frequencies	9-15
9-11	S-IC Stage Structure Vibration Envelopes	9-18
9-12	S-IC Stage Engine Vibration Envelopes	9-19
9-13	S-IC Stage Components Vibration Envelopes	9-20
9-14	S-IC Vibration and Strain Measurement Locations	9-21
9-15	S-II Stage Structure Vibration Envelopes	9-23
9-16	S-II Stage Engine Vibration Envelopes	9-25
9-17	S-II Stage Component Vibration Envelopes	9-26
9-18	S-IVB Stage Vibration Envelopes	9-29
9-19	S-IVB Stage Engine Vibration Envelopes	9-30
9-20	Instrument Unit Vibration Envelopes	9-35
10-1	Navigation, Guidance, and Control System Block Diagram	10-7
10-2	Platform Gimbal Configuration	10-9
10-3	Tracking and ST-124M-3 Platform Velocity Comparison (Trajectory Minus Guidance)	10-10
10-4	Attitude Errors During IGM Flight	10-19
10-5	Saturn V Inertial Gimbal Vibrations	10-22
11-1	Liftoff Vertical Motion and Slow Release Forces	11-5
11-2	Liftoff Lateral Motion (Position III)	11-7

LIST OF ILLUSTRATIONS (CONTINUED)

Figure		Page
11-3	S-IC Plume Angular Variation; Center Engine Trajectory and Fin Tip A Trajectory	11-8
11-4	Pitch Plane Dynamics During S-IC Burn	11-10
11-5	Yaw Plane Dynamics During S-IC Burn	11-11
11-6	Roll Plane Dynamics During S-IC Burn	11-12
11-7	Free Stream Angle-of-Attack and Pitch and Yaw Plane Wind Velocity During S-IC Burn	11-13
11-8	Normal Acceleration During S-IC Powered Flight	11-14
11-9	S-IC Engine Deflection Response to Propellant Slosh	11-15
11-10	Pitch Plane Dynamics During S-II Burn	11-17
11-11	Yaw Plane Dynamics During S-II Burn	11-18
11-12	Roll Plane Dynamics During S-II Burn	11-19
11-13	S-II Engine Deflection Response to Propellant Slosh	11-21
11-14	Pitch Plane Dynamics During S-IVB First Burn	11-23
11-15	Yaw Plane Dynamics During S-IVB First Burn	11-24
11-16	Roll Plane Dynamics During S-IVB First Burn	11-25
11-17	Pitch Attitude Control During Maneuver to Local Horizontal Following S-IVB First Burn	11-27
11-18	Yaw Attitude Control During Maneuver to Local Horizontal Following S-IVB First Burn	11-28
11-19	Roll Attitude Control During Maneuver to Local Horizontal Following S-IVB First Burn	11-29
11-20	Pitch Plane Dynamics During S-IVB Second Burn	11-30
11-21	Yaw Plane Dynamics During S-IVB Second Burn	11-31
11-22	Roll Plane Dynamics During S-IVB Second Burn	11-32

LIST OF ILLUSTRATIONS (CONTINUED)

Figure		Page
11-23	Pitch Attitude Control During Maneuver to Local Horizontal Following S-IVB Second Burn	11-34
11-24	Yaw Attitude Control During Maneuver to Local Horizontal Following S-IVB Second Burn	11-35
11-25	Roll Attitude Control During Maneuver to Local Horizontal Following S-IVB Second Burn	11-36
11-26	Pitch Attitude Control During Maneuver to CSM/S-IVB Separation Attitude	11-33
11-27	Yaw Attitude Control During Maneuver to CSM/S-IVB Separation Attitude	11-39
11-28	Roll Attitude Control During Maneuver to CSM/S-IVB Separation Attitude	11-40
11-29	Pitch Attitude Control During CSM/S-IVB Separation	11-41
11-30	Yaw Attitude Control During CSM/S-IVB Separation	11-42
11-31	Roll Attitude Control During CSM/S-IVB Separation	11-43
11-32	Pitch Attitude Control During Propellant Removal	11-44
11-33	Yaw Attitude Control During Propellant Removal	11-45
11-34	Roll Attitude Control During Propellant Removal	11-46
11-35	Pitch Attitude Control During APS Ullage Burn for Slingshot	11-47
11-36	Yaw Attitude Control During APS Ullage Burn for Slingshot	11-48
11-37	Roll Attitude Control During APS Ullage Burn for Slingshot	11-49

LIST OF ILLUSTRATIONS (CONTINUED)

Figure		Page
12-1	S-IC Retro Motor Thrust	12-4
12-2	S-II Ullage Motor Thrust	12-6
12-3	S-IC/S-II Relative Velocity and Separation Distance During First Plane Separation	12-7
12-4	S-IC Pitch and Yaw Angular Dynamics Following S-IC/S-II Separation	12-8
12-5	S-II Angular Dispersions During S-IC/S-II First Plane Separation	12-8
12-6	Interstage/S-II Relative Velocity and Separation Distance During Second Plane Separation	12-10
12-7	S-II Retro Motor Thrust	12-11
12-8	S-II/S-IVB Longitudinal Acceleration	12-13
12-9	S-II and S-IVB Angular Dispersions During S-II/S-IVB Separation	12-14
12-10	S-IVB-IU-LTA After Separation	12-15
13-1	S-IC Stage Battery No. 1 Voltage and Current, Bus 1D10	13-3
13-2	S-IC Stage Battery No. 2 Voltage and Current, Bus 1D20	13-3
13-3	S-II Stage Main DC Bus Voltage and Current	13-5
13-4	S-II Stage Instrumentation Bus Voltage and Current	13-5
13-5	S-II Stage Recirculation DC Bus Voltage and Current	13-6
13-6	S-II Stage Ignition DC Voltage and Current	13-6
13-7	S-II Stage Temperature Bridge Power Supplies Voltage	13-8

LIST OF ILLUSTRATIONS (CONTINUED)

Figure		Page
13-8	S-IVB Stage Bridge Power Supply Mounting and Chassis, Typical	13-9
13-9	S-IVB Stage Fwd Battery No. 1 Voltage, Current, and Temperature	13-10
13-10	S-IVB Stage Fwd Battery No. 2 Voltage, Current, and Temperature	13-11
13-11	S-IVB Stage Aft Battery No. 1 Voltage, Current, and Temperature	13-12
13-12	S-IVB Stage Aft Battery No. 2 Voltage, Current, and Temperature	13-13
13-13	IU Battery 6D10 Voltage, Current, and Temperature	13-17
13-14	IU Battery 6D20 Voltage, Current and Temperature	13-18
13-15	IU Battery 6D30 Voltage, Current, and Temperature	13-19
13-16	IU Battery 6D40 Voltage, Current, and Temperature	13-20
16-1	S-IC Engine Fairing Compartment Pressure Differential	16-2
16-2	S-IC Engine Fairing Pressure Loading	16-4
16-3	S-IC Compartment Pressure Differential	16-6
16-4	S-IC Compartment Pressure Loading	16-7
16-5	S-II Compartment Pressure Loading	16-9
16-6	S-IVB Compartment Pressure Differential	16-10
16-7	S-IC Base Pressure Differentials	16-11
16-8	S-IC Base Heat Shield Pressure Loading	16-12

LIST OF ILLUSTRATIONS (CONTINUED)

Figure		Page
16-9	S-II Base Heat Shield Forward Face and Thrust Cone Pressures	16-13
16-10	S-II Heat Shield Aft Face Pressures	16-14
16-11	Vehicle External Overall Sound Pressure Level at Liftoff	16-15
16-12	Vehicle External Sound Pressure Spectral Densities at Liftoff	16-16
16-13	Vehicle External Overall Fluctuating Pressure Level	16-19
16-14	Vehicle External Fluctuating Pressure Spectral Densities at Maximum Aerodynamic Noise	16-21
16-15	S-IC Heat Shield Panels Acoustic Environment	16-23
16-16	S-IC Internal Acoustic Environment	16-23
16-17	S-II Compartment Overall Acoustic Levels	16-24
16-18	S-IVB Forward and Aft Skirt Acoustic Levels	16-25
17-1	S-IC Base Heat Shield Thermal Environment	17-3
17-2	F-1 Engine Thermal Environment	17-3
17-3	Base of Fin D Total Heating Rate	17-4
17-4	S-IC Heat Shield Forward Surface Temperature	17-5
17-5	S-IC Heat Shield Bondline Temperature	17-5
17-6	S-IC Heat Shield, M-31 Temperature	17-6
17-7	S-IC Base Heat Shield Measurement Locations	17-7
17-8	S-IC Temperature Under Insulation, Inboard Side Engine No. 1	17-8
17-9	S-IC AFT Face of Base Heat Shield Inflight TV Coverage	17-8

LIST OF ILLUSTRATIONS (CONTINUED)

Figure		Page
17-10	S-IC Upper Compartment Ambient Air Temperature During S-IC/S-II Stage Separation	17-9
17-11	S-IC Forward Skirt Skin Temperature after S-IC/S-II Stage Separation	17-10
17-12	S-IC LOX Tank Forward Dome Temperature During S-IC/S-II Stage Separation	17-11
17-13	S-II Heat Shield Base Region Heating Rates	17-12
17-14	S-II Thrust Cone Heating Rate	17-13
17-15	S-II Base Gas Temperature	17-14
17-16	S-II Heat Shield Aft Face Temperatures	17-16
17-17	S-II Heat Shield Forward Face Temperatures	17-17
17-18	S-IC Forward Skirt Aerodynamic Heating Near Finline D	17-18
17-19	S-IC Forward Skirt Aerodynamic Heating Near Finline B	17-18
17-20	S-IC Forward Skirt Aerodynamic Heating Near Finlines A and D	17-19
17-21	S-IC Intertank Aerodynamic Heating, Forward	17-21
17-22	S-IC Intertank Aerodynamic Heating, Aft	17-21
17-23	S-IC Engine Fairing (Fin B) Aerodynamic Heating	17-22
17-24	S-IC Engine Fairing (Fin D) Aerodynamic Heating	17-22
17-25	S-IC Fin B Aerodynamic Heating	17-23
17-26	S-IC Fin D Aerodynamic Heating	17-23
17-27	Forward Point of Separated Flow	17-24
17-28	S-IC Forward Skirt Skin Temperature	17-25
17-29	S-IC Forward Skirt Thermocouple Plate	17-25
17-30	S-IC LOX Tank Skin Temperature	17-26

LIST OF ILLUSTRATIONS (CONTINUED)

Figure		Page
17-31	S-IC Intertank Skin Temperature	17-26
17-32	S-IC Fuel Tank Skin Temperature	17-27
17-33	S-IC Thrust Structure Skin Temperature	17-27
17-34	S-IC Forward Fairing Skin Temperature	17-29
17-35	S-IC Aft Fairing Skin Temperature	17-29
17-36	S-IC Fin Wedge Section Skin Temperature	17-30
17-37	S-IC Fin Aft Face Structural Temperature	17-30
17-38	S-II Aft Interstage Aeroheating Environment	17-31
17-39	S-II Aft Interstage Aeroheating Environment, Ullage Motor Fairing	17-32
17-40	S-II LH_2 Feedline Aft Fairing Heating Rates	17-33
17-41	S-II LH_2 Feedline Forward Fairing Heating Rates	17-34
17-42	S-II Body Structural Temperature	17-34
17-43	S-II Aft Interstage Structural Temperature	17-35
17-44	S-II LH_2 Feedline Fairing Structural Temperature	17-35
17-45	IU Inner Skin Temperatures for Ascent	17-36
17-46	IU Inner Skin Temperature, Earth Orbit	17-37
18-1	S-IC Forward Compartment Canister Temperature	18-2
18-2	S-IC Forward Compartment Ambient Temperature	18-3
18-3	S-IC Aft Compartment Temperature Range	18-5
18-4	IU Environmental Control System Schematic Diagram	18-8
18-5	Thermal Conditioning System Methanol/Water Control Temperature	18-9
18-6	IU Sublimator Performance During Ascent	18-10
18-7	Thermal Conditioning System GN_2 Pressure	18-11

LIST OF ILLUSTRATIONS (CONTINUED)

Figure		Page
18-8	Selected Component Temperatures	18-12
18-9	Pressure Differential Across Gas Bearings	18-13
18-10	Gas Bearing System GN_2 Pressure	18-13
20-1	Average Base Differential Pressure	20-2
20-2	Forebody Axial Force Coefficient	20-3
20-3	S-IC Fin Pressure Differential	20-4
21-1	Total Vehicle Mass, Center of Gravity, and Mass Moment of Inertia During S-IC Stage Powered Flight	21-17
21-2	Total Vehicle Mass, Center of Gravity, and Mass Moment of Inertia During S-II Stage Powered Flight	21-18
21-3	Total Vehicle Mass, Center of Gravity, and Mass Moment of Inertia During S-IVB Stage Powered Flight	21-19
A-1	Scalar Wind Speed at Launch Time of AS-503	A-11
A-2	Wind Direction at Launch Time of AS-503	A-12
A-3	Pitch Wind Speed Component (W_x) at Launch Time of AS-503	A-13
A-4	Yaw Wind Speed Component at Launch Time of AS-503	A-14
A-5	Pitch (S_x) and Yaw (S_z) Component Wind Shears at Launch Time of AS-503	A-15
A-6	Relative Deviation of AS-503 Temperature and Density From PAFB (63) Reference Atmosphere	A-16
A-7	Relative Deviation of Pressure and Absolute Deviation of the Index of Refraction from the PAFB (63) Reference Atmosphere, AS-503	A-17
B-1	Saturn V Apollo Flight Configuration	B-2
B-2	S-IC Stage Configuration	B-3

LIST OF ILLUSTRATIONS (CONTINUED)

Figure		Page
B-3	S-II Stage Configuration	B-7
B-4	S-IVB Stage Configuration	B-10
B-5	Instrument Unit Configuration	B-14
B-6	Apollo Space Vehicle	B-17

LIST OF TABLES

Table		Page
2-1	Time Base Summary	2-3
2-2	Significant Event Times Summary	2-5
2-3	Sequence of Switch Selector Events	2-12
2-4	Variable Time and Commanded Switch Selector Events	2-27
3-1	AS-503 Milestones	3-2
3-2	S-IC Stage Propellant Mass at Ignition Command	3-7
3-3	S-II Stage Propellant Mass at S-IC Ignition Command	3-7
3-4	S-IVB Stage Propellant Mass at S-IC Ignition Command	3-7
4-1	Summary of AS-503 Orbital C-Band Tracking Data Available	4-2
4-2	Comparison of Significant Trajectory Events	4-4
4-3	Comparison of Cutoff Events	4-5
4-4	Comparison of Separation Events	4-6
4-5	Stage Impact Location	4-12
4-6	Parking Orbit Insertion Conditions	4-14
4-7	Translunar Injection Conditions	4-14
4-8	Comparison of Slingshot Maneuver	4-17
4-9	Lunar Closest Approach Parameters	4-17
4-10	Heliocentric Orbit Parameters	4-18
5-1	S-IC Stage Engine Startup Event Times	5-4
5-2	S-IC Engine Performance Deviations	5-6
5-3	Comparison of S-IC Stage Flight Reconstruction Data with Trajectory Simulation Results	5-7
5-4	S-IC Cutoff Impulse	5-9
5-5	S-IC Stage Propellant Mass History	5-9

LIST OF TABLES (CONTINUED)

Table		Page
5-6	S-IC Residuals at Outboard Engine Cutoff	5-10
6-1	S-II Engine Start Sequence Events	6-6
6-2	S-II Engine Performance Deviations (ESC +61 Seconds)	6-10
6-3	S-II Flight Reconstruction Comparison with Simulation Trajectory Match Results	6-11
6-4	S-II Cutoff Impulse	6-18
6-5	S-II Propellant Mass History	6-20
6A-1	Calculated Longitudinal Structural Response and Thrust Oscillations Using AS-503 Measured Data	6A-8
7-1	S-IVB Engine Start Sequence Events - First Burn	7-8
7-2	S-IVB Steady State Performance - First Burn (ESC +30 Second Time Slice at Standard Altitude Conditions)	7-10
7-3	Comparison of S-IVB Stage Flight Reconstruction Data with Performance Simulation Results - First Burn	7-11
7-4	S-IVB Simulation Burn Time Deviations - First Burn	7-11
7-5	S-IVB Cutoff Impulse - First Burn	7-15
7-6	S-IVB Engine Start Sequence - Second Burn	7-24
7-7	S-IVB Steady State Performance - Second Burn (ESC +80 Second Time Slice at Standard Altitude Conditions)	7-30
7-8	Comparison of S-IVB Stage Flight Reconstruction Data with Performance Simulation Results - Second Burn	7-31
7-9	S-IVB Simulation Burn Time Deviations - Second Burn	7-32
7-10	S-IVB Cutoff Impulse - Second Burn	7-33
7-11	S-IVB Stage Propellant Mass History	7-34
7-12	S-IVB Pneumatic Helium Bottle Mass	7-46
7-13	S-IVB APS Helium Bottle Mass	7-47

LIST OF TABLES (CONTINUED)

Table		Page
7-14	S-IVB APS Propellant Consumption	7-48
7-15	S-IVB Pneumatic Control Sphere Conditions During Dump	7-53
8-1	S-IVB Hydraulic System Pressures	8-4
9-1	Saturn V First Longitudinal Mode Response Comparison During S-IC Powered Flight	9-12
9-2	AS-503 S-IC Stage Propellant Line Frequencies	9-12
9-3	S-IC Stage Vibration Summary	9-17
9-4	S-II Stage Vibration Summary	9-22
9-5	S-IVB Vibration Summary	9-31
10-1	Inertial Platform Velocity Comparisons	10-12
10-2	Guidance Comparisons	10-14
10-3	Start and Stop Times for IGM Guidance Commands	10-16
10-4	S-IVB First Burn Guidance Cutoff Conditions	10-18
10-5	Guidance Comparisons Elliptical Orbit Parameters at S-IVB Second Cutoff	10-18
11-1	Summary of Liftoff Clearances	11-4
11-2	AS-503 Misalignment Summary	11-6
11-3	Maximum Control Parameters During S-IC Boost Flight	11-9
11-4	Maximum Control Parameters During S-II Boost Flight	11-20
11-5	Maximum Control Parameters During S-IVB First Burn	11-22
11-6	Maximum Control Parameters During S-IVB Second Burn	11-33
12-1	Separation Event Times	12-2
12-2	S-IC Retro Motor Performance	12-3
12-3	S-II Ullage Motor Performance	12-5
12-4	AS-503 S-II Retro Motor Performance	12-11
13-1	S-IC Stage Battery Power Consumption	13-4
13-2	S-II Stage Battery Power Consumption	13-4
13-3	S-IVB Stage Battery Power Consumption	13-14

LIST OF TABLES (CONTINUED)

Table		Page
13-4	IU Battery Power Consumption	13-16
14-1	Command and Communications System Command History, AS-503	14-3
15-1	Performance Summary of Thrust OK Pressure Switches	15-3
15-2	Maximum Angular Rates	15-4
15-3	EDS Related Event Times	15-4
16-1	S-II Acoustic Noise Levels Comparison of AS-503 with AS-501 and AS-502 Data	16-24
19-1	AS-503 Flight Measurement Summary	19-3
19-2	AS-503 Flight Measurements Waived Prior to Launch	19-4
19-3	AS-503 Flight Measurements Malfunctions	19-5
19-4	AS-503 Flight Measurements with Improper Range	19-8
19-5	AS-503 Questionable Flight Measurements	19-9
19-6	AS-503 Launch Vehicle Telemetry Links	19-11
19-7	Tape Recorder Summary	19-14
19-8	Final RF LOS, VHF Telemetry	19-16
19-9	Last Usable VHF Telemetry Data	19-16
19-10	VHF Telemetry Systems RF Summary	19-18
19-11	C-Band Tracking System RF Summary	19-20
19-12	CCS RF Summary	19-23
21-1	Total Vehicle Mass, S-IC Burn Phase, Kilograms	21-3
21-2	Total Vehicle Mass, S-IC Burn Phase, Pounds Mass	21-4
21-3	Total Vehicle Mass, S-II Burn Phase, Kilograms	21-5
21-4	Total Vehicle Mass, S-II Burn Phase, Pounds Mass	21-6
21-5	Total Vehicle Mass, S-IVB First Burn Phase, Kilograms	21-7
21-6	Total Vehicle Mass, S-IVB First Burn Phase, Pounds Mass	21-8

LIST OF TABLES (CONTINUED)

Table		Page
21-7	Total Vehicle Mass, S-IVB Second Burn Phase, Kilograms	21-9
21-8	Total Vehicle Mass, S-IVB Second Burn Phase, Pounds Mass	21-10
21-9	Flight Sequence Mass Summary	21-11
21-10	Mass Characteristics Comparison	21-13
22-1	Mission Objectives Accomplishment Summary	22-2
23-1	Summary of Failures and Anomalies	23-2
23-2	Hardware Criticality Categories for Flight Hardware	23-3
23-3	Summary of Deviations	23-4
A-1	Surface Observations at AS-503 Launch Time	A-3
A-2	Solar Radiation at AS-503 Launch Time, Launch Pad 39A	A-4
A-3	Systems Used to Measure Upper Air Wind Data	A-4
A-4	Maximum Wind Speed in High Dynamic Pressure Region for Saturn 1 Through Saturn 10 Vehicles	A-5
A-5	Maximum Wind Speed in High Dynamic Pressure Region for Apollo/Saturn 201 Through Apollo/Saturn 205 Vehicles	A-6
A-6	Maximum Wind Speed in High Dynamic Pressure Region for Apollo/Saturn 501 Through Apollo/Saturn 503 Vehicles	A-6
A-7	Extreme Wind Shear Values in the High Dynamic Pressure Region for Saturn 1 Through Saturn 10 Vehicles	A-7
A-8	Extreme Wind Shear Values in the High Dynamic Pressure Region for Apollo/Saturn 201 Through Apollo/Saturn 205 Vehicles	A-8
A-9	Extreme Wind Shear Values in the High Dynamic Pressure Region for Apollo/Saturn 501 Through Apollo/Saturn 503 Vehicles	A-8

LIST OF TABLES (CONTINUED)

Table		Page
A-10	Selected Atmospheric Observations for Saturn 1 Through Saturn 10 Vehicle Launches at Kennedy Space Center, Florida	A-9
A-11	Selected Atmospheric Observations for Apollo-Saturn 201 Through Apollo-Saturn 205 Launches at Kennedy Space Center, Florida	A-10
A-12	Selected Atmospheric Observations for Apollo-Saturn 501 Through Apollo-Saturn 503 Launches at Kennedy Space Center, Florida	A-10
B-1	S-IC Significant Configuration Changes	B-5
B-2	S-II Significant Configuration Changes	B-11
B-3	S-IVB Significant Configuration Changes	B-13
B-4	IU Significant Configuration Changes	B-15

ACKNOWLEDGEMENT

This report is published by the Saturn Flight Evaluation Working Group--composed of representatives of Marshall Space Flight Center, John F. Kennedy Space Center, and MSFC's prime contractors--and in cooperation with the Manned Spacecraft Center. Significant contributions to the evaluation have been made by:

George C. Marshall Space Flight Center

Research and Development Operations

Aero-Astrodynamics Laboratory
Astrionics Laboratory
Computation Laboratory
Propulsion and Vehicle Engineering Laboratory

Industrial Operations

John F. Kennedy Space Center

Manned Spacecraft Center

The Boeing Company

McDonnell Douglas Astronautics Company

International Business Machines Corporation

North American Rockwell/Rocketdyne Division

North American Rockwell/Space Division

ABBREVIATIONS

ACN	Ascension
ANT	Antigua
AOS	Acquisition of Signal
APS	Auxiliary propulsion system
ASI	Augmented spark igniter
BDA	Bermuda
BSC	O_2H_2 Burner Start Command
CAL	Goldstone, California
CCS	Command and communications system
CDDT	Countdown demonstration test
CG	Center of gravity
CIF	Central instrumentation facility
CKAFS	Cape Kennedy Air Force Site
CM	Command Module
CNV	Canaveral
CRO	Carnarvon
CSM	Command and service module
CSP	Control Signal Processor
CVS	Continuous vent system
CYI	Grand Canary Island
DEE	Digital events evaluator
DCS	Digital Command System
EBW	Exploding bridge wire
ECO	Engine cutoff
ECP	Engineering change proposal
ECS	Environment control system
EDS	Emergency detection system
EMR	Engine mixture ratio
ESC	Engine start command
EST	Eastern Standard Time
FCC	Flight Control Computer
FM/FM	Frequency modulation/ frequency modulation
GBI	Grand Bahama Island
GFCV	GOX flow control valve
GG	Gas generator
GMT	Greenwich Mean Time
GRR	Guidance reference release
GSE	Ground support equipment
GTI	Grand Turk Island
GYM	Guaymas
HAW	Hawaii
HDA	Holddown Arm
HEP	Hardware Evaluation Program
HFCV	Helium flow control valve
HSK	Honeysuckle (Canberra)
IECO	Inboard engine cutoff
IGM	Iterative guidance mode
IP&C	Instrument Program and Components
IRIG	Inter range instrumentation group
IU	Instrument Unit
KSC	Kennedy Space Center
LES	Launch escape system
LET	Launch escape tower

LIEF	Launch Information Exchange Facility
LM	Lunar module
LOS	Loss of signal
LTA	Lunar module test article
LUT	Launch umbilical tower
LV	Launch vehicle
LVDA	Launch vehicle data adapter
LVDC	Launch vehicle digital computer
MAD	Madrid
MCC-H	Mission control center-Houston
MER	Mercury (ship)
MFV	Main fuel valve
MILA	Merritt Island Launch Area
MLV	Main LOX Valve
MOV	Main oxidizer valve
MR	Mixture ratio
MSC	Manned Spacecraft Center
MSFC	Marshall Space Flight Center
MSS	Mobile Service Structure
MTF	Mississippi Test Facility
NPSP	Net positive suction pressure
NASA	National Aeronautics and Space Administration
OAT	Overall test
OCP	Orbital Correction Program
ODOP	Offset frequency doppler
OECO	Outboard engine cutoff
OMNI	Omni directional
PAM/FM/FM	Pulse amplitude modulation/frequency modulation/frequency modulation
PAFB	Patrick Air Force Base
PCM	Pulse code modulation
PCM/FM	Pulse code modulation/ frequency modulation
PMR	Programmed mixture ratio
PSD	Power spectral density
PTCS	Propellant tanking computer system
PTL	Prepare to launch
PU	Propellant utilization
RCS	Reaction Control System
RED	Redstone (ship)
RF	Radio frequency
RMS	Root mean square
RP-1	Designation for S-IC stage fuel (kerosene)
RPM	Revolutions per minute
SA	Service arm
SEC	Seconds
SLA	Spacecraft LM adapter
SM	Service module
SMC	Steering misalignment correction
SPS	Service propulsion system
SRSCS	Secure range safety command system
SS	Switch selector
SS/FM	Single sideband/frequency modulation
STDV	Start tank discharge valve
STP	Special Test Pattern
SV	Space vehicle

T_1I	Time to go in 1st stage IGM
T_2I	Time to go in 2nd stage IGM
TAN	Tananarive
TDM	Time division multiplexer
TEL 4	Cape telemetry 4
TEP	Telemetry Executive Program
TEX	Corpus Christi (Texas)
TLI	Translunar Injection
TMR	Triple modular redundant
TSM	Tail service mast
TVC	Thrust vector control
TV	Television
UHF	Ultra high frequency
UT	Universal time
VAB	Vehicle assembly building at KSC
VAN	Vanguard (ship)
VHF	Very high frequency
WHS	White Sands

MISSION PLAN

AS-503 was the third flight vehicle (Apollo 8 Mission) of the Apollo-Saturn V flight test program. It was to be the first manned Apollo Saturn V vehicle with the spacecraft performing the world's first manned circumlunar flight. The crew was to consist of Air Force Col. Frank Borman, Navy Capt. James Lovell and Air Force Maj. William Anders.

The space vehicle was to be composed of the AS-503 launch vehicle, Command and Service Module (CSM) 103 and a Lunar Module Test Article (LTA-B) in place of an operational Lunar Module (LM). Payload weight, exclusive of the Launch Escape Tower (LET) was to be approximately 39,010 kilograms (87,700 lbm).

Launch was to be from Launch Complex 39, Pad A at the Kennedy Space Center (KSC). Because this was to be a lunar mission, it was necessary for the vehicle to be launched within a particular daily launch window within a monthly launch window. Part of the constraints were dictated by the desire to pass over selected lunar sites with lighting conditions similar to those planned for the later landing missions. Lunar orbit inclination, inclination of the free return trajectory, and spacecraft propellant reserves were other primary factors considered in the mission design.

The first monthly window planned for was December 1968 with launch dates of December 20th through December 27th. January was planned for as a backup. Subsequently, it was decided to make the first attempt on December 21st to have the total available daily window during daylight. Targeting for this day was to cause flight over lunar landing site II-P-2 (2.63 degrees selenographic latitude, 34.03 degrees selenographic longitude). The actual window for December 21st lasted from 7:50:22 AM to 12:31:40 PM Eastern Standard Time (EST) (4 hours 39 minutes duration). Launch was scheduled for 7:51 AM EST slightly into the available window.

The vehicle was to be launched on an azimuth of 90 degrees, then rolled to a flight azimuth of from 72 to 108 degrees depending on time of launch.

The vehicle's mass at launch was to be about 2,782,000 kilograms (6,134,000 lbm). The durations of the S-IC and S-II burns were to be approximately 151 seconds and 366 seconds, respectively. The planned S-IVB first burn was about 156 seconds, culminating in the insertion of the S-IVB and spacecraft into a 185 kilometer (100 n mi) circular parking orbit.

The total vehicle mass at insertion was to be about 127,500 kilograms (281,100 lbm). At 20 seconds after S-IVB first cutoff, the vehicle was to align itself with the local horizontal with position I down. This attitude was to be maintained through S-IVB restart preparation.

Chilldown and reignition sequencing were to begin over the Indian Ocean in preparation for reignition between Hawaii and the Phillipines during the second or third revolution (first or second opportunity). The S-IVB second burn, which was to result in Translunar Injection (TLI), was to have a duration of approximately 315 seconds. The total vehicle mass at injection was to be about 58,800 kilograms (130,000 lbm). The astronauts were to initiate separation of the CSM from the S-IVB 25 minutes after S-IVB second burn cutoff (start of Time Base 7 [T_7]). During the separation, the vehicle was to be oriented to provide the lighting necessary for the docking maneuver on future flights.

After spacecraft separation the S-IVB/IU/LTA-B was to align itself in a near retrograde attitude for a sequence in which residual LOX was to be dumped through the J-2 engine, and the two APS ullage engines were to be turned on to burn to depletion. The LOX dump was to occur between 132 and 137 minutes after the cutoff of the S-IVB second burn. The added velocity increment from the propellant dump and ullage burn was to slow the stage down slightly to allow it to pass behind the moon. On this slingshot trajectory the stage would pick up energy from the moon's gravitational field and enter a heliocentric orbit rather than impacting the moon or remaining in an earth orbit.

The CSM after separation was to continue on its translunar trajectory for about 66 hours. For a nominal mission, the CSM was to perform a Lunar Orbit Insertion (LOI) burn to insert into an initial orbit around the moon of approximately 111 by 315 kilometers (60 by 170 n mi). After two revolutions in this orbit, a coplanar circularization burn was to be made to place the CSM in approximately a 111 kilometer (60 n mi) circular lunar orbit. A Transearth Injection (TEI) burn was to be planned near the end of revolution 10, or after about 20 hours in lunar orbit, to place the CSM on a transearth trajectory. Landing was scheduled in the Pacific Ocean about 57 hours later.

The figure shows the gross profile of the Mission C Prime.

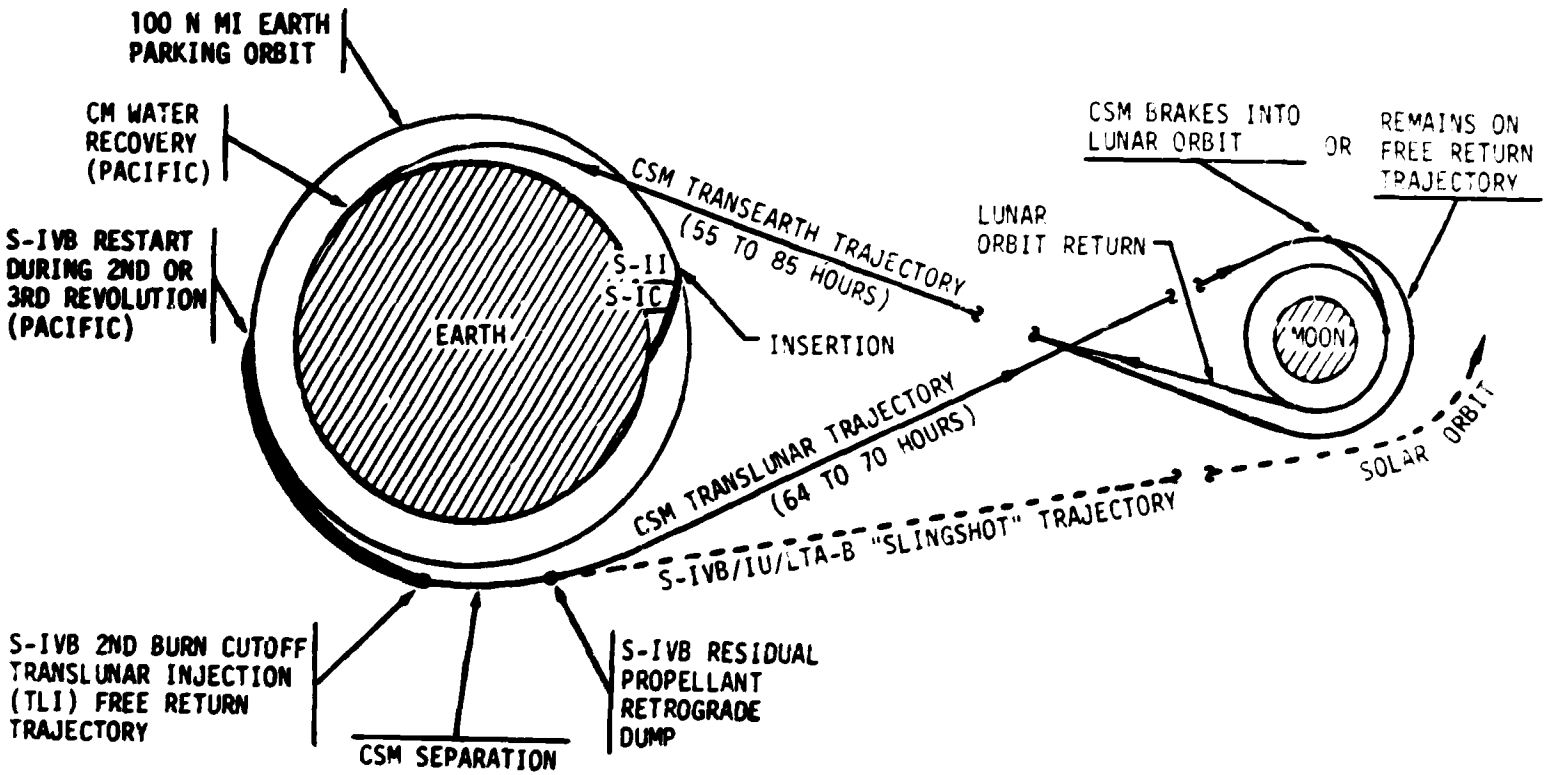

AS-503 Mission C Prime Option 1 Profile

FLIGHT TEST SUMMARY

The first manned Saturn V Apollo space vehicle, AS-503 (Apollo 8 Mission), was launched at Kennedy Space Center (KSC), Florida on December 21, 1968 at 07:51:00 Eastern Standard Time (EST) from Launch Complex 39, Pad A. This was the third launch of a Saturn V Apollo. The nine principle and one secondary detailed test objectives were completely accomplished.

The launch countdown was completed without any unscheduled countdown holds. Ground systems performance was highly satisfactory. The relatively few problems encountered in countdown were overcome such that vehicle launch readiness was not compromised.

The vehicle was launched on an azimuth of 90 degrees east of north and after 12.11 seconds of vertical flight, (which included a small yaw maneuver for tower clearance) the vehicle began to roll into a flight azimuth of 72.124 degrees east of north. Actual trajectory parameters of the AS-503 were close to nominal. Space-fixed velocity at S-IC Outboard Engine Cutoff (OECO) was 12.57 m/s (41.24 ft/s) greater than nominal. At S-II Engine Cutoff (ECO) the space-fixed velocity was 10.58 m/s (34.71 ft/s) greater than nominal. At S-IVB first cutoff the space-fixed velocity was 0.44 m/s (1.44 ft/s) greater than nominal. The altitude at S-IVB first cutoff was 0.02 kilometers (0.01 n mi) lower than nominal and the surface range was 2.61 kilometers (1.41 n mi) greater than nominal. Parking orbit insertion conditions were very close to nominal. The space-fixed velocity at insertion was 0.01 m/s (0.03 ft/s) less than nominal. At translunar injection the total space-fixed velocity was 5.23 m/s (17.16 ft/s) less than nominal and the altitude was 3.62 kilometers (1.96 n mi) higher than nominal. C_3 (twice the specific energy of orbit) was 49,631 m^2/s^2 (534,224 ft^2/s^2) less than nominal.

All S-IC propulsion systems performed satisfactorily. In general, all flight performance data, as determined from the propulsion reconstruction analysis, were close to the nominal predictions. At the 35 to 38-second time slice, average engine thrust reduced to standard pump inlet conditions was 0.73 percent lower than predicted. Average reduced specific impulse was 0.11 percent lower than predicted, and reduced propellant consumption rate was 0.67 percent less than predicted. Inboard engine cutoff, as indicated by engine No. 5 cutoff solenoid activation signal, occurred 0.03 second later than predicted. Outboard engine cutoff, as indicated

by outboard engines No. 1, 2, 3, and 4 cutoff solenoid activation signals occurred 2.42 seconds later than predicted. An outboard engine LOX low level cutoff was predicted, but a combination of propellant loading errors and, to a lesser extent, a fuel-rich mixture ratio resulted in a fuel low level initiated cutoff.

The S-II propulsion system performed satisfactorily during the entire flight. Engine thrust at 61 seconds after Engine Start Command (ESC), was 0.04 percent above prediction. Total engine propellant flowrate was 0.38 percent above and specific impulse 0.34 percent below predictions at this time slice. Average engine mixture ratio was 0.69 percent above predicted. Engine No. 4 evidenced a change in performance level at approximately 200 seconds after S-II ESC of approximately -6672 Newtons (-1500 lbf) thrust. At this time the exact nature of this shift has not been determined but is receiving additional investigation. The pressure gauges in the S-II stage propulsion system and the accelerometers at certain structural locations showed oscillations during the latter portion of S-II powered flight. Oscillations of about 18 hertz were evident in engine No. 5 (center engine) parameters beginning at approximately 450 seconds. Amplitude of the center engine oscillations began increasing at about 478 seconds. An 18 hertz response in the S-II crossbeam region peaked at 482 seconds which showed a like trend of amplitude and frequency to that of the center engine chamber pressure. Accelerations were at much smaller amplitudes in the outboard engines at 18 hertz and chamber pressures were in the noise level. Accelerations were noted in the spacecraft flight data of approximately 9 hertz peaking at 493 seconds and another of approximately 11 hertz peaking at 510 seconds. Chamber pressures were well within the noise level for these two frequency trends. Engine No. 5 experienced a thrust level decrease of about 27,050 Newtons (6081 lbf) and propellant mixture ratio change of -0.1 units coincident with the onset of the high amplitude 18 hertz oscillations. The oscillations dampened out about 4 seconds prior to S-II engine cutoff. Although the results of the evaluation are not conclusive, it appears that the oscillations were induced by the LOX pumps and possibly amplified by the center engine support structure. Self-induced LOX pump oscillations may be related to the low Engine Mixture Ratio (EMR) and low Net Positive Suction Pressure (NPSP) existing during this time period, although the NPSP is considerably above the level at which self driven oscillations are normally produced. Engine and pump tests to investigate this possibility are being conducted at the engine manufacturer's test facility and at Huntsville. A recommendation to increase LOX tank ullage pressure for the latter portion of the S-II burn by commanding the LOX regulator full open at S-II ESC + 98.6 seconds is being implemented for AS-504. Engine cutoff, as sensed by the Launch Vehicle Digital Computer (LVDC), was at 524.04 seconds, with a burn time only 0.42 second longer than predicted.

The IVB J-2 engine operated satisfactorily throughout the operational phase of first and second burn with normal shutdowns. S-IVB first burn

time was 156.69 seconds which was 2.11 seconds less than predicted. The engine performance during first burn, as determined from standard altitude reconstruction analysis, deviated from the predicted ESC + 80-second time slice by +0.01 percent for thrust and +0.04 percent for specific impulse. The S-IVB stage first burn ECO was initiated by the LVDC at 684.98 seconds. The Continuous Vent System (CVS) adequately regulated LH_2 tank ullage pressure at 13.4 N/cm^2 (19.5 psia) during orbit, and the Oxygen/Hydrogen (O_2/H_2) Burner, in its first flight operation, satisfactorily achieved LH_2 tank repressurization for restart. Repressurization of the LOX tank was not required. Engine restart conditions were within specified limits. The restart at full open Propellant Utilization (PU) valve position was successful and there were no indications of overtemperature conditions in the gas generator. S-IVB second burn time was 317.72 seconds which was 2.07 seconds longer than predicted. The engine performance during second burn, as determined from the standard altitude reconstruction analysis, deviated from the predicted ESC + 80-second time slice by -0.03 percent for thrust and +0.28 percent for specific impulse. The S-IVB stage ECO was initiated by the LVDC at 10,555.51 seconds. Subsequent to second burn, the stage propellant tanks were safed satisfactorily, with sufficient impulse being derived from the LOX dump to impart 20.4 m/s (66.9 ft/s) to stage velocity. This slowed the vehicle down and was a major contributory factor toward avoiding lunar impact and establishing a solar orbit. The instrumentation added to this stage to monitor the effectiveness of the engine's Augmented Spark Igniter (ASI) line modification showed no indications of line failure on this engine. Special instrumentation added to the cold helium system to detect any leakage in the system indicated that no leakage was observed on AS-503. Sphere temperature and pressure data likewise indicated no leakage.

The hydraulic systems on all stages performed satisfactorily throughout the flight.

The structural loads and dynamic environment experienced by the AS-503 launch vehicle were well within the vehicle structural capability. Vehicle loads, due to the combined rigid body and dynamic longitudinal load and bending moment, were well below limit design values. Vehicle dynamic characteristics followed the trends established by preflight analyses. The POGO suppression system apparently performed well, as the first mode frequency of the outboard LOX suction ducts was lowered to approximately 2 hertz as predicted, and there was no evidence of an unstable coupled thrust-structure-feed system oscillation (POGO) during S-IC powered flight. Fin bending and torsional modes compared well with analytical predictions. On previous flights the fin vibrations exceeded the range of the accelerometers. On AS-503 the measurement range was increased and the measured vibration levels remained within range and below design values at all times. No fin flutter occurred. S-IC stage vibrations were generally as expected except at the heat shield. The shield flight vibration environment, measured for the first time on AS-503, was considerably higher than expected. This high vibration may have contributed to the loss of M-31

insulation. S-II stage and S-IVB stage environmental vibrations were also generally as expected considering the fact that certain measurements were relocated and improved measurement systems were used. The S-IVB stage ASI lines dynamic strains measured in flight were within the range of similar data recorded during static firing. Instrument Unit vibrations compared favorably with those of previous Saturn V flights.

The guidance and navigation system performed satisfactorily during all periods for which data are available. The boost navigation and guidance schemes were executed properly and terminal parameters were very good for both parking orbit and translunar injection. The vehicle trajectory exhibited a slightly flatter altitude profile than that predicted in the operational trajectory. Analysis reveals that the most probable cause was the vehicle state vector at Iterative Guidance Mode (IGM) initiation being different than predicted. At S-IC OECO, the vehicle altitude was less than predicted and the velocity was greater. The resulting optimum fuel usage trajectory determined by the LVDC flight program was predictable and resulted in satisfactory end conditions.

The ST-124M-3 inertial platform and associated electronic equipment performed as expected. Telemetry from the LVDC indicated that inertial reference was still being maintained at 25,420 seconds (7:03:40). The accelerometer loop signals indicated that the accelerometers correctly measured vehicle acceleration throughout the flight.

The AS-503 Flight Control Computer (FCC), Thrust Vector Control (TVC), and Auxiliary Propulsion System (APS) satisfied all requirements for vehicle attitude control during boost and orbital control modes. Vehicle-tower clearances during liftoff were satisfactory with less than 25 percent of the available margins utilized. To improve S-IC outboard engine out characteristics, the FCC control outputs to the F-1 engines were biased to provide a 2-degree outboard cant beginning at 20.64 seconds. S-IC/S-II first and second plane separations were satisfactory, resulting in minimum disturbance to the control system. S-II/S-IVB separation was nominal and caused only small attitude disturbances. Control system activity during first and second S-IVB burns was nominal. Following CSM separation the launch vehicle maintained a frozen inertial attitude until 6541 seconds after second cutoff, when the vehicle was commanded to the "slingshot" maneuver attitude (180 degrees pitch, 0 degree yaw, and 180 degrees roll attitudes relative to local horizontal). This attitude was inertially held through the maneuver. At approximately 19,556 seconds the S-IVB ullage engines were ignited to provide additional ΔV for the "slingshot" maneuver. Ullage engine No. 2 propellant depleted at 20,288.56 seconds, and engine No. 1 depletion occurred at 20,314.00 seconds.

In general, all AS-503 launch vehicle electrical systems performed satisfactorily. The power profiles of all stages were normal and all stage and switch selector commands were properly executed. The only

deviations or out-of-tolerance conditions noted during the flight were intermittent operation of 3 temperature bridge power supplies on the S-II stage (two of these supplies were affected for approximately 30 seconds through maximum dynamic pressure [Max Q] and the third for approximately 30 seconds starting at low PU step) and the S-IVB aft 5 volt excitation module dropped below the minimum of 4.975 vdc from approximately 9410 to 10,691 seconds.

Data indicated that the redundant Secure Range Safety Command Systems (SRSCS) on the S-IC, S-II, and S-IVB stages were ready to perform their functions properly on command if flight conditions during the launch phase had required vehicle destruct. The system properly safed the S-IVB SRSCS on command from KSC. The performance of the Command and Communications System (CCS) in the IU was satisfactory.

The Emergency Detection System (EDS) performance was nominal; no abort limits were reached. The AS-503 EDS configuration was essentially the same as AS-502 except that the presence of the crew provided the capability for EDS manual abort and there was a display of launch vehicle tank pressures in the spacecraft.

The vehicle internal, external, and base region pressure environments were generally in good agreement with the predictions and compared well with previous flight data. The pressure environment was well below design levels. The measured acoustic levels were generally in good agreement with the liftoff and inflight predictions, and with data from previous flights.

The vehicle thermal environment was generally less severe than that for which the vehicle was designed. As on the previous flights, M-31 insulation was lost from the heat shield but caused no problems.

The S-IC canister conditioning system and the aft environmental conditioning system performed satisfactorily during the AS-503 countdown. The S-II thermal control and compartment conditioning system maintained temperatures within the design limits throughout the prelaunch operations. The IU Environmental Control System (ECS) performed well throughout the flight. Coolant temperatures, pressures, and flowrates remained within the predicted ranges and design limits for the first 3 hours of available flight data.

The AS-503 launch vehicle data system consisted of 2670 active flight measurements, 21 telemetry links, onboard tape recorders, film and television cameras, and tracking. With the exception of the onboard film cameras, all data system elements performed very satisfactorily. However, only one of the four S-IC film cameras was recovered. The performance of all vehicle telemetry systems was excellent. The last usable VHF data were received by the Guaymas and Texas stations from telemetry links CF-1 and CP-1 at 15,660 seconds (4:21:00). Performance of the Radio Frequency (RF) system was satisfactory. Measured flight data, with few exceptions,

agreed favorably with expected trends. Final loss of RF carrier signals after translunar injection were as follows: VHF telemetry was last received by Guaymas at approximately 29,230 seconds (8:07:10); CCS was lost by Guaymas at approximately 44,357 seconds (12:19:17), and the C-Band radar transmission was last received by Grand Turk Island (GTI) at approximately 21,325 seconds (5:55:25). Ground camera coverage was good as evidenced by 81.5 percent system efficiency. The onboard television (TV) systems performed satisfactorily and provided useful data.

SECTION 1

INTRODUCTION

1.1 PURPOSE

This report provides the National Aeronautics and Space Administration (NASA) Headquarters, and other interested agencies, with the launch vehicle evaluation results of the AS-503 flight test. The basic objective of flight evaluation is to acquire, reduce, analyze, evaluate and report on flight test data to the extent required to assure future mission success and vehicle reliability. To accomplish this objective, actual flight malfunctions and deviations must be identified, their causes accurately determined, and complete information made available so that corrective action can be accomplished within the established flight schedule.

1.2 SCOPE

This report presents the results of the early engineering flight evaluation of the AS-503 launch vehicle. The contents are centered on the performance evaluation of the major launch vehicle systems, with special emphasis on failures, anomalies, and deviations. Summaries of launch operations and spacecraft performance are included for completeness.

The official MSFC position at this time is represented by this report. It will not be followed by a similar report unless continued analysis or new information should prove the conclusion presented herein to be significantly incorrect. Final stage evaluation reports will, however, be published by the stage contractors. Reports covering major subjects and special subjects will be published as required.

SECTION 2

EVENT TIMES

2.1 SUMMARY OF EVENTS

Range zero time, the basic time reference for this report, is 7:51:00 Eastern Standard Time (EST) (12:51:00 Universal Time [UT]). This time is based on the nearest second prior to S-IC tail plug disconnect which occurred at 7:51:00.67 EST. Range time is calculated as the elapsed time from range zero time and reflects the time at which the event occurred at the vehicle, plus the time necessary to transmit the data from the vehicle to the ground stations. Figure 2-1 shows transmission delays plotted versus range time. Unless otherwise noted, range time is used throughout the report.

Guidance Reference Release (GRR)occurred at -16.97 and start of Time Base 1 (T_1) occurred 17.64 seconds later at 0.67 second. These times were established by the Digital Events Evaluator (DEE-6), except for the time from GRR to T_1 which was determined by the Launch Vehicle Digital Computer (LVDC).

Range time for each time base used in the flight sequence program and the signal for initiating each time base are presented in Table 2-1.

Start of T_3 was initiated approximately 2.45 seconds later than predicted by a fuel level sensor cutoff rather than the expected LOX level sensor cutoff. Reasons for the longer than expected S-IC burn time and fuel level cutoff are discussed in Section 5 of this document.

Start of T_4 was approximately 2.85 seconds later than predicted due to a combination of the late S-IC Outboard Engine Cutoff (OECO) and a longer than expected S-II burn as discussed in Section 6 of this document.

Start of T_5 was approximately 1 second later than predicted. A shorter than predicted S-IVB burn, as discussed in Section 7, resulted in reducing the effect of the prolonged burns of the lower stages.

Start of T_6 and T_7 were within nominal expectations for these events.

T_{5A} was initiated at spacecraft separation detection by discrete input DIN 4, and upon completion proper return to T_7 was accomplished.

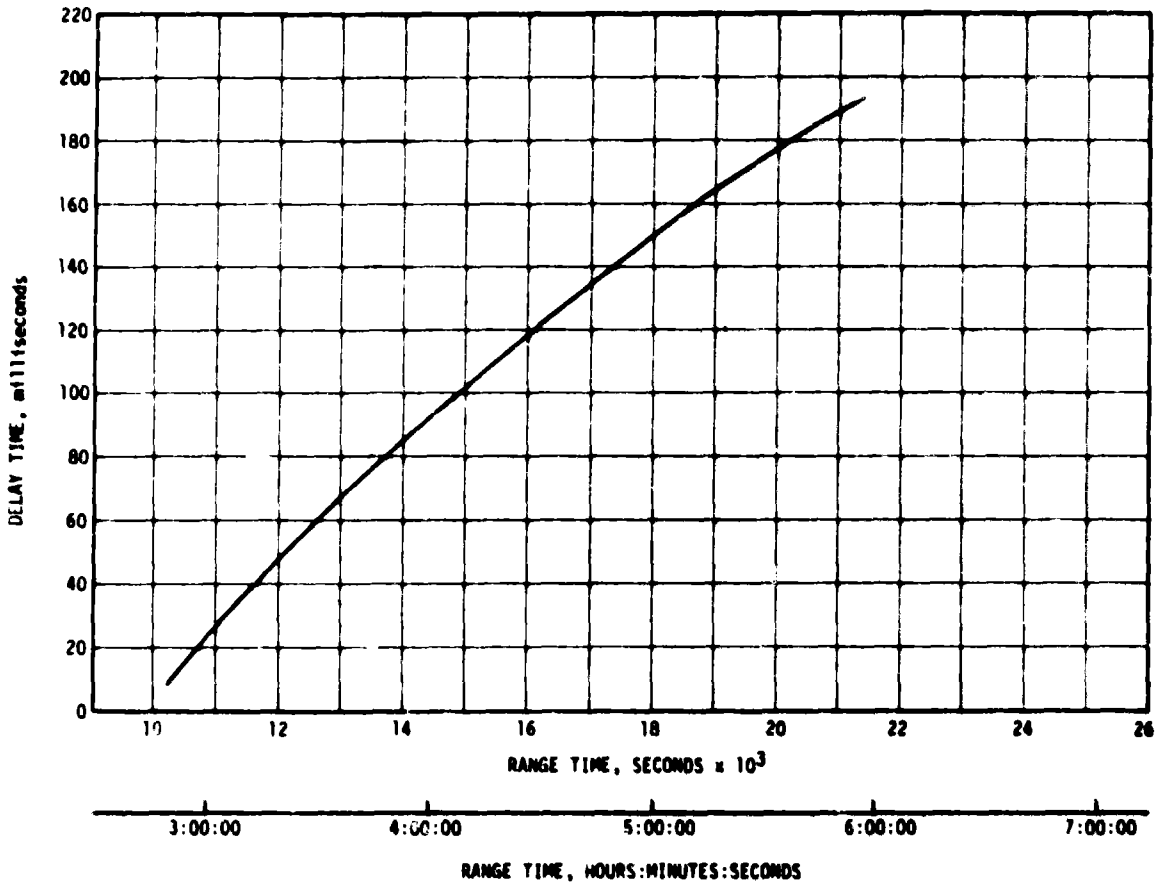

Figure 2-1. AS-503 Transmission Delay Time

A summary of significant events for AS-503 is given in Table 2-2. The actual-minus-predicted times listed in this table in the time-from-base columns are not all IU commanded switch selector functions, and deviations are not to be construed as failures to meet specified switch selector tolerances. The events associated with guidance, navigation, and control have been identified as being accurate to within a major computation cycle time or accurate to within ± 0.5 second (see Table 2-2).

The spacecraft separation sequence was manually initiated at 12,056.3 seconds, and physical separation was accomplished 3 seconds later at 12,059.3. The 3-second interval between initiation of the sequence and actual separation was engendered by a 3-second timer which inhibited the separation initiation signal to the separation pyrotechnics. A parallel initiation signal, inhibited by a 30-millisecond timer, was sent to the Instrument Unit (IU) digital events register.

2.2 SEQUENCE OF EVENTS

Table 2-3 lists the sequence of switch selector events. Terminology in this table agrees with the terminology in document 40M33623C "Interface

Table 2-1. Time Base Summary

TIME BASE	RANGE TIME SEC (HR:MIN:SEC)	SIGNAL START
T_0	-16.97	Guidance Reference Release
T_1	0.67	IU Umbilical Disconnect Sensed by LVDC
T_2	125.88	S-IC IECO Command by LVDC
T_3	153.82	S-IC OECO Sensed by LVDC
T_4	524.04	S-II ECO Sensed by LVDC
T_5	685.19	S-IVB ECO (Velocity) Sensed by LVDC
T_6	9659.54 (2:40:59.54)	Restart Equation Solution
T_7	10,555.73 (2:55:55.73)	S-IVB ECO (Velocity) Sensed by LVDC
T_{5A}	12,057.70 (3:20:57.70)	Spacecraft Separation Sensed by LVDC

Control Definition of Saturn SA-503 Flight Sequence Program". The times reported are accurate to within 10 milliseconds. Ten events, including S-II engine start, were not verified because of telemetry dropout during S-IC/S-II staging, although subsequent events indicate that these events did in fact occur. Additionally, some orbital events and some events after translunar injection were not verified because of station visibility constraints and loss of data due to flight perturbations. Probable times for these events were calculated from the flight program and are so identified in the table.

Table 2-4 lists the known switch selector events which were issued during flight but were not programmed for specific times. The water coolant valve open and close switch selector commands were issued based on the condition of two thermal switches in the Environmental Control System (ECS). The outputs of these switches were sampled once every 300 seconds beginning at 480 seconds; and a switch selector command was issued to open the water valve if the sensed temperature was too high and close the water valve if the temperature was too low.

This table also contains the special sequence switch selector events which were programmed to be initiated by telemetry station acquisition. The issuance of these commands assured telemetry calibration data while the vehicle was in range of the station.

Table 2-2. Significant Event Times Summary

EVENT	RANGE TIME		TIME FROM BASE	
	ACTUAL SEC	ACT-PRED SEC	ACTUAL SEC	ACT-PRED SEC
1. Guidance Reference Release	-16.97	-0.05	-17.64	-0.98
2. S-IC Engine Start Sequence Command	-8.89	-0.09	-9.56	-0.04
3. Range Zero	0.0	0.0	-0.67	-
4. All Holddown Arms Released	0.27	-0.06	-	-
5. First Motion	0.33	0.0	-	-
6. IU Umbilical Disconnect Start of Time Base 1 (T_1)	0.67	-0.05	T_1	-
7. Begin Tower Clearance Yaw Maneuver	1.76*	0.04	1.09*	0.09
8. End Yaw Maneuver	9.72*	0.00	9.05*	0.05
9. Begin Pitch and Roll Maneuver (Tilt and Roll)	12.11*	1.28	11.44*	0.04
10. S-IC Outboard Engine Cant, ON	20.64	-0.08	19.97	-0.03
11. Begin Second Segment of Pitch Polynomial	26.03*	-1.43	25.36*	0.31
12. End Roll Maneuver	31.52*	1.19	30.85*	0.65
13. Mach 1 Achieved	61.48	0.90	60.81	0.81
14. Begin Third Segment of Pitch Polynomial	70.23*	-1.85	69.56*	0.51
15. Maximum Dynamic Pressure (Max Q)	78.90	2.82	78.23	2.23
16. Begin Fourth Segment of Pitch Polynomial	100.29*	-2.43	99.62*	-0.43
17. Computer Switch Point 1 Command	105.64*	-0.08	104.97*	-0.03

* Accurate to within ± 0.5 second

Table 2-2. Significant Event Times Summary (Continued)

EVENT	RANGE TIME		TIME FROM BASE	
	ACTUAL SEC (HR:MIN:SEC)	ACT-PRED SEC	ACTUAL SEC	ACT-PRED SEC
18. Computer Switch Point 2 Command	120.62	-0.10	119.95	-0.05
19. Start of Time Base 2 (T_2)	125.88	-0.04	T_2	-
20. S-IC Inboard Engine Cutoff Command (IECO)	125.93	0.01	0.05	0.05
21. End Pitch Maneuver (Tilt Arrest)	145.50*	-0.96	19.62*	-0.88
22. S-IC Outboard Engine Cutoff (OECO) (Sensed by LVDC), Start of Time Base 3 (T_3)	153.82	2.45	T_3	-
23. S-II Ullage Ignition Command	154.29	2.42	0.47	-0.03
24. S-IC/S-II Separation Command to Fire Separation Devices and Retro Motors	154.47	2.40	0.65	-0.05
25. S-IC Retro Motor Burn Time Initiation (Thrust Buildup Begins)	154.56	2.39	0.64	-0.07
26. S-II Engine Start Command (ESC)	155.19	2.42	1.37	-0.03
27. S-II Ignition (STDV Opens) (Average of 5)	156.19	2.42	2.38	-0.03
28. S-II Engine at 90 Percent Thrust (Average of 5)	158.47	2.70	4.65	0.24
29. S-II Ullage Motor Burn Time Termination (75 Percent Thrust)	158.34	1.97	4.52	0.22

* Accurate to within ± 0.5 second.

Table 2-2. Significant Event Times Summary (Continued)

EVENT	RANGE TIME		TIME FROM BASE	
	ACTUAL SEC (HR:MIN:SEC)	ACT-PRED SEC	ACTUAL SEC	ACT-PRED SEC
30. S-II High Engine Mixture Ratio (EMR) (5.5) Command	160.67	2.40	6.85	-0.05
31. S-II Second Plane Separation Command	184.47	2.40	30.65	-0.05
32. Launch Escape Tower (LET) Jettison	188.6	1.03	34.78	-1.42
33. Initiation of IGM Phase 1	196.22*	3.39	42.40*	1.80
34. Steering Misalignment Correction (SMC) Turn On	214.47**	0.64	60.65**	0.05
35. Computer Switch Point 3 Command	215.17	2.40	61.36	-0.04
36. Computer Switch Point 4 Command	345.20	2.43	191.38	-0.02
37. S-II Low EMR (4.5) Command	443.45†	2.42	289.62†	-0.04
38. Stop First Phase IGM and Initiate IGM Phase 2	443.65*	4.07	289.83*	0.17
39. End of Artificial Tau Mode	484.25**	6.17	330.43**	0.98
40. Begin Chi Freeze, End IGM Phase 2	513.12	0.04*	359.30*	1.28
41. S-II Engine Cutoff (ECO) (Sensed by LVDC), Start of Time Base 4 (T_4)	524.04	2.85	T_4	-
42. S-IVB Ullage Motor Ignition Command	524.78	2.89	0.74	0.04
43. S-II/S-IVB Separation Command to Fire Separation Devices and Retro Motors	524.90	2.91	0.86	0.06

* Accurate to within ± 0.5 second.
** Accurate to major computation cycle dependent upon length of computation cycle.
† Variable switch selector command issued when T_{11} is equal to or less than zero and is a function of the flight program.

Table 2-2. Significant Event Times Summary (Continued)

EVENT	RANGE TIME		TIME FROM BASE	
	ACTUAL SEC (HR:MIN:SEC)	ACT-PRED SEC	ACTUAL SEC	ACT-PRED SEC
44. S-II Retro Motor Burn Time Initiation (Thrust Buildup Begins)	524.98	2.98	0.94	0.13
45. LVDC S-IVB Engine Start Sequence Command	525.00	2.81	0.95	-0.05
46. S-IVB Engine Ignition (STDV Open)	528.29	3.10	4.25	0.25
47. S-IVB Engine at 90 Percent Thrust	530.53	2.84	6.49	-0.01
48. End Chi Freeze; Initiate Third Phase IGM	532.87*	4.04	11.68*	5.18
49. S-IVB Ullage Case Jettison Command	536.80	2.81	12.76	-0.04
50. End Artificial Tau Mode	540.01**	2.43	18.82**	2.32
51. Initiate SMC	542.02**	-0.81	17.97**	2.97
52. Initiate First Chi Bar Steering	652.87*	3.29	131.68*	0.47
53. Initiate Chi Freeze, End Third Phase IGM	677.60*	0.39	156.41	-3.10
54. S-IVB Velocity Cut-off Command (ECO)	684.98	0.99	T_5-0.21	-0.01
55. S-IVB Engine Cutoff Sensed by LVDC, Start of Time Base 5 (T_5)	685.19	1.00	T_5	-
56. S-IVB APS Ullage Motor No. 1 Command	685.46	0.97	0.27	-0.03
57. S-IVB APS Ullage Motor No. 2 Command	685.60	1.01	0.40	0.00
58. Parking Orbit Insertion	694.98	0.99	9.78	-0.02
59. Begin Orbital Navigation	785.19*	0.98	100.00*	0.0

* Accurate to within ± 0.5 second.
** Accurate to major computation cycle dependent upon length of computation cycle.

Table 2-2. Significant Event Times Summary (Continued)

EVENT	RANGE TIME		TIME FROM BASE	
	ACTUAL SEC	ACT-PRED SEC	ACTUAL SEC	ACT-PRED SEC
60. Initiate S-IVB Re-start Sequence and Start of Time Base 6 (T_6)	9659.54	0.71	T_6	-
61. S-IVB Helium Heater On Command	9700.80	0.67	41.25	-0.05
62. S-IVB LH_2 Vent Valve Close Command	9701.72	0.69	42.17	-0.03
63. S-IVB APS Ullage Motor No. 1 Ignition Command	10,155.82	0.69	496.27	-0.03
64. S-IVB APS Ullage Motor No. 2 Ignition Command	10,155.91	0.68	496.36	-0.04
65. S-IVB Helium Heater Off Command	10,160.80	0.67	501.25	-0.05
66. LVDC S-IVB Engine Restart Command	10,229.51	0.68	569.97	-0.03
67. S-IVB APS Ullage Motor No. 1 Cutoff Command	10,232.49	0.66	572.95	-0.05
68. S-IVB APS Ullage Motor No. 2 Cutoff Command	10,232.59	0.66	573.05	-0.05
69. S-IVB Engine Re-ignition (STDV Open)	10,237.79	1.16	578.25	-0.45
70. S-IVB Engine at 90 Percent Thrust	10,240.02	0.89	580.48	0.18
71. Out of Orbit IGM Initiation	10,245.83*	2.50	586.31*	1.97
72. Initiate SMC	10,253.53**	-6.80	594.01**	2.51
73. Flight Control Computer Switch Point 6 Command	10,497.49	0.66	837.95	-0.05
74. S-IVB Velocity Cut-off Command (ECO)	10,555.51	3.23	T_7-0.21	-0.01

* Accurate to within ± 0.5 second.
** Accurate to major computation cycle dependent upon length of computation cycle.

Table 2-2. Significant Event Times Summary (Continued)

EVENT	RANGE TIME		TIME FROM BASE	
	ACTUAL SEC (HR:MIN:SEC)	ACT-PRED SEC	ACTUAL SEC	ACT-PRED SEC
75. S-IVB Engine Cutoff Sensed by LVDC, Start of Time Base 7 (T_7), Begin Orbital Guidance	10,555.73	3.25	T_7	-
76. S-IVB LH_2 Vent Valve Open Command	10,556.19	3.41	0.47	-0.03
77. Translunar Injection	10,565.51	3.23	9.78	-0.02
78. Start Local Horizontal Attitude Maneuver, Begin Orbital Navigation	10,575.77*	3.29	20.05*	0.05
79. S-IVB LH_2 Vent Valve Close Command	11,455.71	2.93	899.95	-0.05
80. Start Maneuver for Separation Attitude	11,458.40*	-2.06	902.64*	-5.34
81. Spacecraft Separation Sequence Start	12,056.3	3.82	1500.58	0.58
82. Start of Time Base 5_A (T_{5A})	12,057.70	-	T_{5A}	-
83. Flight Control Computer Switch Point No. 5 Command	12,057.85	-	T_{5A}+0.15	-0.05
84. LV-LTA/CSM Separation	12,059.3	3.82	1503.58	0.58
85. Start Slingshot Attitude Maneuver	17,096.63*	4.15	6540.92*	0.92
86. Begin Slingshot Mode (LH_2 Vent Valve Open Command)	17,756.02	3.54	7200.15	-0.05
87. Apply Slingshot ΔV (Helium Control Valve Open Command for LOX Dump)	18,476.03	3.35	7920.15	-0.05

* Accurate to within ± 0.5 second.

Table 2-2. Significant Event Times Summary (Continued)

EVENT	RANGE TIME		TIME FROM BASE	
	ACTUAL SEC (HR:MIN:SEC)	ACT-PRED SEC	ACTUAL SEC	ACT-PRED SEC
88. End Propellant Dump (Mainstage Control Valve Close Command)	18,776.03	3.55	8220.15	-0.05
89. S-IVB Ullage Engine No. 1 on Command	19,555.85	3.37	8999.96	-0.04
90. S-IVB Ullage Engine No. 2 on Command	19,556.06	3.38	9000.17	-0.03
91. S-IVB Ullage Engine No. 2 Depleted	20,288.56	-	9732.83	-
92. S-IVB Ullage Engine No. 1 Depleted	20,314.00	-	9758.27	-

Table 2-3. Sequence of Switch Selector Events

FUNCTION	STAGE	RANGE TIME ACTUAL (SEC)	TIME FROM BASE ACTUAL (SEC)	TIME FROM BASE ACT-PRED SEC
1. Liftoff - Start of Time Base 1 (T_1)		0.67	0.0	0.0
2. Sensor Bias, ON	IU	5.63	4.95	-0.05
3. Multiple Engine Cutoff, ENABLE	S-IC	14.63	13.95	-0.05
4. S-IC Outboard Engines Cant, ON "A"	IU	20.42	19.75	-0.05
5. S-IC Outboard Engines Cant, ON "B"	IU	20.64	19.97	-0.03
6. S-IC Outboard Engines Cant, ON "C"	IU	20.82	20.15	-0.05
7. Telemeter Calibrate, ON	S-IC	24.62	23.95	-0.05
8. Telemetry Calibrator In-Flight Calibrate, ON	IU	27.64	26.97	-0.03
9. Telemeter Calibrate, OFF	S-IC	29.62	28.95	-0.05
10. Launch Vehicle Engines EDS Cutoff, ENABLE	IU	30.62	29.95	-0.05
11. Telemetry Calibrator In-Flight Calibrate, OFF	IU	32.64	31.97	-0.03
12. Fuel Pressurizing Valve No. 2 Open + Tape Recorder, RECORD	S-IC	50.12	49.45	-0.05
13. START Data Recorders	S-II	74.63	73.96	-0.04
14. Cooling System Electronic Assembly Power, OFF	IU	75.63	74.95	-0.05
15. Telemetry Calibrator In Flight Calibrate, ON	IU	90.64	89.97	-0.03
16. Telemetry Calibrator In-Flight Calibrate, OFF	IU	95.64	94.97	-0.03
17. Fuel Pressurizing Valve No. 3, OPEN	S-IC	95.94	95.27	-0.03
18. Flight Control Computer Switch Point No. 1	IU	105.64	104.97	-0.03
19. Telemeter Calibrate, ON	S-IC	115.75	115.07	-0.03
20. Flight Control Computer Switch Point No. 2	IU	120.62	119.95	-0.05
21. Telemeter Calibrate, OFF	S-IC	120.73	120.06	-0.04
22. Fuel Pressurizing Valve No. 4, OPEN	S-IC	124.12	123.45	-0.05
23. Tape Recorder Record, ON	IU	124.43	123.75	-0.05
24. LOX Tank Strobe Lights, OFF	S-IC	124.72	124.05	-0.05

Table 2-3. Sequence of Switch Selector Events (Continued)

FUNCTION	STAGE	RANGE TIME ACTUAL (SEC)	TIME FROM BASE ACTUAL (SEC)	TIME FROM BASE ACT-PRED SEC
25. S-IC Two Engines Out Auto-Abort Inhibit, ENABLE	IU	124.93	124.26	-0.04
26. S-IC Two Engines Out Auto-Abort INHIBIT	IU	125.13	124.45	-0.05
27. Excess Rate (P, Y, R) Auto-Abort Inhibit, ENABLE	IU	125.33	124.66	-0.04
28. Excess Rate (P, Y, R) Auto-Abort Inhibit and Switch Rate Gyros SC, INDICATION "A"	IU	125.53	124.85	-0.05
29. Two Adjacent Outboard Engines Out Cutoff, ENABLE	S-IC	125.73	125.06	-0.04
30. START of Time Base 2 (T_2)		125.88	0.0	0.0
31. Inboard Engine Cutoff (IECO)	S-IC	125.93	0.05	0.05
32. Inboard Engine Cutoff, BACKUP	S-IC	126.03	0.15	-0.05
33. START First PAM-FM/FM Calibration	S-II	126.23	0.35	-0.05
34. Auto-Abort Enable Relays, RESET	IU	126.45	0.57	-0.03
35. Excess Rate (Roll) Auto-Abort Inhibit, ENABLE	IU	126.63	0.75	-0.05
36. Excess Rate (Roll) Auto-Abort Inhibit and Switch Rate Gyros SC, INDICATION "B"	IU	126.84	0.96	-0.04
37. STOP First PAM-FM/FM Calibration	S-II	131.23	5.35	-0.05
38. S-II Ordnance, ARM	S-II	141.74	15.86	-0.04
39. Separation and Retro No. 1 EBW Firing Units, ARM	S-IC	141.93	16.05	-0.05
40. Separation and Retro No. 2 EBW Firing Units, ARM	S-IC	142.14	16.26	-0.04
41. Telemetry Measurement, SWITCHOVER	S-IC	144.93	19.05	-0.05
42. Separation Camera, ON	S-IC	145.13	19.25	-0.05
43. Q-Ball Power, OFF	IU	145.23	19.35	-0.05
44. Outboard Engines Cutoff, ENABLE	S-IC	145.33	19.45	-0.05
45. Outboard Engines Cutoff Backup, ENABLE	S-IC	145.54	19.66	-0.04
46. Outboard Engines Cutoff - START of Time Base 3 (T_3)		153.82	0.0	0.0

Table 2-3. Sequence of Switch Selector Events (Continued)

FUNCTION	STAGE	RANGE TIME ACTUAL (SEC)	TIME FROM BASE ACTUAL (SEC)	TIME FROM BASE ACT-PRED SEC
47. LH_2 Tank High Pressure Vent Mode	S-II	153.90	0.08	-0.02
48. S-II LH_2 Recirculation Pumps, OFF	S-II	154.00	0.18	-0.02
49. S-II Ullage, TRIGGER	S-II	154.29	0.47	-0.03
50. S-IC/S-II Separation (No. 1)	S-IC	154.47	0.65	-0.05
51. S-IC/S-II Separation (No. 2)	S-IC	154.57	0.75	-0.05
52. S-II Engines Cutoff, RESET	S-II	154.69*	0.87*	-0.03
53. Engines Ready, BYPASS	S-II	154.79*	0.97*	-0.03
54. Prevalves Lockout, RESET	S-II	154.89*	1.07*	-0.03
55. Switch Engine Control To S-II and S-IC Outboard Engine Cant, OFF "A"	IU	154.99*	1.17*	-0.03
56. S-IC Outboard Engines Cant, OFF "B"	IU	155.09*	1.27*	-0.03
57. S-II Engine, START	S-II	155.19*	1.37*	-0.03
58. S-II Engine Out Indication "A", ENABLE; S-II AFT Interstage Separation Indication "A", ENABLE	IU	155.29*	1.47*	-0.03
59. S-II Engine Out Indication "B", ENABLE; S-II AFT Interstage Separation Indication "B", ENABLE	IU	155.49*	1.67*	-0.03
60. Engines Ready Bypass, RESET	S-II	155.69*	1.87*	-0.03
61. Measurement Transfer Mode Position "B"	S-IVB	155.79*	1.97*	-0.03
62. S-II Hydraulic Accumulators, UNLOCK	S-II	156.78	2.95	-0.05
63. PU System Open Loop, ARM	S-II	159.99	6.17	-0.03
64. Chilldown Valves, CLOSE	S-II	160.17	6.35	-0.05
65. S-II Start Phase Limiter Cutoff, ARM	S-II	160.50	6.67	-0.03
66. High (5.5) Engine Mixture Ratio, ON	S-II	160.67	6.85	-0.05
67. S-II Start Phase Limiter Cutoff, ARM RESET	S-II	161.50	7.67	-0.03
68. Prevalves Close, ARM	S-II	161.60	7.78	-0.02
69. Tape Recorder Record, OFF	IU	165.47	11.65	-0.05
70. STOP Data Recorders	S-II	165.69	11.87	-0.03
71. S-II AFT Interstage Separation	S-II	184.47	30.65	-0.05

*Derived times verified that these events occurred.

Table 2-3. Sequence of Switch Selector Events (Continued)

FUNCTION	STAGE	RANGE TIME ACTUAL (SEC)	TIME FROM BASE ACTUAL (SEC)	TIME FROM BASE ACT-PRED SEC
72. Water Coolant Valve, OPEN	IU	184.77	30.95	-0.05
73. Flight Control Computer Switch Point No. 3	IU	215.17	61.36	-0.04
74. START Second PAM-FM/FM Calibration	S-II	278.78	124.96	-0.04
75. STOP Second PAM-FM/FM Calibration	S-II	283.77	129.95	-0.05
76. Flight Control Computer Switch Point No. 4	IU	345.20	191.38	-0.02
77. Telemetry Calibrator In-Flight Calibrate, ON	IU	356.49	202.67	-0.03
78. Telemetry Calibrator In-Flight Calibrate, OFF	IU	361.49	207.66	-0.04
79. Measurement Control Switch No. 2, ACTIVATE	S-II	366.49	212.66	-0.04
80. START Third PAM-FM/FM Calibration	S-II	378.78	224.96	-0.04
81. STOP Third PAM-FM/FM Calibration	S-II	383.78	229.96	-0.04
82. High (5.5) Engine Mixture Ratio, OFF	S-II	443.24**	289.42**	-0.03
83. Low (4.5) Engine Mixture Ratio, ON	S-II	443.45**	289.62**	-0.04
84. Telemetry Calibrator In-Flight Calibrate, ON	IU	444.69	290.87	-0.03
85. Telemetry Calibrator In-Flight Calibrate, OFF	IU	449.68	295.85	-0.05
86. S-II LH_2 Step Pressurization	S-II	453.78	299.96	-0.04
87. Charge Ullage Ignition, ON	S-IVB	484.99	331.17	-0.03
88. S-II/S-IVB Ordnance, ARM	S-II	485.18	331.35	-0.05
89. Tape Recorder Record, ON	IU	486.09	332.26	-0.04
90. START Data Recorders	S-II	486.27	332.45	-0.05
91. S-II LOX Depletion Sensors Cutoff, ARM	S-II	488.88	335.05	-0.05
92. S-II LH_2 Depletion Sensors Cutoff, ARM	S-II	489.08	335.26	-0.04
93. START of Time Base 4 (T_4)		524.04	0.0	0.0
94. Cutoff S-II J-2 Engines, BACKUP	S-II	524.13	0.08	0.08
95. START Recorder Timers	S-II	524.22	0.18	0.08
96. Prevalves Close, OFF	S-IVB	524.31	0.27	0.07

** Variable switch selector command issued when T_1 is equal to or less than zero and is a function of the flight program.

Table 2-3. Sequence of Switch Selector Events (Continued)

FUNCTION	STAGE	RANGE TIME	TIME FROM BASE	
		ACTUAL (SEC)	ACTUAL (SEC)	ACT-PRED SEC
97. S-IVB Engine Cutoff, OFF	S-IVB	524.41	0.36	0.06
98. LOX Tank Flight Pressure System, ON	S-IVB	524.50	0.46	0.06
99. Engine Ready, BYPASS	S-IVB	524.59	0.55	0.05
100. LOX Chilldown Pump, OFF	S-IVB	524.69	0.64	0.04
101. Fire Ullage Ignition, ON	S-IVB	524.78	0.74	0.04
102. S-II/S-IVB Separation	S-II	524.90	0.86	0.06
103. S-IVB Engine Start, ON	S-IVB	525.00	0.95	-0.05
104. Flight Control Computer S-IVB Burn Mode, ON "A"	IU	525.21	1.16	-0.04
105. Flight Control Computer S-IVB Burn Mode, ON "B"	IU	525.30	1.26	-0.04
106. Fuel Chilldown Pump, OFF	S-IVB	526.22	2.17	-0.03
107. S-IVB Engine Out Indication "A", ENABLE	IU	526.52	2.47	-0.03
108. S-IVB Engine Out Indication "B", ENABLE	IU	526.70	2.65	-0.05
109. Fuel Injection Temperature OK, BYPASS	S-IVB	528.01	3.96	-0.04
110. S-IVB Engine Start, OFF	S-IVB	528.20	4.15	-0.05
111. First Burn Relay, ON	S-IVB	529.80	5.75	-0.05
112. Charge Ullage Jettison, ON	S-IVB	533.80	9.75	-0.05
113. Fire Ullage Jettison, ON	S-IVB	536.80	12.76	-0.04
114. Ullage Charging, RESET	S-IVB	537.80	13.75	-0.05
115. Ullage Firing, RESET	S-IVB	538.02	13.97	-0.03
116. Fuel Injection Temperature OK Bypass, RESET	S-IVB	538.20	14.15	-0.05
117. Tape Recorder Record, OFF	IU	538.42	14.37	-0.03
118. Telemetry Calibrator In-Flight Calibrate, ON	IU	540.82	16.77	-0.03
119. Telemetry Calibrator In-Flight Calibrate, OFF	IU	545.80	21.75	-0.05
120. Heat-Exchanger Bypass Valve Control, ENABLE	S-IVB	548.02	23.97	-0.03

Table 2-3. Sequence of Switch Selector Events (Continued)

	FUNCTION	STAGE	RANGE TIME ACTUAL (SEC)	TIME FROM BASE ACTUAL (SEC)	TIME FROM BASE ACT-PRED SEC
121.	In-Flight Calibration Mode, ON	S-IVB	549.71	25.66	-0.04
122.	TM Calibrate, ON	S-IVB	550.21	26.17	-0.03
123.	TM Calibrate, OFF	S-IVB	555.22	31.17	-0.03
124.	In-Flight Calibration Mode, OFF	S-IVB	555.70	31.65	-0.05
125.	Engine Pump Purge Control Valve, ENABLE ON	S-IVB	678.42	-6.78	0.22
126.	S-IVB Engine Cutoff Velocity	S-IVB	684.98	-0.21	-0.01
127.	Velocity Cutoff of S-IVB Engine START of Time Base 5 (T_5)	S-IVB	685.19	0.0	0.0
128.	S-IVB Engine Cutoff	S-IVB	685.28	0.09	-0.01
129.	Point Level Sensor, DISARMING	S-IVB	685.37	0.18	-0.02
130.	S-IVB Ullage Engine No. 1, ON	S-IVB	685.46	0.27	-0.03
131.	S-IVB Ullage Engine No. 2, ON	S-IVB	685.60	0.40	0.00
132.	S-IVB Ullage Thrust Present Indication, ON	IU	685.77	0.58	-0.02
133.	First Burn Relay, OFF	S-IVB	685.94	0.75	-0.05
134.	LOX Tank Flight Pressure System, OFF	S-IVB	686.35	1.16	-0.04
135.	LOX Tank Pressurization Shutoff Valves, CLOSE	S-IVB	686.57	1.37	-0.03
136.	Engine Pump Purge Control Valve Enable, ON	S-IVB	686.74	1.55	-0.05
137.	Flight Control Computer S-IVB Burn Mode, OFF "A"	IU	688.65	3.46	-0.04
138.	Flight Control Computer S-IVB Burn Mode, OFF "B"	IU	688.86	3.67	-0.03
139.	Aux. Hydraulic Pump Flight Mode, OFF	S-IVB	689.24	4.05	-0.05
140.	Telemetry Calibrator In-Flight Calibrate, ON	IU	689.34	4.15	-0.05
141.	S/C Control of Saturn, ENABLE	IU	690.16	4.97	-0.03
142.	In-Flight Calibration Mode, ON	S-IVB	691.65	6.46	-0.04
143.	TM Calibrate, ON	S-IVB	692.14	6.95	-0.05
144.	Telemetry Calibrator In-Flight Calibrate, OFF	IU	694.34	9.15	-0.05

Table 2-3. Sequence of Switch Selector Events (Continued)

FUNCTION	STAGE	RANGE TIME ACTUAL (SEC)	TIME FROM BASE ACTUAL (SEC)	TIME FROM BASE ACT-PRED SEC
145. S-IVB Engine Out Indication "A", ENABLE RESET	IU	695.14	9.95	-0.05
146. S-IVB Engine Out Indication "B", ENABLE RESET	IU	695.38	10.19	-0.01
147. S-1 RF Assembly Power, OFF	IU	695.54	10.35	-0.05
148. Tape Recorder Playback Reverse, ON	IU	696.45	11.26	-0.04
149. TM Calibrate, OFF	S-IVB	697.16	11.97	-0.03
150. In-Flight Calibration Mode, OFF	S-IVB	697.65	12.46	-0.04
151. Single Sideband FM Transmitter, OFF	S-IVB	707.14	21.95	-0.05
152. LH_2 Tank Continuous Vent Orifice Shutoff Valve, OPEN ON	S-IVB	744.15	58.96	-0.04
153. LH_2 Tank Continuous Vent Relief Override Shutoff Valve, OPEN ON	S-IVB	744.28	59.09	-0.01
154. LH_2 Tank Continuous Vent Orifice Shutoff Valve Open, OFF	S-IVB	746.15	60.95	-0.05
155. LH_2 Tank Continuous Vent Relief Override Shutoff Valve Open, OFF	S-IVB	746.25	61.05	-0.05
156. Tape Recorder Playback Reverse, OFF	IU	767.25	82.05	-0.05
157. S-IVB Ullage Engine No. 1, OFF	S-IVB	772.18	86.99	-0.01
158. S-IVB Ullage Engine No. 2, OFF	S-IVB	772.26	87.06	-0.04
159. S-IVB Ullage Thrust Present Indication, OFF	IU	772.35†	87.15†	-0.05
160. PU Inverter and DC Power, OFF	S-IVB	1185.15†	499.95†	-0.05
161. Engine Pump Purge Control Valve Enable, OFF	S-IVB	1287.75†	602.55†	-0.05
162. Aux. Hydraulic Pump Flight Mode, ON	S-IVB	3285.15†	2599.95†	-0.05
163. Aux. Hydraulic Pump Flight Mode, OFF	S-IVB	3333.15	2647.95	-0.05
164. PU Inverter and DC Power, ON	S-IVB	5685.15	4999.95	-0.05
165. Aux. Hydraulic Pump Flight Mode, ON	S-IVB	6085.15	5399.95	-0.05
166. Aux. Hydraulic Pump Flight Mode, OFF	S-IVB	6133.17	5447.95	-0.05
167. Begin Restart Preparations - START of Time Base 6 (T6)		9659.54	0.0	0.0
168. S-IVB Restart Alert, ON	IU	9659.63	0.08	-0.02

† Derived time, event not verified.

Table 2-3. Sequence of Switch Selector Events (Continued)

FUNCTION	STAGE	RANGE TIME ACTUAL (SEC)	TIME FROM BASE ACTUAL (SEC)	TIME FROM BASE ACT-PRED SEC
169. S/C Control of Saturn, DISABLE	IU	9659.79	0.25	-0.05
170. In-Flight Calibration Mode, ON	S-IVB	9660.50	0.96	-0.04
171. Telemetry Calibrator In-Flight Calibrate, ON	IU	9660.69	1.15	-0.05
172. TM Calibrate, ON	S-IVB	9660.90	1.36	-0.04
173. Telemetry Calibrator In-Flight Calibrate, OFF	IU	9665.69	6.15	-0.05
174. TM Calibrate, OFF	S-IVB	9665.91	6.36	-0.04
175. In-Flight Calibration Mode, OFF	S-IVB	9666.50	6.95	-0.05
176. S-IVB Engine Cutoff, OFF	S-IVB	9669.50	9.95	-0.05
177. Single Sideband FM Transmitter, ON	S-IVB	9670.00	10.45	-0.05
178. LH_2 Tank Vent and Latching Relief Valve Boost, CLOSE ON	S-IVB	9695.81	36.26	-0.04
179. LOX Tank Vent and NPV Valves Boost, CLOSE ON	S-IVB	9696.00	36.45	-0.05
180. S-IVB Restart Alert, OFF	IU	9696.80	37.25	-0.05
181. LH_2 Tank Vent and Latching Relief Valve Boost Close, OFF	S-IVB	9697.80	38.25	-0.05
182. LOX Tank Vent and NPV Valves Boost Close, OFF	S-IVB	9698.00	38.46	-0.04
183. Repressurization System Mode Selector, OFF (AMB)	S-IVB	9700.62	41.08	-0.02
184. Burner LH_2 Propellant Valve, OPEN ON	S-IVB	9700.80	41.25	-0.05
185. Burner Exciters, ON	S-IVB	9701.10	41.55	-0.05
186. Burner LOX Shutdown Valve, OPEN ON	S-IVB	9701.50	41.96	-0.04
187. LH_2 Tank Continuous Vent Valve, CLOSE ON	S-IVB	9701.72	42.17	-0.03
188. Burner LH_2 Propellant Valve Open, OFF	S-IVB	9702.30	42.76	-0.04
189. Burner LOX Shutdown Valve Open, OFF	S-IVB	9703.02	43.47	-0.03
190. LH_2 Tank Continuous Vent Valve Close, OFF	S-IVB	9703.70	44.15	-0.05
191. Burner Exciters, OFF	S-IVB	9704.90	45.35	-0.05
192. Burner Automatic Cutoff System, ARM	S-IVB	9707.51	47.96	-0.04

Table 2-3. Sequence of Switch Selector Events (Continued)

FUNCTION	STAGE	RANGE TIME ACTUAL (SEC)	TIME FROM BASE ACTUAL (SEC)	TIME FROM BASE ACT-PRED SEC
193. LH_2 Tank Repressurization Control Valve, OPEN ON	S-IVB	9707.65	48.10	0.00
194. LOX Tank Repressurization Control Valve, OPEN ON	S-IVB	9707.82	48.27	-0.03
195. Aux. Hydraulic Pump Flight Mode, ON	S-IVB	9878.52	218.97	-0.03
196. LOX Chilldown Pump, ON	S-IVB	9908.50	248.95	-0.05
197. Fuel Chilldown Pump, ON	S-IVB	9913.50	253.95	-0.05
198. Prevalves, CLOSE ON	S-IVB	9918.52	258.97	-0.03
199. In-Flight Calibration Mode, ON	S-IVB	10,059.50	399.95	-0.05
200. Telemetry Calibrator In-Flight Calibrate, ON	IU	10,059.72	400.17	-0.03
201. TM Calibrate, ON	S-IVB	10,059.90	400.35	-0.05
202. Telemetry Calibrator In-Flight Calibrate, OFF	IU	10,064.72	405.17	-0.03
203. TM Calibrate, OFF	S-IVB	10,064.90	405.35	-0.05
204. In-Flight Calibration Mode, OFF	S-IVB	10,065.50	405.95	-0.05
205. Second Burn Relay, ON	S-IVB	10,109.50	449.96	-0.04
206. PU Valve Hardover Position, ON	S-IVB	10,109.60	450.05	-0.05
207. S-IVB Restart Alert, ON	IU	10,153.10	493.55	-0.05
208. S-IVB Ullage Engine No. 1, ON	S-IVB	10,155.82	496.27	-0.03
209. S-IVB Ullage Engine No. 2, ON	S-IVB	10,155.91	496.36	-0.04
210. S-IVB Ullage Thrust Present Indication, ON	IU	10,156.00	496.45	-0.05
211. LOX Tank Repressurization Control Valve Open, OFF	S-IVB	10,156.10	496.55	-0.05
212. LH_2 Tank Repressurization Control Valve Open, OFF	S-IVB	10,156.20	496.65	-0.05
213. Burner LH_2 Propellant Valve, CLOSE ON	S-IVB	10,156.30	496.75	-0.05
214. Burner Automatic Cutoff System, DISARM	S-IVB	10,156.51	496.96	-0.04
215. LH_2 Tank Continuous Vent Valve, CLOSE ON	S-IVB	10,156.69	497.15	-0.05

Table 2-3. Sequence of Switch Selector Events (Continued)

FUNCTION	STAGE	RANGE TIME ACTUAL (SEC)	TIME FROM BASE ACTUAL (SEC)	TIME FROM BASE ACT-PRED SEC
216. Repressurization System Mode Select, ON (AMB)	S-IVB	10,157.10	497.56	-0.04
217. LH_2 Tank Continuous Vent Valve Close, OFF	S-IVB	10,158.72	499.17	-0.03
218. Burner LH_2 Propellant Valve Close, OFF	S-IVB	10,159.30	499.75	-0.05
219. LOX Tank Repressurization Control Valve, OPEN ON	S-IVB	10,159.51	499.96	-0.04
220. Burner LOX Shutdown Valve, CLOSE ON	S-IVB	10,160.80	501.25	-0.05
221. Burner LOX Shutdown Valve Close, OFF	S-IVB	10,163.80	504.25	-0.05
222. LH_2 Tank Repressurization Control Valve, OPEN ON	S-IVB	10,179.52	519.97	-0.03
223. Prevalves Close, OFF	S-IVB	10,218.90	559.35	-0.05
224. S-IVB Restart Alert, OFF	IU	10,219.50	559.96	-0.04
225. Engine Ready, BYPASS	S-IVB	10,228.11	568.57	-0.03
226. Fuel Chilldown Pump, OFF	S-IVB	10,228.90	569.37	-0.03
227. LOX Chilldown Pump, OFF	S-IVB	10,229.09	569.55	-0.05
228. S-IVB Engine Start, ON	S-IVB	10,229.51	569.97	-0.03
229. S-IVB Ullage Engine No. 1, OFF	S-IVB	10,232.49	572.95	-0.05
230. S-IVB Ullage Engine No. 2, OFF	S-IVB	10,232.59	573.05	-0.05
231. S-IVB Ullage Thrust Present Indication, OFF	IU	10,232.69	573.15	-0.05
232. S-IVB Engine Out Indication "A", ENABLE	IU	10,236.71	577.17	-0.03
233. LOX Tank Repressurization Control Valve Open, OFF	S-IVB	10,236.80	577.26	-0.04
234. S-IVB Engine Out Indication "B", ENABLE	IU	10,236.90	577.36	-0.04
235. LH_2 Tank Repressurization Control Valve Open, OFF	S-IVB	10,236.99	577.45	-0.05
236. Flight Control Computer S-IVB Burn Mode, ON "A"	IU	10,237.09	577.55	-0.05

Table 2-3. Sequence of Switch Selector Events (Continued)

FUNCTION	STAGE	RANGE TIME ACTUAL (SEC)	TIME FROM BASE ACTUAL (SEC)	TIME FROM BASE ACT-PRED SEC
237. Flight Control Computer S-IVB Burn Mode, ON "B"	IU	10,237.30	577.76	-0.04
238. Fuel Injection Temperature OK, BYPASS	S-IVB	10,237.49	577.95	-0.05
239. LOX Tank Flight Pressure System, ON	S-IVB	10,237.71	578.17	-0.03
240. LOX Tank Pressurization Shutoff Valves, OPEN	S-IVB	10,237.89	578.35	-0.05
241. S-IVB Engine Start, OFF	S-IVB	10,238.11	578.57	-0.03
242. PU Valve Hardover Position, OFF	S-IVB	10,242.49	582.95	-0.05
243. Fuel Injection Temperature OK Bypass, RESET	S-IVB	10,247.50	587.96	-0.04
244. Flight Control Computer Switch Point No. 6	IU	10,497.49	837.95	-0.05
245. Second Burn Relay. OFF	S-IVB	10,509.51	849.97	-0.03
246. S-IVB Velocity Cutoff	S-IVB	10,551.51	-0.21	-0.01
247. S-IVB Engine Cutoff START of Time Base 7 (17)		10,555.73	0.0	0.0
248. S-IVB Engine Cutoff, BACKUP	S-IVB	10,555.81	0.09	-0.01
249. LH_2 Tank Continuous Vent Orifice Shutoff Valve, OPEN ON	S-IVB	10,556.19	0.46	-0.04
250. LH_2 Tank Continuous Vent Relief Override Shutoff Valve, OPEN ON	S-IVB	10,556.32	0.60	0.00
251. LOX Tank NPV Valve, OPEN ON	S-IVB	10,556.42	0.69	-0.01
252. LH_2 Tank Latching Relief Valve, OPEN ON	S-IVB	10,556.51	0.79	-0.01
253. Point Level Sensor, DISARMING	S-IVB	10,556.63	0.91	0.01
254. LOX Tank Pressurization Shutoff Valves, CLOSE	S-IVB	10,556.72	1.00	0.00
255. LOX Tank Flight Pressure System, OFF	S-IVB	10,556.85	1.13	0.03
256. Second Burn Relay, OFF	S-IVB	10,556.95	1.22	0.02
257. LH_2 Tank Continuous Vent Orifice Shutoff Valve Open, OFF	S-IVB	10,558.19	2.46	-0.04
258. LH_2 Tank Continuous Vent Relief Override Shutoff Valve Open, OFF	S-IVB	10,558.29	2.56	-0.04

Table 2-3. Sequence of Switch Selector Events (Continued)

FUNCTION	STAGE	RANGE TIME ACTUAL (SEC)	TIME FROM BASE ACTUAL (SEC)	TIME FROM BASE ACT-PRED SEC
259. LOX Tank NPV Valve Latch, OPEN ON	S-IVB	10,558.38	2.65	-0.05
260. LH_2 Tank Latching Relief Valve Latch, ON	S-IVB	10,558.48	2.75	-0.05
261. Flight Control Computer S-IVB Burn Mode, OFF "A"	IU	10,559.28	3.55	-0.05
262. LOX Tank NPV Valve Open, OFF	S-IVB	10,559.38	3.65	-0.05
263. LH_2 Tank Latching Relief Valve Open, OFF	S-IVB	10,559.50	3.78	-0.02
264. Flight Control Computer S-IVB Burn Mode, OFF "B"	IU	10,559.60	3.87	-0.03
265. Aux. Hydraulic Pump Flight Mode, OFF	S-IVB	10,559.80	4.07	-0.03
266. LOX Tank NPV Valve Latch Open, OFF	S-IVB	10,560.39	4.66	-0.04
267. LH_2 Tank Latching Relief Valve Latch, OFF	S-IVB	10,560.49	4.76	-0.04
268. S/C Control Of Saturn, ENABLE	IU	10,560.70	4.97	-0.03
269. S-IVB Engine Out Indication "A" Enable, RESET	IU	10,565.69	9.96	-0.04
270. S-IVB Engine Out Indication "B" Enable, RESET	IU	10,565.88	10.15	-0.05
271. Single Sideband FM Transmitter, OFF	S-IVB	10,580.68	24.95	-0.05
272. LOX Tank NPV Valve, OPEN ON	S-IVB	10,705.39†	149.65†	-0.05
273. LOX Tank NPV Valve Open, OFF	S-IVB	10,706.39†	150.65†	-0.05
274. LOX Tank Vent and NPV Valves Boost, CLOSE ON	S-IVB	10,709.39†	153.65†	-0.05
275. LOX Tank Vent and NPV Valves Boost Close, OFF	S-IVB	10,711.39†	155.65†	-0.05
276. LH_2 Tank Latching Relief Valve, OPEN ON	S-IVB	11,454.69	898.95	-0.05
277. LH_2 Tank Continuous Vent Valve, CLOSE ON	S-IVB	11,455.51	899.75	-0.05
278. LH_2 Tank Latching Relief Valve Open, OFF	S-IVB	11,455.71	899.95	-0.05
279. LH_2 Tank Continuous Vent Valve Close, OFF	S-IVB	11,457.51	901.75	-0.05
280. LH_2 Tank Vent and Latching Relief Valve Boost, CLOSE ON	S-IVB	11,458.72	902.96	-0.04

† Derived time, event not verified.

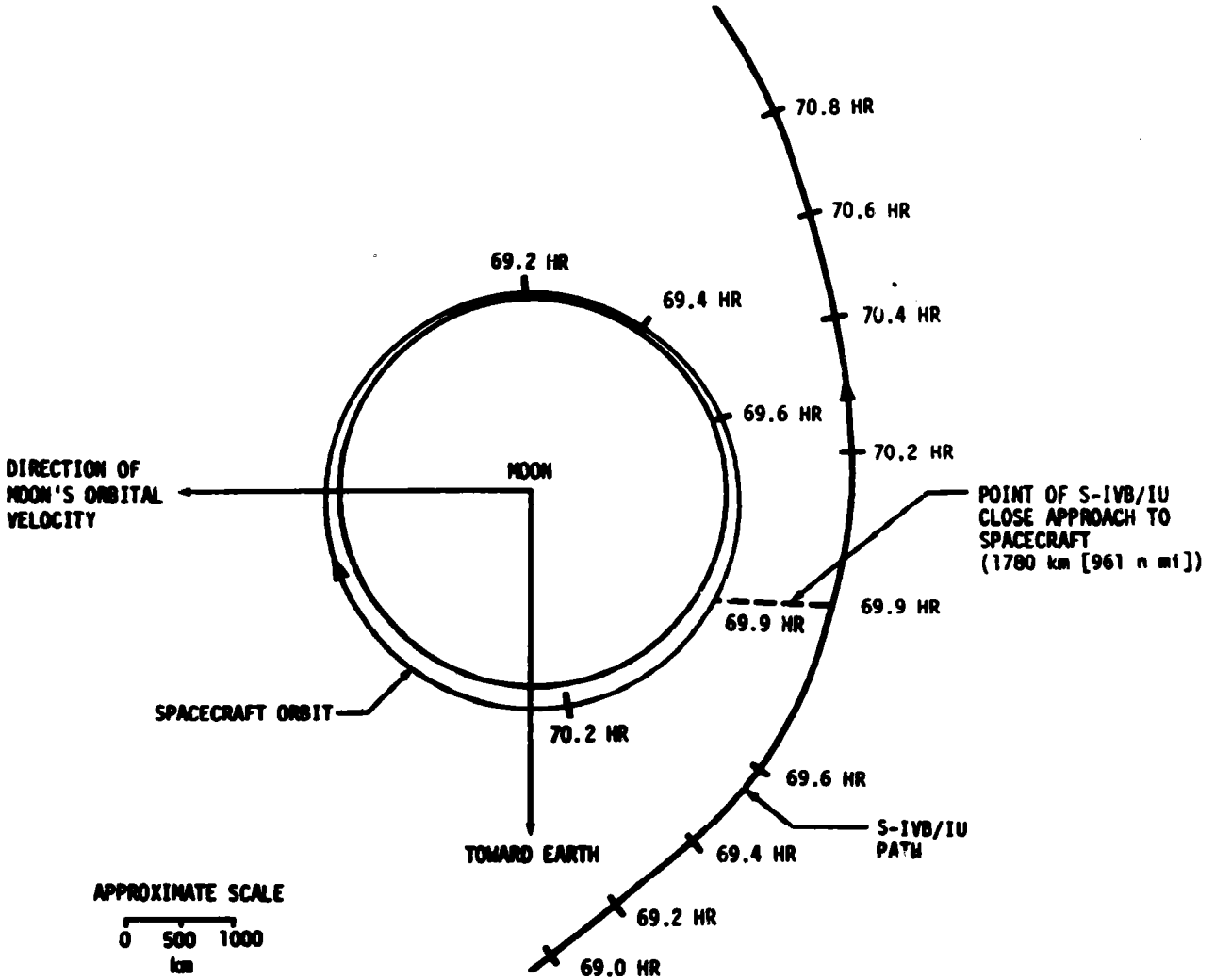

Figure 4-13. Projection of Spacecraft - S-IVB/IU Positions

Table 2-3. Sequence of Switch Selector Events (Continued)

FUNCTION	STAGE	RANGE TIME ACTUAL (SEC)	TIME FROM BASE ACTUAL (SEC)	TIME FROM BASE ACT-PRED (SEC)
304. LH_2 Tank Continuous Vent Relief Override Shutoff Valve, OPEN ON	S-IVB	17,756.13	7200.26	-0.04
305. S-IVB Engine EDS Cutoff No. 2, DISABLE	S-IVB	17,756.31	7200.45	-0.05
306. LH_2 Tank Continuous Vent Orifice Shutoff Valve Open, OFF	S-IVB	17,758.02	7202.15	-0.05
307. LH_2 Tank Continuous Vent Relief Override Shutoff Valve Open, OFF	S-IVB	17,758.12	7202.25	-0.05
308. Aux. Hydraulic Pump Flight Mode, ON	S-IVB	18,445.82	7889.95	-0.05
309. Passivation, ENABLE	S-IVB	18,465.82	7909.95	-0.05
310. Engine Mainstage Control Valve, OPEN ON	S-IVB	18,475.82	7919.95	-0.05
311. Engine He Control Valve, OPEN ON	S-IVB	18,476.03	7920.15	-0.05
312. Start Bottle Vent Control Valve, OPEN ON	S-IVB	18,505.82	7949.95	-0.05
313. Start Bottle Vent Control Valve Open, OFF	S-IVB	18,655.83	8099.95	-0.05
314. Engine Pump Purge Control Valve, ENABLE ON	S-IVB	18,745.83	8189.95	-0.05
315. Engine Mainstage Control Valve Open, OFF	S-IVB	18,776.03	8220.15	-0.05
316. Engine He Control Valve Open, OFF	S-IVB	18,776.23	8220.35	-0.05
317. Aux. Hydraulic Pump Flight Mode, OFF	S-IVB	18,778.83	8222.95	-0.05
318. LOX Tank NPV Valve, OPEN ON	S-IVB	18,779.03	8223.15	-0.05
319. LH_2 Tank Latching Relief Valve, OPEN ON	S-IVB	18,779.23	8223.35	-0.05
320. LOX Tank NPV Valve Latch, OPEN ON	S-IVB	18,781.03	8225.15	-0.05
321. LH_2 Tank Latching Relief Valve Latch, ON	S-IVB	18,781.23	8225.35	-0.05
322. LOX Tank NPV Valve Open, OFF	S-IVB	18,782.03	8226.15	-0.05
323. LH_2 Tank Latching Relief Valve Open, OFF	S-IVB	18,782.23	8226.35	-0.05
324. LOX Tank NPV Valve Latch Open, OFF	S-IVB	18,783.03	8227.15	-0.05
325. LH_2 Tank Latching Relief Valve Latch, OFF	S-IVB	18,783.23	8227.35	-0.05

Table 2-3. Sequence of Switch Selector Events (Continued)

FUNCTION	STAGE	RANGE TIME ACTUAL (SEC)	TIME FROM BASE ACTUAL (SEC)	TIME FROM BASE ACT-PRED (SEC)
326. Repressurization System Mode Select, OFF (AMB)	S-IVB	18,783.43	8227.55	-0.05
327. LH_2 Tank Repressurization Control Valve. OPEN ON	S-IVB	18,783.63	8227.75	-0.05
328. S-IVB Ullage Engine No. 1, ON	S-IVB	19,555.85	8999.96	-0.04
329. S-IVB Ullage Engine No. 2, ON	S-IVB	19,556.06	9000.17	-0.03
330. CCS Coax, SWITCH, High Gain Antenna	IU	19,635.85	9079.96	-0.04
331. PCM Coax, SWITCH, High Gain Antenna	IU	19,636.06	9080.17	-0.03
332. Repressurization System Mode Select, ON (AMB)	S-IVB	21,783.68†	11,227.76†	-0.04
333. LH_2 Tank Repressurization Control Valve Open, OFF	S-IVB	21,983.68†	11,427.76†	-0.04
334. Engine He Control Valve, OPEN ON	S-IVB	21,983.88†	11,427.96†	-0.04
335. Engine Pump Purge Control Valve, ENABLE OFF	S-IVB	22,265.88†	11,709.96†	-0.04
336. Engine He Control Valve Open, OFF	S-IVB	22,283.88†	11,727.96†	-0.04
337. Passivation, DISABLE	S-IVB	22,284.88†	11,728.96†	-0.04

† Derived time, event not verified.

Table 2-4. Variable Time and Commanded Switch Selector Events

EVENT	STAGE	RANGE TIME (SEC)	TIME FROM BASE (SEC)
Inflight Calibration Mode, ON	S-IVB	5362.57	T_5+4677.36
Telemetry Calibrator In-Flight Calibrate, ON	IU	5362.77	T_5+4677.56
TM Calibrate, ON	S-IVB	5362.97	T_5+4677.76
Telemetry Calibrator In-Flight Calibrate, OFF	IU	5367.77	T_5+4682.56
TM Calibrate, OFF	S-IVB	5367.97	T_5+4682.76
In-Flight Calibration Mode, OFF	S-IVB	5368.57	T_5+4683.36
Telemetry Calibrator In-Flight Calibrate, OFF	IU	8955.90	T_5+8270.70
TM Calibrate, OFF	S-IVB	8956.10	T_5+8270.90
In-Flight Calibration Mode, OFF	S-IVB	8956.70	T_5+8271.50
In-Flight Calibration Mode, ON	S-IVB	9650.72	T_5+8965.52
Telemetry Calibrator In-Flight Calibrate, ON	IU	9650.93	T_5+8965.72
TM Calibrate, ON	S-IVB	9651.13	T_5+8965.92
Telemetry Calibrator In-Flight Calibrate, OFF	IU	9655.91	T_5+8970.70
TM Calibrate, OFF	S-IVB	9656.11	T_5+8970.90
In-Flight Calibration Mode, OFF	S-IVB	9656.71	T_5+8971.50
Spacecraft Control of Saturn, ENABLE	S-IVB	9659.79	T_5+8974.59
PCM High Gain Antenna, SWITCH	IU	10,497.49	T_6+837.95
Water Coolant Valve, OPEN	IU	13,102.83	T_7+2547.04
Water Coolant Valve, CLOSED	IU	13,403.47	T_7+2847.68

Table 2-4. Variable Time and Commanded Switch Selector Events (Continued)

EVENT	STAGE	RANGE TIME (SEC)	TIME FROM BASE (SEC)
Water Coolant Valve, OPEN	IU	16,711.39	T_7+6155.54
Water Coolant Valve, CLOSED	IU	17,012.39	T_7+6456.53
Water Coolant Valve, OPEN	IU	18,214.08	T_7+7658.21
Water Coolant Valve, CLOSED	IU	18,515.00	T_7+7959.12
PCM Low Gain Antenna SWITCH	IU	19,096.57	T_7+8540.69
CCS Low Gain Antenna SWITCH	IU	19,096.67	T_7+8540.79
PCM Low Gain Antenna SWITCH	IU	19,096.79	T_7+8540.90
CCS Low Gain Antenna SWITCH	IU	19,096.86	T_7+8540.97
PCM Low Gain Antenna SWITCH	IU	19,097.96	T_7+8542.08
CCS Low Gain Antenna SWITCH	IU	19,098.03	T_7+8542.15
Water Coolant Valve, OPEN	IU	20,017.78	T_7+9461.89
Water Coolant Valve, CLOSED	IU	20,318.32	T_7+9762.42
PCM Low Gain Antenna Switch	IU	21,177.86	T_7+10,621.95
PCM Low Gain Antenna SWITCH	IU	21,179.03	T_7+10,623.12
CCS Low Gain Antenna SWITCH	IU	21,179.12	T_7+10,623.21

SECTION 3

LAUNCH OPERATIONS

3.1 SUMMARY

The launch countdown for AS-503 was completed with no holds or significant delays encountered. Ground systems performance was highly satisfactory. The relatively few problems encountered in countdown were overcome such that vehicle launch readiness was not compromised.

Launch damage to the complex and support equipment was minor. Blast damage appears to be less than that encountered on AS-501 and AS-502.

3.2 PRELAUNCH MILESTONES

The launch vehicle checkout started at Kennedy Space Center (KSC) with the arrival of the S-II-3 stage December 26, 1967. At that time the flight of AS-503 in early May was to be unmanned, utilizing boilerplate BP-30 in lieu of an operational spacecraft. By mid April virtually all testing in the Vehicle Assembly Building (VAB) had been completed. Final preparations to move to Pad A were held pending completion of the AS-502 flight test data analysis and the AS-503 manned/unmanned decision. The decision was received April 27, 1968 that the AS-503 flight would be manned and that CSM-103/LM-3 would be used instead of BP-30. Man-rating the S-II-3 stage which involved an additional cryogenic proof pressure test at Mississippi Test Facility (MTF) was required. This test was successfully completed May 30, 1968 and the stage was returned to KSC June 27, 1968. Testing of the complete launch vehicle was again started in mid August, 3 1/2 months after destacking.

The LM-3 testing started June 11, 1968, but after 2 months of testing, it appeared doubtful that the Lunar Module (LM) would be operationally ready to support the planned launch readiness date of early December. Therefore, the decision was made August 19, 1968 that the Lunar Module Test Article (LTA-B) would be substituted for LM-3. Following satisfactory checkout, the spacecraft was erected atop the launch vehicle October 8, 1968 and the space vehicle was transferred to the pad October 9, 1968. Checkout operation of the space vehicle at the pad proceeded without any significant problems that would impact the launch readiness date which was based on the earliest lunar window. Table 3-1 lists all the significant activities or events which occurred at KSC leading up to the successful launch of Apollo 8.

Table 3-1. AS-503 Milestones

DATE	ACTIVITY OR EVENT
December 26, 1967	S-II Arrival
December 27, 1967	S-IC Arrival
December 30, 1967	S-IVB Arrival, S-IC Erection on LUT-1
January 4, 1968	IU Arrival
January 6, 1968	BP-30 Arrival
January 9, 1968	LTA-B Arrival
January 19, 1968	LTA-B Mate With SLA-10
January 31, 1968	S-II Erection
February 1, 1968	S-IVB, IU Erection
February 5, 1968	BP-30, Summary LES Erection
February 12, 1968	LV Electrical Mate Completion
March 11, 1968	SV OAT 1 Completion
March 25, 1968	SV Pull Test Completion
April 8, 1968	SV OAT 2 Completion
April 10, 1968	Decision to Deerect BP-30 for SPS Tank Skirt Mod
April 27, 1968	C Mission Changed to C Prime Mission
April 28, 1968	SLA-10, IU, S-IVB Deerection
April 29, 1968	S-II Deerection
May 1, 1968	S-II Departure for MTF
June 9, 1968	LM-3 Descent Stage Arrival
June 14, 1968	LM-3 Ascent Stage Arrival
June 27, 1968	S-II-3 Arrival from MTF
July 24, 1968	S-II-3 Erection
August 6, 1968	CSM 103 Quad Arrival
August 11, 1968	SM 103 Arrival
August 12, 1968	CM 103 Arrival
August 14, 1968	S-IVB Erection
August 15, 1968	IU Erection
August 16, 1968	Facility Verification Vehicle Erection

Table 3-1. AS-503 Milestones (Continued)

DATE	ACTIVITY OR EVENT
August 19, 1968	Apollo 8 Designation for AS-503. Decision to Replace LM-3 with SLA-11A and LTA-B.
August 22, 1968	CM 103 Mate with SM 103
August 23, 1968	LV Electrical Systems Test Completion
September 5, 1968	CSM 103 Combined Systems Test Completion
September 14, 1968	Facility Verification Vehicle Deerection
September 15, 1968	BP-30 Erection for SA Checkout
September 18, 1968	SLA-11A Arrival
September 29, 1968	LTA-B Mate with SLA-11A
October 2, 1968	Service Arm OAT Completion
October 4, 1968	BP-30 Deerection, CSM 103
October 7, 1968	CSM 103 Erection in VAB
October 9, 1968	Space Vehicle Transfer to Pad A
October 12, 1968	MSS Transfer to Pad A
October 22, 1968	SV Cutoff and Malfunction Test Completion
October 29, 1968	CSM MCC-H Test Completion
November 5, 1968	SV Electrical Mate Completion
November 7, 1968	SV OAT 1, Plugs-In, Completion
November 11, 1968	LV MCC-H Test Completed
November 12, 1968	LUT/Pad Water System Test Completion
November 19, 1968	SV Flight Readiness Test Completion
November 30, 1968	SV Hypergolic Loading Completion
December 2, 1968	RP-1 Loading Completion
December 5, 1968	SV CDDT (Wet) Start
December 10, 1968	SV CDDT (Wet) Completion
December 11, 1968	SV CDDT (Dry) Completion
December 15, 1968	SV Launch Countdown Start (-103 Hours)
December 21, 1968	Apollo 8 (AS-503) Launched at 0751 EST

3.3 COUNTDOWN EVENTS

The launch countdown started at 1900 Eastern Standard Time (EST) Sunday, December 15, 1968, at -103 hours. There were six preplanned holds incorporated into the countdown. The countdown proceeded as scheduled with relatively few problems. Many of the countdown operations were being accomplished consistently ahead of the clock. At 2051 EST December 19, 1968, the terminal countdown sequence was started at -28 hours. At that time, the space vehicle operations were functionally ahead of the clock. Later in the count, it was discovered that the onboard LOX supply for the spacecraft Environmental Control System (ECS) and fuel cell systems was contaminated with N_2 and preparations were made to replace the LOX. The LOX reservicing operations were completed with the tanks pressurized at approximately -10 hours. During the planned 6-hour hold period that started at -9 hours, virtually all of the countdown tasks, which were delayed by the LOX detanking and retanking operations, had been brought back in line. When the count was picked up again at -9 hours, the space vehicle operations were essentially on schedule. At -8 hours S-IVB LOX loading operations were started. The cryogenic loading operations were completed at 0329 EST, December 21, 1968, (8 minutes into the 1-hour scheduled hold). The count (-3:30 hours) was again picked up at 0421 EST, December 21, 1968. The crew entered the spacecraft at -2:53 hours. Successful launch of the Apollo 8 (AS-503) occurred at 0751 EST, December 21, 1968.

3.4 PROPELLANT LOADING

3.4.1 RP-1 Loading

The RP-1 system successfully completed all operations in support of CDDT and launch. One minor fuel leak occurred during CDDT which required rescheduling of the S-IC tail service mast fuel operation. The level adjust drain operation during CDDT and countdown was completed at -1 hour establishing the required flight mass of RP-1 onboard. About 20 minutes was required to level adjust, drain, and inert the RP-1 system line. At ignition, KSC mass readout indicated that approximately 616,908 kilograms (1,360,049 lbm) of RP-1 were onboard the S-IC stage.

3.4.2 LOX Loading

The LOX system supported CDDT and launch satisfactorily. A minor problem developed during LOX loading concerning the failure of two main pump clutch temperature switches but it did not affect loading operations. LOX fill sequence for launch was initiated at -8 hours, with all stage replenish normal mode attained 3 hours 2 minutes later. Approximately 1332.5 m^3 (352,000 gal) of LOX were used during the two CDDT (wet) propellant loadings. Approximately 2119.8 m^3 (560,000 gal) of LOX were consumed throughout countdown to securing. At launch, approximately 1627.7 m^3 (430,000 gal) of LOX were onboard AS-503.

3.4.3 LH_2 Loading

The LH_2 system performed satisfactorily throughout CDDT and launch countdown. The vehicle fill sequences were performed on schedule. Flight mass was within specification at liftoff. Preconditioning of the S-II LH_2 tank began at -7 hours 42 minutes and was completed 2 hours 40 minutes later. LH_2 auto load was started at -4 hours 49 minutes with S-II chilldown; 100 percent of flight mass was reached 46 minutes later. S-IVB loading began with S-II completion, and 100 percent flight mass was reached at -3 hours 30 minutes. Total fill sequence required 86 minutes. The same fill time was required for each propellant loading of the wet CDDT. Boiloff usage of LH_2 was about 473.2 m^3 (125,000 gal) for each of the two propellant loadings during wet CDDT. The countdown and launch consumed approximately 1779.1 m^3 (470,000 gal) of LH_2.

During both propellant loadings of the wet CDDT, the LH_2 loading logic initiated a revert of the S-II and S-IVB automatic replenishing during the S-IVB stage vent valve test. The cause was traced to a momentary pickup of the S-IVB overfill sensor. This resulted from the Propellant Tanking Computer System (PTCS) sensing a low stage LH_2 level while the S-IVB stage vents were closed and the S-IVB tank was partially pressurized. The replenish valve opened for about 1 minute when it was not required. When the S-IVB stage vent was opened and the tank depressurized, there was a series of momentary actuations of the overfill sensor causing the revert. A command (procedural requirement) to override the S-IVB replenish valve to the closed position while the stage vents were closed was not given by S-IVB personnel before they closed the vents. The override close command was given in the proper sequence during countdown and, although preparations had been made to lockout an S-IVB revert, the S-IVB overfill signal was not actuated.

A minor hydrogen leak was detected during the first propellant loading of the wet CDDT at the packing of the S-IVB fill valve, when the valve was in the "reduced" position with the S-IVB about 95 percent full. The valve packing was retorqued before the second propellant loading of the wet CDDT, and the leak did not reappear during CDDT. During launch countdown, there was a significant vapor leak at the same valve during S-IVB slow fill to 100 percent. The valve was closed and the leak stopped immediately. The slow fill sequence was continued using the redundant fill valve.

3.4.4 Auxiliary Propulsion System Propellant Loading

Propellant loading of the S-IVB Auxiliary Propulsion System (APS) was accomplished satisfactorily. Total propellant mass in both modules at liftoff was 175.2 kilograms (386.3 lbm) of Nitrogen Tetroxide (N_2O_4) and 113.8 kilograms (250.8 lbm) of Monomethyl Hydrazine (MMH). The initial APS loads and the propellant usage during flight are discussed in paragraph 7.12.

3.4.5 S-IC Stage Propellant Load

S-IC stage propellant loads obtained from the KSC weight and balance log were compared to those determined from continuous level sensor data. This comparison showed the LOX load to be 2304 kilograms (5079 lbm) greater, and the fuel load 1095 kilograms (2415 lbm) less than KSC loads. The propulsion performance reconstruction, utilizing a combined RPM chamber pressure match, was able to follow the continuous level sensor data for both LOX and fuel with an accuracy of ±1.27 centimeters (±0.5 in.). The reconstruction matched also the residuals calculated from level sensor and line pressure data indicating that the propellant loads determined from the level sensor data are accurate. Total propellants onboard at ignition command are shown in Table 3-2. The reconstructed LOX load is 0.16 percent above, and the reconstructed fuel load is 0.18 percent below the KSC indicated values.

3.4.6 S-II Stage Propellant Load

The Propellant Utilization (PU) system (fine mass) indication of propellant mass onboard the S-II stage at liftoff was 858 kilograms (1891 lbm) LOX and 746 kilograms (1643 lbm) LH_2 greater than predicted. S-II stage total propellant loads at S-IC ignition command are shown in Table 3-3 and includes trapped propellants below the tanks. The best estimate values, based on engine flowmeter data, are greater than predicted by 0.14 percent for LOX, and less than predicted by 0.46 percent for LH_2.

3.4.7 S-IVB Stage Propellant Load

The PU system indication of initial S-IVB stage propellant mass was only 4 kilograms (7 lbm) greater for LOX and 13 kilograms (30 lbm) greater for LH_2 than the predicted values. Table 3-4 lists the S-IVB propellant loads at S-IC ignition command. Best estimates were 0.04 percent less for LOX and 0.10 percent greater for LH_2 than the predicted propellant masses.

3.5 S-II INSULATION PURGE AND LEAK DETECTION

The S-II insulation purge system performed satisfactorily throughout the countdown. Outlet purge pressure was lost in the LH_2 tank sidewall circuit 3 hours 30 minutes prior to liftoff, approximately 34 minutes after completion of S-II LH_2 loading. Operational television employed to inspect the sidewall insulation revealed that numerous cracks developed in the circumferential flexible closeouts of the insulation near Vehicle Station 55.3 meters (2177 in.), and also in the vertical closeout adjacent to engine No. 4.

The cause of cracking is assessed to local stresses resulting from extremely low surface temperatures created by a heavy frost layer. Both the closeout

Table 3-2. S-IC Stage Propellant Mass at Ignition Command

PROPELLANT	UNITS	MASS REQUIREMENTS		MASS INDICATIONS		MASS DEVIATIONS	
		PREDICTED PRIOR TO LAUNCH[1]	LOADING TABLE AT IGNITION[2,3]	LEVEL SENSOR DATA	BEST ESTIMATE	BEST ESTIMATE MINUS PREDICTED	BEST EST. MINUS LOADING TABLE
LOX	kg	1,420,593	1,416,556	1,418,860	1,418,852	-1741	2296
	lbm	3,131,873	3,122,971	3,128,050	3,128,034	-3839	5063
	%					-0.12	0.16
RP-1	kg	612,982	616,908	615,812	615,812	2920	-1096
	lbm	1,351,395	1,360,049	1,357,634	1,357,634	6239	-2415
	%					0.46	-0.18
Total	kg	2,033,575	2,033,464	2,034,672	2,034,665	1090	1201
	lbm	4,483,268	4,483,020	4,485,684	4,485,668	2400	2648
	%					0.05	0.06

[1] Based on LOX density of 1137.3 kg/m^3 (71.0 lbm/ft^3) and RP-1 density of 802.5 kg/m^3 (50.1 lbm/ft^3).
[2] Based on LOX density of 1138.2 kg/m^3 (71.06 lbm/ft^3) and RP-1 density of 808.1 kg/m^3 (50.445 lbm/ft^3).
[3] KSC propellant mass readouts are same as loading table data at ignition.

Table 3-3. S-II Stage Propellant Mass at S-IC Ignition Command

PROPELLANT	UNITS	PREDICTED PRIOR TO LAUNCH	PU SYSTEM	LEVEL SENSOR DATA	BEST ESTIMATE	PU SYS. MINUS PRED.	BEST EST. MINUS PRED.
LOX	kg	359,569	360,427	359,302	360,059	858	490
	lbm	792,714	794,605	792,125	793,795	1891	1081
	%					0.24	0.14
LH_2	kg	70,587	71,333	70,434	70,265	745	-322
	lbm	155,618	157,261	155,281	154,907	1643	-711
	%					1.06	-0.46
Total	kg	430,156	431,760	429,736	430,324	1604	168
	lbm	948,332	951,866	947,406	948,702	3534	370
	%					0.37	0.04

NOTE: Values include propellants below tanks.

Table 3-4. S-IVB Stage Propellant Mass at S-IC Ignition Command

PROPELLANT	UNITS	PREDICTED PRIOR TO LAUNCH	PU INDICATED (CORRECTED)	FLOW INTEGRAL	BEST ESTIMATE	PU IND. MINUS PRED.	BEST EST. MINUS PRED.
LOX	kg	87,508	87,512	87,501	87,470	4	-38
	lbm	192,923	192,930	192,906	192,840	7	-83
	%					0.00	-0.04
LH_2	kg	19,665	19,678	19,611	19,684	13	19
	lbm	43,353	43,383	43,235	43,395	30	42
	%					0.07	0.10
Total	kg	107,173	107,190	107,112	107,154	17	-19
	lbm	236,276	236,313	236,141	236,235	37	-41
	%					0.02	-0.02

strips and adhesive on the S-II-3 stage were silicone compounds which lose elastomeric properties and become brittle at temperatures below 211°K (-80°F). One sidewall temperature measurement indicated 194°K (-110°F).

This insulation problem was experienced earlier on the S-II-4 stage at the MTF and initiated a change in the closeout configuration effective on S-II-4 and subsequent stages. The change was not made on the S-II-3 stage because of potential schedule impact and acceptance that the probability of calm wind, high humidity, and low temperatures (causing heavy frost) would be minimal at KSC. Figure 3-1 shows the insulation panel joint closeout used on S-II-3 together with the modified configuration.

Contaminant gas concentrations in the system remained below launch mission rule limits at all times. Concentrations of hydrogen gas were low in all purge circuits following pressure stabilization during LH_2 fill. Activation of back purge in the sidewall circuit after LH_2 loading precluded further monitoring of that circuit. A high concentration of nitrogen was present in the combined forward bulkhead circuits during LH_2 fill, and the forward bulkhead uninsulated area indicated a nitrogen content in excess of 1 percent just prior to liftoff. Cause is assessed to leaks in either the forward bulkhead insulation or the membrane seal since the forward interstage is purged with nitrogen during ground hold and is at slightly higher pressure than the purge circuits.

3.6 GROUND SUPPORT EQUIPMENT

Ground systems performance was highly satisfactory. The holddown arms, tail service masts, service arms, propellant tanking systems, and all other ground equipment functioned well in support of AS-503 launch. All Holddown Arms (HDA) release occurred at 0.27 seconds. All arms released pneumatically although the drop and lanyard pull for HDA 2 was sufficiently slow to allow detonation of the backup explosive nut link. This had no detrimental effect on arm release.

Tail Service Mast (TSM) retraction was normal. Mast retraction times were 2.62 seconds for TSM 1-2, 2.77 seconds for TSM 3-2, and 2.54 seconds for TSM 3-4, measured from "umbilical plate separation" to "mast retract" indication.

Service arm retraction was normal except slight deviations of service arm 4 and service arm 1. The service arm 4 retraction was initiated by the secondary supply and return hydraulic pilot valve which is fired by means of the HDA service arm control switch (1-inch liftoff) in sequence with the primary main unbilical carrier, LOX coupler, and LH_2 coupler release switches. The primary retract supply valve and the primary retract return valve, which are normally fired by means of the HDA 4 service arm control switch (1-inch liftoff) in sequence with the secondary main umbilical

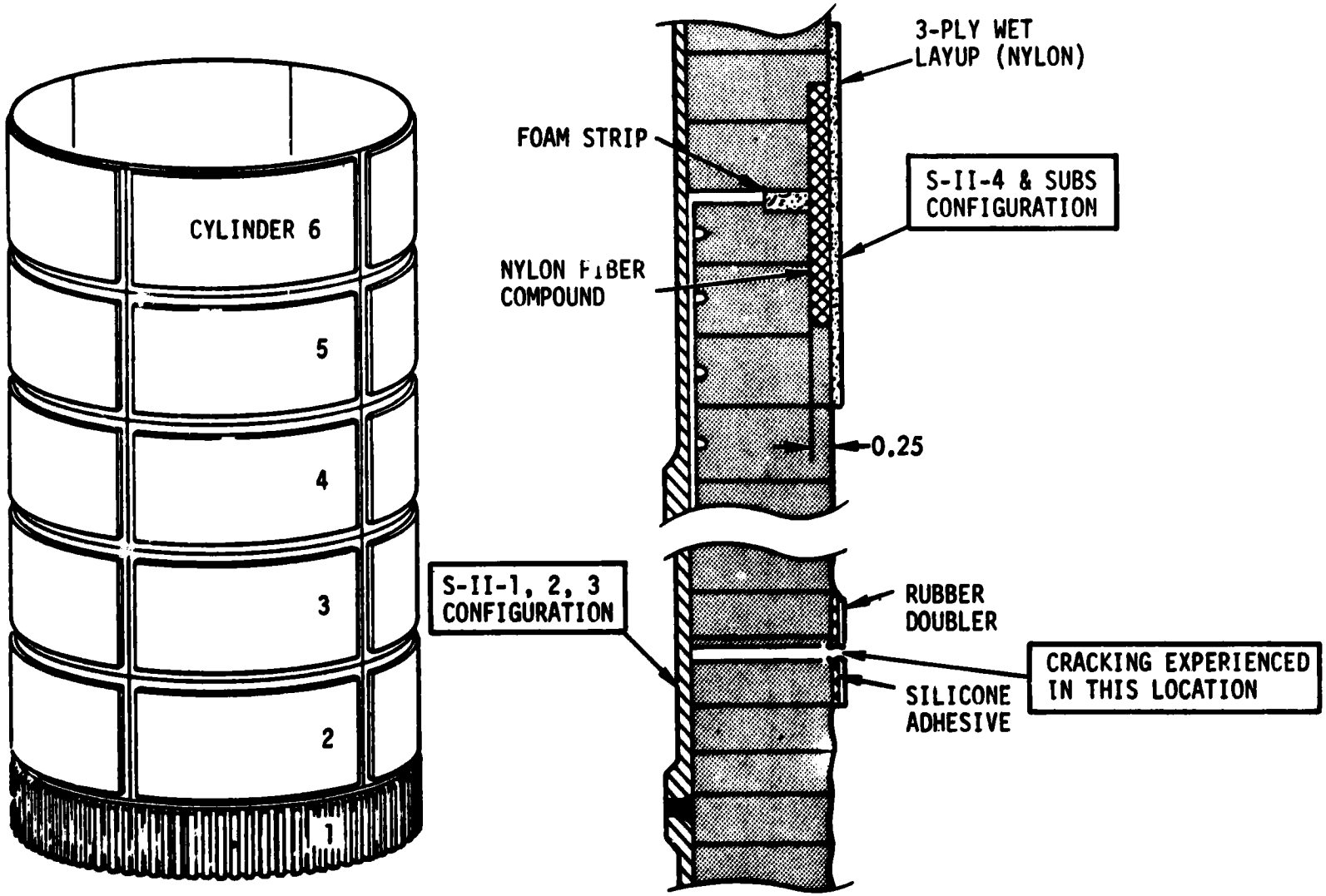

Figure 3-1. S-II LH_2 Tank Sidewall Insulation Closeouts

carrier, LOX coupler, and LH_2 coupler release switches, did not fire until the HDA 2 secondary service arm control switch was actuated (22-inch liftoff). This bypassed the secondary main umbilical carrier, LOX coupler, and LH_2 coupler release switches. Failure to initiate service arm 4 primary retract, before closure of the 22-inch liftoff switch, has been attributed to faulty operation of one or more of the umbilical secondary release switches. In addition, postlaunch inspection revealed that the S-II LOX umbilical coupler on service arm 4 was not latched securely in the retract position. Investigation is continuing to determine the exact nature and extent of this problem.

The withdrawal time for the service arm 1 carrier was 6.14 seconds. Normal withdrawal time is about 4.2 seconds. This did not affect overall service arm 1 retract time enough to cause terminal countdown sequence cutoff. Total service arm 1 retract time to safe angle was 11.1 seconds, 0.6 second greater than specification limit, but 2.69 seconds before service arm 2 retract command. (Failure to achieve service arm 1 safe angle prior to time for service arm 2 retract at 16.2 seconds would cause cutoff.) The cause of the slow withdrawal has not been established.

Detailed information of ground equipment performance, problems encountered during launch preparations, and blast damage to the complex and equipment is given in Apollo/Saturn V Ground Systems Evaluation Report AS-503, Kennedy Space Center, February 10, 1969.

Overall damage to the launch complex and support equipment was less than that occurred at AS-501 and AS-502 launch. Modifications incorporated to reduce blast damage below that experienced on the previous launches were effective. Ablative coating on the HDA and tail service masts provided adequate blast protection. The ablative coating was removed from HDA 1, possibly because of poor bonding. It is estimated that less than 50 percent of the coating on the tail service masts needs replacement. Damage to the service arm systems were significantly less than on AS-501 and AS-502. Although there were several service arm hydraulic leaks, no hydraulic fires occurred as on previous launches. The fire protection system in LUT Room 4A activated at liftoff and covered the RP-1 and hydraulic equipment with dry chemical fire extinguishing powder. This also happened during AS-501 and AS-502 launches.

In general, damage to the Marshall Space Flight Center (MSFC) furnished Ground Support Equipment (GSE) (mechanical and electrical) was minor. On LUT level 60, equipment storage rack damage was similar to that during previous launches. Again, welds were broken and door latching assemblies were torn off. On the LUT level 100, damage was characterized by broken welds, damaged door latches, and rack frames bowed out of shape. On level 120, welds and door latches were broken as occurred during previous launches.

SECTION 4

TRAJECTORY

4.1 SUMMARY

The actual trajectory parameters of the AS-503 were close to nominal. The vehicle was launched on an azimuth of 90 degrees east of north. At 12.11 seconds, the vehicle started a roll maneuver to a flight azimuth of 72.124 degrees east of north.

The space-fixed velocity at S-IC Outboard Engine Cutoff (OECO) was 12.57 m/s (41.24 ft/s) greater than nominal. At S-II Engine Cutoff (ECO) the space-fixed velocity was 10.58 m/s (34.71 ft/s) greater than nominal. At S-IVB first cutoff the space-fixed velocity was 0.44 m/s (1.44 ft/s) greater than nominal. The altitude at S-IVB first cutoff was 0.02 kilometer (0.01 n mi) lower than nominal and the surface range was 2.61 kilometers (1.41 n mi) greater than nominal.

The parking orbit insertion conditions were very close to nominal. The space-fixed velocity at insertion was 0.01 m/s (0.03 ft/s) less than nominal and the flight path angle was 0.001 degree greater than nominal. The eccentricity was 0.00001 greater than nominal. The apogee and perigee were 0.03 kilometer (0.02 n mi) and 0.16 kilometer (0.09 n mi) less than nominal, respectively.

The translunar injection targeting parameters were also very close to nominal. The eccentricity was 0.00083 less than nominal, the inclination was 0.025 degree greater than nominal, the node was 0.043 degree greater than nominal, and C_3 was 49,631 m^2/s^2 (534,224 ft^2/s^2)less than nominal. At translunar injection the total space-fixed velocity was 5.23 m/s (17.16 ft/s) less than nominal and the altitude was 3.62 kilometers (1.96 n mi) higher than nominal.

The actual surface range of the impact point for the S-IC stage, as determined from a theoretical free-flight simulation, was within 8.34 kilometers (4.50 n mi) of the nominal. The free-flight trajectory indicated S-II stage impact of 111.80 kilometers (60.36 n mi) further downrange than the nominal impact point.

4.2 TRACKING DATA UTILIZATION

4.2.1 Tracking During the Ascent Phase of Flight

Tracking data were obtained during the period from the time of first motion through parking orbit insertion.

The ascent trajectory was established by merging the launch phase trajectory with the best estimate trajectory. The launch phase trajectory was established by integrating the telemetered body-fixed accelerometer data, and verified by optical and Offset Frequency Doppler (ODOP) tracking data. The best estimate trajectory utilized telemetered guidance velocities as the generating parameters to fit data from ODOP and seven different C-Band tracking stations. These data points were fit through a guidance error model and constrained to the insertion vector obtained from the orbital solution. Comparison of the ascent trajectory with data from all the tracking systems yielded reasonable agreement.

4.2.2 Tracking During Orbital Flight

Table 4-1 presents a summary of the C-Band radar stations which furnished data for use in determining the orbital trajectory. There were also considerable S-Band tracking data available during the orbital flight which were not used in determining the orbital trajectory due to the abundance of C-Band radar data.

Table 4-1. Summary of AS-503 Orbital C-Band Tracking Data Available

STATION	TYPE OF RADARS	REV 1	REV 2	POST TLI
Bermuda	FPS-16M	X		
Tananarive	FPS-16M	X	X	
Carnarvon	FPQ-6	X	X	
White Sands	FPS-16M	X		
Patrick	FPQ-6		X	
Merritt Island	TPQ-18		X	
Bermuda	FPQ-6		X	
Vanguard Ship	FPS-16M		X	
Grand Turk	TPQ-18		X	
Pretoria	MPS-25M		X	
Mercury Ship	FPS-16M		X	
Hawaii	FPS-16M			X

4.2.2 (Continued)

The orbital trajectory was obtained by integrating corrected insertion conditions forward. The insertion conditions, as determined by the Orbital Correction Program (OCP), were obtained by a differential correction procedure which adjusted the estimated insertion conditions to fit the C-Band radar tracking data in accordance with the weights assigned to the data. After all the C-Band radar tracking data were analyzed, some stations and passes were eliminated completely from use in the determination of the insertion conditions.

4.2.3 Tracking During the Injection Phase of Flight

C-Band radar data were obtained from Hawaii station during the period from S-IVB restart through translunar injection.

The injection trajectory was established by utilizing telemetered guidance velocities as the generating parameters to fit the tracking data in a best estimate sense. These data points were fit through a guidance error model and initialized by the S-IVB restart vector obtained from the orbital solution. Comparison of the injection trajectory with tracking data yielded reasonable agreement.

4.3 TRAJECTORY EVALUATION

4.3.1 Ascent Trajectory

Actual and nominal altitude, surface range, and cross range for the ascent phase are presented in Figure 4-1. The actual and nominal total earth-fixed velocities, and the elevation angles (elevation of earth-fixed velocity vector from the local horizontal) of the velocity vectors are shown in Figure 4-2. Actual and nominal space-fixed velocity and flight path angle during ascent are shown in Figure 4-3. Comparisons of total inertial accelerations are shown in Figure 4-4. The maximum acceleration during S-IC burn according to the postflight trajectory was 3.96 g. The accuracy of the trajectory at S-IVB first cutoff is estimated to be ±1.0 m/s (±3.3 ft/s)in velocity components and ±500 meters (±1640 ft) in position components.

Mach number and dynamic pressure are shown in Figure 4-5. These parameters were calculated using measured meteorological data to an altitude of 89.75 kilometers (48.46 n mi). Above this altitude the measured data were merged into the U.S. Standard Reference Atmosphere.

Actual and nominal values of parameters at significant trajectory event times, cutoff events, and separation events are shown in Tables 4-2, 4-3, and 4-4, respectively.

The free-flight trajectories of the discarded S-IC and S-II stages were simulated using initial conditions from the final postflight trajectory.

Table 4-2. Comparison of Significant Trajectory Events

EVENT		PARAMETER	ACTUAL	NOMINAL*	ACT-NOM
First Motion		Range Time, sec	0.33	0.33	0.00
		Total Inertial Acceleration, m/s² (ft/s²)	11.41 (37.43)	11.40 (37.40)	0.01 (0.03)
Mach 1		Range Time, sec	61.48	60.58	0.90
		Altitude, km (n mi)	7.35 (3.97)	7.38 (3.98)	-0.03 (-0.01)
Maximum Dynamic Pressure		Range Time, sec	78.90	76.08	2.82
		Dynamic Pressure, N/cm² (lbf/ft²)	3.720 (776.938)	3.562 (743.939)	0.158 (32.999)
		Altitude, km (n mi)	13.43 (7.25)	12.77 (6.90)	0.66 (0.35)
Maximum Total Inertial Acceleration:	S-IC	Range Time, sec	153.92	150.00	3.92
		Acceleration, m/s² (ft/s²)	38.85 (127.46)	38.73 (127.07)	0.12 (0.39)
	S-II	Range Time, sec	524.14	521.29	2.85
		Acceleration, m/s² (ft/s²)	18.20 (59.71)	18.50 (60.70)	-0.30 (-0.99)
	S-IVB 1st Burn	Range Time, sec	685.08	684.09	0.99
		Acceleration, m/s² (ft/s²)	7.04 (23.10)	7.09 (23.26)	-0.05 (-0.16)
	S-IVB 2nd Burn	Range Time, sec	10,555.61	10,552.38	3.23
		Acceleration, m/s² (ft/s²)	15.17 (49.77)	15.32 (50.26)	-0.15 (-0.49)
Apex:	S-IC Stage	Range Time, sec	266.54	269.33	-2.79
		Altitude, km (n mi)	119.81 (64.69)	125.94 (68.00)	-6.13 (-3.31)
		Surface Range, km (n mi)	325.39 (175.70)	329.15 (177.92)	-3.76 (-2.22)
	S-II Stage	Range Time, sec	560.34	543.33	17.01
		Altitude, km (n mi)	193.00 (104.21)	193.49 (104.48)	-0.49 (-0.27)
		Surface Range, km (n mi)	1729.88 (934.06)	1627.84 (878.96)	102.04 (55.10)
Maximum Earth-Fixed Velocity:	S-IC	Range Time, sec	154.47	152.07	2.40
		Velocity, m/s (ft/s)	2355.30 (7727.36)	2346.18 (7697.44)	9.12 (29.92)
	S-II	Range Time, sec	524.90	521.99	2.91
		Velocity, m/s (ft/s)	6421.57 (21,068.14)	6411.35 (21,034.61)	10.22 (33.53)
	S-IVB 1st Burn	Range Time, sec	685.50	684.51	0.99
		Velocity, m/s (ft/s)	7389.65 (24,244.26)	7388.97 (24,242.03)	0.68 (2.23)
	S-IVB 2nd Burn	Range Time, sec	10,556.00	10,552.79	3.21
		Velocity, m/s (ft/s)	10,417.68 (34,178.74)	10,422.51 (34,194.59)	-4.83 (-15.85)

* The nominal trajectory is based on the actual flight azimuth of 72.124 degrees.

Table 4-3. Comparison of Cutoff Events

PARAMETER	ACTUAL	NOMINAL	ACT-NOM	ACTUAL	NOMINAL	ACT-NOM
	S-IC IECO			S-IC OECO (LVDC SENSED)		
Range Time, sec	125.93	125.92	0.01	153.82	151.37	2.45
Altitude, km (n mi)	41.48 (22.40)	43.43 (23.45)	-1.95 (-1.05)	65.75 (35.50)	66.74 (36.04)	-0.99 (-0.54)
Surface Range, km (n mi)	42.05 (22.71)	42.72 (23.07)	-0.68 (-0.36)	89.46 (48.30)	85.95 (46.41)	3.51 (1.89)
Space-Fixed Velocity, m/s (ft/s)	1893.96 (6213.78)	1940.83 (6367.55)	-46.87 (-153.77)	2712.65 (8899.77)	2700.08 (8858.53)	12.57 (41.24)
Flight Path Angle, deg	24.527	25.417	0.110	20.699	21.819	-1.120
Heading Angle, deg	76.572	76.391	0.181	75.387	75.414	-0.027
Cross Range, km (n mi)	0.49 (0.26)	0.06 (0.03)	0.43 (0.23)	0.62 (0.33)	0.15 (0.08)	0.47 (0.25)
Cross Range Velocity, m/s (ft/s)	5.10 (16.73)	1.79 (5.87)	3.31 (10.86)	4.94 (16.21)	5.22 (17.13)	-0.28 (-0.92)
	S-II ECO (LVDC SENSED)			S-IVB 1ST ECO (VELOCITY CUTOFF)		
Range Time, sec	524.04	521.19	2.85	684.98	683.99	0.99
Altitude, km (n mi)	191.54 (103.42)	192.95 (104.18)	-1.41 (-0.76)	191.36 (103.33)	191.38 (103.34)	-0.02 (-0.01)
Surface Range, km (n mi)	1504.32 (812.27)	1490.39 (804.75)	13.93 (7.52)	2577.30 (1391.63)	2574.69 (1390.22)	2.61 (1.41)
Space-Fixed Velocity, m/s (ft/s)	6821.15 (22,379.10)	6810.57 (22,344.39)	10.58 (34.71)	7791.43 (25,562.43)	7790.99 (25,560.99)	0.44 (1.44)
Flight Path Angle, deg	0.646	0.412	0.234	-0.001	-0.003	0.002
Heading Angle, deg	81.777	81.731	0.046	88.098	88.091	0.007
Cross Range, km (n mi)	23.11 (12.48)	23.00 (12.42)	0.11 (0.06)	57.08 (30.82)	57.60 (31.10)	-0.52 (-0.28)
Cross Range Velocity, m/s (ft/s)	160.43 (526.35)	162.92 (534.51)	-2.49 (-8.16)	265.72 (871.78)	266.69 (874.97)	-0.97 (-3.19)
	S-IVB 2nd ECO (VELOCITY CUTOFF)					
Range Time, sec	10,555.51	10,552.28	3.23			
Altitude, km (n mi)	332.19 (179.37)	328.75 (177.51)	3.44 (1.86)			
Space-Fixed Velocity, m/s (ft/s)	10,830.28 (35,532.41)	10,835.05 (35,548.06)	-4.77 (-15.65)			
Flight Path Angle, deg	7.445	7.341	0.104			
Heading Angle, deg	67.162	67.125	0.037			
Eccentricity	0.97425	0.97497	-0.00072			
C_3* m^2/s^2 (ft^2/s^2)	-1,556,426 (-16,753,229)	-1,513,447 (-16,290,597)	-42,979 (-462,622)			
Inclination, deg	30.639	30.615	0.024			
Descending Node, deg	38.988	38.946	0.042			

* C_3 is twice the specific energy of orbit.

$$C_3 = V^2 - \frac{2\mu}{R}$$

Where: V = Inertial Velocity
μ = Gravitational constant
R = Radius vector from center of earth

Table 4-4. Comparison of Separation Events

PARAMETER	ACTUAL	NOMINAL	ACT-NOM
S-IC/S-II SEPARATION			
Range Time, sec	154.47	152.07	2.40
Altitude, km (n mi)	66.37 (35.84)	67.45 (36.42)	-1.08 (-0.58)
Surface Range, km (n mi)	90.84 (49.05)	87.42 (47.20)	3.42 (1.85)
Space-Fixed Velocity, m/s (ft/s)	2721.91 (8930.15)	2709.66 (8889.96)	12.25 (40.19)
Flight Path Angle, deg	20.605	21.720	-1.115
Heading Angle, deg	75.384	75.410	-0.026
Cross Range, km (n mi)	0.62 (0.33)	0.15 (0.08)	0.47 (0.25)
Cross Range Velocity, m/s (ft/s)	5.04 (16.53)	5.33 (17.49)	-0.29 (-0.96)
Geodetic Latitude, deg N	28.852	28.847	0.005
Longitude, deg E	-79.717	-79.751	0.034
S-II/S-IVB SEPARATION			
Range Time, sec	524.90	521.99	2.91
Altitude, km (n mi)	191.61 (103.46)	192.99 (104.21)	-1.38 (-0.75)
Surface Range, km (n mi)	1509.67 (815.16)	1495.36 (807.43)	14.31 (7.73)
Space-Fixed Velocity, m/s (ft/s)	6824.96 (22,391.50)	6814.89 (22,358.56)	10.07 (33.04)
Flight Path Angle, deg	0.636	0.404	0.232
Heading Angle, deg	81.807	81.759	0.048
Cross Range, km (n mi)	23.24 (12.55)	23.13 (12.49)	0.11 (0.06)
Cross Range Velocity, m/s (ft/s)	160.89 (527.85)	163.38 (536.02)	-2.49 (-8.17)
Geodetic Latitude, deg N	31.728	31.707	0.021
Longitude, deg E	-65.334	-65.482	0.148
S-IVB/SPACECRAFT SEPARATION			
Range Time, sec	12,056.3	12,052.48	3.82
Altitude, km (n mi)	7017.31 (3789.04)	7005.74 (3782.80)	11.57 (6.24)
Space-Fixed Velocity, m/s (ft/s)	7617.07 (24,990.40)	7624.36 (25,014.30)	-7.29 (-23.90)
Flight Path Angle, deg	45.076	45.051	0.025
Heading Angle, deg	107.090	107.071	0.019
Geodetic Latitude, deg N	25.884	25.866	0.018
Longitude, deg E	-66.293	-66.342	0.049

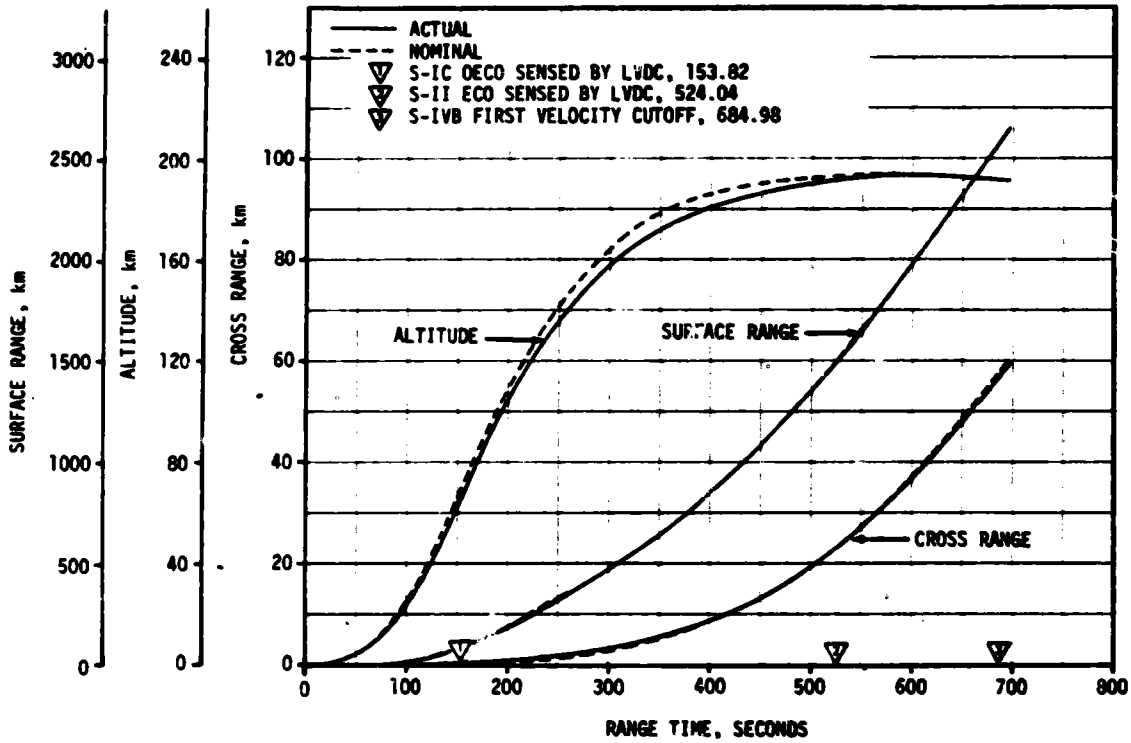

Figure 4-1. Ascent Trajectory Position Comparison

The simulation was based upon the separation impulses for both stages and nominal tumbling drag coefficients. No tracking data were available for verification. Table 4-2 presents a comparison of free-flight parameters to nominal at apex for the S-IC and S-II stages. Table 4-5 presents a comparison of free-flight parameters to nominal at impact for the S-IC and S-II stages.

4.3.2 Parking Orbit Trajectory

The acceleration due to venting during parking orbit is presented in Figure 4-6. These accelerations were obtained by differentiating the telemetered guidance velocity data and removing accelerometer biases and the effects of drag.

A family of values for the insertion parameters was obtained depending upon the combination of data used and the weights applied to the data. The solutions that were considered reasonable had a spread of about ±500 meters (±1640 ft) in position components and ±1.0 m/s (±3.3. ft/s) in velocity components. The actual and nominal parking orbit insertion parameters are presented in Table 4-6. The ground track from parking orbit insertion to S-IVB/spacecraft separation is given in Figure 4-7.

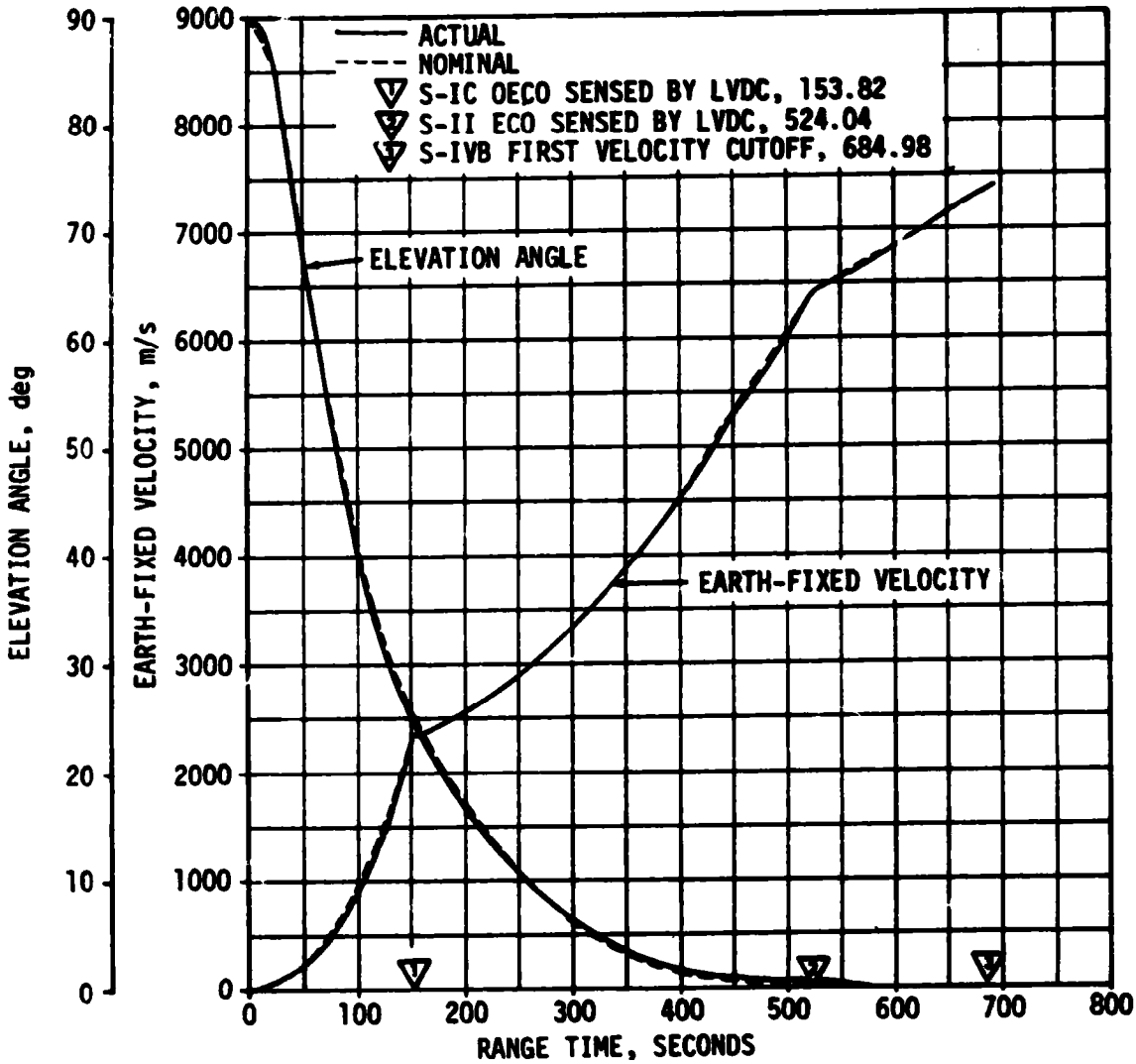

Figure 4-2. Ascent Trajectory Earth-Fixed Velocity Comparison

4.3.3 Injection Trajectory

Comparisons between the actual and nominal total space-fixed velocity and flight path angle are shown in Figure 4-8. The actual and nominal total inertial acceleration comparisons are presented in Figure 4-9. Throughout the injection phase of flight, the space-fixed velocity, flight path angle, and total inertial acceleration were slightly less than nominal.

The trajectory and targeting parameters at S-IVB second cutoff and translunar injection are presented in Tables 4-3 and 4-7, respectively.

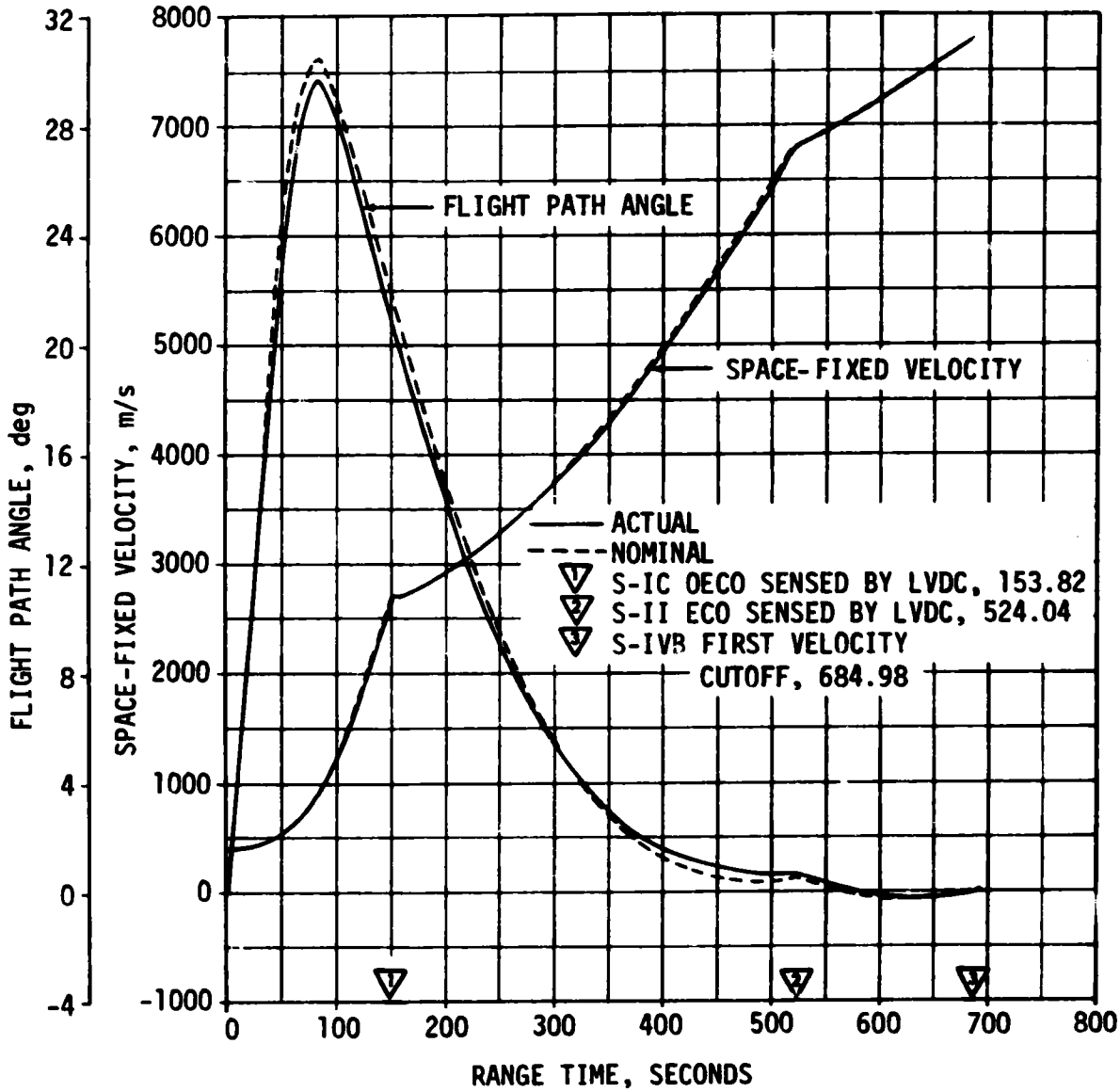

Figure 4-3. Ascent Trajectory Space-Fixed Velocity Comparison

4.3.4 Post TLI Trajectory

The post Translunar Injection (TLI) trajectory spans the time interval from TLI to S-IVB/spacecraft separation. The post TLI trajectory was obtained by integrating the translunar injection conditions, derived from the injection trajectory solution, to S-IVB/spacecraft separation. A comparison of S-IVB/spacecraft separation conditions is presented in Table 4-4.

4.3.5 S-IVB/IU Post Separation Trajectory

The S-IVB/IU was placed in a lunar slingshot trajectory close to nominal. This was accomplished by a combination of a continuous LH_2 vent, a LOX

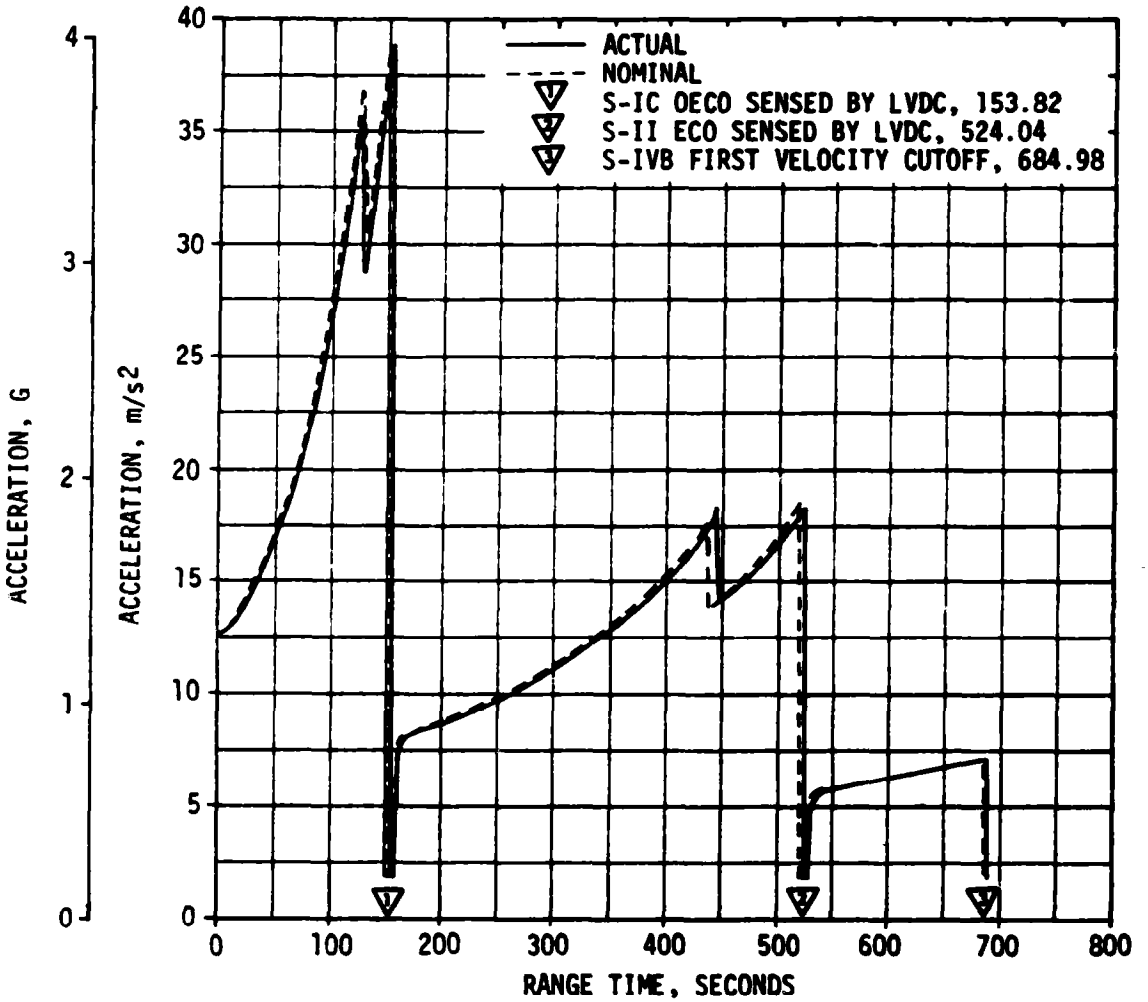

Figure 4-4. Ascent Trajectory Acceleration Comparison

dump and APS ullage burn. A time history of the longitudinal velocity increments of the slingshot maneuver is presented in Figure 4-10. Table 4-8 presents the velocity increments compared with nominal. The purpose of this maneuver was to slow down the S-IVB/IU to make it pass by the trailing edge of the moon and obtain sufficient energy to continue to a solar orbit. Figure 4-11 presents the resultant conditions for various velocity increments at the attitude of the vehicle for the maneuver. The nominal and the 3σ band about the nominal are included.

The S-IVB/IU closest approach of 1262 kilometers (682 n mi) above the lunar surface occurred at 69.982 hours into the mission. This point was at 19.2 degrees north latitude and 88.0 degrees east longitude. The path of the S-IVB/IU was inclined 44.56 degrees to the lunar equatorial plane. The trajectory parameters were obtained by integrating forward a vector which was obtained from CCS tracking data during the active lifetime of the S-IVB/IU. The actual and nominal conditions at closest approach are

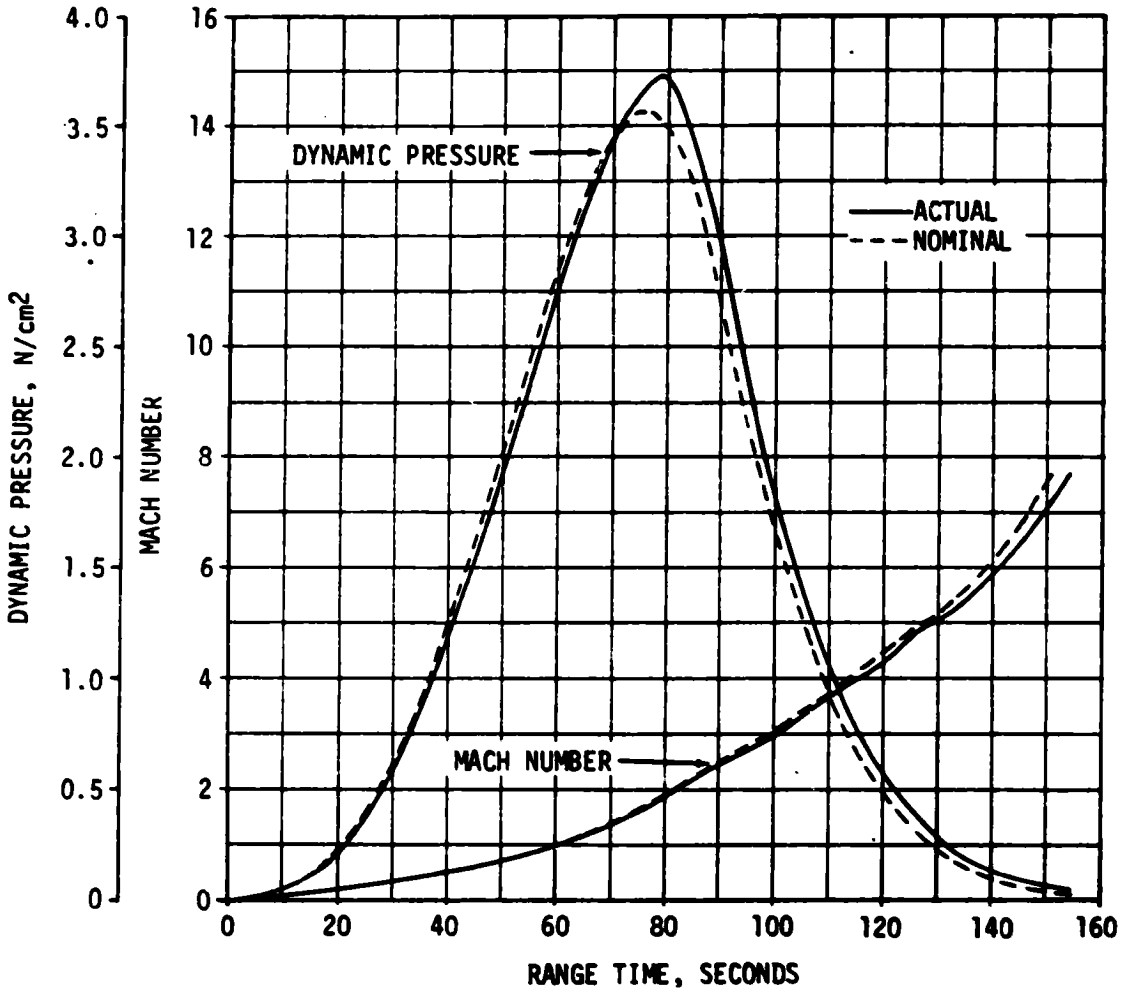

Figure 4-5. Dynamic Pressure and Mach Number Versus Range Time

presented in Table 4-9. The velocity of the S-IVB/IU relative to the earth is presented in Figure 4-12. This vividly illustrates how the influence of the moon imparted energy to the S-IVB/IU. Figure 4-13 presents the relative positions of the spacecraft and the S-IVB/IU in the vicinity of the moon.

Some of the heliocentric orbit parameters of the S-IVB/IU are presented in Table 4-10. Similar parameters for the earth's orbit are also presented for comparison.

Table 4-5. Stage Impact Location

PARAMETER	ACTUAL	NOMINAL	ACT-NOM
S-IC STAGE IMPACT			
Range Time, sec	540.41	546.55	-6.14
Surface Range, km (n mi)	654.61 (353.46)	662.95 (357.96)	-8.34 (-4.50)
Cross Range, km (n mi)	7.13 (3.85)	7.08 (3.82)	0.05 (0.03)
Geodetic Latitude, deg N	30.204	30.223	-0.019
Longitude, deg E	-74.109	-74.027	-0.082
S-II STAGE IMPACT			
Range Time, sec	1165.11	1147.13	17.98
Surface Range, km (n mi)	4159.43 (2245.91)	4047.63 (2185.55)	111.80 (60.36)
Cross Range, km (n mi)	128.62 (69.45)	124.51 (67.23)	4.11 (2.22)
Geodetic Latitude, deg N	31.834	31.955	-0.121
Longitude, deg E	-37.277	-38.453	1.176

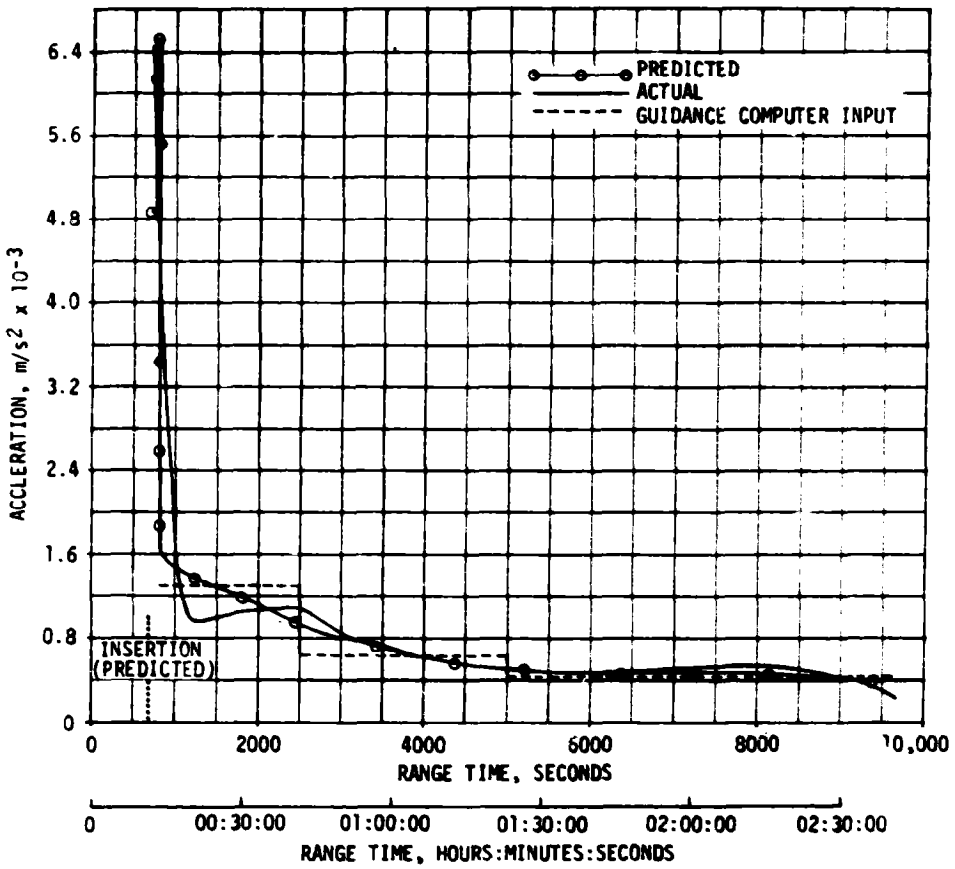

Figure 4-6. Acceleration Due to Venting

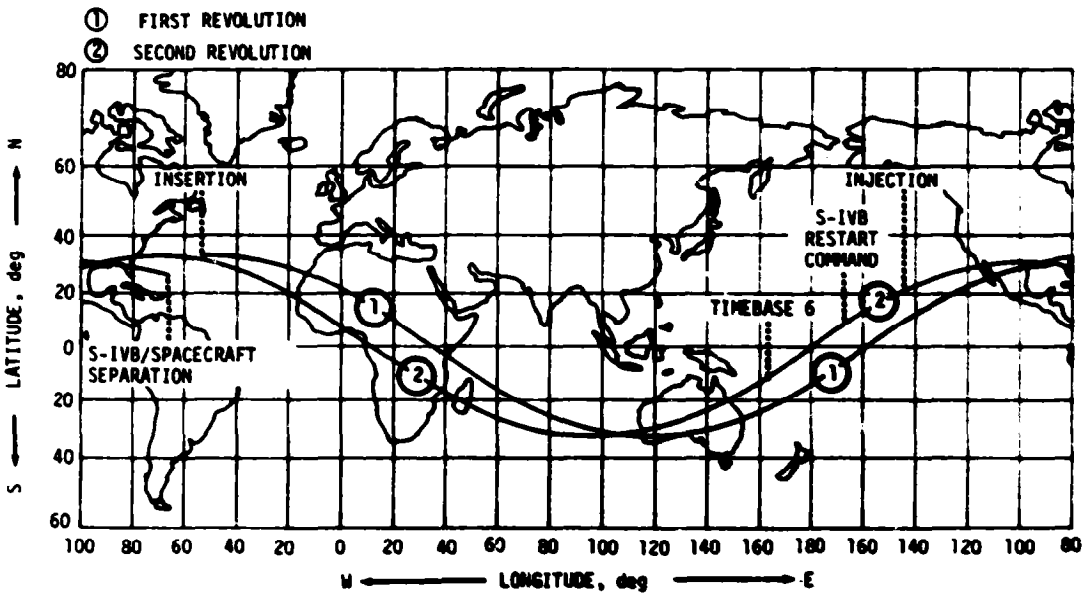

Figure 4-7. Ground Track

Table 4-6. Parking Orbit Insertion Conditions

PARAMETER	ACTUAL	NOMINAL	ACT-NOM	TOLERANCES** -3 SIGMA	TOLERANCES** +3 SIGMA
Range Time, sec	694.38	693.99	0.99	-11.61	+13.96
Space-Fixed Velocity, m/s (ft/s)	7792.84 (25,567.06)	7792.85 (25,567.09)	-0.01 (-0.03)	-1.38 (-4.53)	+1.38 (+4.53)
Flight Path Angle, deg	0.0006	-0.0005	0.0011	-0.0159	+0.0159
Heading Angle, deg	88.5319	88.5247	0.0072	-0.3231	+0.3869
Inclination, deg	32.509	32.503	0.006	-0.010	+0.010
Descending Node, deg	42.415	42.397	0.018	-0.038	+0.038
Eccentricity	0.00006	0.00005	0.00001	-0.00032	+0.00032
Apogee*, km (n mi)	185.18 (99.99)	185.21 (100.01)	-0.03 (-0.02)	-1.5 (-0.8)	+1.5 (+0.8)
Perigee*, km (n mi)	184.41 (99.57)	184.57 (99.66)	-0.16 (-0.09)	-3.4 (-1.8)	+3.5 (+1.9)
Period, min	88.19	88.19	0.00		
Geodetic Latitude, deg N	32.649	32.643	0.006	-0.018	+0.019
Longitude, deg E	-53.292	-53.320	0.028	-0.554	+0.662
Altitude, km (n mi)	191.36 (103.33)	191.39 (103.34)	-0.03 (-0.01)	-0.72 (-0.39)	+0.72 (+0.39)

* Based on a spherical earth of radius 6378.165 km (3443.934 n mi).

** These do not include evaluation inaccuracies.

Table 4-7. Translunar Injection Conditions

PARAMETER	ACTUAL	NOMINAL	ACT-NOM
Range Time, seconds	10,565.51	10,562.28	3.23
Space-Fixed Velocity, m/s (ft/s)	10,822.05 (35,505.41)	10,827.28 (35,522.57)	-5.23 (-17.16)
Altitude, km (n mi)	346.73 (187.22)	343.11 (185.26)	3.62 (1.96)
Flight Path Angle, deg	7.897	7.794	0.103
Heading Angle, deg	67.494	67.456	0.038
Eccentricity	0.97553	0.97636	-0.00083
C_3, m^2/s^2 (ft^2/s^2)	-1,478,917 (-15,918,930)	-1,429,286 (-15,384,706)	-49,631 (-534,224)
Inclination, deg	30.636	30.611	0.025
Descending Node, deg	38.983	38.940	0.043

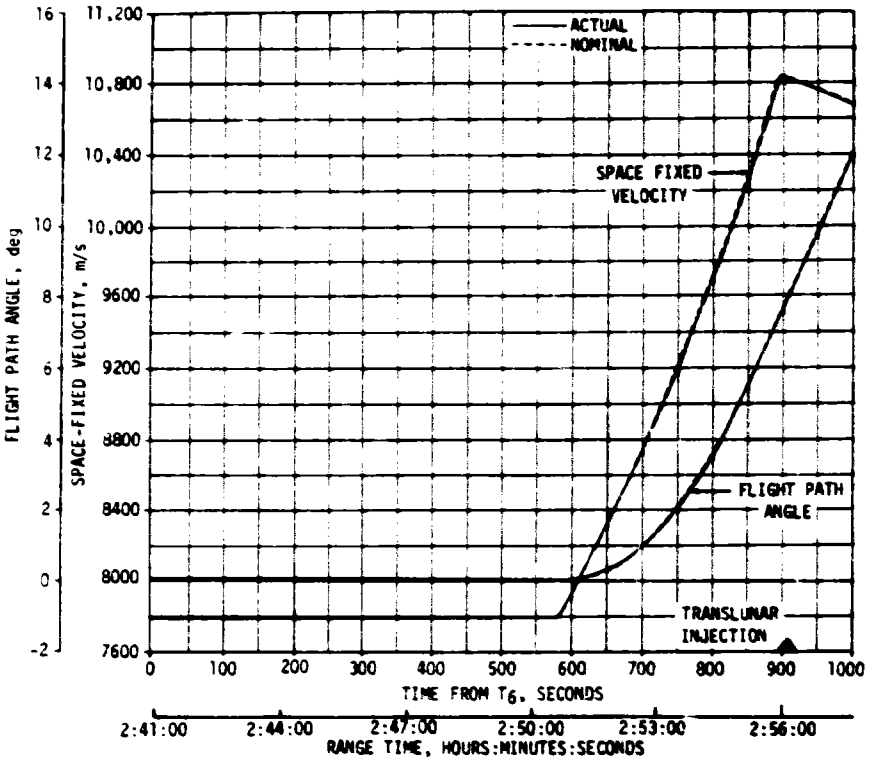

Figure 4-8. Injection Phase Space-Fixed Velocity Comparison

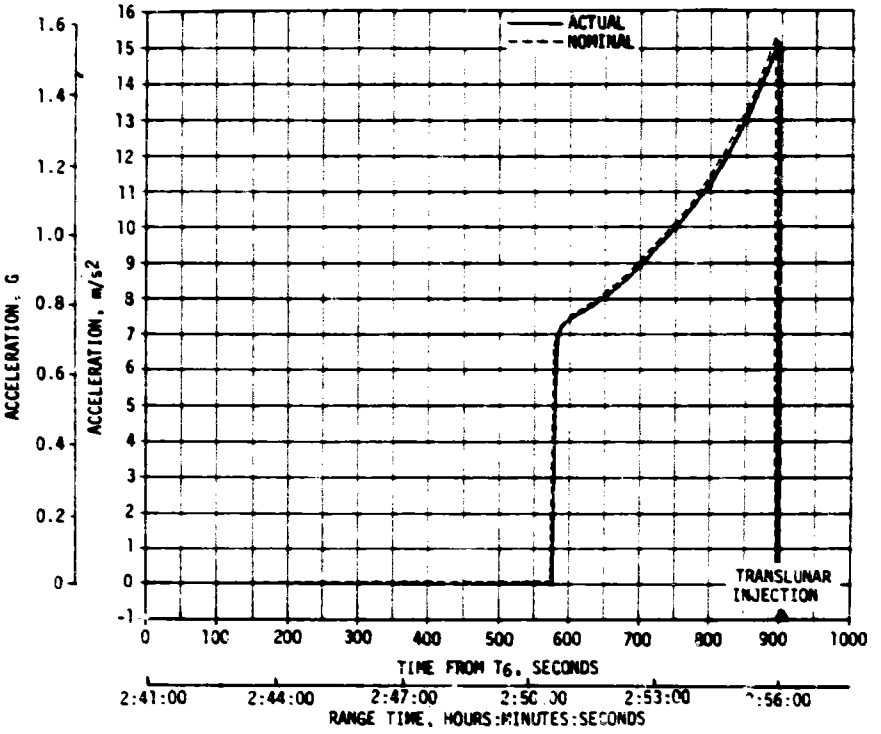

Figure 4-9. Injection Phase Acceleration Comparison

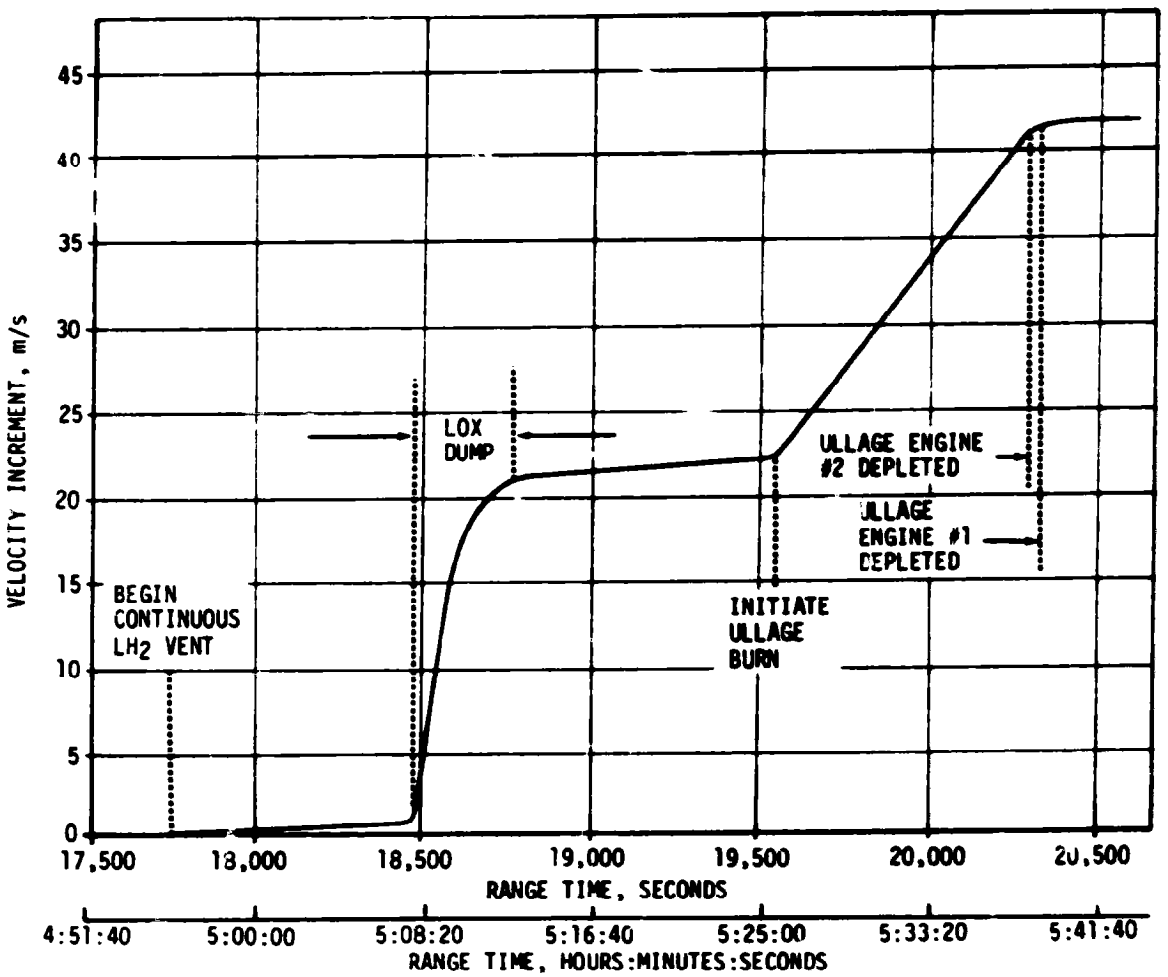

Figure 4-10. Slingshot Maneuver Velocity Increment

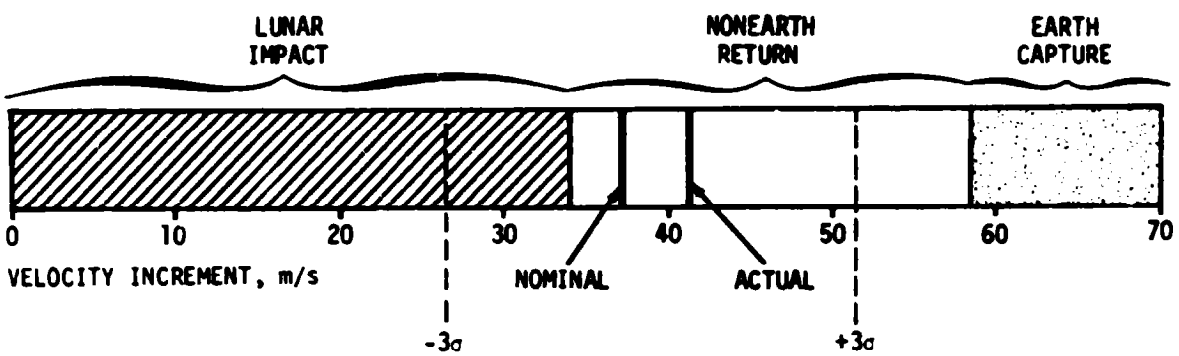

Figure 4-11. Resultant Slingshot Maneuver Conditions

Table 4-8. Comparison of Slingshot Maneuver

PARAMETER	ACTUAL	NOMINAL	TOLERANCES	
			-3 SIGMA	+3 SIGMA
Velocity Increment, m/s (ft/s)	41.9 (137.5)	37.0 (121.4)	-10.5 (-34.4)	+14.5 (+47.6)
Misc. (LH_2 and Guidance Hardware Error), m/s (ft/s)	2.1 (6.9)	1.1 (3.6)	-8.8 (-28.9)	+13.3 (+43.6)
LOX Dump, m/s (ft/s)	20.4 (66.9)	18.0 (59.1)	-4.9 (-16.1)	+5.5 (+18.0)
APS Ullage Burn, m/s (ft/s)	19.4 (63.6)	17.9 (58.7)	-3.0 (-9.8)	+1.4 (+4.6)
APS Ullage Burn Time				
Engine No. 1, sec	758.2	714	-114	+64
Engine No. 2, sec	732.5	714	-114	+64

Table 4-9. Lunar Closest Approach Parameters

PARAMETER	ACTUAL	NOMINAL
Lunar Radius of Closest Approach, km (n mi)	3000 (1620)	2139 (1155)
Altitude above Lunar Surface, km (n mi)	1262 (682)	401 (217)
Time from Launch, hr	69.982	69.964
Velocity Increase Relative to Earth from Lunar Influence, km/s (n mi/s)	1.46 (0.79)	1.84 (0.99)

Table 4-10. Heliocentric Orbit Parameters

PARAMETER	S-IVB/IU	EARTH
Semi-Major Axis, km (n mi)	1.4284×10^8 (0.7713×10^8)	1.4900×10^8 (0.8045×10^8)
Aphelion, km (n mi)	1.4774×10^8 (0.7977×10^8)	1.5115×10^8 (0.8161×10^8)
Perihelion, km (n mi)	1.3795×10^8 (0.7449×10^8)	1.4684×10^8 (0.7929×10^8)
Inclination, deg	23.47	23.44
Period, days	340.8	365.25

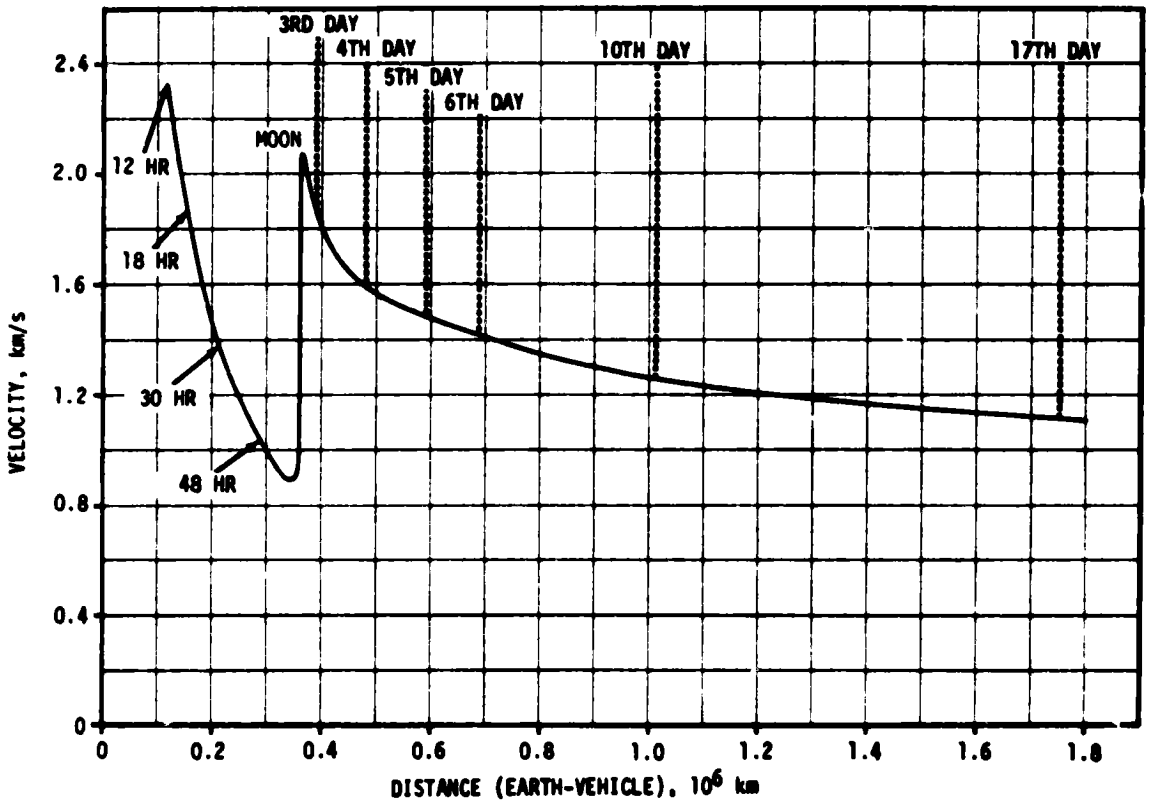

Figure 4-12. S-IVB/IU Velocity Relative to Earth Distance

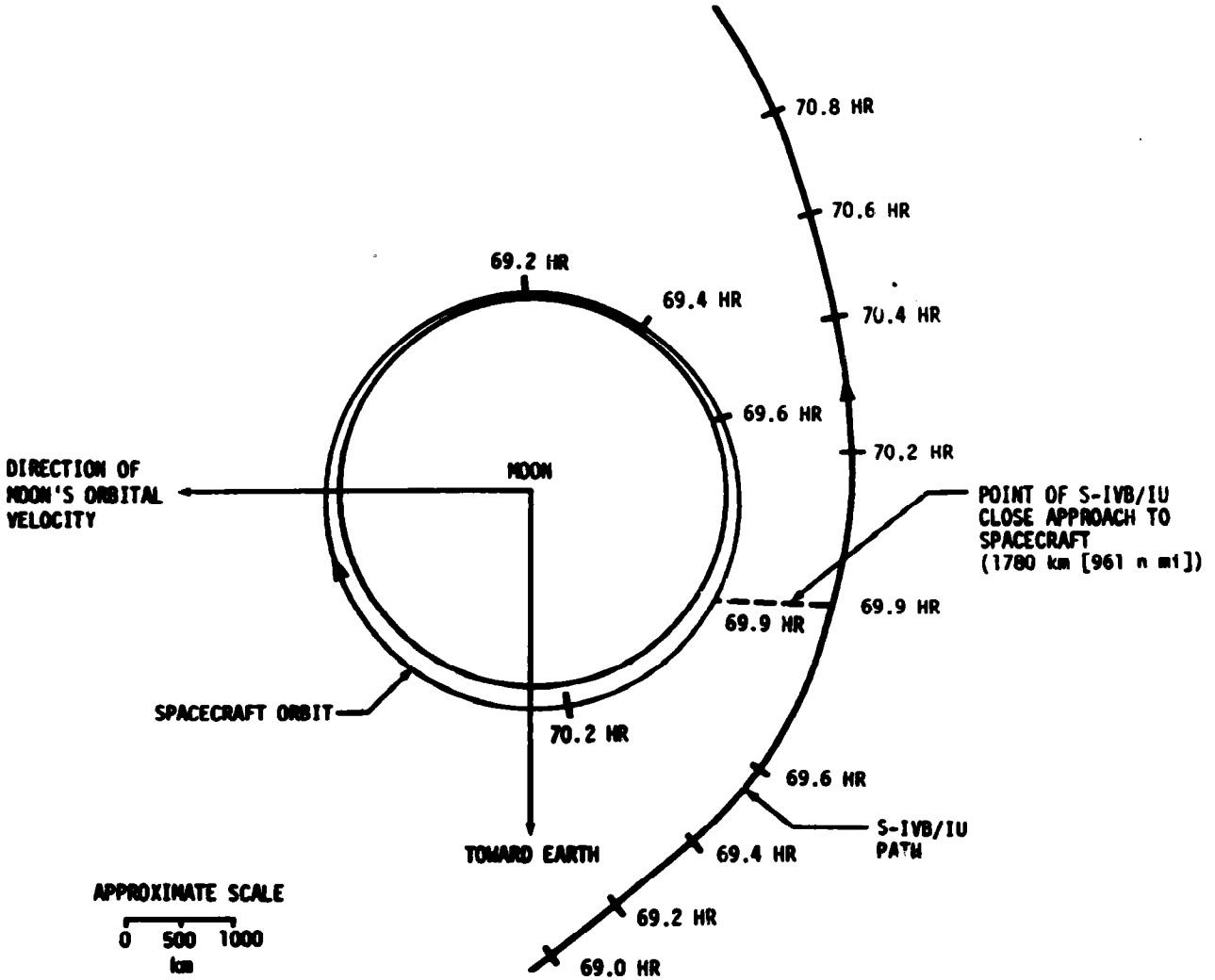

Figure 4-13. Projection of Spacecraft - S-IVB/IU Positions

SECTION 5

S-IC PROPULSION

5.1 SUMMARY

The S-IC propulsion system was equipped with a new subsystem to suppress oscillations similar to those experienced during the 110 to 140-second period of AS-502 flight. This subsystem performed as expected.

All S-IC propulsion systems performed satisfactorily. In general, all flight performance data, as determined from the propulsion reconstruction analysis, were close to the nominal predictions. At the 35 to 38-second time slice, average engine thrust reduced to standard pump inlet conditions was 0.73 percent lower than predicted. Average reduced specific impulse was 0.11 percent lower than predicted, and reduced propellant consumption rate was 0.67 percent less than predicted.

Inboard engine cutoff, as indicated by engine No. 5 cutoff solenoid activation signal, occurred 0.03 second later than predicted. Outboard engine cutoff, as indicated by outboard engines No. 1, 2, 3, and 4 cutoff solenoid activation signals occurred 2.42 seconds later than predicted. An outboard engine LOX low level cutoff was predicted, but a combination of propellant loading errors and, to a lesser extent, a fuel-rich mixture ratio resulted in a fuel low level initiated cutoff. The usable LOX residual at Outboard Engine Cutoff (OECO) was 3018 kilograms (6653 lbm) compared to the usable zero predicted, and the usable fuel residual was zero compared to the usable 2419 kilograms (5333 lbm) predicted.

5.2 S-IC IGNITION TRANSIENT PERFORMANCE

The fuel pump inlet preignition pressure and temperature were 30.3 N/cm^2 (44.0 psia) and 272.6°K (31.0°F), respectively. These fuel pump inlet conditions were within the F-1 engine model specification limits (start box requirements) as shown in Figure 5-1. The preignition temperature at the fuel pump inlet was considerably lower than the fuel bulk temperature of 288°K (59°F) due to the cooling effect of the LOX in the suction lines and engine. The LOX pump inlet preignition pressure and

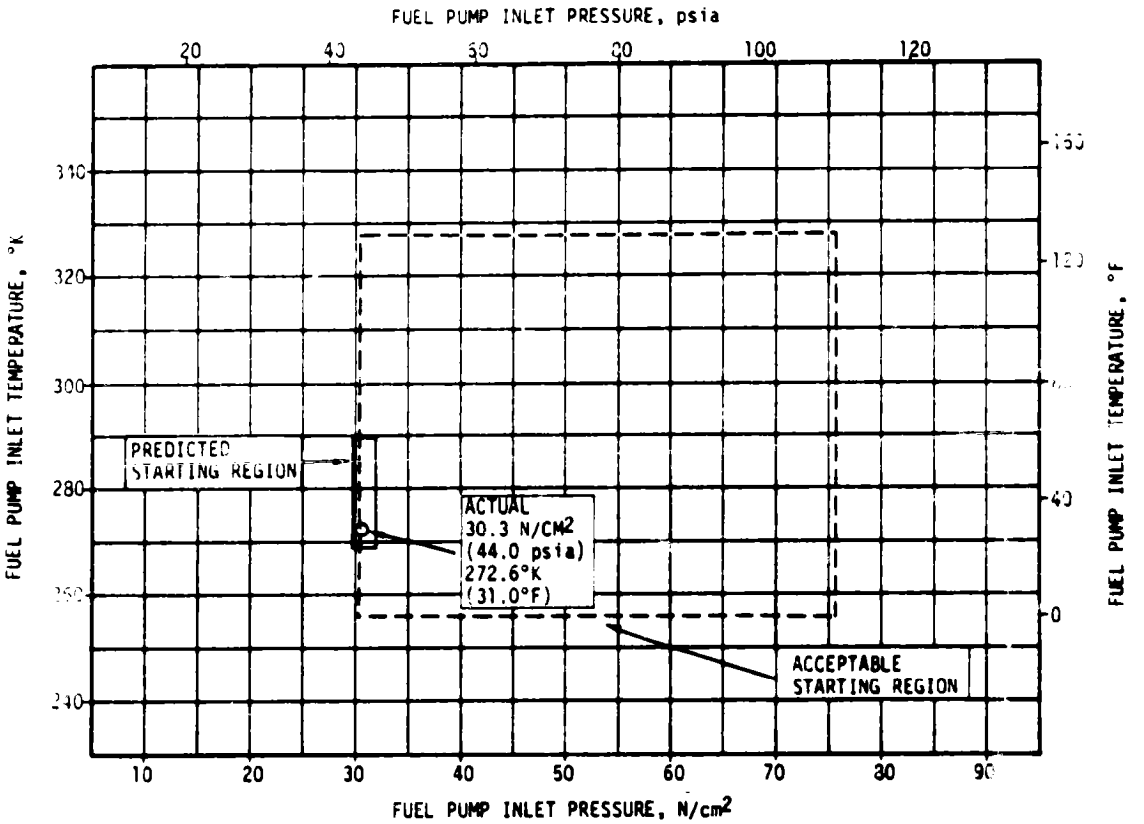

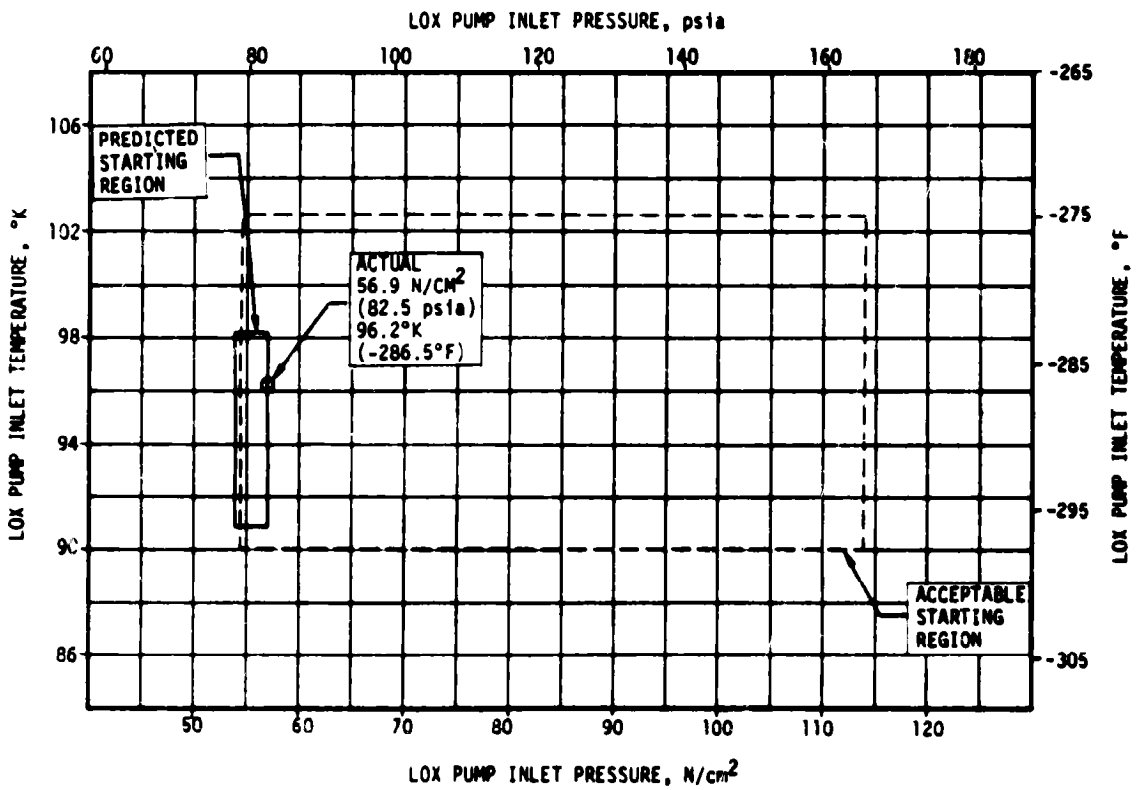

Figure 5-1. S-IC Start Box Requirements

temperature were 56.9 N/cm^2 (82.5 psia) and 96.2°K (-286.5°F), respectively. The LOX pump inlet conditions were also within the F-1 engine model specification limits as shown in Figure 5-1.

The engine startup sequence was normal. A 1-2-2 start was planned and attained. Engine position starting order was 5, 3-1, 2-4. Two engines are considered to start together if their combustion chamber pressures reach 69 N/cm^2 (100 psig) within 100 milliseconds of each other. All engines started an average of 125 milliseconds slower than predicted. Figure 5-2 shows the thrust buildup of each engine, indicating the successful 1-2-2 start. The shift in thrust buildup near the 4,893,044 Newton (1,100,000 lbf) thrust level on the outboard engines was caused primarily by a combination ingestion of Gaseous Oxygen (GOX) and helium from the LOX prevalves which are used as helium filled accumulators for POGO suppression. The thrust shift is absent on the inboard engine for which the POGO suppression system was rendered inoperative prior to flight. Major events during the engine startup sequence are listed in Table 5-1. The best estimate of propellants consumed between ignition and holddown arms release was 40,520 kilograms (89,332 lbm). These consumptions are more than the predicted consumption of 38,985 kilograms (85,949 lbm). The higher than predicted consumption during holddown resulted in best estimate liftoff propellant loads of 1,386,971 kilograms (3,057,349 lbm) for LOX and 605,355 kilograms (1,338,987 lbm) for fuel.

5.3 S-IC MAIN STAGE PERFORMANCE

Two analytical techniques were employed in evaluating S-IC stage propulsion system performance. The primary method, propulsion reconstruction analysis, utilized telemetered engine and stage data to compute longitudinal thrust, specific impulse, and stage mass flowrate. In the second method, flight simulation, a six-degree-of-freedom trajectory simulation was utilized to fit propulsion and aerodynamic (drag and base pressure profiles) reconstruction analysis results to the trajectory. Using a differential correction procedure, this simulation determined adjustments to the reconstruction analysis of thrust and mass flow histories to yield a simulated trajectory which closely matched the observed postflight trajectory.

S-IC stage propulsion performance, as determined by reconstruction, was completely satisfactory. Performance parameters and the nominal predictions are shown in Figure 5-3. All performance parameters were within the predicted values ± 3 sigma deviations. Average engine thrust, reduced to standard pump inlet conditions, at a 35 to 38-second time slice was 0.73 percent lower than predicted, as shown in Table 5-2. Individual engine deviations from predicted thrust ranged from 1.44 percent lower (engine No. 4) to 0.39 percent lower (engine No. 3). Average reduced engine specific impulse was 0.11 percent lower than predicted. Individual engine deviations from predicted specific impulse ranged from 0.18 percent lower (engine No. 4) to 0.07 percent lower (engines No. 2 and No. 3).

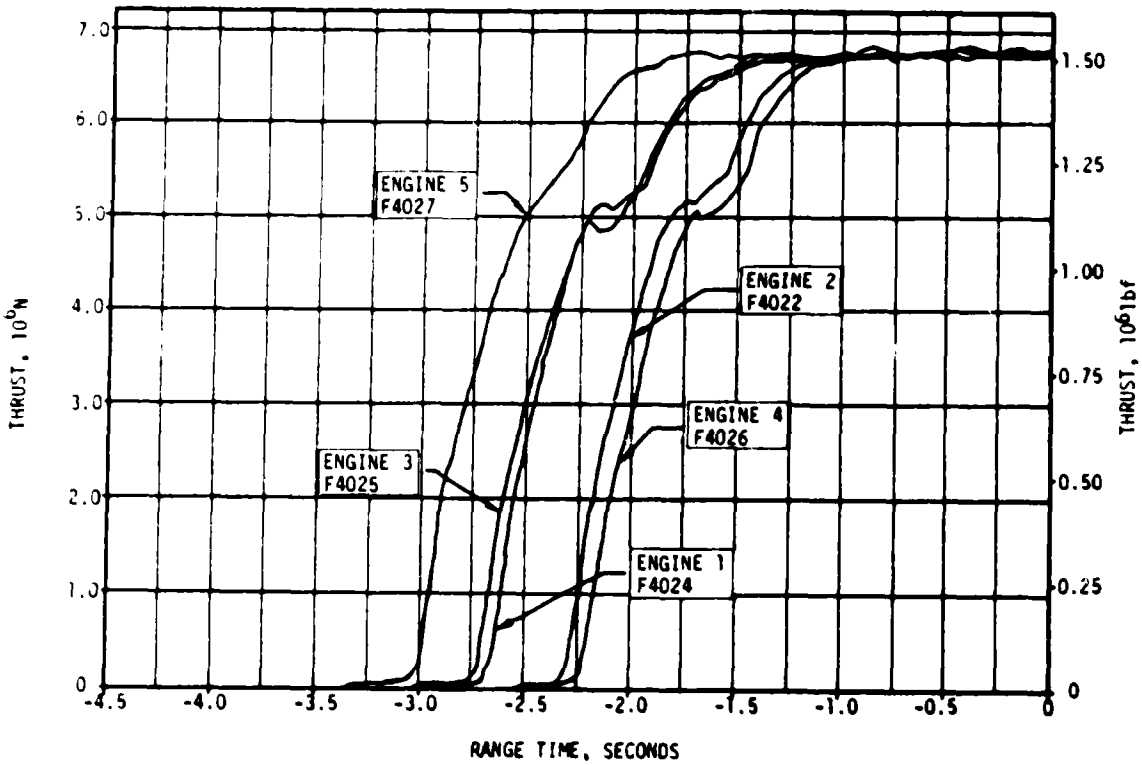

Figure 5-2. S-IC Engine Buildup Transient

Table 5-1. S-IC Stage Engine Startup Event Times

EVENT	RANGE TIME, SECONDS				
	ENGINE 1	ENGINE 2	ENGINE 3	ENGINE 4	ENGINE 5
Start Solenoid Energized	-5.817	-5.765	-6.235	-5.927	-6.585
MLV 1 Starts Open	-5.669	-5.601	-6.083	-5.773	-6.439
2 Starts Open	-5.669	-5.605	-6.089	-5.785	-6.421
Thrust Chamber Ignition	-2.975	-2.615	-3.035	-2.525	-3.315
MFV 1 Starts Open	-2.817	-2.459	-2.877	-2.401	-3.161
2 Starts Open	-2.821	-2.447	-2.879	-2.397	-3.155
Final Thrust OK	-1.831	-1.427	-1.803	-1.387	-2.201
All Engines Running	-1.381				
Launch Commit	0.019				

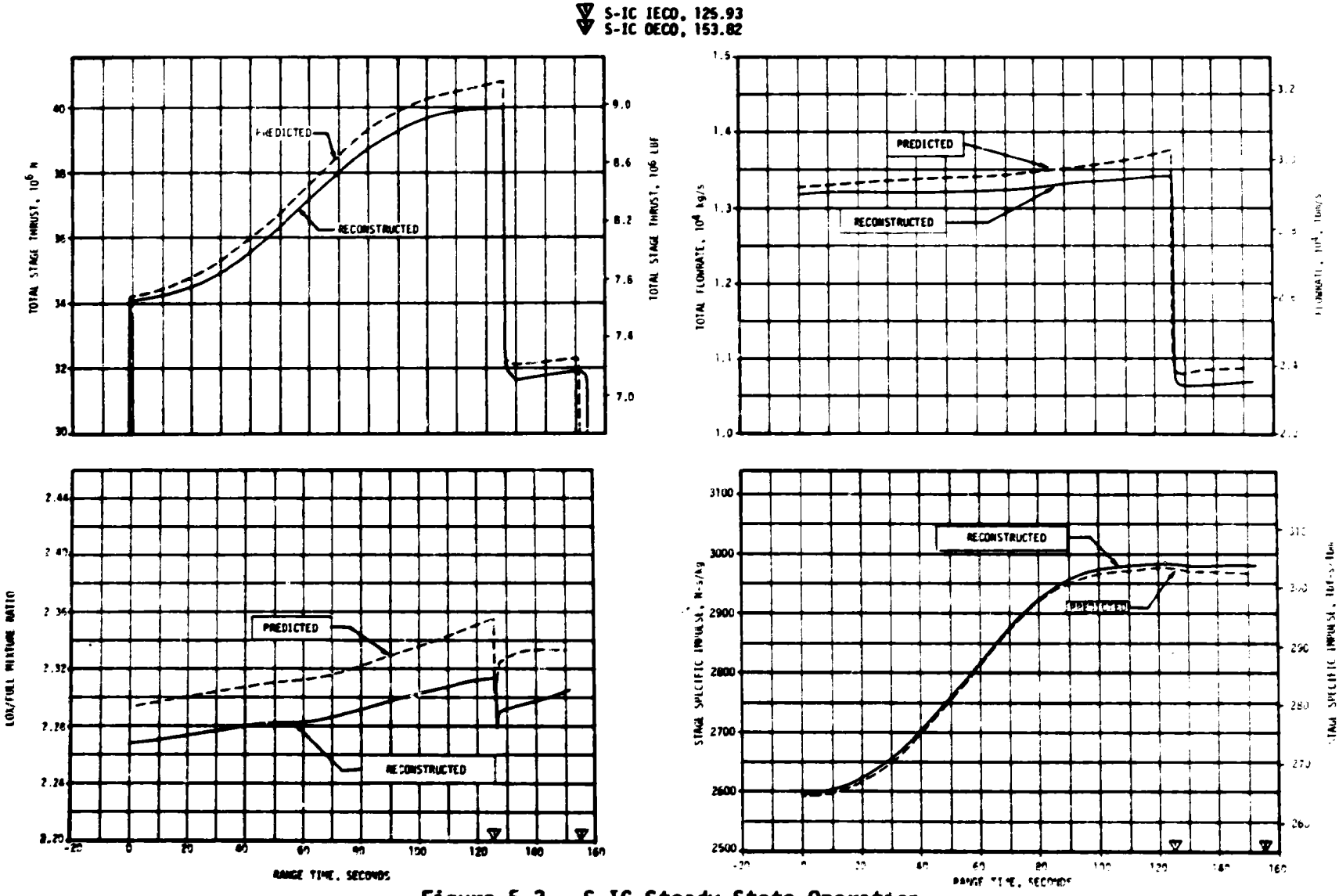

Figure 5-3. S-IC Steady State Operation

Table 5-2. S-IC Engine Performance Deviations

PARAMETER	ENGINE	PREDICTED	RECONSTRUCTED	DEVIATION PERCENT	AVERAGE DEVIATION PERCENT
Thrust 10^3 N (10^3 lb_f)	1	6787 (1526)	6752 (1518)	-0.52	
	2	6731 (1513)	6695 (1505)	-0.53	
	3	6816 (1532)	6788 (1526)	-0.39	
	4	6808 (1530)	6708 (1508)	-1.44	
	5	6762 (1520)	6690 (1504)	-0.77	-0.73
Specific Impulse N-s/kg (lbf-s/lbm)	1	2587 (263.8)	2584 (263.5)	-0.11	
	2	2580 (263.1)	2578 (262.9)	-0.07	
	3	2594 (264.5)	2592 (264.3)	-0.07	
	4	2592 (264.3)	2587 (263.8)	-0.18	
	5	2605 (265.6)	2601 (265.2)	-0.15	-0.11
Flowrate kg/s (lbm/s)	1	2624 (5785)	2613 (5761)	-0.41	
	2	2609 (5751)	2597 (5725)	-0.45	
	3	2628 (5794)	2619 (5774)	-0.34	
	4	2626 (5790)	2593 (5716)	-1.27	
	5	2596 (5724)	2572 (5671)	-0.92	-0.67
Mixture Ratio LOX/Fuel	1	2.239	2.227	-0.53	
	2	2.266	2.254	-0.10	
	3	2.278	2.265	-0.57	
	4	2.288	2.275	-0.56	
	5	2.274	2.262	-0.52	-0.45

Note: Analysis was reduced to standard sea level conditions (standard pump inlet conditions) at liftoff plus 35 to 38 seconds.

From a clustered engine performance analysis (flight simulation), utilizing the results of the propulsion reconstruction and reduced to sea level ambient pressure, the stage average longitudinal thrust for the flight was 1.36 percent lower than predicted and the stage average longitudinal specific impulse was 0.04 percent higher than predicted. Table 5-3 presents a summary of the flight simulation results, reduced to sea level ambient pressure conditions, of the average values and deviations for longitudinal thrust, propellant flowrate, and vehicle longitudinal specific impulse.

5.4 S-IC ENGINE SHUTDOWN TRANSIENT PERFORMANCE

In response to the Inboard Engine Cutoff (IECO) command from the IU at 125.93 seconds, the inboard engine shut down at 125.95 seconds as indicated by the engine cutoff solenoid activation signal. The outboard engines shut down at 153.79 seconds as indicated by engines No. 1, 2, 3, and 4 solenoid activation signals. This was 2.42 seconds later than predicted. These events were sensed by the Launch Vehicle Digital Computer (LVDC) at 153.82 seconds (OECO, start of Time Base 3 [T_3]) which was 2.45 seconds later than the predicted time of 151.37 seconds. The late OECO was caused by fuel density, thrust, specific impulse, mixture ratio, and propellant

Table 5-3. Comparison of S-IC Stage Flight Reconstruction Data With Trajectory Simulation Results

PARAMETERS	UNITS	PREDICTED	RECONSTRUCTION	RECONSTRUCTION DEVIATION FROM PREDICTED	FLIGHT SIMULATION	SIMULATION DEVIATION FROM PREDICTED
Average * longitudinal thrust	N (lbf)	34,794,249 (7,822,058)	34,371,122 (7,726,936)	-1.23%	34,322,108 (7,715,917)	-1.36%
Vehicle mass at hold-down arm release	kg (lbm)	2,782,424 (6,134,195)	2,781,694 (6,132,585)	0.03%	2,779,469 (6,127,680)	-0.11%
Average mass loss rate	kg/s (lbm/s)	13,403.26 (29,549.13)	13,213.19 (29,130.10)	-1.42%	13,216.14 (29,136.60)	-1.40%
Average * specific impulse	N-s/kg (lbf-s/lbm)	2595.9 (264.71)	2601.3 (265.26)	0.21%	2597.0 (264.82)	0.04%

*Parameters reduced to sea level ambient pressure.

loading deviations. Figure 5-4 shows the relative contribution of each influencing parameter to the cutoff deviation. The combined effects of a slightly LOX-rich loading mixture ratio and, to a lesser extent, a fuel-rich propellant consumption mixture ratio resulted in a fuel low level cutoff of the outboard engines rather than the more probable LOX low level cutoff mode (see paragraph 5.5).

Thrust decay of the F-1 engines is shown in Figure 5-5. The decay transient was normal. The oscillations which occur near the end of "tailoff" are characteristic of the engine shutdown sequence.

The total stage impulse from OECO to separation was indicated by engine analysis to be less than predicted. Telemetered guidance data also indicated that the cutoff impulse was lower than expected, as shown in Table 5-4. These deviations are within the acceptable range.

5.5 S-IC STAGE PROPELLANT MANAGEMENT

The reconstructed propellant loads were 2297 kilograms (5063 lbm) greater than Kennedy Space Center (KSC) indicated loads at ignition (corresponding to the actual density at ignition) for LOX and 1095 kilograms (2415 lbm) less for fuel. This loading increased the probability of a fuel low level cutoff from a nominal 11 percent to approximately 44 percent. A summary of the propellants remaining at major event times is presented in Table 5-5 and the residuals are presented in Table 5-6. The predicted masses in Table 5-5 are based on nominal LOX and fuel densities. The nominal fuel temperature was 294°K (70°F) and the actual temperature was 288°K (59°F).

5.6 S-IC PRESSURIZATION SYSTEMS

5.6.1 S-IC Fuel Pressurization System

The helium pressurization system satisfactorily maintained the required ullage pressure in the fuel tank during the flight. Helium Flow Control

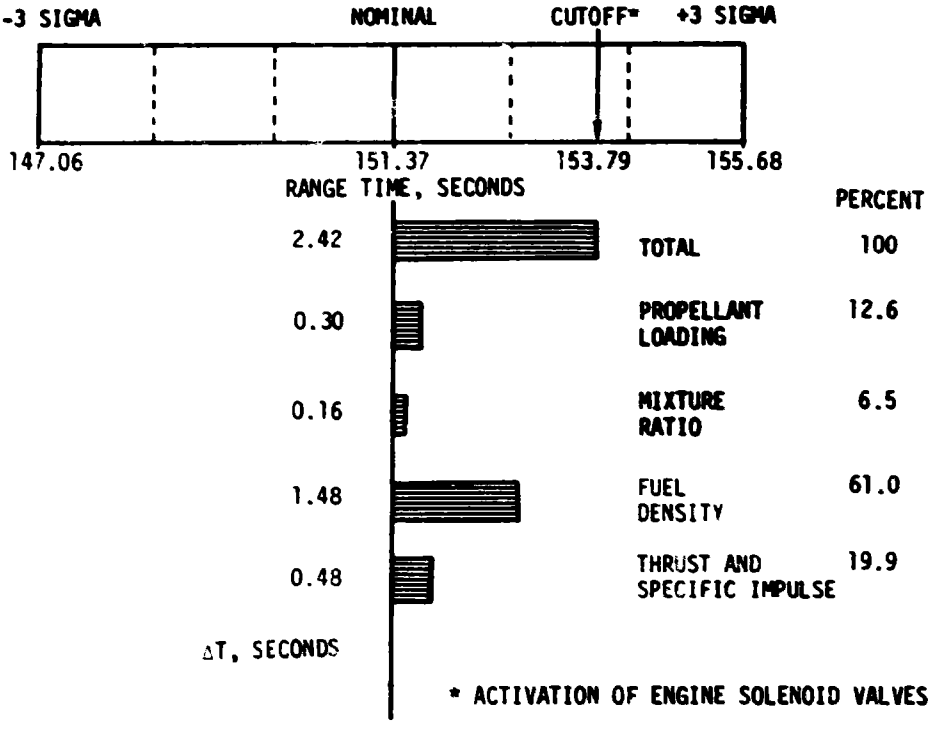

Figure 5-4. S-IC Outboard Engine Cutoff Deviations

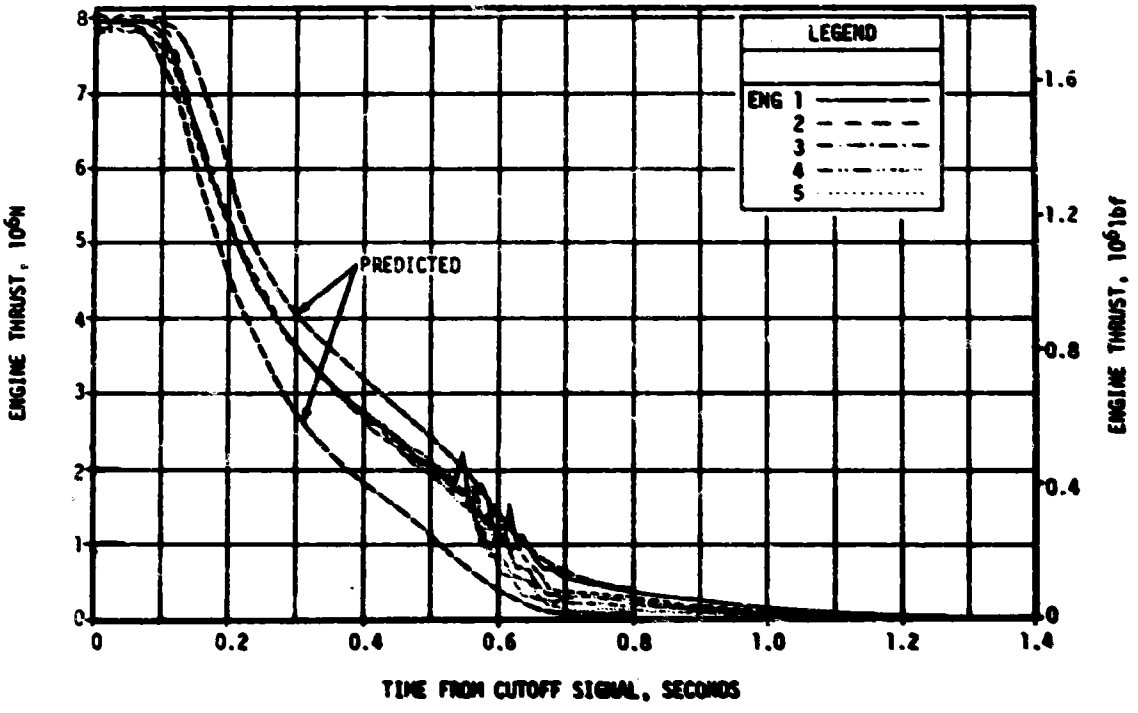

Figure 5-5. S-IC Engine Shutdown Transient Performance

Valves (HFCV) No. 1 through 4 opened as programmed and the fifth flow control valve was required only once, between 47.11 seconds and 50.79 seconds.

In Section 2, Table 2-3, Sequence of Switch Selector Events, these valves are designated "Fuel Pressurizing Valves". The heat exchangers performed as expected.

The low flow prepressurization system was commanded on at -96.99 seconds and performed satisfactorily. The Ground Support Equipment (GSE) fuel high flow prepressurization supply valve was commanded open at -4.09 seconds and maintained the ullage pressure within the required band.

Table 5-4. S-IC Cutoff Impulse

PARAMETER	PREDICTED	FLIGHT		PERCENT DEVIATION FROM PREDICTED	
		ENGINE	GUID. DATA	ENGINE	GUID. DATA
Cutoff N-s Impulse (lbf-s)	10,382,145 (2,334,000)	10,324,091 (2,320,948)	10,365,326 (2,330,218)	-0.06	-0.02
Velocity m/s Increase (ft/s)	10.13 (33.25)	10.61 (34.81)	10.56 (34.67)	0.47	0.52

Note: The parameters quoted are for the time period beginning at OECO and ending at separation signal.

Table 5-5. S-IC Stage Propellant Mass History

EVENT		PREDICTED *		RECONSTRUCTED**		LEVEL SENSOR DATA		BEST ESTIMATE	
		LOX	FUEL	LOX	FUEL	LOX	FUEL	LOX	FUEL
Ignition Command	kg (lbm)	1,420,593 (3,131,873)	612,982 (1,351,395)	1,418,853 (3,128,034)	615,813 (1,357,634)	1,418,860 (3,128,050)	615,812 (1,357,634)	1,418,853 (3,128,034)	615,813 (1,357,634)
Holddown Arm Release	kg (lbm)	1,390,120 (3,064,690)	604,470 (1,332,629)	1,386,791 (3,057,349)	607,355 (1,338,987)	1,385,778 (3,055,118)	606,873 (1,337,927)	1,386,791 (3,057,349)	607,355 (1,338,987)
IECO	kg (lbm)	211,823 (466,990)	97,276 (214,450)	228,735 (504,276)	102,315 (225,566)	226,223 (498,737)	102,550 (226,084)	228,735 (504,276)	102,315 (225,566)
OECO	kg (lbm)	17,656 (38,924)	14,220 (31,350)	20,994 (46,065)	12,073 (26,616)	21,448 (47,284)	11,861 (26,149)	20,994 (46,065)	12,073 (26,616)
Separation	kg (lbm)	15,462 (34,087)	13,116 (28,917)	18,578 (40,958)	10,946 (24,132)			18,578 (40,958)	10,946 (24,132)

Note: Values do not include pressurization gas (GOX) so they will compare with level sensor data.
* Based on LOX density of 1137.3 kg/m^3 (71.0 lbm/ft^3) and fuel density of 802.5 kg/m^3 (50.1 lbm/ft^3).
** based on LOX density of 1138.2 kg/m^3 (71.06 lbm/ft^3) and fuel density of 808.0 kg/m^3 (50.445 lbm/ft^3).

Table 5-6. S-IC Residuals at Outboard Engine Cutoff

PROPELLANTS		PREDICTED	ACTUAL	DEVIATION
LOX RESIDUALS*				
Usable Mainstage	kg	0	3018	3018
	(lbm)	0	6653	6653
Thrust Decay and Unusable	kg	17,656	17,876	220
	(lbm)	38,924	39,412	488
FUEL RESIDUALS				
Usable Mainstage	kg	2419	0	-2419
	(lbm)	5333**	0	-5333
Thrust Decay and Unusable	kg	11,801	12,073	272
	(lbm)	26,017	26,616	599

* Does not include GOX pressurization gas.
** Fuel bias.

At 0.70 seconds the No. 1 HFCV of the onboard pressurization system was opened. HFCV's No. 2, 3, and 4 were commanded open by the switch selector within acceptable times as shown in Table 2-3. These flows held the ullage and pump inlet pressures within the operating limits as shown in Figures 5-6 and 5-7. Helium bottle pressure, as shown in Figure 5-8, stayed within expected limits.

5.6.2 S-IC LOX Pressurization System

The LOX pressurization system performed satisfactorily, and all performance requirements were met. The ground prepressurization system maintained ullage pressure within acceptable limits until launch commit. The onboard pressurization system subsequently maintained ullage pressure within the GOX Flow Control Valve (GFCV) band during the flight. The heat exchangers performed as expected.

The prepressurization system was initiated by opening of the ground supply valve at -67.94 seconds. The ullage pressure increased until it entered

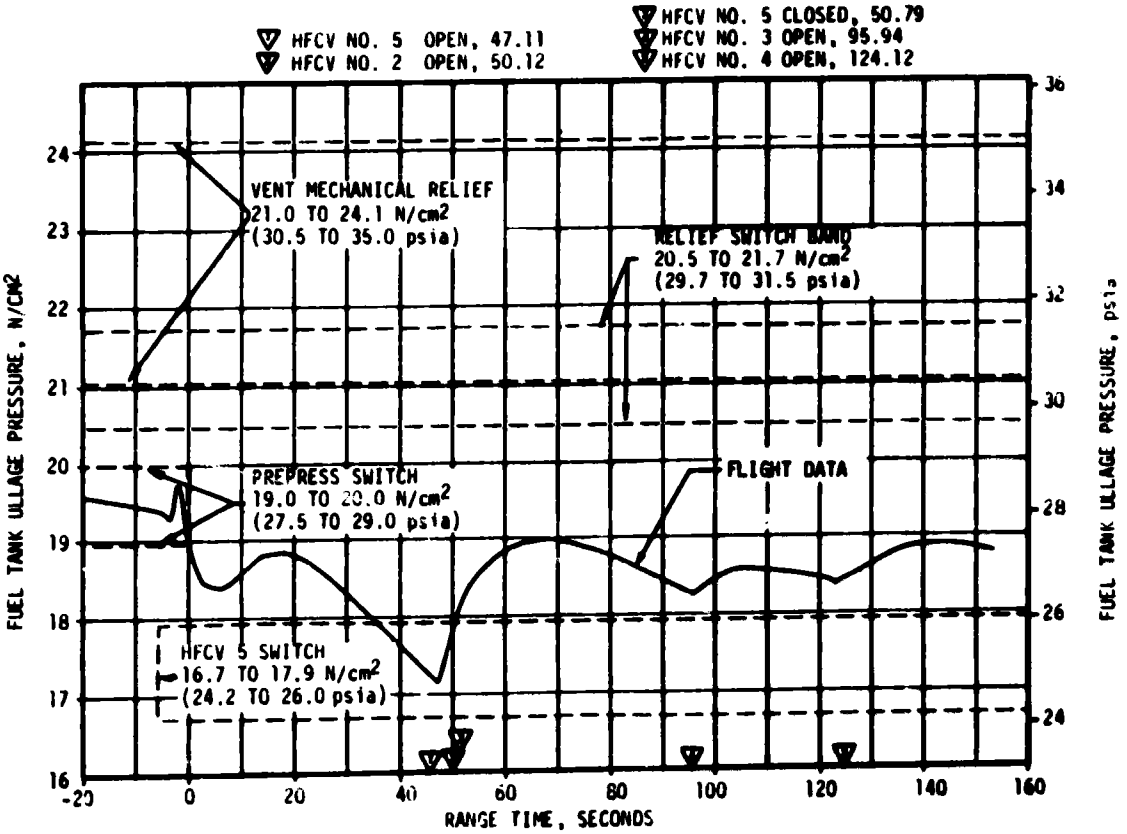

Figure 5-6. S-IC Fuel Ullage Pressure

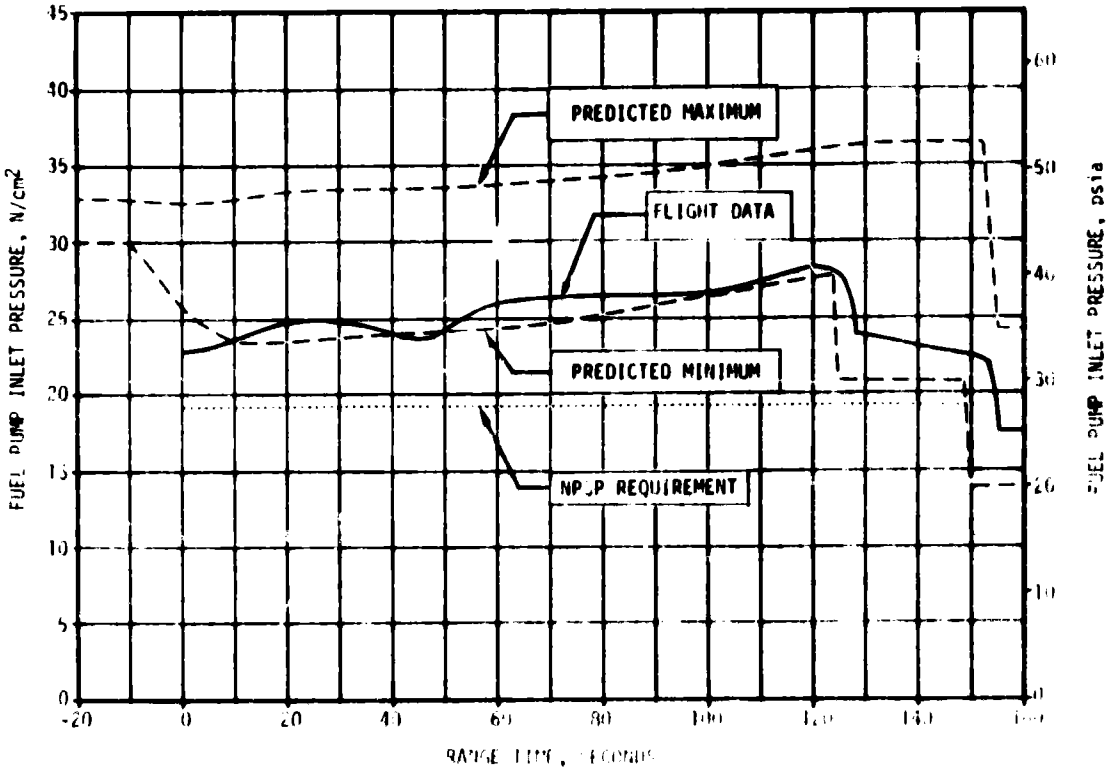

Figure 5-7. S-IC Fuel Pump Inlet Pressure Engine No. 1

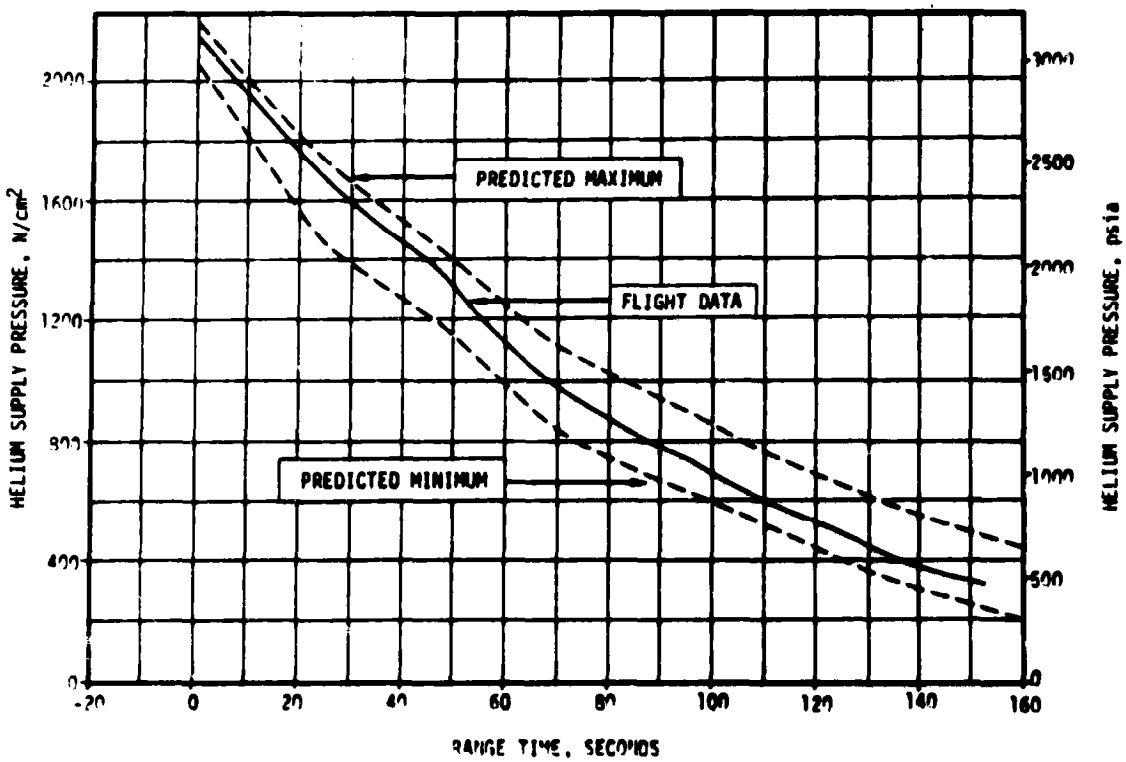

Figure 5-8. S-IC Helium Bottle Pressure for Fuel Pressurization

the switch band zone which terminated the flow at approximately -59.51 seconds. The ullage pressure increased approximately 1.24 N/cm^2 (1.80 psid) above the prepressurization switch setting to 19.5 N/cm^2 (28.3 psia). This overshoot is similar to that seen on AS-501 and AS-502.

The LOX tank ullage pressure history is shown in Figure 5-9. During flight, the ullage pressure was maintained within required limits by the GFCV and followed the anticipated trend.

The maximum GOX flowrate was 24.7 kg/s (54.5 lbm/s). After IECO, the GOX flow requirements for the remaining four engines increased until OECO.

The LOX pump inlet pressure met the Net Positive Suction Pressure (NPSP) requirements as shown in Figure 5-10. This figure is for engine No. 1, but is typical of the four outboard engines. Engine No. 5 LOX pump inlet pressure decayed unexpectedly after IECO. This pressure is shown in Figure 5-11 along with the preflight predictions and pump requirements. Analysis of the problem has shown that the most probable cause of this pressure decay is a LOX leak of approximately 98 cm^3/s (6 in.^{3}/s) somewhere below the LOX prevalve.

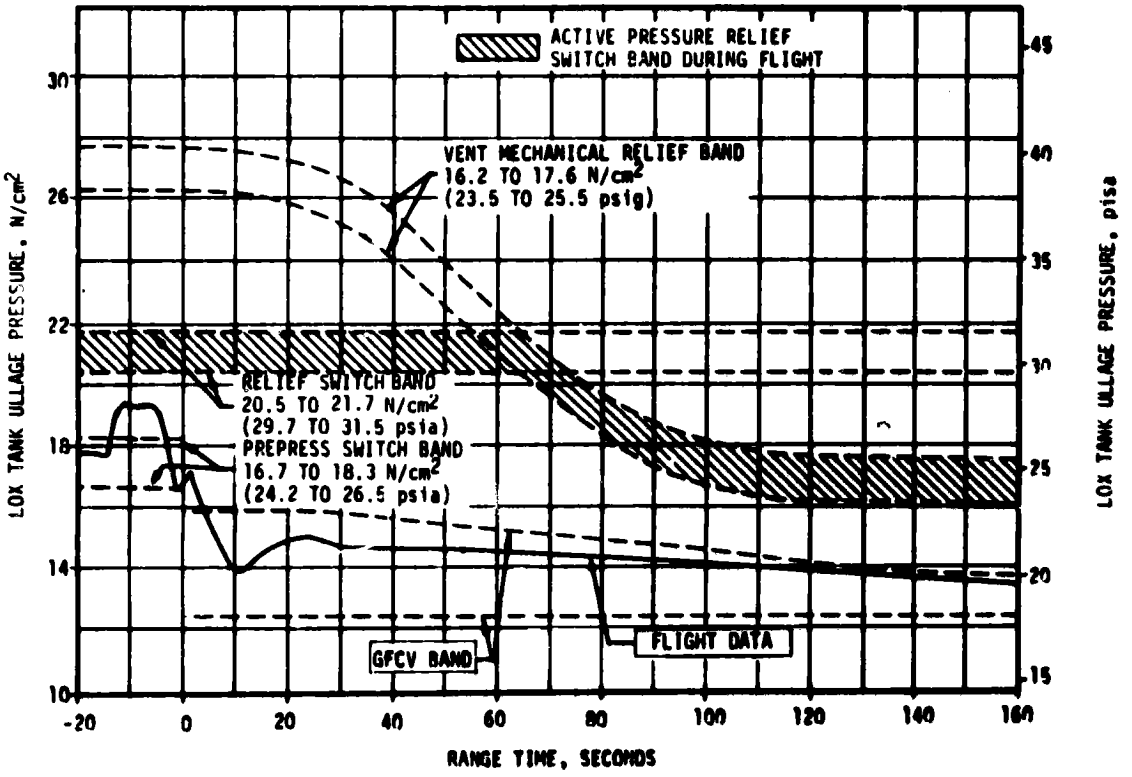

Figure 5-9. S-IC LOX Tank Ullage Pressure

5.7 S-IC PNEUMATIC CONTROL PRESSURE SYSTEM

The pneumatic control pressure system performed satisfactorily during S-IC flight. The pneumatic control regulator outlet pressure was 518 N/cm^2 (751 psia) at liftoff and decreased to 511 N/cm^2 (741 psia) at 120 seconds. There were two slight dips in outlet pressure at IECO and at OECO as the control pressure system actuated the prevalves after engine cutoff. All instrumented prevalves indicated closed positions.

The control sphere pressure was 2055 N/cm^2 (2981 psia) at liftoff and remained steady until IECO when it decreased to 1974 N/cm^2 (2863 psia) due to inboard engine prevalve actuation.

There was a further decrease to 1718 N/cm^2 (2492 psia) after OECO. As shown in Figure 5-12, the rapid decay of sphere pressure after OECO experienced on the AS-502 flight did not recur.

5.8 S-IC PURGE SYSTEM

The turbopump LOX seal, Gas Generator (GG) actuator housing, and radiation calorimeter purge systems performed satisfactorily during S-IC flight. The LOX dome and GG LOX injector purge system also met all requirements.

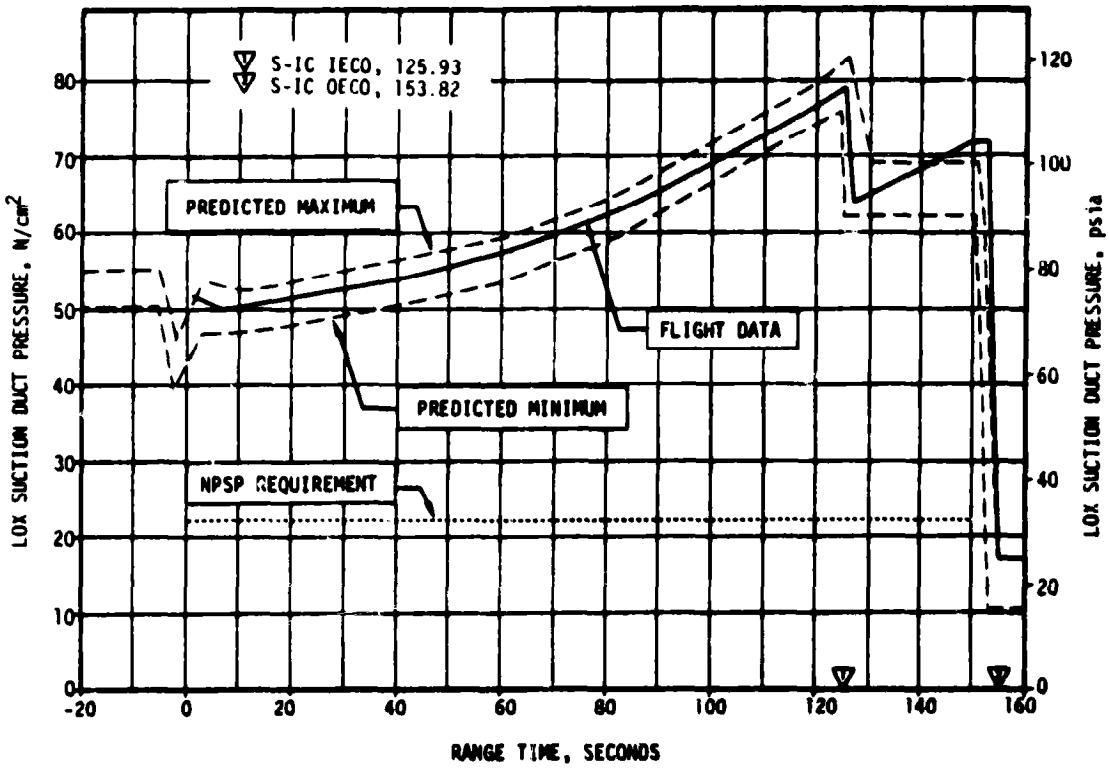

Figure 5-10. S-IC LOX Suction Duct Pressure, Engine No. 1

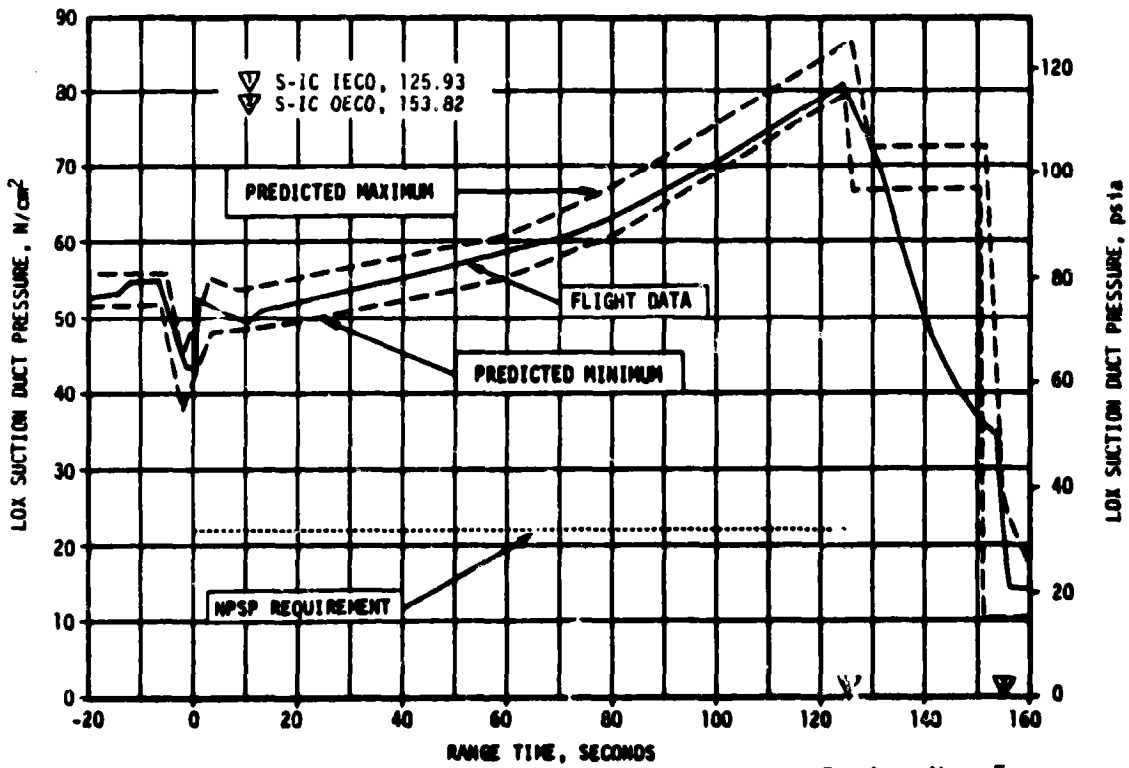

Figure 5-11. S-IC LOX Suction Duct Pressure, Engine No. 5

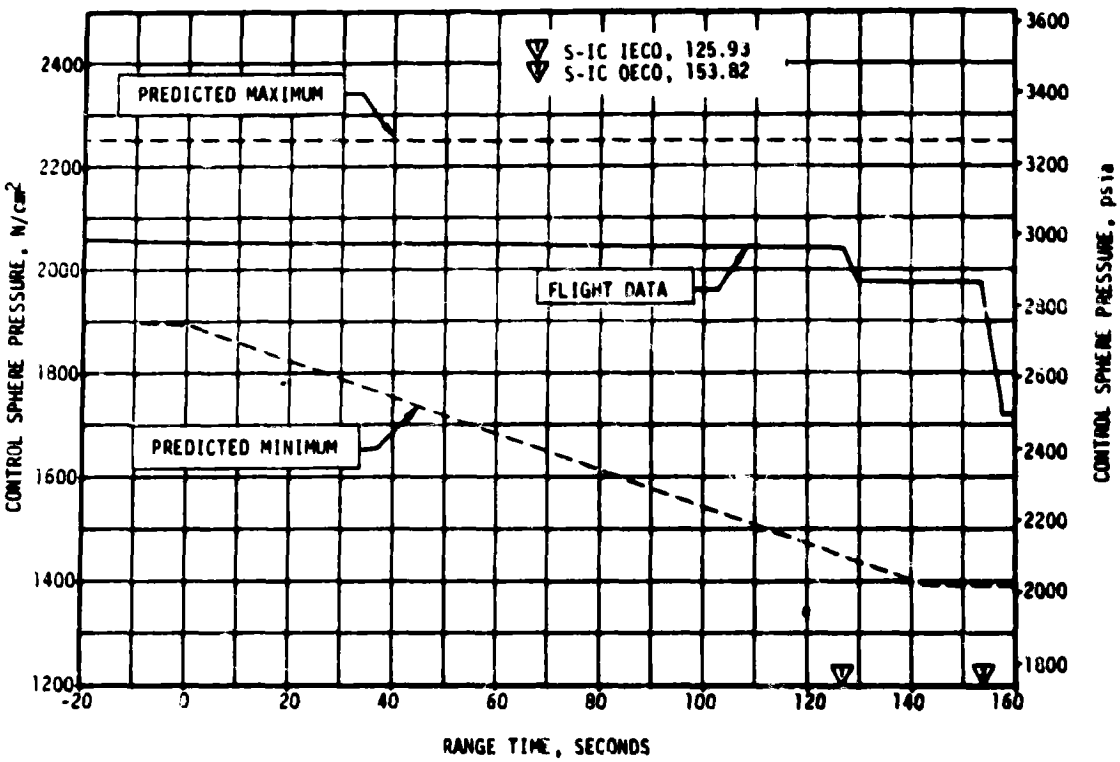

Figure 5-12. S-IC Control Sphere Pressure

5.9 POGO SUPPRESSION SYSTEM

The POGO suppression system supplies helium gas to the four outboard LOX prevalve cavities. The helium is obtained from the onboard fuel pressurization system. Four resistance thermometers in each prevalve determine the presence of gas or liquid in the prevalve cavity at each measurement location. A schematic of the system is shown in Figure 5-13.

The POGO suppression system performed satisfactorily prior to and during S-IC flight. The system was initially turned on approximately 26 minutes prior to launch to be sure the prevalves would fill with helium. Redline measurements indicated that the four outboard lines filled as scheduled. The pressure measurement downstream of the solenoid valves indicated that flow was properly established in the system. Eleven minutes prior to launch, the system was turned on again and flow was established. The temperature measurements did not change since the system still contained helium from the earlier initiation. The four resistance thermometers performed as expected during flight. In the outboard lines, the three upper measurements went cold momentarily at liftoff indicating that the LOX level shifted on the probes. The probes remained warm throughout flight, indicating helium in the prevalves. Figure 5-14 shows a plot of liquid level in the prevalve. At cutoff, the increased pressure forced

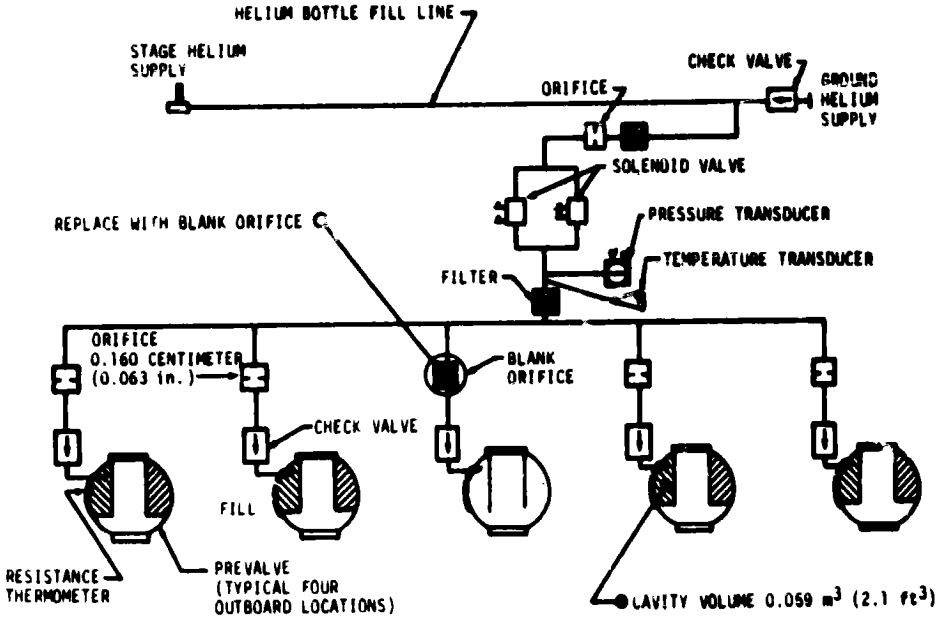

Figure 5-13. S-IC POGO Suppression System

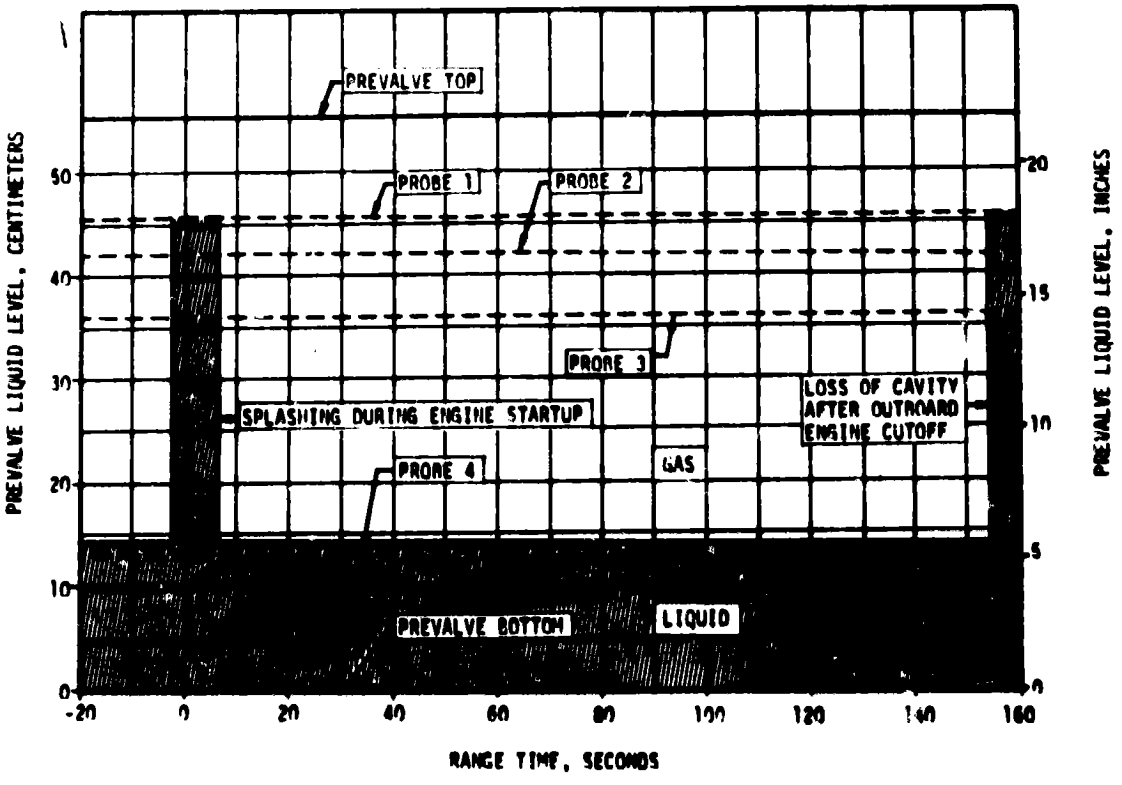

Figure 5-14. S-IC Prevalve Liquid Level, Typical Outboard Engine

LOX into prevalves. The fourth resistance thermometer, at the lip of the valve cavity, was cold throughout flight.

5.10 S-IC CAMERA PURGE AND EJECTION SYSTEM

Although only one of the four film cameras was recovered, there is good evidence that there was adequate pneumatic pressure to eject them all.

Frame rate measurements for the two separation cameras went to zero at approximately 180 seconds. This indicates sufficient pressure in both of the eject lines to shear the restraining pins and provide motion of the cameras within the ejection tubes thus disconnecting the electrical plugs. The No. 2 LOX tank camera was recovered. For a discussion of the film recovered from this camera see paragraph 19.6. Both LOX tank camera frame rate measurements went to zero at 79 seconds. Because of this, it was not possible to determine if the No. 1 LOX tank camera moved in its canister at eject signal. The camera cover ejection signal was given at 160 seconds, but there is no way to ascertain that the covers opened.

Camera eject signal occurred at 179.5 seconds. Separation camera purge was initiated on at 145.2 seconds and turned off at 154.8 seconds. The purge and eject sphere pressure was 2079 N/cm^2 (3015 psia) prior to liftoff. The calculated pressure at eject signal was 1633 N/cm^2 (2369 psia). This is more than the 762 N/cm^2 (1105 psia) required to eject all cameras. AS-503 is the last flight to have these cameras.

SECTION 6

S-II PROPULSION

6.1 SUMMARY

The S-II propulsion system performed satisfactorily during the entire flight. Engine thrust, as determined by computer analysis of telemetered propulsion measurements at 61 seconds after Engine Start Command (ESC), was 0.04 percent above prediction. Total engine propellant flowrate was 0.38 percent above and specific impulse 0.34 percent below predictions at this time slice. Average engine mixture ratio was 0.69 percent above predicted.

Engine No. 4 evidenced a change in performance level at approximately 200 seconds after S-II ESC of approximately -6672 Newtons (-1500 lbf) thrust. At this time the exact nature of this shift has not been determined but is receiving additional investigation.

Engine No. 5 experienced a thrust level decrease of about 27,050 Newtons (6081 lbf) and propellant mixture ratio change of -0.1 units coincident with the onset of the high amplitude 18 hertz oscillations (discussion of the 18 hertz oscillation problem is contained in Section 6A). Beginning at 450 seconds engine No. 5 thrust chamber pressure began oscillating at 18 hertz. At 478 seconds the apparent amplitude of the oscillations was about 48.3 N/cm^2 (70 psi) peak-to-peak. The oscillations dampened out about 4 seconds prior to S-II Engine Cutoff (ECO). Oscillations of this same frequency were also evident in LOX pump discharge pressure along with several other engine No. 5 parameters.

Although the results of the evaluation are not conclusive, it appears that the oscillations were induced by the LOX pumps and possibly amplified by the center engine support structure. Self-induced LOX pump oscillations may be related to the low Engine Mixture Ratio (EMR) and low Net Positive Suction Pressure (NPSP) existing during this time period, although the NPSP is considerably above the level at which self driven oscillations are normally produced. Engine and pump tests to investigate this possibility are being conducted at the engine manufacturer's test facility and at Huntsville. A recommendation to increase LOX tank ullage pressure for the latter portion of the S-II burn by commanding the LOX regulator full open at S-II ESC + 98.6 seconds is being implemented for AS-504.

The propellant management system met all performance requirements. System operation differed from previous flights since EMR control was open-loop versus closed-loop on AS-501 and AS-502. The EMR step from high to low EMR occurred at 443.45 seconds as commanded by the Instrument Unit (IU). Engine cutoff, as sensed by the Launch Vehicle Digital Computer (LVDC), was at 524.04 seconds, with a burn time only 0.42 second longer than predicted. Cutoff was initiated by the LOX low level cutoff sensors located in the LOX tank sump. Residual propellants remaining in the tanks at S-II ECO signal were 3505 kilograms (7727 lbm) compared to a prediction of 3866 kilograms (8524 lbm).

The performance of the LOX and LH_2 tank pressurization systems were satisfactory. AS-503 was the first flight using the dual sensing gage LH_2 vent valves. Ullage pressure in both tanks was more than adequate to meet engine inlet NPSP requirements throughout mainstage. As on the two previous flights LOX ullage pressure dropped below the regulator band. This was expected as a result of operating at the low EMR used for this flight. The ullage pressure drop occurred earlier, however, than expected due to LOX surface agitation and subsequent ullage gas condensation caused by the 18 hertz oscillation.

6.2 S-II CHILLDOWN AND BUILDUP TRANSIENT PERFORMANCE

The prelaunch servicing operations satisfactorily accomplished the engine conditioning requirements. Thrust chamber temperatures were within predicted limits both at launch and S-II engine start as shown in Figure 6-1. Chamber temperatures increased during S-IC boost at rates from 9.8 to 11.8°K/min (17.7 to 21.2°F/min), which agrees closely with those experienced on previous flights. Engine No. 4 thrust chamber jacket temperature transducer indicated about 11°K (20°F) warmer than the other four engines due to poor thermal contact between the transducer and its mounting on the chamber jacket. This condition also occurred on one engine of AS-501 flight and several static firings and is of no consequence to normal system operation.

Both temperature and pressure conditions of the J-2 engine start tanks were within the required prelaunch and engine start boxes as shown in Figure 6-2. Start tank temperatures at the conclusion of chilldown ranged from 89 to 95°K (-300 to -288°F) and were nearly identical to AS-501 results. Start tank pressures at completion of the pressurizing operation were lower than those for AS-501 as a result of adjusting the ground supply regulator setting from 831 N/cm^2 (1205 psia) to 810 N/cm^2 (1175 psia). This lower pressurization level accomplished the desired effect of increasing start tank temperatures at end of pressurization over those obtained for AS-501. Start tank temperatures at engine start were 4.2°K (7.5°F) warmer than on the AS-501 flight. The ground supply regulator had the lower setting on AS-502, but the planned temperature increase was offset by a lower than predicted start tank chilldown caused by a Ground Support Equipment (GSE) heat exchanger malfunction.

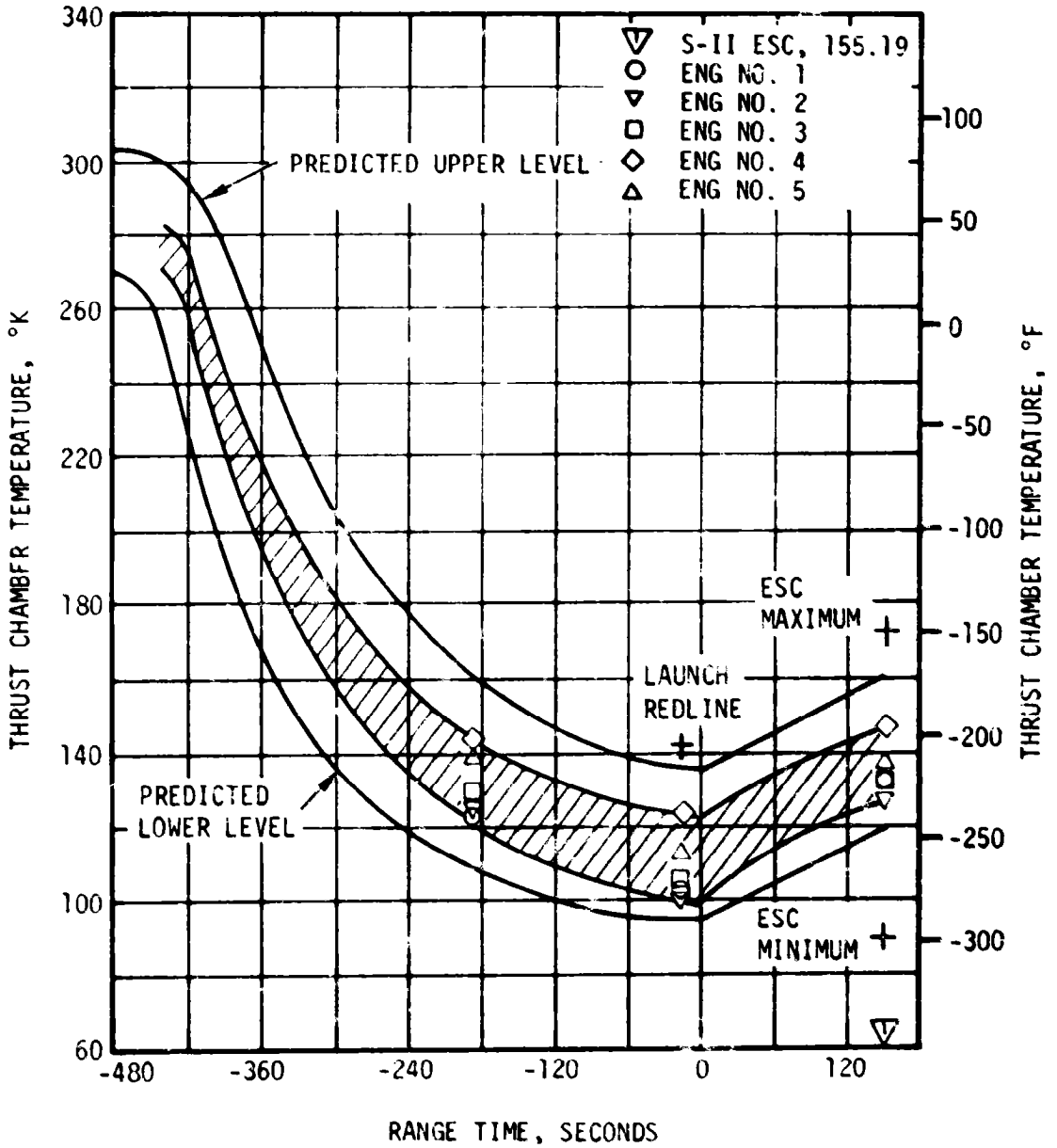

Figure 6-1. S-II Thrust Chamber Jacket Temperature

Except for engine No. 3, the start tank warmup rates during both prelaunch and S-IC boost were in good agreement with those for AS-501. Engine No. 3 start tank pressure rise rate was about 35 percent less than the others, indicating that relief valve operation was occurring on this tank.

All engine helium tank pressures were within the redline limit of 1931 to 2379 N/cm^2 (2800 to 3450 psia) established for prelaunch pressurization.

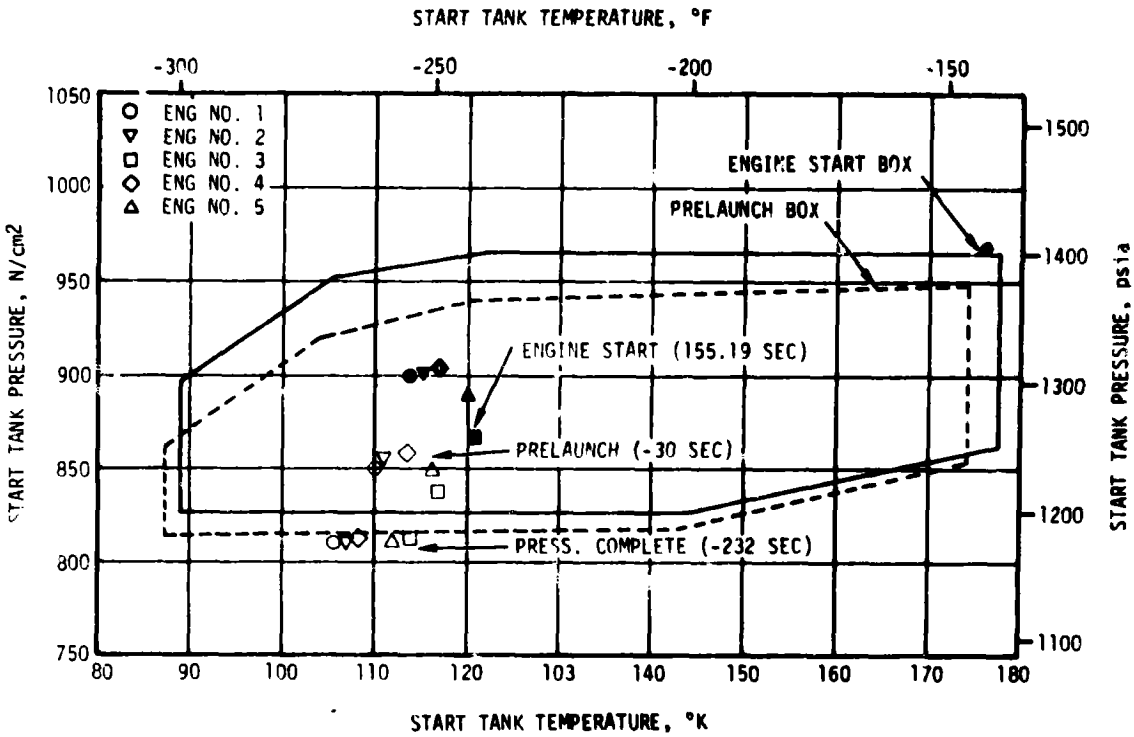

Figure 6-2. S-II Engine Start Tank Performance

Helium tank prelaunch pressure levels were higher than for AS-502 due to a change of the regulator setting in the GSE pneumatic servicing system. This regulator setting was increased approximately 138 N/cm^2 (200 psi) to insure meeting the minimum pressure redline of the helium injection bottle. The helium injection system was reorificed to provide a higher flow rate to the LOX recirculation lines (see paragraph 6.8). The initial high pressurization levels in conjunction with a pressure increase due to warmup during prelaunch and S-IC boost, resulted in helium tank pressures being near the upper limit of 2379 N/cm^2 (3450 psia) at ESC. Engine No. 2 helium tank pressure exceeded this value by 28 N/cm^2 (40 psi). This high pressure did not adversely affect flight operations.

The LOX and LH_2 recirculation systems used to chill the feed ducts, turbopumps, and other engine components performed satisfactorily. Pump inlet temperatures and pressures at engine start were well within the predicted as shown in Figure 6-3.

Performance of the LOX recirculation system was considerably improved over that experienced on AS-502. The helium injection system that supplements natural convective LOX recirculation was modified for AS-503 and subsequent stages to improve recirculation system performance (see paragraph 6.8). LOX recirculation system performance evinced during the AS-503 Countdown Demonstration Test (CDDT) led to a revision of the LOX pump discharge

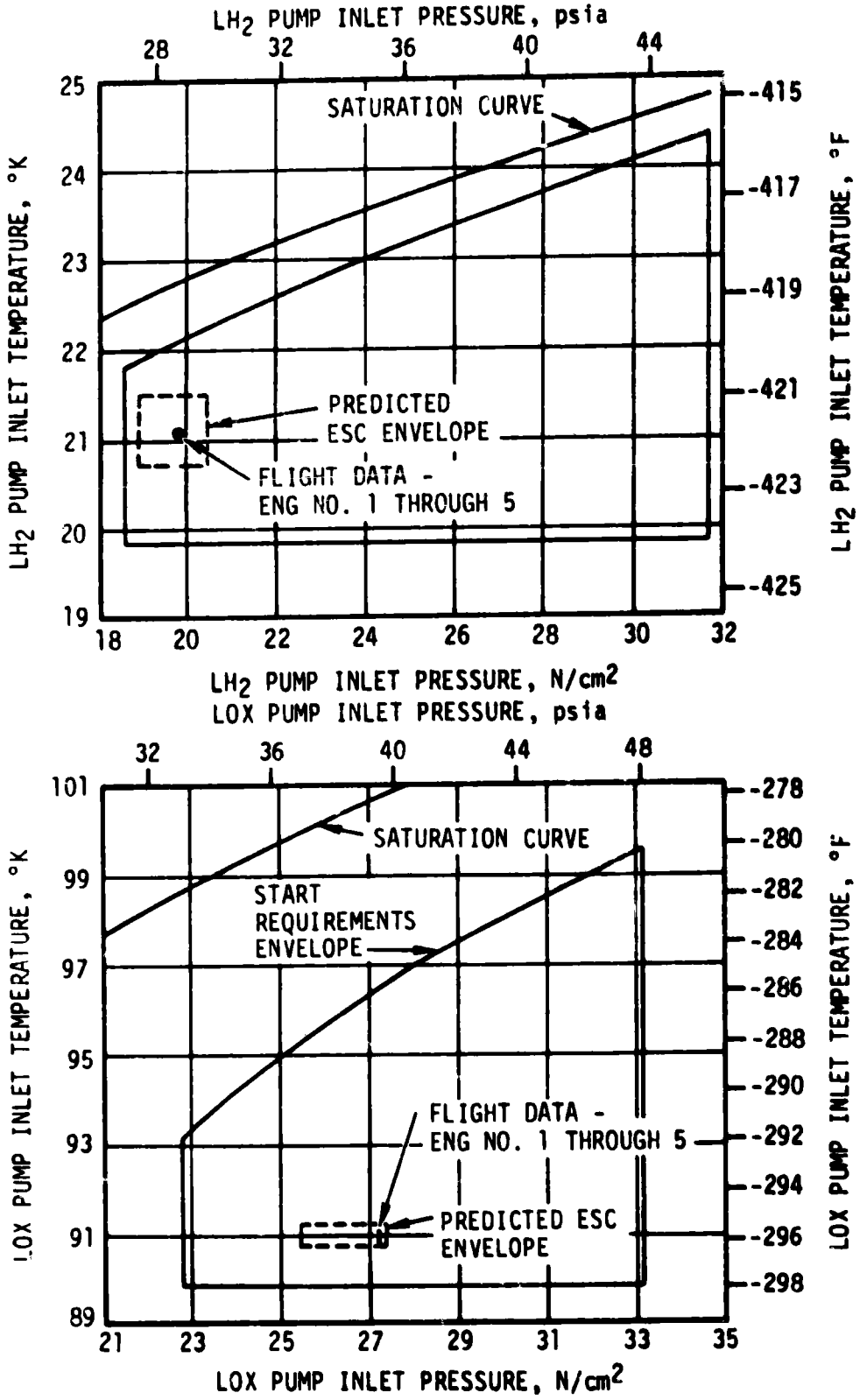

Figure 6-3. S-II Engine Pump Start Requirements

temperature redline limit from 97.6°K (-284.0°F) to 98.7°K (-282.0°F) maximum at -22 seconds. Changes instituted on AS-503 and subsequent vehicles also upgraded the LH_2 recirculation system performance. Improved vacuum line maintenance procedures, lower vacuum levels, and new design evacuation valves reduced heat leaks into the system and resulted in improved LH_2 pump inlet temperatures.

S-II ESC was issued by the LVDC at 155.19 seconds, and the Start Tank Discharge Valve (STDV) solenoid activation signal occurred 1.0 second later. Major engine start event times are summarized in Table 6-1. The thrust buildup profile of each J-2 engine is shown in Figure 6-4. All engines performed within the required thrust buildup envelope. S-II mainstage, average time for engines to reach 90 percent thrust, occurred at 158.47 seconds, 3.28 seconds after ESC. The engine thrust levels were between 864,289 and 908,772 Newtons (194,300 and 204,300 lbf) prior to "HIGH EMR" command at 160.67 seconds.

6.3 S-II MAIN STAGE PERFORMANCE

Two analytical techniques were used to evaluate the S-II stage propulsion system performance. The primary method, propulsion reconstruction analysis, used telemetered engine and stage data to calculate longitudinal thrust, stage mass flowrate and specific impulse. The second method used was trajectory simulation which adjusted the propulsion reconstruction data using a differential correction procedure. This six-degrees-of-freedom trajectory simulation determined adjustments to thrust and mass flow histories to yield a simulated trajectory which closely matched the observed postflight trajectory.

Table 6-1. S-II Engine Start Sequence Events

EVENT	TIME OF EVENT IN RANGE TIME (SECONDS)				
	ENGINE 1	ENGINE 2	ENGINE 3	ENGINE 4	ENGINE 5
Engine Start Command	155.19	155.19	155.19	155.19	155.19
Start Tank Discharge Solenoid	156.19	156.18	156.18	156.19	156.19
Mainstage Control Solenoid	156.63	156.63	156.63	156.65	156.64
Main LOX Valve Open	158.90	158.90	158.81	158.81	158.94
Mainstage OK	157.94	158.02	157.93	157.94	157.94
90 Percent Thrust	158.64	158.50	158.58	158.26	158.35

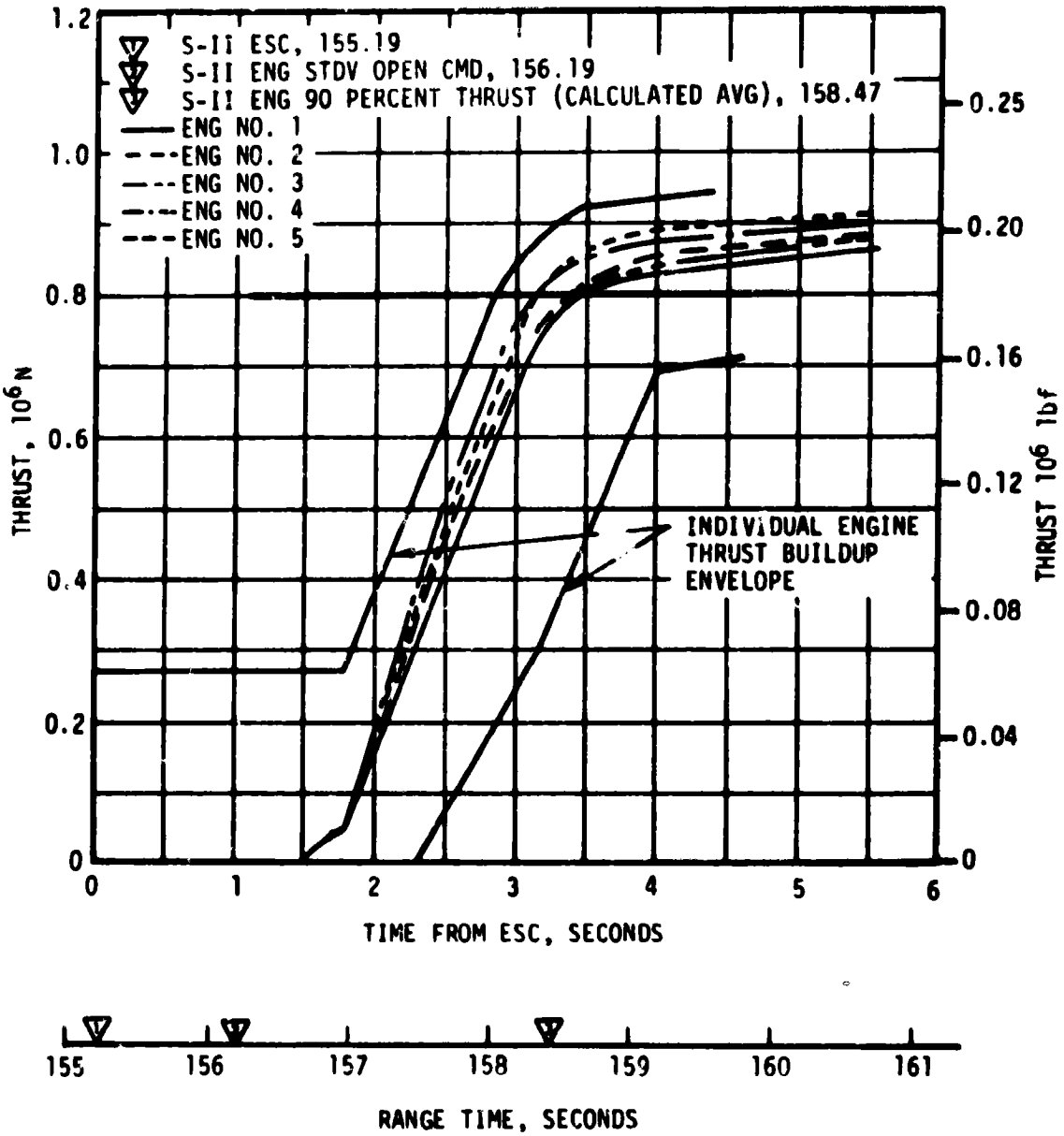

Figure 6-4. S-II Engine Buildup Transients

S-II stage performance during the high EMR portion of the flight was very close to predicted as shown in Figure 6-5. At a time slice of ESC +61 seconds the total vehicle thrust was 5,086,888 Newtons (1,143,578 lbf), which is only 1890 Newtons (425 lbf) or 0.04 percent above the final preflight prediction. Average engine specific impulse was 4155.0 N-s/kg (423.7 lbf-s/lbm), or 0.34 percent below the predicted level.

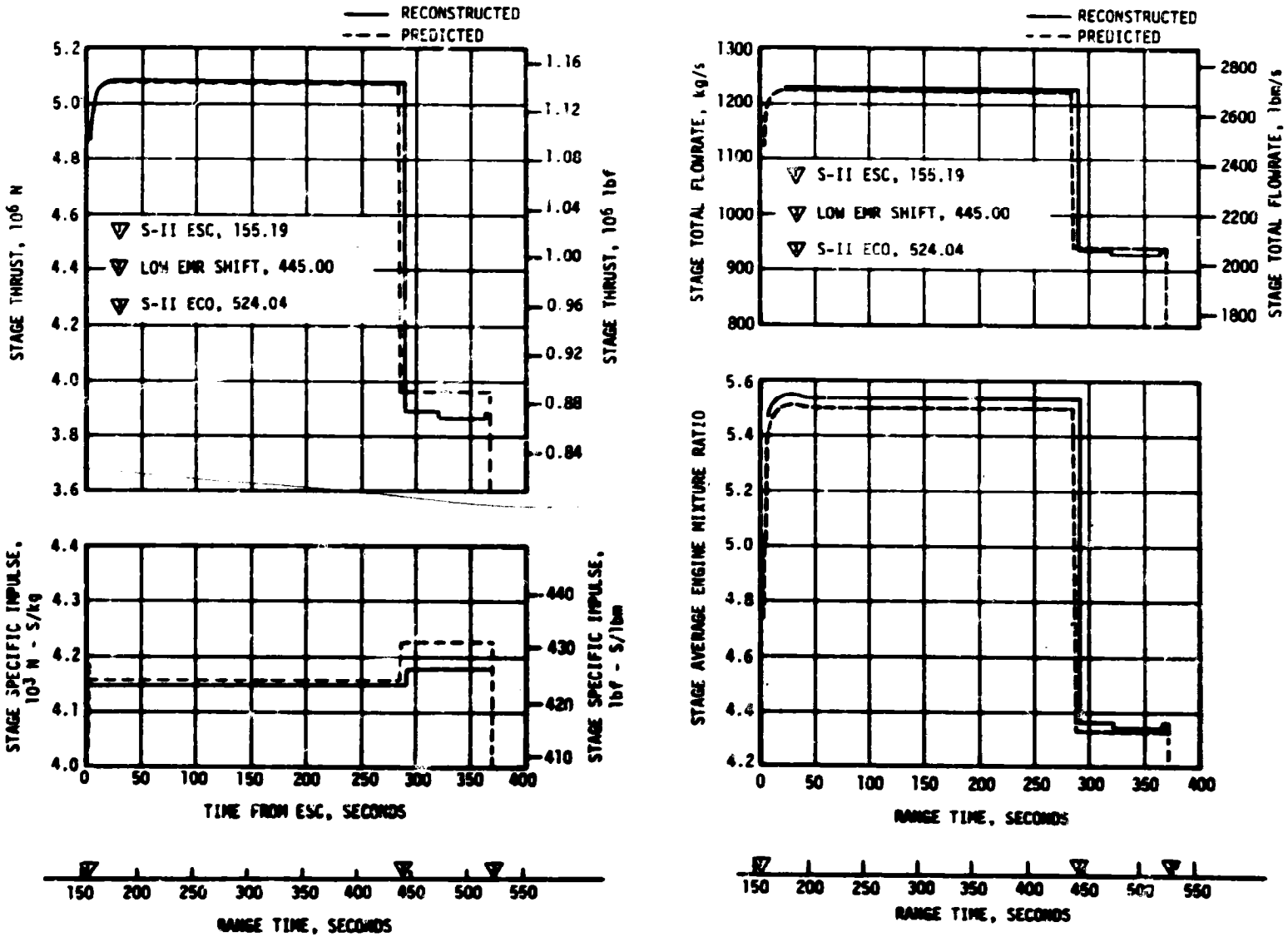

Figure 6-5. S-II Steady State Operation

Propellant flowrate to the engines was 1224.3 kg/s (2699.2 lbm/s) which is 0.38 percent above prediction, and the propellant mixture ratio was 5.56 to 1 or 0.69 percent in excess of prediction.

The high to low EMR step command was initiated by the IU at 443.45 seconds, and the Propellant Utilization (PU) valves started shifting to the open position at 445 seconds. Actual EMR shift, as determined by engine thrust chamber pressures, occurred at 445.60 seconds. This action reduced the total vehicle thrust to 3,877,101 Newtons (871,607 lbf) a change of 1,209,777 Newtons (271,969 lbf). Throughout the low mixture ratio portion of the flight the vehicle thrust was 74,654 Newtons (16,783 lbf) below the final flight prediction. An additional thrust loss of 27,050 Newtons (6081 lbf) is associated with the performance decrease of the center engine during the oscillation period (see Section 6A). The relatively large deviations, shown in Figure 6-5, between actual and predicted performance levels during low mixture ratio operation are considered to be the result of inaccurate predictions. Deviations between predicted and actual performance at low engine mixture ratios has been a problem on previous S-II flights. The S-II stage performance during the AS-503 flight is in good agreement with the S-II-6 vehicle performance during stage acceptance static testing. These are the only current examples of the 5.5 to 4.5 engine propellant mixture ratio excursion.

Individual J-2 engine data is presented in Table 6-2 for the ESC + 61-second time point. Very good correlation between prediction and flight is evidenced by the generally low magnitude of the deviations. Flight data reconstruction procedures were directed toward matching the engine and stage acceptance specific impulse values while maintaining the engine flow and pump speed data as a baseline.

Predicted average performance characteristics of the S-II stage propulsion system are compared in Table 6-3 with data obtained from the propulsion reconstruction and the trajectory simulation analyses. Results of the trajectory simulation analysis indicate that the total average thrust and mass flowrate were 0.63 percent and 0.41 percent above predicted values. Deviations of the simulated trajectory from the postflight observed trajectory were very small. Maximum variation in velocity and acceleration were 1.1 m/s (3.6 ft/s) and 0.17 m/s^2 (0.56 ft/s^2).

Data presented in Table 6-2 is actual flight data and has not been corrected to standard J-2 engine conditions. Data that has been corrected to standard J-2 engine conditions, through use of a computer program, shows that engine No. 1 thrust increased approximately 6672 Newtons (1500 lbf) over the stage acceptance levels and engine No. 3 decreased approximately 4448 Newtons (1000 lbf). These magnitudes were maintained throughout the S-II burn and are considered normal test-to-test variations.

Table 6-2. S-II Engine Performance Deviations (ESC + 61 Seconds)

PARAMETER	ENGINE	PREDICTED	RECONSTRUCTION ANALYSIS	PERCENT DEVIATION FROM PREDICTED	AVERAGE PERCENT DEVIATION FROM PREDICTED
Thrust N (lbf)	1	1,011,494 (227,393)	1,021,276 (229,592)	0.97	0.04
	2	1,010,169 (227,095)	1,010,858 (227,250)	0.07	
	3	1,005,409 (226,025)	1,000,908 (225,013)	-0.45	
	4	1,020,458 (229,408)	1,020,102 (229,328)	-0.03	
	5	1,037,468 (233,232)	1,033,744 (232,395)	-0.36	
Specific Impulse N-s/kg (lbf-s/lbm)	1	4169.8 (425.2)	4161.9 (424.4)	-0.19	-0.34
	2	4181.6 (426.4)	4157.0 (423.9)	-0.59	
	3	4165.9 (424.8)	4155.1 (423.7)	-0.26	
	4	4161.9 (424.4)	4159.0 (424.1)	-0.07	
	5	4166.8 (424.9)	4141.3 (422.3)	-0.51	
Flowrate kg/s (lbm/s)	1	242.6 (534.8)	245.4 (541.0)	1.16	0.38
	2	241.6 (532.6)	243.2 (536.1)	0.66	
	3	241.4 (532.1)	240.9 (531.0)	-0.21	
	4	245.2 (540.5)	245.3 (540.8)	0.06	
	5	249.0 (548.9)	249.6 (550.3)	0.26	
Mixture Ratio LOX/Fuel	1	5.61	5.61	0	0.69
	2	5.51	5.56	0.91	
	3	5.48	5.48	0	
	4	5.52	5.60	1.45	
	5	5.47	5.53	1.10	

Table 6-3. S-II Flight Reconstruction Comparison With Simulation Trajectory Match Results

PARAMETERS	UNITS	PREDICTED			RECONSTRUCTION ANALYSIS			PERCENT DEV FROM PRED		
		HIGH MIXTURE RATIO	LOW MIXTURE RATIO	TOTAL FLIGHT AVERAGE	HIGH MIXTURE RATIO	LOW MIXTURE RATIO	TOTAL FLIGHT AVERAGE	HIGH MIXTURE RATIO	LOW MIXTURE RATIO	TOTAL FLIGHT AVERAGE
Average Longitudinal Stage Thrust	N (lbf)	5,062,530 (1,138,102)	3,918,087 (880,821)	4,808,145 (1,080,914)	5,074,980 (1,140,901)	3,871,114 (870,261)	4,822,388 (1,084,116)	0.24	-0.12	0.29
Average Vehicle Mass Loss Rate	kg/s (lbm/s)	1219.3 (2680.1)	927.6 (2045.1)	1152.8 (2541.4)	1220.3 (2690.4)	918.3 (2024.6)	1157.0 2550.8	0.08	-1.00	0.36
Average Stage Longitudinal Specific Impulse	N-s/kg (lbf-s/lbm)	4152.1 (423.4)	4223.7 (430.7)	4170.8 (425.3)	4159.0 (424.1)	4214.9 (429.8)	4170.8 (425.3)	0.16	-0.21	0.00

PARAMETERS	UNITS	SIMULATION-TRAJECTORY MATCH			PERCENT DEV FROM PRED		
		HIGH MIXTURE RATIO	LOW MIXTURE RATIO	TOTAL FLIGHT AVERAGE	HIGH MIXTURE RATIO	LOW MIXTURE RATIO	TOTAL FLIGHT AVERAGE
Average Longitudinal Stage Thrust	N (lbf)	5,094,321 (1,145,249)	3,889,725 (874,445)	4,838,642 (1,087,770)	0.62	-0.72	0.63
Average Vehicle Mass Loss Rate	kg/s (lbm/s)	1221.4 (2692.7)	920.6 (2029.5)	1157.5 (2551.8)	0.17	-0.75	0.41
Average Stage Longitudinal Specific Impulse	N-s/kg (lbf-s/lbm)	4170.8 (425.3)	4225.7 (430.9)	4182.5 (426.5)	0.45	0.05	0.28

Several additional engine performance shifts of the in-run type were also observed during the S-II flight. Engine No. 1 exhibited approximately 30 Gas Generator (GG) system resistance shifts varying in magnitude from 3.4 to 6.9 N/cm^2 (5 to 10 psia) in main thrust chamber pressure. These were dispersed throughout the S-II operation. Gas generator shifts of this type are common to J-2 engine operation and are not considered to be detrimental to engine or stage performance.

Engine No. 4 evidenced a change in performance level at approximately 200 seconds after ESC of approximately -6672 Newtons (-1500 lbf) thrust and -0.03 mixture ratio unit. This is being investigated as a possible change in the fuel pump primary seal and/or turbine seal leakage rate. An additional factor being examined is the possibility of changes in the fuel pump balance piston flowrate. At this time the exact nature of this performance shift has not been determined.

Engine No. 5 experienced a thrust level decrease of about 27,050 Newtons (6081 lbf) and propellant mixture ratio change of -0.1 units coincident with the onset of the high amplitude 18 hertz oscillations (see Section 6A). Beginning at 450 seconds, engine No. 5 thrust chamber pressure began oscillating at 18 hertz with an apparent amplitude of about 10.3 N/cm^2 (15 psi) peak-to-peak. At 478 seconds, apparent amplitude of these oscillations increased from this value to approximately 48.3 N/cm^2 (70 psi) peak-to-peak. The oscillations then dampened out 4 seconds prior to S-II ECO. Oscillations of this same frequency were also evident in the LOX pump discharge pressure along with other engine No. 5 parameters (Figures 6-6 and 6-7). The LOX pump inlet pressure measurement frequency response (recorded at 12 sps) was inadequate to conclusively verify an 18 hertz component. It appears that the oscillations are induced by the LOX pump and possibly amplified by the center engine support structure. Self-induced LOX pump oscillations may be related to the low EMR and low NPSP existing during this time period, although the NPSP is considerably above the level at which self driven oscillations are normally produced. A configuration difference between S-II-3 and preceeding S-II flight stages was the removal of the radial tank baffles and upper screens from the LOX tank. At this time, it is not known whether the configuration change influenced the occurrence of the 18 hertz oscillations.

The 18 hertz oscillations, as indicated by engine No. 5 data, are considered realistic from a frequency standpoint. However, the amplitudes at 18 hertz indicated by the LOX feed system parameters and the main chamber pressure are questionable since they are affected by the geometry and conditions existing at the transducer taps and/or in the pressure transmission lines. It has been determined that the center engine LOX pump inlet pressure measurement (static level) is affected by disturbance from the pump during oscillations.

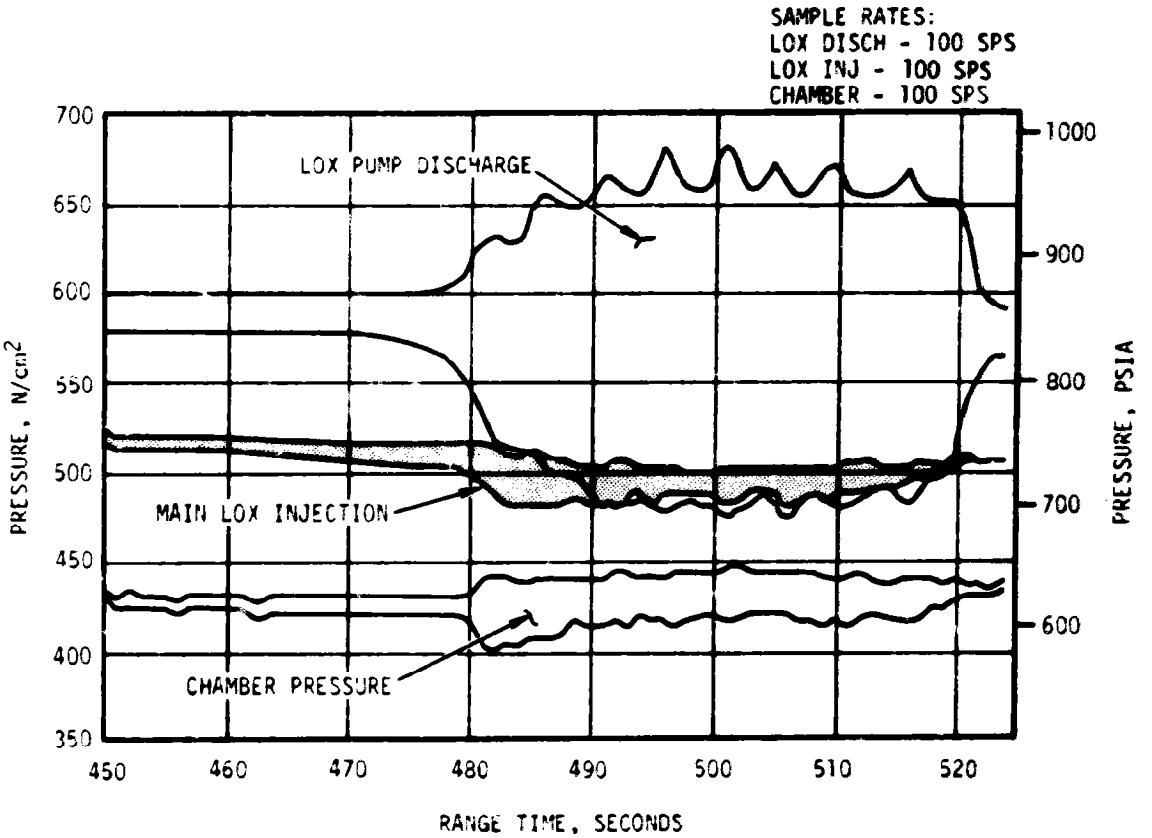

Figure 6-6. Engine No. 5 Pressure Parameter After EMR Step

Reviews of previous flight and static firing data (including Battleship) indicate the presence of 18 hertz oscillations but at low amplitudes. AS-503 apparent amplitudes were considerably greater than those of previous operations.

Two potential corrective actions for AS-504 are as follows:

a. Change the engine mixture ratio.

b. Increase LOX NPSP.

In effect these changes are being accomplished. AS-504 will operate with a closed loop PU system which will provide a higher EMR (4.7) during the latter part of flight as compared to the AS-503 EMR of 4.3. The higher mixture ratio will preclude the LOX ullage pressure and NPSP decay that occurred on AS-503. A further increase in LOX NPSP is being implemented for AS-504 by step pressurization (refer to paragraph 6.6.2). A comparison of LOX NPSP for all S-II flight stages is shown on Figure 6-8. The most significant 18 hertz oscillations are shown to have occurred in the low

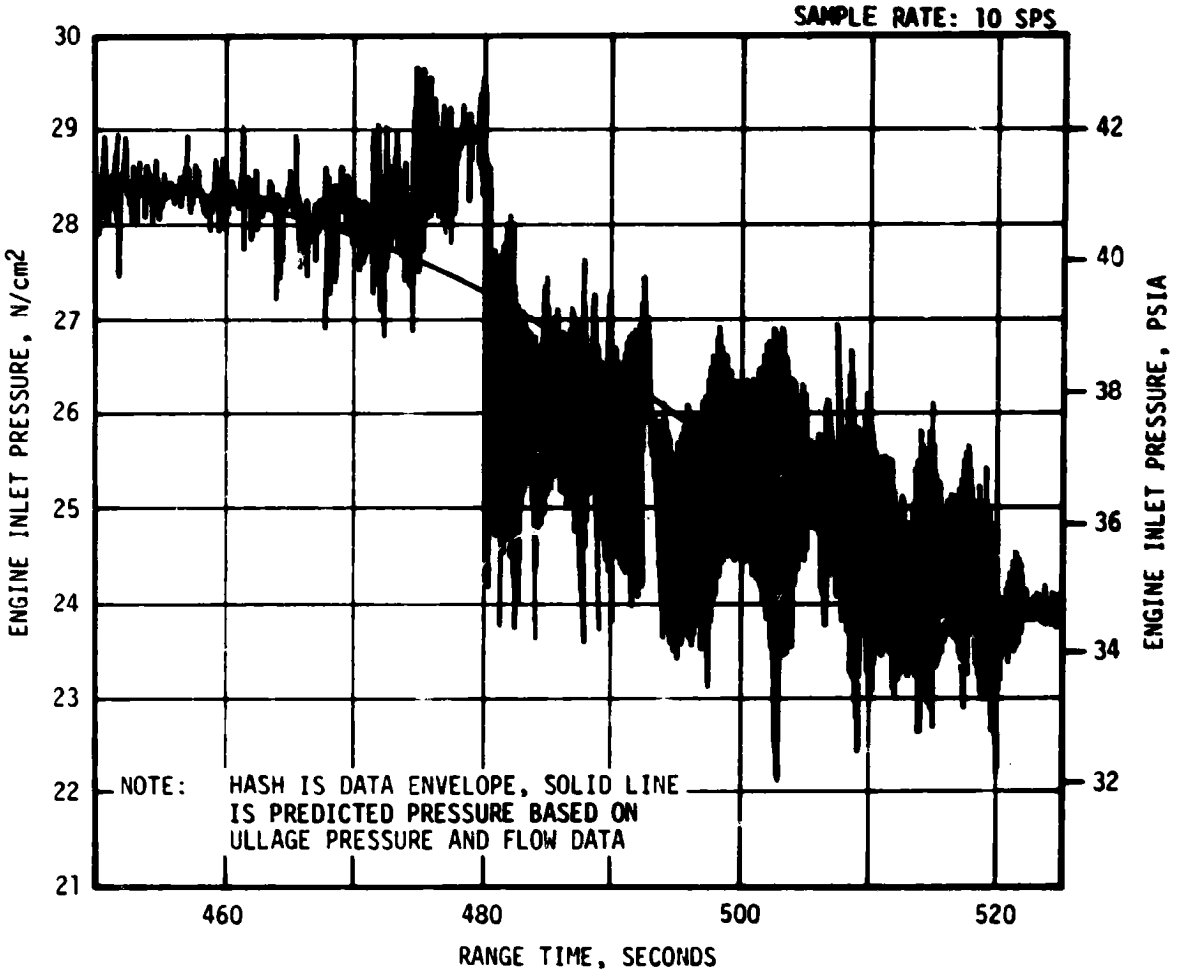

Figure 6-7. Engine No. 5 LOX Inlet Pressure

EMR portion of flight where NPSP is dropping and is in the range of approximately 17.2 to 17.9 N/cm^2 (25 to 26 psi). Operating at higher LOX pump NPSP levels, such as occurs during the first portion of flight, has not resulted in significant amplitudes at 18 hertz frequencies.

To understand better the engine interaction with the variables of NPSP and mixture ratio, Rocketdyne is conducting a single engine test program with J-2 engine J025. The program will determine whether the J-2 engine generates and/or amplifies disturbances in the 18 hertz frequency range at various mixture ratios and LOX pump NPSP levels. Results of the test program will be used to determine critical NPSP and/or engine mixture ratios (if any).

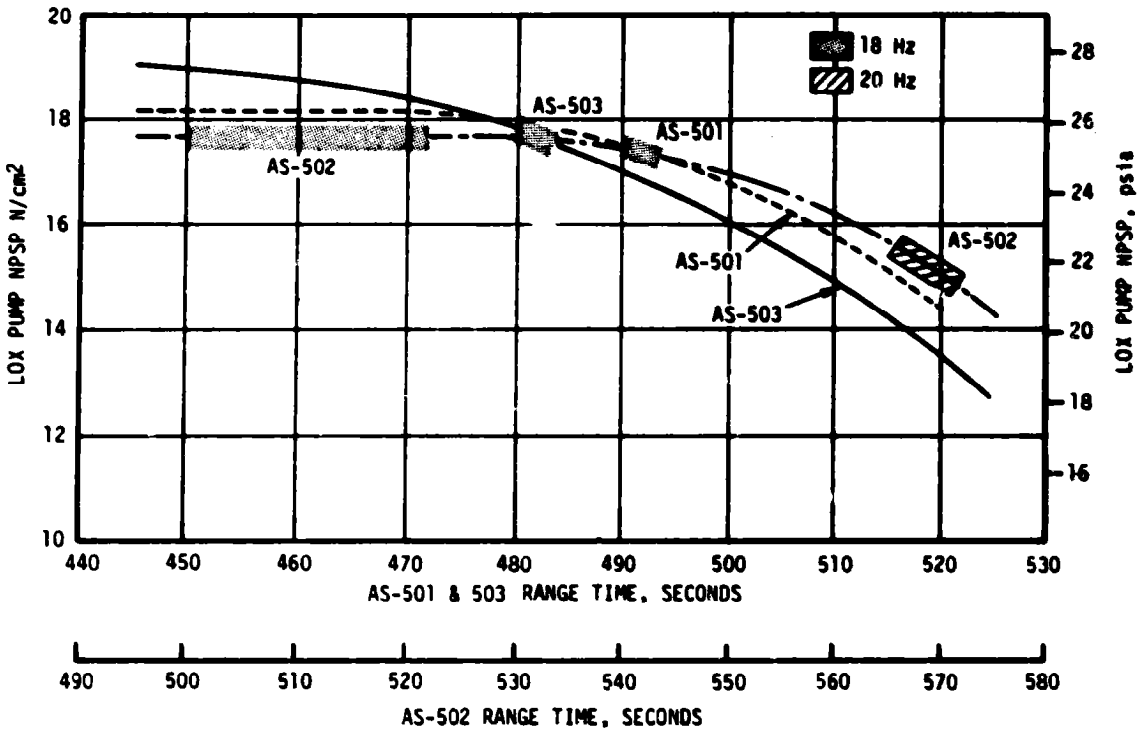

Figure 6-8. LOX NPSP History

During AS-502 flight, failure of an Augmented Spark Igniter (ASI) fuel line resulted in premature shutdown of S-II engine No. 2. Engine No. 3 was lost also when its LOX prevalve was inadvertently closed by the shutdown of engine No. 2. Consequently, redesigned configurations for both the fuel and LOX ASI supply lines were incorporated for AS-503 and subsequent vehicles. The redesigned fuel and LOX ASI line configurations are shown in Section 7, Figure 7-8 and 7-9, respectively. Postflight data analysis indicates that the AS-503 ASI systems performed satisfactorily. The ASI supply line and thrust chamber temperatures were normal, and ASI line vibrations were generally as expected.

6.4 S-II STAGE SHUTDOWN TRANSIENT PERFORMANCE

S-II engine shutdown sequence was initiated by stage LOX low level sensors at 524.02 seconds, and 0.02 second later (524.04 seconds) the LVDC sensed ECO and started Time Base 4 (T_4). At the time of cutoff, all J-2 engines were operating at the extreme low mixture ratio level and individual thrusts ranged from a high of 795,756 Newtons (178,893 lbf) to a low of 752,074 Newtons (169,073 lbf). Thrust decay transients of the four outboard engines were completely nominal. The center engine, however, exhibited an extended period of thrust below the 10 percent level. This resulted in the 5 percent stage thrust level occurring 0.60 second after cutoff signal in contrast to a value of 0.41 second for AS-501 flight. Figure 6-9 presents the individual engine cutoff transients.

The total stage thrust at ECO was 3,849,189 Newtons (865,332 lbf). The stage thrust decay is presented in Figure 6-10. Vehicle cutoff impulse through the 5 percent stage thrust level is estimated to be 760,646 N-s (171,000 lbf-s). For the period from cutoff until S-II/S-IVB separation at 524.90 seconds, a total cutoff impulse of 813,491 N-s (182,880 lbf-s) is indicated which corresponds to an equivalent velocity change of 3.8 m/s (12.5 ft/s). Guidance data indicates the velocity increment for this time period to be 3.44 m/s (11.29 ft/s). Comparisons of flight and predicted values of cutoff impulse and velocity change are shown in Table 6-4.

6.5 S-II STAGE PROPELLANT MANAGEMENT

The propellant management system performed satisfactorily during the propellant loading operation and adequately controlled propellant usage during flight. The S-II stage of AS-503 was the first to employ an open-loop PU system that received fixed commands from the IU for changing EMR rather than feedback signals from the tank mass probes.

The facility Propellant Tanking Control System (PTCS) together with the propellant management system successfully accomplished S-II loading and replenishment. Best estimates of propellant loaded in the S-II tanks, based on flowmeter data, are 359,322 kilograms (792,170 lbm) LOX and 70,160 kilograms (154,676 lbm) LH_2. These propellants were 0.46 percent by mass higher than predicted for LOX and 0.14 percent less than predicted for LH_2.

During the prelaunch auto-sequence, the PTCS did not indicate 100 ± 0.2 percent pressurized LH_2 mass at the expected time, thereby delaying the stage LH_2 fill valve closure command by about 7 seconds. In addition, the LH_2 fill valve closed approximately 5 seconds slower prior to launch than it did during CDDT. Valve closure time was 19.9 seconds compared to a specification requirement of 20 seconds maximum. The closed position was attained at liftoff -34 seconds. This was just 4 seconds prior to the S-II "ready-for-launch" interlock which is required at liftoff -30 seconds. This slower closure time is attributed to relatively colder gas present in the valve actuator due to the launch countdown being approximately two hours longer than the CDDT. Fill valve actuation time is extremely sensitive to the temperature of the gas being vented from the opening side of the actuator through a 2.03×10^{-4} meters (0.008 in.) control orifice. This marginal condition will be relieved for AS-504 and subsequent vehicles by an earlier closing of the fill valves at the start of auto-sequence.

The "HIGH EMR" command was received 5.5 seconds after ESC causing the PU valves to move from the nominal engine start position of 5.0 EMR to the closed position, providing a nominal EMR of 5.5 for the first phase of S-II Programmed Mixture Ratio (PMR). "LOW EMR" was commanded by the IU at 443.45 seconds versus the originally planned time of 438.19 seconds.

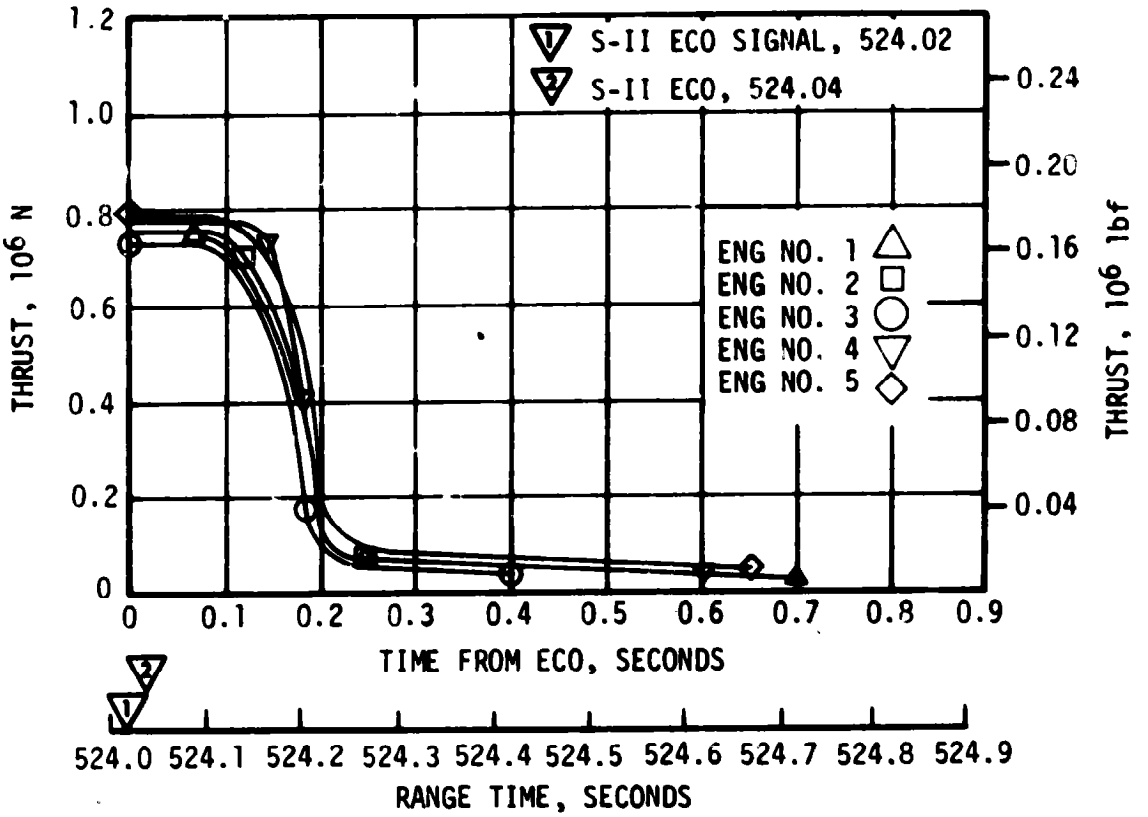

Figure 6-9. S-II Engine Shutdown Transient

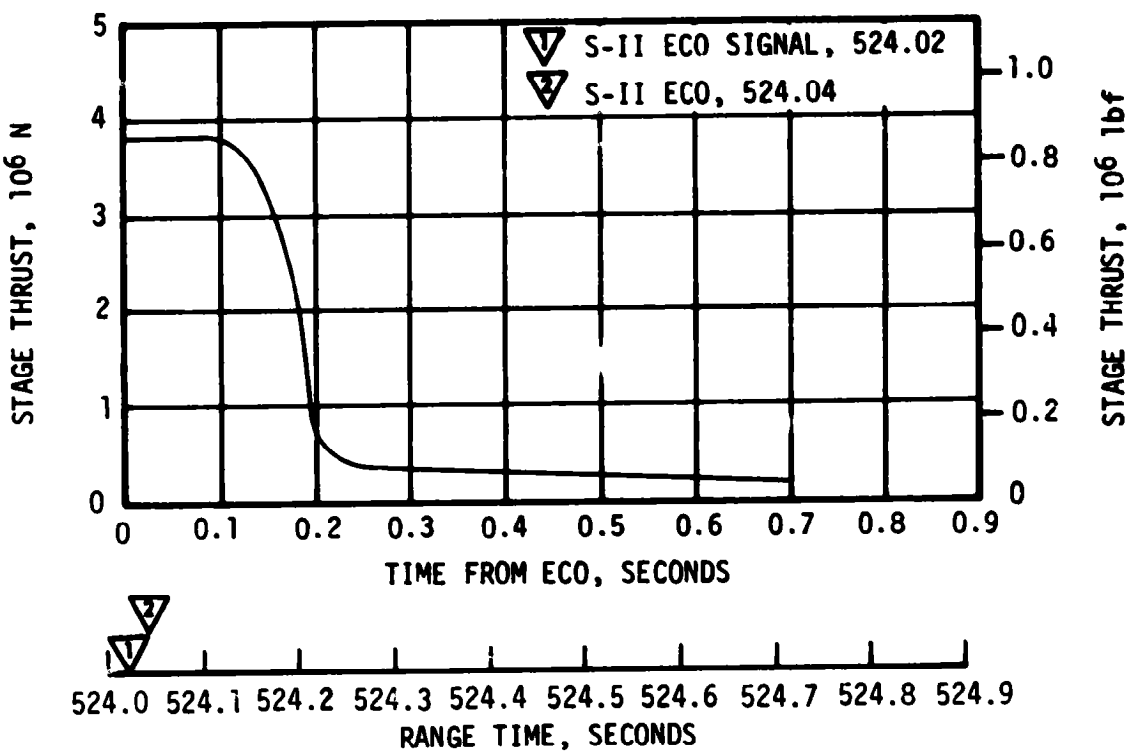

Figure 6-10. S-II Stage Thrust Decay

Table 6-4. S-II Cutoff Impulse

PARAMETER	PREDICTED	FLIGHT		PERCENT DEVIATION FROM PREDICTED	
		ENGINE	GUID. DATA	ENGINE	GUID. DATA
Cutoff N-s Impulse (lbf-s)	822,018 184,797	813,491 182,880	731,621 164,475	-1.1	-11.0
Velocity m/s Increase (ft/s)	3.86 12.66	3.8 12.5	3.44 11.29	-0.9	-10.9

This later than predicted PU valve step was due to changes in IU programming. The PU valves responded 1.55 seconds after IU command, with a slew time of about 1.8 seconds to the low EMR stop (open position) where the valves remained for the rest of S-II boost. Figure 6-11 gives a comparison of actual versus predicted S-II PU valve position for AS-503 flight. The open loop PU error at ECO was approximately +20.4 kilograms (+45 lbm) LH_2 versus a 3 sigma tolerance of approximately ±1134 kilograms (±2500 lbm).

The PU control system responded as predicted during flight and no instabilities were noted. PU valve response to open-loop IU commands was evaluated by comparing valve loop characteristics obtained from flight data with results obtained from tests of an actual PU computer in a breadboard setup using five servoactuators and an analog computer to simulate vehicle conditions. The comparison shows PU valve response times during flight to be within 0.1 second of the simulated times, which is essentially equal to the telemetry resolution capability for PU valve position measurements.

During AS-503 CDDT slew check, the engine No. 5 PU valve failed to move from the null position when the "PU activate" command was given. At the same time the PU package voltage dropped steadily from 115 vac to approximately 95 vac. The valve responded sluggishly to the second slew command but operated normally during all subsequent CDDT slew checks. The PU computer and the engine No. 5 PU valve were replaced before flight.

At 3 hours 30 minutes before AS-503 launch, the engine No. 5 PU valve replacement also responded sluggishly to the first slew check. However, upon subsequent slew checks and during flight, the valve responded normally. Unlike the CDDT failure, the PU package voltage remained constant throughout launch preparations and flight.

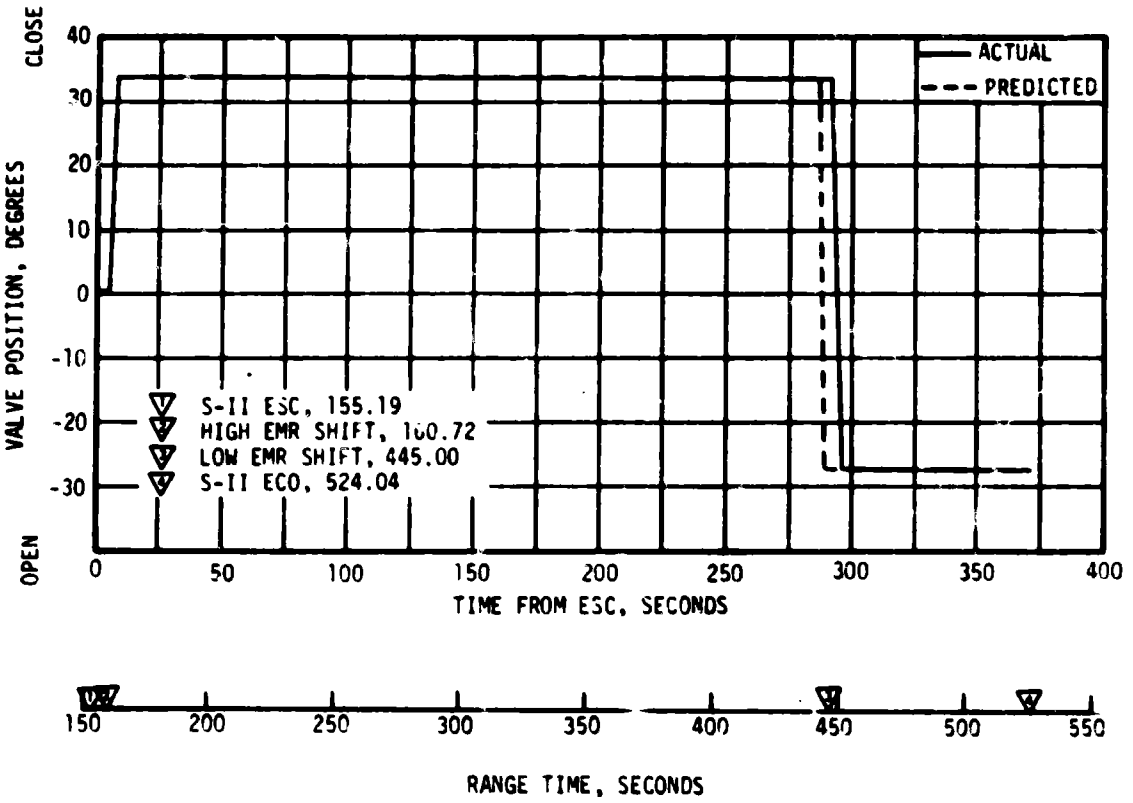

Figure 6-11. S-II PU Valve Position

The PU valve removed after CDDT was disassembled by Rocketdyne and found to have insufficient axial overtravel in the actuator motor shaft plus misalignment of the motor end cap. Under cryogenic conditions, differential contraction caused excessive loading of motor bearings causing mechanical binding. Tests are now underway on the S-II Battleship Stage to develop field procedures that would verify correct PU valve operation on all existing engines. Actuator inspection procedures will be revised and existing stock and new production valves will be acceptance-tested to meet more stringent environmental requirements.

Engine shutdown sequence was initiated by the LOX low level sensors at 524.02 seconds. Based on point level sensor data, propellant residuals (mass in tanks and sumps) at ECO signal were 1544 kilograms (3405 lbm) LOX and 1960 kilograms (4322 lbm) LH_2 versus the predicted of 1905 kilograms (4200 lbm) LOX and 1961 kilograms (4324 lbm) LH_2.

Table 6-5 presents a comparison of propellant masses as measured by the PU probes, flowmeters and point level sensors. The best estimate of S-II stage propellant mass is based on integration of flowmeter data, utilizing propellant residuals determined from the point level sensor data.

Table 6-5. S-II Propellant Mass History

EVENT RANGE TIME	UNITS	PREDICTED		PU SYSTEM (FINE MASS)		ENGINE FLOW INTEGRAL		POINT SENSOR ANALYSIS		PROPELLANT MANAGEMENT BEST ESTIMATE	
		LOX	LH_2	LOX	LH_2	LOX	LH_2	LOX	LH_2	LOX	LH_2
S-II ESC 155.19	kgs (lbm)	358,832 (791,089)	70,482 (155,387)	360,286 (794,295)	71,236 (157,048)	359,322 (792,170)	70,160 (154,676)	360,180 (794,061)	70,508 (155,443)	359,322 (792,170)	70,160 (154.676)
Hi EMR Select 160.67	kgs (lbm)	355,311 (783,326)	69,527 (153,281)	356,959 (786,959)	70,662 (155,783)	356,980 (787,006)	69,487 (153,193)	357,693 (788,577)	69,858 (154,010)	356,980 (787,006)	69,487 (153,193)
PU Shift (off high stop) 445.00	kgs (lbm)	67,398 (148,588)	17,018 (37,518)	62,867 (138,598)	16,124 (35,548)	64,386 (141,947)	16,125 (35,549)	61,504 (135,594)	15,990 (35,251)	64,386 (141,947)	16,125 (35,549)
S-II Engine Cutoff Signal 524.02	kgs (lbm)	1905 (4200)	1961 (4324)	1228 (2707)	2050 (4519)	1544 (3405)	1960 (4322)	1544 (3405)	1960 (4322)	1544 (3405)	1960 (4322)
Residuals After Thrust Decay*	kgs (lbm)	1762 (3885)	1898 (4184)	1104 (2434)	1984 (4379)	1421 (3132)	1895 (4178)	1421 (3132)	1896 (4178)	1421 (3132)	1895 (4178)

NOTE: Propellant mass in tanks. *Residuals in tank and sump.

On the basis of a statistical analysis using data from PU capacitance probes, flowmeters, point level sensors, and a six-degree-of-freedom trajectory simulation, the total launch vehicle masses at S-II ignition and cutoff were estimated to be 645,610 kilograms (1,423,327 lbm) and 212,860 kilograms (469,275 lbm), respectively. These values can be compared with a mass at ignition of 645,610 kilograms (1,423,327 lbm) and a cutoff mass of 212,799 kilograms (469,141 lbm) for a trajectory simulation best fitting the observed postflight trajectory.

6.6 S-II PRESSURIZATION SYSTEMS

The function of the S-II pressurization systems is to provide the necessary positive pressure to the J-2 engines propellant pumps and to increase the structural integrity of the tanks. Prior to launch, the propellant tanks are prepressurized by Gaseous Helium (GHe) supplied from the GSE. During powered flight of the S-II stage, the LOX tank is pressurized by GOX routed from the LOX heat exchangers. The LH_2 tank is pressurized during flight by Gaseous Hydrogen (GH_2) tapped from the thrust chamber hydrogen injector manifold.

6.6.1 S-II Fuel Pressurization System

Prepressurization of the LH_2 tank was initiated upon closure of the vent valves at -97 seconds and an ullage pressure of 24.0 N/cm^2 (34.8 psia) was obtained in approximately 35 seconds. Figure 6-12 presents actual and predicted tank ullage pressures from the beginning of prepressurization through S-II ECO.

AS-503 was the first flight using dual sensing gage LH_2 vent valves. During S-IC boost the LH_2 tank vent valves were kept in the low differential pressure vent mode of 19.0 to 20.3 N/cm^2 (27.5 to 29.5 psid) as referenced to the vent valve sense line. The first vent cycle occurred at 58.04 seconds when the tank ullage pressure had decayed to 22.5 N/cm^2 (32.6 psia).

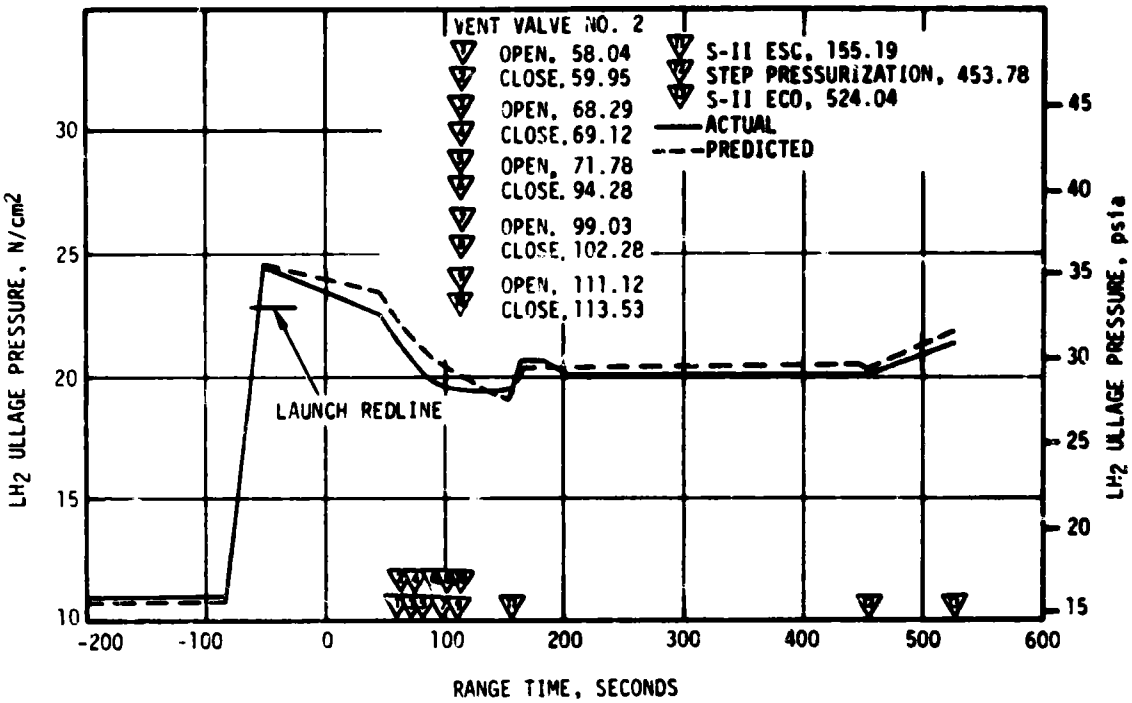

Figure 6-12. S-II Fuel Tank Ullage Pressure

There were five vent cycle events with the No. 2 vent valve during S-IC boost phase; the No. 1 vent valve did not open. When vent valve No. 2 final reseat occurred at 113.53 seconds, the ullage pressure was 19.5 N/cm^2 (28.3 psia) and remained essentially constant until S-II engine start.

At engine start the LH_2 vent valves were switched to high pressure vent mode which limits the maximum ullage pressure to 22.8 N/cm^2 (33.0 psid), referenced to the vent valve sense line. From ESC until step pressurization, the ullage pressure was maintained within the range of 19.6 to 20.7 N/cm^2 (28.5 to 30.0 psia) by the LH_2 tank pressure regulator. This regulator was stepped open as programmed at 453.78 seconds and ullage pressure increased to 21.6 N/cm^2 (31.2 psia) at S-II ECO.

Figure 6-13 shows LH_2 pump inlet temperature, total inlet pressure and NPSP. The NPSP supplied to the engines was close to predicted throughout the S-II burn phase.

6.6.2 S-II LOX Pressurization System

Following LOX tank chilldown the vent valves were closed at -187 seconds and the LOX tank ullage prepressurized to 26.5 N/cm^2 (38.4 psia) in

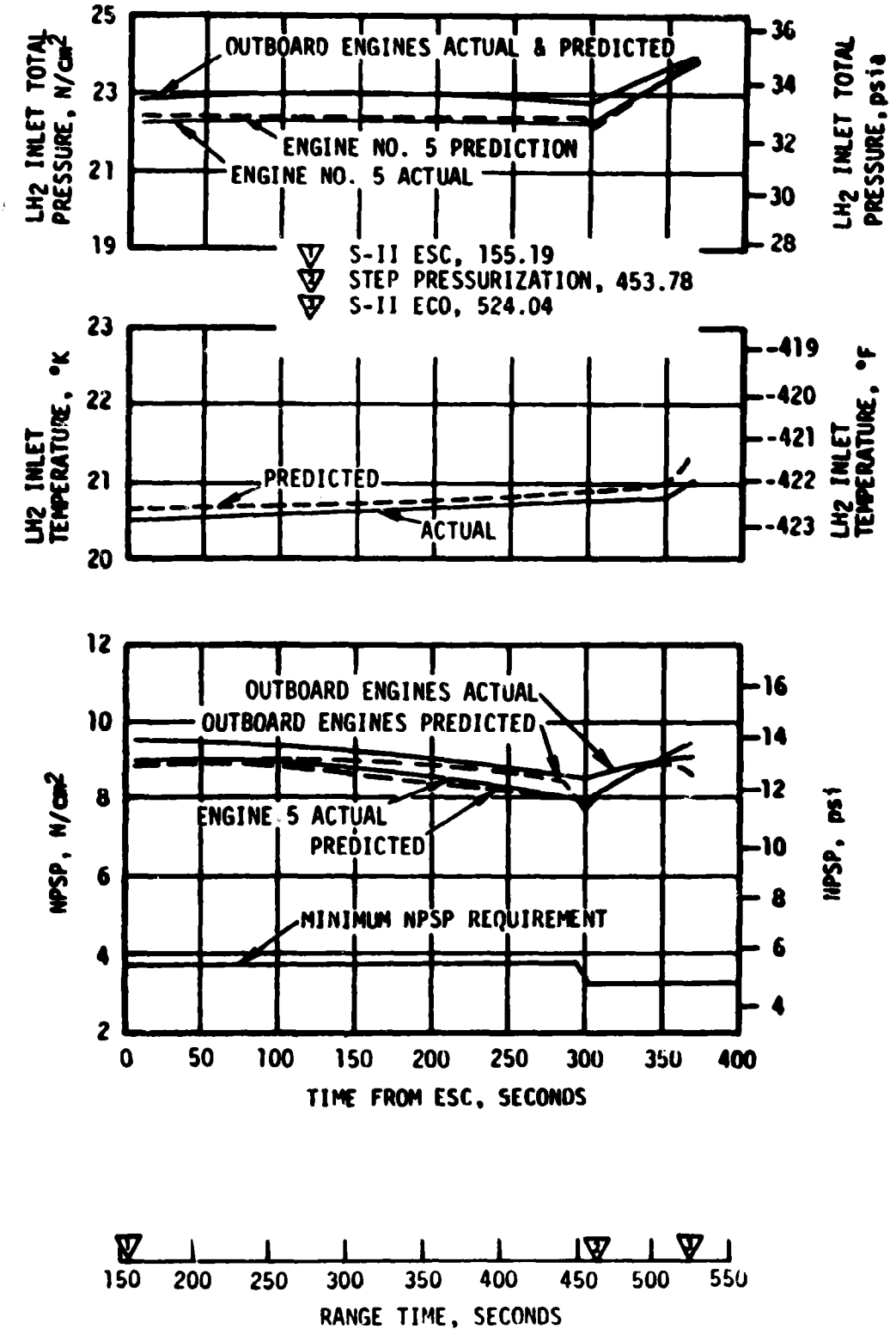

Figure 6-13. S-II Fuel Pump Inlet Conditions

approximately 70 seconds. One prepressurization makeup cycle was required after which the ullage pressure stabilized at 26.5 N/cm^2 (38.4 psia) and remained essentially constant until engine start. Figure 6-14 presents the LOX tank ullage pressure as compared to predicted from prepressurization until S-II ECO.

With the exception of the characteristic pressure slump associated with S-II engine start, the LOX tank ullage pressure remained within the regulator range of 24.8 to 25.9 N/cm^2 (36.0 to 37.5 psia) during S-II burn until low EMR shift. The ullage pressurant gas supplied by the engine heat exchangers is marginal at low EMR, and although the LOX tank pressure regulator opened to its maximum position at about 480 seconds, ullage pressure gradually decreased to 22.5 N/cm^2 (32.6 psia) at ECO. Although tank ullage pressure dropped further below the regulator range than on the two previous flights, it was adequate to meet the engine inlet NPSP requirements. The LOX pump inlet temperature, total inlet pressure, and NPSP are shown in Figure 6-15. The NPSP supplied exceeded that required throughout S-II powered flight.

The 18 hertz oscillations had two separate but related effects on the pressurization system:

a. The engine inlet LOX temperature was 1.3°K (2.4°F) higher than predicted at cutoff.

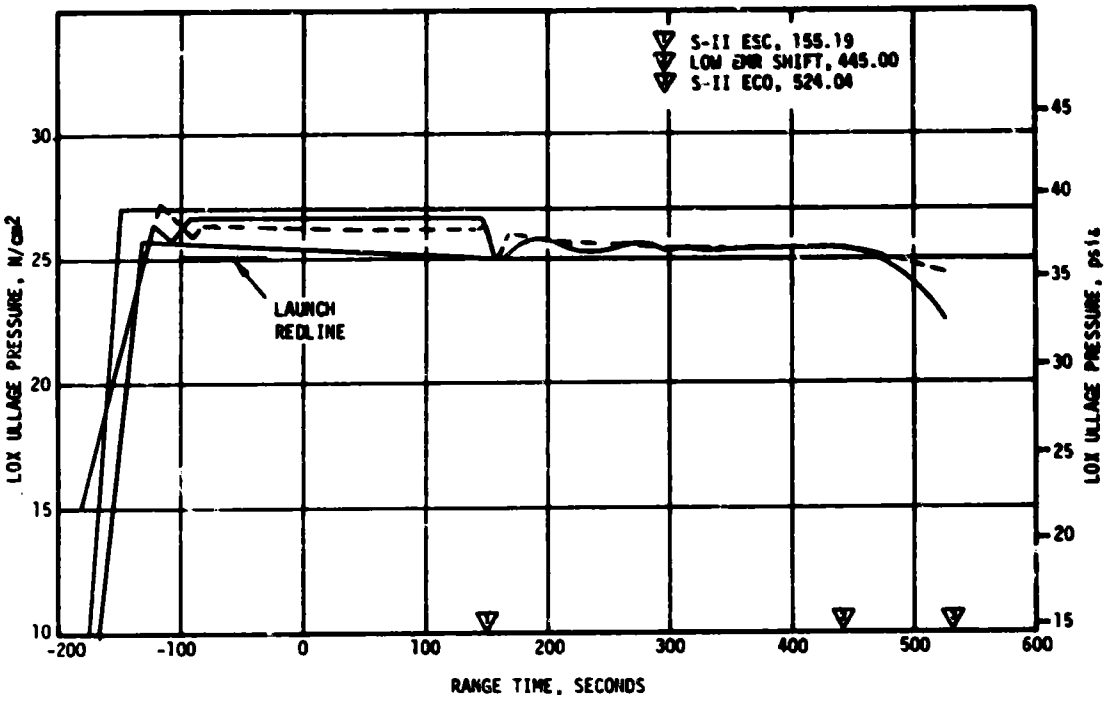

Figure 6-14. S-II LOX Tank Ullage Pressure

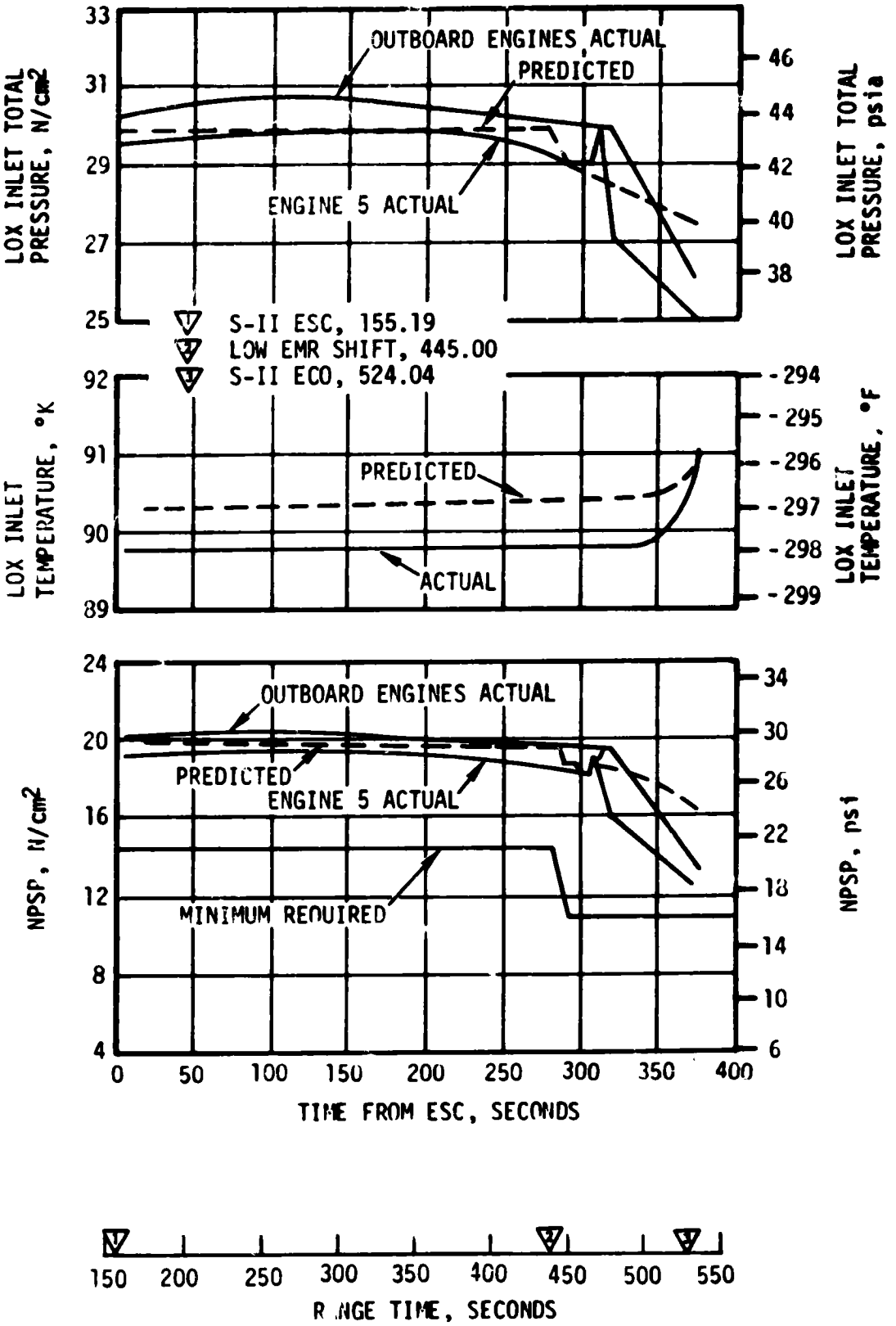

Figure 6-15. S-II LOX Pump Inlet Conditions

b. The LOX tank ullage pressure decayed 1.8 N/cm^2 (2.7 psi) more than predicted (based on S-II-6 static firing results).

The warmer LOX inlet temperature was attributed to surface agitation. Agitation tends to break up the stable "hot" LOX layer at the surface and consequently brings cold LOX in contact with the GOX pressurant, thereby causing condensation of the GOX. The extra heat added to the LOX by condensation plus the heat normally contained in the LOX residual was distributed into the usable LOX by the oscillation, thereby raising the engine inlet LOX temperature near the end of the S-II portion of flight.

This condensation of GOX pressurant caused a more rapid ullage pressure decay then predicted. When the ullage pressure decayed to approximately 24.2 N/cm^2 (36 psia), the GOX regulator went full open in an effort to maintain ullage pressure. This high flow demand at low EMR causes the output temperature of the GOX heat exchanger on the J-2 engine to drop to saturation temperature. This operating point of the heat exchanger does not provide adequate volumetric flow to maintain ullage pressure; therefore the ullage pressure decayed even more rapidly. The main effect of the oscillation was to cause the full-open condition of the regulator earlier in the flight, thereby resulting in the lower end-boost ullage pressure.

Even though the ullage pressure was less than expected and the LOX inlet temperature was warmer than expected, engine NPSP requirements were satisfied. For AS-504 and subsequent stages it has been proposed to institute step pressurization for the LOX tank at T_3 + 100 seconds (S-II ESC + 98.6 seconds). This will permit the LOX ullage pressure to be raised to the vent valve range before that pressure decay associated with low EMR operation takes place. The net effect will be an increase in LOX NPSP for the latter portion of S-II burn. This modification was successfully tested during S-II-7 acceptance test and will be incorporated for AS-504.

There were some pronounced steps in the position of the LOX tank pressure regulator during the S-II burr phase. It has been verified that similar regulator step changes occurred during S-II-3 and S-II-4 static firings. No detrimental effects on pressurization system performance have resulted from this type of regulator operation. It is concluded that regulator performance was acceptable and satisfactory during AS-503 flight.

6.7 S-II PNEUMATIC CONTROL PRESSURE SYSTEM

Performance of the S-II pneumatic control pressure system was satisfactory. Figure 6-16 shows main receiver pressure and regulator outlet pressure of the system from before liftoff until S-II ECO. The main receiver pressure was well above the predicted minimum performance limit. The actual data show receiver pressure to have a lower rate of decay than predicted, indicating that system leakage was less than expected. The regulator outlet pressure was within a very narrow band of 486 to 493 N/cm^2 (705 to 715 psia) except during actuation of the propellant recirculation valves and engine prevalves.

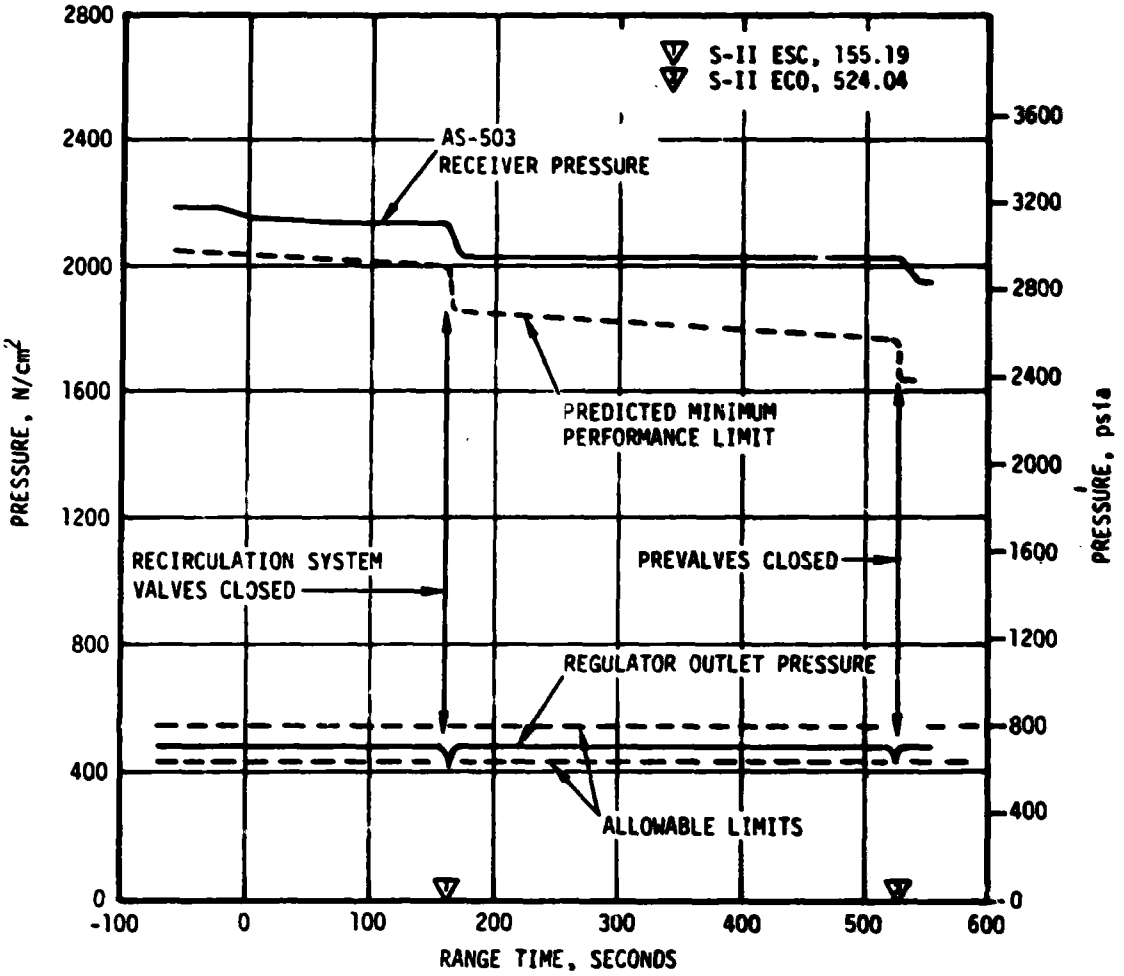

Figure 6-16. S-II Pneumatic Control Pressure

During launch, the Marshall Space Flight Center Launch Information Exchange Facility (MSFC LIEF) propulsion console lights indicated that engine No. 4 LH_2 recirculation pump discharge valve stayed open throughout S-II burn. It was determined that this was not an instrumentation problem. Evaluation of valve discrete data shows that the open position switch did not drop out but the closed position switch did pick up, indicating the valve had closed. The open and closed position switches are activated by the same linkage for each valve, and it is concluded that the engine No. 4 valve actually closed. For the above reasons, and because these position switches have a past history of failure, it has been concluded that this erroneous indication is the result of a malfunction of the open position switch. Improved switches have been installed on S-II-4 and are scheduled for subsequent stages.

6.8 S-II HELIUM INJECTION SYSTEM

Operating performance of the helium injection system was satisfactory and in good agreement with predictions. Helium injected into the LOX recirculation lines supplemented natural thermopumping and successfully maintained the temperature of the LOX feed system within the required limits. The supply bottle was pressurized to 2206 N/cm^2 (3200 psia) prior to liftoff and at ESC the pressure was 655 N/cm^2 (950 psia). From this usage, the average helium flowrate was determined to be 1.93 SCMM (68 SCFM).

During AS-502 prelaunch operations, difficulties were experienced in maintaining engines No. 3 and 4 LOX pump discharge temperatures below the launch redlines. To increase recirculation system performance, the following procedural and hardware changes to the helium injection system were incorporated for AS-503 and subsequent vehicles.

a. Helium injection system total flow was increased from 1.13 to 1.70 SCMM (40 to 60 SCFM) to 1.42 to 1.98 SCMM (50 to 70 SCFM) by increasing the primary orifice size.

b. Screens were added upstream of each injection orifice.

c. Checkout procedures were revised in order to assure even helium flow distribution to all engines.

d. Solenoid valves outlet pressure instrumentation and solenoid valves outlet pressure redline values were deleted.

e. Primary orifice outlet pressure instrumentation was added and established as a redline measurement from liftoff -30 minutes to liftoff -15 minutes. Its redline value is 138 N/cm^2 (200 psia) to 207 N/cm^2 (300 psia).

f. The supply bottle pressure redline value was changed from 1999 to 2389 N/cm^2 (2900 to 3465 psia) to 1931 to 2389 N/cm^2 (2800 to 3465 psia).

SECTION 6A

STRUCTURAL RESPONSE TO S-II ENGINE OSCILLATIONS

6A.1 SUMMARY

The pressure gauges in the S-II stage propulsion system and the accelerometers at certain structural locations showed oscillations during the latter portion of S-II powered flight. Oscillations of about 18 hertz were evident in engine No. 5 (center engine) parameters beginning at approximately 450 seconds. Amplitude of the center engine oscillations began increasing at about 478 seconds, as illustrated by the engine chamber pressure data in Figure 6A-1. An 18 hertz response in the S-II crossbeam region peaked at 482 seconds which showed a like trend of amplitude and frequency to that of the center engine chamber pressure. Accelerations were at much smaller amplitudes in the outboard engines at 18 hertz and chamber pressures were in the noise level. Accelerations were noted in the spacecraft flight data of approximately 9 hertz peaking at 493 seconds and another of approximately 11 hertz peaking at 510 seconds. Chamber pressures were well within the noise level for these two frequency trends.

6A.2 S-II STAGE STRUCTURAL RESPONSE

Acceleration amplitudes of the S-II stage in the 18 hertz region cannot be accurately determined from flight data because of the rolloff characteristics of the instrumentation. The accelerometers were only accurate in amplitude at frequencies from 0 to 6.5 hertz and the response characteristics rolled off sharply above this frequency. In Figures 6A-1 and 6A-2, the accelerations and chamber pressures shown are results of a Power Spectral Density (PSD) analysis of 5-second slice times in the flight time of interest. Amplitudes of the accelerations are noted as uncorrected amplitudes because of the rolloff problem. However, the frequency and amplitude trend shows the high oscillations in engine chamber pressure and crossbeam accelerations and their correlations. It appears the engine chamber pressure or forcing function is close to the crossbeam natural frequency but not necessarily following the crossbeam frequency. This is evident in both the measured flight data and the calculated data. Both Dynamic Test Vehicle (DTV) data and analytical frequency calculations show that the crossbeam frequency was almost constant with time. The chamber pressure oscillations frequency seemed

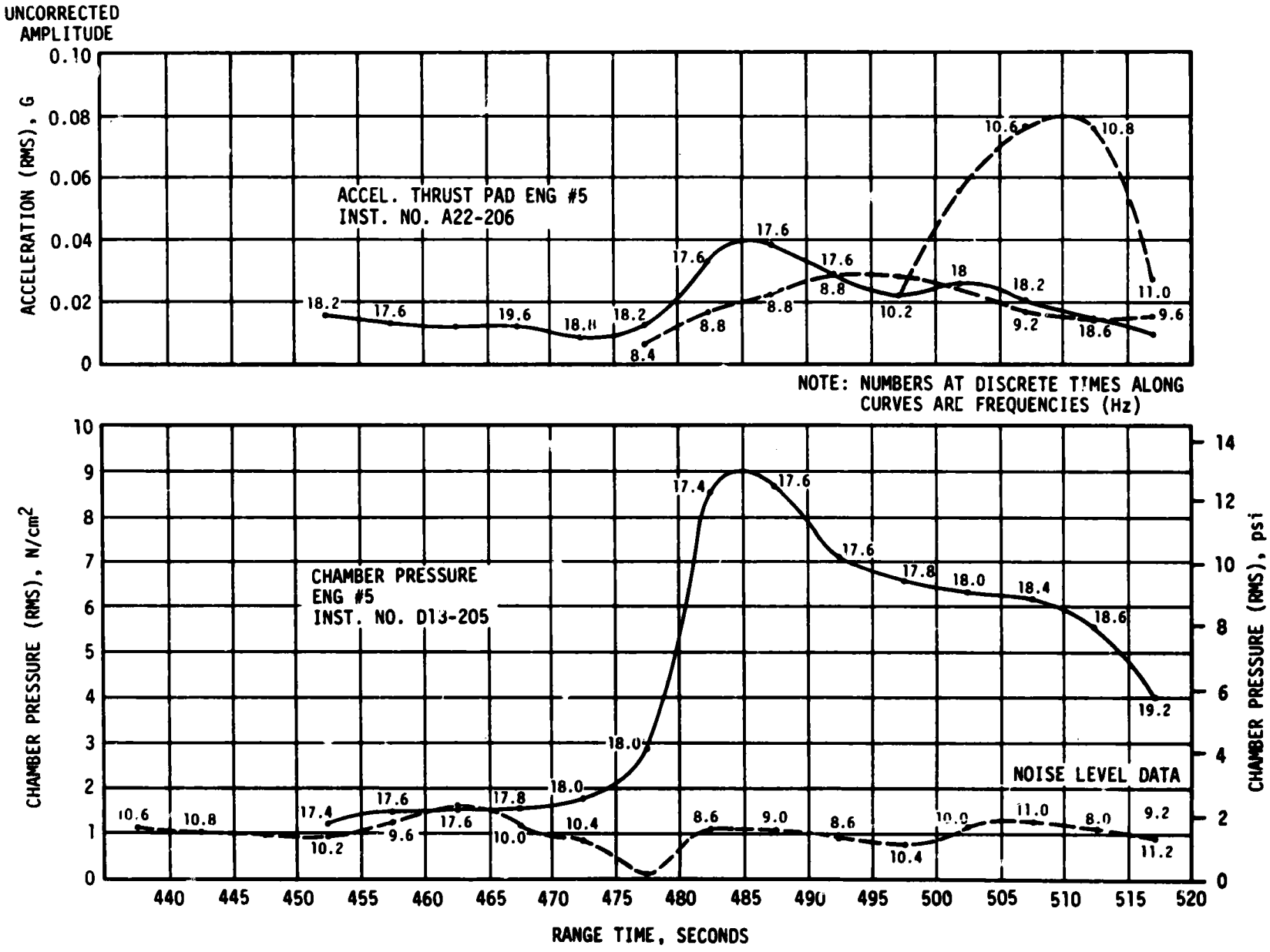

Figure 6A-1. S-II Stage Engine No. 5 Longitudinal Oscillation Time Histories

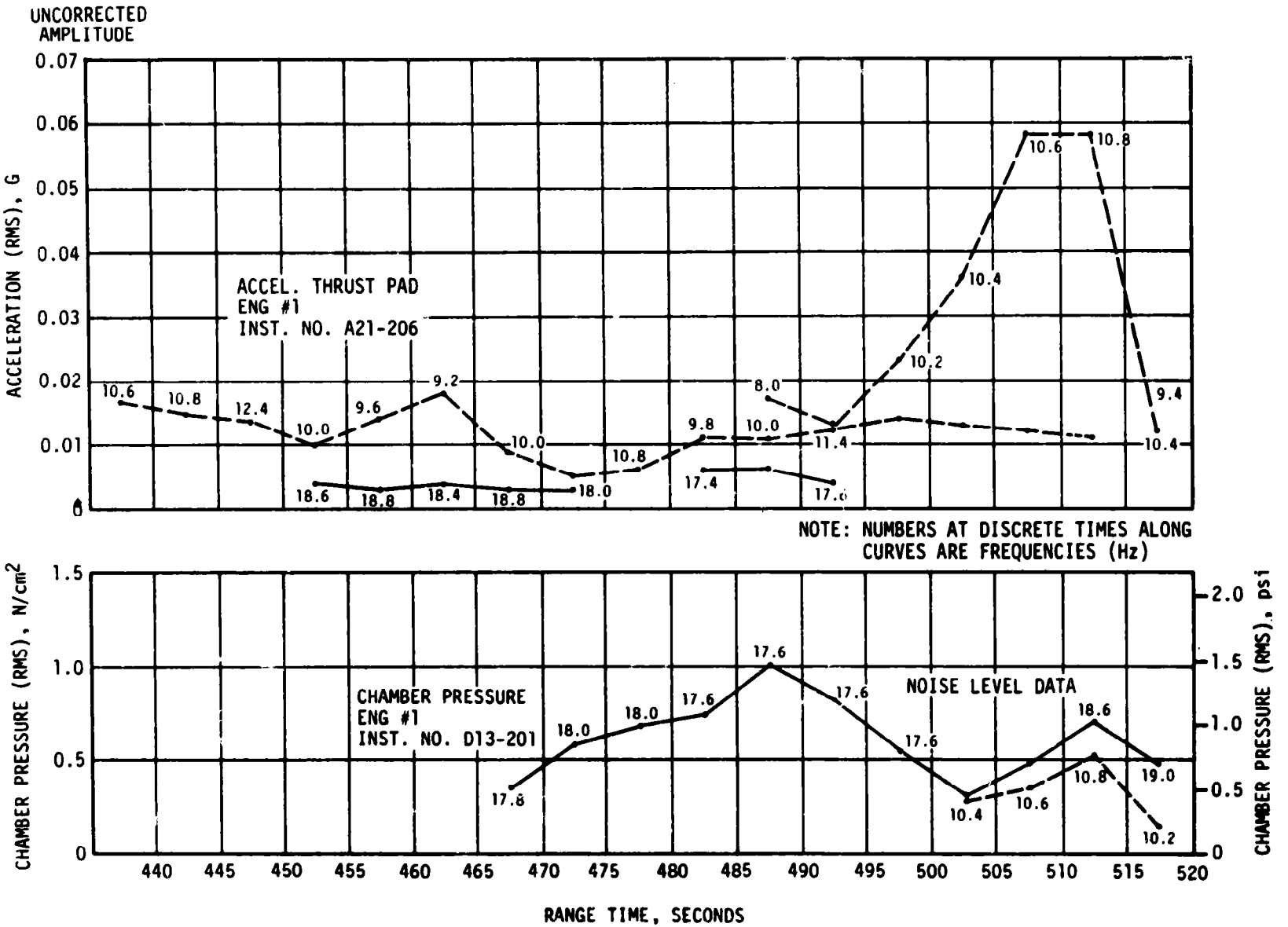

Figure 6A-2. S-II Stage Engine No. 1 Longitudinal Oscillation Time Histories

to be somewhat erratic, crossing the frequency (approximately 18 hertz) of the center engine support structure at least twice and separating in the latter part of flight (see Figure 6A-3).

The S-II stage thrust structure including the center engine crossbeam is shown in Figure 6A-4. This figure shows also the thrust structure differences between the S-II-3 and S-II-4 stages. The modal frequency of the S-II-4 crossbeam is approximately 17 hertz.

The evaluation to date has not concluded a definite cause of the large magnitude oscillations. However, the data does give some indications that it is not classical POGO (a fluid loop feedback through the tanks and propellant lines). The ratio of discharge pressure to pump inlet pressure as measured on the AS-503 flight were greater than that shown by previous test results by more than an order of magnitude. Another reason that this was probably not a line dominated oscillation is the fact that the frequency of engine chamber pressure was increasing while Net Positive Suction Pressure (NPSP) was decreasing during the time of interest. Line frequencies should decrease with decreasing NPSP. The J-2 engine LOX pump has demonstrated a susceptibility to small amplitude oscillations between 15 and 20 hertz independent of the support structure on which the engine is mounted when operating at certain NPSP values. At this point of the evaluation, it appears that this self induced pump oscillation of the center engine was initiated or greatly influenced by the NPSP and was magnified by the local center engine support structure (cross-beam) which has a modal frequency of approximately 18 hertz. Similar oscillations of smaller magnitudes were seen in AS-501 and AS-502 data at approximately the same LOX tank liquid levels and NPSP values. No conclusion can be made at this time as to the exact cause of the 18 hertz phenomenon. Flight and test data evaluation and analytical investigations continue.

6A.3 SPACECRAFT STRUCTURAL RESPONSE

The 8 and 11 hertz oscillation time histories measured at the Command Module (CM) are shown in Figure 6A-5. The 8 hertz response at ±0.06 g's agrees in time with that reported by the astronaut. The 8 and 11 hertz response corresponds to the first and second longitudinal mode of the vehicle at this flight time. These oscillations are forced responses and are caused by uncoupled oscillatory thrust well within the noise level of the engines. No 18 hertz response was evident in spacecraft data.

6A.4 RESPONSE THRUST CALCULATIONS

Since it was impossible to ascertain acceleration levels in the S-II thrust structure in the 18 hertz frequency range due to the rolloff characteristics of the accelerometers, calculations were made of these g levels by analytically forcing the vehicle with the oscillatory thrust from valid engine chamber pressure measurements. This computation resulted in an engine gimbal block acceleration of ±3.5 g's as shown in Table 6A-1.

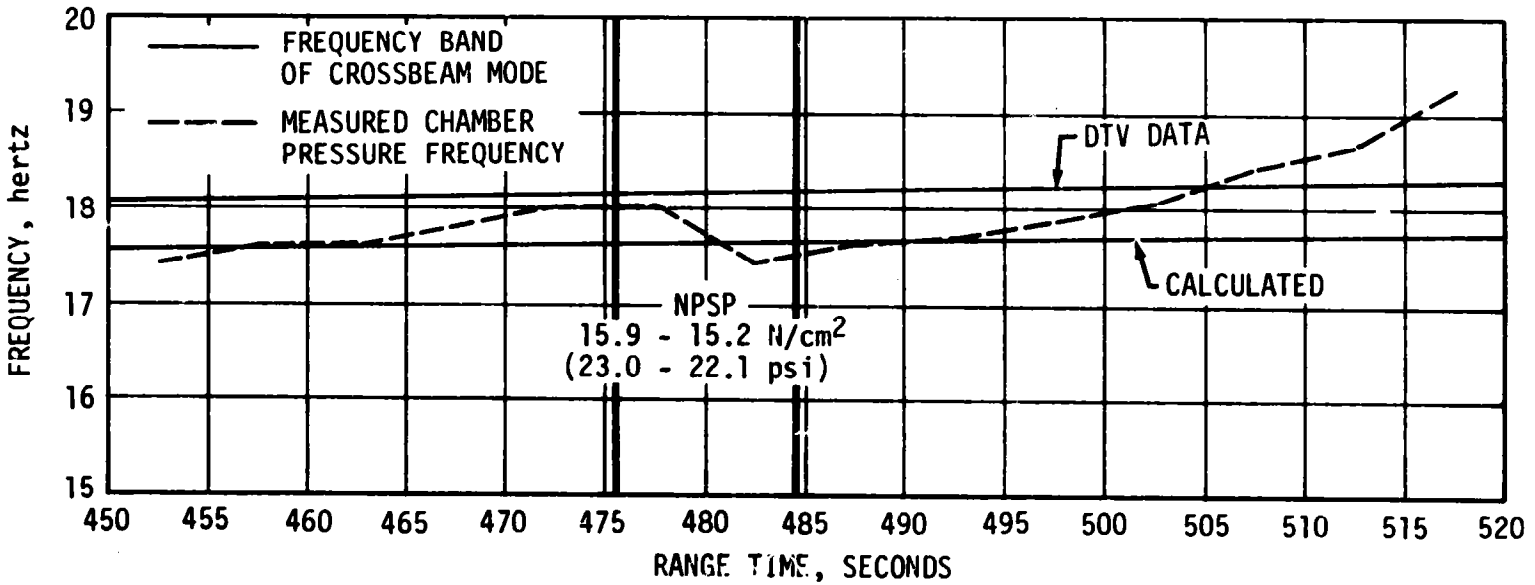

Figure 6A-3. S-II Stage Crossbeam and Center Engine Chamber Pressure Frequency

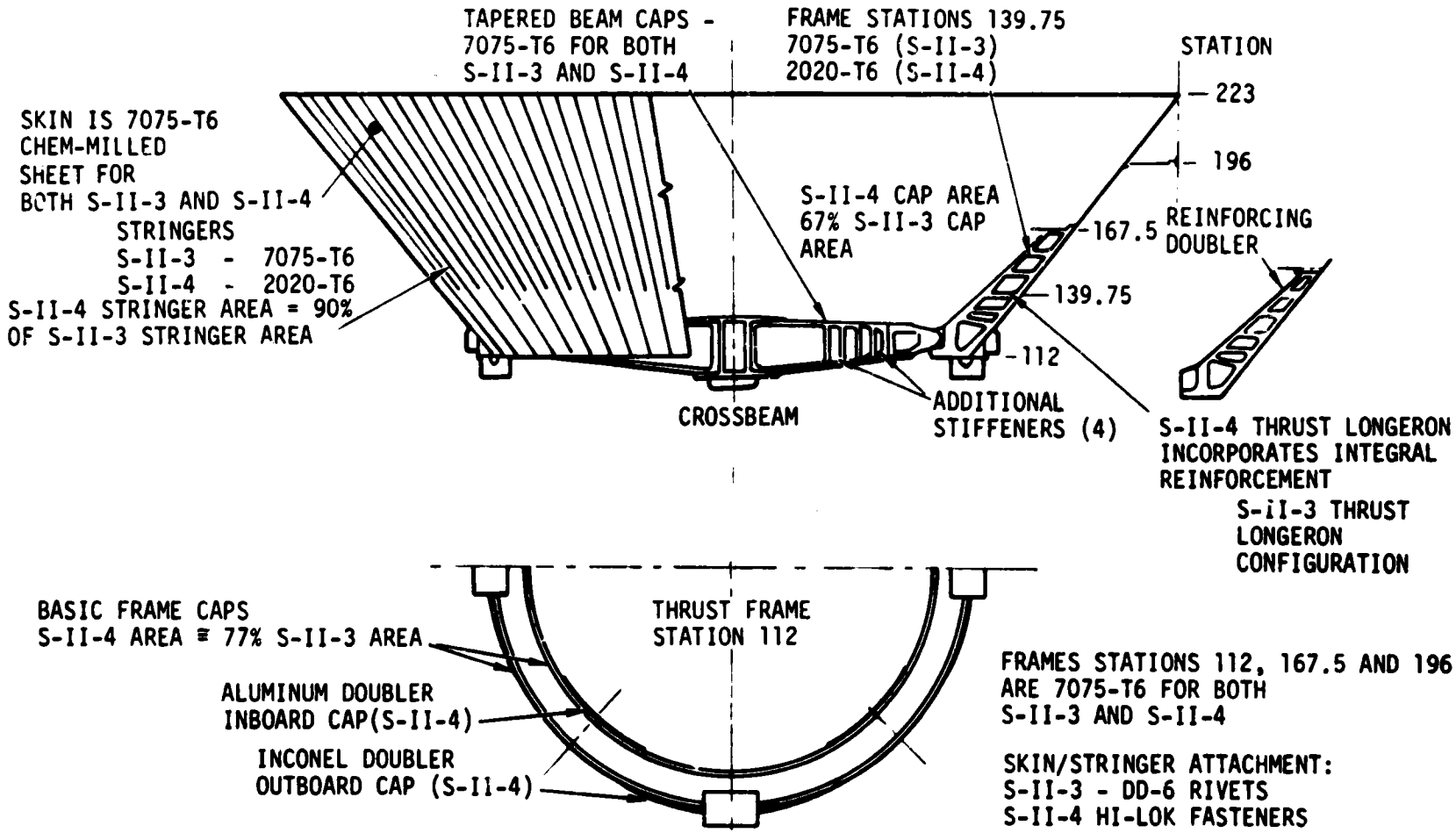

Figure 6A-4. S-II-3 and S-II-4 Thrust Structure Comparison

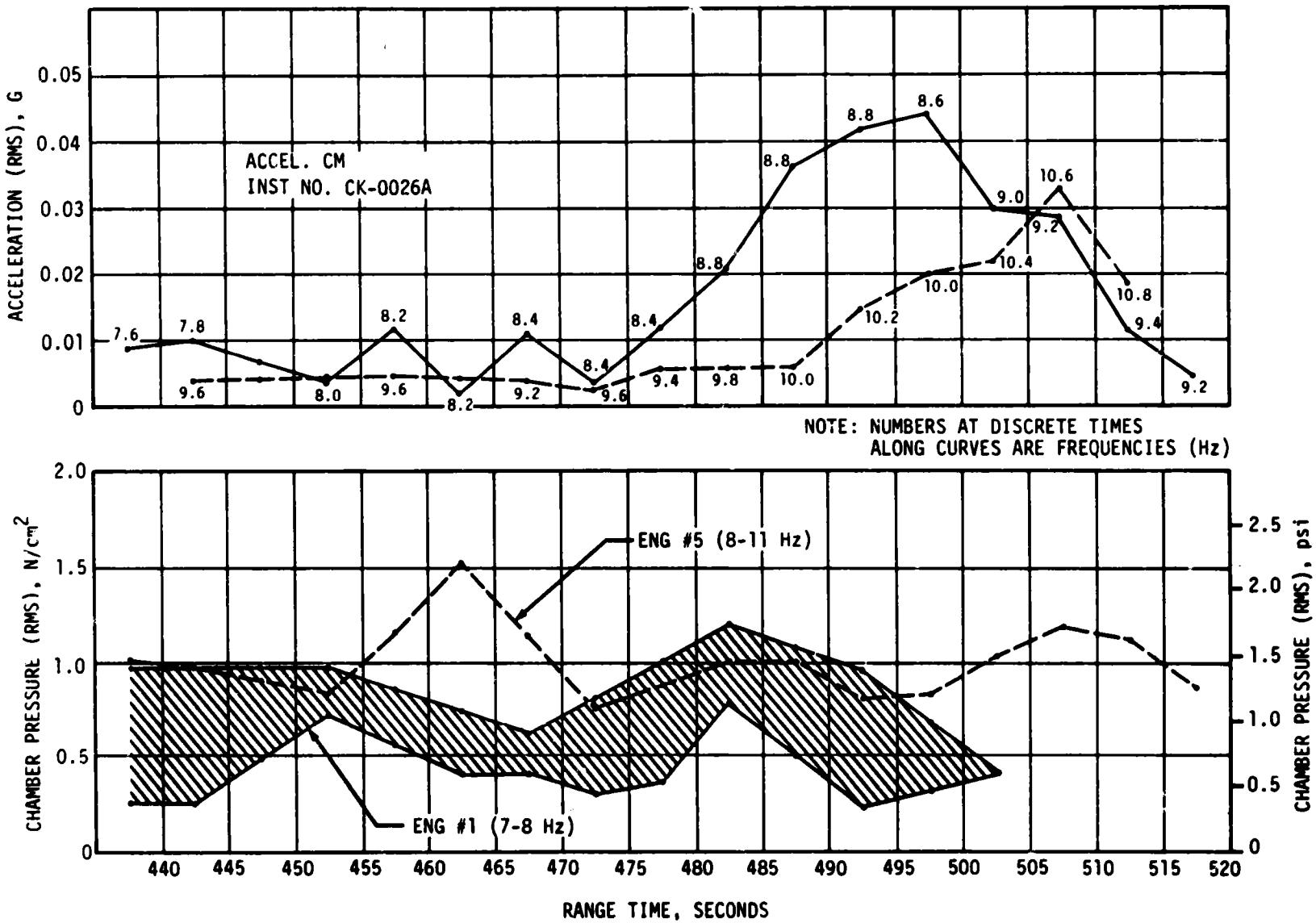

Figure 6A-5. Command Module Longitudinal Oscillation Time Histories

Table 6A-1. Calculated Longitudinal Structural Response and Thrust Oscillations Using AS-503 Measured Data

FREQUENCY	MOST VALID AS-503 FLIGHT DATA	RESULTS OF RESPONSE/THRUST CALCULATIONS
17-18 hertz	S-II Center Engine Chamber Pressure	1. The measured chamber pressure produces an oscillating thrust of ±22,241 Newtons (±5000 lbf). 2. Forcing the 17.7 hertz mode (c/c_c = 1.5 percent) with ±5000 lbf gives a calculated thrust pad acceleration of ± 3.5 g's.
8-9 hertz	Accelerometers in the Command Module (CM)	1. The measured acceleration in the command module is ± .06 g's at 8-9 hertz. 2. The calculated force level required to give ± .06 g's CM response in the 8.6 hertz mode (c/c_c = 0.8 percent) is ±667 Newtons (±150 lbf).
10-11 hertz	Accelerometers in the CM	1. The measured acceleration in the command module is ± .05 g's at 10-11 hertz. 2. The calculated force level required to give ± .05 g's CM response in the 11.0 hertz mode (c/c_c = 0.8 percent) is ± 845 Newtons (±190 lbf).

This loading, combined with thrust loading on the crossbeam, gave only 82 percent of the design load. The crossbeam is the most critical load carrying structure at this time of flight, therefore, a very adequate structural margin was maintained during the S-II oscillation phenomenon.

The 8 and 11 hertz accelerations measured in the CM were valid, however, engine chamber pressure amplitudes were in the noise level and could not be determined. This chamber pressure level was determined analytically by back calculating the oscillatory engine thrust required to reproduce the measured responses in the CM. This resulted in a total oscillatory thrust of ± 667 Newtons (± 150 lbf) for the 8 hertz response and ± 845 Newtons (± 190 lbf) for the 11 hertz response as shown in Table 6A-1. The 8 and 11 hertz oscillations were insignificant from a structural loads consideration.

SECTION 7

S-IVB PROPULSION

7.1 SUMMARY

The J-2 engine operated satisfactorily throughout the operational phase of first and second burn with normal shutdowns. S-IVB first burn time was 156.69 seconds which was 2.11 seconds less than predicted. The engine performance during first burn, as determined from standard altitude reconstruction analysis, deviated from the predicted ESC + 80-second time slice by +0.01 percent for thrust and +0.40 percent for specific impulse. The S-IVB stage first burn ECO was initiated by the Launch Vehicle Digital Computer (LVDC) at 684.98 seconds.

The Continuous Vent System (CVS) adequately regulated LH_2 tank ullage pressure at 13.4 N/cm^2 (19.5 psia) during orbit, and the Oxygen/Hydrogen (O_2/H_2) Burner, in its first flight operation, satisfactorily achieved LH_2 tank repressurization for restart. Repressurization of the LOX tank was not required.

Engine restart conditions were within specified limits. The restart at full open Propellant Utilization (PU) valve position was successful and there were no indications of overtemperature conditions in the gas generator. S-IVB second burn time was 317.72 seconds which was 2.07 seconds longer than predicted. The engine performance during second burn, as determined from the standard altitude reconstruction analysis, deviated from the predicted ESC + 80-second time slice by -0.03 percent for thrust and +0.28 percent for specific impulse. The S-IVB stage ECO was initiated by the LVDC at 10,555.51 seconds.

Subsequent to second burn, the stage propellant tanks were safed satisfactorily, with sufficient impulse being derived from the LOX dump to impart 20.4 m/s (66.9 ft/s) to stage velocity. This slowed the vehicle down and was a major contributing factor toward avoiding lunar impact and establishing a solar orbit.

The instrumentation added to this stage to monitor the effectiveness of the engine's Augmented Spark Igniter (ASI) line modification showed no indications of line failure on this engine.

Special instrumentation added to the cold helium system to detect any leakage in the system indicated that no leakage was observed on AS-503. Sphere temperature and pressure data likewise indicated no leakage.

7.2 S-IVB CHILLDOWN AND BUILDUP TRANSIENT PERFORMANCE FOR FIRST BURN

The propellant recirculation systems performed satisfactorily, meeting start and run box requirements for fuel and LOX as shown in Figure 7-1.

The thrust chamber temperature at launch was well below the maximum allowable redline limit of 172°K (-150°F). At S-IVB first burn ESC the temperature was 158.2°K (-175°F), which is within the requirement of 166 ± 27.5°K (-160.9 ± 49.5°F) as shown in Figure 7-2.

The chilldown and loading of the engine Gaseous Hydrogen (GH_2) start sphere and pneumatic control sphere prior to liftoff were satisfactory. Figure 7-3 shows the start tank performance for first burn. At first ESC the start tank conditions were within the required S-IVB region of 896.3 ± 68.9 N/cm^2 and 133.2 ± 44.4°K (1300 ± 100 psia and -220 ± 80°F) for initial start. The discharge was completed and the refill initiated at first burn ESC +3.86 seconds. The refill was satisfactory and in good agreement with the acceptance test.

As a modification on this stage, the J-2 control helium sphere was tied into the stage LOX and LH_2 ambient helium repressurization spheres as shown in Figure 7-4. This resulted in a continual replenishing of the J-2 control sphere in flight. The engine control bottle pressure and temperature at liftoff were 2034 N/cm^2 (2950 psia) and 152.8°K (-184.6°F), respectively. LOX and LH_2 systems chilldown, which were continuous from before liftoff until just prior to S-IVB first burn ESC were satisfactory. At ESC the LOX pump inlet temperature was 91.1°K (-295.7°F) and the LH_2 pump inlet temperature was 20.82°K (-422.2°F).

The first burn start transient was satisfactory. The thrust buildup was within the limits set by the engine manufacturer. Faster thrust buildup to the 90 percent level as compared to the acceptance test results was observed on this flight and is shown in Figure 7-5. This buildup was similar to the thrust buildups observed on AS-501 and 502. Table 7-1 shows the major sequences of events during the buildup transients. The PU valve was in proper null position prior to first start. The total impulse from STDV to STDV +2.5 seconds was 820,972 N-s (184,562 lbf-s) for first start. This was greater than the value of 671,681 N-s (151,000 lbf-s) obtained during the same interval for the acceptance test.

First burn fuel lead generally followed the predicted pattern and resulted in satisfactory conditions as indicated by the thrust chamber temperatures and the associated fuel injector temperatures.

7.3 S-IVB MAIN STAGE PERFORMANCE FOR FIRST BURN

Two analytical techniques were employed in evaluating S-IVB stage propulsion system performance. The primary method, propulsion reconstruction analysis, utilized telemetered engine and stage data to compute longitudinal thrust,

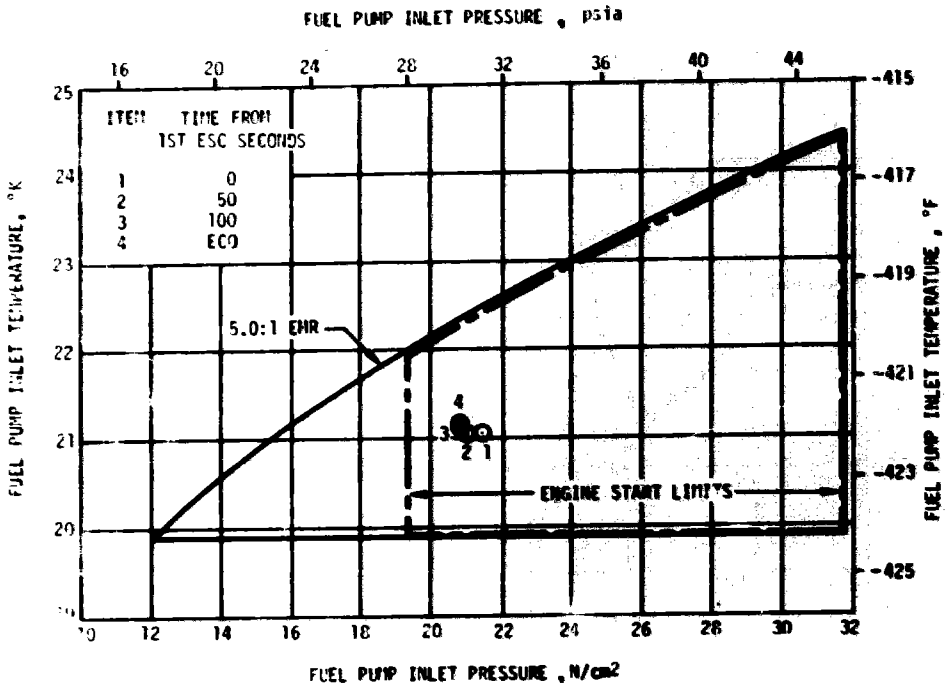

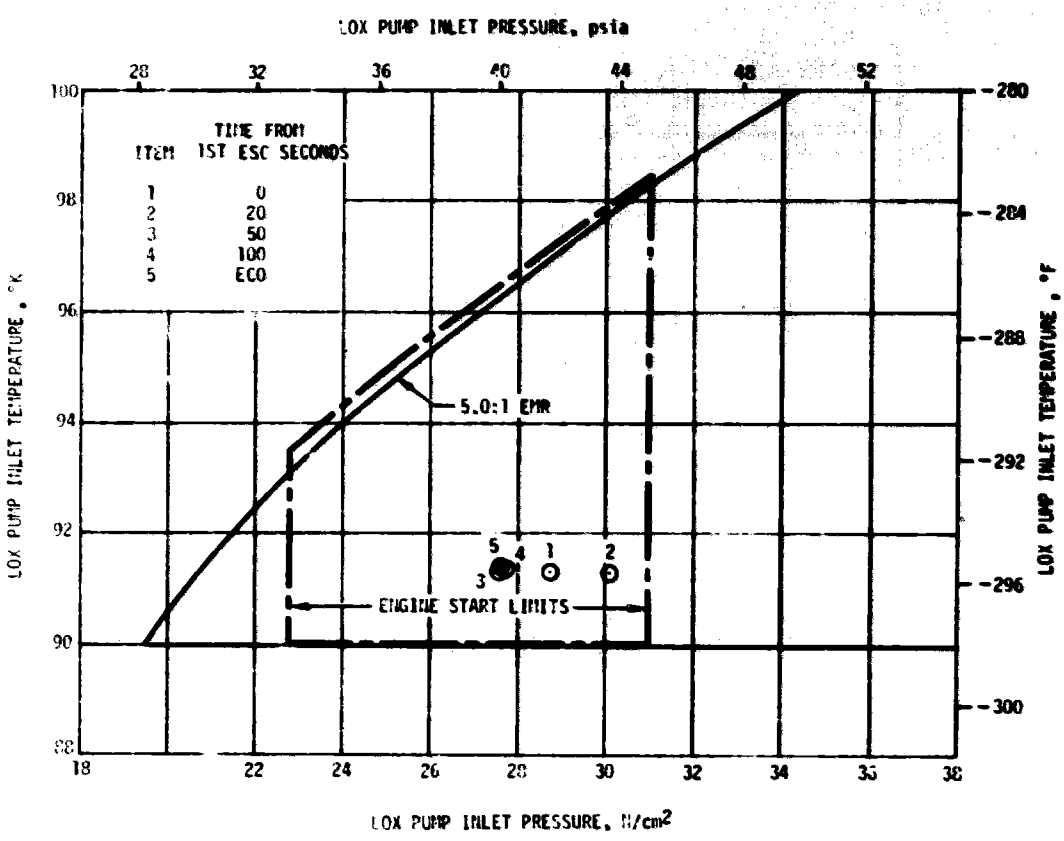

Figure 7-1. S-IVB Start Box and Run Requirement - First Burn

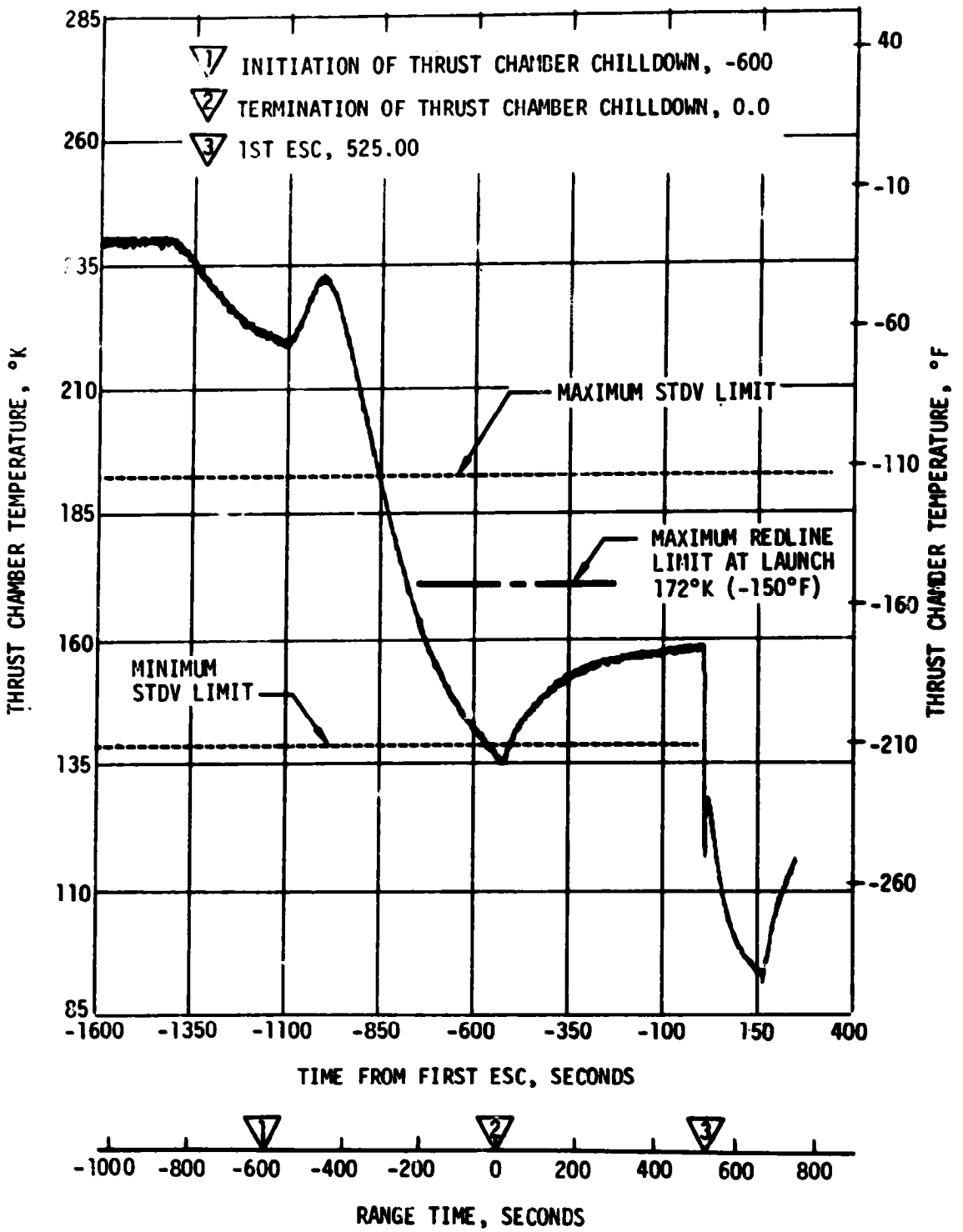

Figure 7-2. S-IVB Thrust Chamber Temperature - First Burn

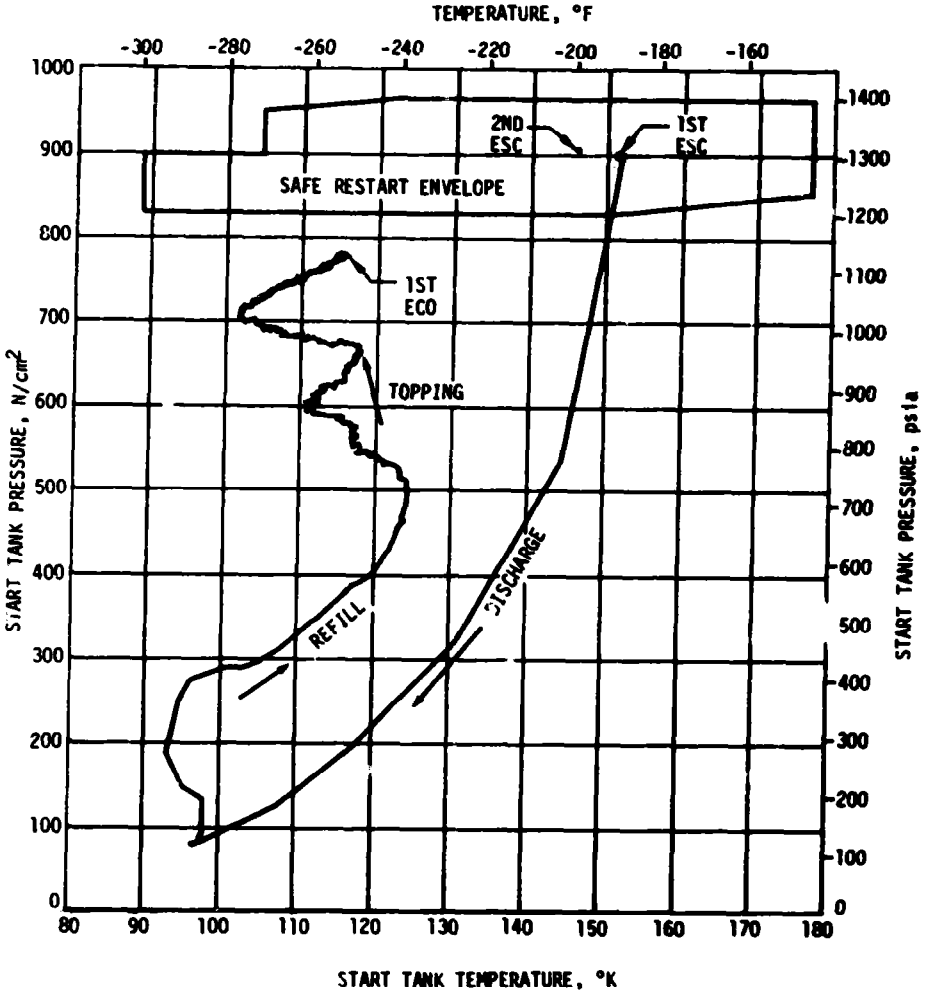

Figure 7-3. S-IVB Start Tank Performance - First Burn

specific impulse, and stage mass flowrate. In the second method, flight simulation, a five-degree-of-freedom trajectory simulation was utilized to fit propulsion reconstruction analysis results to the trajectory. Using a differential correction procedure, this simulation determined adjustments to the reconstruction analysis of thrust and mass flow histories to yield a simulated trajectory which closely matched the observed postflight trajectory.

The propulsion reconstruction analysis showed that the stage performance during mainstage operation was satisfactory. A comparison of predicted and actual performance of thrust, total flowrate, specific impulse, and mixture ratio versus time is shown in Figure 7-6. Table 7-2 shows the specific impulse, flowrates and mixture ratio deviations from the predicted at the ESC +80-second time slice. This time slice performance is the standardized altitude performance which is comparable to engine acceptance tests. The

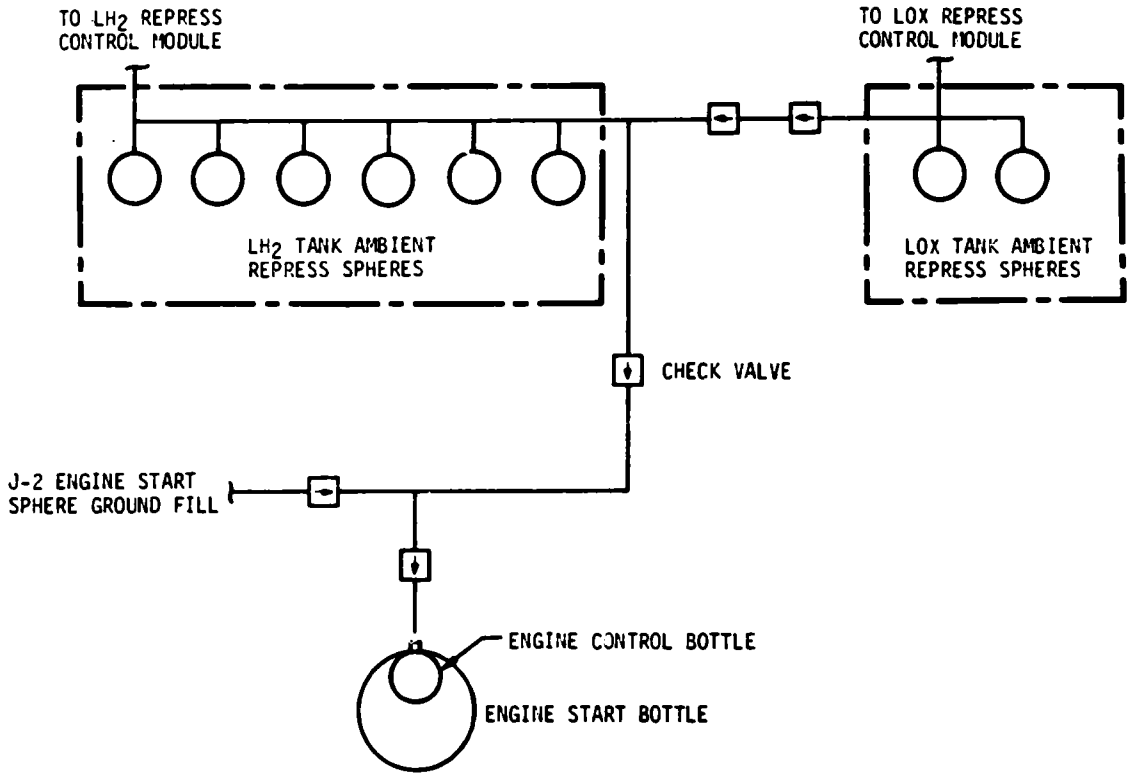

Figure 7-4. J-2 Engine Control and Stage Ambient Bottles Tie-In Schematic

80-second time slice performance for first burn thrust was 0.01 percent greater than predicted. Specific impulse performance for first burn was 0.40 percent greater than predicted.

The overall propulsion reconstruction of longitudinal thrust compared to the predicted was +0.09 percent for first burn. Longitudinal specific impulse for first burn when compared to predicted was +0.44 percent.

The flight simulation analysis showed an increase of 0.59 percent, compared to the prediction, in specific impulse. Other comparisons are shown in Table 7-3.

The S-IVB burn time was 2.11 seconds shorter than predicted. Table 7-4 shows that the primary contributors to the shorter burn time were deviations in the preconditions for the S-IVB portion of flight. The total contributors show a burn time deviation of -1.707 seconds. This is 0.403 second less than the actual deviations. The additional 0.403 second of burn time may be accounted for by uncertainties in preconditions of flight and uncertainties in the thrust average obtained from trajectory reconstruction.

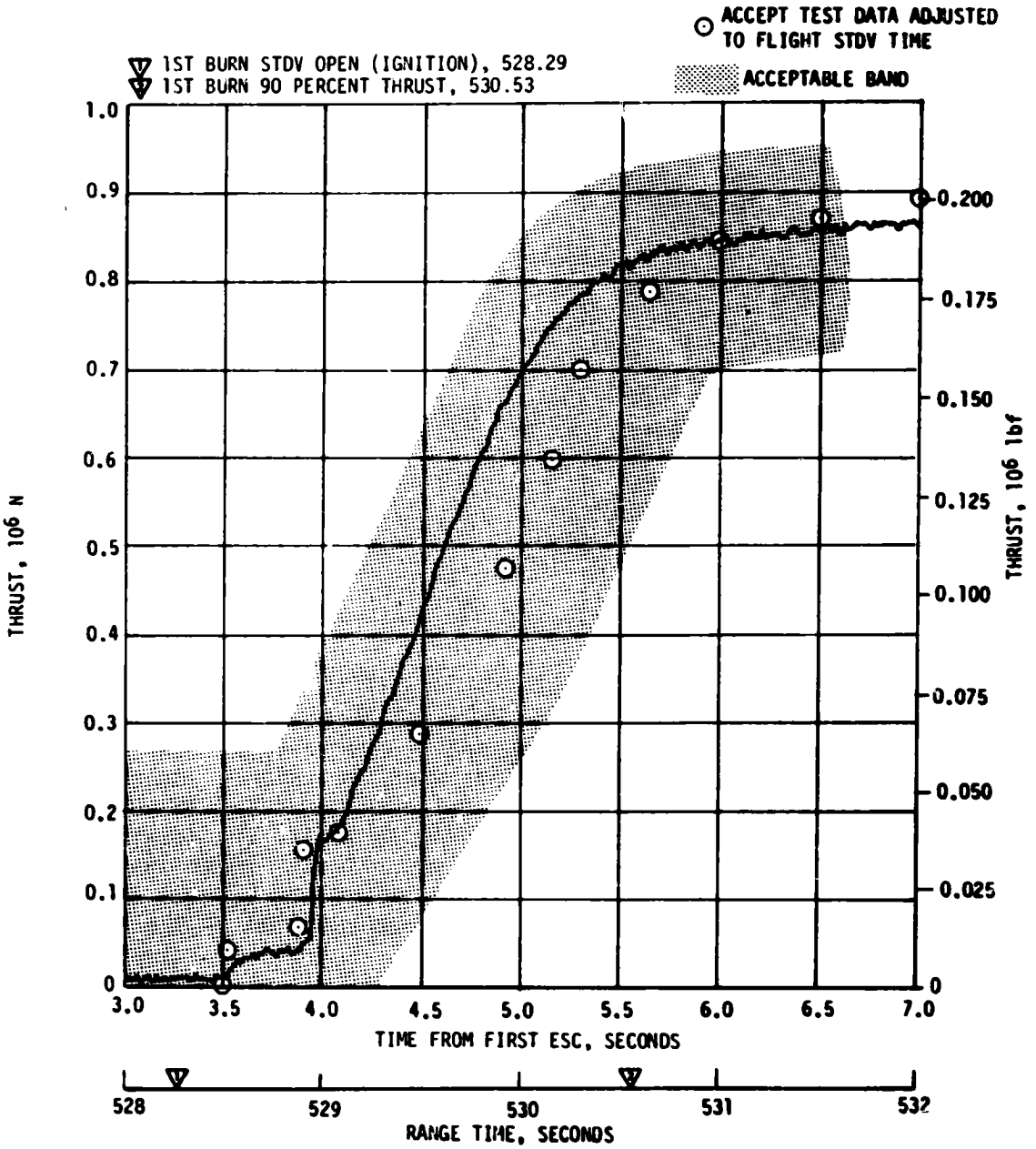

Figure 7-5. S-IVB Buildup Transient - First Burn

During both burns the engine experienced in-run shifts of approximately 8896 Newtons (2000 lbf) of thrust due to 4.5 N/cm^2 (6.5 psia) shifts in chamber pressure. These shifts are attributed to shifts in the PU valve resistance to flow. Figure 7-7 shows the PU valve calculated pressure drop and chamber pressure for both burns. The calculated pressure drops correlate with the observed changes in chamber pressure.

A reduction in PU valve flow resistance at a fixed valve position results in an increase in LOX bypass flow. Since the LOX pump during mainstage

Table 7-1. S-IVB Engine Start Sequence Events - First Burn

EVENT	TIME OF EVENT IN RANGE TIME (SECONDS)	
	PREDICTED	ACTUAL
S-IVB Engine Start Sequence Command (ESC)	522.19	525.00
S-IVB Engine Start Indication	522.19	525.03
Start Tank Discharge Valve (STDV) Open	525.19	528.29
Mainstage Control Solenoid	525.64	528.46
Mainstage OK	526.60	529.78
90 Percent Thrust	527.69	530.53
Main LOX Valve Open	527.74	530.85

is essentially a constant flow pump an increase in bypass flow allows less flow to be delivered to the chamber causing a lower chamber pressure. Figure 7-7 shows that during those periods when the valve ΔP decreased the chamber pressure decreased, and when the valve ΔP increased the chamber pressure increased. Thus the engine performance shifts are attributed to shifts in the hydraulic flow resistance of the valves. These in-run shifts have been experienced on previous acceptance tests, and ECP-601 which relocates the baffle in the PU valve will be incorporated on the AS-504 and subsequent S-IVB stages.

Due to the S-II engine failure and restart problems on AS-502 flight, the ASI system on the J-2 engine was redesigned. Photographs of the redesigned LOX and fuel lines are shown in Figures 7-8 and 7-9. Instrumentation installed to monitor ASI system performance responded as expected. Both LOX and LH_2 supply line temperatures chilled to expected levels during both burns and did not indicate any abnormal condition. Combustion chamber temperature responded during fuel lead indicating proper ignition of the ASI. The measurement was cooled by its local environment during mainstage (see Figure 7-10). Paragraph 9.3.3 discusses the structural integrity of the redesigned lines.

The helium control system for the J-2 engine performed satisfactorily during mainstage operation. Since the engine bottle was connected with the stage ambient repressurization bottles there was little pressure

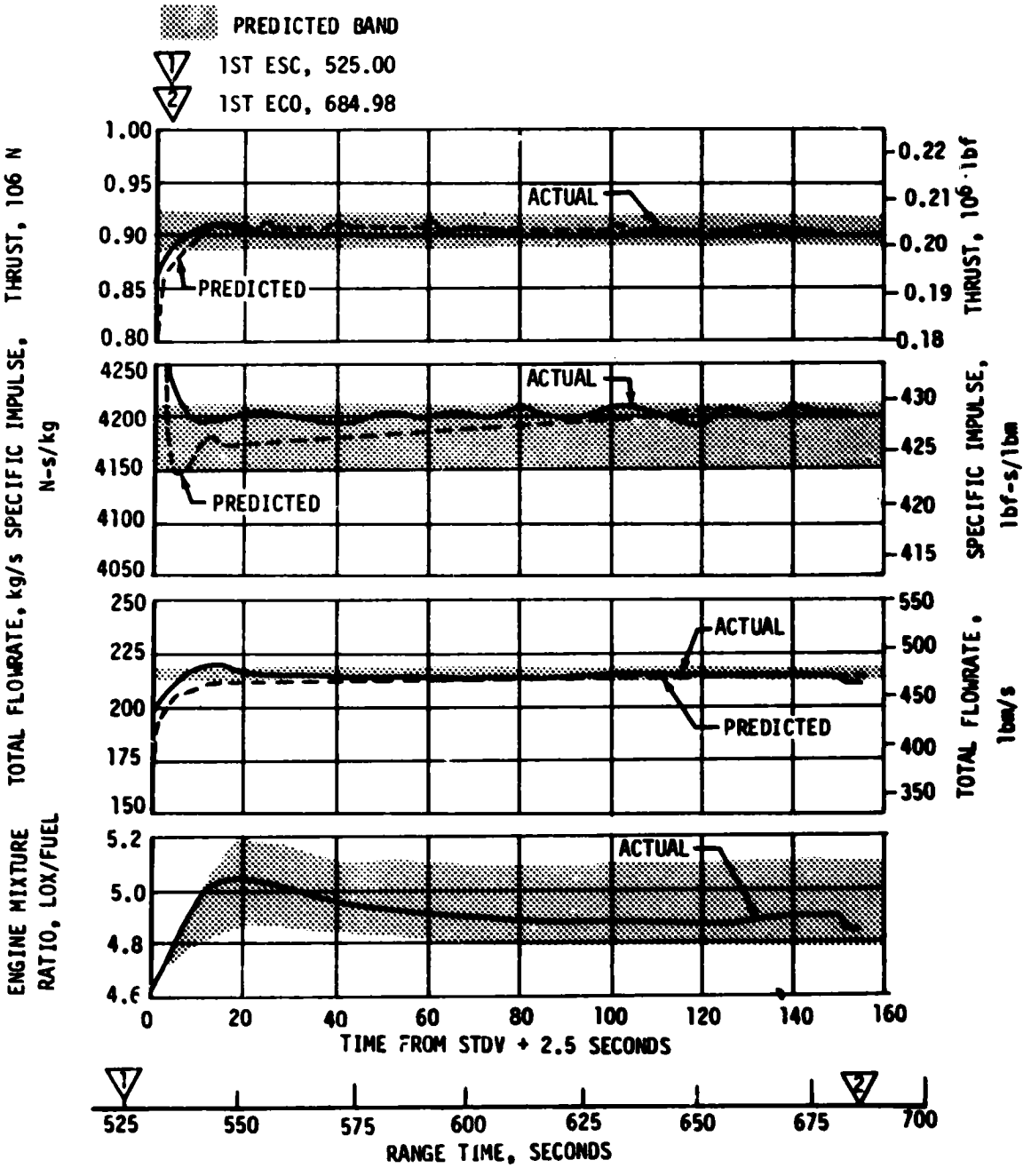

Figure 7-6. S-IVB Steady State Performance - First Burn

decay. Helium usage was estimated from flowrates during engine operation. Approximately 0.20 kilogram (0.44 lbm) was consumed during first burn.

7.4 S-IVB SHUTDOWN TRANSIENT PERFORMANCE FOR FIRST BURN

S-IVB ECO was initiated at 684.98 seconds by a guidance velocity cutoff command which resulted in a 2.11-second shorter than predicted first burn time.

Table 7-2. S-IVB Steady State Performance - First Burn
(ESC + 80 Second Time Slice at Standard Altitude Conditions)

PARAMETER	PREDICTED	RECONSTRUCTION	FLIGHT DEVIATION	PERCENT DEVIATION FROM PREDICTED
Thrust N (lbf)	900,609 (202,465)	901,557 (202,678)	948 (213)	0.01
Specific Impulse N-s/kg (lbf-s/lbm)	4,187.4 (427.0)	4,204.1 (428.7)	16.7 (1.70)	0.40
LOX Flowrate kg/s (lbm/s)	178.89 (394.38)	178.16 (392.78)	-0.73 (-1.60)	-0.41
Fuel Flowrate kg/s (lbm/s)	36.17 (79.74)	36.30 (80.03)	0.13 (0.29)	0.36
Engine Mixture Ratio LOX/Fuel	4.946	4.908	-0.038	-0.77

The ECO transient was satisfactory and agreed closely with the acceptance test and predictions. The total cutoff impulse to zero percent of rated thrust was 183,427 N-s (41,236 lbf-s). Cutoff occurred with the PU valve in the null position.

The Main Oxidizer Valve (MOV) actuator temperature at cutoff for first burn was 182°K (-133°F). The cutoff impulse was adjusted from these conditions to standard conditions for comparison with the log book values at null PU valve position and 255°K (0°F) MOV actuator temperature. After these adjustments, the flight value was near the log book value. The thrust during first cutoff is shown in Figure 7-11.

Telemetered guidance velocity data indicated the cutoff impulse was very close to that expected as presented in Table 7-5.

7.5 S-IVB PARKING COAST PHASE CONDITIONING

The LH_2 Continuous Vent System (CVS) performed satisfactorily, maintaining the fuel tank ullage pressure at an average level of 13.4 N/cm^2 (19.5 psia).

Table 7-3. Comparison of S-IVB Stage Flight Reconstruction Data With Performance Simulation Results - First Burn

PARAMETERS	UNITS	PREDICTED	FLIGHT RECONSTRUCTION	PERCENT DEV FROM PRED
		FIRST BURN FLIGHT AVE	FIRST BURN FLIGHT AVERAGE	FIRST BURN FLIGHT AVERAGE
Longitudinal Vehicle Thrust	N (lbf)	902,42 (202,87	903,225 (203,053)	0.09
Vehicle Mass Loss Rate	kg/s (lbm/s)	215.55 (475.20)	214.79 (473.54)	-0.35
Longitudinal Vehicle Specific Impulse	N-s/kg (lbf-s/lbm)	4186.5 (426.9)	4205.1 (428.8)	0.44
PARAMETERS	UNITS	FLIGHT SIMULATION	PERCENT DEV FROM PRED	
		FIRST BURN FLIGHT AVERAGE	FIRST BURN FLIGHT AVERAGE	
Longitudinal Vehicle Thrust	N (lbf)	900,881 (202,526)	-0.17	
Vehicle Mass Loss Rate	kg/s (lbm/s)	213.94 (471.65)	-0.75	
Longitudinal Vehicle Specific Impulse	N-s/kg (lbf-s/lbm)	4211 (429.4)	0.59	

Table 7-4. S-IVB Simulation Burn Time Deviations - First Burn

CONTRIBUTOR	BURN TIME DELTA (SECONDS)
Preconditions of Flight (S-II/ S-IVB Separation Command) Velocity Magnitude (Space Fixed)	-1.41
Start Sequence Uncertainties	-0.29
S-IVB Thrust	0.053
S-IVB Mass Flow	-0.06
S-IVB Initial Mass	Zero
	Explained -1.707
	Unexplained -0.403

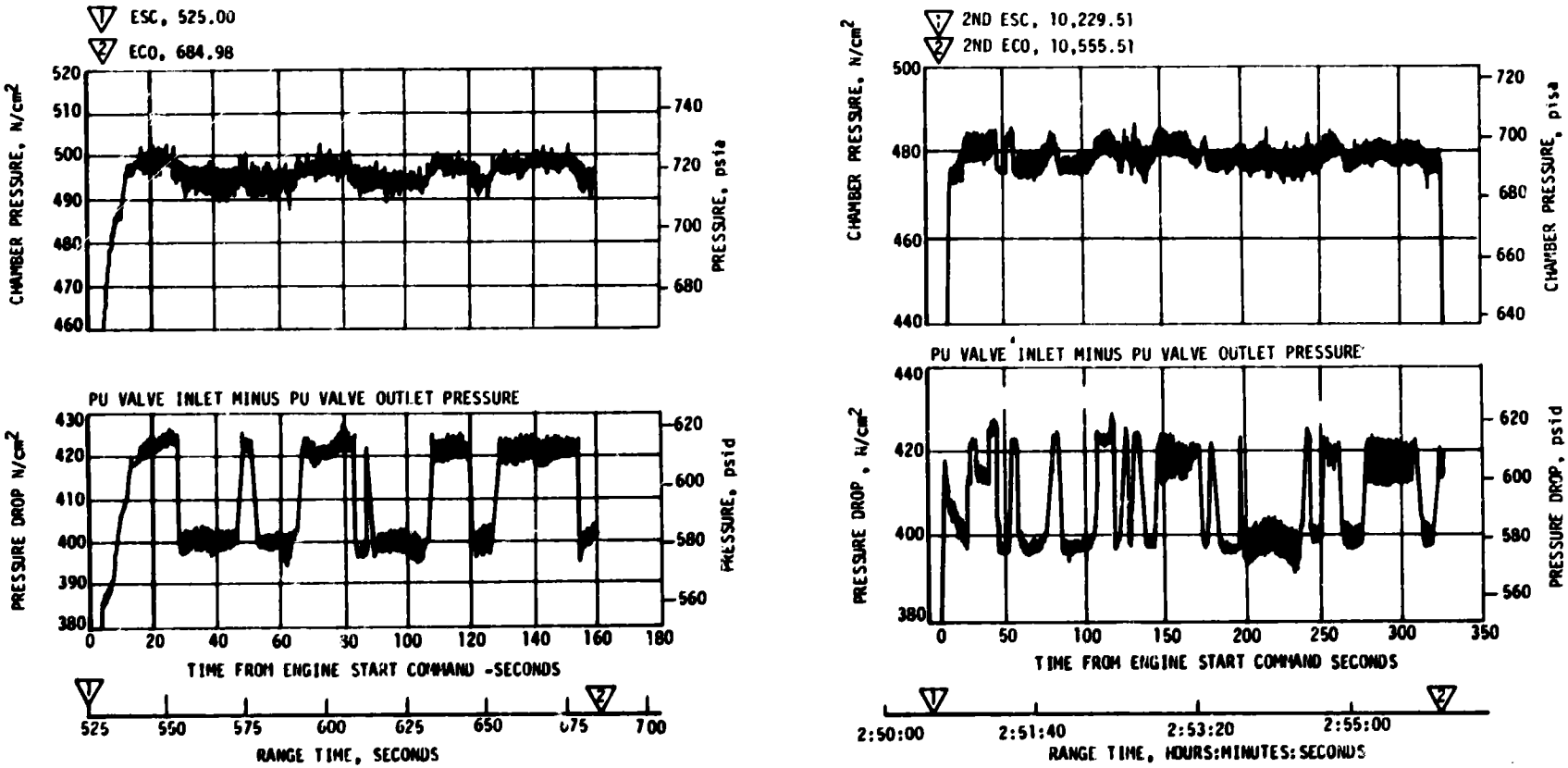

Figure 7-7. S-IVB Performance Shifts - First Burn and Second Burn

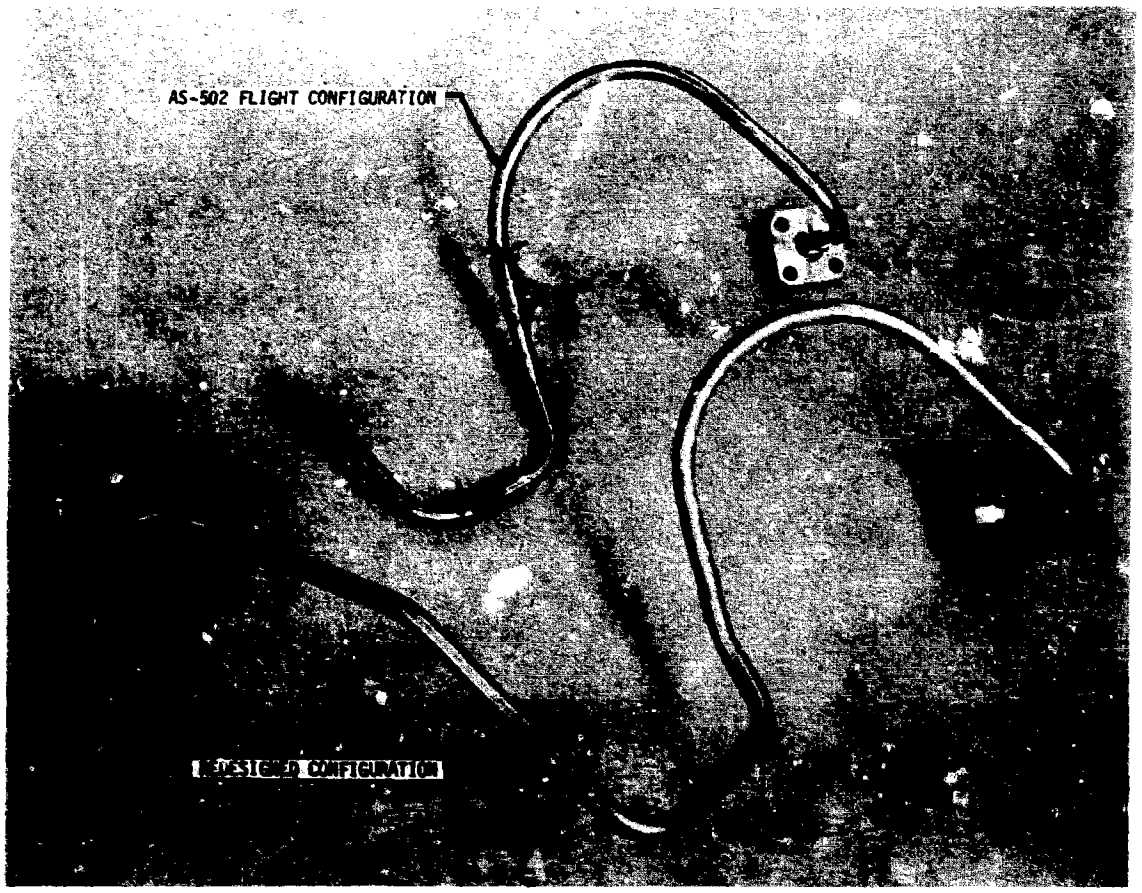

Figure 7-8. Revised J-2 LOX ASI Line

The continuous vent regulator was activated at 744.15 seconds. Regulation continued, with the expected operation of the main poppet periodically opening, cycling, and reseating. Continuous venting was terminated at 9701.72 seconds.

Calculations based on estimated temperatures indicate that the mass vented during parking orbit was 983 kilograms (2169 lbm) and that the boiloff mass was 1040 kilograms (2293 lbm).

J-2 engine control sphere pressure buildup during coast periods was lower than predicted. This is attributed to the fact that there was less mass in the control sphere than expected. Because there was a pressure loss in the lines between the ambient bottles and the engine control sphere of approximately 41 N/cm^2 (60 psid), there was a drop in temperature. There was less warming from the ambient bottles than anticipated.

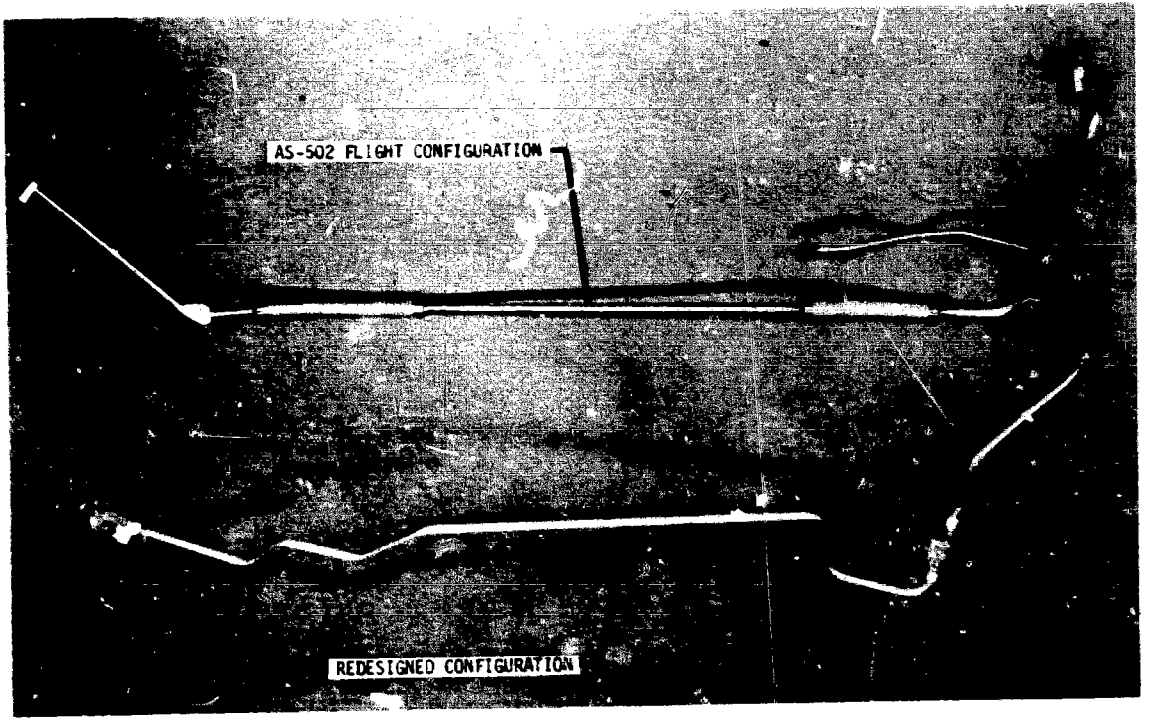

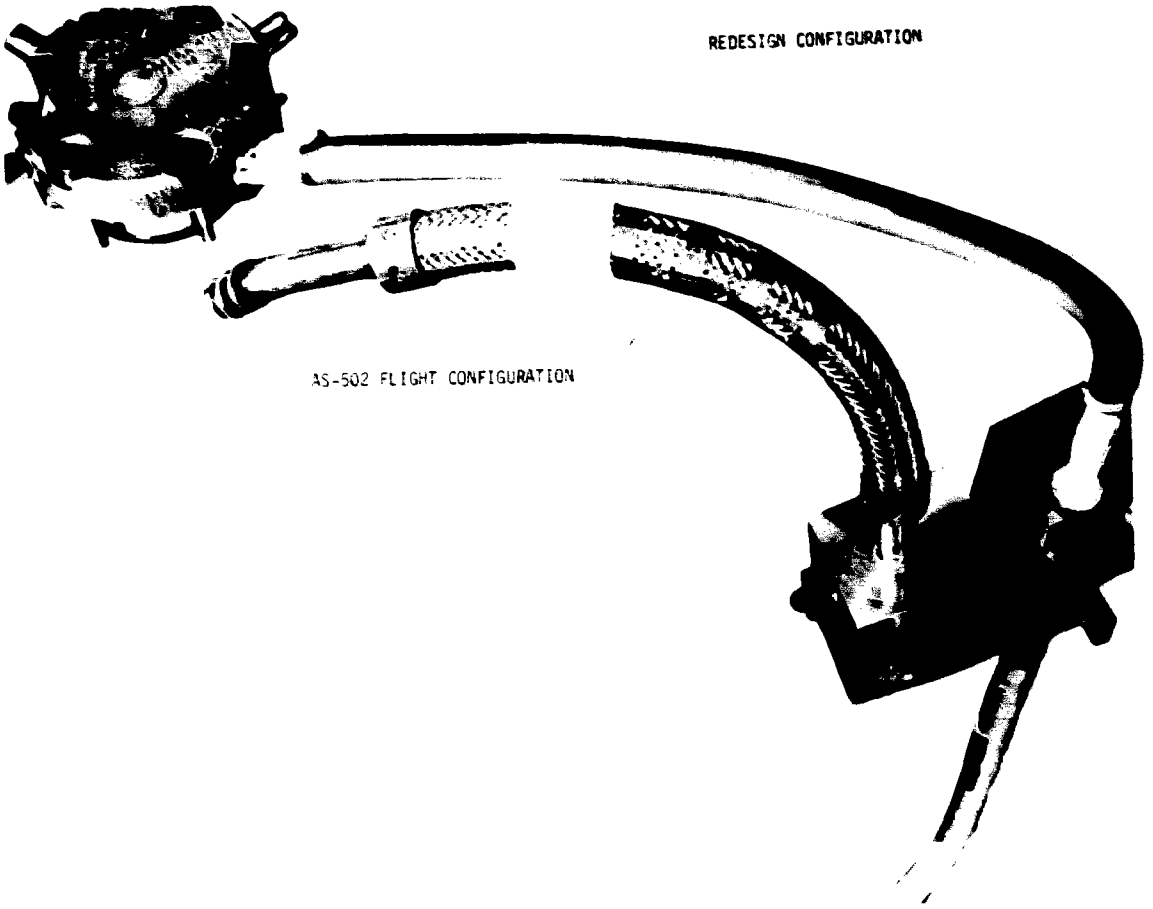

Figure 7-9. Revised J-2 LH_2 ASI Line

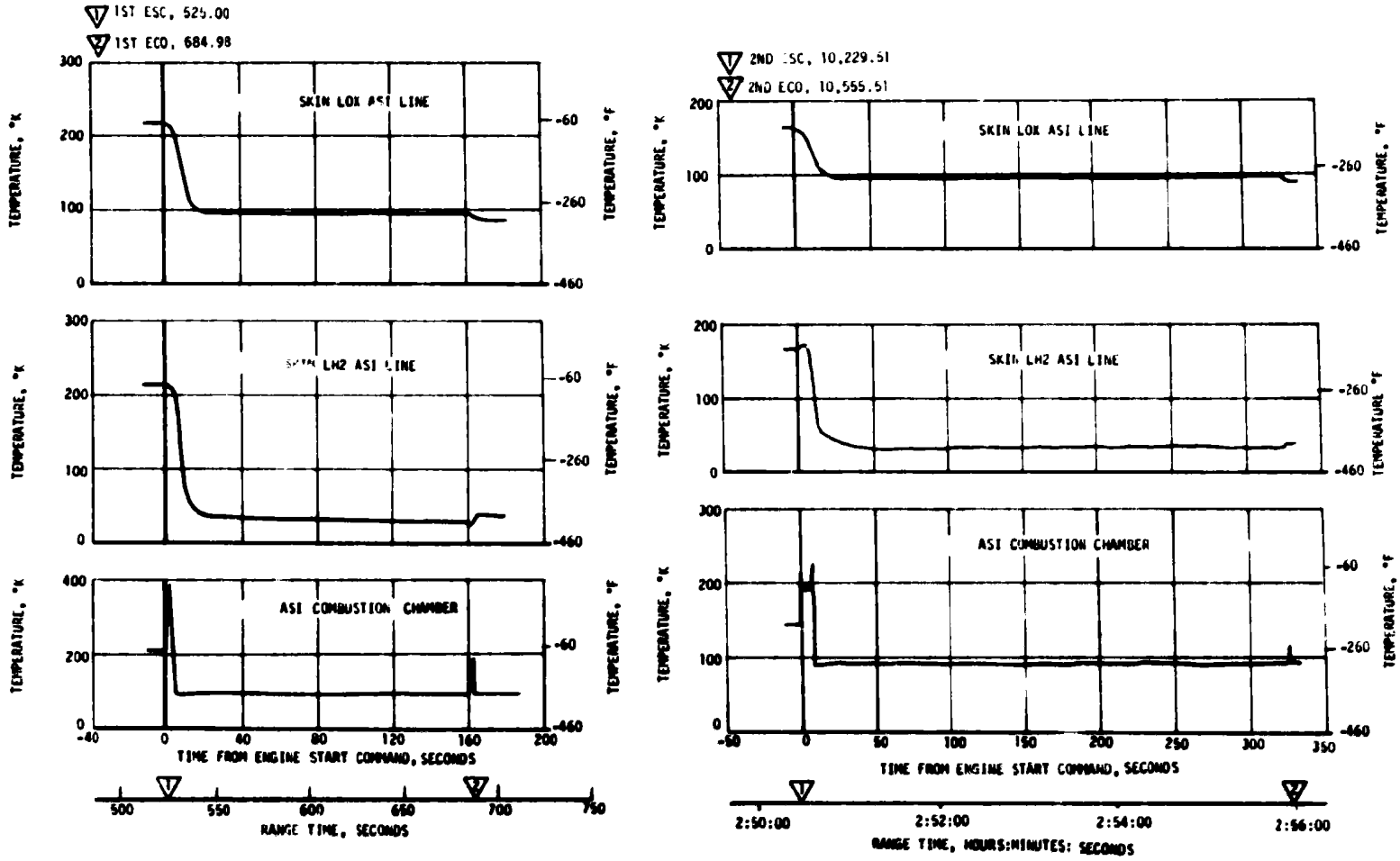

Figure 7-10. ASI Line Conditions - First Burn and Second Burn

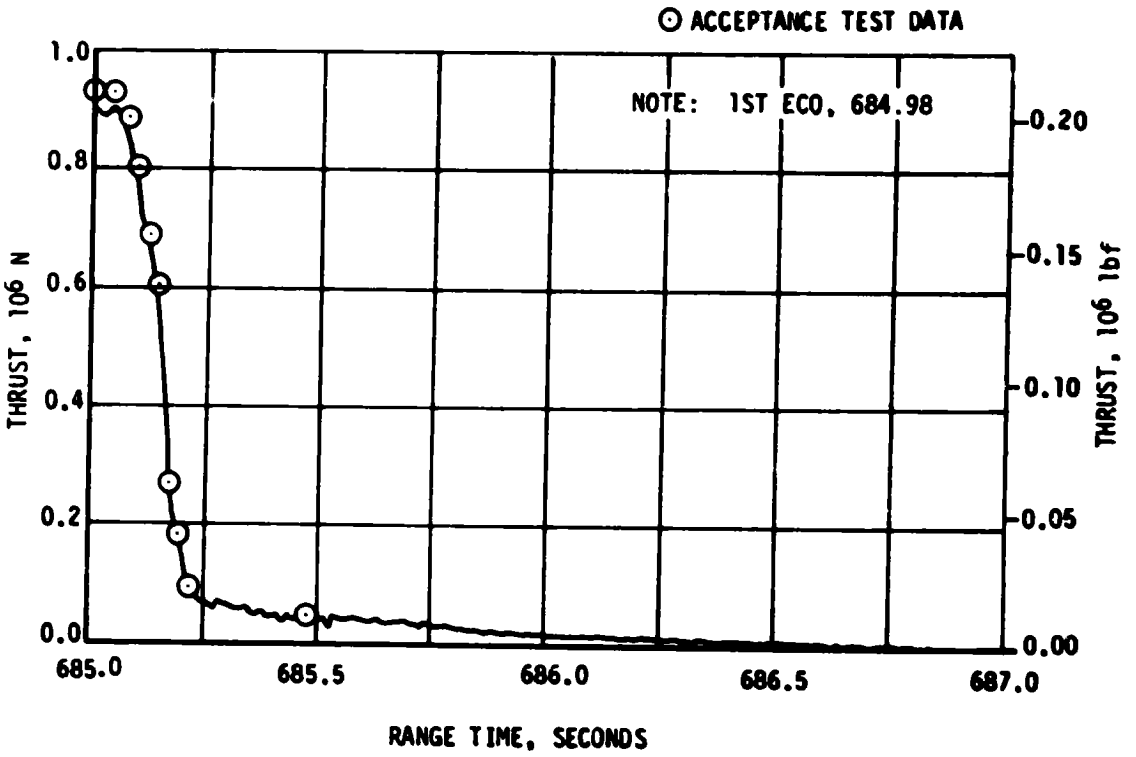

Figure 7-11. S-IVB Shutdown Transient Performance - First Burn

Table 7-5. S-IVB Cutoff Impulse - First Burn

PARAMETER	PREDICTED	FLIGHT		PERCENT DEVIATION FROM PREDICTED	
		ENGINE	GUID. DATA	ENGINE	GUID. DATA
Cutoff Impulse N-s (lbf-s)	187,564 (42,166)	183,427 (41,236)	183,111 (41,165)	-2.21	-2.37
Velocity Increase m/s (ft/s)	1.47 (4.82)	1.43 (4.69)	1.43 (4.69)	-2.72	-2.72

Note: The parameters quoted are from velocity cutoff command to zero percent of rated thrust.

7.6 S-IVB CHILLDOWN AND RESTART FOR SECOND BURN

The O_2/H_2 burner system was implemented on AS-503 and subsequent stages to provide a new means of repressurizing the oxidizer and fuel tanks for orbital restart. The ambient helium repressurization system was retained as a redundant system. The O_2/H_2 burner is mounted on the aft thrust structure where it heats cold helium that is used to repressurize the propellant tanks. Onboard propellants, LOX and LH_2, are fed to the burner through vacuum jacketed, low pressure ducts at existing tank pressures and then through regenerative coils where they are heated before being injected through two injectors into the combustion chamber of the burner. The propellants are ignited and the resulting combustion products pass over four sets of helium coils, heating the cold helium, and then are exhausted through a nozzle. Three of these helium coils are connected in parallel to pressurize the fuel tank; the fourth coil is utilized to pressurize the oxidizer tank (see Figure 7-12). Figure 7-13 shows an illustration of the O_2/H_2 burner.

Repressurization was satisfactorily accomplished by the O_2/H_2 burner. Burner Start Command (BSC) was initiated at 9700.80 seconds. LOX tank ullage pressure at BSC was approximately 26.9 N/cm^2 (39 psia), therefore, repressurization of the LOX tank was not required. The LH_2 repressurization control valves were opened at BSC +6.85 seconds. The fuel tank was repressurized from 13.4 to 20.8 N/cm^2 (19.4 to 30.2 psia) in 168.4 seconds which yields a ramp rate of 2.65 N/cm^2/min (3.85 psi/min) as shown in Figure 7-14. Figures 7-15 and 7-16 show the performance of the O_2/H_2 burner pressurant coil. There were 11.34 kilograms (25 lbm) of cold helium used from the cold helium spheres during repressurization. The burner continued to operate for a total of 460 seconds providing nominal propellant settling forces.

The performance of the AS-503 O_2/H_2 burner during flight was satisfactory although an unusual increase in combustion chamber pressure and temperature were observed during a 20-second period subsequent to the termination of LH_2 tank repressurization as shown in Figures 7-17 and 7-18.

Normally, at the conclusion of LH_2 tank repressurization the combustion chamber pressure and temperature momentarily increase by 0.69 to 1.7 N/cm^2 (1 to 2.5 psid) and 111.1°K (-259.7°F), respectively. The higher than normal combustion chamber pressure and temperature transients, 2.76 N/cm^2 (4 psid) and 305°K (90.31°F), respectively, were caused by:

a. An increase in oxygen flowrate, due to two-phase flow, approximately 10 seconds after the termination of repressurization.

b. LH_2 tank self-pressurization, 0.34 N/cm^2 (0.5 psid), after the conclusion of repressurization.

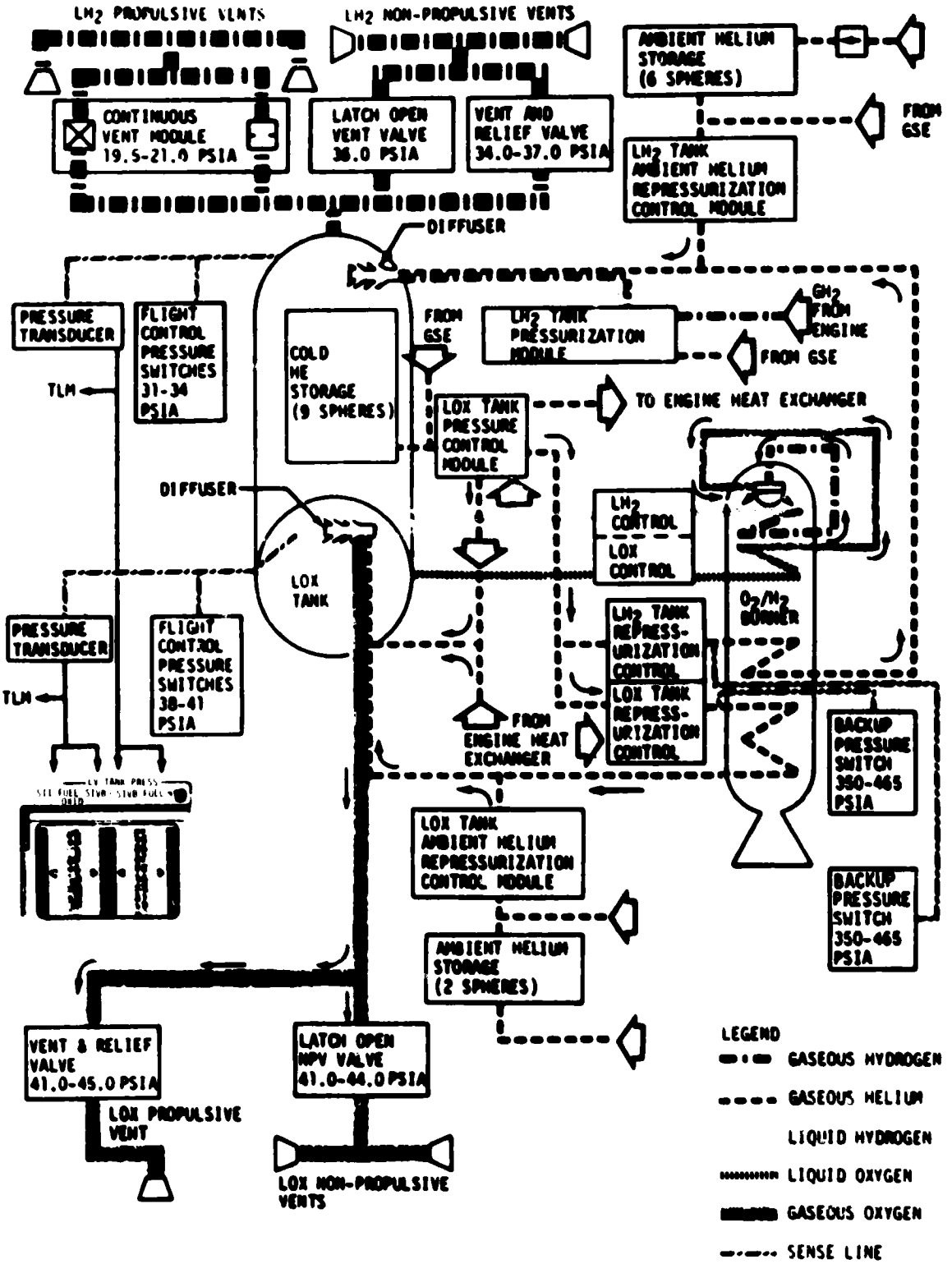

Figure 7-12. O_2/H_2 Burner Propellant Tanks Pressurization

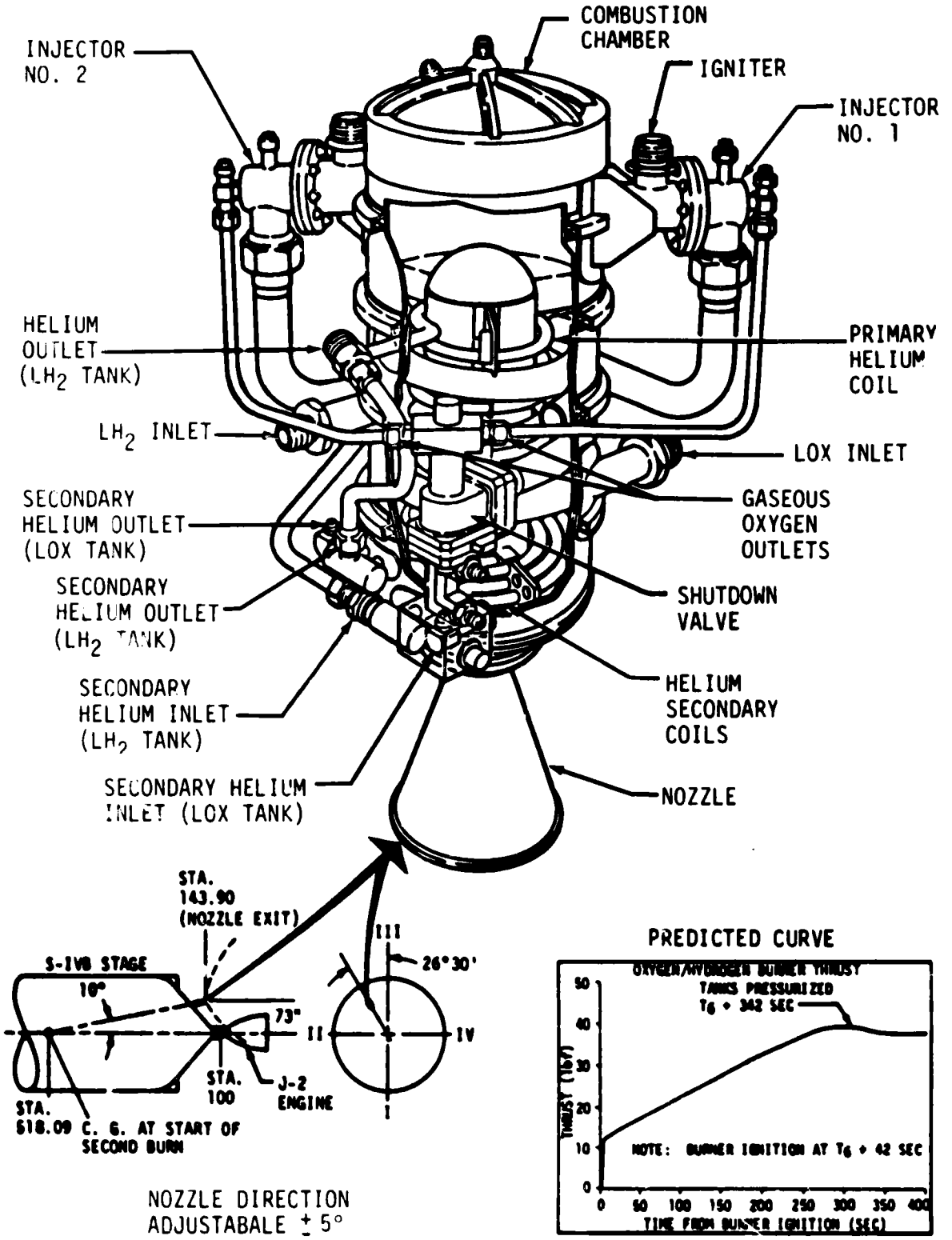

Figure 7-13. S-IVB Stage O_2/H_2 Burner

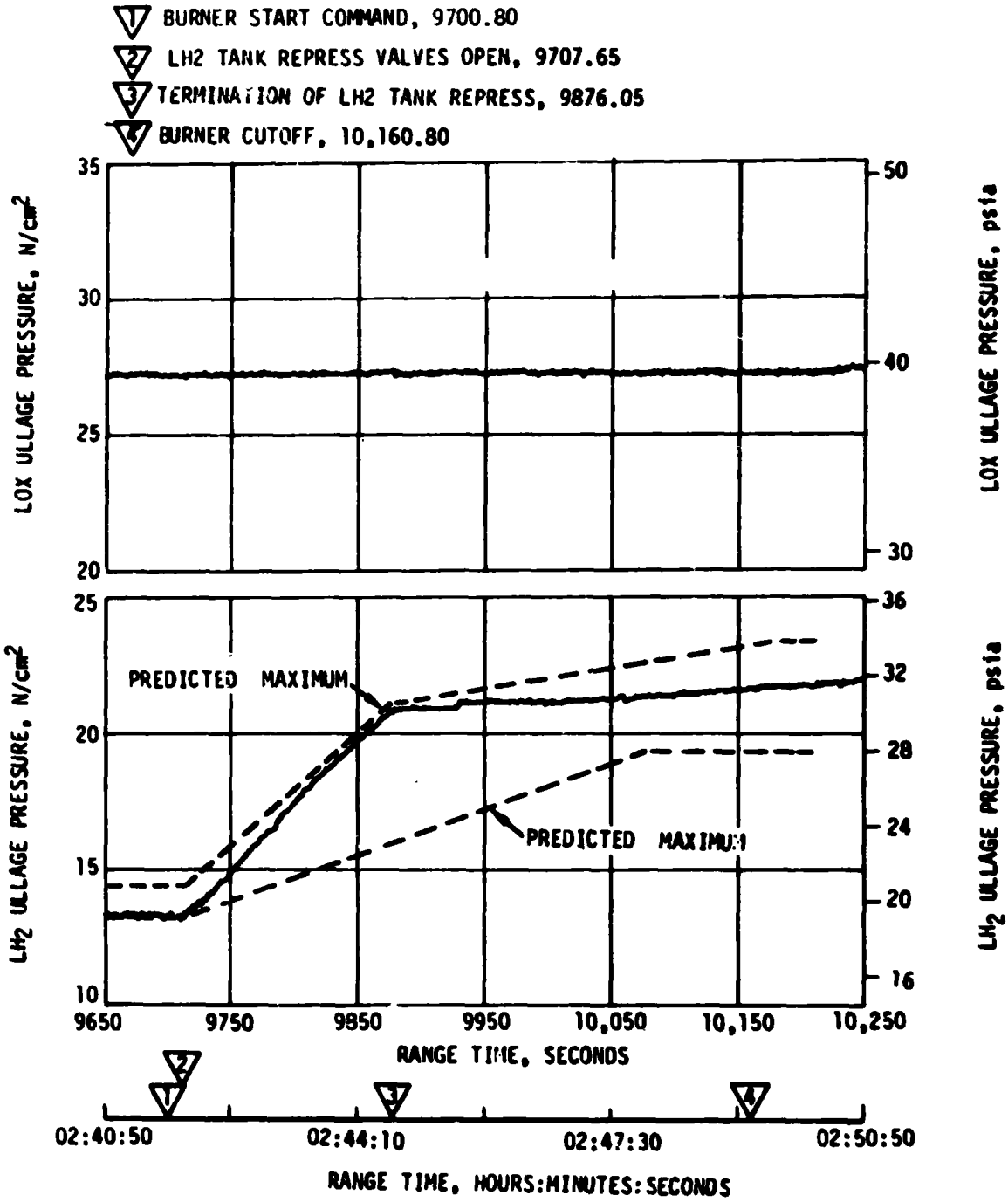

Figure 7-14. S-IVB Ullage Conditions During Repressurization Using O_2/H_2 Burner

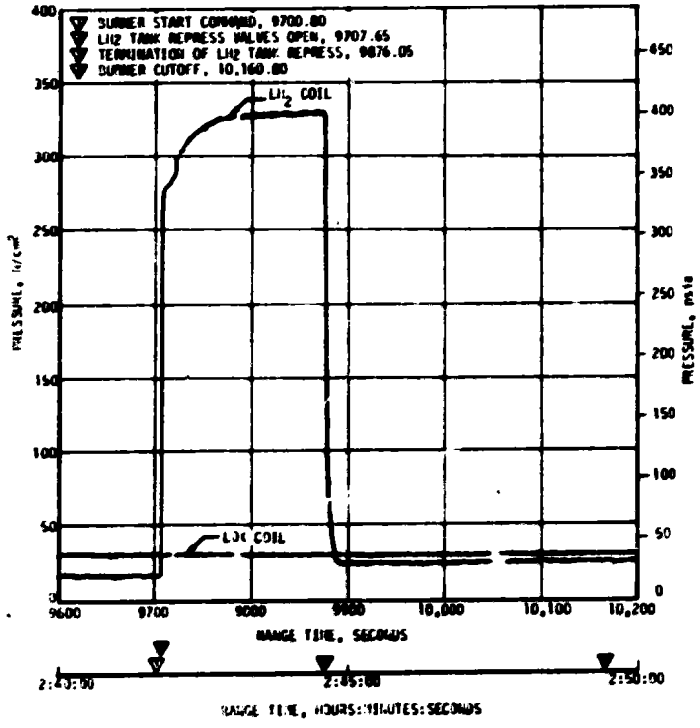

Figure 7-15. O_2/H_2 Burner LOX and LH_2 Pressurant Coil Pressure

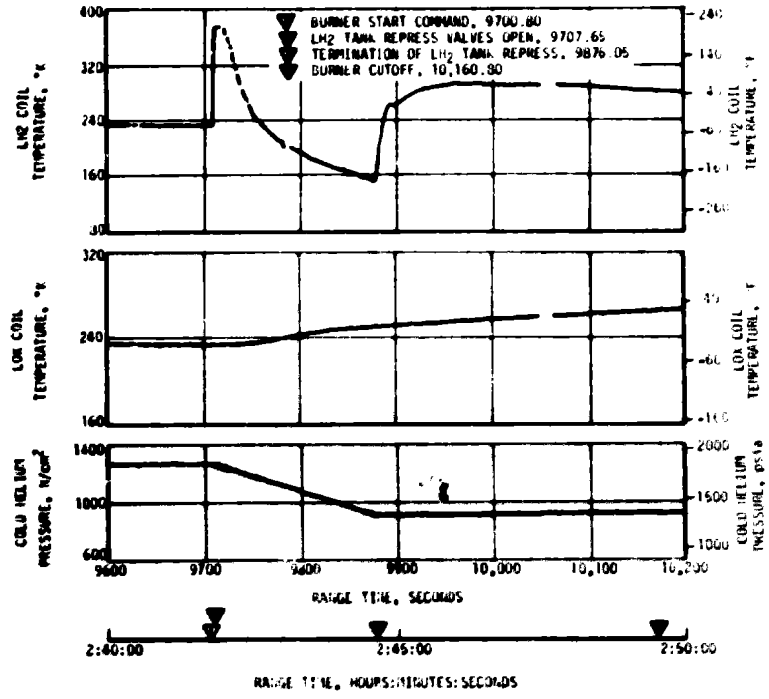

Figure 7-16. LOX and LH_2 Pressurant Coil Temperatures and Cold Helium Pressure

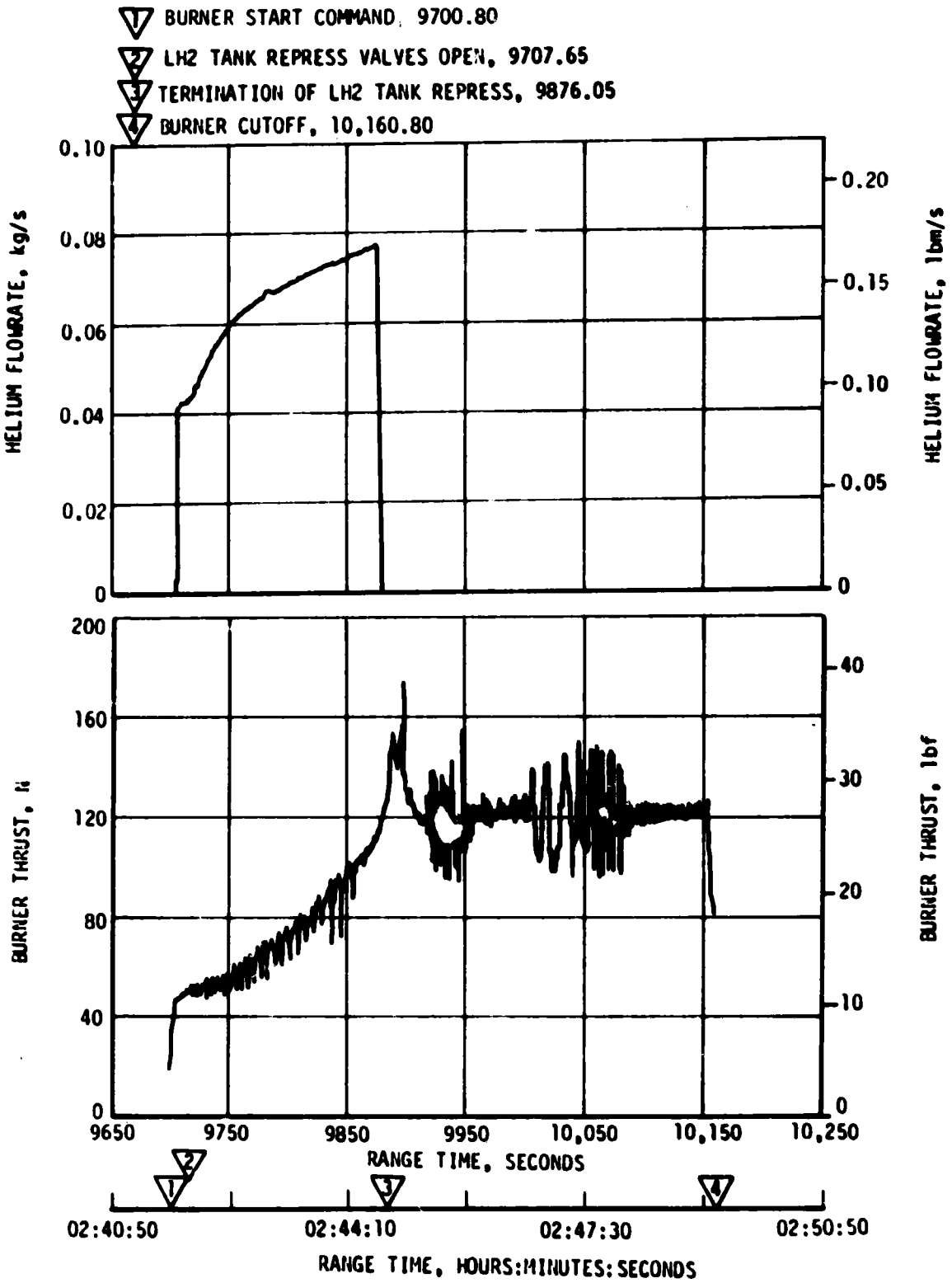

Figure 7-17. S-IVB O_2/H_2 Burner Thrust and Pressurant Flowrate

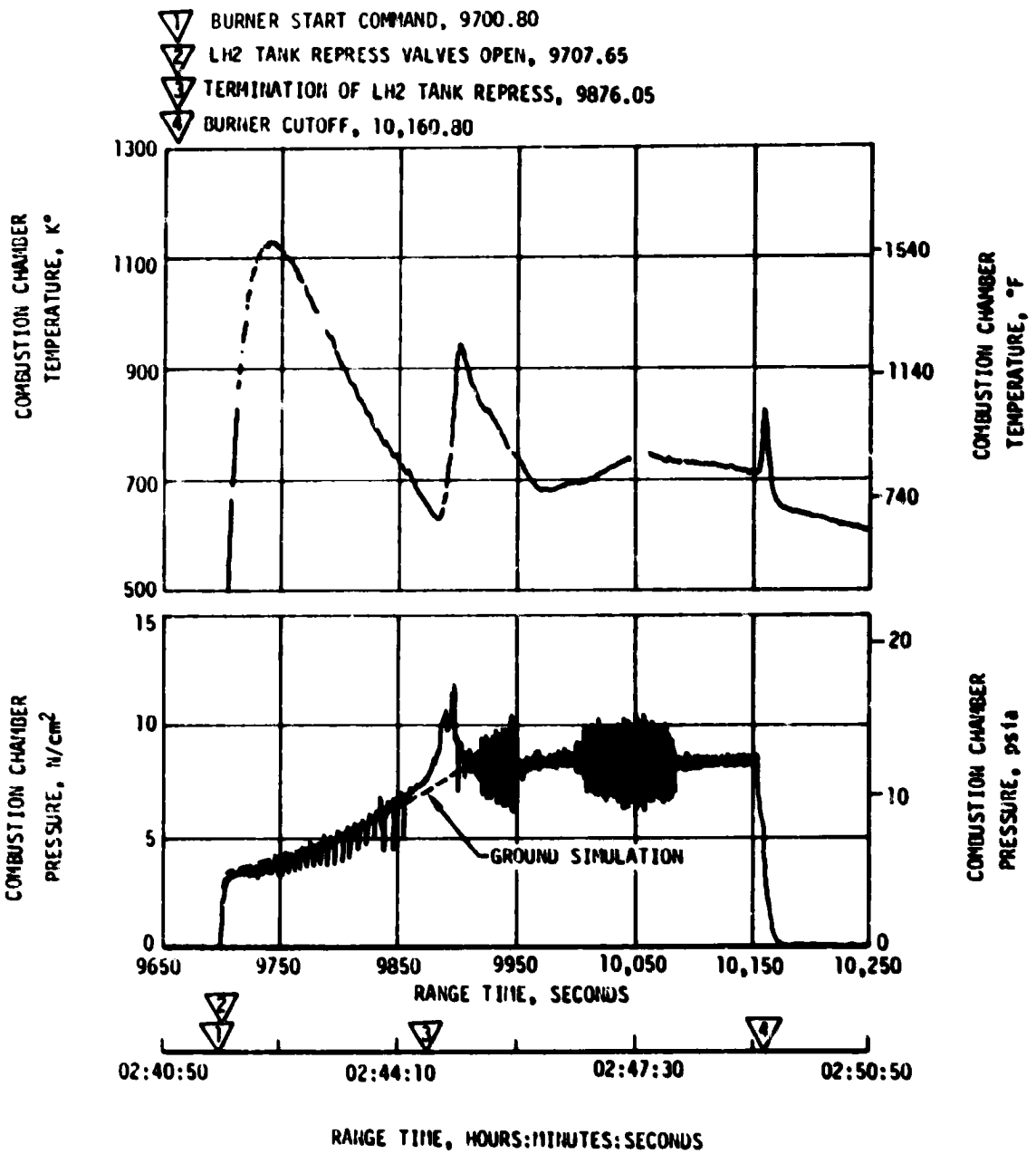

Figure 7-18. S-IVB O_2/H_2 Burner Chamber Pressure and Temperature

The S-IVB stage provided adequate conditioning of propellants to the J-2 engine for the restart attempt. The engine start sphere was recharged properly and maintained sufficient pressure during coast. The engine control sphere gas usage was as predicted during the first burn; the ambient helium spheres recharged the control sphere to a nominal level adequate for a proper restart.

Table 7-6, showing the major events during the start transient, indicates that all events occurred as required and performance was as predicted.

The propellant recirculation systems performed satisfactorily and met start and run box requirements for fuel and LOX as shown in Figure 7-19. Second burn fuel lead generally followed the predicted pattern and resulted in satisfactory conditions as indicated by the thrust chamber temperatures and the associated fuel injector temperatures shown in Figure 7-20. The LH_2 chilldown system performance for second burn was satisfactory. The LH_2 pump inlet temperature at second burn ESC was 22.5°K (-419.5°F). Second burn LOX pump chilldown was also satisfactory. At S-IVB second burn ESC the LOX pump inlet temperature was 91.9°K (-294.6°F). The start tank performed satisfactorily during the second burn blowdown and recharge sequence, as shown in Figure 7-21.

The second burn start transient was satisfactory. The thrust buildup was within the limits set by the engine manufacturer. Faster thrust buildup to the 90 percent level as compared to the acceptance test result was observed on this flight and is shown in Figure 7-22. This buildup was similar to the thrust buildup on AS-501 and AS-502. The PU valve was in the proper full open (4.5 EMR) position prior to the second start.

Table 7-6. S-IVB Engine Start Sequence - Second Burn

EVENT	TIME OF EVENT IN RANGE TIME, SECONDS	
	PREDICTED	ACTUAL
S-IVB Engine Restart Command (ESC)	10,228.83	10,229.51
S-IVB Engine Start Indication	10,228.83	10,229.52
STDV Open	10,236.63	10,237.79
Mainstage Control Solenoid	10,237.08	10,237.94
Mainstage OK	10,238.16	10,239.34
90 Percent Thrust	10,239.13	10,240.02
Main LOX Valve Open	10,239.18	10,240.32

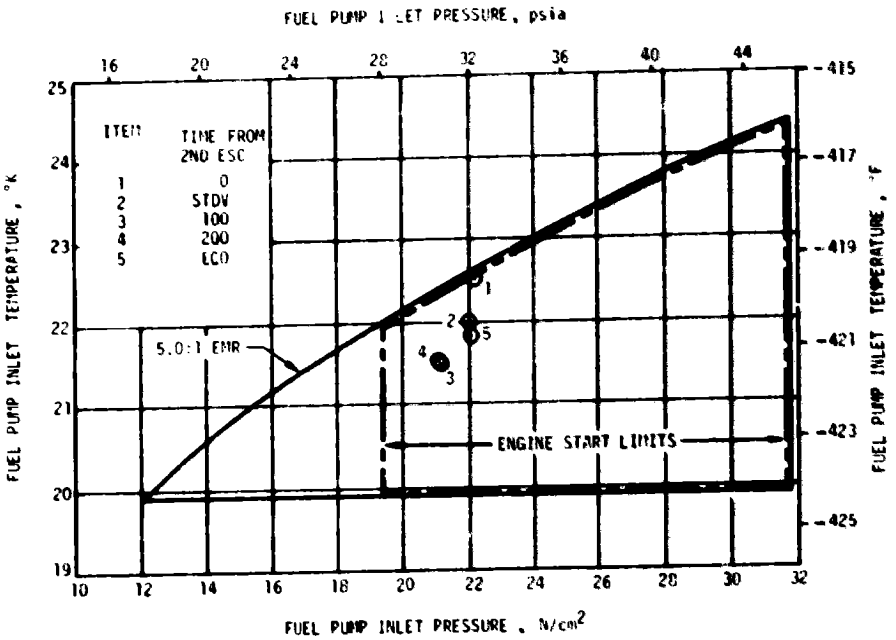

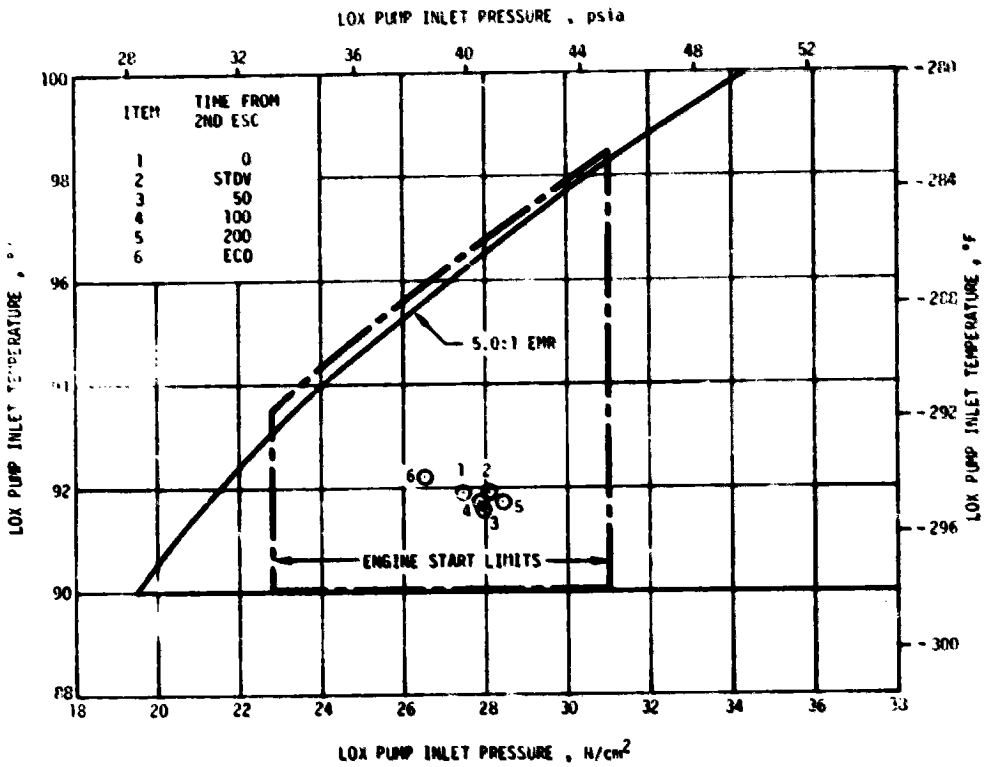

Figure 7-19. S-IVB Start Box and Run Requirements Restart

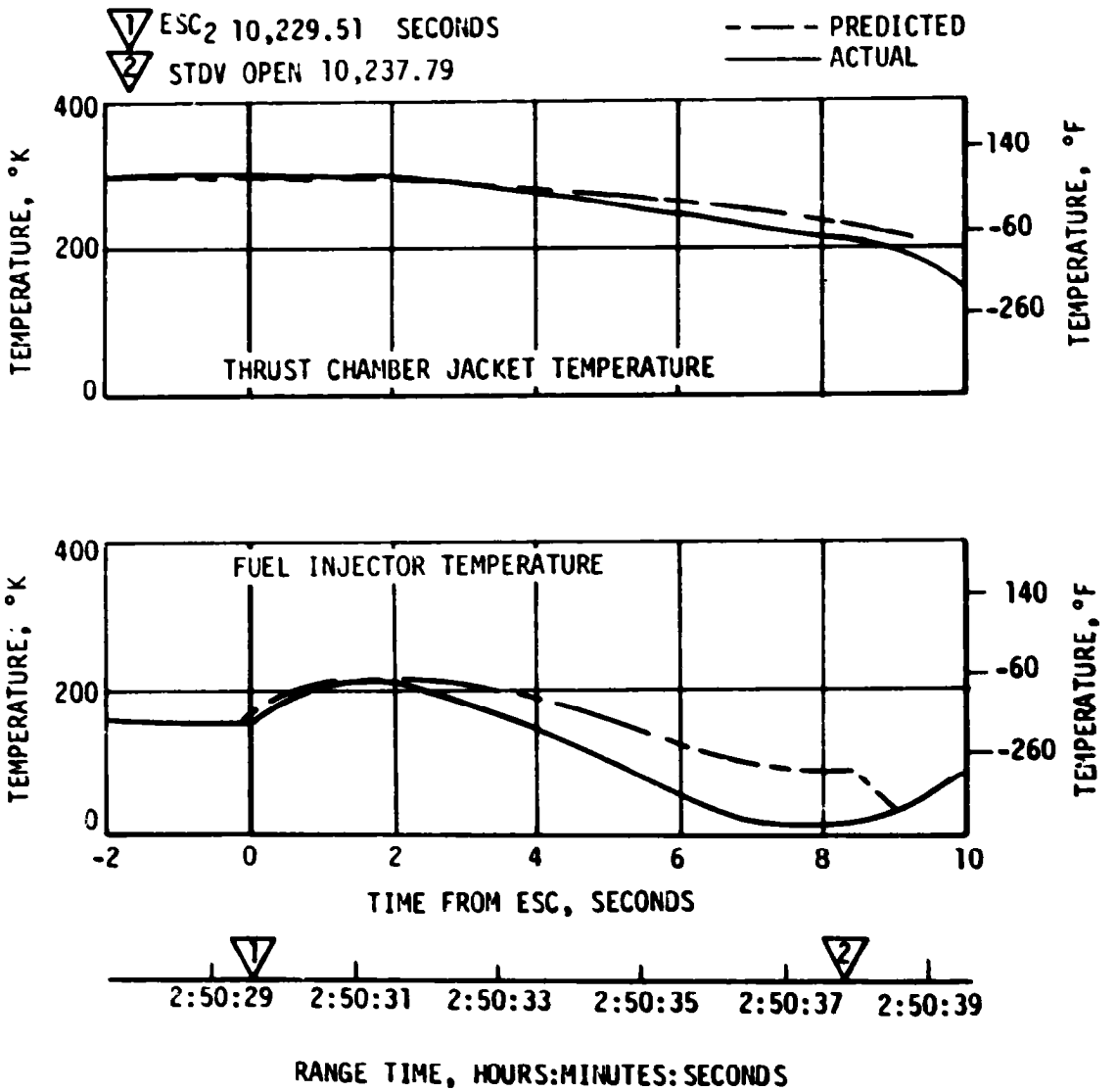

Figure 7-20. S-IVB J-2 Fuel Lead Restart - Second Burn

The total impulse from STDV to STDV +2.5 seconds was 821,124 N-s (184,596 lbf-s). This was greater than the value of 671,681 N-s (151,000 lbf-s) obtained during the same interval for the acceptance test.

The helium control system performed satisfactorily during second burn mainstage. There was little pressure decay during the burn due to the connection to the stage repressurization system. Helium usage was estimated from flowrates during engine operation. Approximately 0.19 kilogram (0.41 lbm) was consumed during second burn.

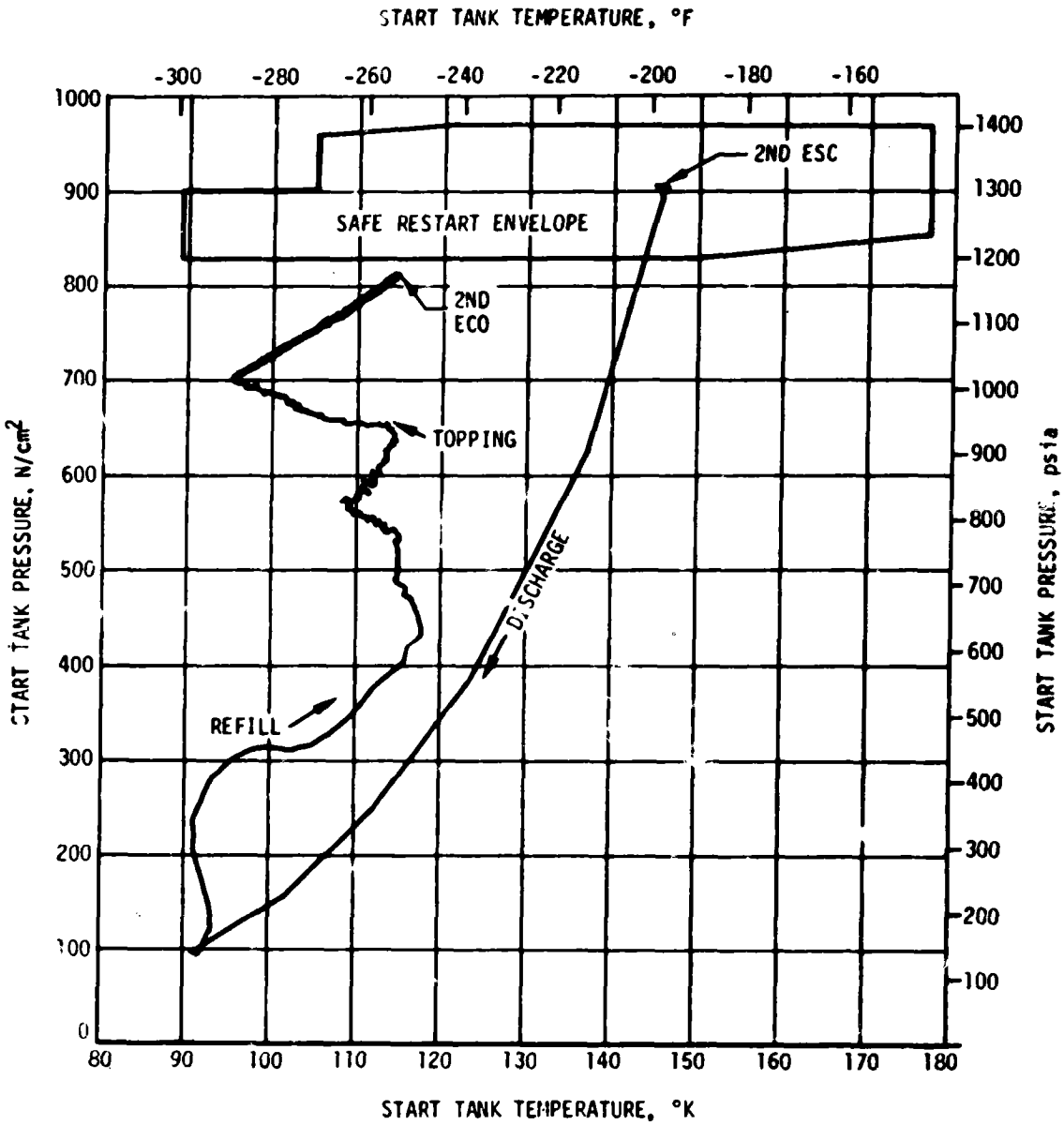

Figure 7-21. S-IVB Start Tank Performance - Second Burn

7.7 S-IVB MAIN STAGE PERFORMANCE FOR SECOND BURN

The propulsion reconstruction analysis showed that the stage performance during mainstage operation was satisfactory. A comparison of predicted and actual performance of thrust, total flowrate, specific impulse, and mixture ratio versus time is shown in Figure 7-23. Table 7-7 shows the specific impulse, flowrates and mixture ratio deviations from the predicted at the 80-second time slice. This time slice performance is the standardized altitude performance which is comparable to engine acceptance tests.

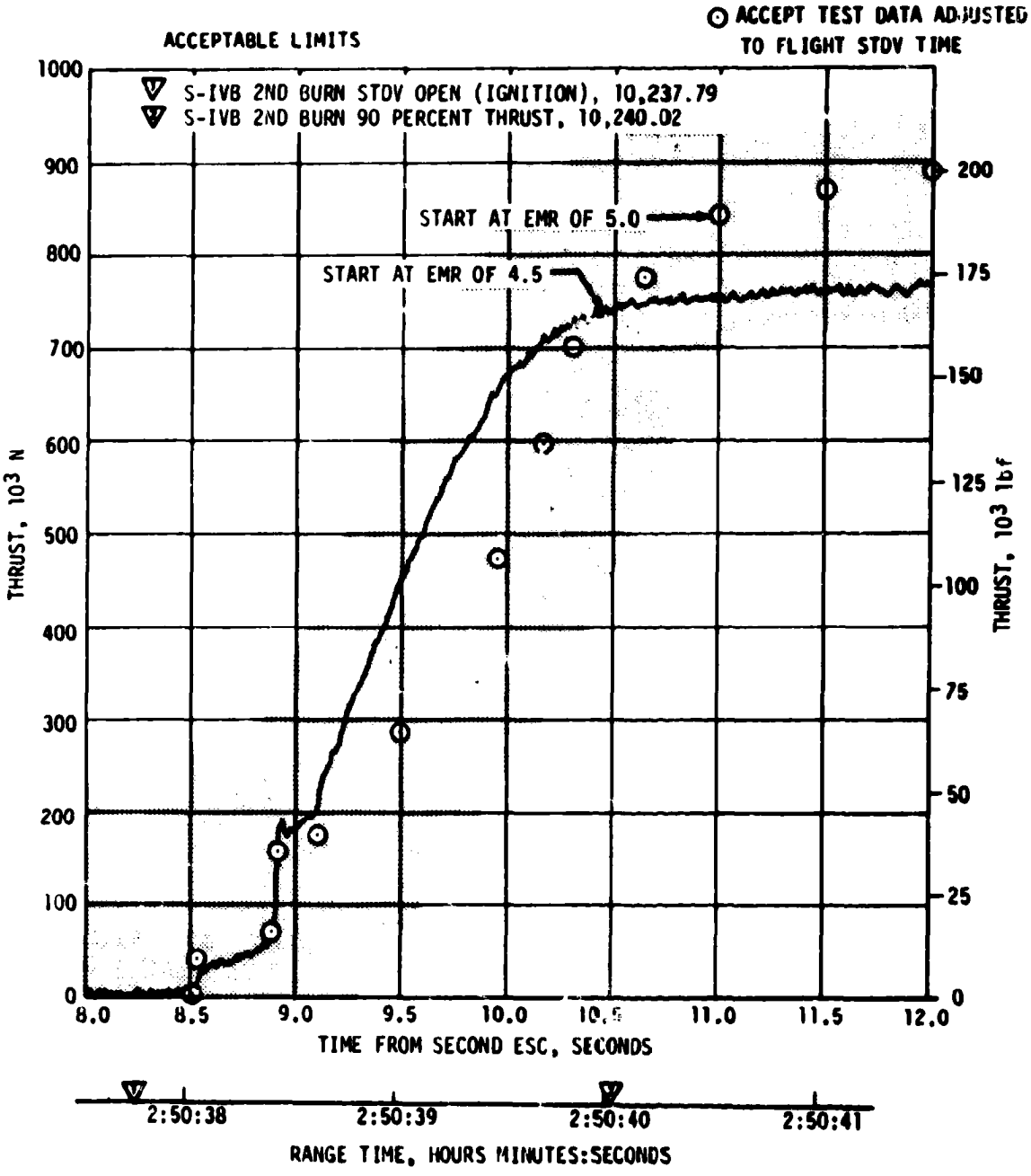

Figure 7-22. S-IVB Buildup Transients - Second Burn

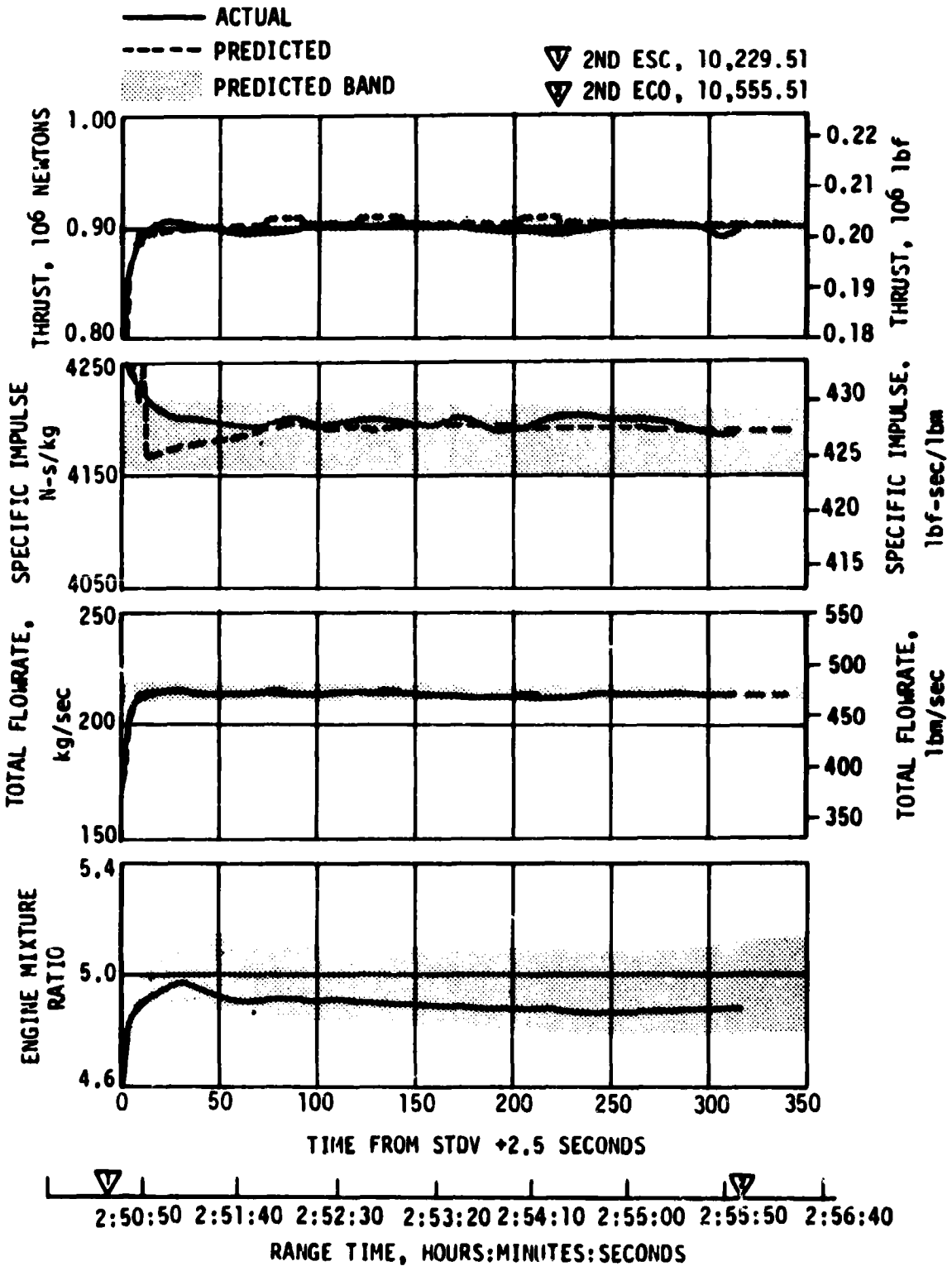

Figure 7-23. S-IVB Steady State Performance - Second Burn

The 80-second time slice performance for second burn thrust was 0.03 percent less than predicted. Specific impulse performance for second burn was 0.28 percent greater than predicted. A shift in performance occurred between first and second burn which resulted in an average lower level of thrust during second burn of 6775 Newtons (1523 lbf).

The overall propulsion reconstruction of longitudinal thrust compared to the predicted was -0.88 percent for second burn. Longitudinal specific impulse for second burn when compared to predicted was +0.26 percent.

The flight simulation analysis showed a increase of 0.22 percent, compared to the prediction, in specific impulse. Other comparisons are shown in Table 7-8.

S-IVB burn time was 2.07 seconds longer than predicted. Table 7-9 shows that the primary contributors to the longer burn time were deviations in thrust and initial mass for the S-IVB second burn portion of flight. The total contributors show a burn time deviation of 2.79 seconds. This is 0.72 second more than the actual deviation. The additional 0.72 second of burn time may be accounted for by uncertainties in preconditions of flight and uncertainties in the thrust average obtained from trajectory reconstruction.

Table 7-7. S-IVB Steady State Performance - Second Burn
(ESC + 80 Second Time Slice at Standard Altitude Conditions)

PARAMETER	PREDICTED	2ND BURN RECONSTRUCTION	FLIGHT DEVIATION	PERCENT DEVIATION FROM PREDICTED
Thrust N (lbf)	900,609 (202,465)	897,548 (201,777)	-3,061 (-688)	-0.03
Specific Impulse N-s/kg (lbf-s/lbm)	41,187.4 (427.0)	4199.2 (428.2)	11.8 (1.2)	0.28
LOX Flowrate kg/s (lbm/s)	178.89 (394.38)	177.70 (391.77)	-1.19 (-2.61)	-0.66
Fuel Flowrate kg/s (lbm/s)	36.17 (79.74)	36.01 (79.40)	-0.16 (-0.34)	-0.43
Engine Mixture Ratio LOX/Fuel	4.946	4.934	-0.012	-0.24

7.8 S-IVB SHUTDOWN TRANSIENT PERFORMANCE FOR SECOND BURN

S-IVB ECO was initiated at 10,555.51 seconds by a guidance velocity cutoff command which resulted in a 2.07-second longer than predicted second burn time. The transient was satisfactory and agreed closely with the acceptance test and predictions. The total cutoff impulse to zero percent of rated thrust was 184,463 N-s (41,469 lbf-s). Cutoff occurred with the PU valve in the null position. The MOV actuator temperature was 170°K (-153.7°F) at cutoff. The thrust during second cutoff is shown in Figure 7-24, and impulse data is included on Table 7-10.

7.9 S-IVB STAGE PROPELLANT UTILIZATION

On AS-503 the PU system was operated in the open-loop mode, which means the LOX flowrate is not controlled to insure simultaneous depletion of propellants. The PU system successfully accomplished the requirements associated with propellant loading.

A comparison of propellant mass values at critical flight events, as determined by various analyses, is presented in Table 7-11. The best estimate full load propellant masses were 0.04 percent lower for LOX and 0.10 percent higher for LH_2 than the predicted values, as shown in Table 3-4 of Launch Operations, Section 3. This deviation was well within the required loading accuracy. Figure 7-25 shows a graphical representation of the PU mass sensor nonlinearities during S-IVB powered flight.

Table 7-8. Comparison of S-IVB Stage Flight Reconstruction Data With Performance Simulation Results - Second Burn

PARAMETERS	UNITS	PREDICTED	FLIGHT RECONSTRUCTION	PERCENT DEV FROM PRED
		SECOND BURN FLIGHT AVERAGE	SECOND BURN FLIGHT AVERAGE	SECOND BURN FLIGHT AVERAGE
Longitudinal Vehicle Thrust	N (lbf)	904,412 (203,320)	896,450 (201,530)	-0.88
Vehicle Mass Loss Rate	kg/s (lbm/s)	214.73 (473.40)	213.34 (470.33)	-0.65
Longitudinal Vehicle Specific Impulse	N-s/kg (lbf-s/lbm)	4191.4 (427.4)	4202.1 (428.5)	0.26
PARAMETERS	**UNITS**	**FLIGHT SIMULATION**	**PERCENT DEV FROM PRED**	
		SECOND BURN FLIGHT AVERAGE	SECOND BURN FLIGHT AVERAGE	
Longitudinal Vehicle Thrust	N (lbf)	895,841 (201,393)	-0.90	
Vehicle Mass Loss Rate	kg/s (lbm/s)	214.22 (472.27)	-0.24	
Longitudinal Vehicle Specific Impulse	N-s/kg (lbf-s/lbm)	4182.14 (426.46)	-0.22	

Table 7-9. S-IVB Simulation Burn Time Deviations - Second Burn

CONTRIBUTOR	BURN TIME DELTA (SECONDS)
S-IVB Thrust	1.04
S-IVB Mass Flow	0.43
S-IVB Initial Mass	1.32
	Explained 2.79 Unexplained -0.72

The third stage statistical weighted average masses at ignition were 161,398 and 126,867 kilograms (355,821 and 279,694 lbm) and the cutoff masses were 128,126 and 59,254 kilograms (282,469 and 130,633 lbm) for first and second burns, respectively. Extrapolation of propellant level sensor data to depletion, using the propellant flowrates to depletion, indicated that a LOX depletion would have occurred approximately 19.24 seconds after second burn velocity cutoff.

During first burn the PU valve was positioned at null for start and remained there, as programmed, during first burn. The PU valve was commanded to the 4.5 EMR position 119.91 seconds prior to second burn start command, and remained there for 132.89 seconds. At 10,242.49 seconds the valve was commanded to the null position (approximately 5.0 EMR) and remained there throughout the remainder of the flight. The actual times are within 50 milliseconds of predicted.

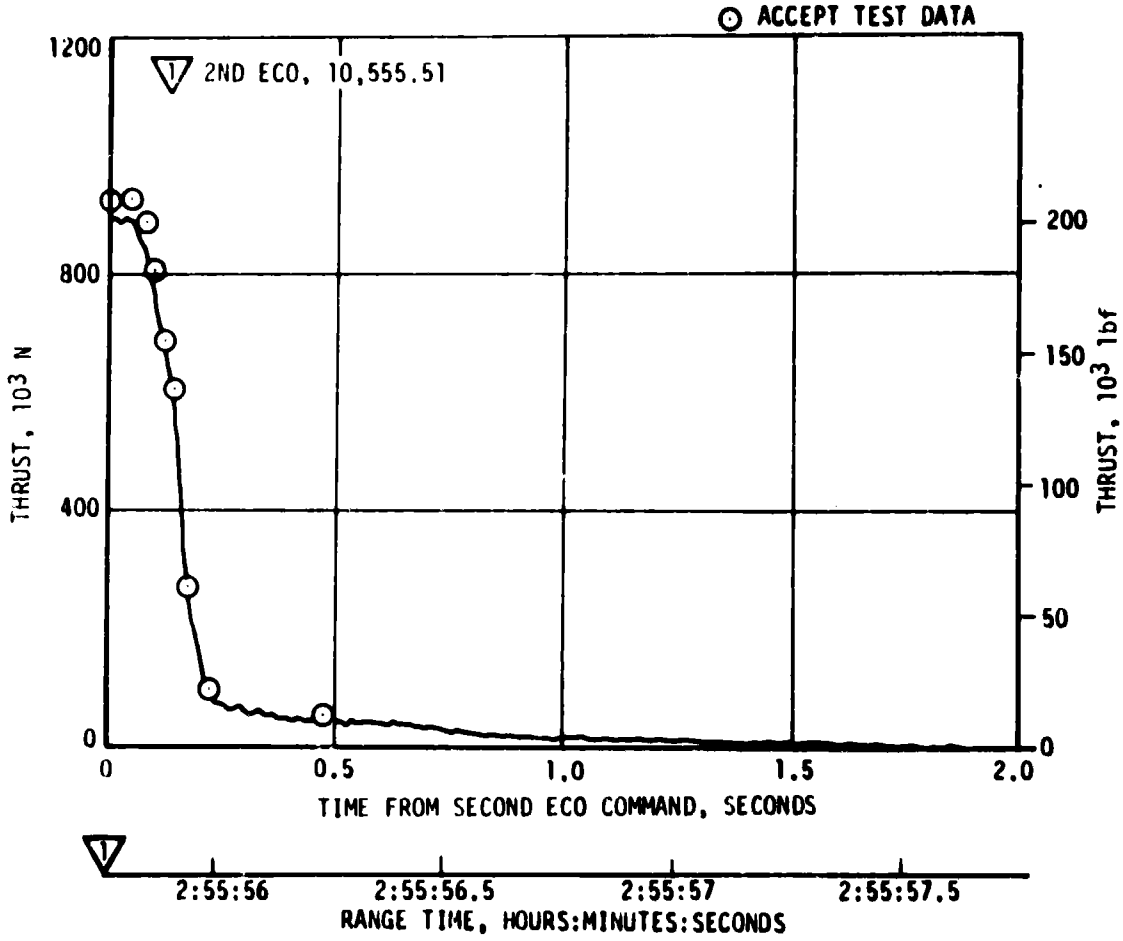

Figure 7-24. S-IVB Shutdown Transient Performance - Second Burn

Table 7-10. S-IVB Cutoff Impulse - Second Burn

PARAMETER		PREDICTED	FLIGHT		PERCENT DEVIATION FROM PREDICTED	
			ENGINE	GUID. DATA	ENGINE	GUID. DATA
Cutoff Impulse	N-s (lbf-s)	223,456 (50,235)	184,463 (41,469)	227,286 (51,096)	-17.45	1.71
Velocity Increase	m/s (ft/s)	3.80 (12.47)	3.12 (10.24)	3.84 (12.60)	-17.89	1.05

Note: The parameters quoted are from velocity cutoff command to zero percent of rated thrust.

Table 7-11. S-IVB Stage Propellant Mass History

EVENT		PREDICTED		PU INDICATED (CORRECTED)		PU VOLUMETRIC		LEVEL SENSOR* (EXTRAPOLATED)		FLOW INTEGRAL		BEST ESTIMATE	
		LOX	LH_2	LOX	LH_2	LOX	LH_2	LOX	LH_2	LOX	LH_2	LOX	LH_2
S-IC Liftoff	kg	87,508	19,665	87,512	19,678	87,430	19,773	-	-	87,501	19,611	87,470	19,684
	(lbm)	(192,923)	(43,353)	(192,930)	(43,383)	(192,750)	(43,593)	-	-	(192,906)	(43,235)	(192,840)	(43,395)
1st Ignition (ESC)	kg	87,508	19,665	87,512	19,678	87,430	19,773	-	-	87,501	19,607	87,470	19,684
	(lbm)	(192,923)	(43,353)	(192,930)	(43,383)	(192,750)	(43,593)	-	-	(102,906)	(43,225)	(192,840)	(43,395)
1st Cutoff (ECO)	kg	59,351	13,931	59,923	13,878	60,039	13,920	-	-	59,791	13,890	59,974	13,915
	(lbm)	(130,846)	(30,712)	(132,108)	(30,596)	(132,363)	(30,688)	-	-	(131,816)	(30,623)	(132,220)	(30,678)
2nd Ignition (ESC)	kg	59,201	12,742	59,811	12,808	59,815	12,937	-	-	59,679	12,820	59,862	12,865
	(lbm)	(130,516)	(28,091)	(131,861)	(28,236)	(131,870)	(28,522)	-	-	(131,569)	(28,263)	(131,975)	(28,358)
2nd Cutoff (ECO)	kg	3,084	1,271	3,652	1,270	3,666	1,279	3,572	1,204	3,619	1,242	3,658	1,251
	(lbm)	(6,798)	(2,802)	(8,051)	(2,800)	(8,083)	(2,821)	(7,874)	(2,654)	(7,979)	(2,738)	(8,064)	(2,759)

NOTE: Mass in and below the tank

* Due to instrumentation reduction on this flight, only the data presented is available.

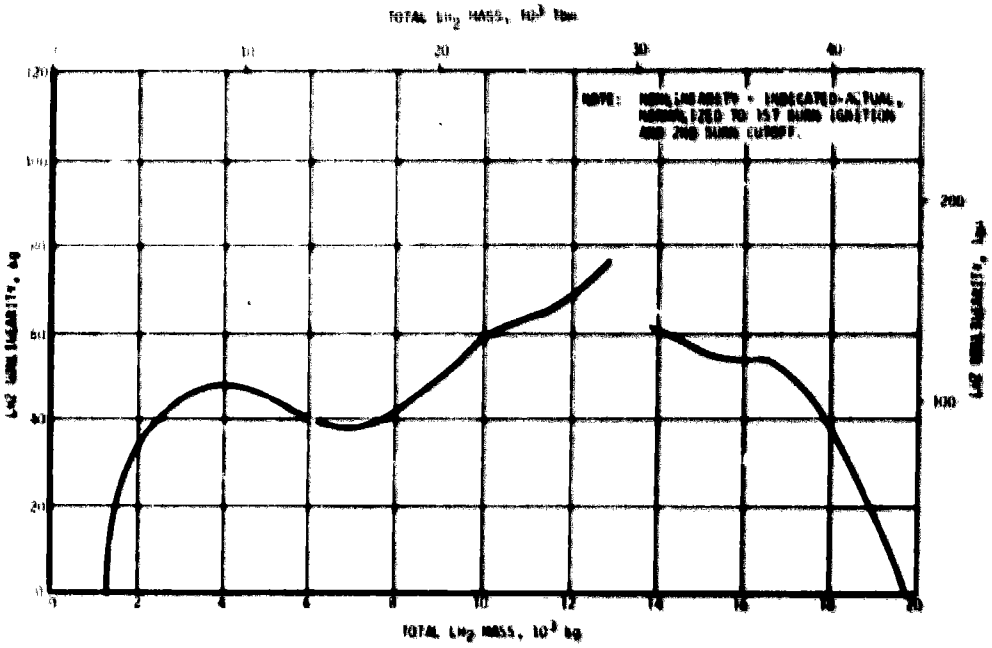

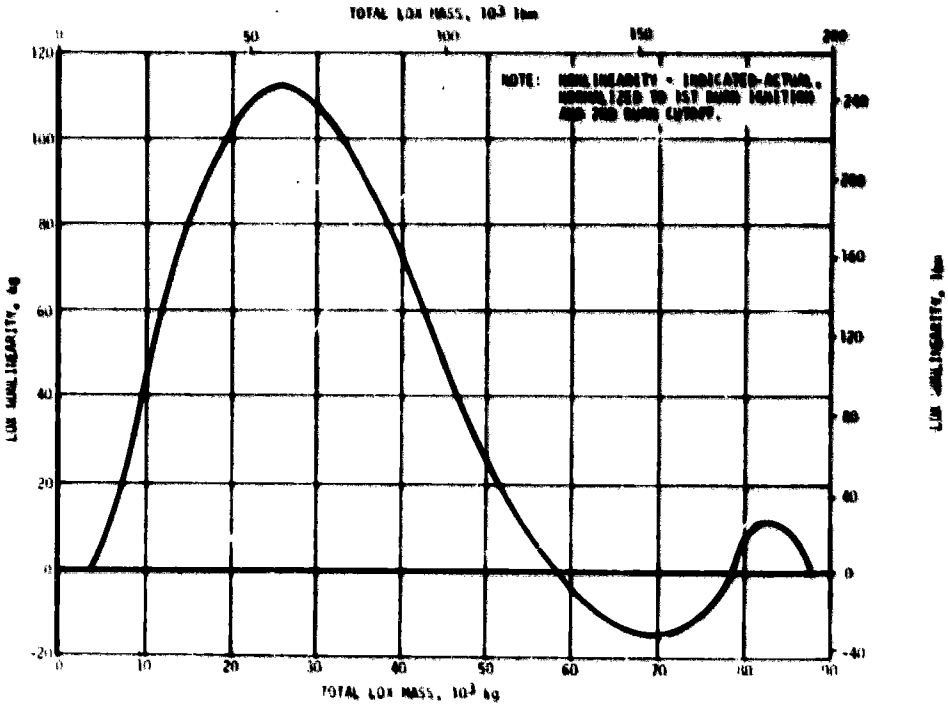

Figure 7-25. S-IVB PU System Nonlinearities

7.10 S-IVB PRESSURIZATION SYSTEM

7.10.1 S-IVB LH_2 Tank Pressurization System

The LH_2 pressurization system operationally met all engine performance requirements. The LH_2 pressurization system indicated acceptable performance during prepressurization, boost, first burn, coast phase, and second burn. The sequence of events and associated system performances are discussed in the following paragraphs. The LH_2 tank prepressurization command was received at -96.4 seconds. The pressurized signal was received 12.9 seconds later.

Following the termination of prepressurization, the ullage pressure reached relief conditions, approximately 21.8 N/cm^2 (31.7 psia) and remained at that level until liftoff as shown in Figure 7-26. A small ullage collapse occurred during the first 70 seconds of boost, and then returned to the relief level by 150 seconds due to self pressurization.

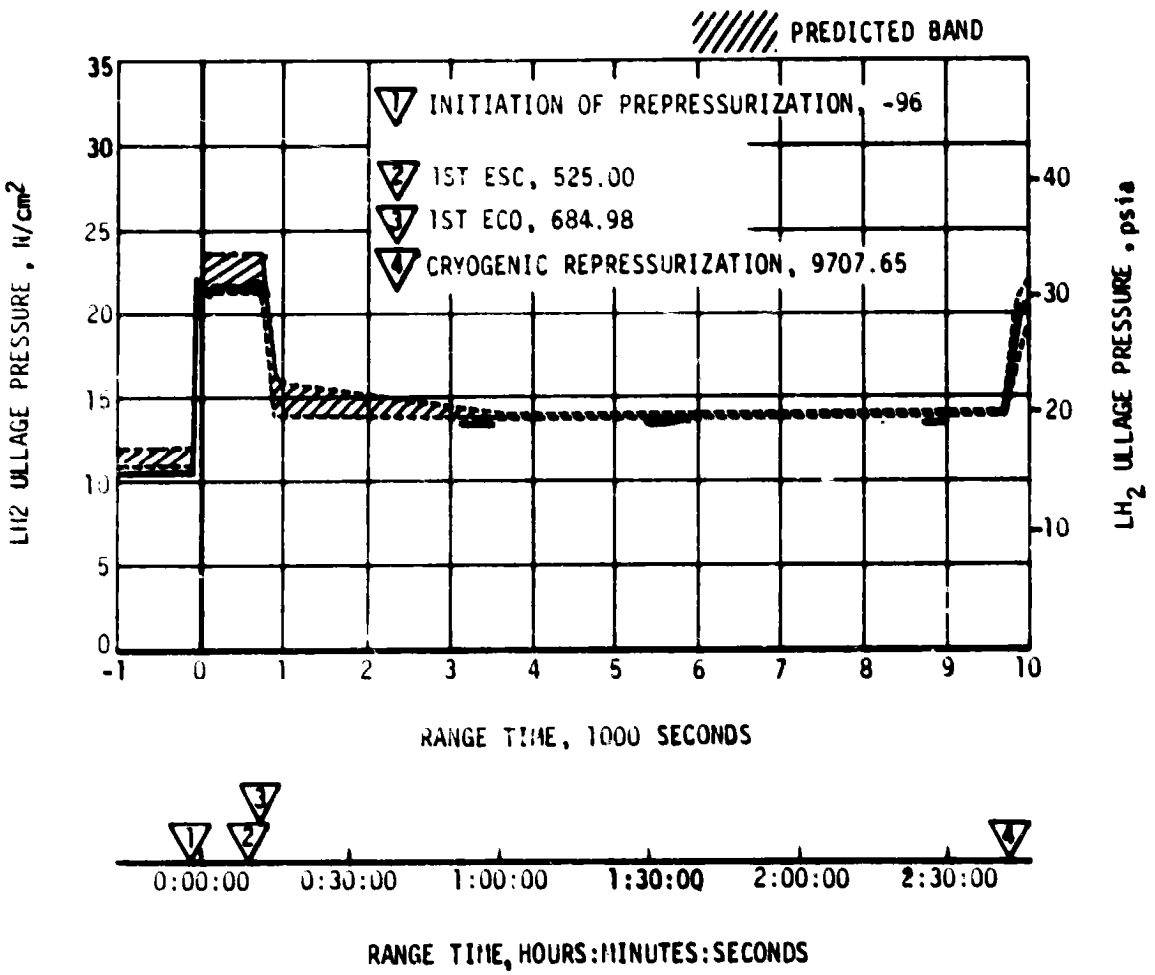

Figure 7-26. S-IVB LH_2 Ullage Pressure - First Burn and Parking Orbit

During first burn, the average pressurization flowrate was approximately 0.31 kg/s (0.69 lbm/s) providing a total flow of 48.5 kilograms (107 lbm). All during the burn the ullage pressure was at the relief level, as predicted.

During O_2/H_2 burner repressurization period, the LH_2 tank was pressurized from 13.3 to 20.8 N/cm^2 (19.3 to 30.2 psia). The LH_2 ullage pressure was 21.7 N/cm^2 (31.5 psia) at second burn ESC as shown in Figure 7-27. Approximately 11.3 kilograms (25.0 lbm) of helium were used in the repressurization operation. The average second burn pressurization flowrate was 0.30 kg/s (0.67 lbm/s) until step pressurization when it increased to 0.48 kg/s (1.06 lbm/s). This provided a total flow of 106 kilograms (234 lbm) during second burn. Significant venting during second burn occurred at second ESC + 280 seconds when step pressurization was initiated. This behavior was as predicted.

The LH_2 pump inlet NPSP was calculated from the pump interface temperature and total pressure. These values indicated that the NPSP at first burn ESC was 13.2 N/cm^2 (19.2 psia). At the minimum point, the NPSP was 5.6 N/cm^2 (8.1 psid) above the required. Throughout the burn, the NPSP had satisfactory agreement with the predicted. The NPSP at second burn ESC was 3.4 N/cm^2 (4.9 psia) which was 0.14 N/cm^2 (0.2 psid) above the required. Figures 7-28 and 7-29 summarize the fuel pump inlet conditions for first and second burns, respectively.

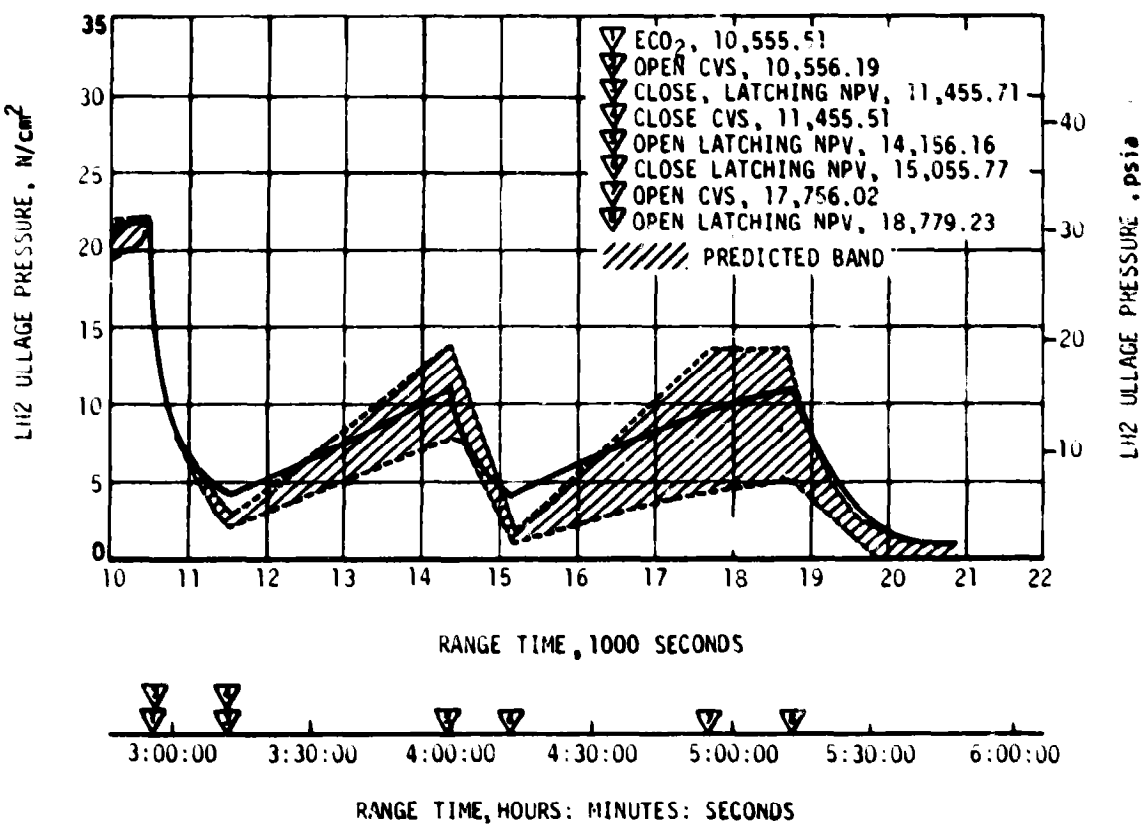

Figure 7-27. S-IVB LH_2 Ullage Pressure - Second Burn and Translunar Coast

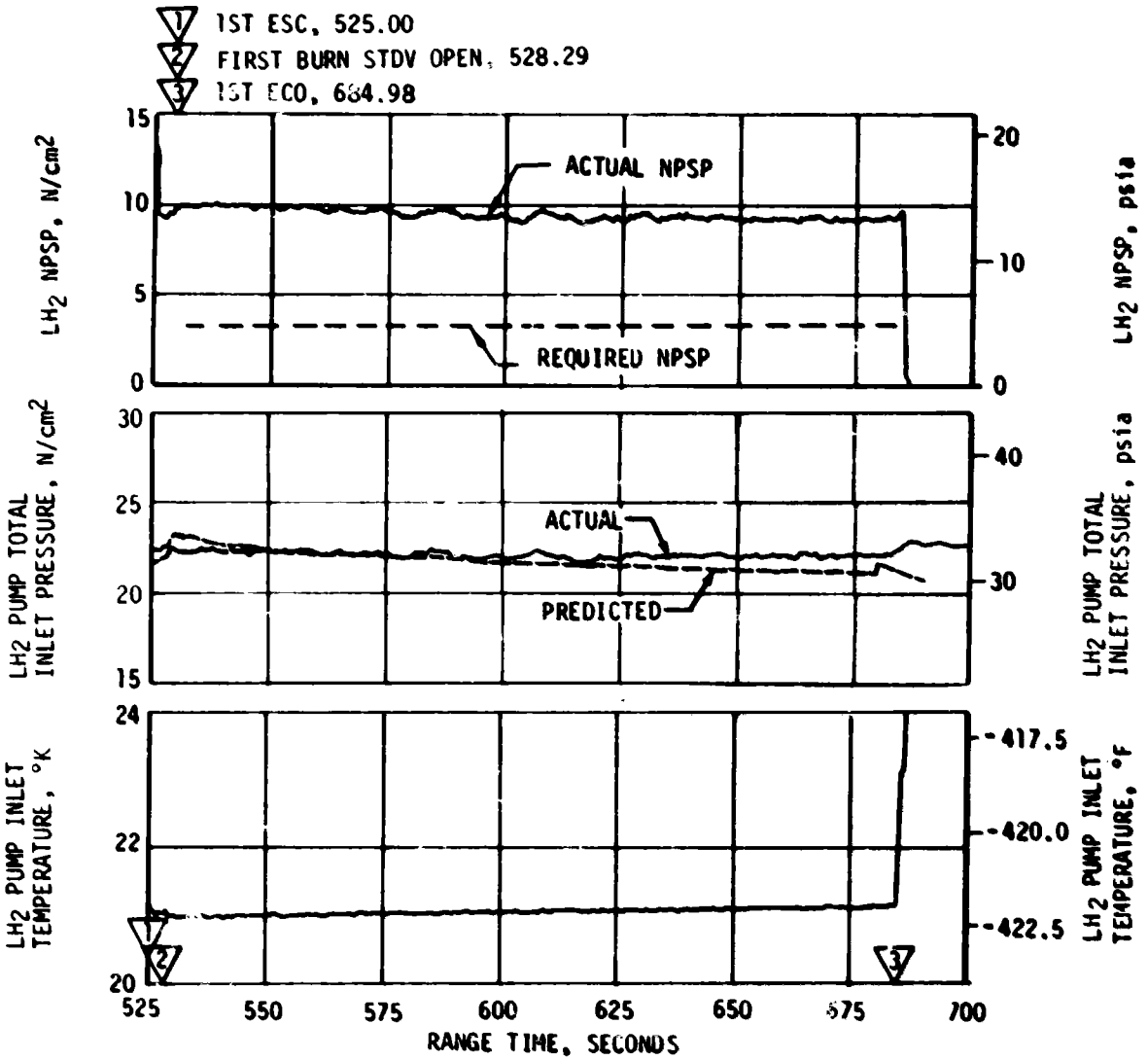

Figure 7-28. S-IVB Fuel Pump Inlet Conditions - First Burn

7.10.2 S-IVB LOX Pressurization System

LOX tank prepressurization was initiated at -167 seconds and increased the LOX tank ullage pressure from ambient to 27.9 N/cm^2 (40.5 psia) within 17 seconds as shown in Figure 7-30. Three makeup cycles were required to maintain the LOX tank ullage pressure before the ullage temperature stabilized. At -96 seconds the LOX tank ullage pressure increased from 27.0 to 29.1 N/cm^2 (39.1 to 42.2 psia) due to fuel tank prepressurization, LOX tank vent purge, and LOX pressure sense line purge. This caused the vent/relief valve to open, dropping the pressure down to 28.8 N/cm^2 (41.8 psia). The pressure remained at this level until liftoff.

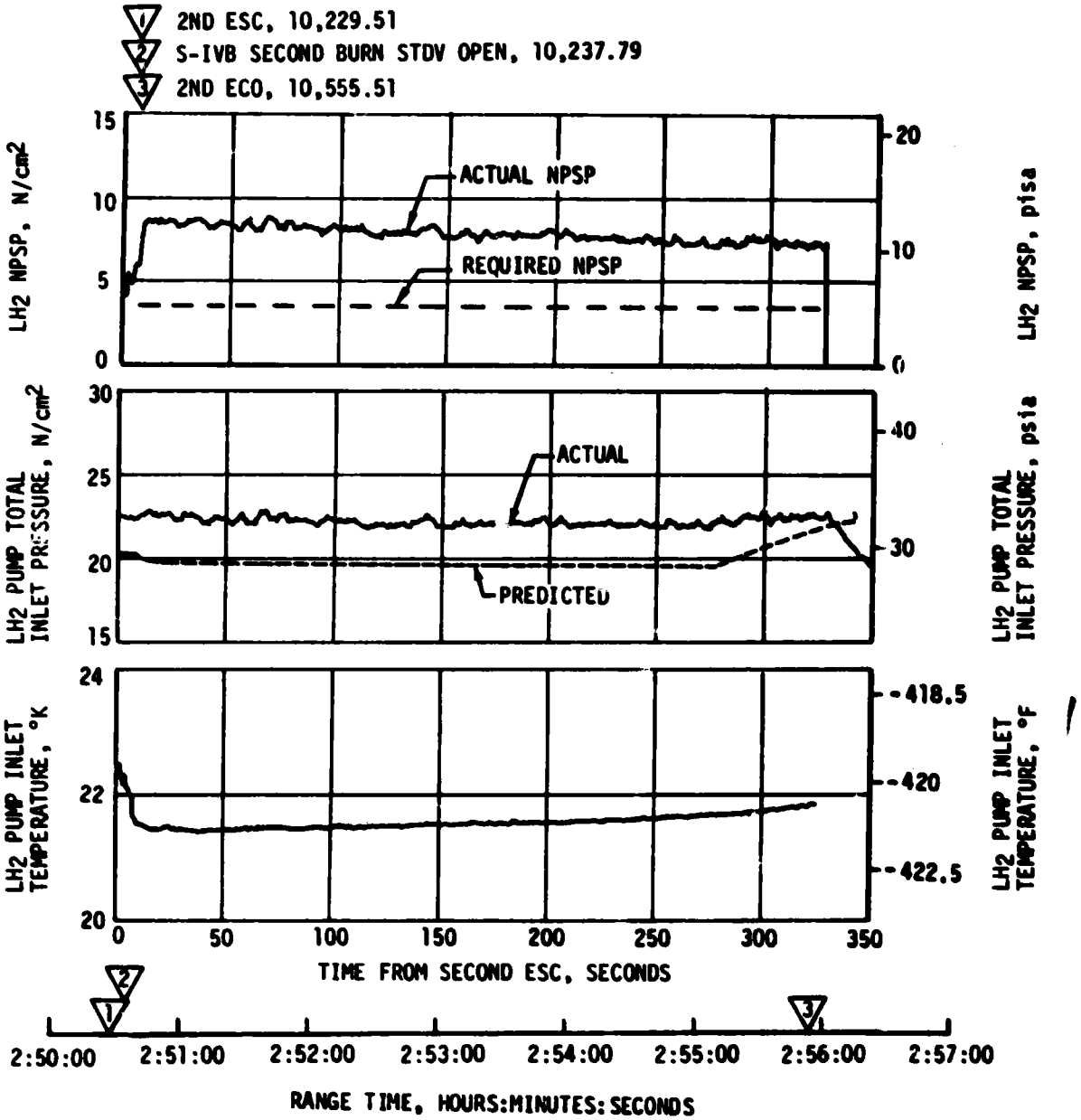

Figure 7-29. S-IVB Fuel Pump Inlet Conditions - Second Burn

During S-IC boost there was a relatively high rate of ullage pressure decay caused by an acceleration effect and temperature collapse, the decay necessitated two makeup cycles from the cold helium spheres as shown in Figure 7-30.

No makeup cycles were required during S-II boost. Although ullage cooling continued during this period, the major cause of the decay again appears to be response to the vehicle acceleration. The LOX tank ullage pressure was 27.8 N/cm^2 (40.4 psia) at ESC.

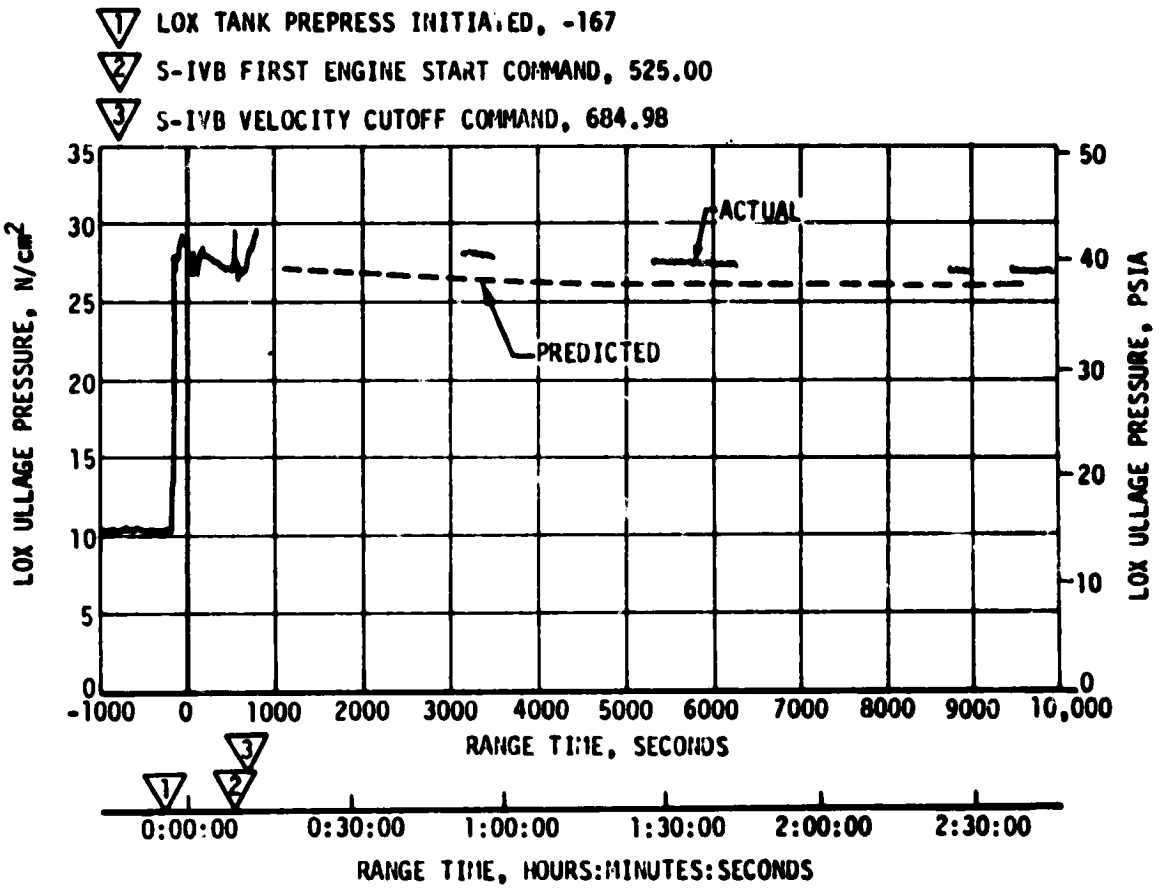

Figure 7-30. S-IVB LOX Tank Ullage Pressure - First Burn and Parking Orbit

During first burn, only one over-control cycle was initiated, as compared to the predicted four cycles. The reason for this performance is that this stage was the first to fly larger flow control orifices and the revised flight pressurization control sequence. This was compounded because, at 5.0 EMR, the energy available in the J-2 heat exchanger is altered. The LOX tank pressurization flowrate variation was 0.18 to 0.19 kg/s (0.40 to 0.42 lbm/s) during under-control system operation. This variation is normal because the bypass orifice inlet temperature changes as it follows the cold helium sphere temperature. Heat exchanger performance during first burn was satisfactory.

Repressurization of the LOX tank prior to second burn was not required. The tank ullage pressure was 26.9 N/cm^2 (39.0 psia) at second ESC, satisfying the engine start requirements as shown in Figure 7-31.

Pressurization system performance during second burn was satisfactory, having the same characteristics noted during first burn. There were no over-control cycles as compared to three predicted. Flowrate varied between 0.16 and 0.20 kg/s (0.35 to 0.45 lbm/s). Heat exchanger performance was satisfactory.

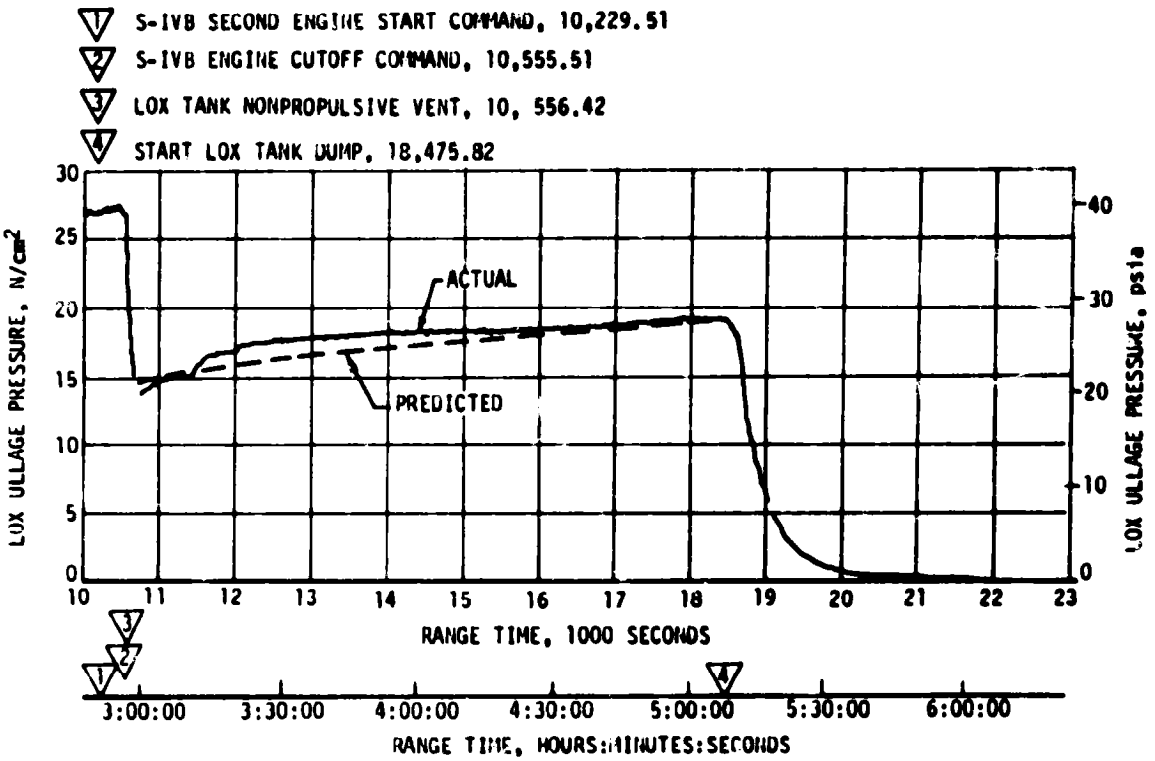

Figure 7-31. S-IVB LOX Tank Ullage Pressure - Second Burn and Translunar Coast

The LOX NPSP calculated at the interface was 17.9 N/cm^2 (25.8 psi) at first burn ESC. The NPSP decreased after start and reached a minimum value of 16.8 N/cm^2 (24.3 psi) at 51 seconds after ESC. This was 6.3 N/cm^2 (9.2 psi) above the required NPSP at that time.

The LOX pump static interface pressure during first burn followed the cyclic trends of the LOX tank ullage pressure. The NPSP calculated at the engine interface was 15.2 N/cm^2 (22.0 psia) at second burn ESC. At all times during second burn, NPSP was above the required level. Figures 7-32 and 7-33 summarize the LOX pump conditions for the first burn and the second burn, respectively. The run requirements for first and second burn were satisfactorily met as previously presented.

The cold helium supply was adequate to meet all flight requirements. At first burn ESC the cold helium spheres contained 171 kilograms (376 lbm) of helium. At the end of the first burn, the helium mass had decreased to 147 kilograms (323 lbm). Figure 7-34 shows helium supply pressure history.

7.11 S-IVB PNEUMATIC CONTROL SYSTEM

The pneumatic control and purge system performed satisfactorily during all phases of the mission. System performance was nominal during boost and first

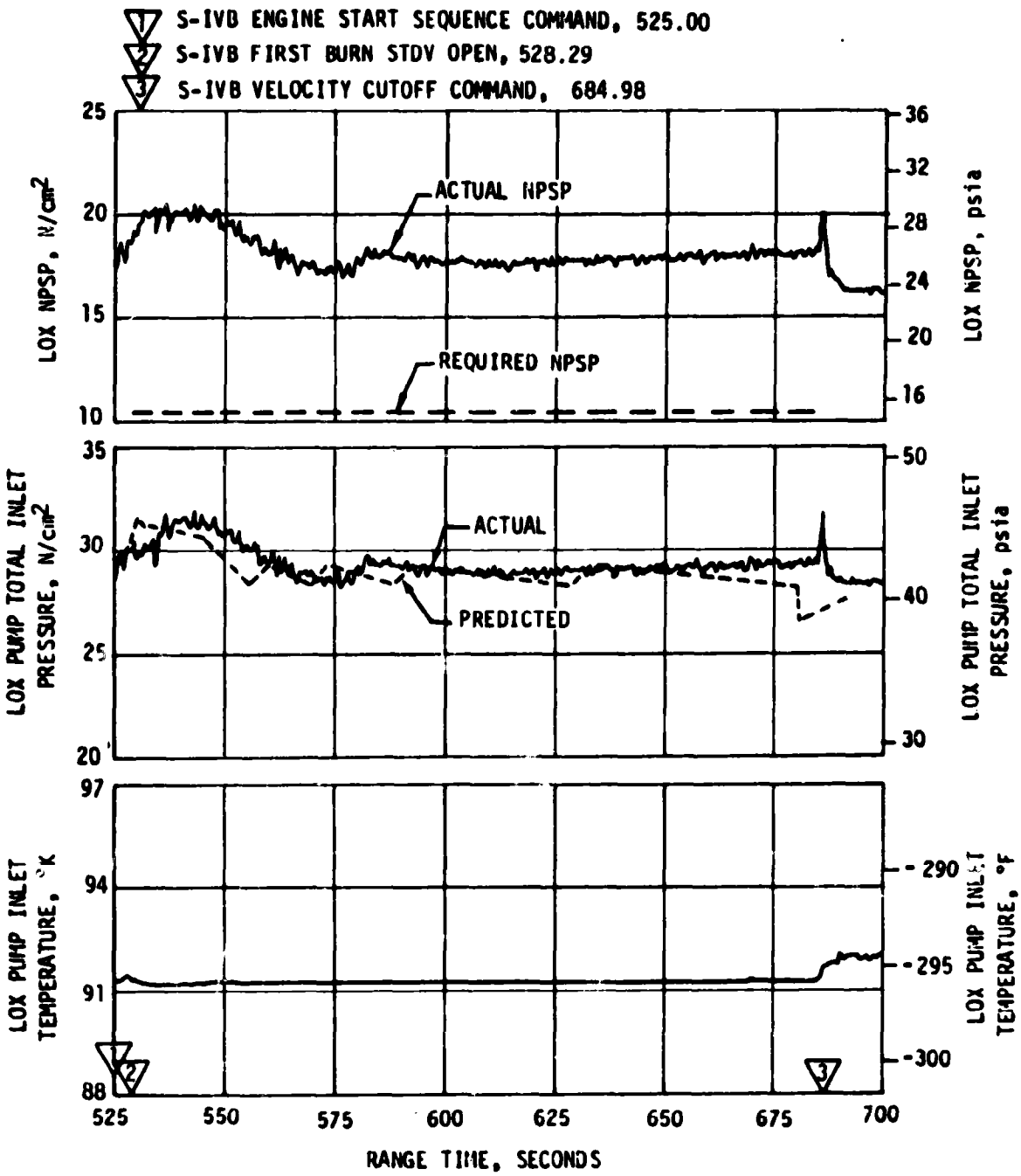

Figure 7-32. S-IVB LOX Pump Inlet Conditions - First Burn

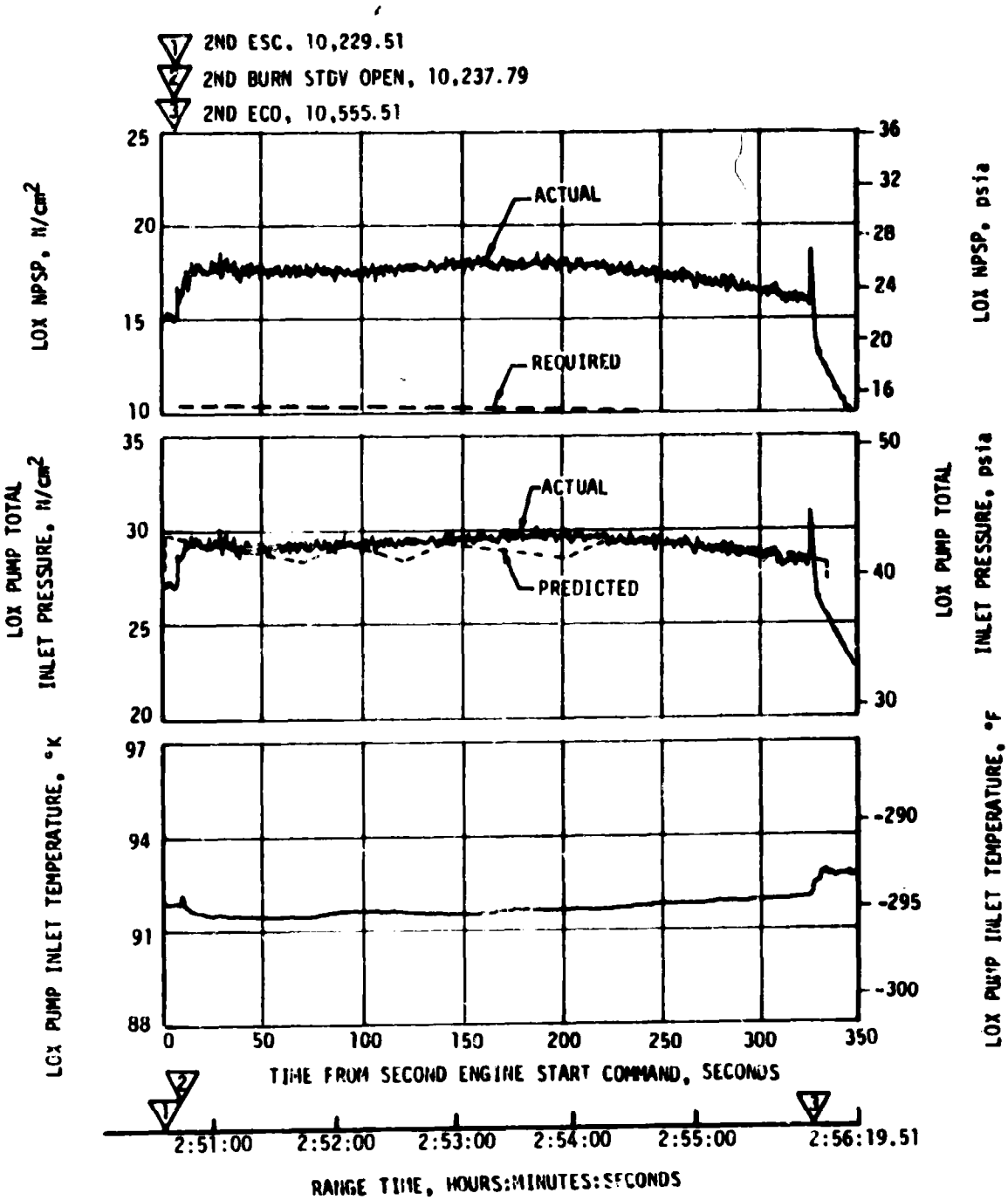

Figure 7-33. S-IVB LOX Pump Inlet Conditions - Second Burn

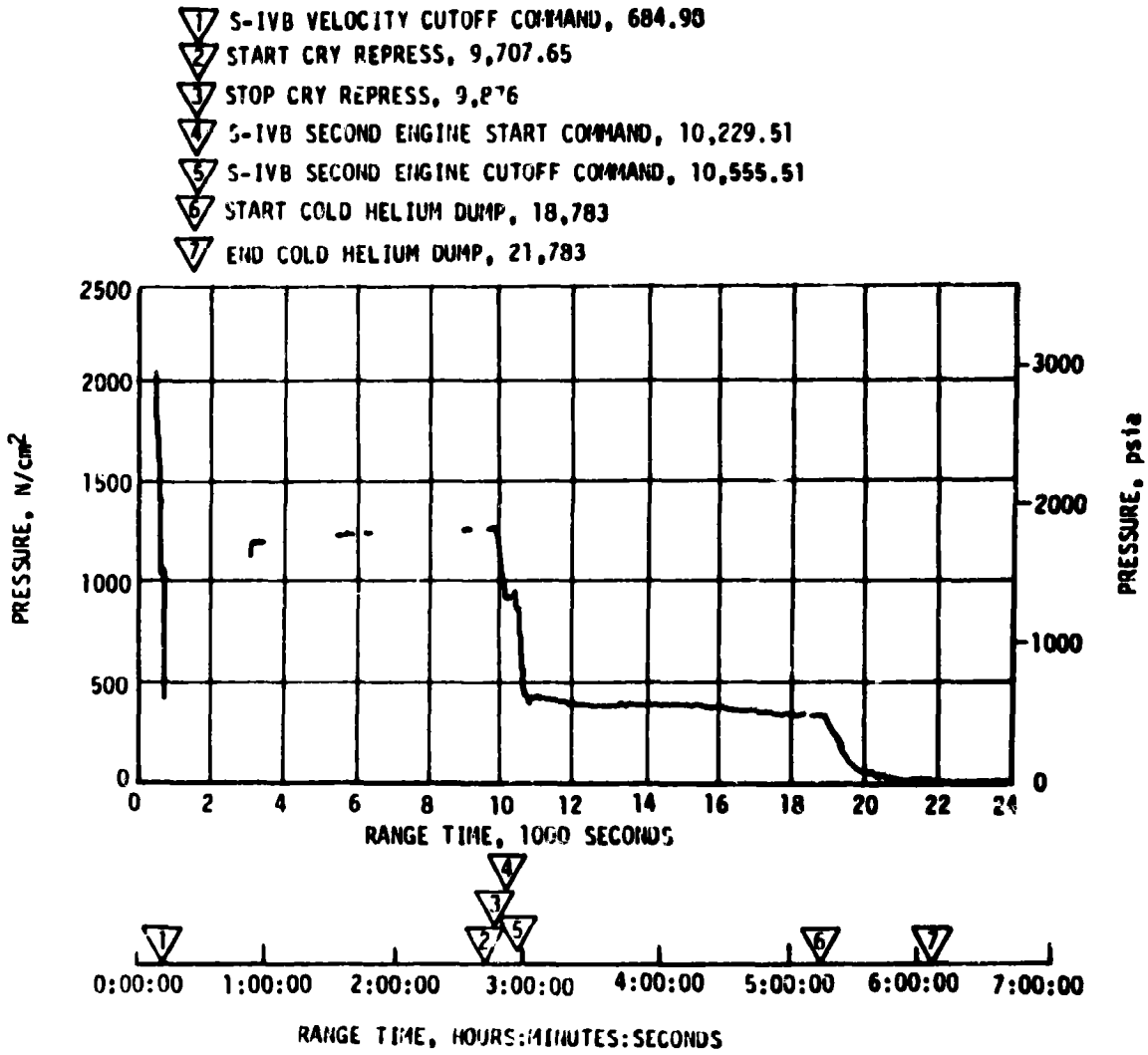

Figure 7-34. S-IVB Cold Helium Supply History

burn operations. The AS-503 stage incorporated the redesigned pneumatic actuation control modules, and experienced no discernible leakage as opposed to earlier stages which had significant degrees of leakage. Pneumatic control bottle temperature, pressure, and regulator outlet pressure are shown in Figure 7-35. Bottle masses at various pertinent times are shown in Table 7-12.

7.12 S-IVB AUXILIARY PROPULSION SYSTEM

The Auxiliary Propulsion System (APS) pressurization systems demonstrated nominal performance throughout the flight and met control system demands as required until APS propellant depletion. The Module No. 1 regulator outlet pressure was maintained at 135 N/cm² (196 psia). Module No. 2

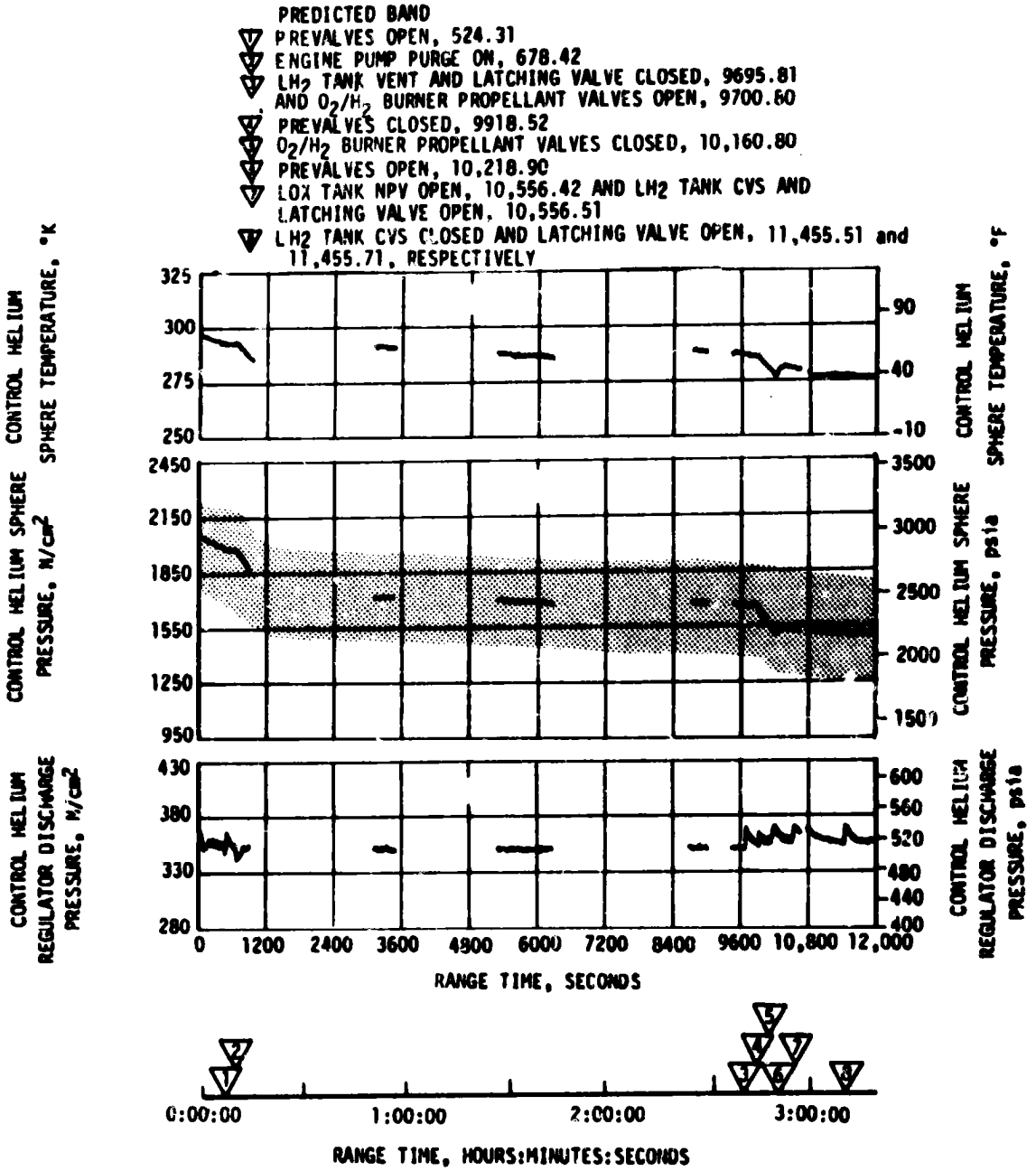

Figure 7-35. S-IVB Pneumatic Control Performance

Table 7-12. S-IVB Pneumatic Helium Bottle Mass

TIME	BOTTLE MASS	
	kg	lbm
Liftoff	3.79	8.36
First Burn ESC, 525.00 sec	3.72	8.20
First Burn ECO, 684.98 sec	3.71	8.19
9910 Sec (2:45:01)	3.29	7.25
Second Burn ESC, 10,229.51 sec, (2:50:29.51)	3.06	6.74
Second Burn ECO, 10,555.51 sec, (2:55:55.51)	3.05	6.73
Start Pneumatic Dump, 18,745.83 sec (5:12:25:83)	2.94	6.47

regulator outlet pressure was 131 to 133 N/cm^2 (190 to 193 psia) which was below the 135 ± 2 N/cm^2 (196 ± 3 psia) regulation band. This is within instrumentation accuracy and other system pressures verify proper regulator operation. The APS ullage pressures in the tanks were acceptable, ranging from 131 to 135 N/cm^2 (190 to 196 psia). The APS helium bottle masses during flight are presented in Table 7-13.

The oxidizer and fuel supply systems performed as expected during the flight. The propellant temperatures measured in the propellant control module were as expected. The maximum temperature recorded was 314°K (105°F). The bulk temperatures of the propellants in the bladder ranged from 304 to 307°K (87 to 93°F).

The APS ullage engines of the modules at position I and III were turned on at 19,555.85 and 19,556.06 seconds, respectively, and burned to propellant depletion to provide additional impulse for the slingshot maneuver. The propellants in Module No. 2 (at position III) were depleted first as shown in Figure 7-36. The fuel was depleted at 20,288.56 seconds resulting in a burn time of 732.5 seconds, while the oxidizer was depleted at 20,455 seconds. The fuel was also depleted first in Module No. 1 (at position I) at 20,314 seconds resulting in a burn time of 758.15 seconds, as shown in Figure 7-37. The oxidizer was depleted at 20,500 seconds. The reason the fuel was depleted first in both modules was that the propellants were loaded for a 1.65 to 1.0 EMR while the attitude control engines normally operate at a 1.60 EMR during minimum impulse bit pulsing. Also the oxidizer was not off-loaded to account for the third ullage burn to propellant depletion at the ullage engine EMR of 1.27 to 1.0. The fuel load for the flight was maximum. Table 7-14 presents the APS oxidizer and fuel consumption at significant events during the flight.

Table 7-13. S-IVB APS Helium Bottle Mass

TIME	BOTTLE MASS			
	kg		lbm	
	MODULE 1	MODULE 2	MODULE 1	MODULE 2
Liftoff	0.450	0.453	0.993	0.999
First Burn ESC	0.450	0.453	0.993	0.999
First Burn ECO	0.450	0.453	0.993	0.999
End of 1st Ullage Burn Approximately, 772 sec	0.430	0.431	0.949	0.950
Start of 2nd Ullage Burn, 10,155.82 sec (2:49:15.82)	0.415	0.427	0.916	0.941
Second Burn ESC, 10,229.51 sec (2:50:29.51)	0.401	0.410	0.885	0.903
Second Burn ECO, 10,555.51 sec (2:55:55.51)	0.398	0.409	0.878	0.901
Separation, 12,056.3 sec (3:20:56.3)	0.389	0.391	0.858	0.862
Loss of CP Signal, 15,660 sec (4:21:00)	0.383	0.388	0.844	0.856

The attitude control engine chamber pressures were normal and ranged from 66 to 69 N/cm^2 (95 to 100 psia) until loss of data. The attitude control engine chamber pressure data were on the CP-1 link which were not received after 4 hours and 21 minutes from liftoff. The ullage engine chamber pressures which were on the DP-1 link were normal at 67 to 71 N/cm^2 (97 to 102 psia) during their burns, including the burn to propellant depletion.

7.13 S-IVB ORBITAL SAFING OPERATION

The S-IVB high pressure systems were safed following J-2 engine cutoff in order to demonstrate this capability. The thrust developed during the LOX dump was utilized to ensure that the spent S-IVB stage would be placed in solar orbit and would not impact the lunar surface. The manner and sequence in which the safing was performed is presented in Figure 7-38.

7.13.1 Fuel Tank Safing

The LH_2 tank was satisfactorily safed by accomplishing three programmed vents, as indicated in Figure 7-38, utilizing both the Non Propulsive Vent (NPV) and CVS. The LH_2 tank ullage pressure during safing is shown

Table 7-14. S-IVB APS Propellant Consumption

TIME PERIOD	MODULE AT POSITION I				MODULE AT POSITION III			
	OXIDIZER		FUEL		OXIDIZER		FUEL	
	kg	(lbm)	kg	(lbm)	kg	(lbm)	kg	(lbm)
Initial Load	87.7	(193.3)	56.9	(125.4)	87.5	(193.0)	56.9	(125.4)
First J-2 Burn. Roll Control	0.2	(0.5)	0.1	(0.3)	0.2	(0.5)	0.1	(0.3)
J-2 ECO to End of First APS Ullaging	6.3	(13.8)	4.6	(10.2)	6.8	(15.1)	5.1	(11.3)
End of 1st Ullage Earth Burn to Start of 2nd	5.3	(11.7)	3.3	(7.3)	1.4	(3.0)	0.9	(1.9)
Restart Preparations	5.1	(11.2)	4.0	(8.8)	5.4	(11.9)	4.3	(9.4)
2nd J-2 Burn (Roll Control)	0.2	(0.5)	0.1	(0.3)	0.2	(0.5)	0.1	(0.3)
ECO to S-IVB/CSM Separation	3.1	(6.8)	1.9	(4.2)	6.3	(13.8)	3.9	(8.6)
From Separation to Propellant Depletion	67.5	(148.8)	42.8	(94.3)	67.2	(148.2)	42.4	(93.6)
TOTAL	87.7	(193.3)	56.9	(125.4)	87.5	(193.0)	56.9	(125.4)

in Figure 7-27. At second ECO, the LH_2 tank ullage pressure was 22.1 N/cm^2 (32.0 psia) and after three vents had decayed to approximately 1.03 N/cm^2 (1.5 psia). The mass of GH_2 and LH_2 vented agrees well with the 1438 kilograms (3170 lbm) of liquid residual and pressurant in the tank at the end of powered flight.

7.13.2 LOX Tank Dump and Safing

Immediately following second burn cutoff, a programmed 155-second vent reduced LOX tank ullage pressure from 26.5 N/cm^2 (38.4 psia) to 13.2 N/cm^2 (19.1 psia) as shown in Figure 7-31. Data levels were as expected with 31.1 kilograms (68.5 lbm) of helium and 58.9 kilograms (129.8 lbm) of GOX being vented overboard. As indicated in Figure 7-31, the ullage pressure then rose gradually, due to self-pressurization, to 19.0 N/cm^2 (27.6 psia) at the initiation of LOX dump.

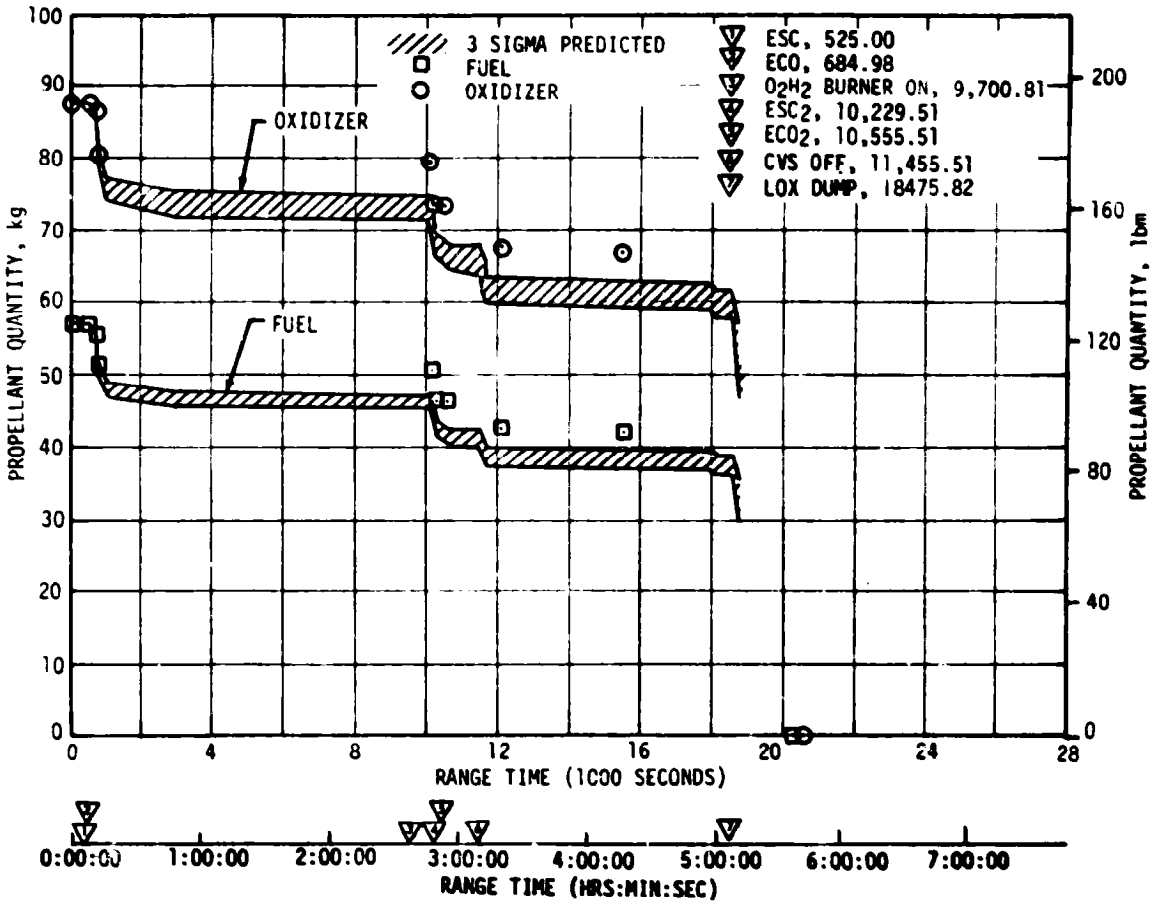

Figure 7-36. S-IVB APS Mass History - Module No. 2

The LOX tank dump was initiated at 18,475.82 seconds and was satisfactorily accomplished. A steady-state liquid flow of 1.40 m^3/s (370 gpm) was reached within 40 seconds.

Approximately 126 seconds after dump initiation, the measured LOX flowrate showed a sudden increase indicating that gas ingestion had begun. Shortly thereafter, the LOX ullage pressure began decreasing at a greater rate. Calculations indicate the LOX residual, approximately 3329 kilograms (7340 lbm), was essentially dumped within 150 seconds. Ullage gases continued to be dumped until the programmed termination. The tank pressure had decayed to 11 N/cm^2 (16.0 psig) at this time.

LOX dump ended at 18,776.03 seconds as scheduled by closure of the MOV. A steady state LOX dump thrust of 3959 Newtons (890 lbf) was obtained. The total impulse before MOV closure was 556,473 N-s (125,100 lbf-s), resulting in a calculated velocity increase of 20.4 m/s (66.9 ft/s). Figure 7-39 shows the LOX flowrate during dump and the mass of liquid and gas in the oxidizer tank. Figure 7-39 shows LOX ullage pressure and the LOX dump

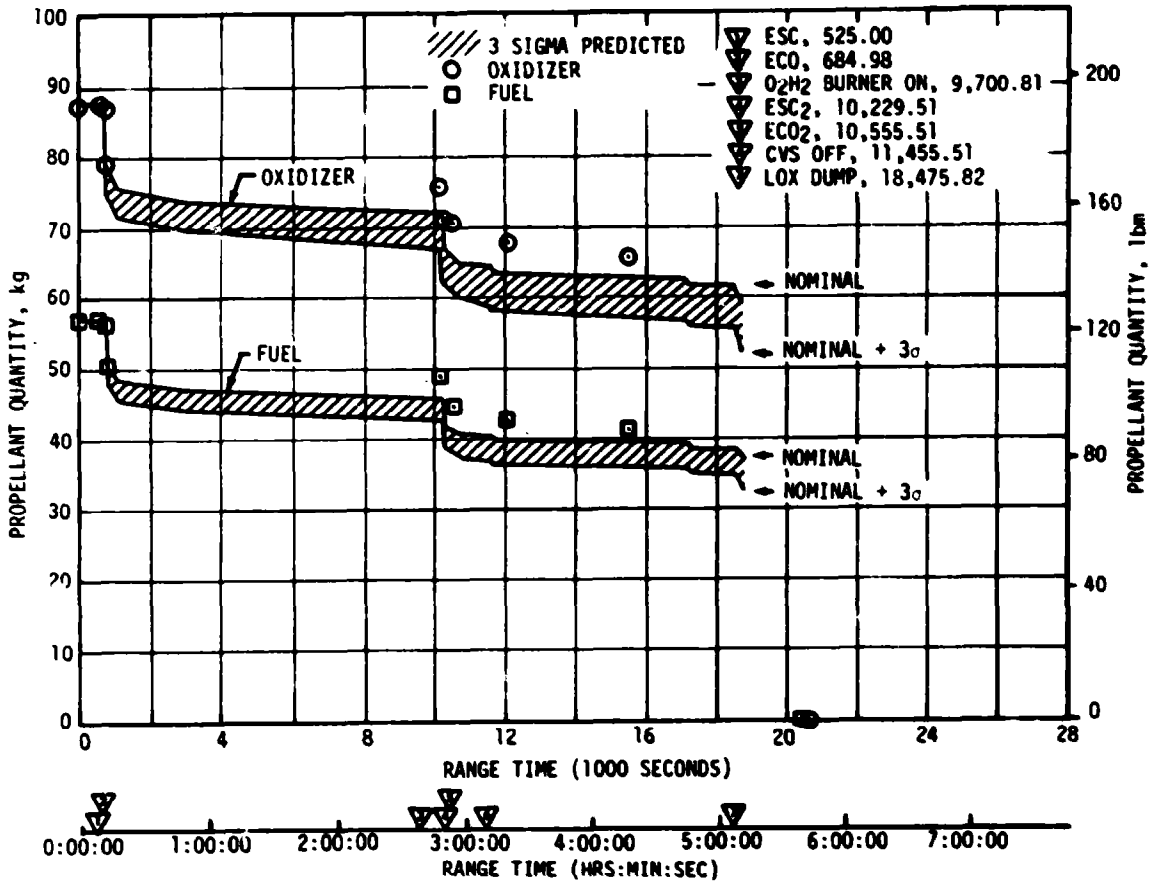

Figure 7-37. S-IVB APS Mass History - Module No. 1

thrust produced. The predicted curves provided for the LOX flowrate and dump thrust correspond to the quantity of LOX dumped and the actual ullage pressure.

Three seconds following termination of LOX dump the LOX NPV valve was opened and remained open for the duration of the mission. LOX tank ullage pressure decayed from 11 N/cm^2 (16.0 psia) at 18,776 seconds to zero pressure at approximately 24,000 seconds.

7.13.3 Cold Helium Dump

With the addition of the O_2/H_2 burner on the S-IVB-503 stage, cold helium was dumped through the burner heating coils and into the LH_2 tank, and overboard through the tank vents. This change from past methods was made to avoid the possibility of freezing LOX in the LOX tank vent system.

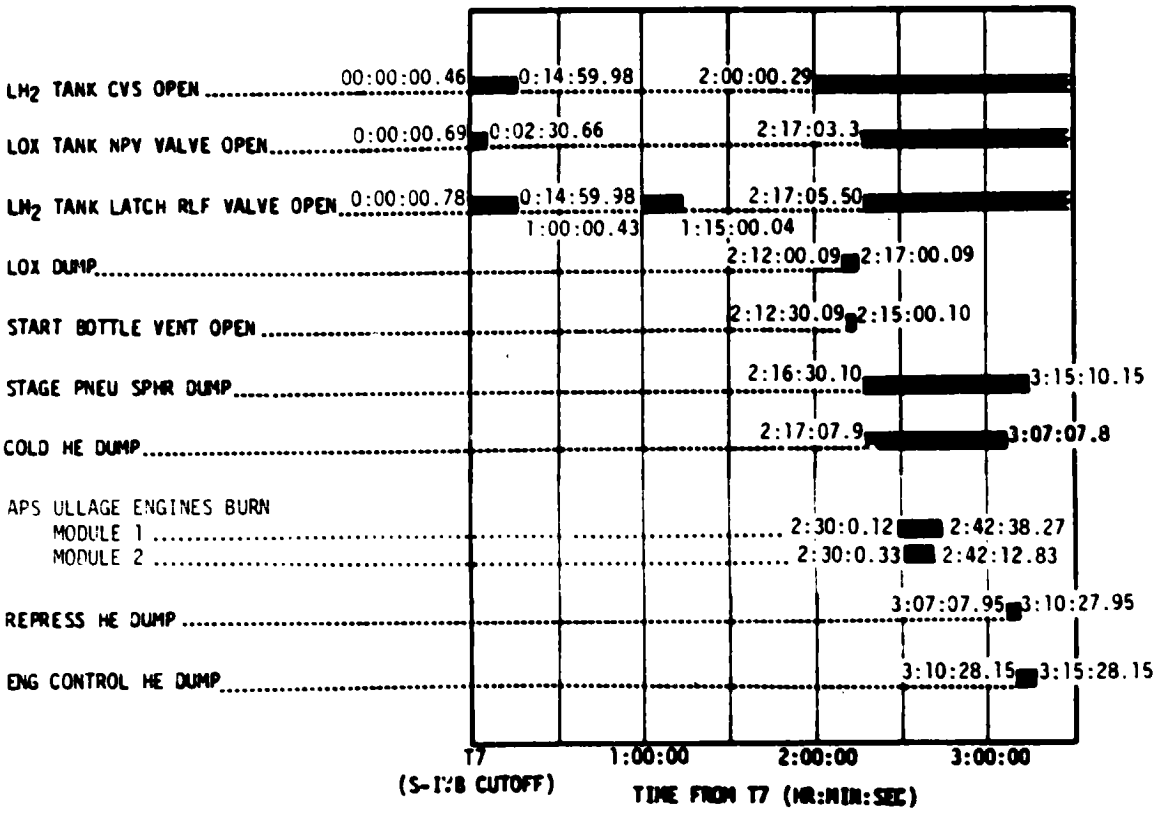

Figure 7-38. S-IVB Orbital Safing and Propellant Dump Sequence

The dump was initiated at 18,783.63 seconds and programmed to continue for approximately 3000 seconds as shown in Figure 7-34. During this period, the pressure decayed normally from 358 to 34 N/cm^2 (520 to 50 psia). Approximately 64 kilograms (140 lbm) of helium was dumped overboard.

7.13.4 Ambient Helium Dump

The ambient helium in the LOX and LH_2 repress spheres was dumped, via the fuel tank. The 200-second dump occurred at 21,783.68 seconds. The pressure decayed from 2136 N/cm^2 (3100 psia) to 172 N/cm^2 (250 psia). Data during this period was not recovered, and a detailed analysis will not be possible.

7.13.5 Stage Pneumatic Control Sphere Safing

The stage pneumatic control sphere was safed by initiating the J-2 engine pump purge and flowing helium through the pump seal cavities to atmosphere. The safing period of 3520 seconds satisfactorily reduced the potential energy in the spheres. Initial and final sphere conditions are listed in Table 7-15.

7.13.6 Engine Start Sphere Safing

The engine start sphere was safed during approximately a 150-second period at 18,505.82 seconds. Safing was accomplished by opening the sphere vent

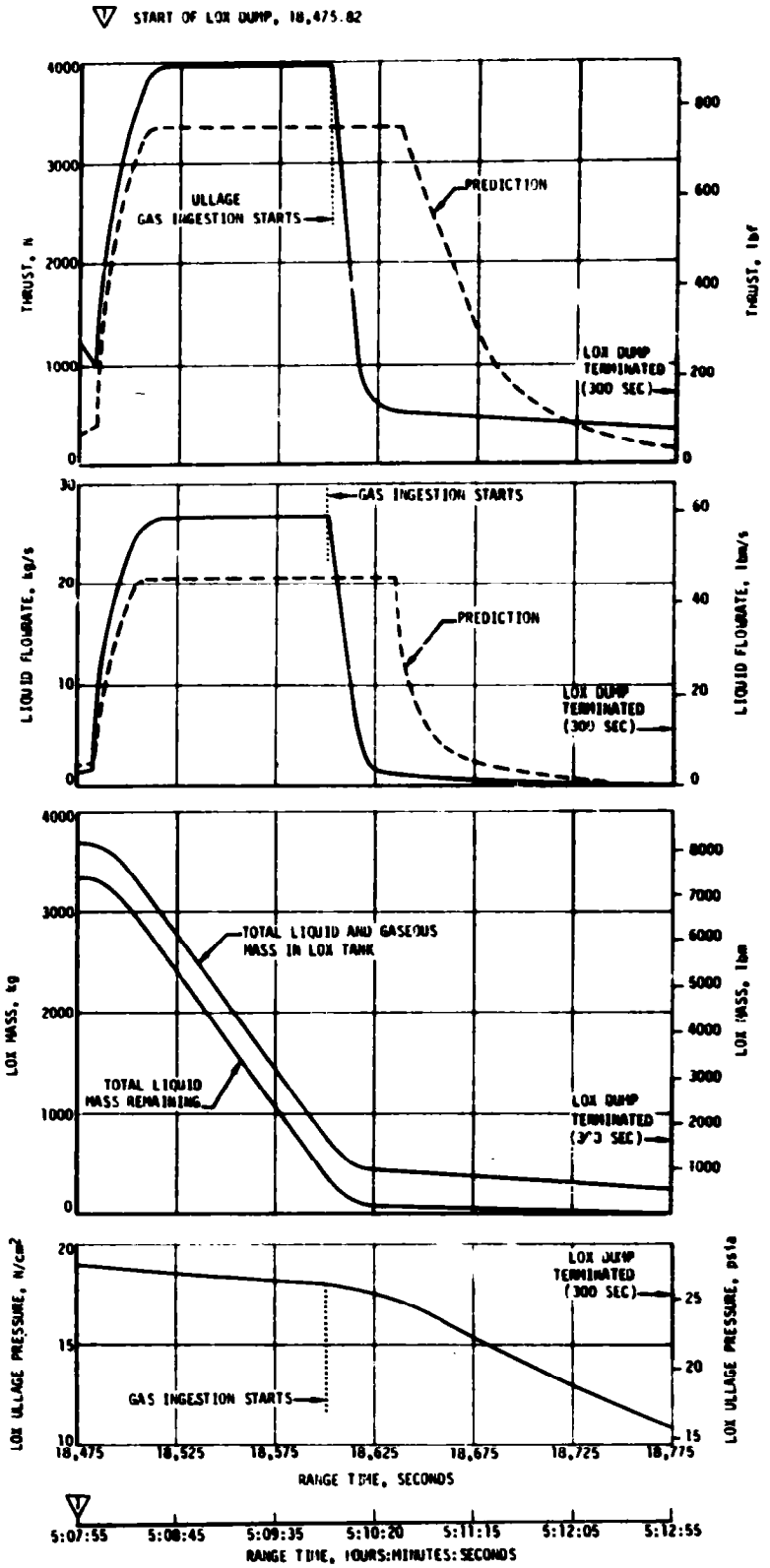

Figure 7-39. S-IVB LOX Dump Parameter Histories

Table 7-15. S-IVB Pneumatic Control Sphere Conditions During Dump

PARAMETER	INITIAL CONDITIONS		FINAL CONDITIONS	
Press N/cm^2 (psia)	1351	(1960)	255	(370)
Temp °K (°F)	263	(13)	205	(-90)
Mass kg (lbm)	2.94	(6.47)	0.74	(1.64)

valve. Pressure was decreased from 902 N/cm^2 (1309 psia) to 11 N/cm^2 (16 psia) with 1.8 kilograms (3.9 lbm) of hydrogen being vented as shown in Figure 7-40.

7.13.7 Engine Control Sphere Safing

The engine control sphere was safed, beginning at 21,983.88 seconds after the completion of the ambient repress spheres safing. The helium control solenoid was energized to flow helium through the engine purge system to atmosphere. The pressure decayed from 2102 N/cm^2 (3048 psia) to 140 N/cm^2 (203 psia) with 0.9 kilogram (2.0 lbm) vented during the 300-second safing period as shown in Figure 7-40.

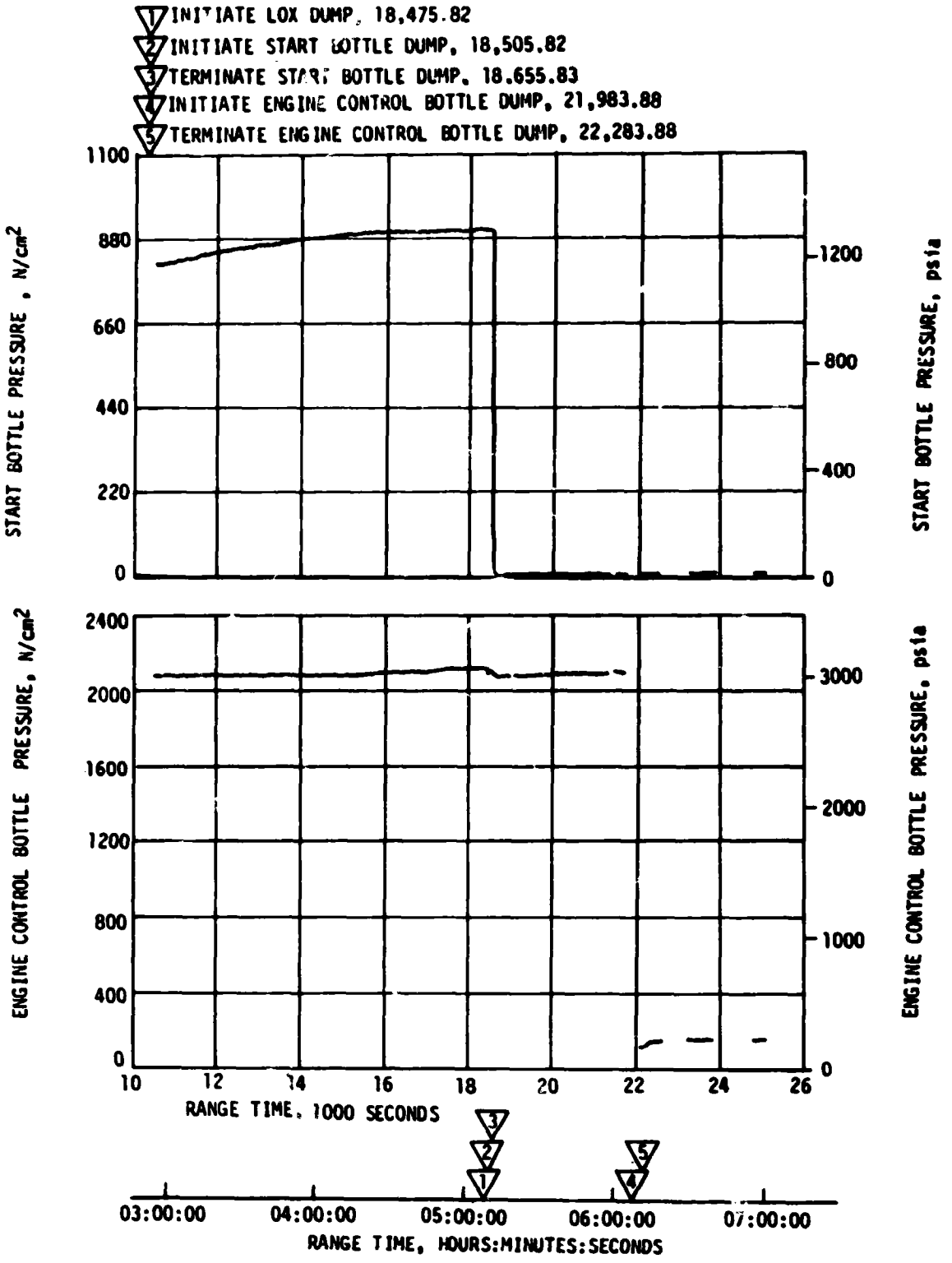

Figure 7-40. S-IVB Start Bottle and Engine Control Bottle Safing

SECTION 8

HYDRAULIC SYSTEMS

8.1 SUMMARY

The S-IC, S-II, and S-IVB hydraulic systems performed satisfactorily during the flight. All parameters were within specification limits although the return fluid temperature of one S-IC actuator began to rise unexpectedly after 117 seconds. There were no other deviations and no anomalies during the flight.

8.2 S-IC HYDRAULIC SYSTEM

The S-IC stage incorporated eight gimbal actuators of the Hydraulic Research Model (60B84500-7C). Analysis indicates that all actuators performed as commanded during the flight. The maximum actuator deflection was equivalent to 2.06 degrees engine gimbal angle at 113 seconds. The average hydraulic supply pressure was 1307 N/cm^2 (1895 psia) and operated in a small band within the operating limits as shown in Figure 8-1. The operating temperature as depicted by the return actuator fluid was 303°K (86°F) and operated in a narrow band except for the engine 103 pitch actuator return fluid temperature (shown separately in Figure 8-1) which began a sudden increase at about 117 seconds into the flight. The measurement went out of the expected range, but not out of specification limits as shown in Figure 8-1. No explanation has been found for this unexpected occurrence. The maximum hydraulic engine valve opening pressure was 1365 N/cm^2 (1980 psia).

8.3 S-II HYDRAULIC SYSTEM

Figure 8-2 shows plots of reservoir fluid volumes and temperatures and accumulator fluid pressures (indicative of system supply pressures) for engine No. 1 through 4. The volumes and pressures were within predicted ranges. Temperature rise rates were close to the predicted rate.

Throughout the flight all servoactuators responded to commands with good precision. The maximum difference between actuator command and position was less than 0.2 degree. Forces acting on the actuators were well below a predicted maximum of 84,516 Newtons (19,000 lbf). The maximum force in tension was 52,044 Newtons (11,700 lbf) acting on the pitch actuator of engine No. 3. The maximum force in compression was 14,234 Newtons (3200 lbf) acting on the yaw actuator of engine No. 1. In addition, force oscillations were detected on all of the actuators during the time that

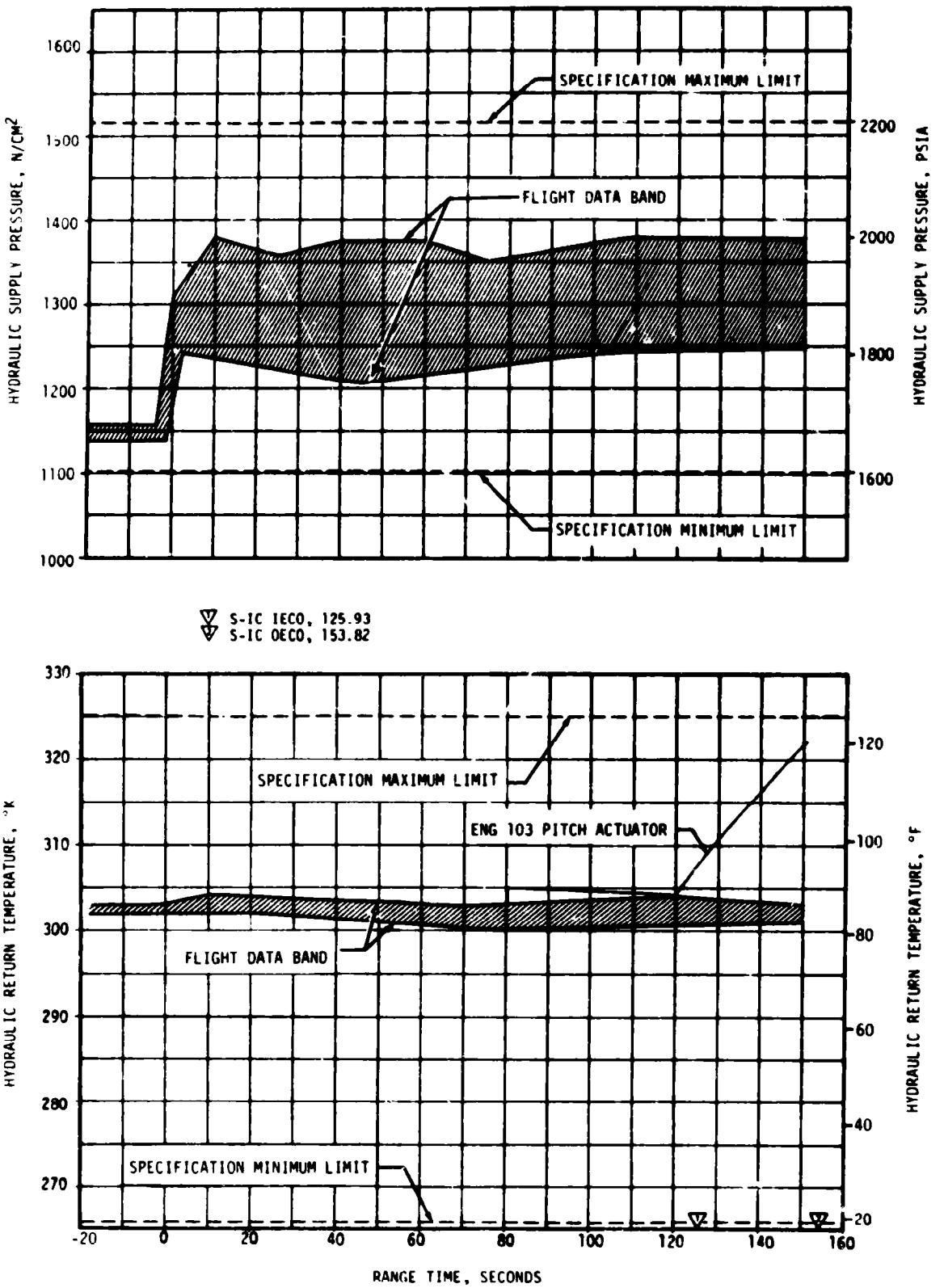

Figure 8-1. S-IC Hydraulic System Performance

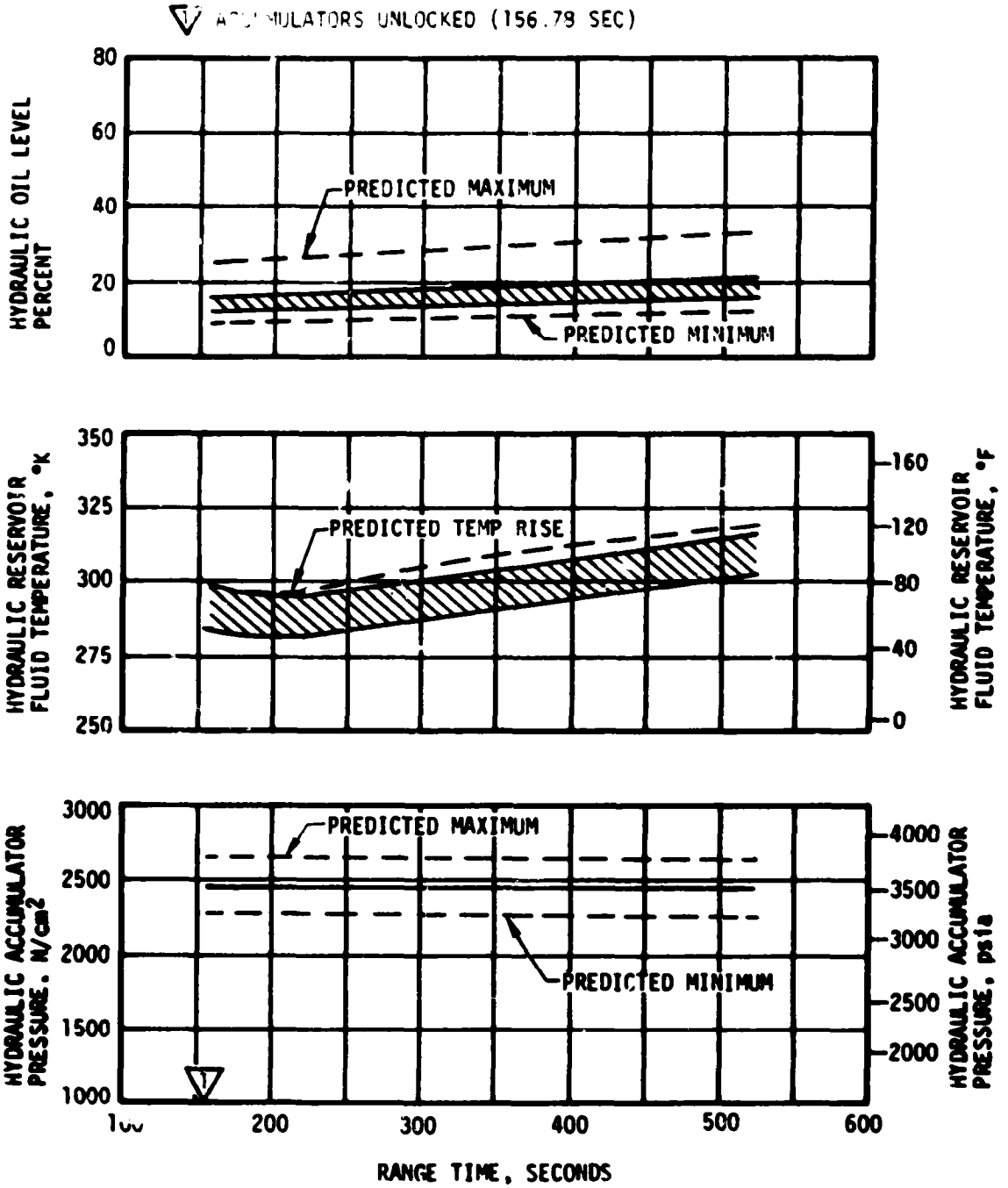

Figure 8-2. S-II Hydraulic System Performance

engine No. 5 chamber pressure oscillations appeared. The frequency of the oscillations was 18 hertz, and the peak-to-peak amplitudes ranged between 23,131 and 34,696 Newtons (5200 and 7800 lbf).

8.4 S-IVB HYDRAULIC SYSTEM (FIRST BURN)

The S-IVB hydraulic system performed within the predicted limits after liftoff with no overboard venting of system fluid as a result of reservoir fluid expansion. Prior to start of propellant loading, the accumulator was precharged to 1655 N/cm^2 (2400 psia) at 294°K (70°F). Reservoir oil level (auxiliary pump off) was 87 percent at 294°K (70°F). Table 8-1 shows minor pressure level variations and compares the liftoff, first burn parking orbit, and second burn system pressures.

Table 8-1. S-IVB Hydraulic System Pressures

PRESSURES	LIFTOFF N/cm^2 (psia)	FIRST BURN N/cm^2 (psia)	PARKING ORBIT N/cm^2 (psia)	AFTER RESTART COMMAND N/cm^2 (psia)	ALLOWABLE DURING BURN N/cm^2 (psia)
System Oil	2496 (3620)	2517 (3650)	-	2517 (3650)	2413 to 2517 (3500 to 3650)
Accumulator GN_2	2496 (3620)	2524 (3660)	1620 (2350)	2517 (3650)	2413 to 2517 (3500 to 3650)
Reservoir Oil	121 (175)	124 (180)	53 (77)	124 (180)	110 to 128 (160 to 185)
Aux Pump Air Tank	290 (420)	288 (418)	308 (446)	310 (450)	138 to 345 (200 to 500)
Aux Pump Motor Air	12.3 (17.9)	23.1 (33.5)	22.2 (32.2)	22.8 (33.0)	7 to 31 (10 to 45)

Note: These values have been corrected to 293°K (68°F).

During S-IC/S-II boost all system fluid temperatures rose steadily, as shown in Figure 8-3, when the auxiliary pump was operating and convection cooling was decreasing. The supply pressure during the first burn was nearly constant at 2517 N/cm^2 (3650 psia) as compared to the allowable 2413 to 2517 N/cm^2 (3500 to 3650 psia). The maximum actuator torque resulting from vehicle attitude commands during first burn was in pitch at 7904 N-m (69,955 lbf-in.).

The system internal fluid leakage rate of 45 cm^3/s (0.71 gpm) (25 to 50 cm^3/s [0.4 to 0.8 gpm] allowable) was delivered by the main engine driven pump during engine burn as indicated by a 27 N/cm^2 (39 psia) jump in system pressure after ignition and the auxiliary pump motor current draw of only 21 amperes. Power extracted from the engine by the main pump during burn was 5.13 horsepower.

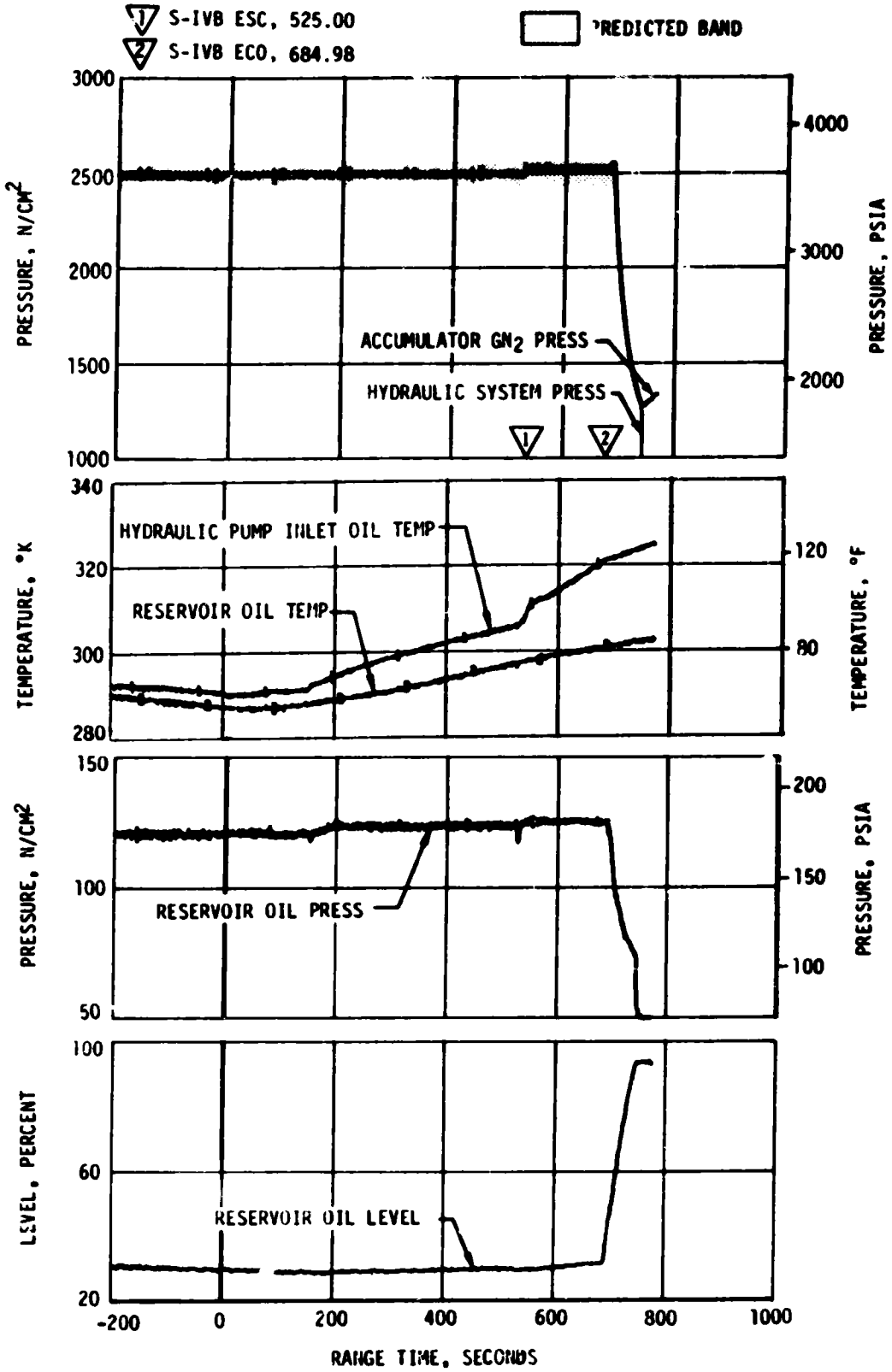

Figure 8-3. S-IVB Hydraulic System Performance - First Burn

Engine deflections were nominal throughout first burn. The actuator positions were offset from null during powered flight due to the displacement of the vehicle's Center of Gravity (CG) off the vehicle's vertical axis, due to J-2 engine installation tolerances, thrust misalignment, and uncompensated gimbal clearances and thrust structure compression effects.

Pitch and yaw actuator transient loads during engine start were negligible as were the loads throughout the powered flight. Proper operation of the pitch and yaw actuator dynamic pressure feedback mechanism is indicated by the actuator differential pressure traces. The hydraulic servoactuators responded properly to incoming Instrument Unit (IU) signals. Good correlation was observed between the S-IVB actuator position data and the IU actuator command data throughout the powered flight.

8.5 S-IVB HYDRAULIC SYSTEM (COAST PHASE)

After engine cutoff, the pump inlet oil temperature increased from 321 to 341°K (118 to 153°F) due to continued heat transfer from the LOX turbine dome to the pump manifold as shown in Figure 8-4. This is well within the system high temperature limit of 408°K (275°F).

During the orbital coast period the auxiliary pump was thermally cycled for 48 seconds at 3285.15 seconds and again at 6085.15 seconds as programmed. These cycles were programmed to circulate the system fluid and to distribute the heat more evenly throughout the system.

8.6 S-IVB HYDRAULIC SYSTEM (SECOND BURN)

The auxiliary pump was activated to the flight mode at 9878.52 seconds. System operation was normal through restart operation and second burn as shown in Figure 8-5. Pump inlet and reservoir oil temperatures rose at the rate of 4.6 and 2.0°K/min (8.4 and 3.6°F/min), respectively, during second burn. System pressure stabilized at 2517 N/cm2 (3650 psia) during burn. After cutoff, reservoir pressure stabilized at 52 N/cm2 (75 psia) following a 48-second bleeddown.

Engine deflections were nominal throughout second burn. The maximum actuator torque resulting from vehicle attitude commands during second burn was in yaw at 12,646 N-m (111,928 lbf-in.).

8.7 TRANSLUNAR INJECTION COAST AND PROPELLANT DUMP

After engine cutoff the pump inlet oil temperature continued to increase until the third and final 48-second thermal cycle as shown in Figure 8-6. At this point the temperature peaked at 372°K (209°F). This was the highest temperature recorded in the system during flight. It rose after the thermal cycle and was back up to the same temperature prior to LOX dump. Pressures during this period were nominal. Hydraulic system performance during the LOX dump was nominal as evidenced in Figures 8-7 and 8-8.

Table 21-9. Flight Sequence Mass Summary

MASS HISTORY	ACTUAL KG	ACTUAL LBM	PREDICTED KG	PREDICTED LBM
S-IC STAGE, TOTAL	2175940.	4797126.	2175030.	4799120.
S-IC/S-II INTERSTAGE-SMALL	654.	1441.	658.	1450.
S-IC/S-II INTERSTAGE-LARGE	4987.	10995.	5062.	11160.
S-II STAGE, TOTAL	471114.	1038628.	471009.	1038389.
S-II/SIIVB INTERSTAGE	3960.	8731.	3973.	8760.
S-IVB STAGE, TOTAL	119652.	263787.	119634.	263749.
VEHICLE INSTRUMENT UNIT	2196.	4842.	2214.	4880.
SPACECRAFT INCLUDING LES	43668.	96272.	43906.	96575.
1ST FLT STG AT IGN	2822171.	6221823.	2821380.	6220078.
S-IC THRUST BUILDUP	-40476.	-89237.	-38955.	-85884.
1ST FLT STG HOLDDOWN ARM REL	2781694.	6132585.	2782424.	6134194.
S-IC FROST	-294.	-650.	-294.	-650.
S-IC MAINSTAGE PROPELLANT	-1957147.	-4314773.	-1958894.	-4318624.
S-IC N2 PURGE	-16.	-37.	-16.	-37.
S-IC INBD ENGINE T.D. PROP	-864.	-1907.	-822.	-1814.
S-IC INBD ENG EXPENDED PROP	-189.	-418.	-189.	-418.
S-II INSULATION PURGE GAS	-53.	-120.	-53.	-120.
S-II FROST	-203.	-450.	-203.	-450.
S-IVB FROST	-90.	-200.	-44.	-100.
1ST FLT STAGE AT S-IC OECOS	822829.	1814028.	821901.	1811981.
S-IC OTBD ENGINE T.D. PROP	-3436.	-7578.	-3290.	-7256.
S-IC/S-II ULLAGE RKT PROP	-32.	-73.	-32.	-73.
1ST FLT STAGE AT SIC/SII SEP	819359.	1806377.	818577.	1804653.
S-IC STAGE AT SEPARATION	-173509.	-382524.	-172563.	-380439.
S-IC/S-II INTERSTAGE SMALL	-653.	-1441.	-657.	-1450.
S-IC/S-II ULLAGE RKT PROP	-277.	-612.	-277.	-612.
2ND FLT STAGE AT S-II IGN	644918.	1421800.	645077.	1422151.
S-II THRUST BUILDUP	-423.	-935.	-423.	-935.
S-II START TANK	-10.	-25.	-10.	-25.
S-IC/S-II ULLAGE RKT PROP	-299.	-662.	-305.	-675.
2ND FLT STAGE 90 PC THRUST	644182.	1420178.	644335.	1420515.
LAUNCH ESCAPE TOWER	-4031.	-8890.	-4025.	-8875.
S-IC/S-II INTERSTAGE LARGE	-4375.	-9648.	-4444.	-9800.
S-II MAINSTAGE & VENTING	-423347.	-933323.	-422799.	-932114.
2ND FLT STAGE AT S-II C.O.S.	212425.	468316.	213064.	469726.
S-II T.D. PROPELLANT	-214.	-474.	-210.	-465.
S-IVB ULLAGE PROPELLANT	-1.	-5.	-1.	-5.
2ND FLT STG AT SII/SIVB SEP	212207.	467836.	212853.	469259.

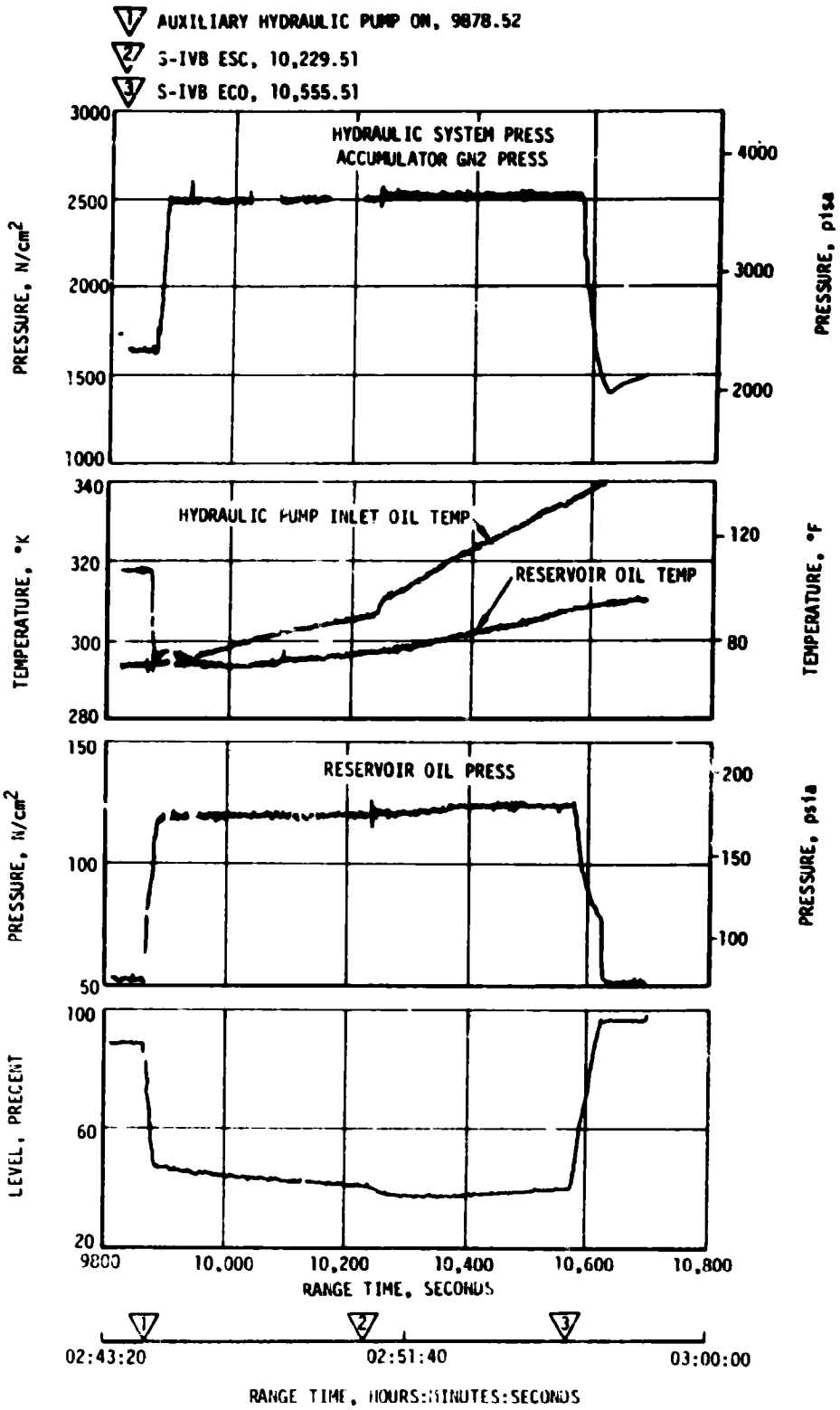

Figure 8-5. S-IVB Hydraulic System Performance - Second Burn

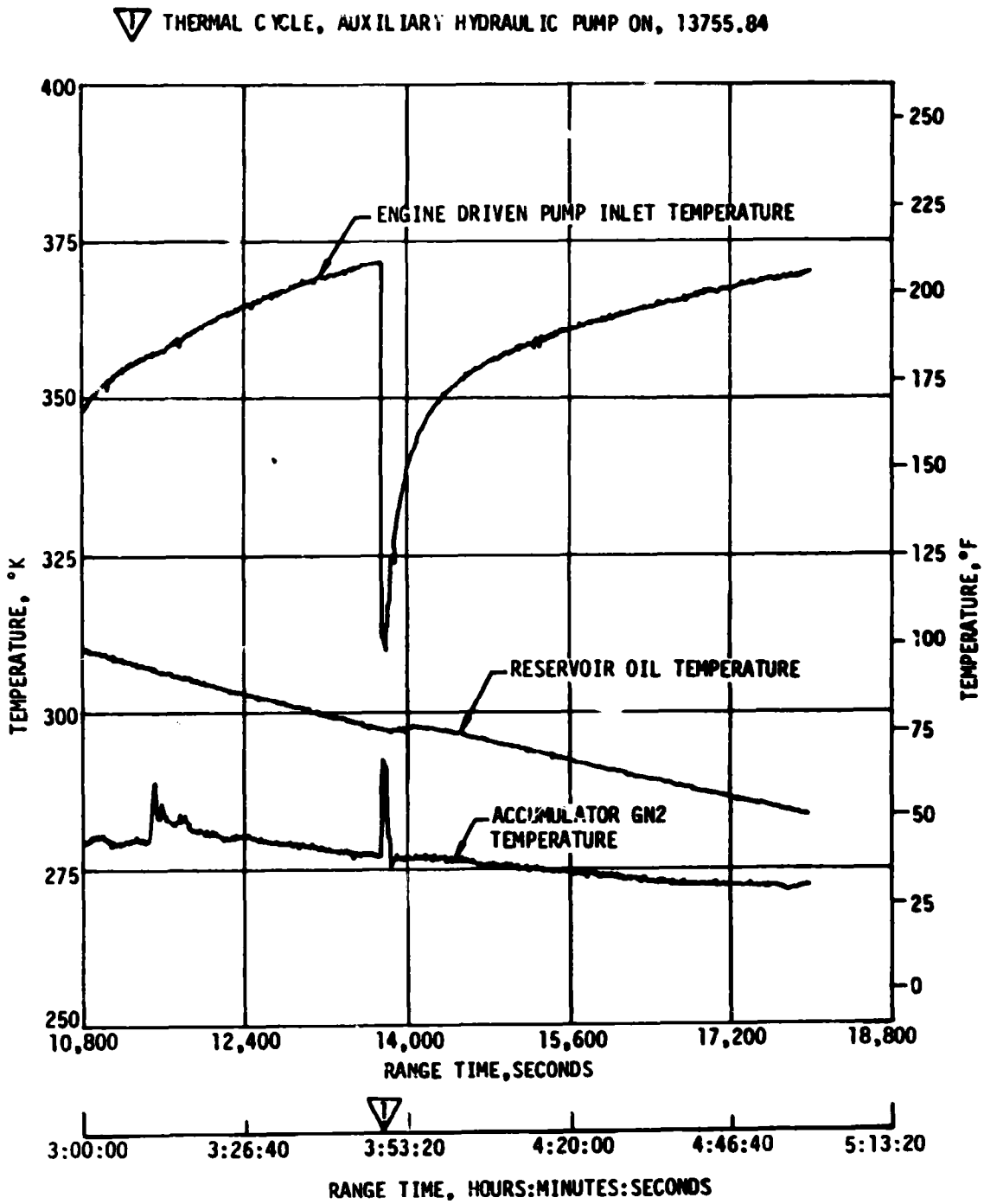

Figure 8-6. S-IVB Hydraulic System Performance During Translunar Coast

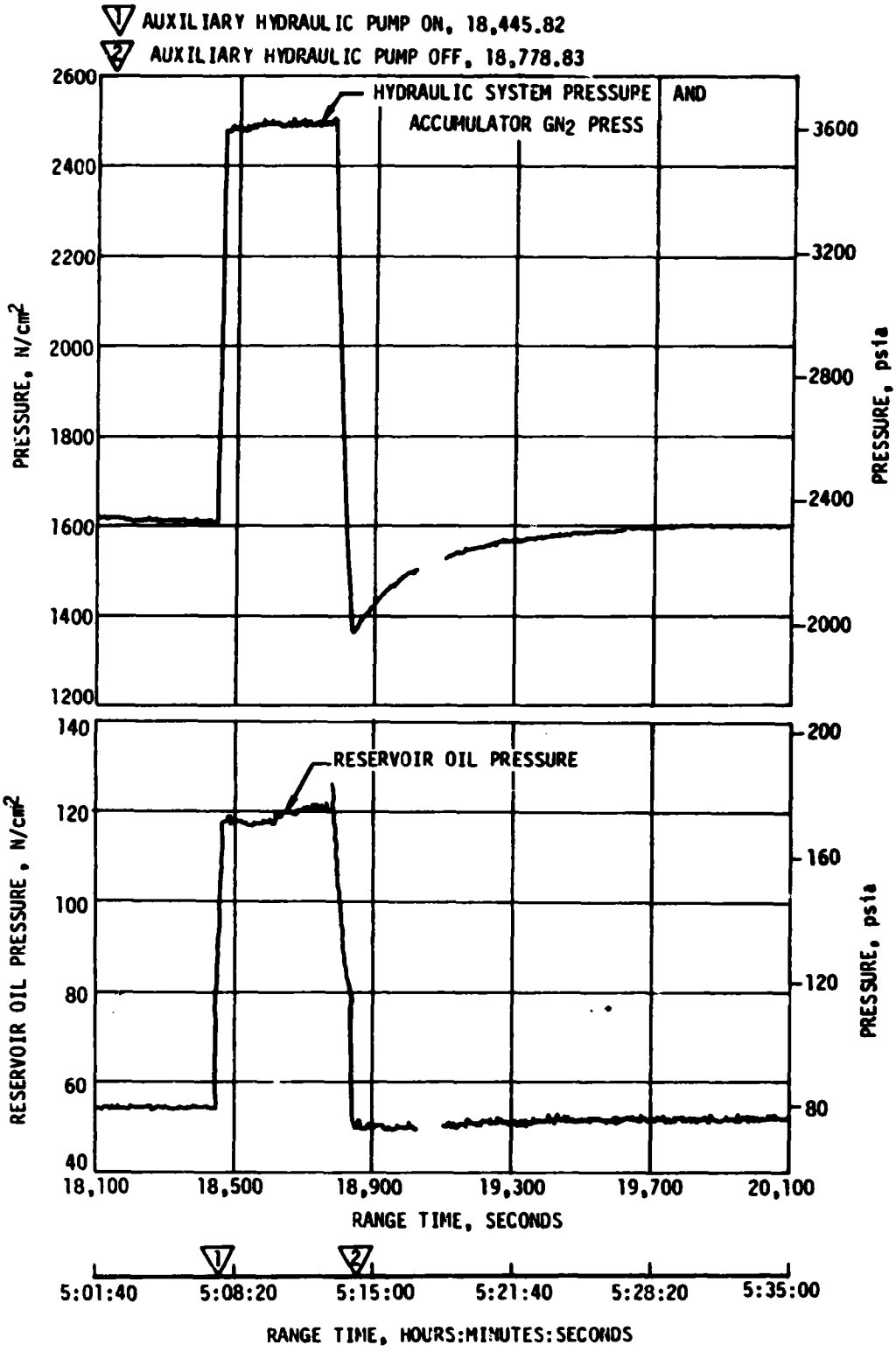

Figure 8-7. S-IVB Hydraulic System Pressures During LOX Dump

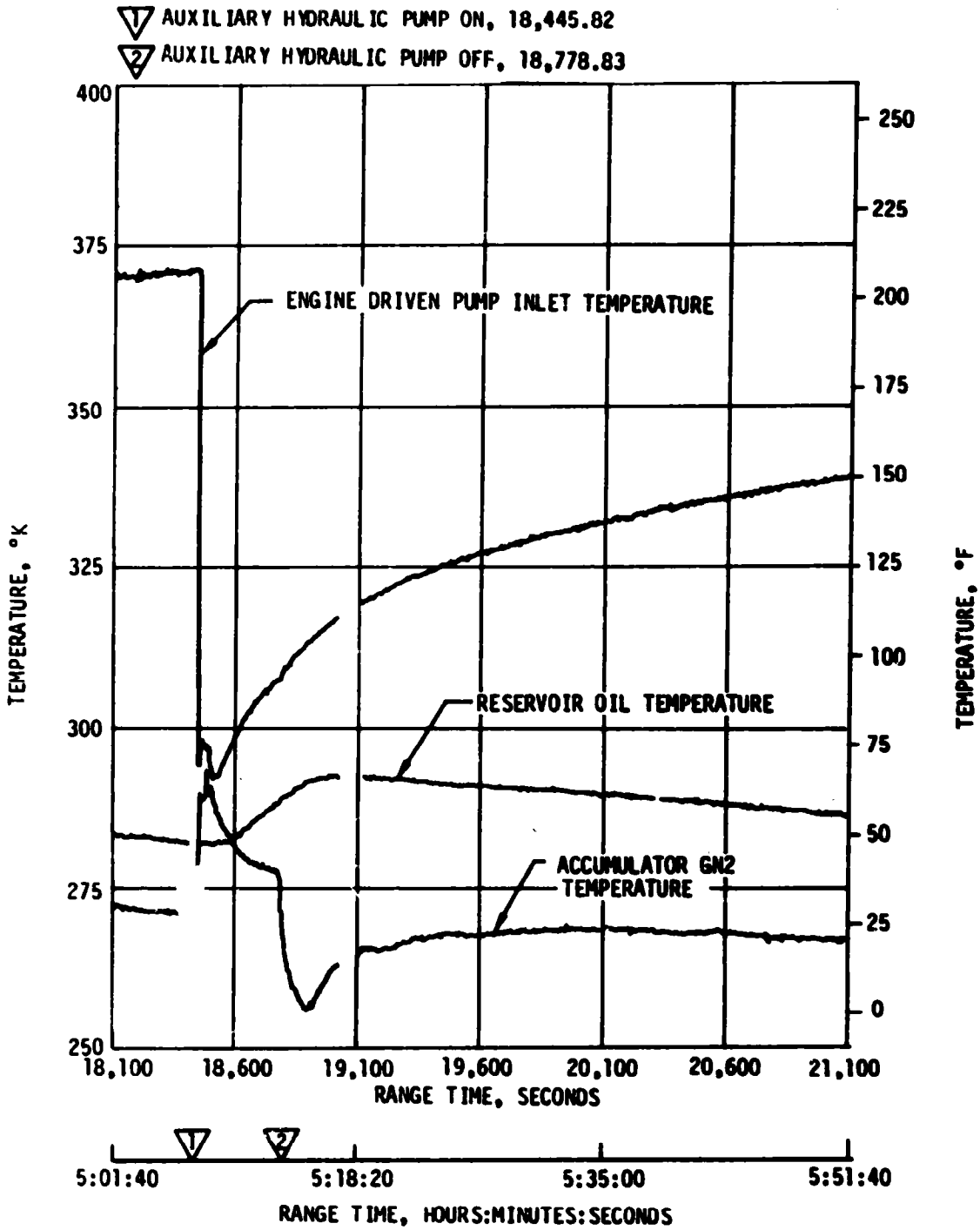

Figure 8-8. S-IVB Hydraulic System Performance During LOX Dump

SECTION 9

STRUCTURES

9.1 SUMMARY

The structural loads and dynamic environment experienced by the AS-503 launch vehicle were well within the vehicle structural capability. Vehicle loads, due to the combined rigid body and dynamic longitudinal load and bending moment, were well below limit design values.

The transients, due to thrust buildup and vehicle release, resulted in maximum longitudinal and lateral (yaw plane) dynamic peak accelerations of ±0.3 g and ±0.24 g, respectively, at the command module. The maximum bending moment condition, 6.78 x 10^6 N-m (60 x 10^6 lbf-in.), was experienced at 74.7 seconds. The maximum longitudinal loads were experienced at 153.82 seconds, Outboard Engine Cutoff (OECO), at an acceleration of 4.0 g.

Vehicle dynamic characteristics followed the trends established by preflight analyses. The POGO suppression system apparently performed well, as the first mode frequency of the outboard LOX suction ducts was lowered to approximately 2 hertz as predicted, and there was no evidence of an unstable coupled thrust-structure-feed system oscillation (POGO) during S-IC powered flight.

Fin bending and torsional modes compared well with analytical predictions. On previous flights the fin vibrations exceeded the range of the accelerometers. On AS-503 the measurement range was increased and the measured vibration levels remained within range and below design values at all times. No fin flutter occurred.

S-IC stage vibrations were generally as expected except at the heat shield. The heat shield flight vibration environment, measured for the first time on AS-503, was considerably higher than expected. This high vibration may have contributed to the loss of M-31 insulation discussed in Section 17. S-II stage and S-IVB stage vibrations were also generally as expected considering the fact that certain measurements were relocated and improved measurement systems were used. The S-IVB stage ASI lines dynamic strains measured in flight were within the range of similar data recorded during static firing. Instrument Unit vibrations compared favorably with those of previous Saturn V flights.

A buildup and subsequent decay of longitudinal and lateral structural oscillations was evident during S-II powered flight shortly after the mixture ratio shift. Details of this buildup are discussed in Section 6A.

9.2 TOTAL VEHICLE STRUCTURES EVALUATION

9.2.1 Longitudinal Loads

The vehicle longitudinal dynamic response due to thrust buildup and release is shown in Figure 9-1. The axial dynamic loads derived from strain gage data are shown at the S-IC intertank and forward skirt. The command module response, where astronaut comfort is of prime concern, is given in terms of acceleration. A frequency analysis of the filtered data indicated a predominance of 3.8 hertz (tank bulging mode) and 4.4 hertz (first longitudinal mode) oscillations, as expected. Oscillations observed in the axial load plots are not as pronounced as in the acceleration data because of the low frequency limitation (2.4 hertz) of the telemetry system from which the strain data was obtained.

In general, the AS-503 vehicle longitudinal dynamic response amplitudes at launch were approximately the same as those experienced on AS-502. The maximum response (simulated) at the command module was approximately ±0.4 g on both AS-503 and AS-502. The maximum measured response at the command module of AS-503 was ±0.3 g. The AS-502 measured data was considered invalid.

The slow release device rod force displacement characteristics shown in Figure 9-2 represent an average per instrumented rod. On AS-503, for the 12 rods used, only 6 were instrumented and, of these, only 3 yielded valid data. The differences in the curves shown for the three Saturn V launches are apparently due to variations in release rod easing techniques.

The longitudinal loads which existed at the time of maximum aerodynamic loading (maximum bending moment), at Inboard Engine Cutoff (IECO), and at OECO are shown in Figure 9-3. These loads were as expected with the maximum longitudinal loads (at the critical stations) occurring at OECO at a rigid body longitudinal acceleration of 4.0 g.

Figure 9-4 shows longitudinal dynamic response time histories at the S-IC inboard and outboard engine gimbal blocks and at the command module (simulated) during S-IC OECO. The amplitudes shown agree favorably with those of previous Saturn V flights.

9.2.2 Bending Moments

The lateral loads experienced during thrust buildup and release were much lower than design because of the favorable winds experienced during launch. The wind speed was low, 5.1 m/s (10 knots) at the 18.3 meters (60 ft) level, and the 360 degrees wind azimuth brought about a tower

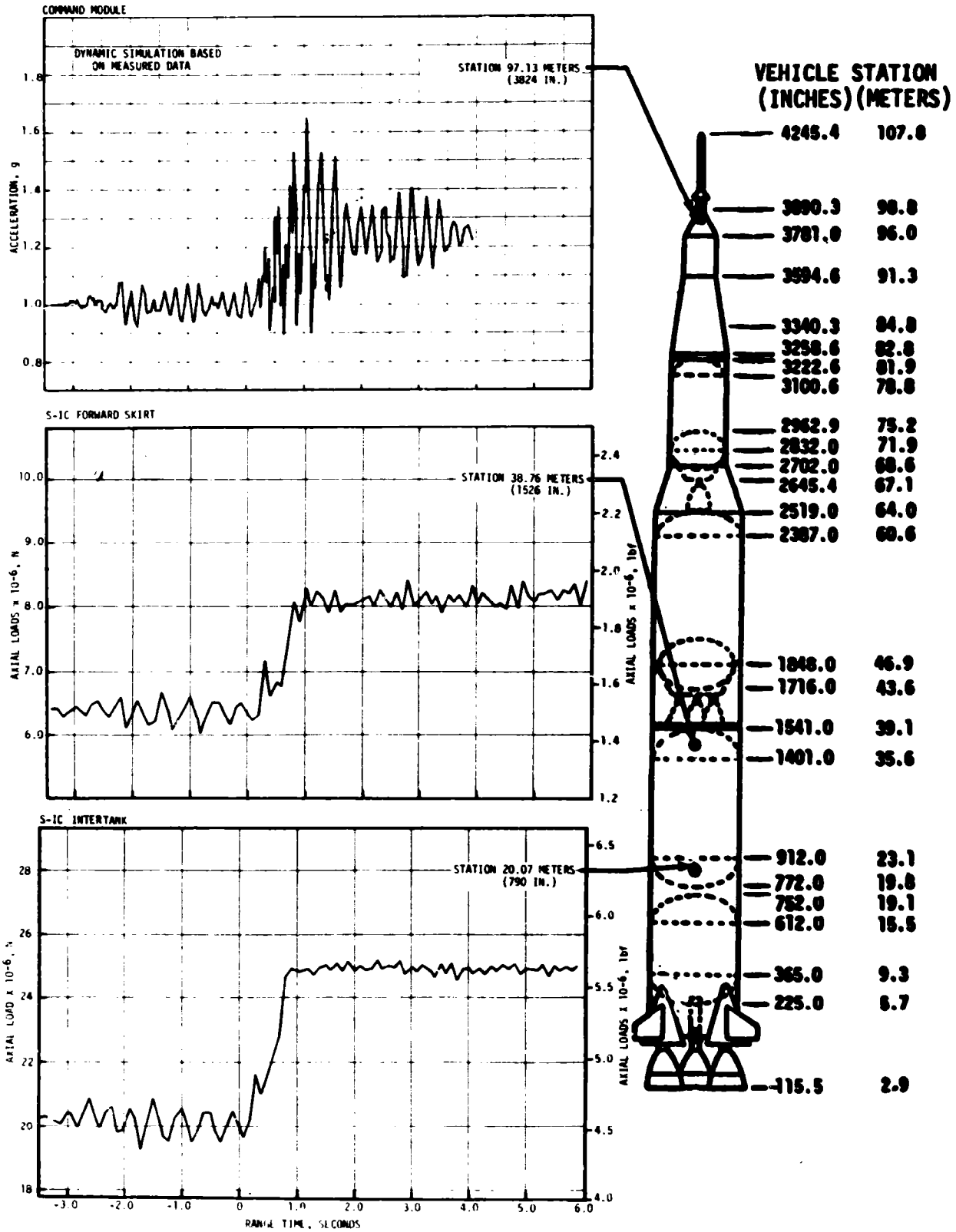

Figure 9-1. Longitudinal Structural Dynamic Response due to Thrust Buildup and Release

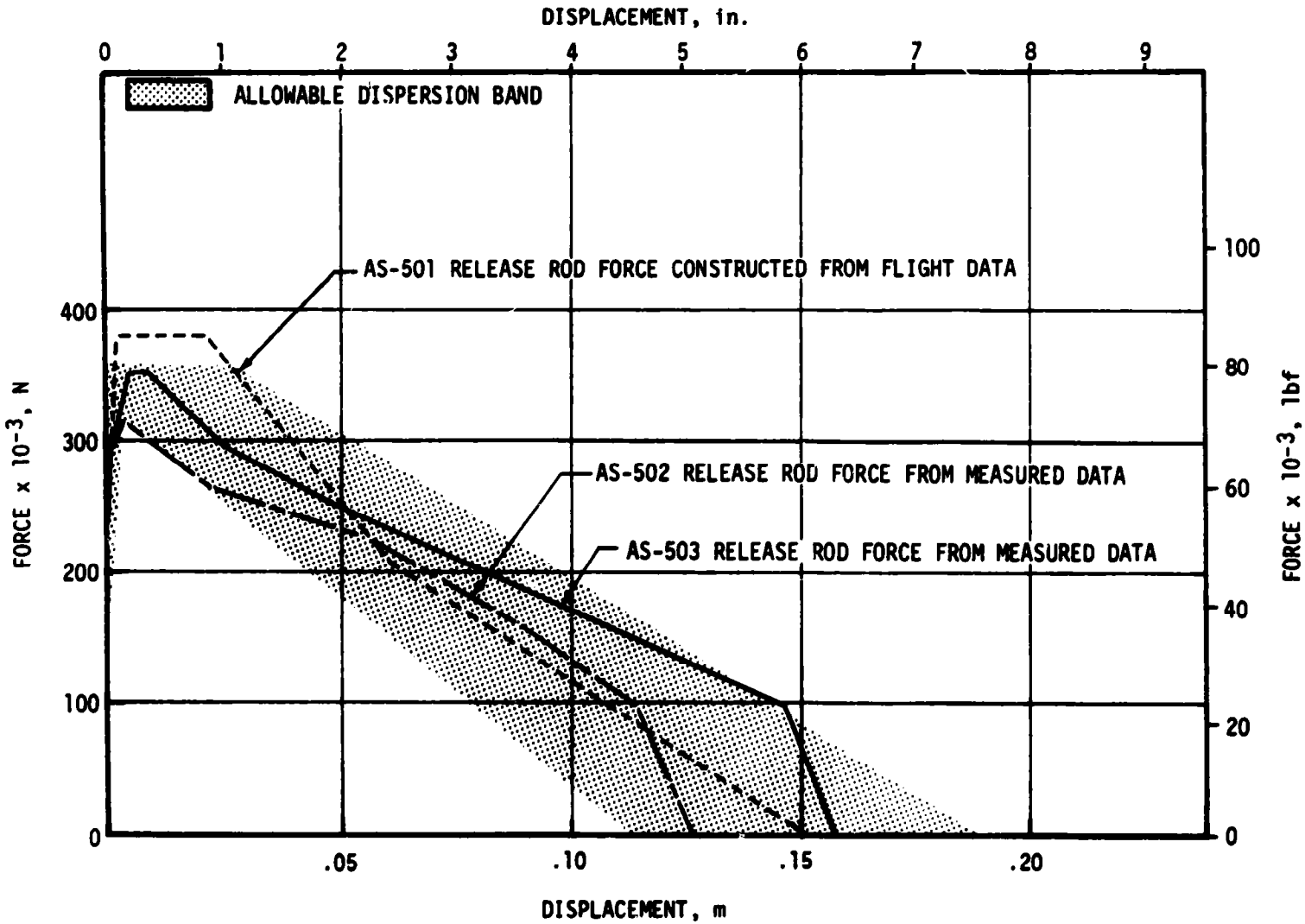

Figure 9-2. Release Rod Force Displacement Curves

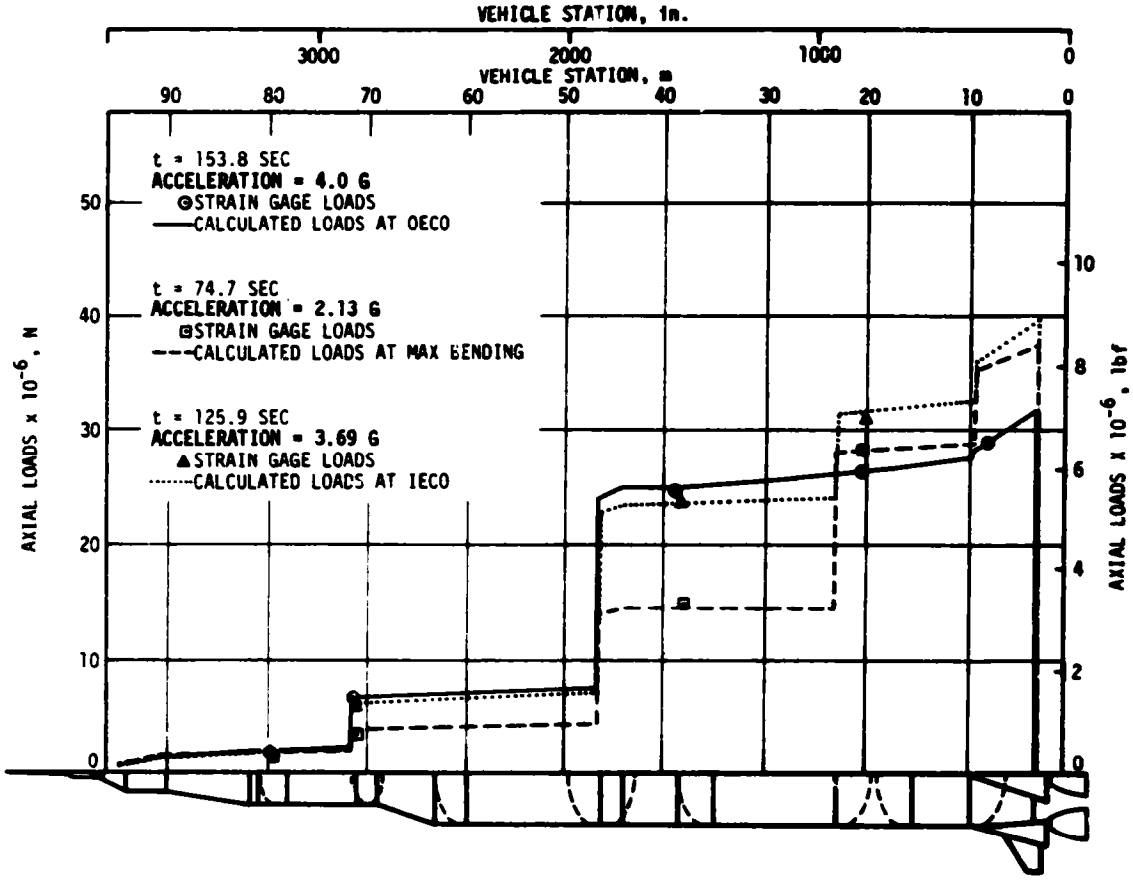

Figure 9-3. Longitudinal Loads at Maximum Bending Moment, Inboard Engine Cutoff, and Outboard Engine Cutoff

shielding effect. The comparable launch vehicle peak design wind is 18.9 m/s (36.8 knots), and the spacecraft peak design wind is 14.4 m/s (28 knots).

Figure 9-5 shows the absolute value of the resultant moments imposed at the S-IC intertank and forward skirt during thrust buildup and release. These loads are based on measured strain gage data, and since they are plotted as absolute values are representative of magnitude only and not frequency. The peak loads occurring just after release are due to lateral response or twang. The longer duration load buildup and decay starting at about 1.8 seconds is caused by the tower clearance yaw maneuver. The pitch plane dynamic response at the command module during launch is also presented in Figure 9-5. The maximum command module response accelerations were found to be ±0.12 g in pitch and ±0.24 g in yaw.

The conditions which existed during the high aerodynamic loading phase of flight were such as to cause near minimal lateral loads. This is illustrated by a comparison of the maximum AS-503 flight bending moments with design values shown in Figure 9-6. The lateral load factor is also shown. The 6.78 x 10^6 N-m (60 x 10^6 lbf-in.) maximum bending moment at

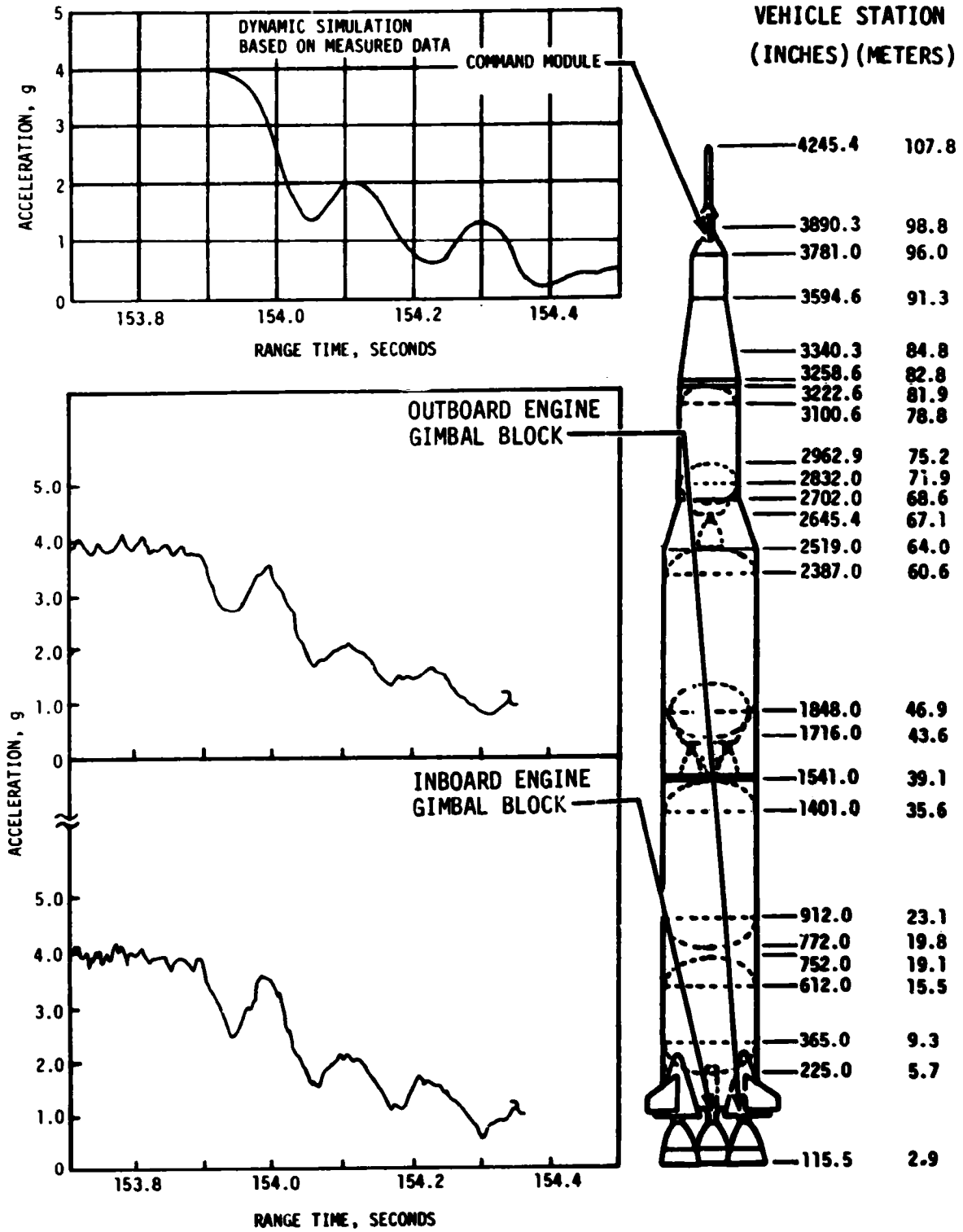

Figure 9-4. Longitudinal Structural Dynamic Response Due To Outboard Engine Cutoff

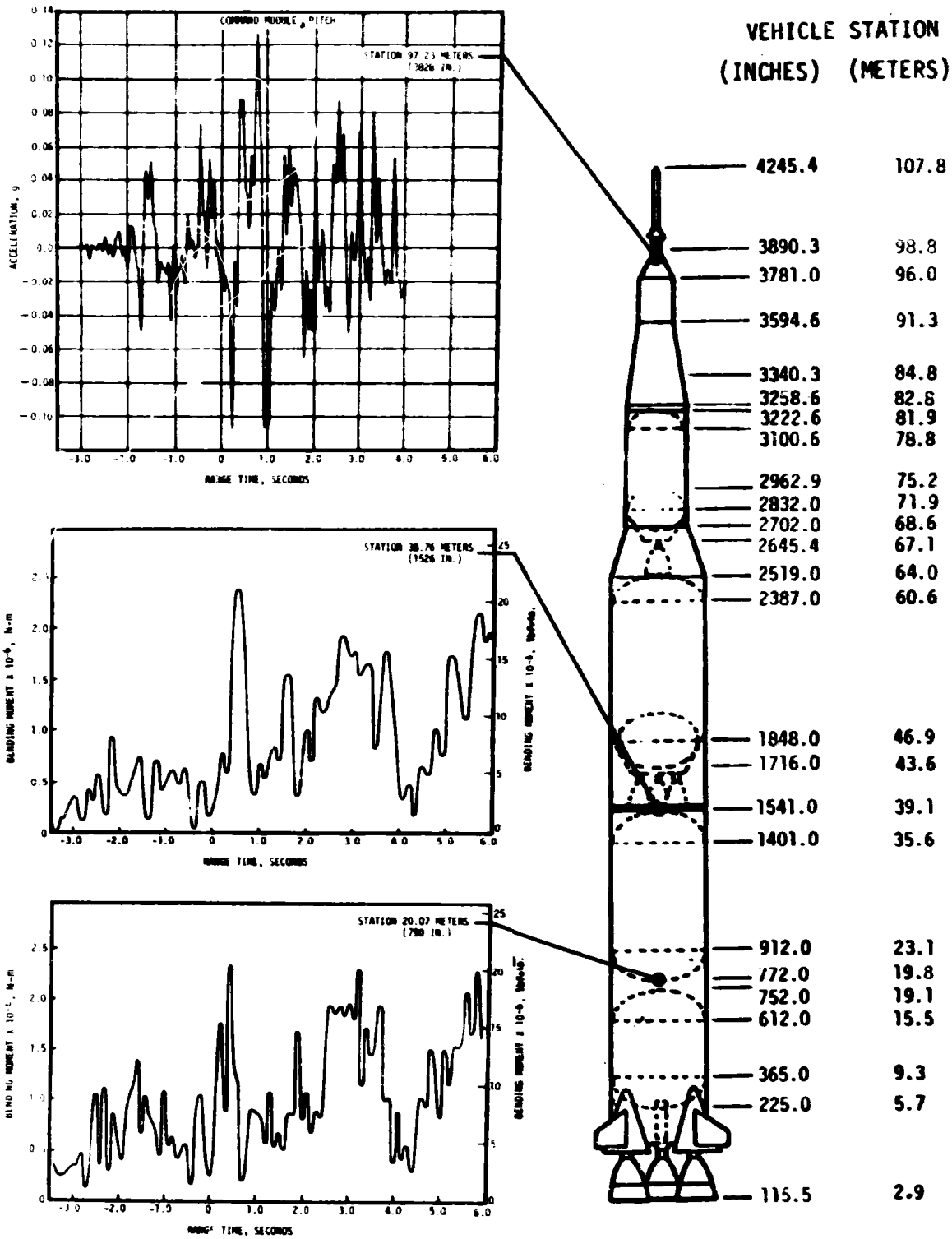

Figure 9-5. Lateral Loads and Structural Dynamic Response During Thrust Buildup and Release

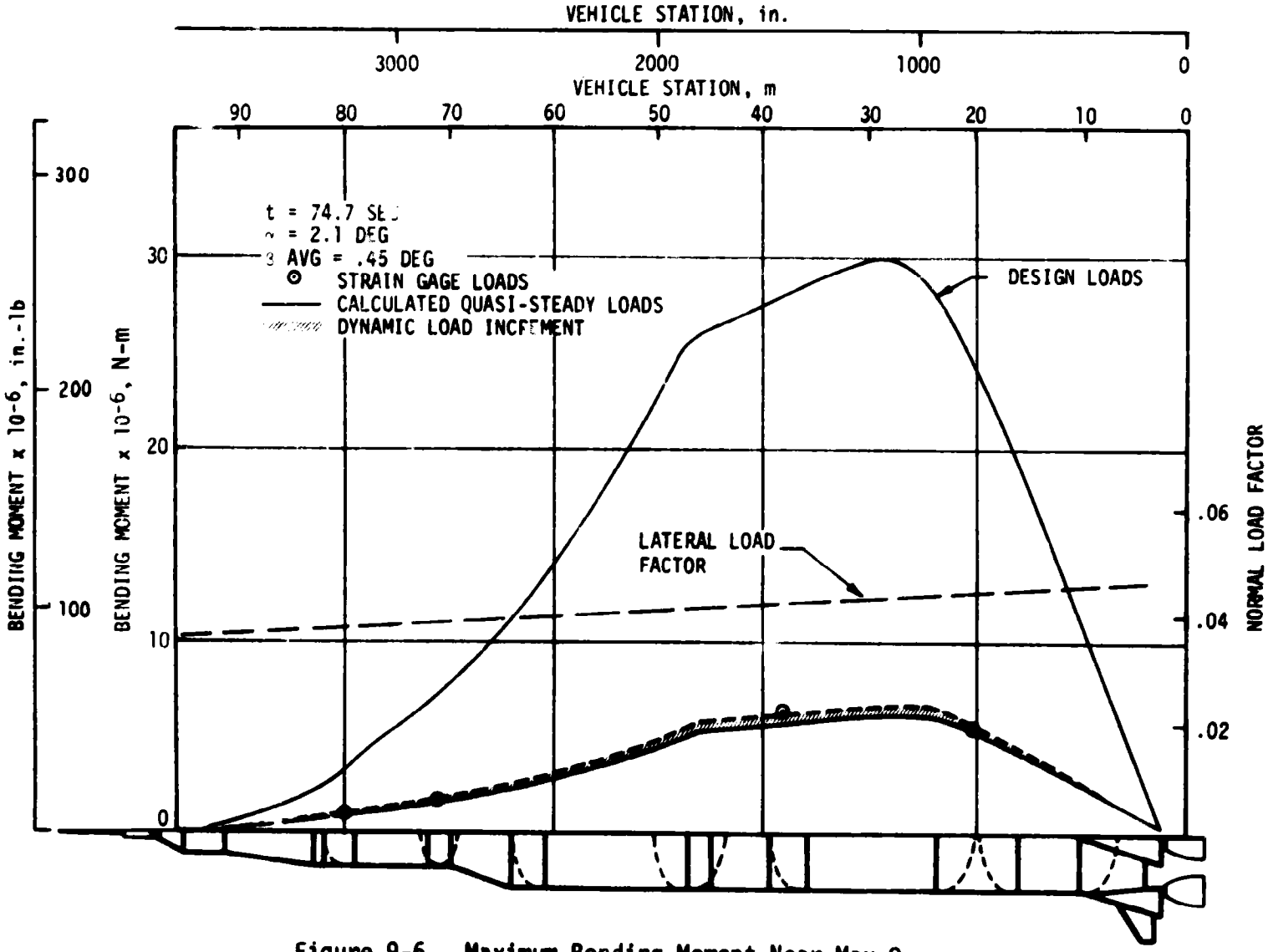

Figure 9-6. Maximum Bending Moment Near Max Q

station 27.94 meters (1100 in.) at 74.7 seconds was less than 25 percent of the design criteria. The calculated loads are from a simulation based on measured flight parameters such as thrust, gimbal angle, dynamic pressure, angle-of-attack, and modal accelerations. The bending moments indicated by circles were derived from measured strain gage data.

9.2.3 Vehicle Dynamic Characteristics

Structural dynamic characteristics are presented in this section for the S-IC stage powered flight. Evaluation of S-II powered flight indicated a pronounced oscillatory buildup in both the lateral and longitudinal directions at approximately 480 seconds. Dynamic characteristics relating to this oscillation are discussed in Section 6A.

9.2.3.1 Longitudinal Dynamic Characteristics. Frequency versus range time for the first longitudinal mode is compared with the analytical data in Figure 9-7. Modal amplitude versus range time is also shown. The measured frequencies, determined by spectral analysis using 5-second time slices, agree well with the analytical prediction. The maximum amplitude in this mode, 0.15 Gpeak, occurred at the command module at 143 seconds and was much lower than the maximum AS-502 amplitude. Figure 9-8 shows a comparison of normalized flight data with analytically predicted longitudinal mode shapes.

The accumulator modification on the outboard LOX suction ducts successfully suppressed the POGO response that the AS-502 vehicle experienced during flight, as there was no evidence of POGO during AS-503 S-IC powered flight. The observed propellant line frequencies from AS-503 flight data agreed well with the predicted frequencies. Since the AS-502 POGO problem involved frequencies in the 5 to 6 hertz frequency range, particular emphasis was placed on evaluation of flight data at these frequencies.

Structural oscillations at the 5 hertz frequency were lower than those measured on AS-501 and much less than those seen on AS-502. These oscillations were approximately the same magnitude after IECO as before IECO. Therefore, this engine did not contribute significantly to the 5 hertz response even though it was unmodified. Table 9-1 shows a comparison of acceleration for several locations on the vehicle with that measured on the AS-501 and AS-502 vehicles.

Chamber pressure measurements were in the noise level in the frequencies from 0 to 15 hertz. Therefore, the oscillatory thrust was very low and could not be determined.

The pump inlet pressure measurements were good throughout flight, and the propellant line frequencies could be detected from these data. All line frequencies were verified as within the predicted ranges with the exception of the second outboard LOX line mode where response was too low to measure. A comparison of predicted and observed line frequencies are shown in Table 9-2.

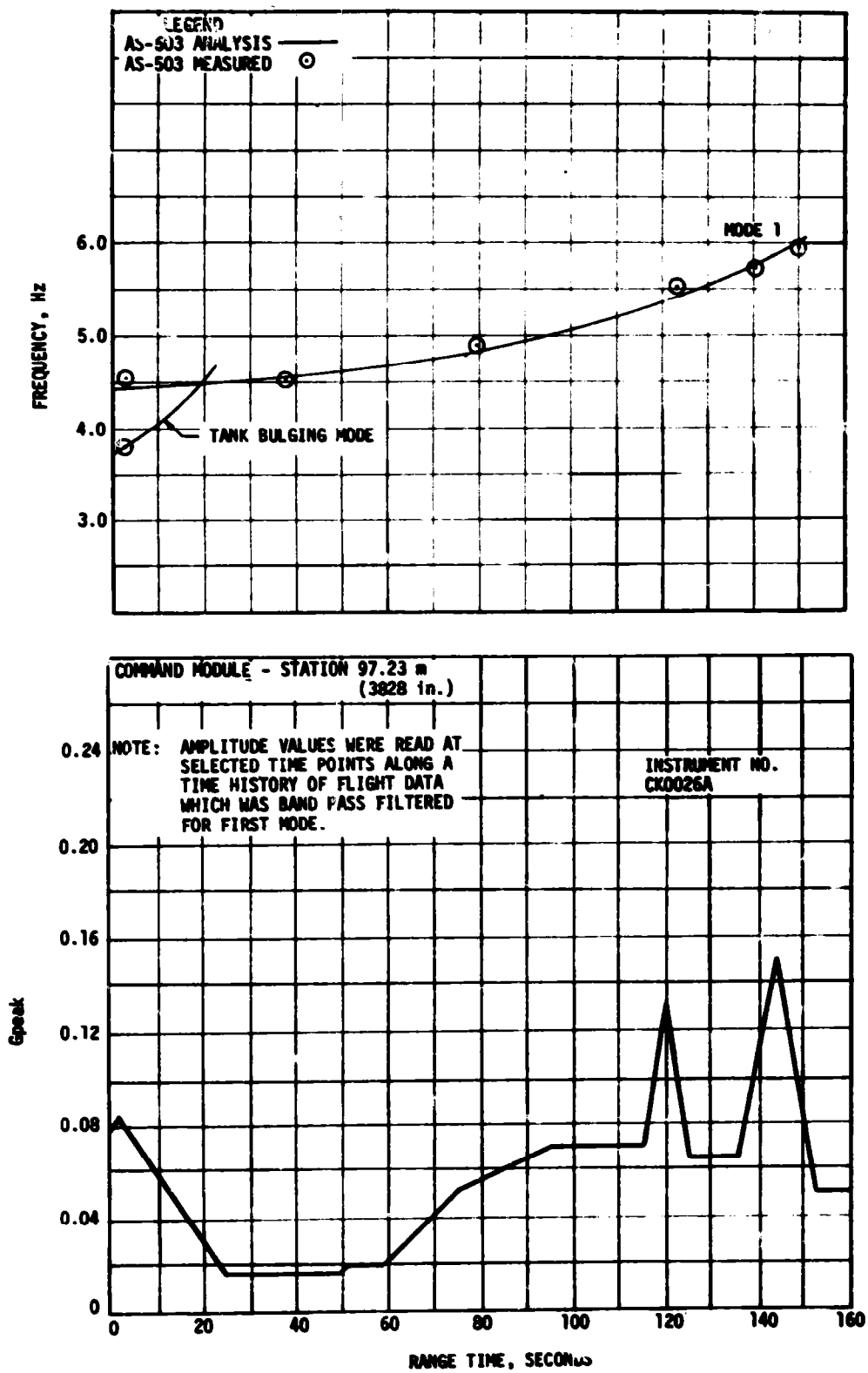

Figure 9-7. First Longitudinal Modal Frequencies and Amplitudes During S-IC Powered Flight

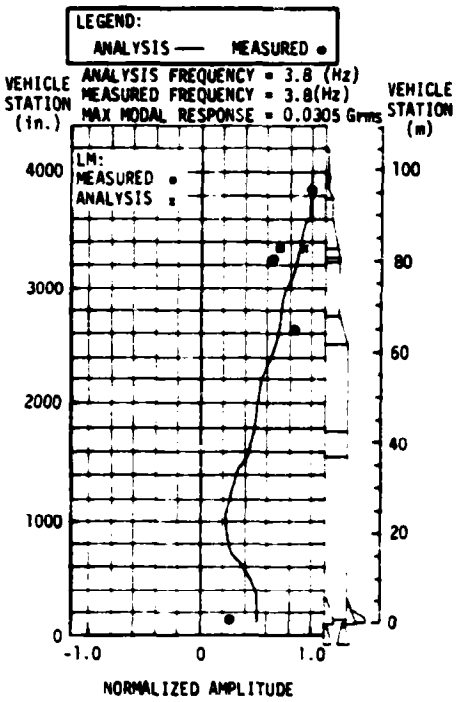

TANK BULGING MODE SHAPE AT LIFTOFF

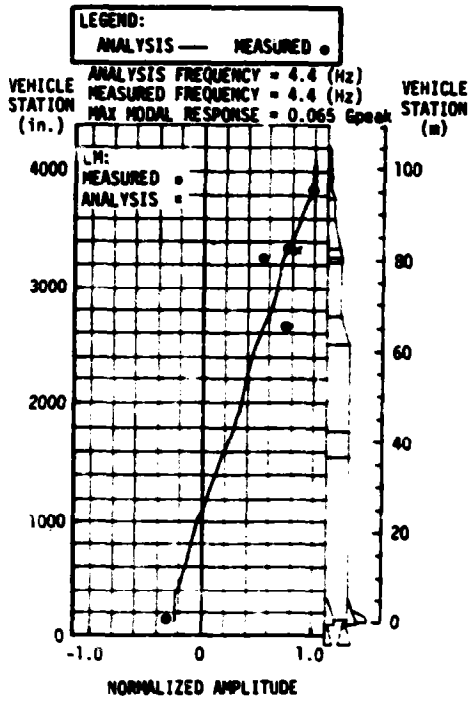

FIRST LONGITUDINAL MODE SHAPE AT LIFTOFF

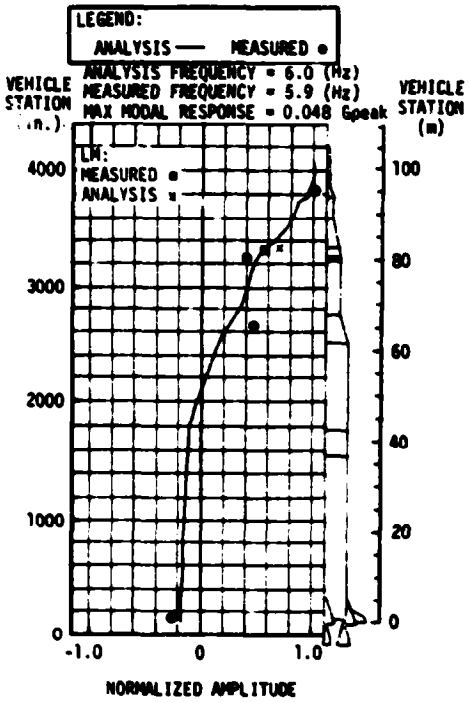

FIRST LONGITUDINAL MODE SHAPE AT 151 SEC

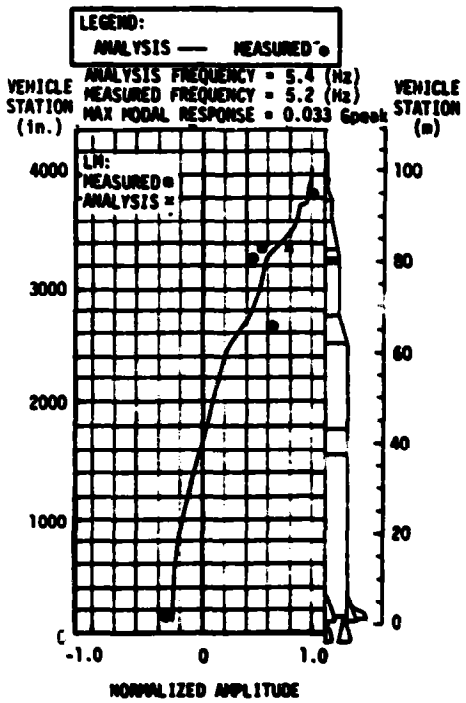

FIRST LONGITUDINAL MODE SHAPE AT 120 SEC

NOTE: TIMES INDICATED ARE FOR THE ANALYTICAL DATA. MEASURED DATA WERE TAKEN FROM A SPECTRAL ANALYSIS OF A TIME SLICE NEAR THE INDICATED TIMES.

Figure 9-8. Longitudinal Mode Shapes During S-IC Powered Flight

Table 9-1. Saturn V First Longitudinal Mode Response Comparison During S-IC Powered Flight

INSTRUMENT NUMBER	STATION-METERS (INCHES)	AS-501 ACCELERATION Gpeak	AS-502 ACCELERATION Gpeak	AS-503 ACCELERATION Gpeak
Command Module		0.2	0.6	0.15
A2-603	82.55 (3250)	0.05	0.14	0.05
E58-118	21.62 (851)	0.04	0.14	0.024
E93-119	Aft LOX Tank Bulkhead 19.61 (772)	*	0.18	0.022
E92-117	Aft Fuel Tank Bulkhead 5.72 (225)	*	0.43	0.028
E57-115	Holddown Post 5.31 (209)	0.06	0.12	0.025
E82-115	3.15 (124)	0.07	0.18	0.025
E83-115	Inboard Engine 3.07 (121)	0.07	0.16	0.025

*Not Instrumented on AS-501

Table 9-2. AS-503 S-IC Stage Propellant Line Frequencies

LINE	MODE	LINE FREQUENCY (Hz) PREDICTED	LINE FREQUENCY (Hz) OBSERVED
LOX	First Inboard	4.9 to 5.5	4.6 to 6.8
	First Outboard	1.8 to 2.2	2.0 to 2.6
	Second Outboard	12.4 to 16	-
	Third Outboard	18.6 to 19.5	17.2 to 20.0
FUEL	First Outboard	10.2	10.6 to 11.8
	First Inboard	12.2	10.8 to 13.6

As in previous flights, the S-IC crossbeam showed responses at approximately 18 hertz throughout flight. A maximum amplitude of ±0.16 g was seen on the inboard engine gimbal block at 10 to 15 seconds. The chamber pressure oscillation is in the noise level at this time. A maximum chamber pressure oscillation of approximately 3.0 N/cm^2 (4.4 psi) at 20 hertz was observed at 100-115 seconds; however, the acceleration on the gimbal block showed a frequency of 17.6 hertz with an amplitude of only ±0.09 g, and no line inlet pressure oscillation could be detected at this time. Therefore, no correlation could be seen with accelerations and propulsion system pressure measurements with regard to flight time, frequency response and amplitude.

Structural response and engine system pressure data showed low responses for all other frequencies in the POGO frequency range; and from the evaluation of the flight data, 5 hertz responses were suppressed without creating any unfavorable responses on other modes of the structural and propulsion system.

9.2.3.2 Lateral Dynamic Characteristics. Oscillations in the first four lateral vehicle modes, as well as the payload mode, were detectable throughout S-IC powered flight. Spectral analyses were performed to determine modal frequencies using 5-second time slices. The frequencies of these oscillations agreed well with the analytical predictions as shown in Figure 9-9.

To obtain maximum acceleration levels, magnetic tape data were filtered using digital filters set at the modal frequency range. The amplitudes of the modal oscillations at the launch escape tower are presented in Figure 9-9. The maximum pitch modal response during S-IC flight was 0.056 Gpeak in the second lateral mode at 5 seconds. This second mode exhibited the most activity during S-IC boost except during Mach 1 and Max Q when the third mode was more active. The yaw modal accelerations exhibited about the same levels of response as did the pitch, except near 2 seconds when the second yaw mode obtained a maximum of 0.10 Gpeak as the vehicle executed the yaw maneuver for tower clearance.

9.2.4 S-IC Fin Dynamics

AS-503 fin vibration levels were below design values. Measured amplitudes were higher at liftoff and in the region of high dynamic pressures than at other flight times as shown in Figure 9-10. This profile of vibration level versus time is similar in shape but somewhat higher than those reported for AS-501 and AS-502. Levels at liftoff and at high dynamic pressure are not available from those flights because of inadequate instrumentation. The fin vibration measurement ranges were increased for AS-503 and measured levels were within range at all times.

Fin frequencies observed on AS-503 are also shown in Figure 9-10 and compared with those measured on the Dynamic Test Vehicle. Frequency variation with velocity is similar to that observed on AS-501 and AS-502. There was no evidence of flutter.

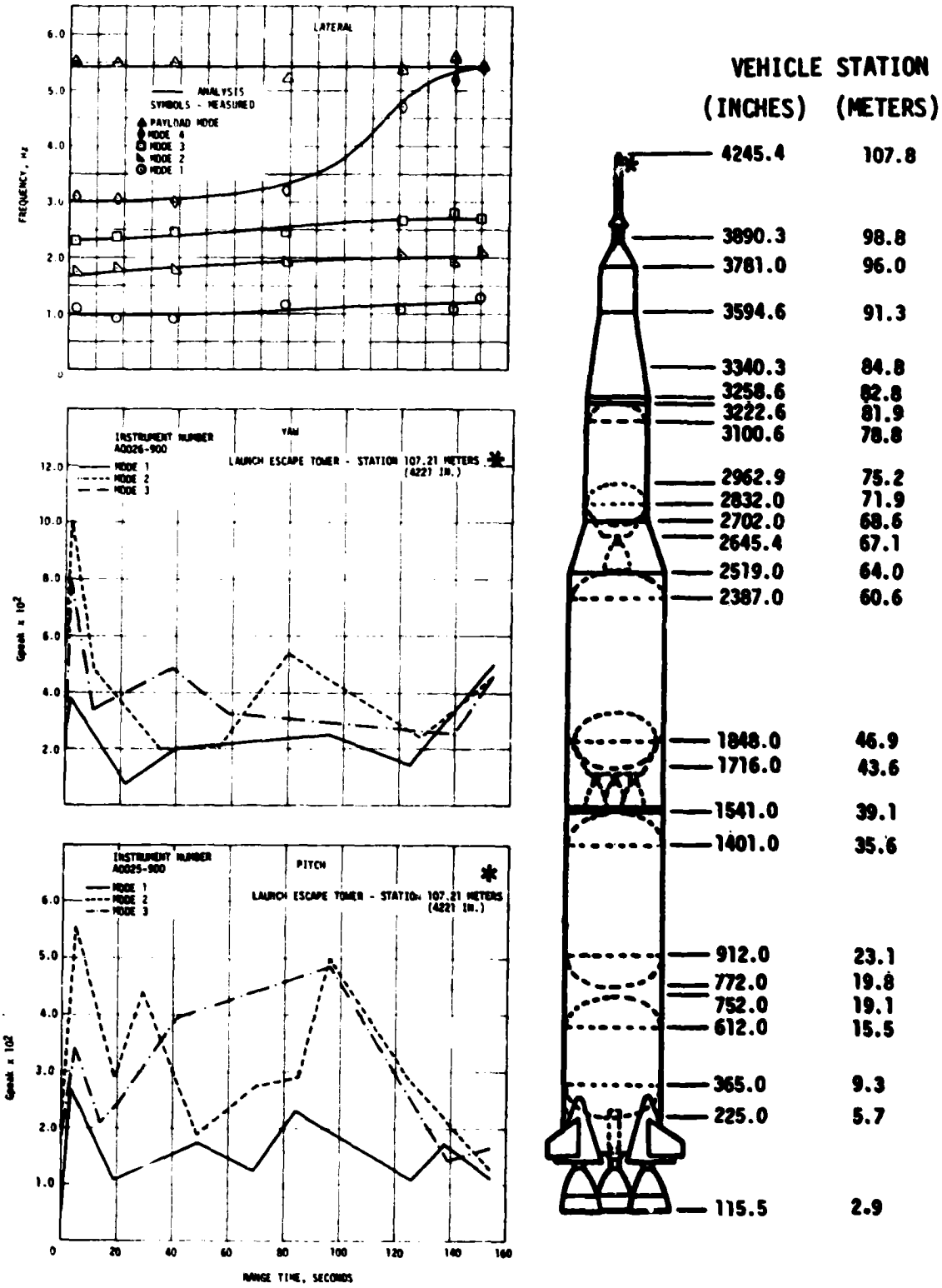

Figure 9-9. Lateral Modal Frequencies and Amplitudes During S-IC Powered Flight

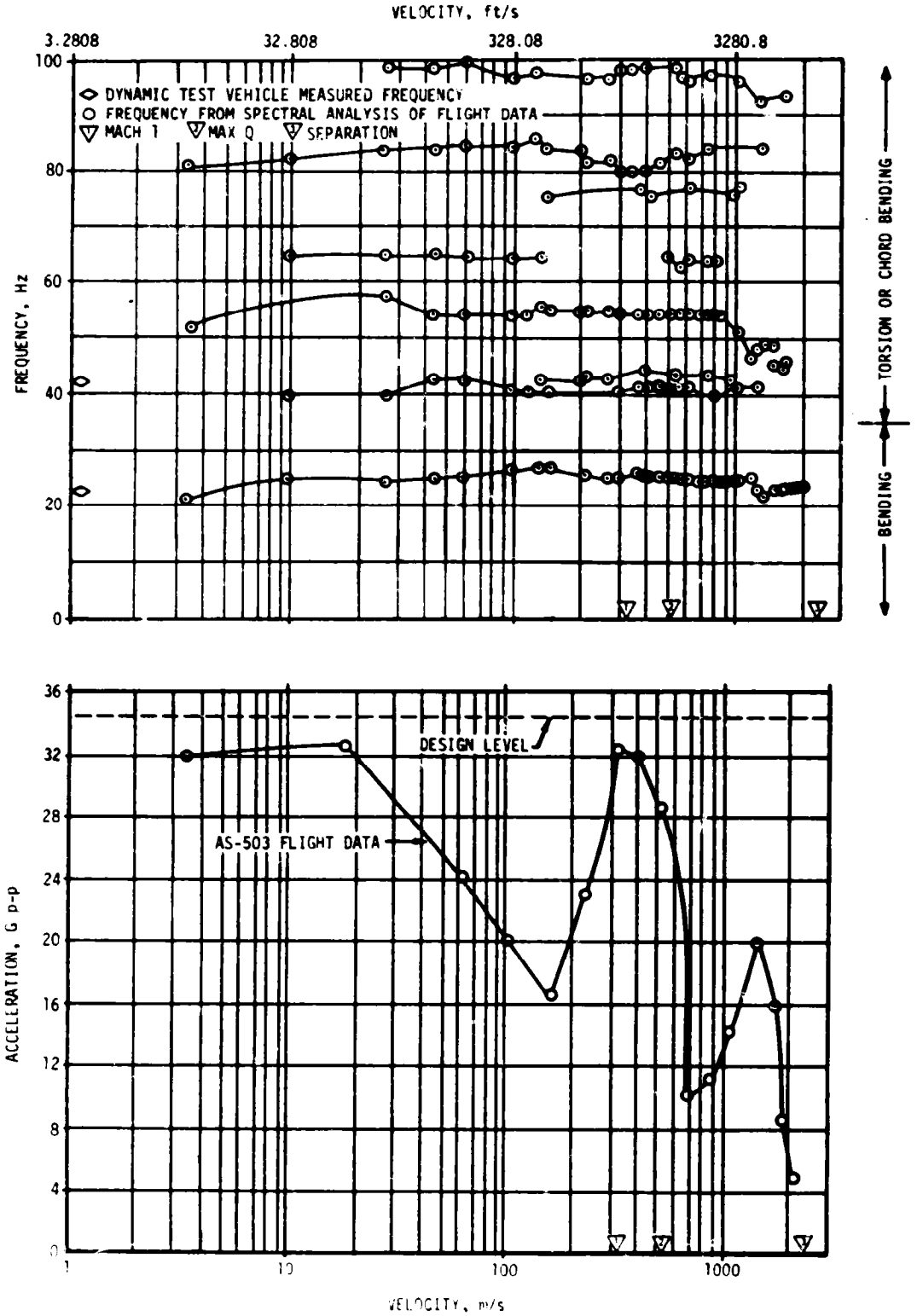

Figure 9-10. S-IC Fin Vibration Response and Bending and Torsional Modal Frequencies

AS-503 fin bending moments were similar to those of AS-501 and AS-502 and were well below design levels.

9.3 VIBRATION EVALUATION

9.3.1 S-IC Stage and Engine Evaluation

Structure, engine, and component vibration measurements taken on the S-IC stage are summarized in Table 9-3 and Figures 9-11 through 9-13. A total of 49 single sideband vibration measurements were taken of which 47 yielded usable data. Measurement locations are shown in Figure 9-14.

9.3.1.1 S-IC Stage Structure. Stage structure vibration data exhibited RMS levels and spectra shapes similar to previous flights. The data, in general, did not appear to be either higher or lower than previous data.

9.3.1.2 F-1 Engines. All five F-1 engine combustion chamber measurements were considered valid. Overall RMS levels of engine No. 2 were somewhat higher than levels of the other engines; however, the overall RMS levels and spectra shapes of all five engine measurements compared favorably to data from flight AS-502. All engine combustion chamber measurements were invalid on AS-501. AS-502 data have been adjusted to correct for a calibration error made in the original analyses.

Turbopump data from two measurements (E37-101 and E38-101) appeared higher from 0 to 30 seconds, but the spectra were similar to static firing data. These measurements have been invalid on past flights. The expected range of data based on static firing was 20 to 30 Grms. Generally, other turbopump measurements compared closely with past flight data in both overall levels and spectra shapes.

9.3.1.3 S-IC Components. The responses of three components on the S-IC, the servoactuators, the cold helium line, and the propellant delivery system showed amplitudes and spectra similar to previous flights. Data from the one measurement on a vibration isolated equipment panel were invalid.

Vibration environments on the heat shield panels were measured for the first time in flight on AS-503. The spectra shapes at launch were similar to those from static firing below about 200 hertz. Above 200 hertz, the flight data at launch are considerably higher than static firing. This resulted in overall RMS levels 1.5 to 2 times as high as expected. The levels drop rapidly to less than 20 percent of launch levels by 30 seconds.

The heat shield vibration experienced at liftoff is in excess of data measured during qualification testing. Some development tests have shown that these levels, when applied to the heat shield for about 10 seconds, have caused severe cracking of the M-31 insulation. This vibration is suspected of causing eventual loss of M-31 as discussed in Section 17.

Table 9-3. S-IC Stage Vibration Summary

MEASUREMENT	MAXIMUM GRMS		DESIGN OVERALL Grms	REMARKS
STRUCTURE	PREVIOUS FLIGHT DATA	AS-503		
Thrust Structure				
E023-115	10.7 at -0.5	14.7 at 0	22	
E024-115	11.2 at 0	8.0 at 0	25	
E049-115	13.9 at 0.5	11.9 at 1	34	
E053-115	6.9 at 149.5	5.5 at 150	17	
E054-115	3.7 at 147.5	3.7 at 150	17	
E079-115	3.2 at 148	3.3 at 148	17	
E080-115	4.2 at 148	3.7 at 148	17	
Intertank Structure				
E020-118	7.7 at 2	4.7 at 3	27	Intertank structure AS-503 data may be invalid at times shown in Figure 9-11; data were less than 5% of calibration level.
E021-118	9.1 at 4	7.0 at -1	27	
Forward Skirt Structure				
E018-120	1.7 at 2.8 and 4.9	1.4 at -1	30	Forward skirt structure AS-503 data may be invalid at times shown in Figure 9-11; data were less than 5% of the calibration level. E047-120 is located near command destruct isolated panel.
E019-120	6.9 at -0.2	5.9 at -1	30	
E047-120	6.1 at 3.9	4.4 at 1	30	
ENGINE				
Combustion Chamber				
E036-101	8.8 at 20.5	7.6 at 60	49	E036-102 invalid on previous flights.
E036-102		9.7 at 0	49	
E036-103	8.3 at 53	7.8 at 120	49	
E036-104	8.4 at 106.8	7.5 at 101	49	
E036-105	8.2 at 130.5	7.6 at 91	49	
Turbopump				
E037-101		41.5 at 20	41	Measurements E037-101, E038-101, E040-101 were invalid on previous flights. E039-101 and E042-104 data were invalid for AS-503.
E038-101		39.0 at 1.0	41	
E039-101	26.5 at 125	--	41	
E040-101		12.5 at 132.5	41	
E041-101	15.4 at 122	19.7 at 152.0	41	E042-102 and E042-103 data were invalid between 0 and 20 seconds.
E041-102	15.2 at 142	17.5 at 144.5	41	
E042-102	9.6 at 86	9.3 at -1.0	41	
E042-103	18.1 at 63	9.3 at 132	41	
E042-104	8.2 at 51	--	41	
E042-105		8.5 at 96.5	41	
COMPONENTS				
Engine Actuators				
E030-101	5.2 at 141.8	9.4 at 111	30	
E030-102	5.0 at 123	4.7 at 113	30	
E031-101	6.2 at 136	4.4 at 129	30	
E031-102	6.5 at 138.9	7.8 at 107	30	
E032-101	10.9 at 141.8	15.1 at 111	30	
E032-102	11.0 at 121	14.0 at 89	30	
E033-101	8.8 at 100	8.7 at 68	30	
E033-102	7.0 at 127	6.7 at 60	30	
E034-101	5.0 at -1.0	4.1 at 63	30	
E034-102	5.5 at 135	5.0 at 125	30	
E035-101	14.6 at 17	15.0 at 68	30	
E035-102	10.5 at 127	9.7 at 0	30	
Helium Line				
E050-116	7.6 at -1.4	5.7 at -1.0	40	AS-503 data from E050-116 may be invalid at times shown in Figure 9-13; they were less than 5% of calibration level.
E051-116	14.0 at 0	12.8 at 1.0	34	
Heat Shield Panels				
E105-106		76.6 at -1	33	Heat shield panel measurements not installed for previous flights. Heat shield panel data may be invalid at times shown in Figure 9-13; data were less than 5% of the calibration level.
E106-106		62.6 at -1	33	
E107-106		68.0 at -1	33	
Propellant Delivery System				
E025-118	2.7 at 13	1.6 at 2.5	9	
E026-118	2.4 at 4.6	2.3 at 0	9	
E027-115	10.4 at -0.5	5.7 at 2.5	22	
E028-115	9.7 at 4.6	9.3 at 92	22	

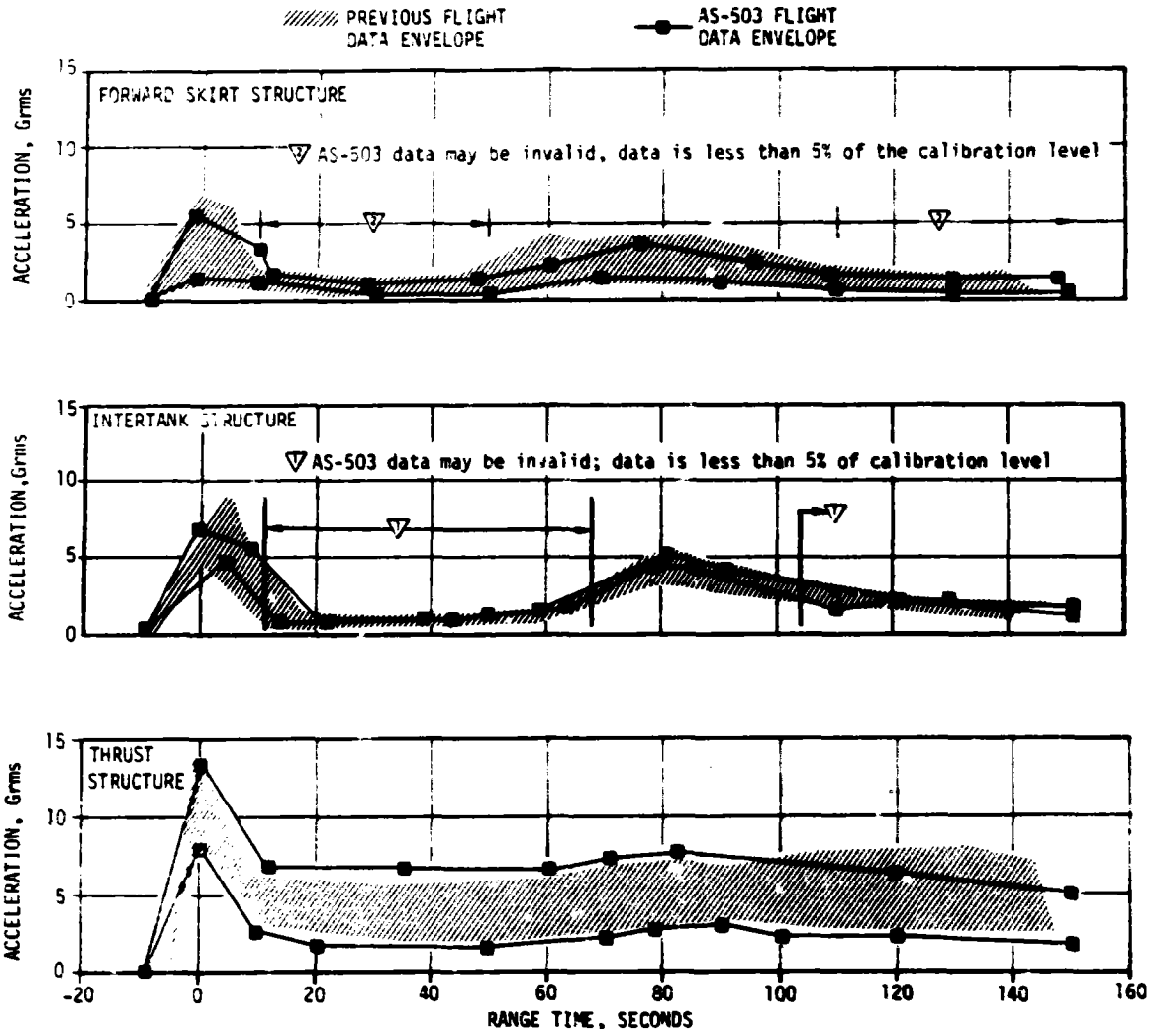

Figure 9-11. S-IC Stage Structure Vibration Envelopes

9.3.2 S-II Stage and Engine Evaluation

Comparisons of Grms values for AS-501, AS-502, and AS-503 are shown in Table 9-4 and Figures 9-15 through 9-17. The variations between the three flights are considered normal.

9.3.2.1 S-II Stage Structure. The AS-503 vibration environment for the interstage in the radial direction exceeds that for the previous flights. This was expected since the measurements were moved to unloaded areas of the interstage structure. No previous measurements were made in the tangential direction.

Although the single measurement on the aft skirt indicated levels comparable with previous flights and static firings, the data is considered to be questionable because the oscillograph trace does not appear to be random data.

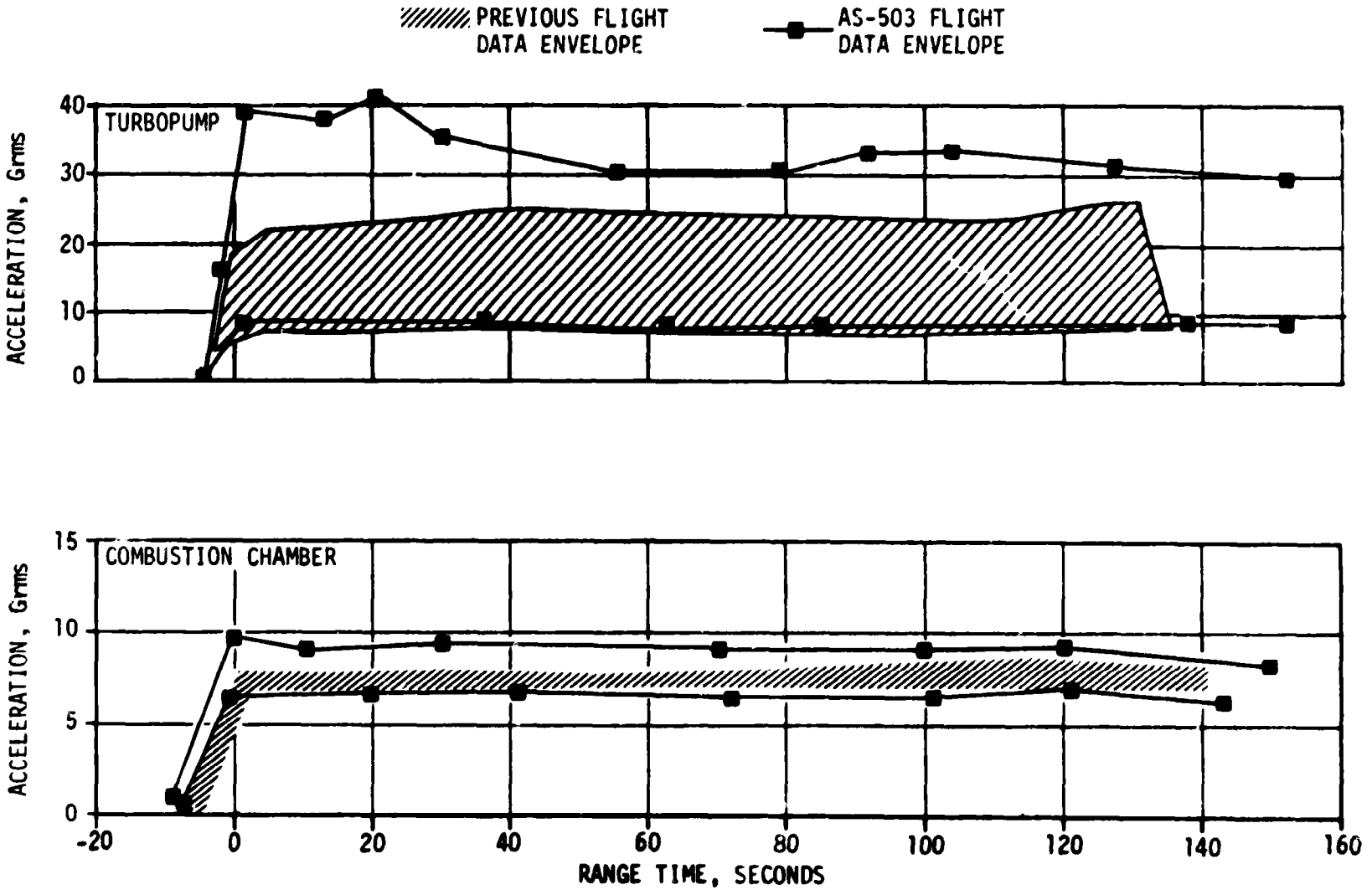

Figure 9-12. S-IC Stage Engine Vibration Envelopes

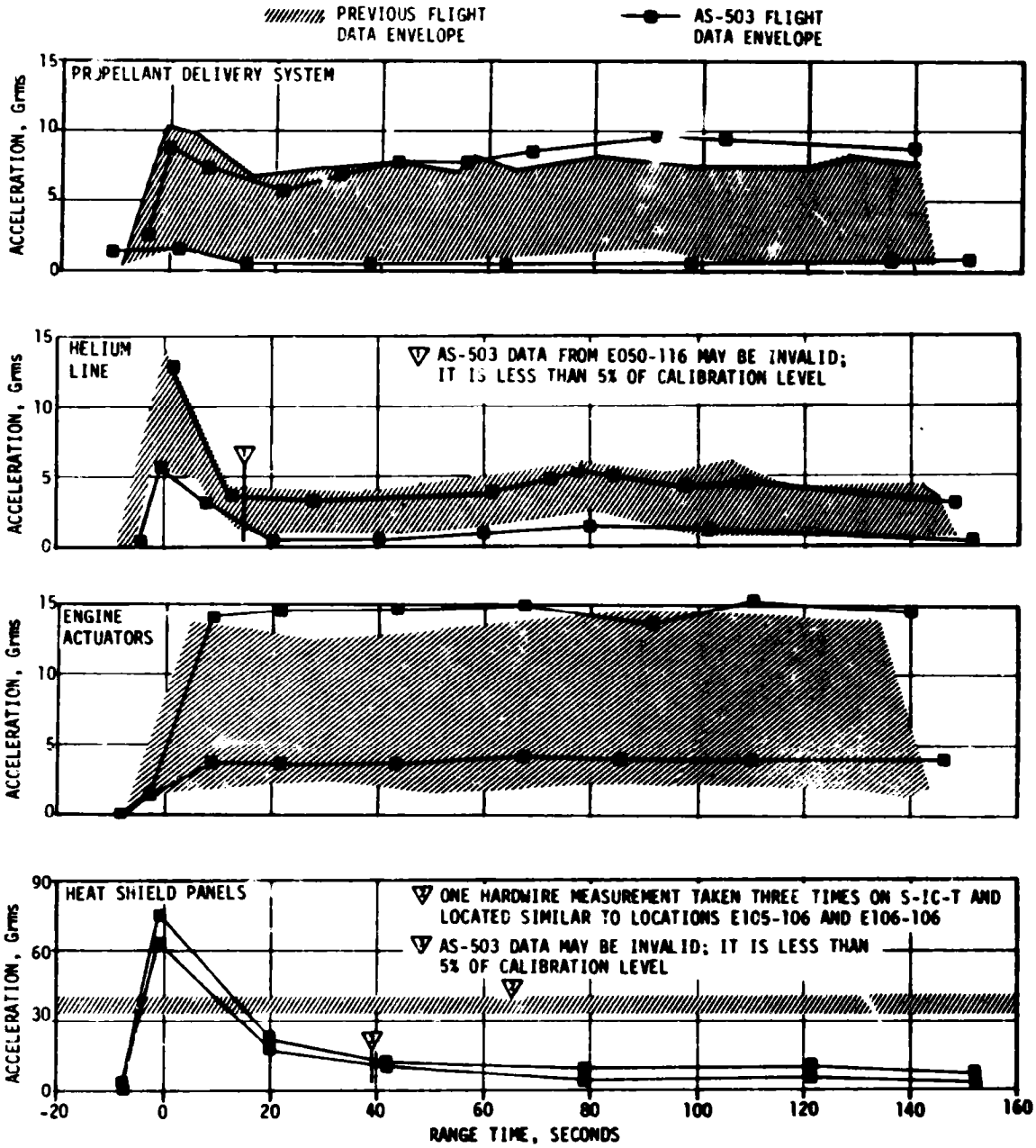

Figure 9-13. S-IC Stage Components Vibration Envelopes

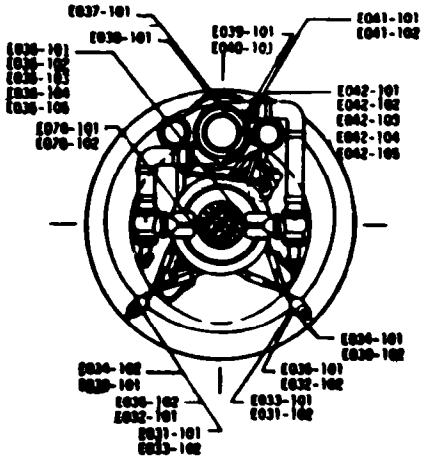

F-1 ENGINE

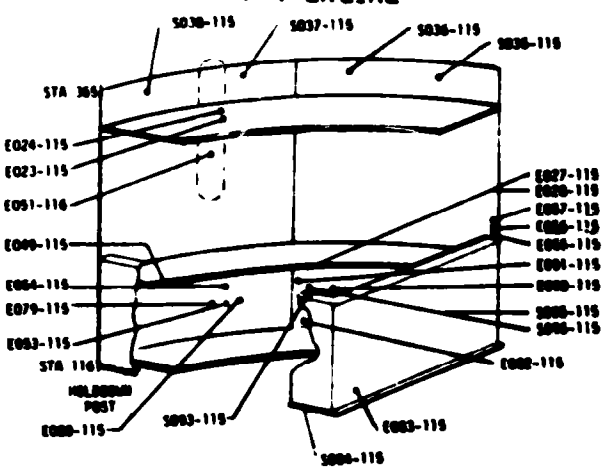

THRUST STRUCTURE

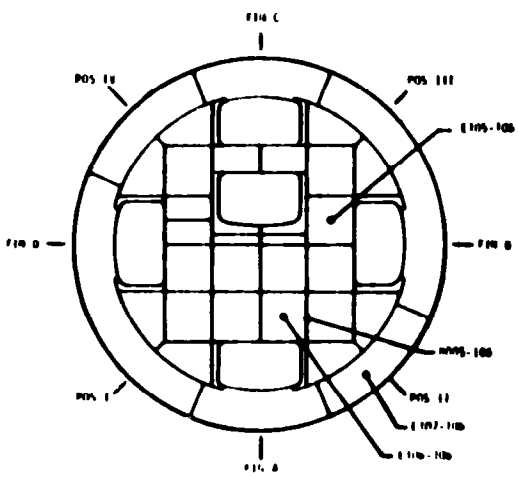

HEAT SHIELD

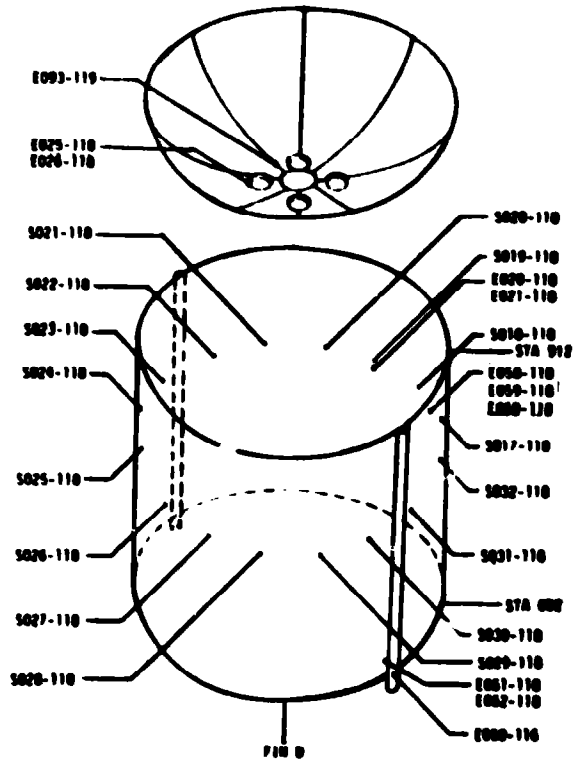

INTERTANK

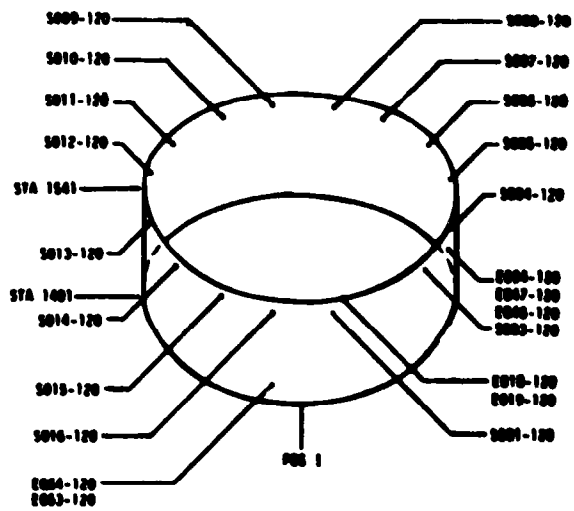

FORWARD SKIRT

Figure 9-14. S-IC Vibration and Strain Measurement Locations

Table 9-4. S-II Stage Vibration Summary

ZONE	NO. OF MEASUREMENTS	S-II, 501, 502 AND 503 STATIC FIRINGS GRMS	OVERALL GRMS				
			VEHICLE	LIFTOFF	TRANSONIC	MAX Q	S-II MAINSTAGE
Forward Skirt Containers	8	0.7 to 2.5	AS-501	1.4 to 8.8	2.1 to 3.7	2.4 to 5.1	0.5 to 0.7
	8		AS-502	2.7 to 9.0	0.7 to 2.5	1.1 to 4.6	0.3 to 0.6
	8		AS-503	0.7 to 9.1	1.0 to 3.7	1.7 to 5.3	0.0 to 0.9
Forward Skirt Stringers	10	1.6 to 4.8	AS-501	3.5 to 11.0	2.3 to 11.3	3.7 to 9.2	0.4 to 0.9
	10		AS-502	3.4 to 13.1	1.8 to 7.6	2.7 to 8.0	0.3 to 0.7
	9		AS-503	1.2 to 8.5	1.0 to 6.8	1.7 to 7.9	0.3 to 1.3
Aft Skirt	4	10.1 to 31.7	AS-501	5.5 to 17.3	3.6 to 6.2	5.7 to 1[illegible].1	1.6 to 2.2
	4		AS-502	5.3 to 14.8	5.2 to 8.3	5.4 to 9.4	0.4 to 1.2
	1		AS-503	Data Questionable			
Interstage	4	Interstage Not Install.	AS-501	3.4 to 5.9	2.0 to 3.5	2.6 to 4.5	2.1 to 3.6
	4		AS-502	3.1 to 4.8	2.2 to 3.3	2.8 to 4.1	1.1 to 1.8
	3		AS-503	7.6 to 16.0	5.6 to 6.5	5.6 to 7.2	1.2 to 2.9
Thrust Structure Containers	10	2.2 to 15.8	AS-501	0.8 to 7.0	0.6 to 1.8	0.6 to 2.2	1.5 to 3.8
	10		AS-502	0.6 to 2.4	0.4 to 1.1	0.5 to 1.4	0.8 to 2.9
	9		AS-503	0.3 to 3.9	0.4 to 2.6	0.3 to 2.2	0.3 to 3.0
Thrust Structure Longitudinal	3	4.1 to 12.3	AS-501	1.6 to 5.1	1.1 to 2.0	1.2 to 2.2	2.8 to 7.2
	3		AS-502	1.0 to 3.7	0.6 to 1.6	0.7 to 1.7	1.6 to 5.1
	3		AS-503	0.2 to 2.9	1.1 to 1.5	1.6 to 2.7	1.0 to 2.3
Engine Beams	5	5.4 to 15.3	AS-501	0.9 to 1.5	0.5 to 0.9	0.6 to 1.0	5.8 to 10.4
	5		AS-502	0.5 to 1.0	0.3 to 0.4	0.4 to 0.5	5.3 to 13.9
	1		AS-503	1.4	0.7	0.7	8.0
Gimbal Pad	1	4.2 to 9.6	AS-501	1.0	0.9	0.9	5.6
	1		AS-502	0.4	0.3	0.3	4.5
	1		AS-503	0.3	0.2	0.4	9.0
Combustion Dome	5	Invalid Data	AS-503	0.8 to 3.6	1.0 to 4.6	1.2 to 3.7	6.5 to 10.3
LOX Pumps	5	Invalid Data	AS-503	0.0 to 2.6	0.0 to 2.6	0.0 to 2.6	3.5 to 16.8
LH_2 Pumps	5	Invalid Data	AS-503	0.0 to 3.1	0.0 to 6.1	0.0 to 6.1	9.2 to 17.2
LOX Sump Prevalve	2	Not Installed	AS-503	0.4 to 0.6	0.5 to 0.7	0.6 to 0.7	0.4 to 2.3
LH_2 Prevalve	3	Not Installed	AS-503	0.2 to 1.0	0.5 to 0.7	0.8 to 0.9	0.6 to 1.8

NOTE: The values listed above for AS-501 & AS-502 are based on PSD overall levels.
The values listed above for AS-503 are based on Grms histories.

9.3.2.2 S-II Stage J-2 Engines. The J-2 engine vibration trends were generally as expected with the maximum levels occurring after S-II engine start. The LOX pump measurements show a sharp amplitude increase at the propellant mixture ratio (PMR) shift time, as expected. This increased vibration results from changed flow characteristics through the LOX pump after the propellant utilization (LOX bypass) valve position is changed.

9.3.2.3 S-II Stage Components. For the AS-503 flight, instrumentation was relocated to better define component and container environments. The levels indicated for the LOX sump prevalves and the LH_2 prevalves were lower than expected. The response levels in the containers were as expected.

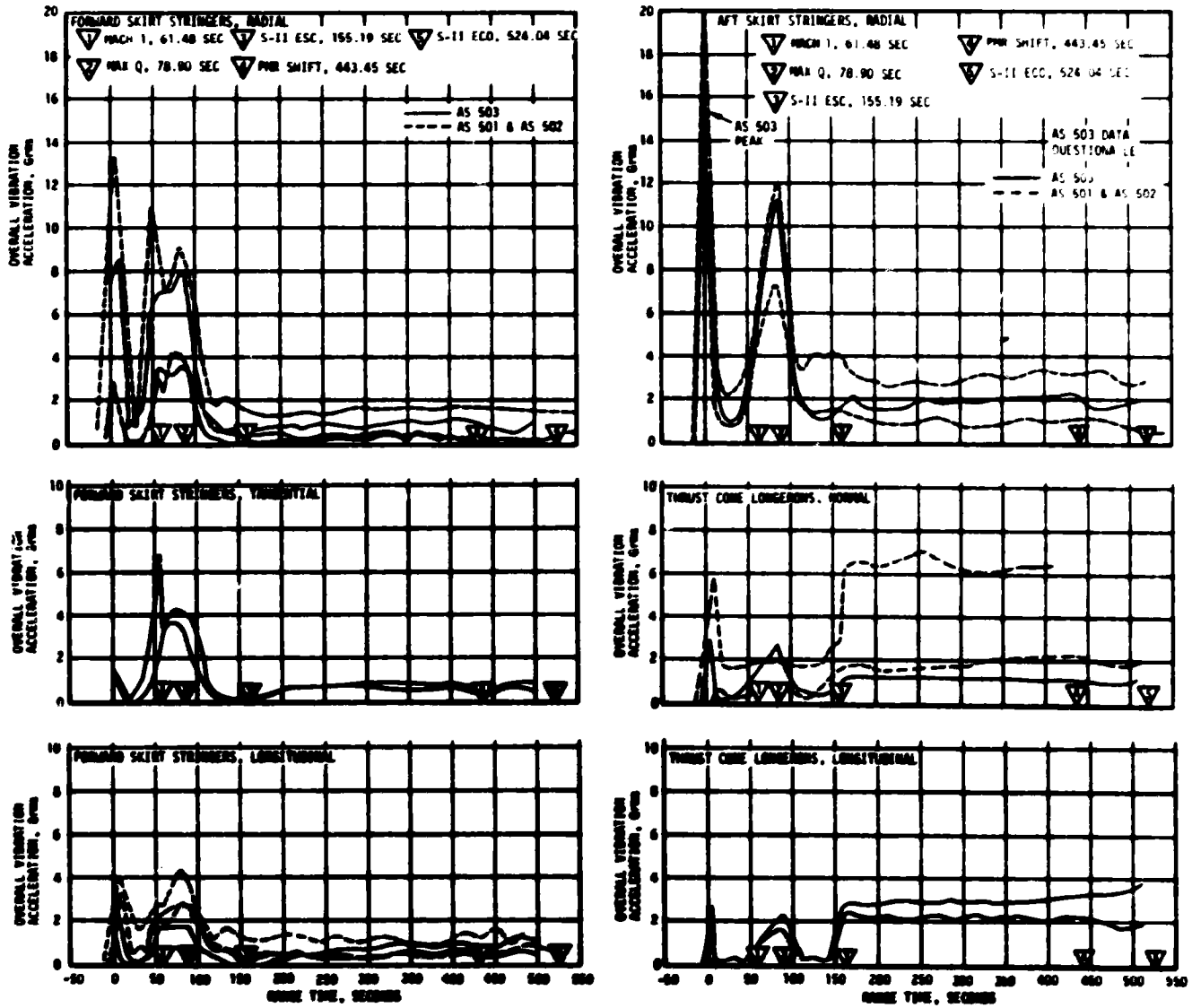

Figure 9-15. S-II Stage Structure Vibration Envelopes (Sheet 1 of 2)

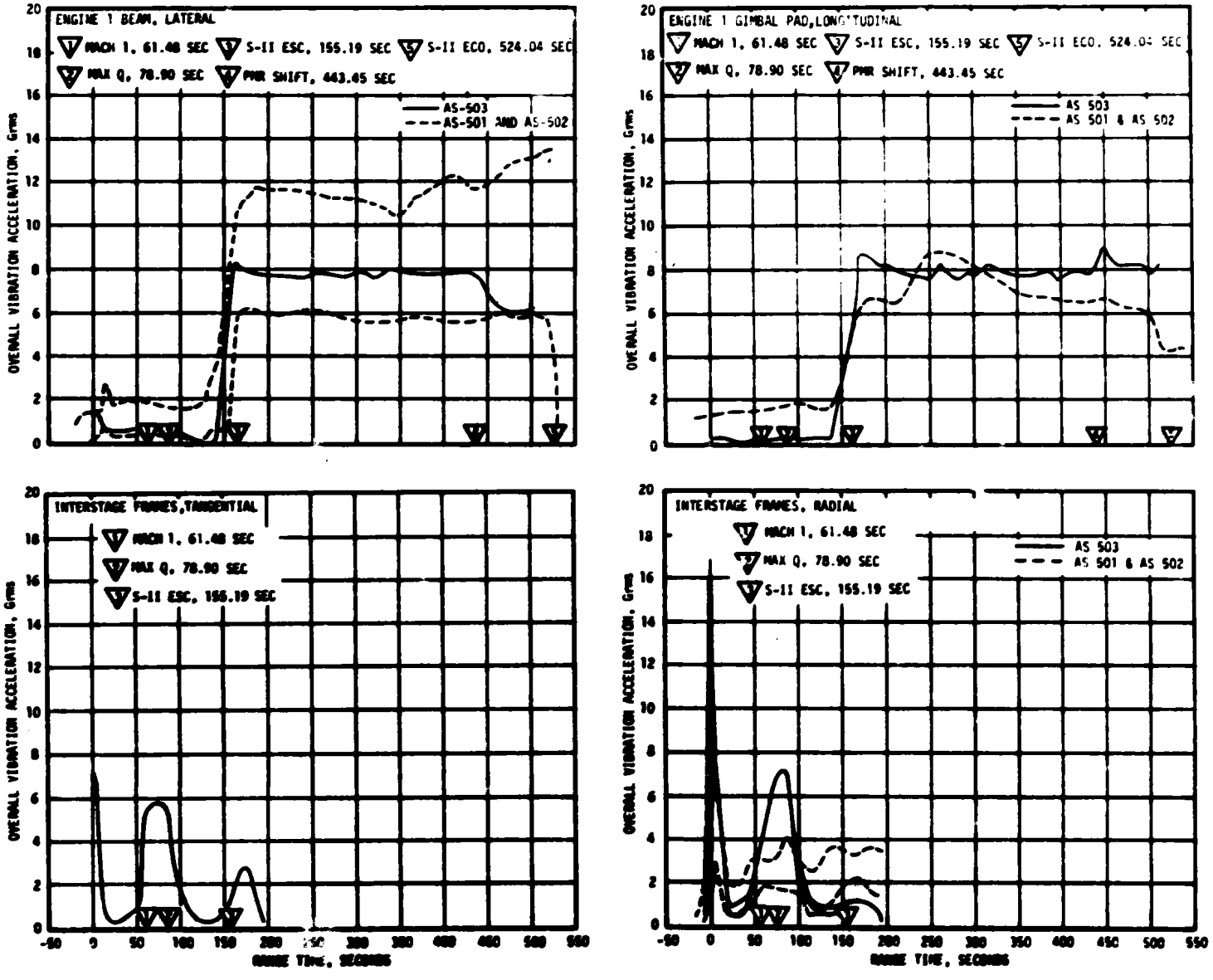

Figure 9-15. S-II Stage Structure Vibration Envelopes (Sheet 2 of 2)

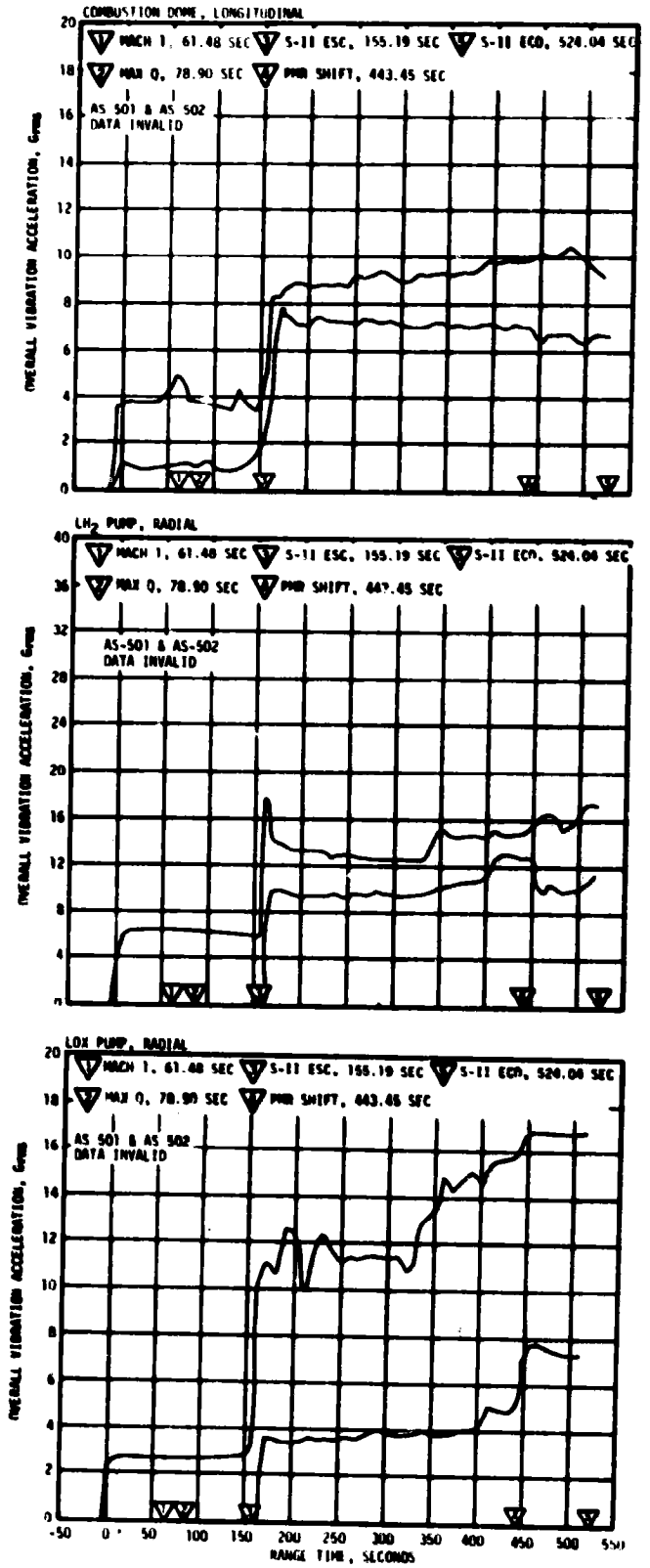

Figure 9-16. S-II Stage Engine Vibration Envelopes

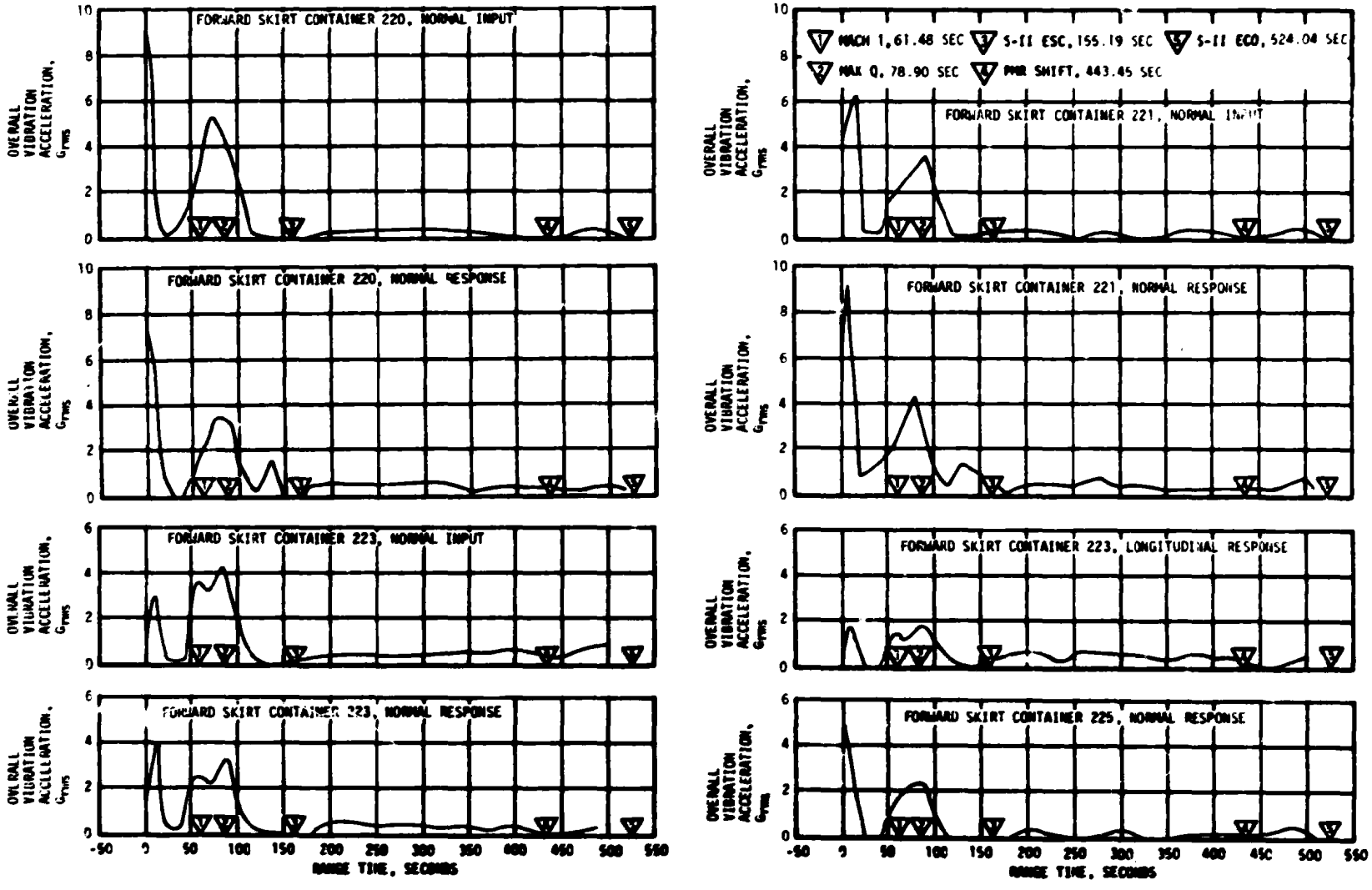

Figure 9-17. S-II Stage Component Vibration Envelopes (Sheet 1 of 2)

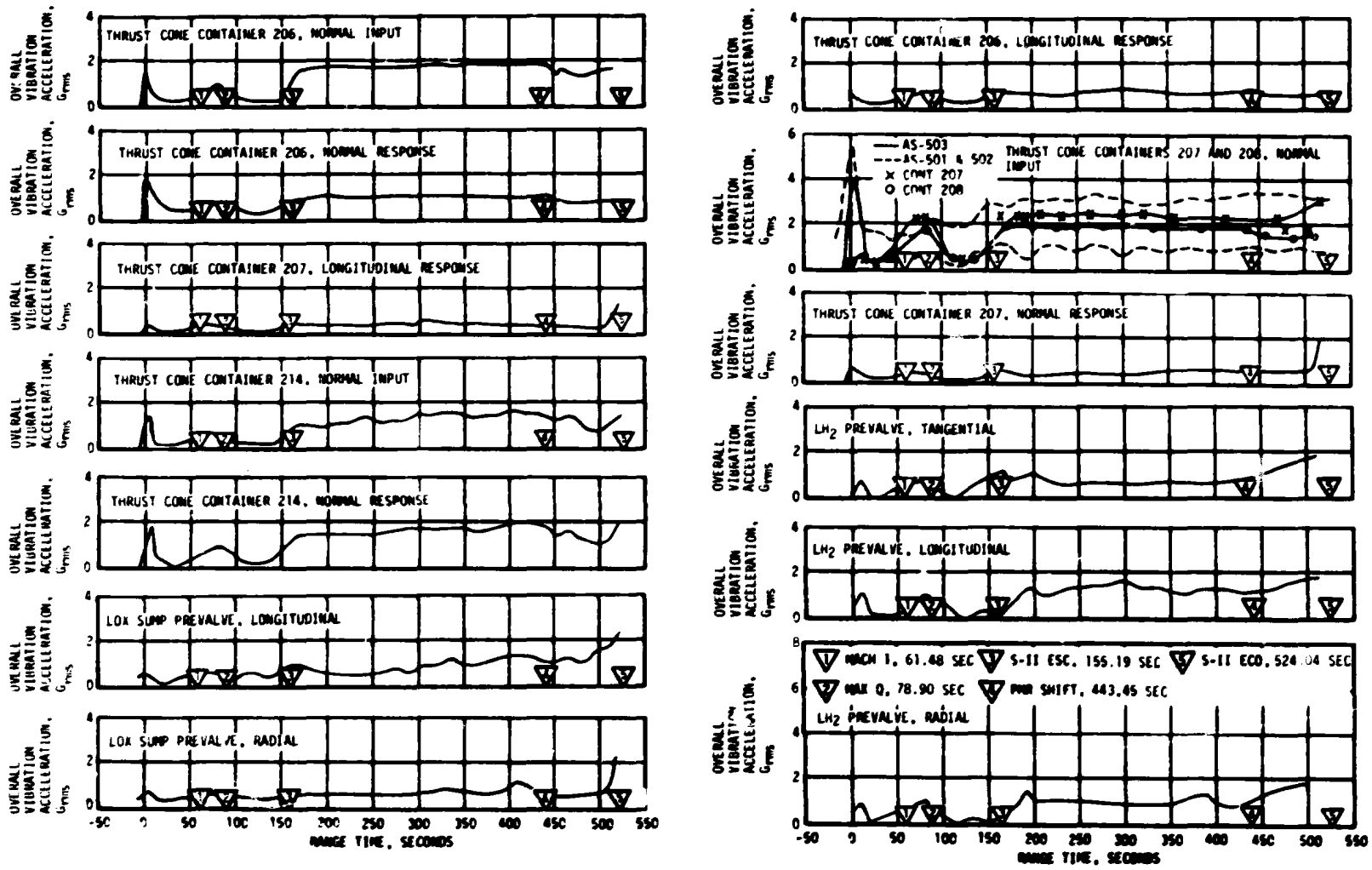

Figure 9-17. S-II Stage Component Vibration Envelopes (Sheet 2 of 2)

9.3.3 S-IVB Stage and Engine Evaluation

Two vibration measurements were made on the structure, fifteen at components mounted on the stage, and thirteen at engine components. The maximum composite levels are indicated in Figures 9-18 and 9-19 and Table 9-5.

9.3.3.1 S-IVB Stage Structure and Components. Figure 9-18 shows the range of vibration levels on the structure. The AS-503 levels were much lower than the maximum measured during the AS-501 and AS-502 flights. This is due to the limited frequency range used in acquiring the AS-503 data. The figure shows the range of vibration levels at the input to forward components and the range of vibration levels at the input to the aft components. The components monitored on AS-503 were not monitored on the AS-501 and AS-502 flights; however, inputs to components that were monitored are shown.

9.3.3.2 S-IVB Stage J-2 Engine. Figure 9-19 presents data measured during the AS-503 flight on the two turbopumps. These measurements were made with a measurement system that was improved over that used for AS-501. The AS-501 levels presented in Figure 9-19 for comparison include data from the turbopumps and the combustion chamber dome. The fact that the AS-503 levels are two to three times higher than the AS-501 levels may be an indication that the earlier measurement system was inadequate. In any case, the differences between the measured vibration environment is within the normal scatter of the engines.

Figure 9-19 also presents first and second burn data from components in the J-2 engine installed on the S-IVB stage. In addition, Figure 9-19 shows the nominal range of levels found during test firings at the engine contractor's test facility. With the exception of the radial measurement on the fuel Augmented Spark Igniter (ASI) block, the AS-503 measurements are within the range of engine contractor's data. The ASI block measurement appears to be within an allowable variation, since component vibration levels vary greatly from J-2 engine to J-2 engine. However, the operation in a vacuum may be reflected by the higher level obtained in flight.

9.3.3.3 S-IVB Stage ASI Lines Dynamics. Dynamic strain measurements were made on LOX ASI lines 1 and 2 and LH_2 lines 1, 2, 3, and 4. The LOX ASI line strains ranged from 10 to 20 μ in./in. RMS. (Engine Contractor's static firing gave 10 to 90 μ in./in. RMS.) The LH_2 ASI line strains ranged from 20 to 50 μ in./in. RMS. (Engine contractor's static firings gave 10 to 175 μ in./in. RMS.)

9.3.4 Instrument Unit (IU) Evaluation

There were 28 vibration measurements on the AS-503 IU. All of these measurements functioned properly and appeared to provide usable data. The telemetered data were of good quality. As on previous flights, a

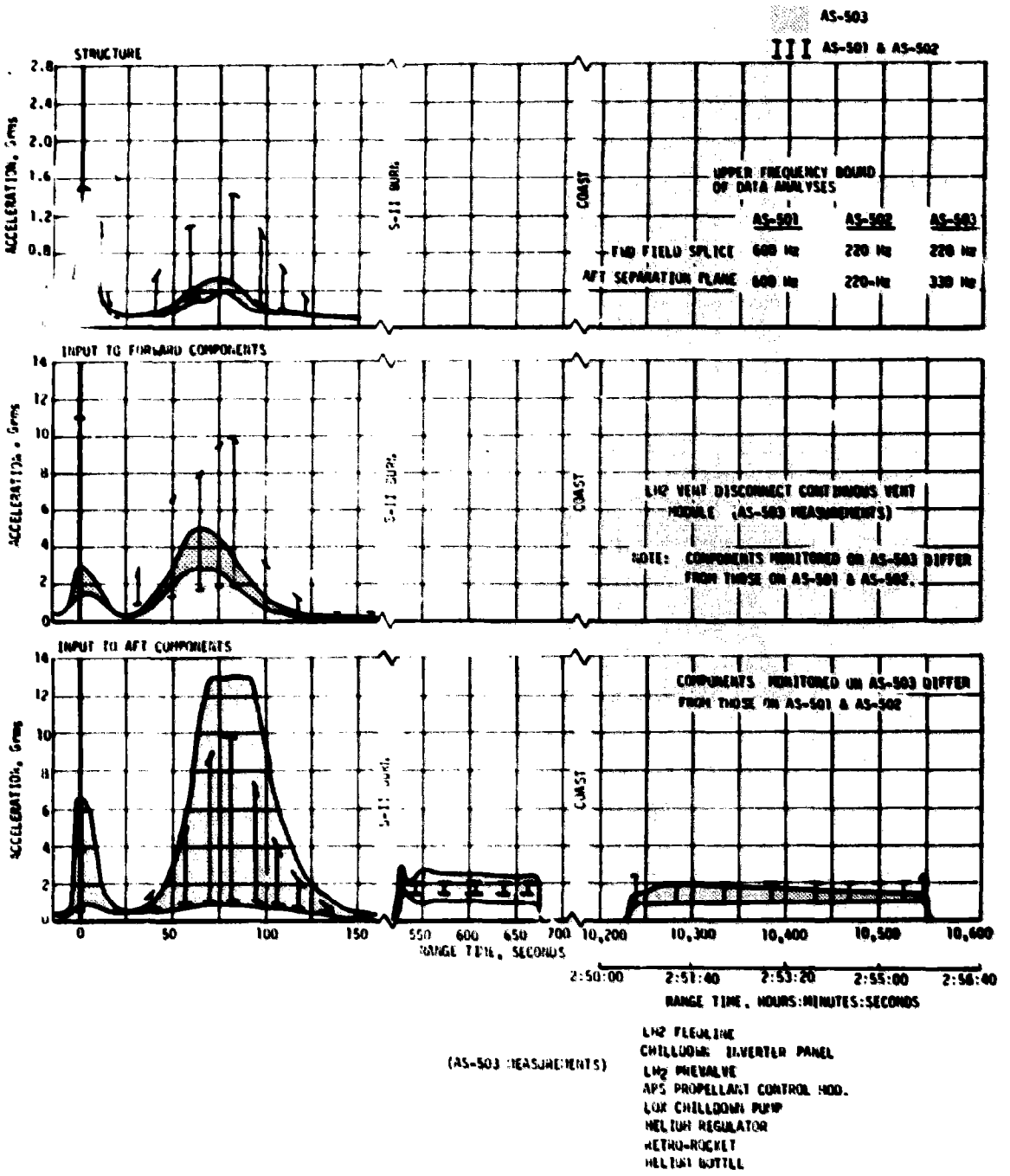

Figure 9-18. S-IVB Stage Vibration Envelopes

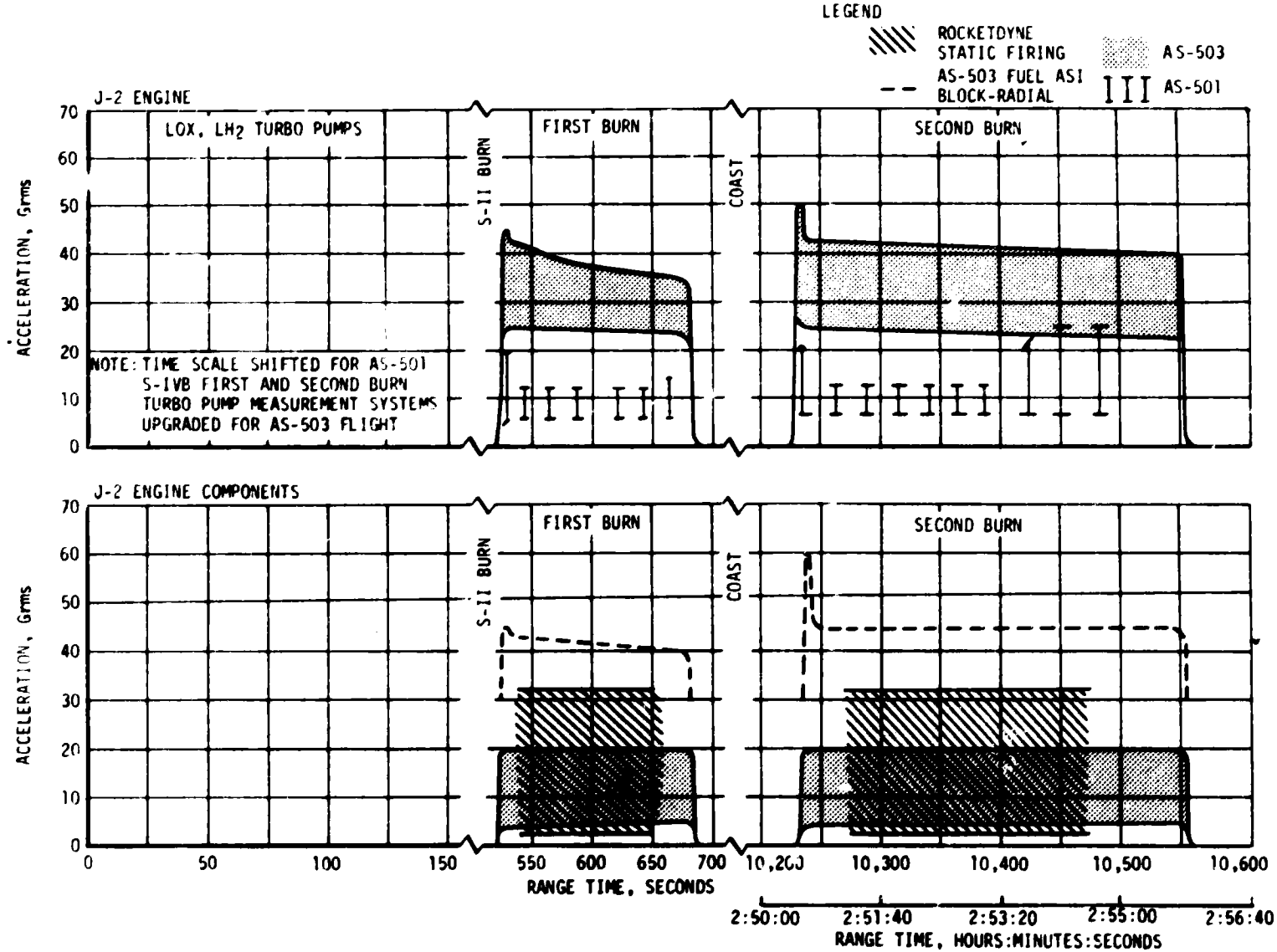

Figure 9-19. S-IVB Stage Engine Vibration Envelopes

Table 9-5. S-IVB Vibration Summary

	AREA MONITORED	MAX LEVEL Grms	RANGE TIME (SEC)	REMARKS
Structure	Field Splice at Position I (Low Frequency), Thrust	0.8	2	Frequency Range Limited to 220
	Station 2748 at Position II on Aft Skirt, Thrust	0.6	2	Frequency Range Limited to 330
Engine	Combustion Chamber Dome (Low Frequency), Thrust	0.28	2	Very Low Data Level
	Combustion Chamber Dome Longitudinal	-	-	Lost Data Channel
	LH_2 Turbopump, Lateral	21.0	530	New Measurement System Used
	LOX Turbopump, Lateral	50.0	10,230	New Measurement System Used
Component (Forward Skirt)	Input to LH_2 Vent Disconnect, Forward Skirt, Thrust	3.7	70	
	Input to LH_2 Vent Disconnect, Forward Skirt, Radial	4.8	70	
	Input to Continuous Vent Module, Forward Skirt, Radial	3.0	62	
Component (Aft Skirt)	Thrust Structure at Helium Bottle, Pitch	-	-	Data Questionable
	Input to LH_2 Feedline at LH_2 Tank, Thrust	1.7	73	
	Input to LH_2 Feedline at LH_2 Tank, Radial	2.6	73	

Table 9-5. S-IVB Vibration Summary (Continued)

	AREA MONITORED	MAX LEVEL Grms	RANGE TIME (SEC)	REMARKS
Component (Aft Skirt) (Cont)	Ambient Panel, Input to Chilldown, Inverter, Thrust	1.1	80	
	Ambient Panel, Input to Chilldown, Inverter, Radial	3.7	2	
	Input LH_2 Prevalve in LH_2 Feedline, Thrust	2.9	540	
	Input LH_2 Prevalve in LH_2 Feedline, Radial	2.4	540	
	APS Input to Propellant Control Module, Radial	4.7	75	
	APS Input to Propellant Control Module, Tangential	8.5	75	
	Input to LOX Chilldown Pump, Aft LOX Pump, Normal to Dome	3.4	2	
	Input to Helium Regulator, Tangential	13.0	78	
	Input to Retromotor Forward Support, Aft I/S, Radial	2.7	82	
Component (J-2 Engine)	Main Fuel Valve, Tangential	5.6	680	
	Main Fuel Valve, Radial	4.8	680	
	Main Fuel Valve, Longitudinal	5.7	680	
	LOX Turbine Bypass Valve, Tangential	9.2	680	

Table 9-5. S-IVB Vibration Summary (Continued)

	AREA MONITORED	MAX LEVEL Grms	RANGE TIME (SEC)	REMARKS
Component (J-2 Engine) (Cont)	LOX Turbine Bypass Valve, Radial	10.0	680	
	LOX Turbine Bypass Valve, Longitudinal	14.2	680	
	ASI LOX Valve, Radial	18.4	680	
	ASI LOX Valve, Longitudinal	19.3	680	
	Fuel ASI Block, Radial	60.0	10,230	Level Greater than Found in Static Test Firings

telemetry dropout occurred during S-IC stage separation. This resulted in a complete loss of all single sideband data between 154.6 and 155.7 seconds.

The maximum composite vibration levels (Grms) occurred for about a 20-second period centered near the time of maximum dynamic pressure. All vibration levels appeared to be nominal. For comparison purposes, the IU structure and component measurements are shown with those taken during previous Saturn V flights. Figure 9-20 shows the Grms time histories of these measurements.

9.3.4.1 Instrument Unit Structure. Eight measurements were used for monitoring structural vibration at the upper and lower interface rings. The AS-503 levels were generally within the envelope of previous flight values except for two peaks at 77 and 85 seconds. All levels appeared to be reasonable and no structural problems existed. After S-IC powered flight, the levels became negligible.

9.3.4.2 Instrument Unit Components. Twenty measurements were used to monitor the IU component vibration levels. Figure 9-20 indicates a broader range of data than that of structure vibration measurements. This is due to the difference in response characteristics of the various components. The AS-503 component composite vibration levels appear to be nominal and within those of AS-501 and AS-502. The vibration levels during S-II and S-IVB stage powered flight were negligible.

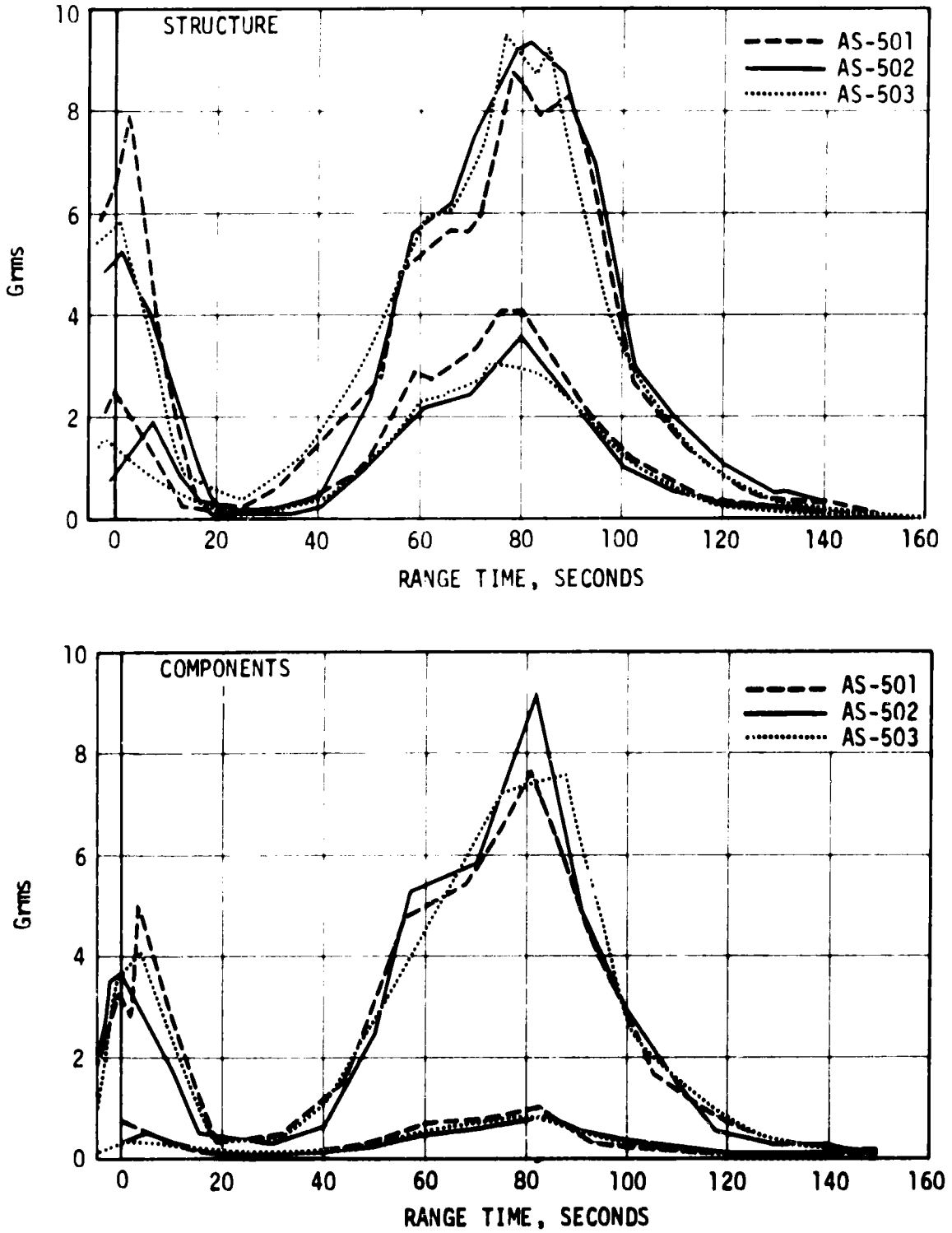

Figure 9-20. Instrument Unit Vibration Envelopes

SECTION 10

GUIDANCE AND NAVIGATION

10.1 SUMMARY

10.1.1 Flight Program

The guidance and navigation system performed satisfactorily during all periods for which data are available. The boost navigation and guidance schemes were executed properly and terminal parameters were very good for both parking orbit and translunar injection. All target parameters were satisfactorily achieved and all orbital operations were nominal. Mission objectives were accomplished and the nominal mission time line was flown.

The vehicle trajectory exhibited a slightly flatter altitude profile than that predicted in the operational trajectory. Analysis reveals that the most probable cause was the vehicle state vector at Iterative Guidance Mode (IGM) initiation being different than predicted. At S-IC Outboard Engine Cutoff (OECO), the vehicle altitude was less than predicted and the velocity was greater. The resulting optimum fuel usage trajectory determined by the Launch Vehicle Digital Computer (LVDC) flight program was predictable and resulted in satisfactory end conditions.

A roll angle offset, varying from 0.3 to 0.5 degree was evident throughout boost. A combination of Center of Gravity (CG) offsets and thrust vector misalignments is the most probable cause.

10.1.2 Instrument Unit Components

Data indicates that the Launch Vehicle Data Adapter (LVDA) and the LVDC performed as predicted. There were numerous error monitor register indications of Triple Modular Redundant (TMR) logic disagreements in the interrupt processor during Time Base 7 (T_7). Such indications on past missions have been associated with the command and communications subsystem operation. All commands were received and processed, thus these indications had no detrimental effect on the flight.

The ST-124M-3 inertial platform and associated electronic equipment performed as expected. Telemetry from the LVDC indicated that inertial reference was still being maintained at 25,420 seconds (7:03:40). The accelerometer loop signals indicated that the accelerometers correctly measured vehicle acceleration throughout the flight. Temperatures, pressures, and voltages were nominal to 13,410 seconds (3:43:30).

10.2 GUIDANCE AND NAVIGATION SYSTEM DESCRIPTION

10.2.1 Flight Program Description

The flight program controls the LVDC from Guidance Reference Release (GRR) until the end of the mission. The program performs seven primary functions: navigation, guidance, event sequencing, attitude control, data management, ground command processing, and hardware evaluation.

10.2.1.1 Preflight Prepare-to-Launch Mode

At approximately -13 minutes, the LVDC is commanded into the Prepare-to-Launch (PTL) mode by a mode command from the RCA-110A ground computer. This ground routine performs certain prelaunch functions and prepares the LVDC for entering the flight mode.

10.2.1.2 Boost Initialize

The flight program contains routines which initialize navigation quantities, boost-to-parking orbit parameters, and translunar injection parameters. The variable azimuth routine computes an azimuth from a predicted liftoff time which is computed from the Greenwich Mean Time (GMT) maintained in the PTL mode. This azimuth is used to compute an inclination and a descending node. The translunar injection targeting routine uses an interpolation scheme to determine orbital energy, right ascension, declination and cosine of the true anomaly of the target vector, and eccentricity of the transfer ellipse from the predicted liftoff time. Boost initialize also computes transformation matrices from the azimuth, inclination, descending node, and launch pad latitude, and target vectors for first and second opportunities from right ascension, declination, launch pad latitude, azimuth, and the angle between the launch meridian and the vernal equinox.

10.2.1.3 Boost Routines

In general, the boost routines perform navigation and guidance, event sequencing, and attitude control. Boost navigation encompasses the computations and logic necessary to determine position, velocity, and acceleration of the vehicle during powered flight phases.

The boost guidance is divided into two distinct modes, pre-IGM and IGM. The pre-IGM guidance, used during S-IC and part of S-II stage operation, computes guidance commands during the interval from GRR to IGM initiation. Programmed commands include a yaw maneuver for tower clearance and roll and tilt commands. The yaw maneuver is initiated 1 second after Instrument Unit (IU) umbilical disconnect and roll and tilt are initiated when the vertical component of the space-fixed position changes by 138 meters (452.8 ft), approximately 11 seconds after liftoff. A time backup of 11.4 seconds is provided in case of an accelerometer failure. The roll command is initiated to align Position 1 with the flight azimuth. The pitch profile is arrested at 146.5 seconds nominally, and the pitch, roll, and yaw commands are frozen from this time until IGM initiation. If an S-IC stage engine failure is detected, the steering angle is frozen for a specified time dependent on the time of the engine failure. The tilt arrest time is also adjusted.

The guidance scheme used in the S-II stage and S-IVB stage burn is a modification of the multistage three-dimensional form of IGM. IGM is a near optimal scheme based on the flat earth optimum steering function for planar motion of a point-mass vehicle. The approximate thrust vector steering function is implemented in both the pitch and yaw planes. IGM is implemented in two flight modes. The first mode (boost-to-parking orbit IGM) starts 40.6 seconds after S-IC stage OECO and is terminated at first S-IVB stage cutoff. The second mode (out-of-orbit IGM), starting approximately 14 seconds after S-IVB stage reignition, is terminated at second S-IVB stage cutoff, Steering Misalignment Correction (SMC) is used during both IGM modes of flight.

The equations and logic needed to implement IGM are essentially the same for both modes. During the boost-to-parking orbit mode the S-II/S-IVB staging sequence causes a rapid variation of the force-to-mass ratio. To smooth the steering commands of these disturbances IGM is supplemented by periods of artificial tau. The sensitivity of the IGM to changes in force-to-mass increases as the desired terminal parameters are approached. A terminal scheme is required (chi bar steering) which uses only the velocity constraint terms. During chi bar steering, the altitude constraint terms are set to zero. The first S-IVB stage cutoff signal is given by the program when the desired terminal velocity is reached. To obtain an accurate cutoff velocity, a high-speed computer loop is entered just prior to cutoff.

Because of perturbations in the parking orbit, it is desirable to revise the out-of-orbit desired trajectory to be near optimum for the actual orbit rather than the desired orbit. Hence, near the reignition point, computations to determine the plane of the transfer ellipse and the dimensions of the ellipse (defined by energy, eccentricity, and argument of perigee) are made. These data are then used by the out-of-orbit IGM

equations. The most significant difference between the out-of-orbit and boost-to-parking orbit equations is that the terminal parameters are recalculated each cycle as a function of the range angle. The point of injection on the waiting orbit ellipse varies with range angle to constrain the argument of perigee. The high-speed loop is again employed to issue the second S-IVB stage cutoff command. For the out-of-orbit case, the terminal velocity is recalculated each cycle through the high-speed loop to force a correct orbital energy at engine cutoff.

A backup IGM is provided to give correct guidance in case of an early S-II stage engine cutoff, This scheme is essentially the same as the out-of-orbit except the argument of perigee constraint is dropped.

Event sequencing is accomplished by the switch selector routine on an interrupt basis. This routine provides the communication link between the LVDC and the control distributors in the IU and in each stage. The routine determines if it is time to issue a switch selector command, verifies that no switch selector stage was hung, verifies that the correct address is sent to the stage switch selector, and issues the read commands.

Attitude control is accomplished in the minor loop section of the program on an interrupt basis. The minor loop support routine (a part of the major loop) includes calculations of such parameters as steering rates to be applied in the minor loop. The boost minor loop is entered at a rate of 25 times per second and processes platform gimbal angles to compute attitude errors to drive the gimbal angles to their desired values. Limiting of the ladder outputs is accomplished when necessary, and backup and failure paths are provided in case gimbal angle discrepancies occur.

10.2.1.4 Orbital Routines

The orbital program consists of two interruptable monitor routines. The first is the IU Hardware Evaluation Program (HEP), and the second is the Telemetry Executive Progrmm (TEP). Navigation, guidance, event sequencing, attitude control, and ground command processing are initiated on an interrupt basis from either HEP or TEP.

During orbital flight and when the vehicle is not over a ground station, the HEP routine is exercised. For this mission, however, no hardware evaluation functions were defined and the HEP routine operated as a dummy monitor routine.

Once the vehicle acquires a ground station, TEP is entered as the program major loop. This routine provides time sharing telemetry of compressed and real time data. In addition, various special data are telemetered on an interrupt basis. Data from the LVDA is telemetered automatically.

Orbital guidance controls the vehicle attitude during the earth parking orbit (T_5) and after S-IVB second burn cutoff (T_7).

During T_5, the vehicle is continuously commanded to track the local horizontal with a zero degree roll. This attitude is maintained until IGM starts in the second S-IVB burn. In T_7, the local horizontal is again commanded until the spacecraft separation maneuver at T_7 + 907.98 seconds. The separation attitude is dependent on lighting constraints for the spacecraft and may be different for each day of launch. This inertial attitude for separation is held until T_7 + 6540 seconds. At that time the slingshot attitude, which is independent of launch day, is assumed.

Orbital navigation encompasses the computations necessary to determine position, velocity, and acceleration in the space-fixed coordinate system during earth orbit. These computations are carried out in an indirect fashion, making use of mathematical models of the earth, its atmosphere, and the vehicle to approximate the effects of the earth on the vehicle. Navigation is accomplished by integrating the space-fixed accelerations. These accelerations are obtained by solving an approximate atmospheric drag equation, by rotating prestored body-fixed vent accelerations through the platform gimbal angles, and by solving for gravitational accelerations. The gravitation model is the same as that used in boost with the addition of two oblateness terms. The integration scheme is a modified Scarborough routine. It is a self-starting scheme that is carried out in two basic steps. The first step obtains predicted values of position and velocity at the midpoint of the integration interval. Gravitational, vent, and drag accelerations are then computed based on these midpoint positions and velocities at the end of the interval. Accelerations are again computed and the second step is completed by calculating corrected end point values of position and velocity. Values for position at points within the 8-second intervals between integrations are calculated assuming a constant velocity over the interval. A routine for telemetry station acquisition, as a function of position, is included. This routine is also entered upon exit from the minor loop at 8-second intervals.

Event sequencing in orbit is accomplished exactly as in the boost phase with the added capability to receive special output sequence commands from ground stations after T_7 + 1200 seconds.

Attitude control for orbital operation is accomplished in the same manner as in the boost phase with the exception of the rate of entry into the minor loop. The orbital minor loop is entered 10 times per second. The first and fifth passes being the attitude update pass (cycled through twice per second) and the remaining eight passes are for attitude hold (cycled through eight times per second) to minimize drift problems.

Ground command processing is accomplished by the Command Decoder interrupt with the Digital Command System (DCS) routine. The DCS routine processes all ground commands, provides data and mode verification, and supplies the necessary information to the various affected routines.

10.2.1.5 Flight Program Differences: AS-503 Compared to AS-502

The following functions were deleted:

a. Computer simplex operations.

b. Compression of computer interface unit data.

c. Navigation update DCS command.

d. Self-test

The following functions were changed:

a. Time of D012 moved to middle of boost initialize.

b. Propellant utilization system operated open loop.

c. Acquisition and telemetry station loss done on navigation calculations.

The following functions were added:

a. Interface with the RCA 110A ground computer in the azimuth laying program was programmed.

b. Variable targeting calculations in boost initialization.

c. Spacecraft commands for S-IVB stage early staging and S-IVB stage cutoff.

d. Translunar injection burn can be inhibited by spacecraft command.

e. Alternate sequences for O_2/H_2 burner malfunction.

f. Capability for second S-IVB stage burn without spacecraft.

g. Logic to provide two restart opportunities.

h. Redundant guidance failure indication.

i. Six dummy telemetry stations added to increase coverage during restart.

j. Variable targeting calculation telemetry.

10.2.2 Instrument Unit System Description

A block diagram of the navigation, guidance and control system is shown in Figure 10-1.

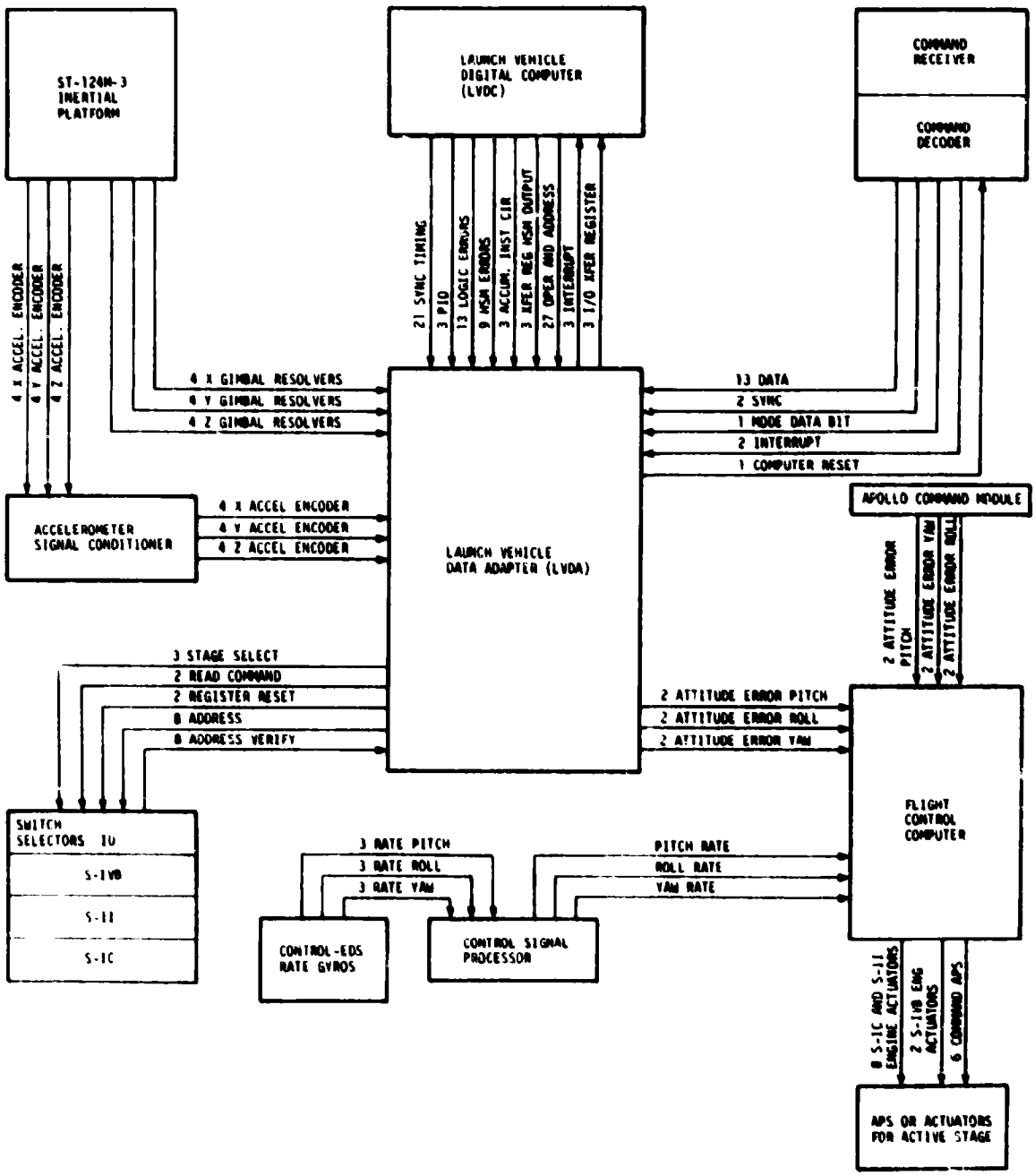

Figure 10-1. Navigation, Guidance and Control System Block Diagram

The LVDC is a high-reliability general purpose random-access digital computer which contains the logic circuits, memory, and timing system required to perform mathematical operations necessary for navigation guidance, and vehicle flight sequencing. The LVDC is also used for prelaunch and orbital checkout.

The LVDA is the input/output device for the LVDC. These two components are digital devices which operate in conjunction to carry out the flight program. This program performs the following functions:

a. Processes the inputs from the platform.

b. Performs navigation calculations.

c. Provides first stage tilt program.

d. Calculates IGM steering commands.

e. Resolves gimbal angles and steering commands into the vehicle system for attitude error commands.

f. Issues cutoff and sequencing signals.

The ST-124M-3 inertial platform assembly is a three-gimbal configuration with gas bearing gyros and pendulous integrating gyro accelerometers mounted on the stable element to provide an inertial space-fixed coordinate reference frame for attitude control and navigation measurements (see Figure 10-2). Vehicle accelerations and rotations are sensed relative to the stable element. Gimbal angles are measured by resolvers which have both fine and coarse outputs. Inertial velocity is obtained from measurements of the angular rotation of the accelerometer measuring head. The data are in the form of encoder outputs which have redundant channels.

10.3 GUIDANCE COMPARISONS

The postflight guidance hardware error analysis is based on comparisons of the ST-124M-3 platform measured velocities with the postflight trajectory (OMPT), established from external tracking data. Figure 10-3 presents comparisons of the platform measured velocities with corresponding values from the final postflight trajectory. A positive difference indicates trajectory data greater than the platform measurement. The velocity differences shown for the pitch plane (range and altitude) are essentially zero from T_3 to parking orbit insertion. The differences during the S-IC stage flight probably result from roughness in the data.

The crossrange velocity difference builds up to -1.45 m/s (-4.76 ft/s) by S-IVB first cutoff. There appears to be a velocity bias of about -0.2 m/s

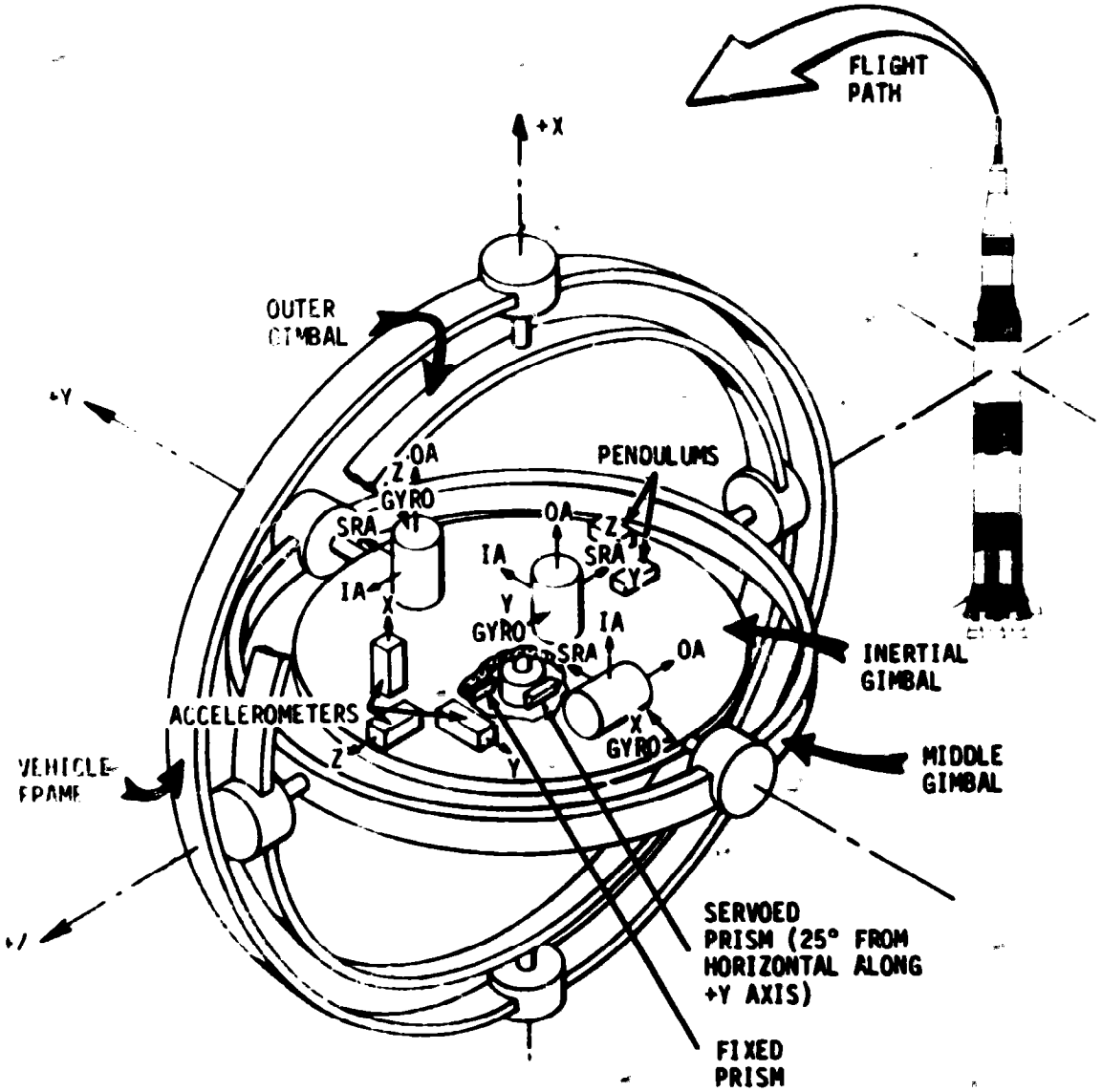

Figure 10-2. Platform Gimbal Configuration

(-0.66 ft/s) which is probably in the trajectory data. However, the differences at parking orbit insertion are well within the accuracy of either the tracking data or 3 sigma hardware errors.

The velocity differences are relatively small and well within the accuracy of the tracking data and/or the alignment of the platform after 9659.54 seconds. Since the platform velocities are set to zero in the LVDC after parking orbit insertion and held to zero until T_6, the comparisons represent the differences accumulated during T_6 only. The crossrange velocity differences exhibit a characteristic shape which could result from an accumulated platform misalignment about the X or Z axes or some combination of small angles. However, this represents a very small platform drift.

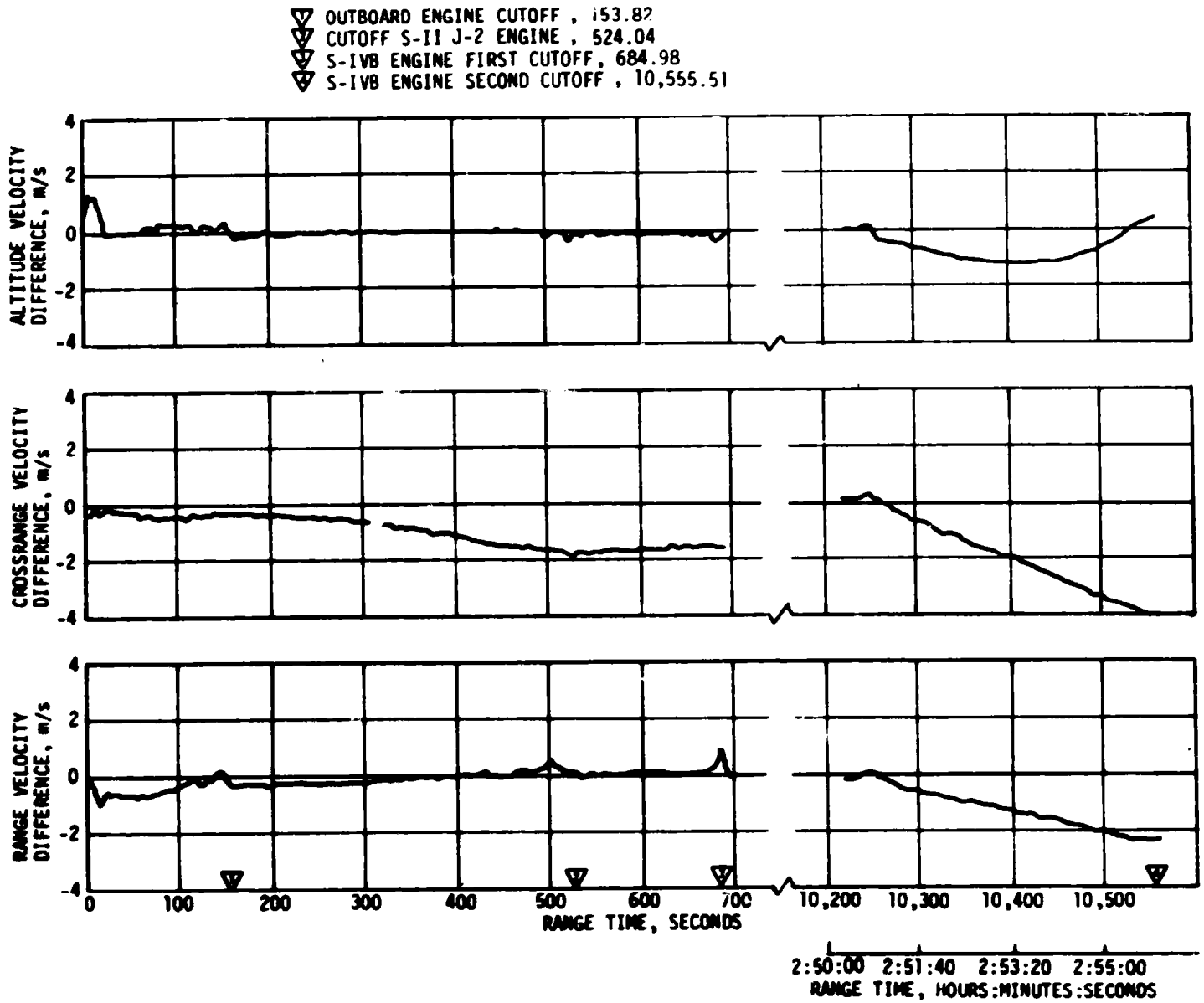

Figure 10-3. Tracking and ST-124M-3 Platform Velocity Comparison (Trajectory Minus Guidance)

The range velocity differences taken alone could result from an accumulated pitch alignment error. However, the trend of the altitude velocity differences are not consistent with the range difference curve. The inertial platform accelerations were positive in all three components during the entire S-IVB second burn mode. The crossrange accelerations were relatively small, which indicates that no reasonable alignment errors would produce the combination of range and altitude velocity differences. The differences are probably the result of limited ground tracking available for trajectory construction. In any case, the differences shown for the boost phase of flight are well within the accuracy of the data compared.

The velocities measured by the ST-124M-3 platform system at significant flight event times are shown in Table 10-1, along with corresponding values computed from the final OMPT and the preflight Operational Trajectory (OT), computed using the actual flight azimuth. The trajectory data were taken directly from both the OMPT and the OT. The OT platform velocities were initialized to zero at liftoff, which results in a platform OT altitude velocity error of 168.9 m/s low. However, the navigation positions and velocities do not reflect this error.

Comparisons of navigation (PACSS 13) positions, velocities, and flight path angle at significant flight event times are presented in Table 10-2. For the boost to parking orbit portion of flight, the guidance LVDC and OMPT parameters were in very good agreement. At parking orbit insertion, the velocity component differences were -0.21 m/s (-0.66 ft/s), -1.24 m/s (-4.07 ft/s) and 0.04 m/s (0.13 ft/s) for altitude, crossrange, and range velocities, respectively. The difference in total velocity was 0.12 m/s (0.39 ft/s). These differences are well within the accuracy of either the trajectory data or the 3 sigma guidance hardware errors.

The vehicle was approximately 1.0 kilometer (3281 ft) lower in altitude than nominal at S-IC OECO. The burn time from T_2 to T_3 was about 2.49 seconds longer than nominal and the total velocity was 12.79 m/s (41.96 ft/s) greater than nominal. However, the optimum fuel usage trajectory determined by the LVDC flight program was predictable and satisfactory end conditions were obtained. At S-IVB first cutoff, the radius and total velocity were 54 meters (177 ft) greater and 0.01 m/s (0.03 ft/s) less than nominal, respectively.

The comparisons for the second burn mode of the S-IVB are very good, with both the postflight and preflight trajectory values. This indicates a near nominal parking orbit computed by the LVDC and also near nominal second burn mode. At S-IVB second cutoff, the respective radius and total velocity differences (trajectory minus LVDC) were 0.301 kilometer (988 ft) and -1.99 m/s (-6.53 ft/s) for the postflight trajectory and -3.118 kilometers (-10,230 ft) and 2.78 m/s (9.12 ft/s) for the preflight trajectory. Since the S-IVB second cutoff was based on energy rather

Table 10-1. Inertial Platform Velocity Comparisons

EVENTS	DATA SOURCE	VELOCITY m/s (ft/s)		
		ALTITUDE ($\dot{X}_m$)	CROSS RANGE ($\dot{Y}_m$)	RANGE ($\dot{Z}_m$)
Start of T_2 125.88 s	Guidance	2158.30 (7081.04)	2.15 (7.05)	1348.50 (4424.21)
	Postflight Trajectory	2158.42 (7081.43)	1.89 (6.20)	1348.28 (4423.49)
	Preflight Trajectory	2035.07 (6676.74)	-1.49 (-4.89)	1379.36 (4525.46)
S-IC OECO 153.82 s	Guidance	2565.30 (8416.34)	-3.75 (-12.30)	2180.73 (7154.63)
	Postflight Trajectory	2565.57 (8417.22)	-3.98 (-13.06)	2180.37 (7153.44)
	Preflight Trajectory	2419.38 (7937.60)	-3.23 (-10.60)	2149.28 (7051.44)
S-II ECO 524.04 s	Guidance	3360.63 (11,025.69)	-2.00 (-6.56)	6652.20 (21,824.80)
	Postflight Trajectory	3360.70 (11,025.92)	-3.72 (-12.20)	6652.31 (21,825.16)
	Preflight Trajectory	3151.46 (10,339.44)	-0.31 (-1.02)	6632.06 (21,758.73)
S-IVB First Cutoff 684.98 s	Guidance	3123.60 (10,248.03)	0.75 (2.46)	7599.72 (24,933.46)
	Postflight Trajectory	3123.35 (10,247.21)	-0.70 (-2.30)	7600.07 (24,934.61)
	Preflight Trajectory	2942.82 (9654.92)	0.44 (1.44)	7598.07 (24,928.05)
Parking Orbit Insertion 694.98 s	Guidance	3123.15 (10,246.56)	0.75 (2.46)	7601.45 (24,939.14)
	Postflight Trajectory	3122.99 (10,246.03)	-0.68 (-2.23)	7601.46 (24,939.17)
	Preflight Trajectory	2942.31 (9653.25)	0.44 (1.44)	7599.90 (24,934.06)

Table 10-1. Inertial Platform Velocity Comparisons (Continued)

EVENTS	DATA SOURCE	VELOCITY m/s (ft/s)		
		ALTITUDE ($\dot{X}_m$)	CROSS RANGE($\dot{Y}_m$)	RANGE ($\dot{Z}_m$)
S-IVB * Second Cutoff 10,555.51 s	Guidance	1857.75 (6094.98)	509.77 (1672.47)	2532.63 (8309.15)
	Postflight Trajectory	1858.37 (6097.01)	505.73 (1659.22)	2530.47 (8302.07)
	Preflight Trajectory	1854.85 (6085.47)	510.65 (1675.36)	2534.37 (8314.86)
Injection * Waiting Orbit 10,565.51 s	Guidance	1859.60 (6101.05)	510.75 (1675.69)	2535.90 (8319.88)
	Postflight Trajectory	1860.07 (6102.59)	506.73 (1662.50)	2533.60 (8312.34)
	Preflight Trajectory	1856.74 (6091.67)	511.71 (1678.84)	2537.74 (8325.92)

* Values represent velocity change from Time Base 6.

Table 10-2. Guidance Comparisons

EVENT	DATA SOURCE	POSITIONS (meters) (ft)				VELOCITIES m/s (ft/s)				FLIGHT PATH ANGLE (deg)
		X_s	Y_s	Z_s	R	$\dot{X}_s$	$\dot{Y}_s$	$\dot{Z}_s$	V_s	
Start of T_2 125.88 s	Guidance	6,413,964 (21,042,933)	35,291 (115,783)	92,785 (304,409)	6,414,732 (21,045,453)	760.51 (2495.08)	123.49 (405.15)	1730.30 (5676.77)	1894.08 (6214.10)	24.522
	Postflight Trajectory	6,413,973 (21,042,963)	35,264 (115,694)	92,731 (304,231)	6,414,740 (21,045,479)	760.63 (2495.47)	123.42 (404.92)	1730.12 (5676.18)	1893.96 (6213.70)	24.527
	Preflight Trajectory	6,415,917 (21,049,340)	34,841 (114,306)	93,470 (306,656)	6,416,692 (21,051,883	806.79 (2646.92)	120.09 (393.99)	1761.10 (5777.82)	1940.83 (6367.48)	25.417
S-IC OECO 153.82 s	Guidance	6,437,045 (21,118,657)	38,646 (126,790)	152,013 (498,724)	6,438,956 (21,124,927)	897.63 (2944.94)	116.56 (382.41)	2557.40 (8390.32)	2712.87 (8900.38)	20.689
	Postflight Trajectory	6,437,062 (21,118,713)	38,613 (126,682)	151,972 (498,590)	6,438,971 (21,124,927)	898.03 (2946.26)	116.34 (381.69)	2557.04 (8389.14)	2712.65 (8899.66)	20.699
	Preflight Trajectory	6,438,162 (21,122,322)	37,863 (124,221)	147,517 (483,974)	6,439,963 (21,128,231)	945.27 (3101.24)	117.28 (384.77)	2526.49 (8288.91)	2700.08 (8858.42)	21.819
S-II ECO 524.04 s	Guidance	6,328,539 (20,762,671)	77,211 (253,314)	1,740,077 (5,708,845)	6,563,858 (21,534,705)	-1735.05 (-5692.35)	91.71 (300.88)	6596.03 (21,640.26)	6821.02 (22,378.40)	0.645
	Postflight Trajectory	6,328,533 (20,762,651)	76,895 (252,277)	1,740,006 (5,708,612)	6,563,830 (21,534,613)	-1734.96 (-5692.06)	90.09 (295.57)	6596.20 (21,640.81)	6821.15 (22,378.83)	0.646
	Preflight Trajectory	6,333,966 (20,780,476)	76,907 (252,316)	1,725,502 (5,661,027)	6,565,242 (21,539,246)	-1743.68 (-5720.67)	94.05 (308.56)	6582.90 (21,597.18)	6810.57 (22,344.12)	0.412
S-IVB First Cutoff 684.98 s	Guidance	5,919,081 (19,419,321	90,858 (298,087)	2,834,490 (9,299,395	6,563,391 (21,533,173)	-3365.83 (-11,042.62)	77.43 (254.03)	7025.99 (23,050.87)	7790.98 (25,560.65)	-0.00054
	Postflight Trajectory	5,919,028 (19,419,147)	90,317 (296,312)	2,834,500 (9,299,428)	6,563,341 (21,533,009)	-3366.13 (-11,043.60)	76.15 (249.83)	7026.36 (23,052.08)	7791.43 (25,562.12)	-0.00126
	Preflight Trajectory	5,920,376 (19,423,570)	90,892 (298,198)	2,831,738 (9,290,366)	6,563,337 (21,532,996)	-3362.85 (-11,032.84)	77.57 (254.49)	7027.43 (23,055.59)	7790.99 (25,560.68)	-0.00274
Parking Orbit Insertion 694.98 s	Guidance	5,885,001 (19,307,511)	91,627 (300,610)	2,904,566 (9,529,300)	6,563,394 (21,533,183)	-3449.51 (-11,317.15)	76.26 (250.19)	6987.24 (22,923.74)	7792.72 (25,566.36)	0.00171
	Postflight Trajectory	5,884,944 (19,307,324)	91,072 (298,789)	2,904,573 (9,529,323)	6,563,337 (21,532,996)	-3449.72 (-11,317.84)	75.02 (246.13)	6987.28 (22,923.87)	7792.84 (25,566.75)	0.00057
	Preflight Trajectory	5,886,326 (19,311,858)	91,662 (300,725)	2,901,828 (9,520,317)	6,563,372 (21,533,111)	-3446.60 (-11,307.61)	76.41 (250.69)	6988.83 (22,928.95)	7792.85 (25,566.78)	-0.00047

X_s = Vertical direction
Y_s = Crossrange direction
Z_s = Range direction

Table 10-2. Guidance Comparisons (Continued)

EVENT	DATA SOURCE	POSITIONS (meters) (ft)				VELOCITIES m/s (ft/s)				FLIGHT PATH ANGLE (deg)
		X_s	Y_s	Z_s	R	$\dot{X}_s$	$\dot{Y}_s$	$\dot{Z}_s$	V_s	
S-IVB Second Cutoff 10,555.51 s	Guidance	6,318,403 (20,729,417)	15,403 (50,534)	-2,250,639 (-7,383,896)	6,707,297 (22,005,300)	4919.74 (16,140.68)	672.57 (2206.57)	9627.15 (31,584.75)	10,832.27 (35,538.51)	7.4559
	Postflight Trajectory	6,316,612 (20,723,541)	15,148 (49,698)	-2,256,558 (-7,403,315)	6,707,598 (22,006,288)	4925.99 (16,161.19)	667.24 (2189.08)	9622.07 (31,568.09)	10,830.28 (35,531.98)	7.4450
	Preflight Trajectory	6,305,608 (20,687,439)	13,928 (45,695)	-2,277,088 (-7,470,670)	6,704,179 (21,995,070)	4943.71 (16,219.32)	673.57 (2209.85)	9617.92 (31,554.47)	10,835.05 (35,547.63)	7.341
Injection Waiting Orbit 10,565.51 s	Guidance	6,367,203 (20,889,520)	22,138 (72,630)	-2,154,184 (-7,067,447)	6,721,776 (22,052,803)	4837.97 (15,872.41)	673.38 (2209.23)	9659.40 (31,690.56)	10,824.21 (35,512.07)	7.9087
	Postflight Trajectory	6,365,470 (20,883,834)	21,828 (71,613)	-2,160,163 (-7,087,063)	6,722,052 (22,053,708)	4844.12 (15,892.59)	668.08 (2191.84)	9654.27 (31,673.73)	10,822.05 (35,504.98)	7.8971
	Preflight Trajectory	6,354,646 (20,848,323)	20,673 (67,824)	-2,180,728 (-7,154,532)	6,718,447 (22,041,881)	4862.04 (15,951.38)	674.48 (2212.83)	9650.68 (31,661.95)	10,827.28 (35,522.14)	7.794

X_s = Vertical direction
Y_s = Crossrange direction
Z_s = Range direction

than total velocity, the 2.78 m/s difference between the LVDC and preflight trajectory values does not represent the error in cutoff conditions. Second burn mode end conditions are given in paragraph 10.4.

10.4 NAVIGATION AND GUIDANCE SCHEME EVALUATION

10.4.1 Flight Program Performance

The flight program performed correctly based on a review of available data. All boost and orbital navigation functions were performed properly. Accelerations were computed correctly throughout all of boost and no unreasonable accelerometer readings were indicated by the reasonableness tests or zero change tests.

The tower avoidance maneuver was executed properly at the expected time. The maneuver to remove the roll bias and the start of the time tilt pitch guidance were both initiated at 12.11 seconds when the altitude was greater than 138 meters (452.8 ft). The roll bias was removed at 31.52 seconds. Tilt arrest occurred at 145.50 seconds. The program detected OECO at 153.82 seconds.

The active guidance phases start and stop times are given in Table 10-3. Included in this table are the start and stop times for the artificial tau phases and chi freezes. There were 0.5 and 0.1 degree changes in commanded pitch and yaw, respectively, when IGM computations were initiated in S-II burn. The SMC's (a correction factor for thrust misalignments, etc.) were initiated at 214.47 seconds, 542.02 seconds, and 10,253.53 seconds in S-II, first S-IVB and second S-IVB burns, respectively.

Table 10-3. Start and Stop Times for IGM Guidance Commands

EVENT	IGM PHASES (sec)		ARTIFICAL TAU* (sec)		TERMINAL GUIDANCE (CHI TILDE STEERING) (sec)		ATTITUDE FREEZE (CHI FREEZE) (sec)	
	START	STOP	START	STOP	START	STOP	START	STOP
First Phase IGM	196.22	443.65						
Second Phase IGM	443.65	513.12	441.91	484.25			513.12	532.87
Third Phase IGM	532.87	677.60	523.63	540.01	652.87	677.60	677.60	684.85**
Fourth Phase IGM	10,245.83	10,247.73	10,244.17	10,246.06				
Fifth Phase IGM	10,247.73	10,553.37	10,246.06	10,247.96	10,528.32	10,553.37	10,553.37	10,555.38**

* Times to nearest computation cycle.
** Start orbital time line

The presetting of tau 3 was approximately 88 seconds too small in the first S-IVB burn and approximately 80 seconds too large in the second. In first S-IVB burn this resulted in a change of 11.5 and 0.29 degrees in the pitch

and yaw commands, respectively. For the second S-IVB burn, the change was 3.0 and 6.6 degrees in pitch and yaw, respectively. The computed cutoff times in first and second burns were 684.98 seconds and 10,555.51 seconds, respectively. The velocity cutoff conditions for first S-IVB burn are given in Table 10-4. The energy cutoff conditions for second S-IVB burn are given in Table 10-5.

The orbital guidance routine was entered at the start of T_5 and T_7. The program commanded the vehicle to local horizontal 20 seconds into each time base. All commands were proper.

10.4.2 Attitude Error Computations

The minor loop performed as expected during flight. No unreasonable gimbal angles were detected. Performance during IGM flight is shown in Figure 10-4.

A roll attitude error from 0.3 to 0.5 degree was present from liftoff through S-II burn. This was probably caused by a combination of CG offset and thrust vector misalignment. In response to this bias, the platform roll gimbal angle was maintained 0.3 to 0.5 degree away from the commanded angle. This gimbal angle bias was recognized correctly by the flight program and entered into the control coordinate transformation. Consequently, no deterioration of control performance occurred.

10.4.3 Program Sequencing

All programmed events occurred properly. The successful translunar injection essentially demonstrated that all program sequencing was followed.

However, the propellant mixture ratio change was programmed to occur when "time-to-go" in the first stage IGM (T_1I) was calculated to be zero. The LVDC program was compatible with the OT and Engine Mixture Ratio (EMR) shift occurred 289.62 seconds, compared with 289.66 seconds for the OT. The time difference (0.04 seconds) is within the length of a LVDC computer cycle (approximately 1.7 seconds) at this time. EMR shift occurred as programmed. However, the propulsion predictions used in the OT assumed a fixed time of 284.05 seconds in T_3.

The actual EMR shift time was consistent with the preset value of 246.5 seconds for T_1I. In order to be consistent with the propulsion predictions, the guidance presetting for T_1I should have been reduced by 4.2 seconds to 242.3 seconds. Also, T_2I presetting would have had to be increased by the same amount to be compatible with the propulsion prediction.

Table 10-4. S-IVB First Burn Guidance Cutoff Conditions

PARAMETER	UNIT	TARGET VALUE	ACTUAL VALUE	DELTA
Range Time	s		684.98	
Velocity	m/s (ft/s)	7791.0608* (25,561.2231)	7790.986 (25560.978)	0.075 (0.245)
Radius	meters (ft)	6,563,366 (21,533,354)	6,563,392 (21,533,439)	26 (85)
Inclination	deg	32.5031	32.5036	0.0005
Descending Node	deg	123.004	123.004	0.0000
Path Angle	deg	0.0	0.00063	0.00063
Azimuth	deg		72.1239	
Apogee	meters (ft)		6,563,411 (21,533,501)	
Perigee	meters (ft)		6,556,488 (21,510,787)	

*The preset velocity, 7793.0429, is biased by 1.98215 to compensate for thrust decay (7793.0429 - 1.98215 = 7791.0608).

Table 10-5. Guidance Comparisons Elliptical Orbit Parameters at S-IVB Second Cutoff

PARAMETER	UNITS	DATA SOURCE		
		LVDC	OMPT	OT
Eccentricity		0.97488614	0.97425438	0.97496599
Argument of Perigee	deg	29.665288	29.595497	29.650827
Inclination	deg	30.620166	30.639100	30.614597
Descending Node*	deg	119.55275	119.59257	119.55035
Energy	m^2/s^2 (ft^2/s^2)	-1,518,371 (-16,343,609)	-1,556,426 (-16,753,229)	-1,513,447 (-16,290,597)

*Includes longitude of launch site (80.604 degrees west)

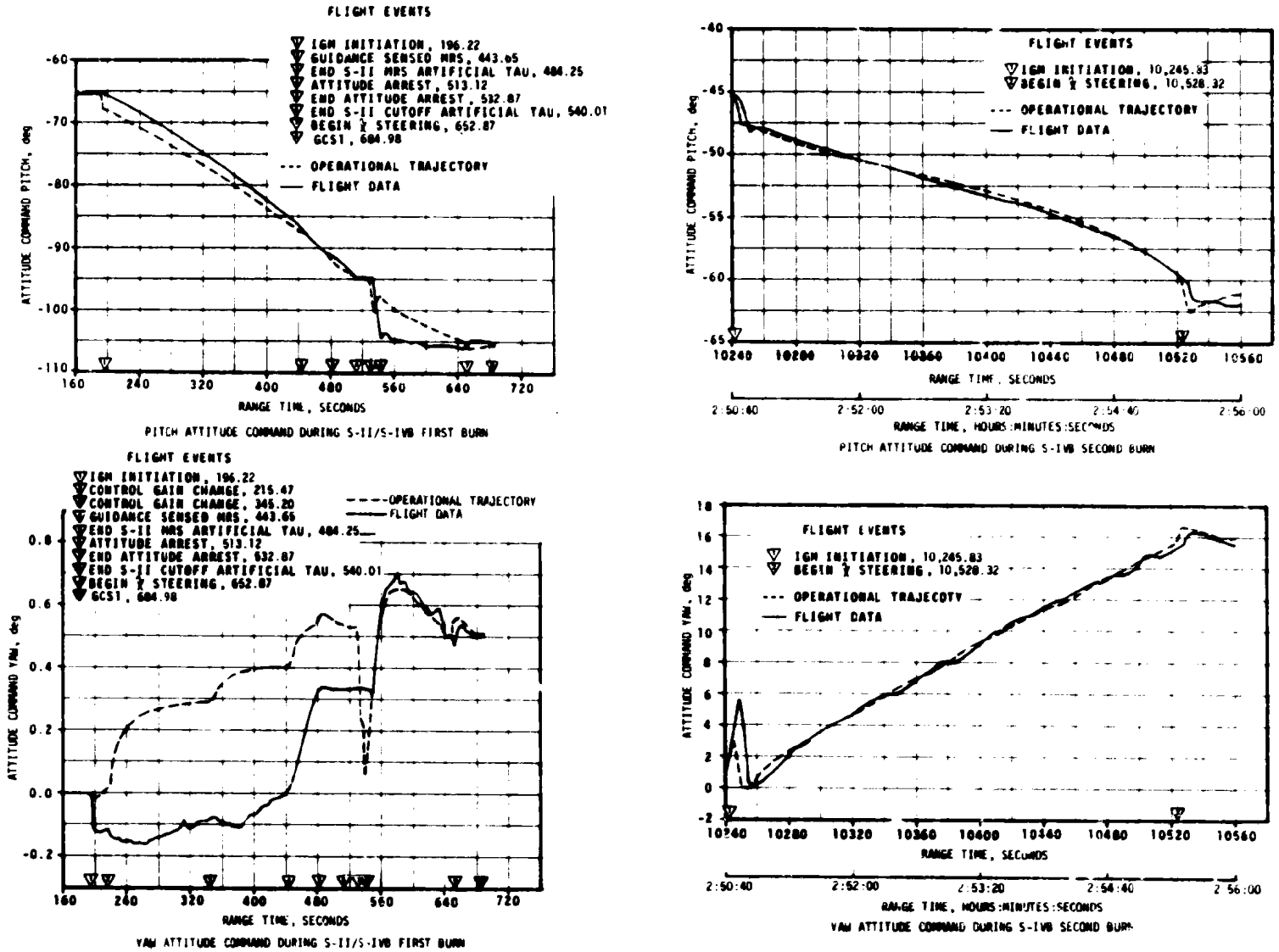

Figure 10-4. Attitude Errors During IGM Flight

10.5 GUIDANCE SYSTEM COMPONENT EVALUATION

10.5.1 LVDC Performance

The LVDC performed as predicted for the AS-503 mission. No valid error monitor words and no self-test error data have been observed that indicate any deviation from correct operation.

10.5.2 LVDA Performance

The LVDA performance was nominal. Error monitor words with associated error time words occurred on this flight as on past flights. These words were associated with the TMR logic inputs to the interrupt processor. These indications had no detectable effect on the performance of the LVDA during the flight.

10.5.3 Ladder Outputs

The ladder networks and converter amplifiers performed satisfactorily. No data have been observed that indicate an out-of-tolerance condition between channel A and the reference channel converter-amplifiers.

10.5.4 Telemetry Outputs

Analysis of the available analog telemetry buffer and flight control computer attitude error plots indicated symmetry between the buffer outputs and the ladder outputs. The analysis of the available LVDC power supply plots indicated satisfactory performance of the power supply telemetry buffers.

10.5.5 Discrete Outputs

No valid discrete output register words (TAGS 043 and 052) were observed to indicate guidance or simultaneous memory failure.

10.5.6 Switch Selector Functions

Switch selector data indicate that the LVDA switch selector functions were performed satisfactorily. No error monitor words were observed that indicate disagreement in the TMR switch selector register positions or in the switch selector feedback circuits. No mode code 24 words or switch selector feedback words were observed that indicated a switch selector feedback was in error. In addition, no indications were observed to suggest that the B channel input gates to the switch selector register postions were selected.

10.5.7 ST-124M-3 Inertial Platform Performance

The inertial platform system performed as designed with no unexpected deviations.

The accelerometer servo loops functioned as designed and maintained the accelerometer float within the measuring head stops (±6 degrees) throughout the flight. The accelerometer encoder outputs indicated that the accelerometers accurately measured the vehicle acceleration.

The X, Y, and Z gyro servo loops for the stable element functioned as designed. The operational limits of the servo loops were not reached at any time during the mission. Telemetry from the LVDC indicates that the inertial reference was still being maintained at 25,420 seconds.

Oscillations of 5.5 hertz could be seen on an oscillogram of the Z gyro pickup signal beginning at 116 seconds and ending at 158.8 seconds. These oscillations were apparently the result of an external force since they were also observed on a longitudinal accelerometer not associated with the platform. Maximum amplitude reached 0.2 degree peak-to-peak at S-IC cutoff. Similar oscillations were observed on AS-502.

The fine and backup gimbal resolver outputs indicated nominal performance.

The portions of the environmental control subsystem associated with the ST-124M-3 stabilized platform subsystem performed nominally through 10,700 seconds. Subsequent data is not available at this time.

Available data indicates that all temperatures and pressures associated with the ST-124M-3 remained within specifications through 13,410 seconds. Gaseous Nitrogen (GN_2) and coolant flowrates also were nominal through 13,410 seconds.

The ST-124M-3 inertial platform assembly vibration levels during (or near) liftoff for AS-503 compared closely to those of AS-501 and AS-502. The vibration levels of all three vehicles (during the liftoff period) were similar in both amplitude and frequency. Four measurements exceeded the test specification for vibration acceptance on AS-503. This is a previously reported condition which is not believed to be detrimental to the stabilized platform subsystem.

Figure 10-5 shows a time history of the composite Grms level of vibration measured on the inertial gimbal during the first 140 seconds of flight for AS-503, AS-502, and AS-501. This figure shows a similarity of the vibration profile for all three flights.

From an analysis of the available data, the following conclusions regarding ST-124M-3 inertial platform assembly vibrations on AS-503 have been reached:

a. There were no vibration-induced malfunctions of the ST-124M-3 inertial platform on AS-503.

b. The low-frequency vibrations at liftoff exceeded the random vibration test specifications in the perpendicular and longitudinal directions.

c. The vibration profile of AS-503 was similar to those of AS-501 and AS-502.

d. Data indicates that the vibration frequency and amplitude of AS-503 will be typical of AS-504.

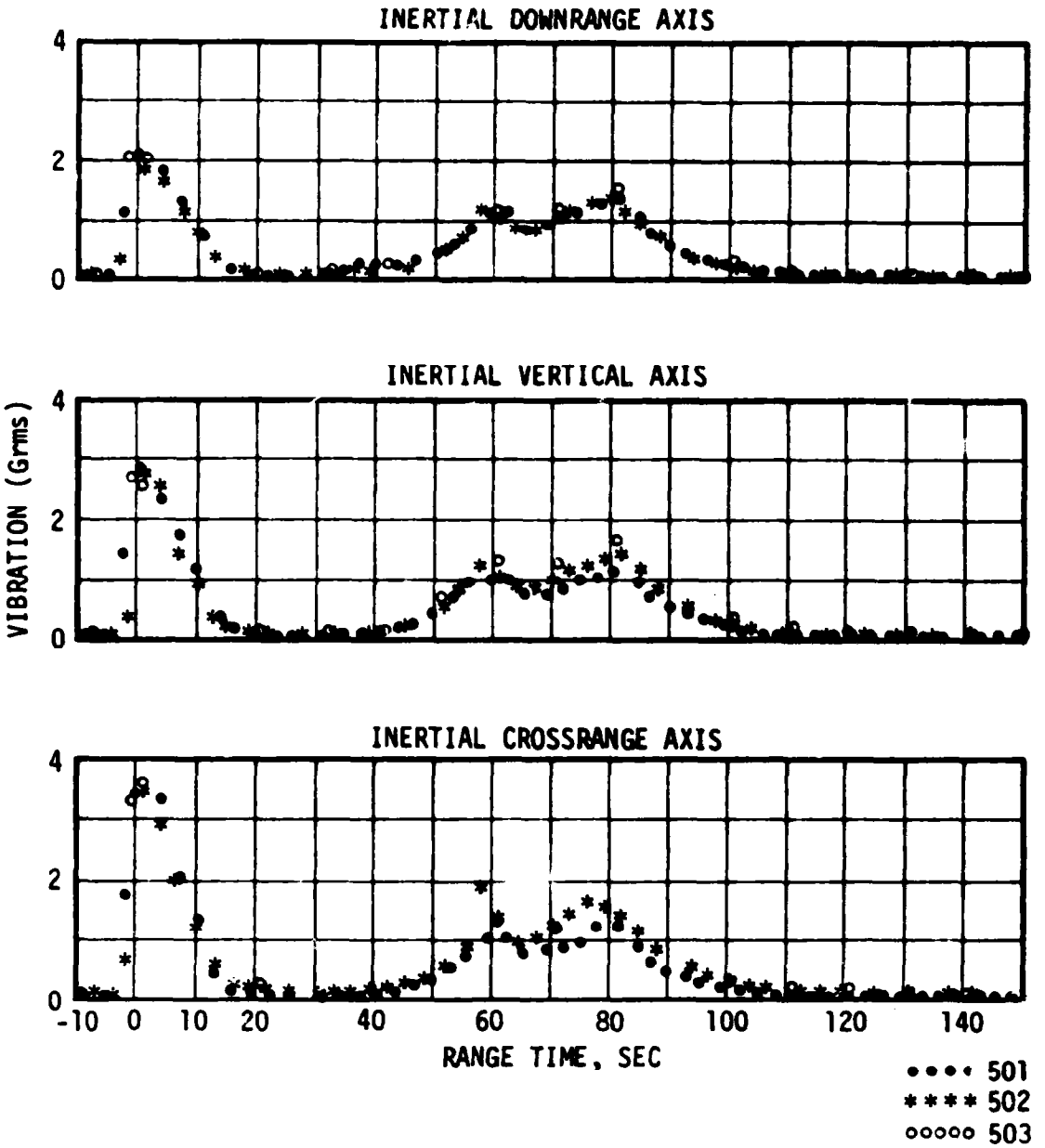

Figure 10-5. Saturn V Inertial Gimbal Vibrations

SECTION 11

CONTROL SYSTEM

11.1 SUMMARY

The AS-503 Flight Control Computer (FCC), Thrust Vector Control (TVC), and Auxiliary Propulsion System (APS) satisfied all requirements for vehicle attitude control during boost and orbital control modes. Bending and slosh dynamics were adequately stabilized. The programmed 1.25 degree yaw maneuver to provide tower clearance was properly executed, making vehicle-tower clearances during liftoff satisfactory with less than 25 percent of the available margins utilized. At 12.11 seconds a simultaneous pitch-roll maneuver was begun. The vehicle rolled about 18 degrees to the 72.124 degree flight azimuth. Vehicle response to the steering commands (attitude error signals) was nominal, and the roll and pitch programs were satisfactorily completed.

To improve S-IC outboard engine out characteristics, the FCC control outputs to the F-1 engines were biased to provide a 2-degree outboard cant beginning at 20.64 seconds. The canting had negligible effect on the control system. The wind biased pitch tilt program resulted in nominal control system activity and low angles-of-attack during the high dynamic pressure region of flight. Throughout S-IC boost the control system was required to correct for a steady state roll torque which resulted in a roll attitude error of +0.4 degree.

S-IC/S-II first and second plane separations were satisfactory, resulting in minimum disturbance to the control system. The Programmed Mixture Ratio (PMR) shift resulted in only a small attitude change. Following PMR shift the rate gyros detected an 18 hertz oscillation; however, the FCC filter networks attenuated the signal so that the oscillation could not be seen in the actuator currents. The S-II stage also experienced a steady state roll torque resulting in a roll attitude error of +0.5 degree.

S-II/S-IVB separation was nominal and caused only small attitude disturbances. Control system activity during first and second S-IVB burns was nominal. At third stage Iterative Guidance Mode (IGM) initiation, there was an attitude disturbance in the pitch plane, reaching a 2.2-degree

attitude error. The first LOX slosh frequency was observed in the pitch rate during the first 20 seconds of S-IVB second burn. The vehicle experienced a small clockwise roll torque of 7 to 8 N-m (5 to 6 lbf-ft) during both burns, resulting in minimal APS propellant consumption for roll control.

At approximately 20 seconds after S-IVB first and second cutoffs, the vehicle was maneuvered to align the longitudinal axis along the local horizontal. At approximately 908 seconds after second S-IVB cutoff, the vehicle was commanded through a 120-degree pitch up and a 180-degree counterclockwise roll maneuver to obtain the desired Command and Service Module (CSM) separation and S-IVB communications attitude. Following CSM separation the launch vehicle maintained a frozen inertial attitude until 6541 seconds after second cutoff, when the vehicle was commanded to the "slingshot" maneuver attitude (180 degrees pitch, 0 degree yaw, and 180 degrees roll attitudes relative to local horizontal). This attitude was inertially held through the maneuver.

At approximately 19,556 seconds the S-IVB ullage engines were ignited to provide additional ΔV for the "slingshot" maneuver. Ullage engine No. 2 propellant depleted at 20,288.56 seconds, and engine No. 1 depletion occurred at 20,314.00 seconds. Since the ullage engines and the APS modules use the same propellant supply, no APS control was available subsequent to depletion. The Launch Vehicle Digital Computer (LVDC) was still issuing valid attitude commands at 21,214 seconds since angular rates following depletion were small and the attitude reference was not lost. However, the pitch, yaw, and roll attitude errors had all reached their 6.0-degree ladder limit at that time.

11.2 CONTROL SYSTEM DESCRIPTION

Figure 10-1 (Section 10) shows the interconnection and signal flow paths of the control components as they relate to the guidance components.

Vehicle attitude correction is accomplished in accordance with the requirements of the guidance system through attitude error signals. These signals are generated by the LVDC and Launch Vehicle Data Adapter (LVDA). During S-IC stage burn, attitude steering commands are the result of the preprogrammed yaw and roll maneuvers and the time tilt pitch program. At the initiation of IGM during S-II burn, attitude steering commands become the result of guidance system computations.

The AS-503 FCC, which is essentially identical to the AS-502 FCC, is an analog computer which generates the proper commands for the S-IC, S-II, and S-IVB stage engine actuators and S-IVB stage APS. In generating the engine commands, the FCC processes and combines attitude error signals from the LVDA and angular velocity signals from the Control-EDS Rate Gyros/Control Signal Processor (CSP).

S-IVB stage attitude control commands to the APS are provided to the roll axis during S-IVB stage burn and to all three control axes during coast.

The Control-EDS Rate Gyros/CSP used on AS-503 were essentially identical to those used on AS-502. The Control-EDS Rate Gyros/CSP combination provides angular velocity signals to the FCC for dynamic feedback. The Control-EDS Rate Gyros contain nine rate gyros, three in each axis. On AS-503 the S-IC outboard engines were canted 2 degrees outboard beginning at about 20 seconds.

11.3 S-IC CONTROL SYSTEM EVALUATION

The AS-503 control system performed satisfactorily during S-IC powered flight with all control variables within predicted envelopes. The 2-degree outboard canting of the control engines was accomplished as planned.

Vehicle liftoff acceleration was as predicted and was similar to the AS-502. The vehicle cleared the launch platform and tower using less than 25 percent of the available clearance. The pitch, yaw, and roll guidance maneuvers were executed as planned.

The vehicle performed within flight dynamic constraints throughout flight. In the region of high dynamic pressure the maximum angles-of-attack were 2.0 degrees in pitch and 2.5 degrees in yaw. The maximum average pitch engine deflection was -0.5 degree due to a wind shear and the maximum average yaw engine deflection was -0.5 degree due to the yaw maneuver.

11.3.1 Liftoff Clearances

The vehicle cleared the mobile launcher structure using less than 25 percent of the available clearance as shown in Table 11-1. The ground wind was from the north with a magnitude of 5.1 m/s (10 knots) at the 18.3 meters (60 ft) level. The liftoff vertical motion, as shown in Figure 11-1, was very close to predicted. The release forces of the 12 lubricated rods were slightly higher than predicted. Table 11-2 compares the vehicle misalignments measured during flight with preflight measurements.

The clearance between the vehicle thrust structure and the holddown post as determined by liftoff cameras is shown in Figure 11-2. Also shown is the motion of engine No. 2 with respect to the holddown post at position III. The motion of the vehicle was nearly vertical with 1.9 centimeters (0.75 in.) of lateral motion at the 61 centimeters (24.0 in.) level. The actual motion was within the predicted clearance envelopes. Following holddown arm release, the vehicle rolled to a trim angle of +0.4 degree. This roll motion resulted in 2.5 centimeters (1 in.) of tangential motion of the engines which compares to an available clearance of 1.2 meters (3.9 ft).

Table 11-1. Summary of Liftoff Clearances

POTENTIAL INTERFERENCE		AVAILABLE CLEARANCE cm (in.)	ACTUAL CLEARANCE cm (in.)
VEHICLE	GROUND EQUIPMENT		
Thrust Structure	Holddown Post	8.26 (3.25)	7.1 (2.8)
Engine Bell	Holddown Post	85.1 (33.5)	74.9 (29.5)
Service Module	SM Swing Arm	Variable	*
S-IVB Stage	S-IVB Forward Swing Arm	Variable	*
S-II/S-IVB Interstage	S-IVB Aft Swing Arm	Variable	*
S-II Stage	S-II Forward Swing Arm	Variable	*
S-II Stage	S-II Intermediate Swing Arm	Variable	*
Fin Tip	Swing Arms	862.79 (339.68)	650 (256)

* Camera data indicates clearance, no quantitative data available.

Figure 11-3 shows that the combination of the yaw maneuver and the wind blowing away from the tower resulted in a clearance of 11.0 meters (36 ft) between S-IC fin tip A and the top of the tower. Flight data were taken from a camera located due east of the mobile launcher. Center engine translation and the exhaust plume angles for each of the five S-IC engines during the first 240 meters (787 ft) of vertical flight are also shown in Figure 11-3. Center engine translation was a maximum of 12 meters (39.4 ft) south and 8 meters (26.2 ft) east.

11.3.2 S-IC Flight Dynamics

Table 11-3 lists maximum control parameters during S-IC burn. Pitch, yaw, and roll time histories are shown in Figures 11-4 through 11-6. Dynamics in the region between liftoff and 35 seconds resulted primarily from guidance commands. Maximum yaw and roll dynamics occurred in this region as follows. Maximum yaw rate was -0.6 degree at 12.4 seconds, maximum yaw error was -1.3 degrees at 3.1 seconds, and maximum yaw engine deflection

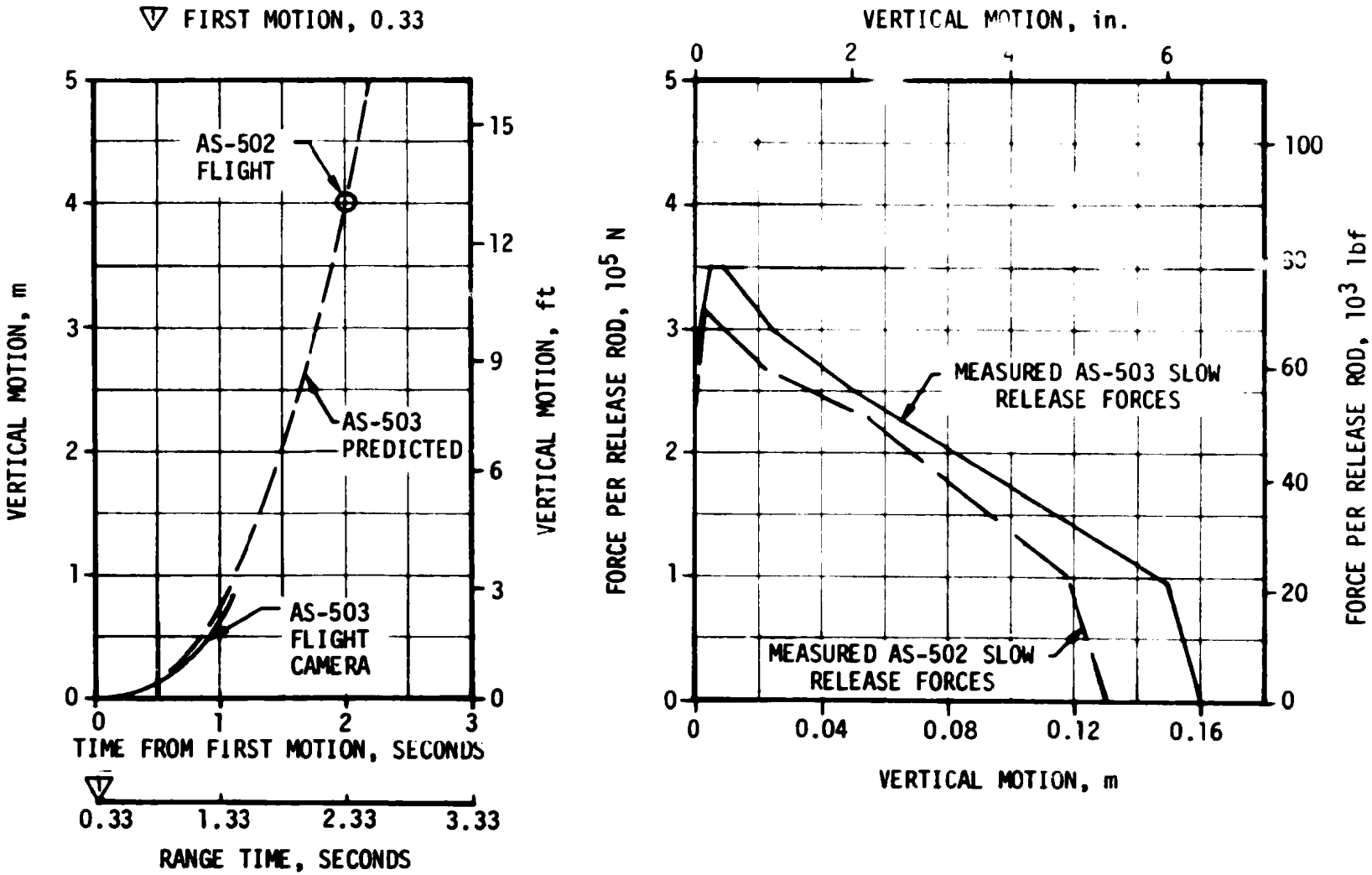

Figure 11-1. Liftoff Vertical Motion and Slow Release Forces

Table 11-2. AS-503 Misalignment Summary

PARAMETER	PREFLIGHT PREDICTED			LAUNCH		
	PITCH	YAW	ROLL	PITCH	YAW	ROLL
Thrust Misalignment, deg	±0.20*	±0.20* **	±0.20*	+0.15	+0.11	-0.10
Inboard Engine Cant, deg	+0.11	-0.08	-	+0.11	-0.08	-
Servo Amp Offset deg/eng	±0.1	±0.1	±0.1	-	-	-
Vehicle Stacking and Pad Misalignment, deg	±0.1	±0.1	-	-0.05	-0.04	+0.0
Peak Soft Release Force per Rod, N (lbf)	316,000 (71,000)			350,000 (78,700)		
Wind	95 Percentile Envelope			5.1 m/s (10 knots) at 18.3 meters (60 ft)		
Thrust to Weight Ratio	1.247			1.247		

* Thrust vector measurement uncertainty.

** A positive polarity was used to determine minimum fin tip/umbilical tower clearance. A negative polarity was used to determine vehicle/GSE clearances.

was -0.5 degree at 3.1 seconds. The maximum roll rate was 1.3 deg/s at 14.2 seconds, and the maximum roll error was 0.7 degree at 32.3 seconds.

The AS-503 was the first Saturn V vehicle to fly with the control engines canting radially outboard 2.0 degrees beginning at 20.64 seconds. This feature was added to improve engine out characteristics and performed as predicted. The canting of the control engines was not perceptible in the pitch and yaw dynamics and caused only a small transient in roll. Roll transients show more oscillation at the roll control frequency than the simulation, indicating that the actual roll damping is lower than predicted.

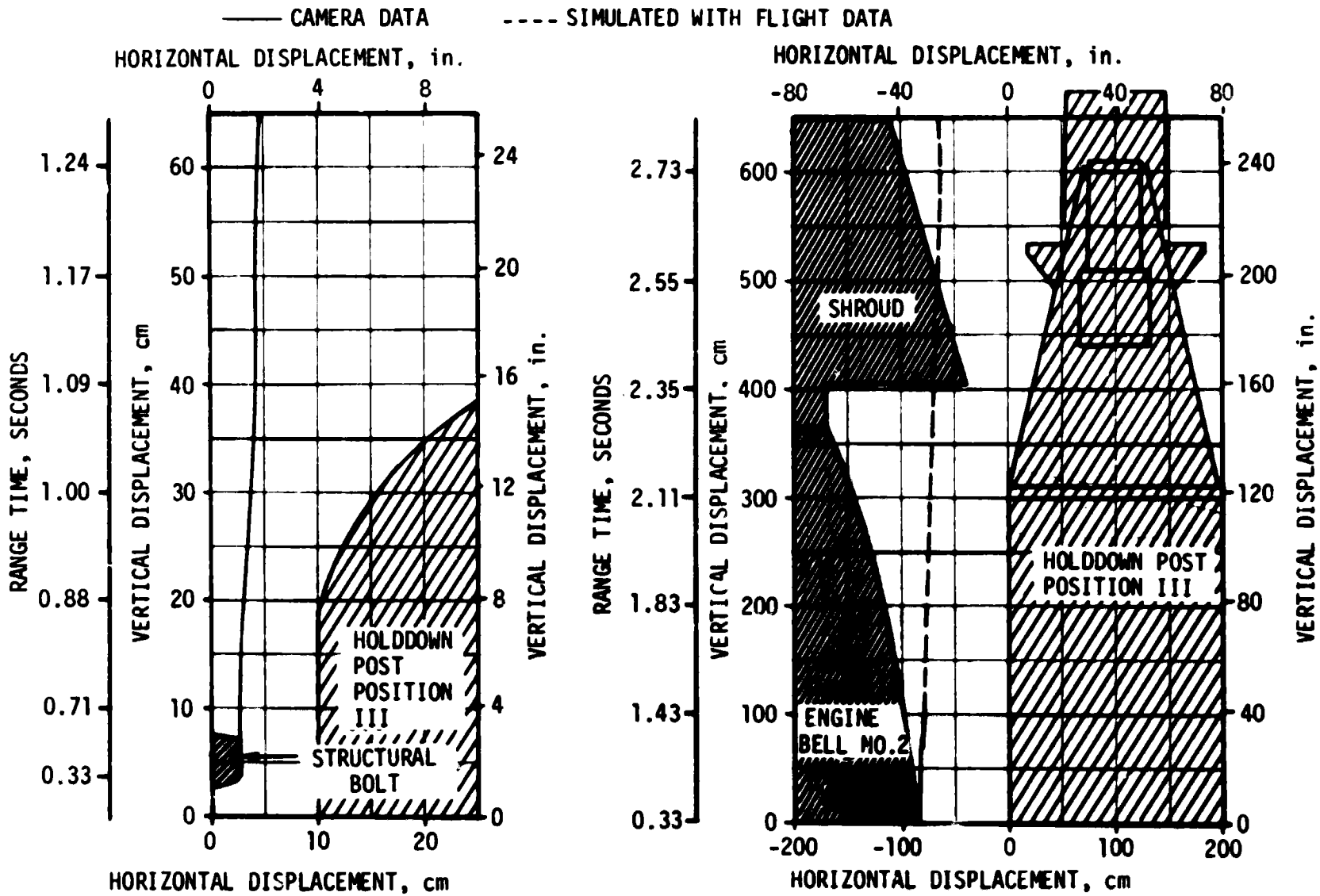

Figure 11-2. Liftoff Lateral Motion (Position III)

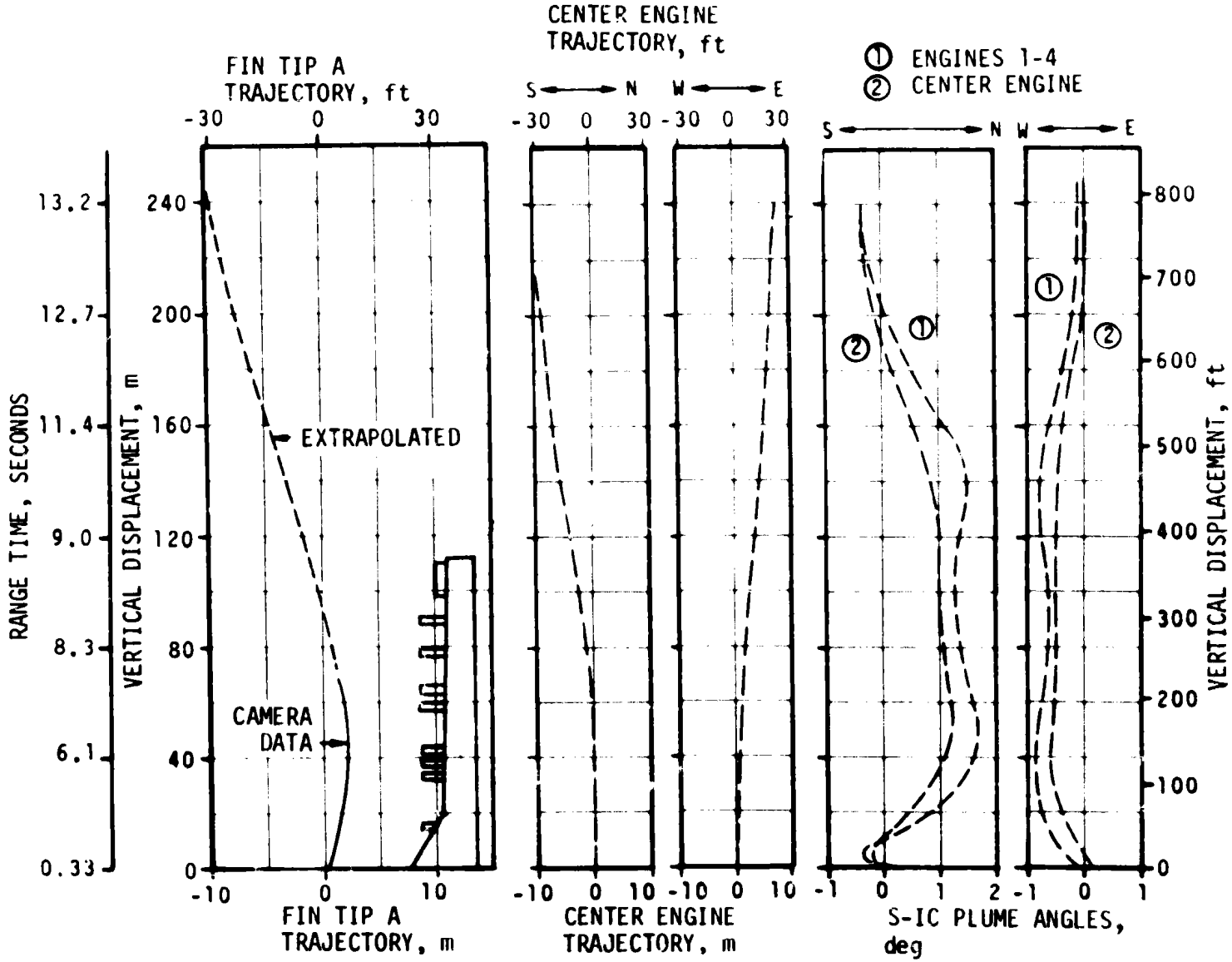

Figure 11-3. S-IC Plume Angular Variation; Center Engine Trajectory and Fin Tip A Trajectory

Table 11-3. Maximum Control Parameters During S-IC Boost Flight

PARAMETERS	UNITS	PITCH PLANE		YAW PLANE		ROLL PLANE	
		MAGNITUDE	RANGE TIME (SEC)	MAGNITUDE	RANGE TIME (SEC)	MAGNITUDE	RANGE TIME (SEC)
Attitude Error	deg	+1.2	+76.4	-1.3	+3.1	+0.7	+32.3
Angular Rate	deg/s	-1.0	+83.0	±0.6	+4 to 13	+1.3	+14.2
Average Gimbal Angle	deg	-0.5	+112.8	-0.5	+3.1	+0.2	+31.9
Angle-of-Attack	deg	+2.0	+74.6	+2.5	+51.4		
Angle-of-Attack Dynamic Pressure Product	deg-N/cm^2 (deg-lbf/in.^{2})	+7.1 (10.3)	+74.6	+5.05 (7.32)	+51.5		
Normal Acceleration	m/s^2 (ft/s^2)	<0.4 (<1.3)		<0.4 (<1.3)			

In the region between 35 and 140 seconds, maximum dynamics were caused by the pitch tilt program, the wind, and wind shears. The pitch and yaw plane wind velocities and angles-of-attack are shown in Figure 11-7. The peak angle-of-attack in pitch was 2.0 degrees at 75 seconds and the peak yaw angle-of-attack was 2.5 degrees at 51 seconds. Peak engine deflection in pitch was -0.5 degree at 113 seconds. The maximum pitch rate was -1.0 deg/s at 83 seconds and resulted from the combined effects of pitch guidance and winds. Maximum pitch error was 1.2 degrees at 76 seconds. Significant dynamics due to wind shears occurred in yaw at 80 seconds and in pitch at 106 seconds. Figure 11-8 shows the normal acceleration components as seen in the IU and extracted from the platform accelerometer data. The maximum normal acceleration was less than 0.04 g in pitch and yaw.

The transient at Inboard Engine Cutoff (IECO) indicates that the actual center engine cant was approximately equal to the predicted cant of +0.11 degree in pitch and -0.08 degree in yaw. At outboard engine cutoff the vehicle had attitude errors to trim out the effects of thrust unbalance, offset center of gravity, thrust misalignment, and control system misalignments.

Engine response to slosh is shown in Figure 11-9. The figure was derived by passing measured engine deflection time histories through bandpass filters, retaining only slosh frequencies. The small engine motion at slosh frequencies other than at the time of known disturbances indicates that slosh was adequately stabilized. The engine response to slosh was approximately 0.05 degree peak-to-peak. The maximum slosh amplitude in the S-IC fuel tank was 0.27 meter (10.5 in.) in pitch at 13.8 seconds and 0.24 meter (9.5 in.) in yaw at 11.4 seconds. The maximum slosh amplitude in the S-IC LOX tank was 0.21 meter (8.4 in.) in pitch at 75.4 seconds and 0.22 meter (8.8 in.) in yaw at 78.6 seconds.

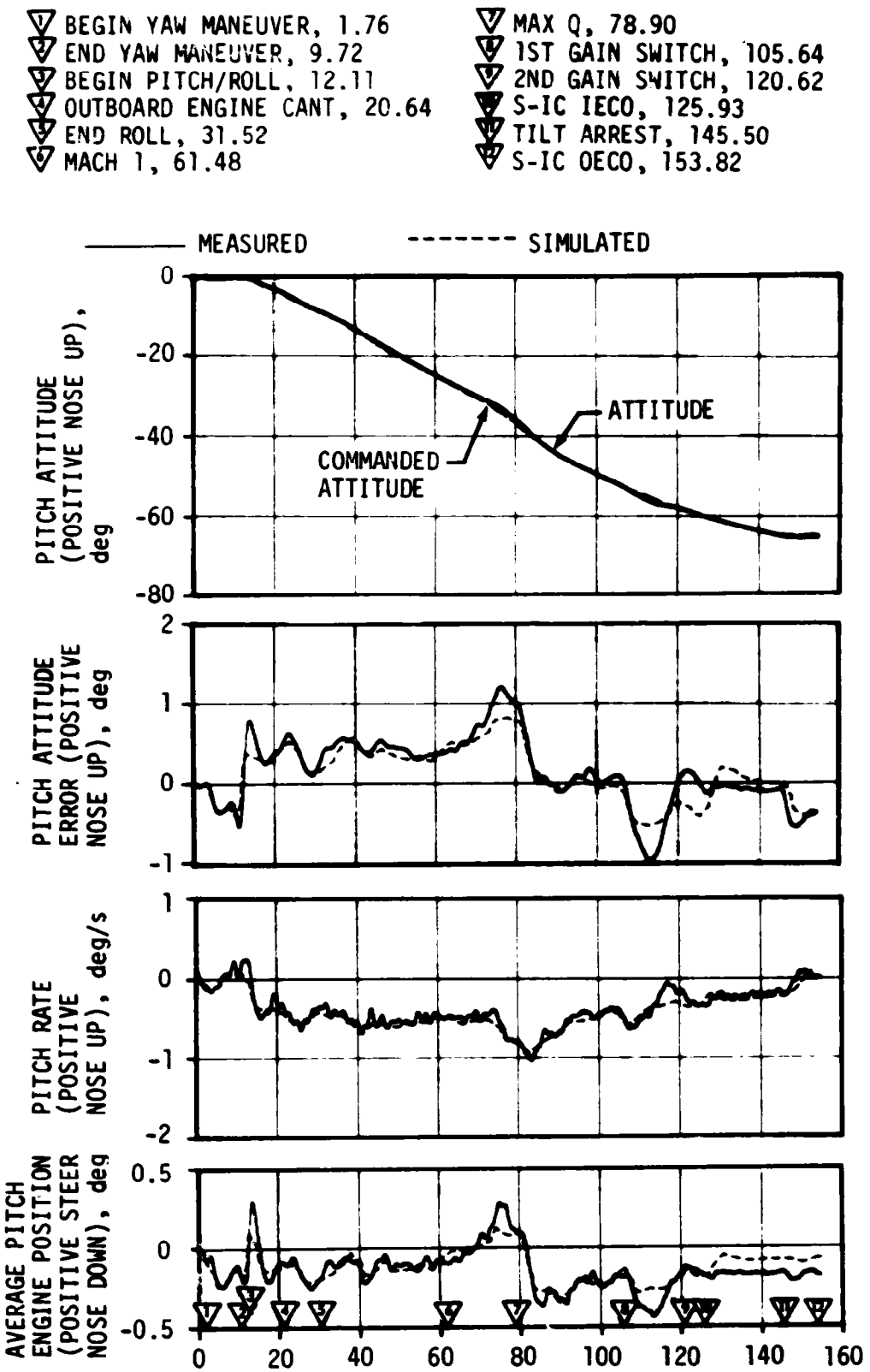

Figure 11-4. Pitch Plane Dynamics During S-IC Burn

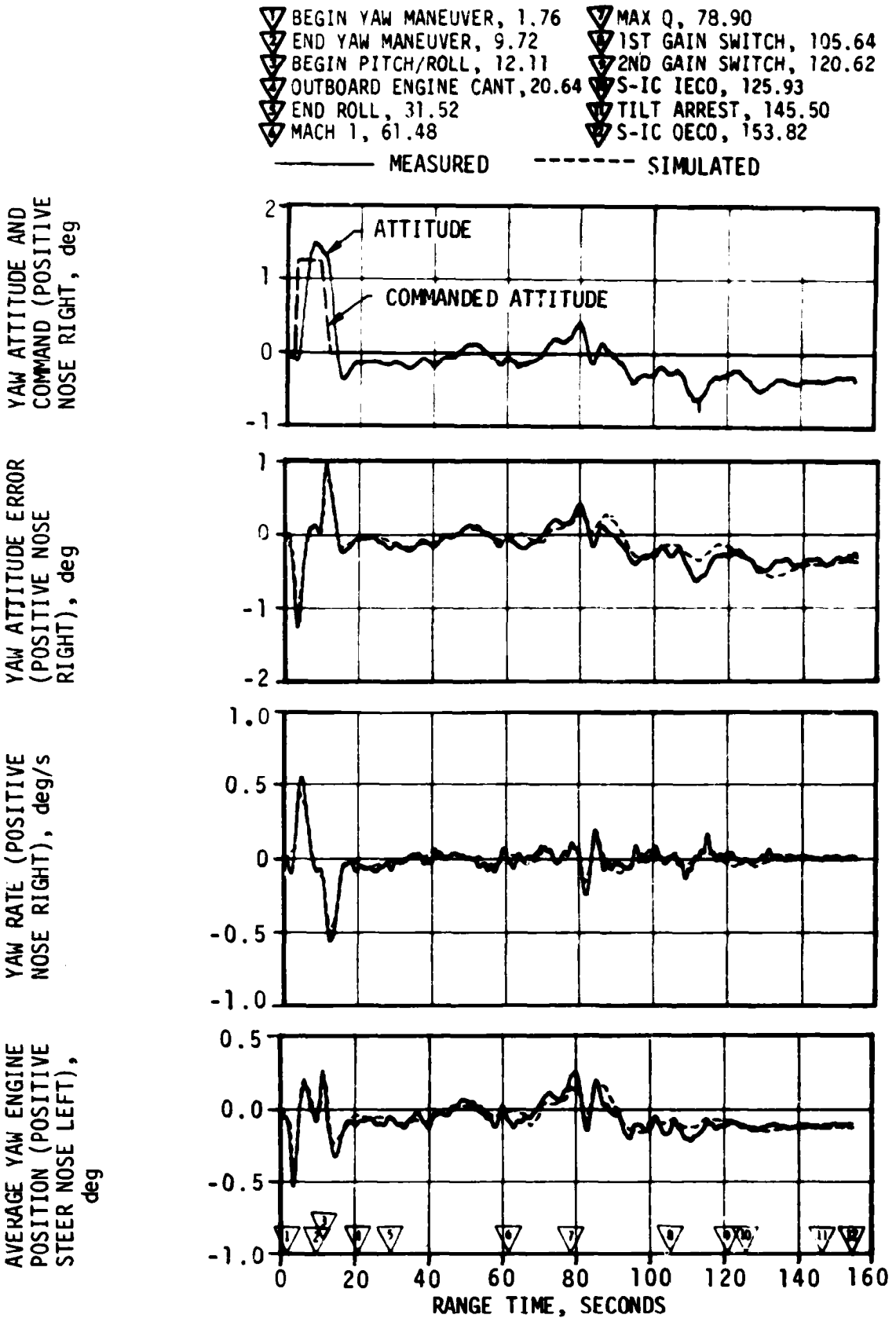

Figure 11-5. Yaw Plane Dynamics During S-IC Burn

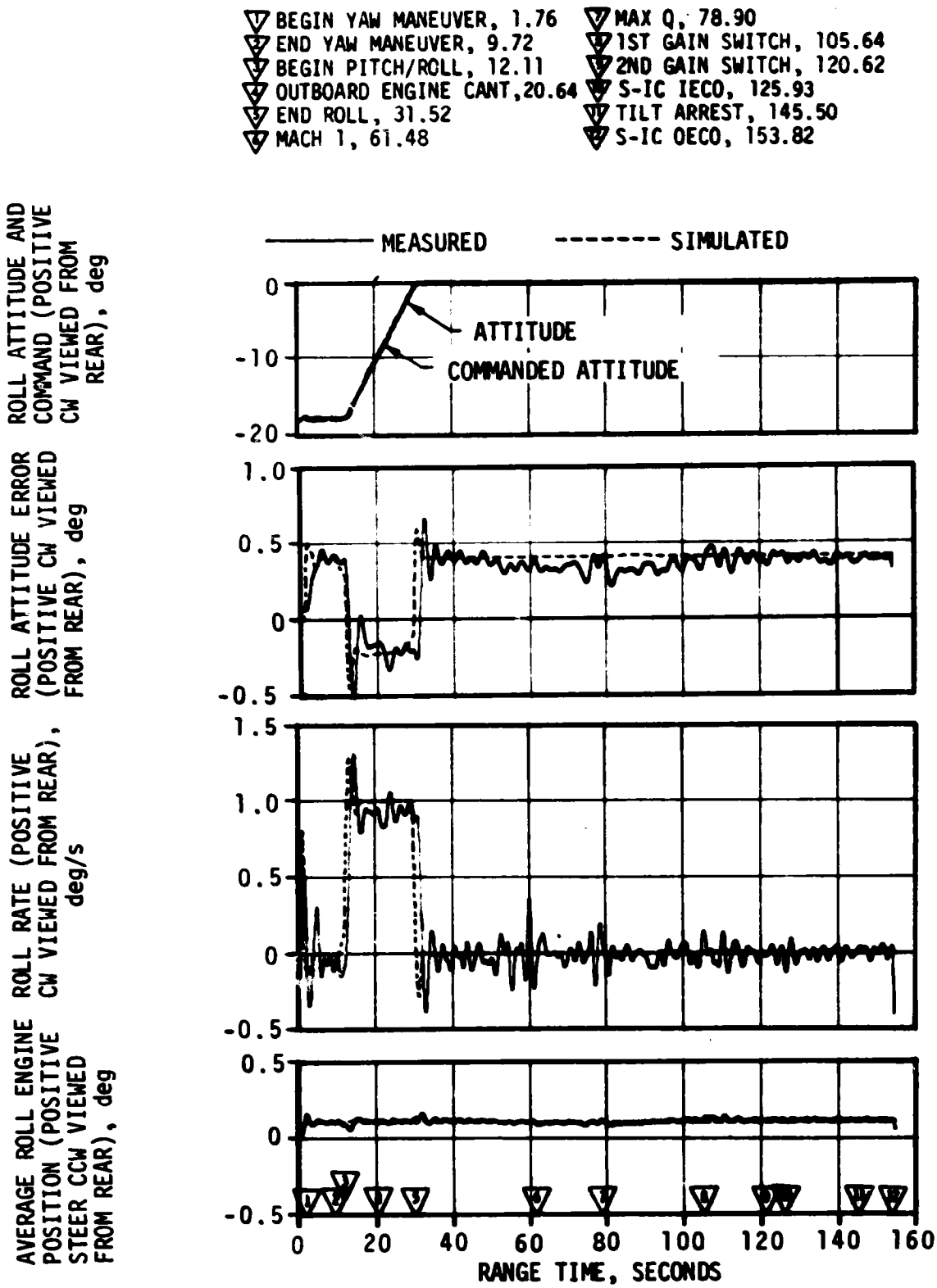

Figure 11-6. Roll Plane Dynamics During S-IC Burn

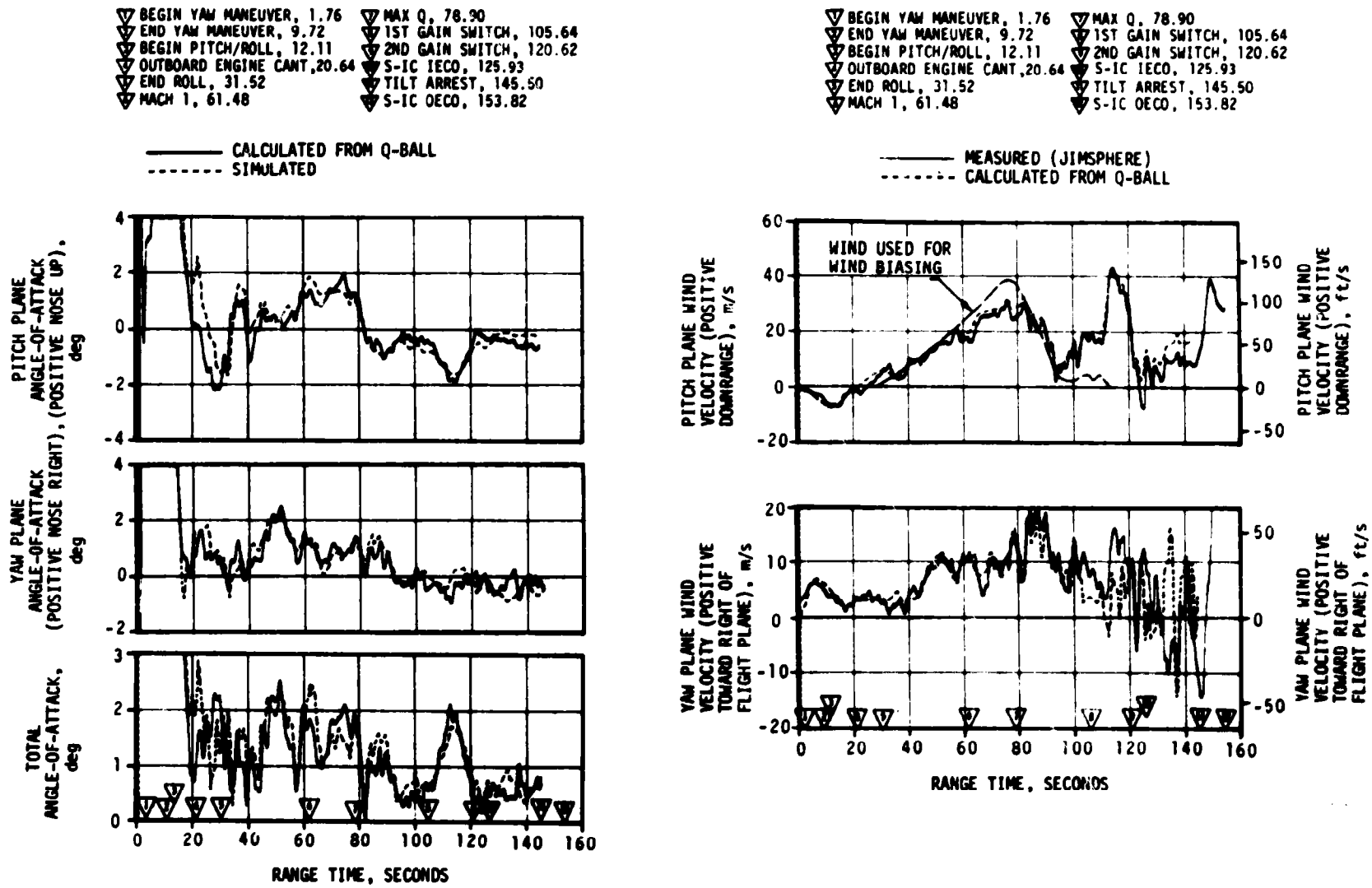

Figure 11-7. Free Stream Angle-of-Attack and Pitch and Yaw Plane Wind Velocity During S-IC Burn

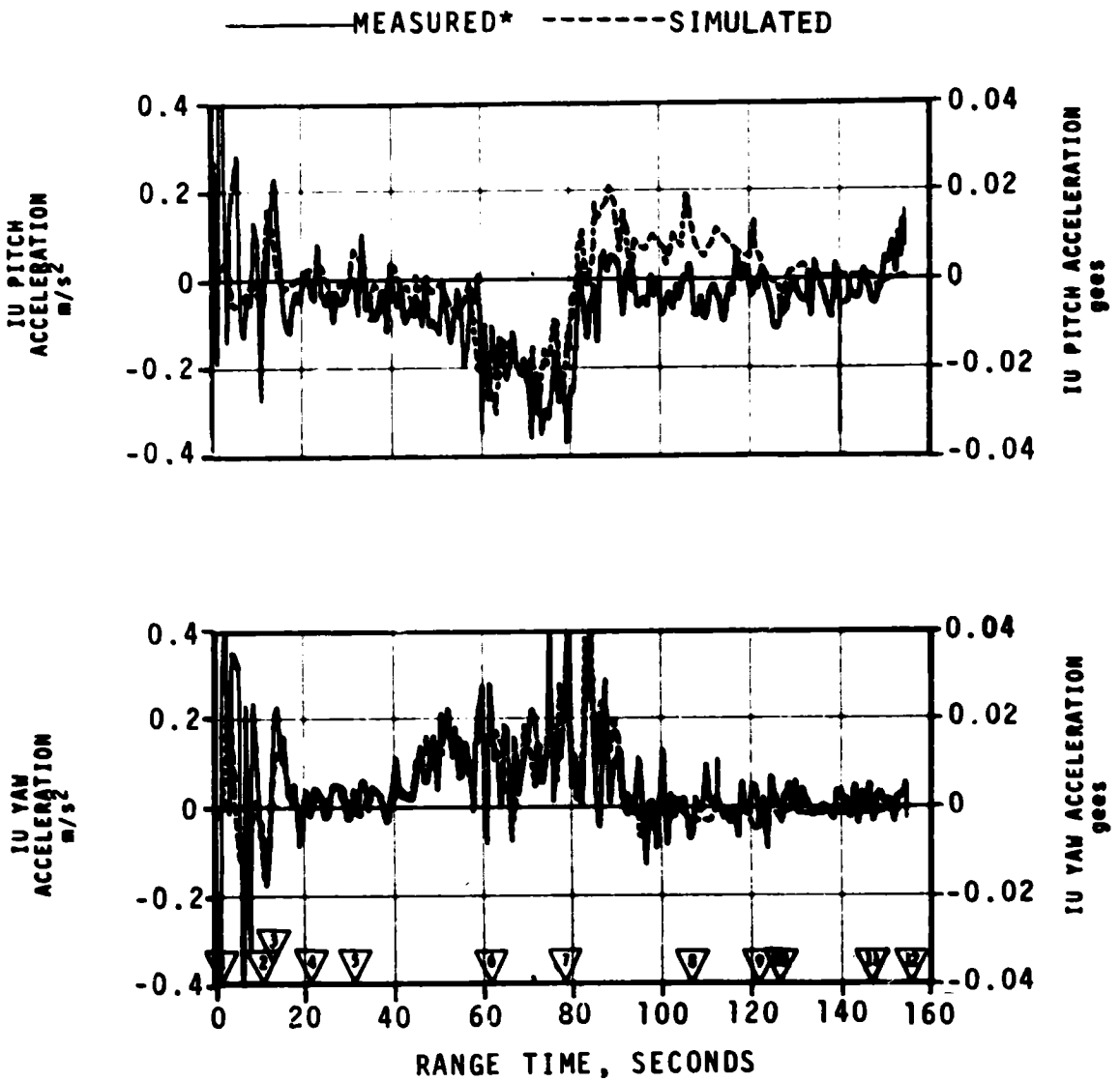

*OBTAINED FROM PLATFORM ACCELEROMETERS

Figure 11-8. Normal Acceleration During S-IC Powered Flight

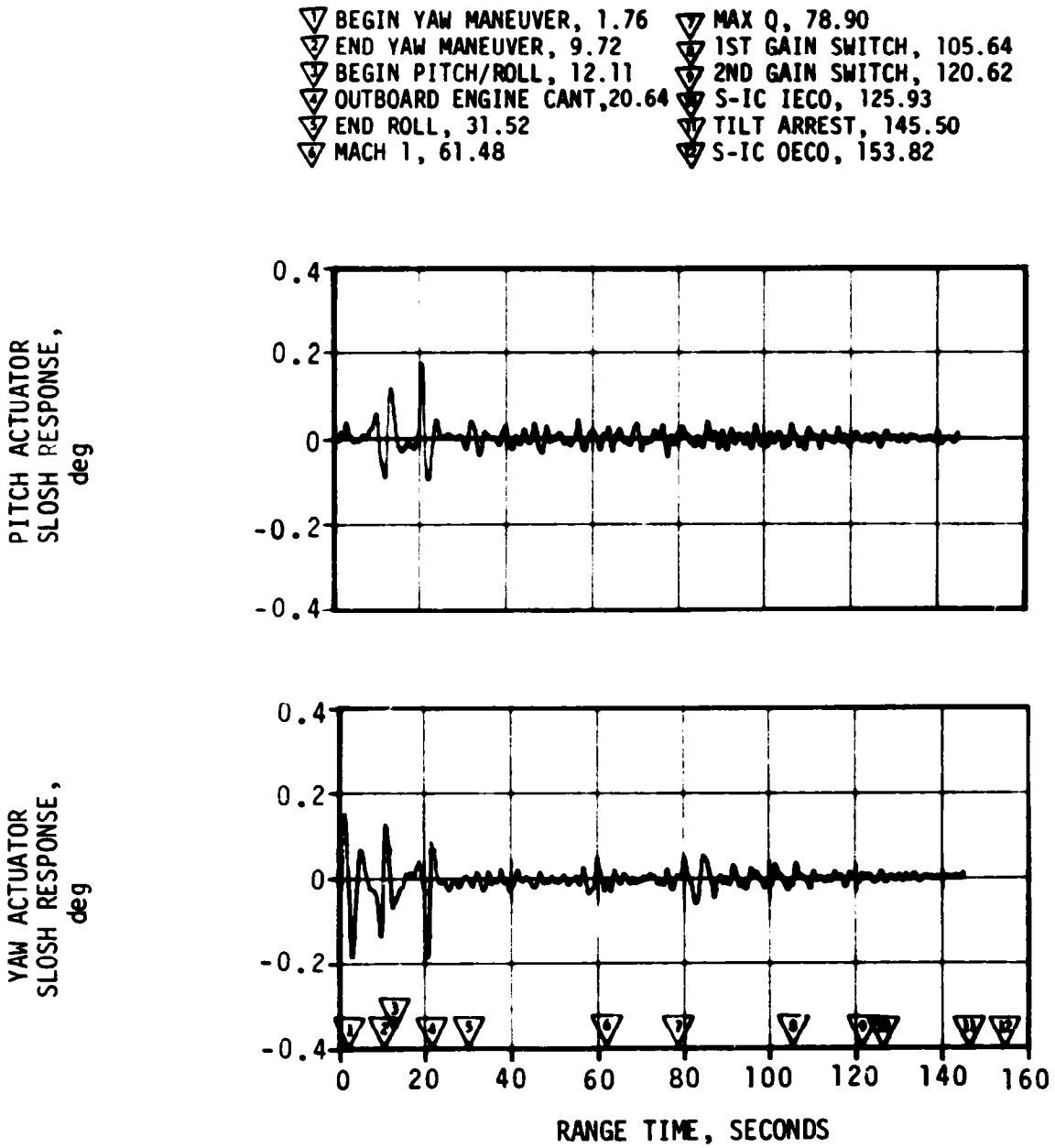

Figure 11-9. S-IC Engine Deflection Response to Propellant Slosh

11.4 S-II CONTROL SYSTEM EVALUATION

The S-II stage attitude control system performance was satisfactory. Analysis of the magnitude of modal components in the engine deflections revealed that vehicle structural bending and propellant sloshing had negligible effect on control system performance. The maximum values of control parameters occurred in response to S-IC/S-II separation disturbances and nonuniform J-2 engine thrust buildups. At that time attitude rates for pitch, yaw, and roll were 0.2, 0.1 and 1.4 deg/s, respectively. The response at other times (such as initiation of IGM guidance, initiation of first artificial tau mode) was within expectations.

11.4.1 Attitude Control Dynamics and Stability

Between the events of S-IC OECO (153.82 seconds) and initiation of IGM (196.22 seconds), attitude commands were held constant. Significant events which occurred during that interval were S-IC/S-II separation, S-II stage J-2 engine start, second plane separation, and Launch Escape Tower (LET) jettison. The attitude control dynamics throughout this interval indicated stable operation as shown in Figures 11-10 through 11-12. Steady state attitudes were achieved within 10 seconds from S-IC/S-II separation. The maximum control excursions occurred in the roll axis following S-IC/S-II separation when 1.4 deg/s rate and -1.0 degree attitude error occurred, as shown in Table 11-4. The principal attitude error of approximately 0.5 degree for the roll axis was maintained throughout the S-II boost due to thrust and engine misalignments producing a constant roll torque. Similar roll offsets existed during the AS-501 and AS-502 flights.

IGM was initiated at 196.22 seconds, and the flight control computer received thrust vector control commands to pitch the vehicle down as shown in Figure 11-10. During IGM, the vehicle pitched down at a constant commanded rate of approximately -0.1 deg/s. During the transient interval following initiation of IGM guidance, the engines deflected 0.3 degree in pitch. This transient magnitude was significantly less than on the AS-501 and AS-502 flights.

The effects of steering misalignment corrections and flight control gain switch points 3 and 4 had no noticeable effect upon control performance. Steering misalignment corrections were less than ±0.1 degree in pitch and ±0.2 degree in yaw. The effects of initiating the first artificial tau mode at 443.7 seconds were most apparent in the pitch axis when a -0.2 deg/s pitch rate occurred. At S-II stage engine cutoff, the attitude errors and rates were at or near null.

During the interval 480 to 520 seconds, the attitude control rate gyros detected an 18 hertz oscillation. The magnitudes sensed were approximately 1.0, 0.6, and 2.5 deg/s for the pitch, yaw, and roll axes, respectively. The filters of the flight control computer filtered this high frequency so that the control system did not respond to these oscillations.

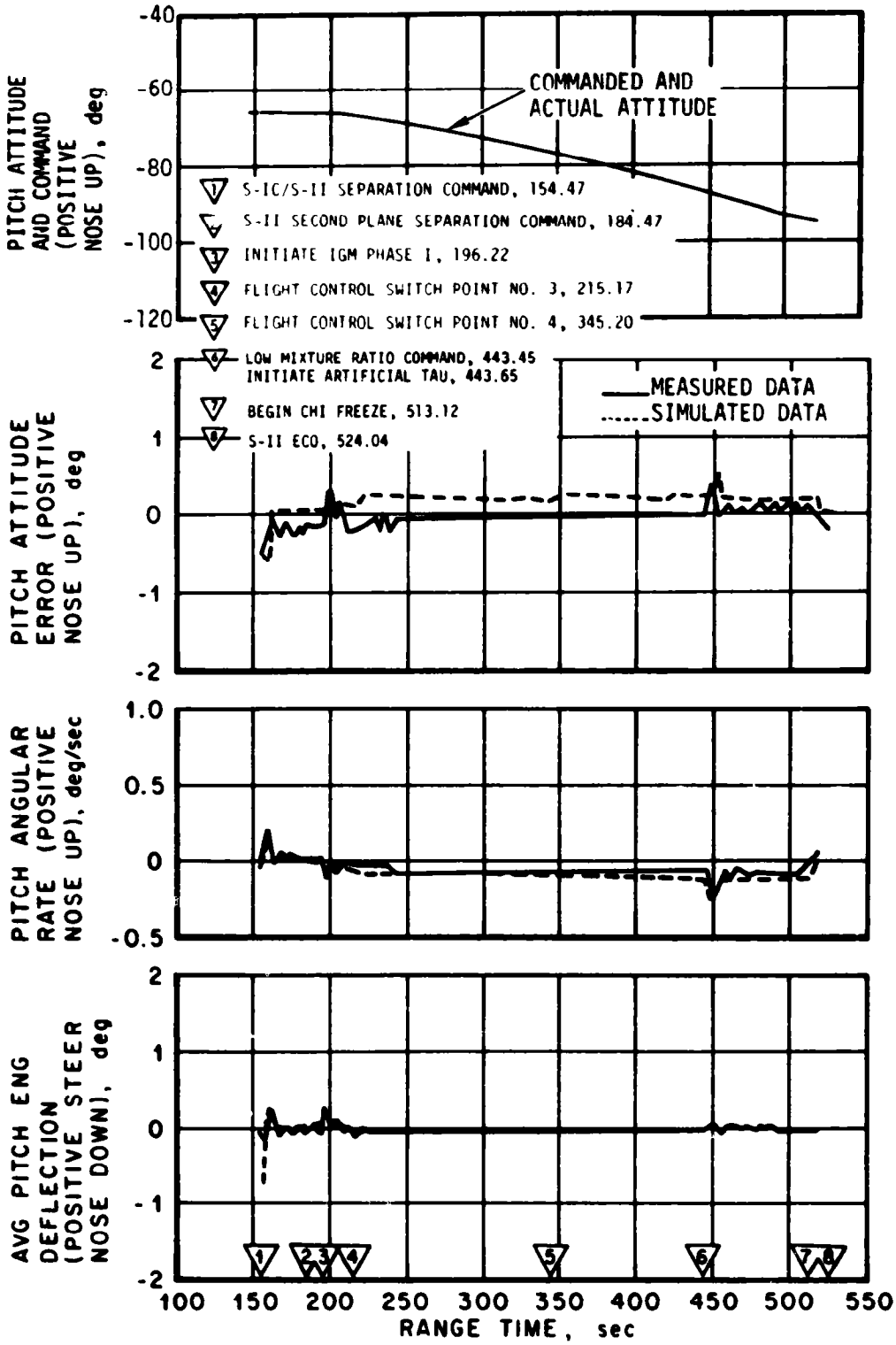

Figure 11-10. Pitch Plane Dynamics During S-II Burn

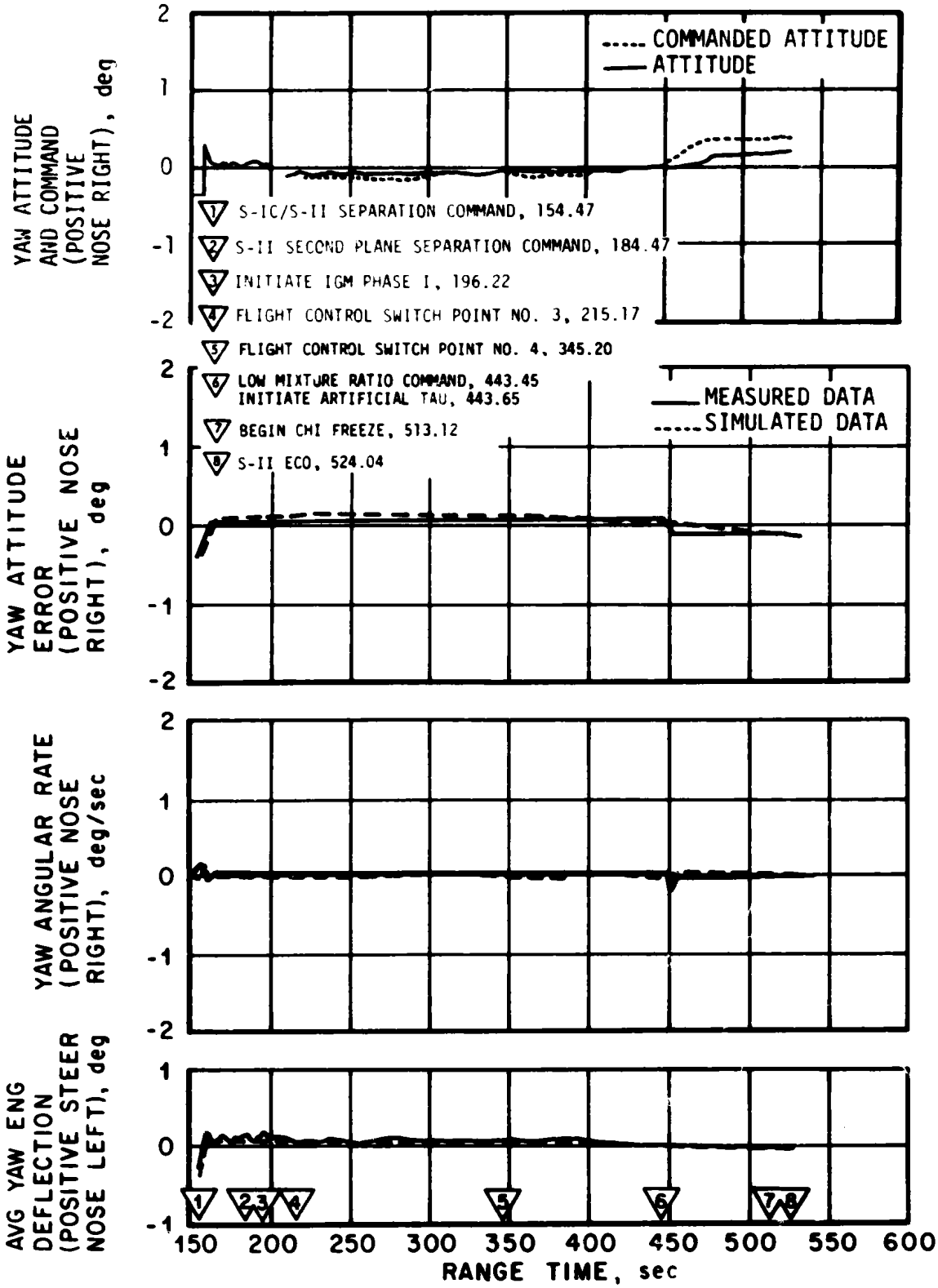

Figure 11-11. Yaw Plane Dynamics During S-II Burn

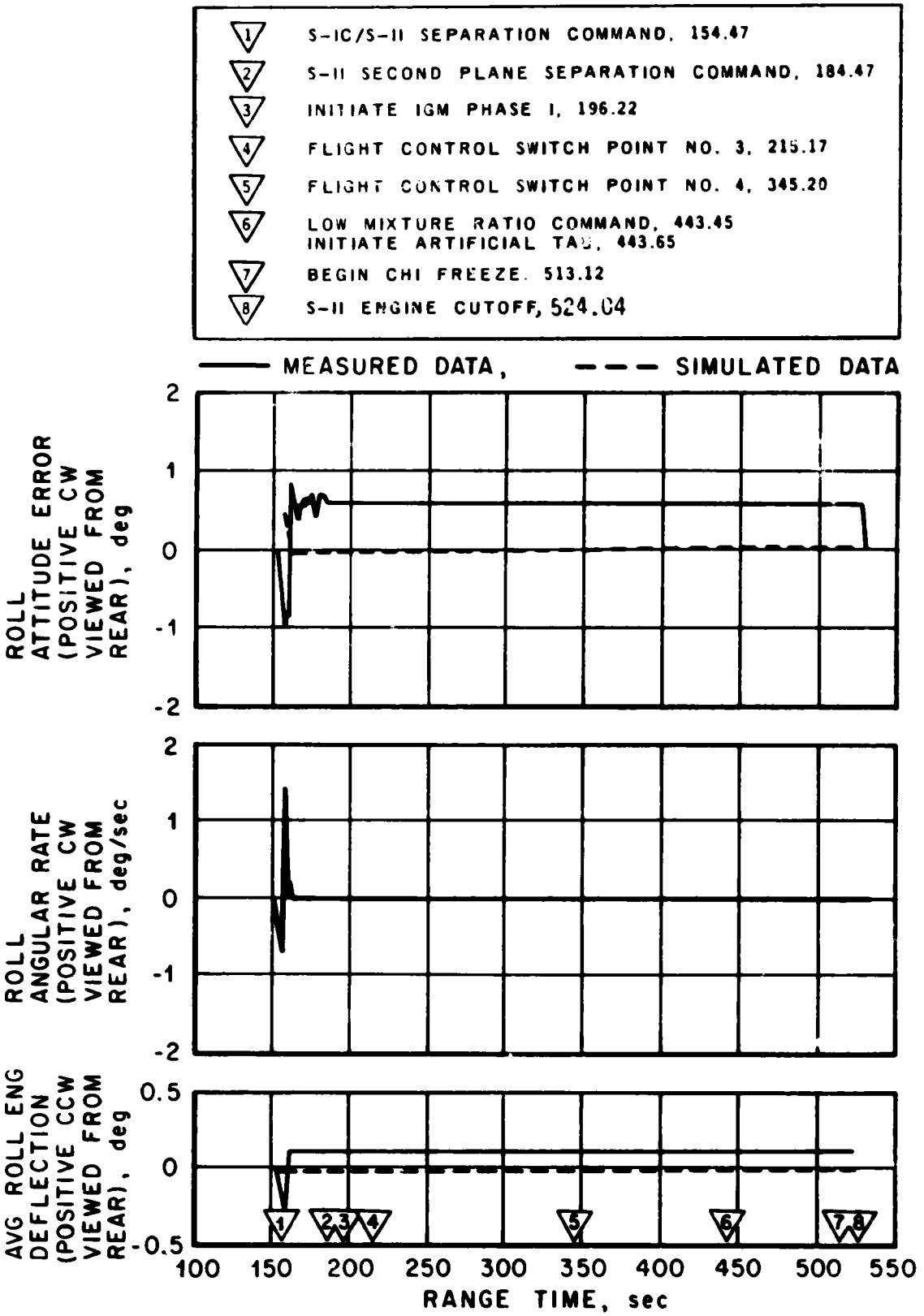

Figure 11-12. Roll Plane Dynamics During S-II Burn

Table 11-4. Maximum Control Parameters During S-II Boost Flight

PARAMETER	S-IC/S-II SEPARATION	FIRST PHASE IGM INITIATE	FIRST ARTIFICIAL TAU INITIATE	S-II CUTOFF
Pitch Plane				
Attitude Error, deg	-0.5	+0.3	+0.4	-0.2
Body Rate, deg/s	+0.[illegible]	-0.1	-0.2	+0.2
Average Gimbal Angle, deg	+0.3	+0.3	+0.1	Null
Slosh Component of Average Gimbal Angle, deg	-	+0.07	+0.02	-
Yaw Plane				
Attitude Error, deg	-0.4	+0.1	-0.1	-0.2
Body Rate, deg/s	+0.1	Null	Null	Null
Average Gimbal Angle, deg	+0.2	+0.1	Null	Null
Slosh Component of Average Gimbal Angle, deg	-	+0.05	+0.01	-
Roll Plane				
Attitude Error, deg	-1.0	+0.5	+0.6	+0.4
Body Rate, deg/s	+1.4	Null	Null	Null
Average Gimbal Angle, deg	-0.3	+0.1	+0.1	+0.1

Simulated data is shown for comparison in Figures 11-10 through 11-12. Differences between the simulated and actual flight data are attributed largely to uncertainties in the J-2 engine thrust buildup and engine and thrust misalignments. Thrust vector misalignments were estimated to be -0.22, -0.11, and 0.13 degree for pitch, yaw, and roll, respectively.

11.4.2 Liquid Propellant Dynamics and Their Effects on Flight Control

The effect of liquid propellant slosh upon the flight control system was estimated from the slosh mode components of the engine deflections as presented in Figure 11-13. The engine deflections were analyzed using bandpass filtering. The largest slosh component magnitudes at initiation of first phase IGM were 0.07 and 0.05 degree for pitch and yaw gimbal angles, respectively. Peak magnitudes of slosh components of engine gimbal angles at S-II engine start were not determinable due to data dropout; however, the data indicated that slosh was adequately stabilized throughout S-II boost flight.

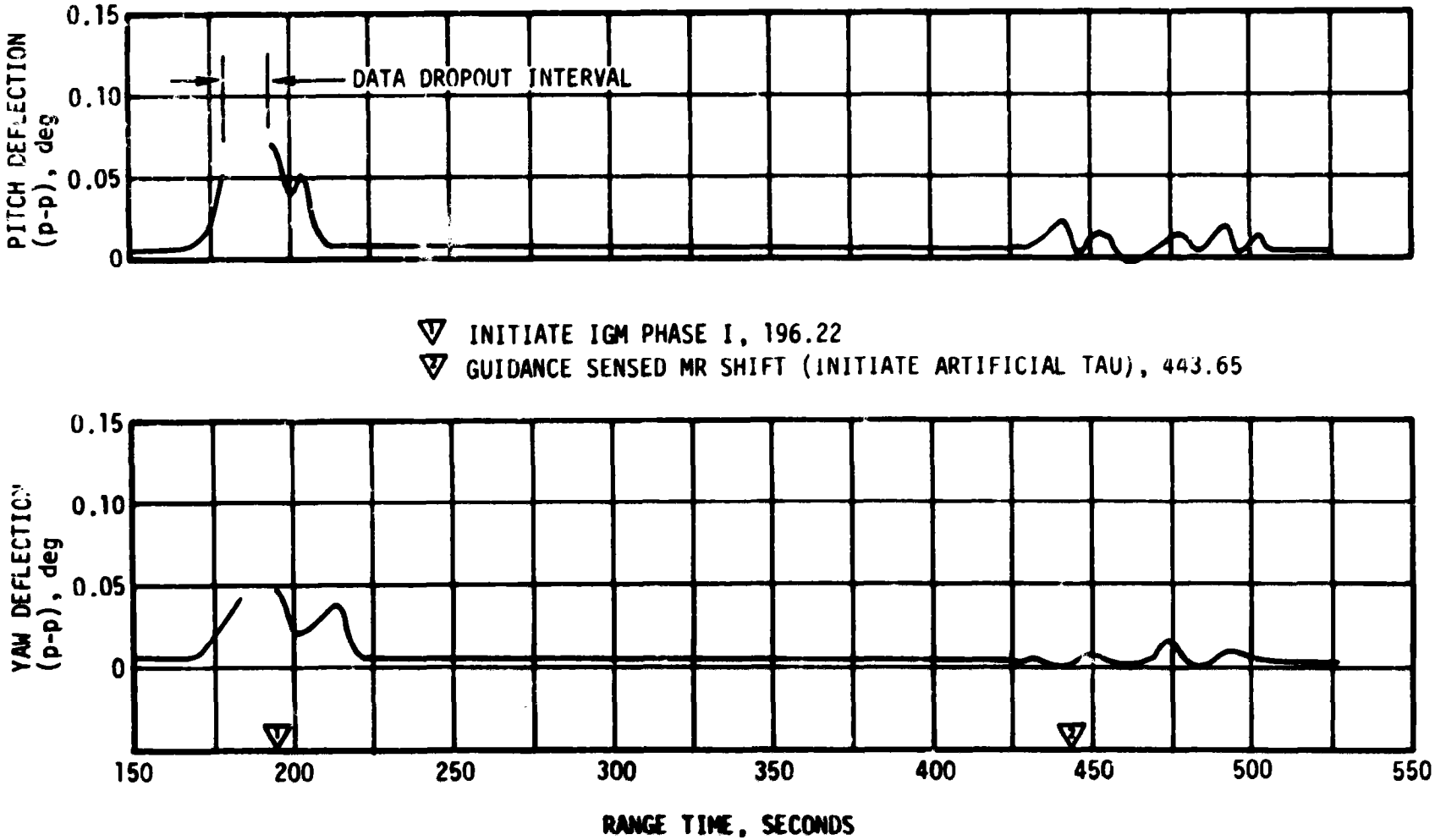

Figure 11-13. S-II Engine Deflection Response to Propellant Slosh

11.5 S-IVB CONTROL SYSTEM EVALUATION

The S-IVB TVC system provided satisfactory pitch and yaw control during powered flight. The APS provided satisfactory roll control during first and second burns.

During S-IVB first and second burns, control system transients were experienced at S-II/S-IVB separation, guidance initiation, chi bar guidance mode, chi freeze, and J-2 engine cutoff. These transients were expected and were well within the capabilities of the control system.

11.5.1 Control System Evaluation During First Burn

The S-IVB first burn attitude control system response to guidance commands for pitch, yaw, and roll are presented in Figures 11-14, 11-15, and 11-16, respectively. The significant events related to control system operation are indicated in each figure. Flight oscillations were experienced on the pitch and yaw guidance commands due to J-2 thrust oscillations. These oscillations were well within the capabilities of the control system. The maximum attitude errors and rates occurred at IGM initiation. A summary of the first burn maximum values of critical flight control parameters is presented in Table 11-5.

Table 11-5. Maximum Control Parameters During S-IVB First Burn

PARAMETER	S-II/S-IVB SEPARATION, GUID. INITIATION AND ART. TAU	BEGIN CHI BAR	S-IVB FIRST CUTOFF
Pitch Attitude Error, deg	+2.2	+0.6	+0.4
Yaw Attitude Error, deg	-0.2	-0.3	-0.3
Roll Attitude Error, deg	-0.8	+0.5	+0.2
Pitch Rate, deg/s	-1.3	+0.4	Null
Yaw Rate, deg/s	+0.1	Null	Null
Roll Rate, deg/s	-0.6	-0.1	+0.1
Pitch Actuator Pos., deg	+1.1	+0.6	+0.4
Yaw Actuator Pos., deg	-0.4	-0.4	-0.4

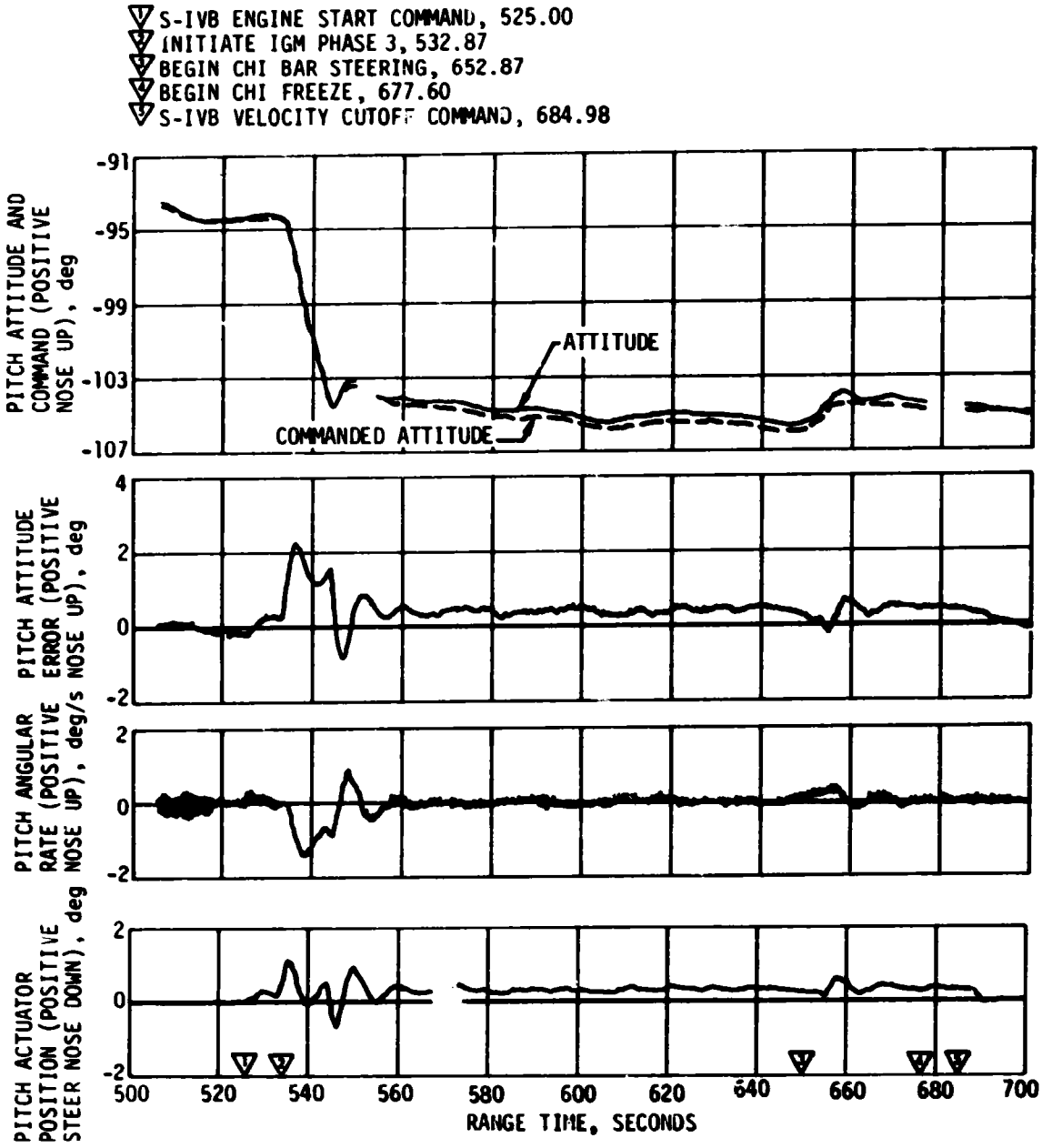

Figure 11-14. Pitch Plane Dynamics During S-IVB First Burn

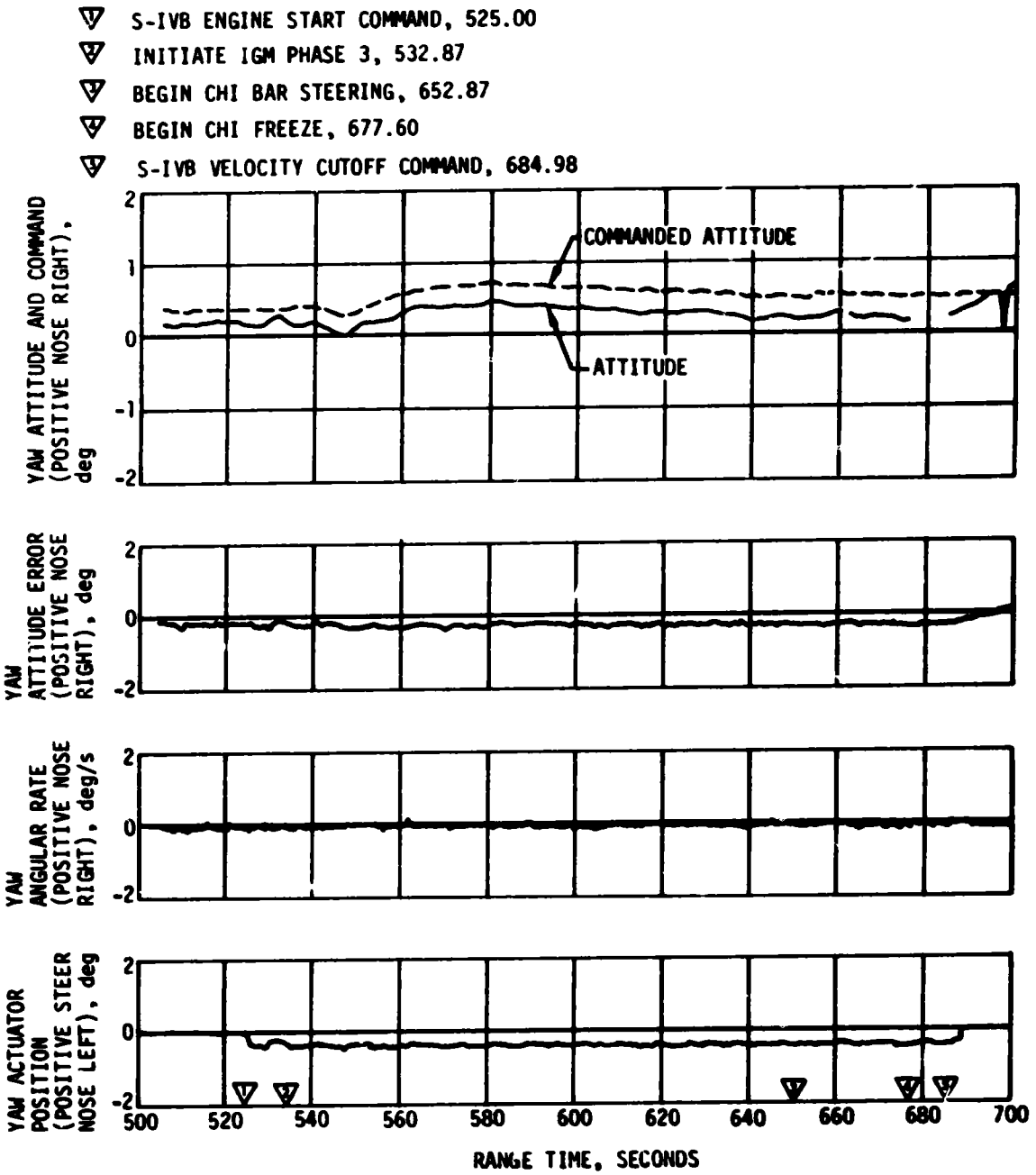

Figure 11-15. Yaw Plane Dynamics During S-IVB First Burn

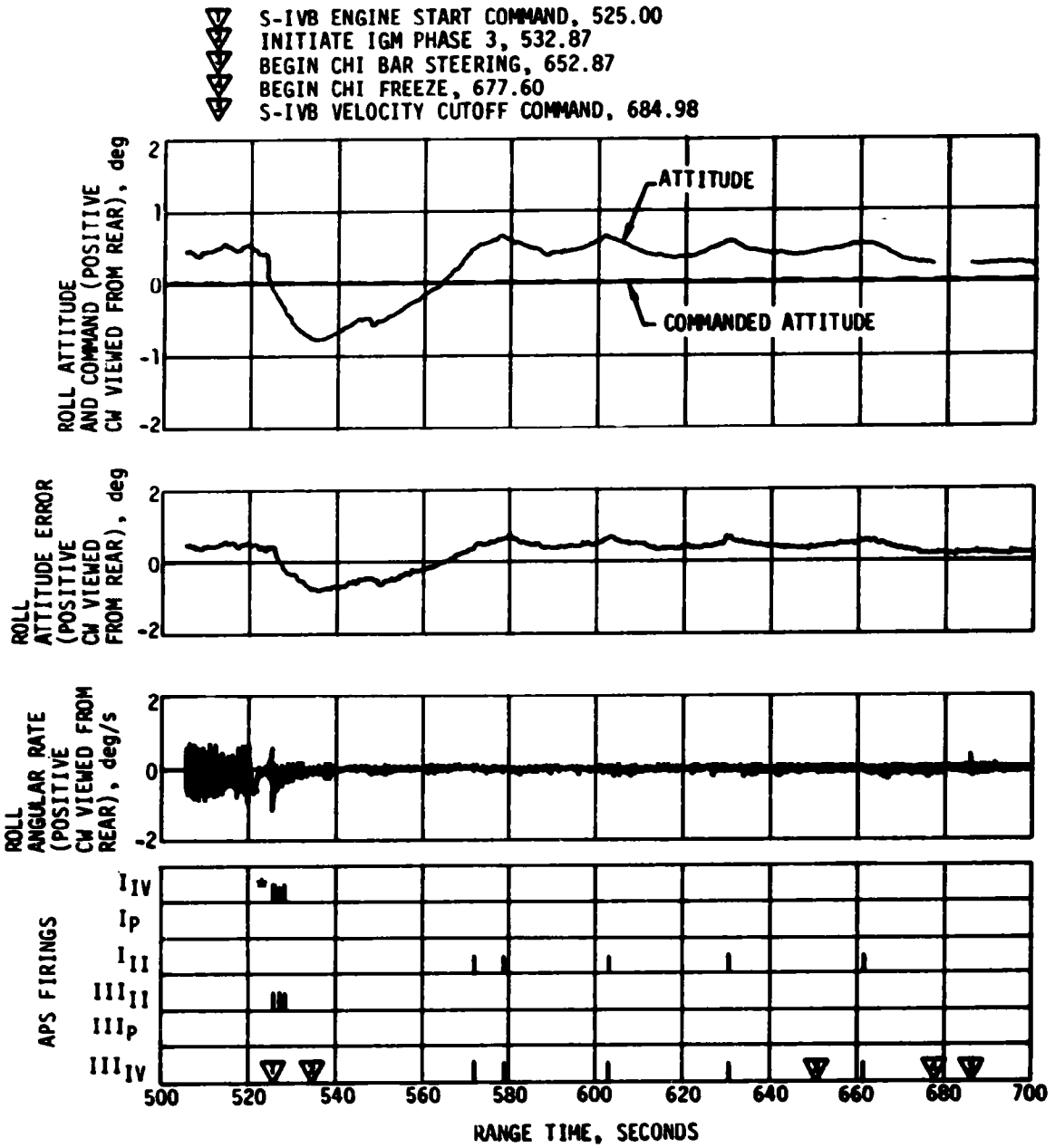

*PULSEWIDTH APPROXIMATELY 600 MS (2 PLACES)

Figure 11-16. Roll Plane Dynamics During S-IVB First Burn

The pitch and yaw effective thrust vector misalignments during first burn were +0.21 and -0.17 degree, respectively.

As experienced on previous flights a steady state roll torque of 8.54 N-m (6.3 lbf-ft), clockwise looking forward, required roll APS firings during first burn. This roll torque is considerably less than the previously experienced maximum of 54.2 N-m (40 lbf-ft) on AS-502. The previously experienced minimum roll torque of 8.1 N-m (6 lbf-ft) was on AS-203.

During S-IVB burn mode and ullage burn following J-2 engine cutoff, an 18 hertz oscillation was also seen in the rate signals; however, this was not unexpected as a similar condition was seen on previous flights. The pitch and yaw control system filter networks properly attenuated the signal. To prevent deterioration of the pseudorate modulator operation and saturation of the spatial amplifiers, low pass filters with a 1.9 hertz cutoff frequency were installed in the spatial amplifiers. The filters apparently were satisfactory as there was no deterioration in the APS operation.

Propellant sloshing during first burn was observed on data obtained from the Propellant Utilization (PU) sensors. The propellant slosh amplitudes and frequencies were comparable to those experienced on previous flights and did not have an appreciable effect on the control system. LH_2 slosh during first burn was well damped by the LH_2 baffle and deflector, as expected, resulting in negligible LH_2 slosh amplitudes during first burn.

11.5.2 Control System Evaluation During Parking Orbit

The APS provided satisfactory orientation and stabilization during parking orbit. Following S-IVB first cutoff, the vehicle was maneuvered to the local horizontal (through approximately 16 degrees), and an orbital pitch rate was established. The pitch, yaw, and roll control system responses are shown in Figures 11-17, 11-18, and 11-19, respectively.

11.5.3 Control System Evaluation During Second Burn

The S-IVB second burn attitude control system response to guidance commands for pitch, yaw, and roll are presented in Figures 11-20, 11-21, and 11-22, respectively. The significant events are indicated in each figure. The effect of the thrust oscillations on the pitch and yaw guidance commands was more pronounced during second burn, as seen in Figures 11-20 and 11-21. The maximum attitude errors and rates occurred near guidance initiation. A summary of the second burn maximum values of critical flight control parameters is presented in Table 11-6.

The pitch and yaw effective thrust vector misalignments during second burn were +0.32 and -0.24 degree, respectively. The steady state roll torque during second burn was 7.34 N-m (5.41 lbf-ft).

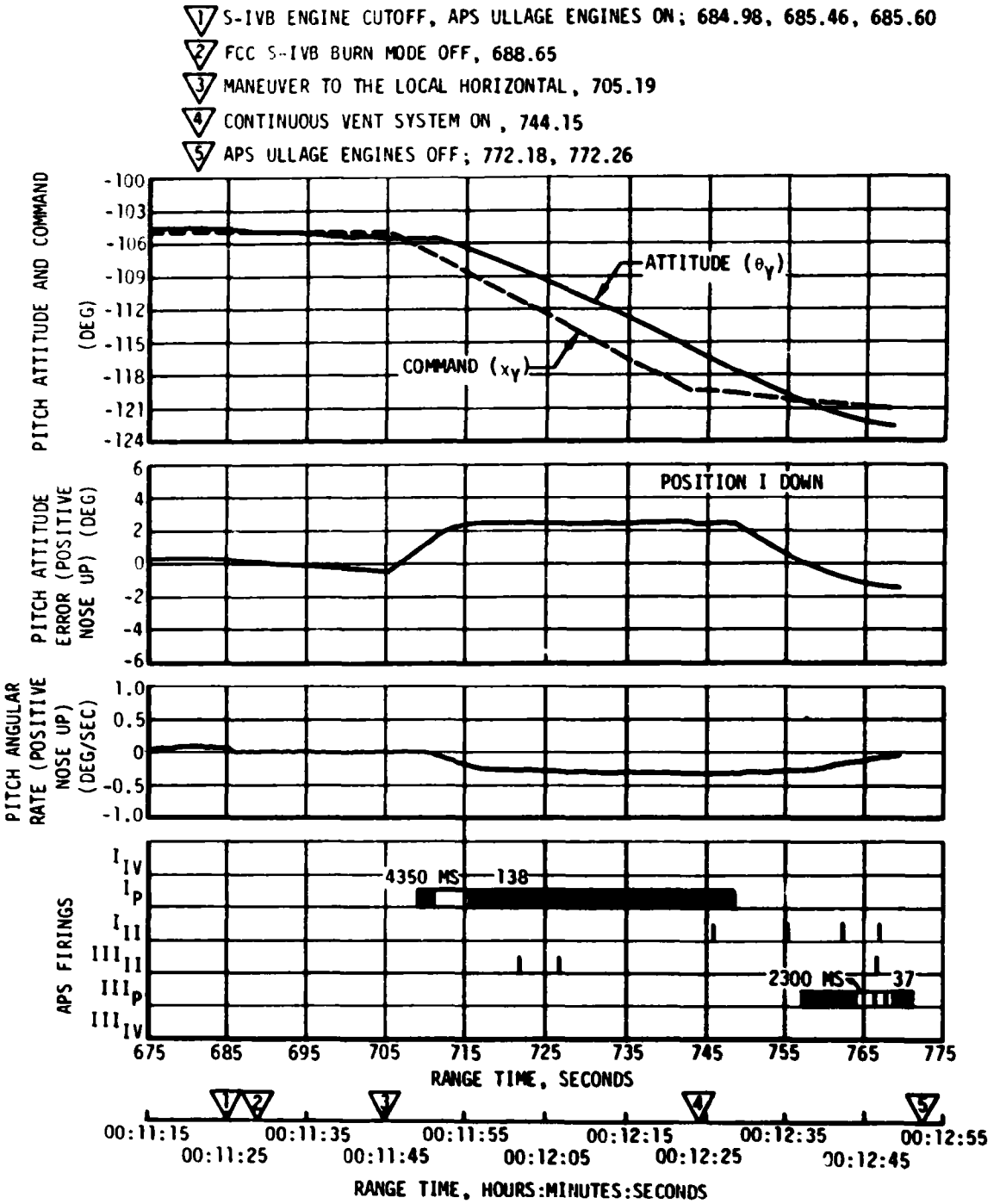

Figure 11-17. Pitch Attitude Control During Maneuver to Local Horizontal Following S-IVB First Burn

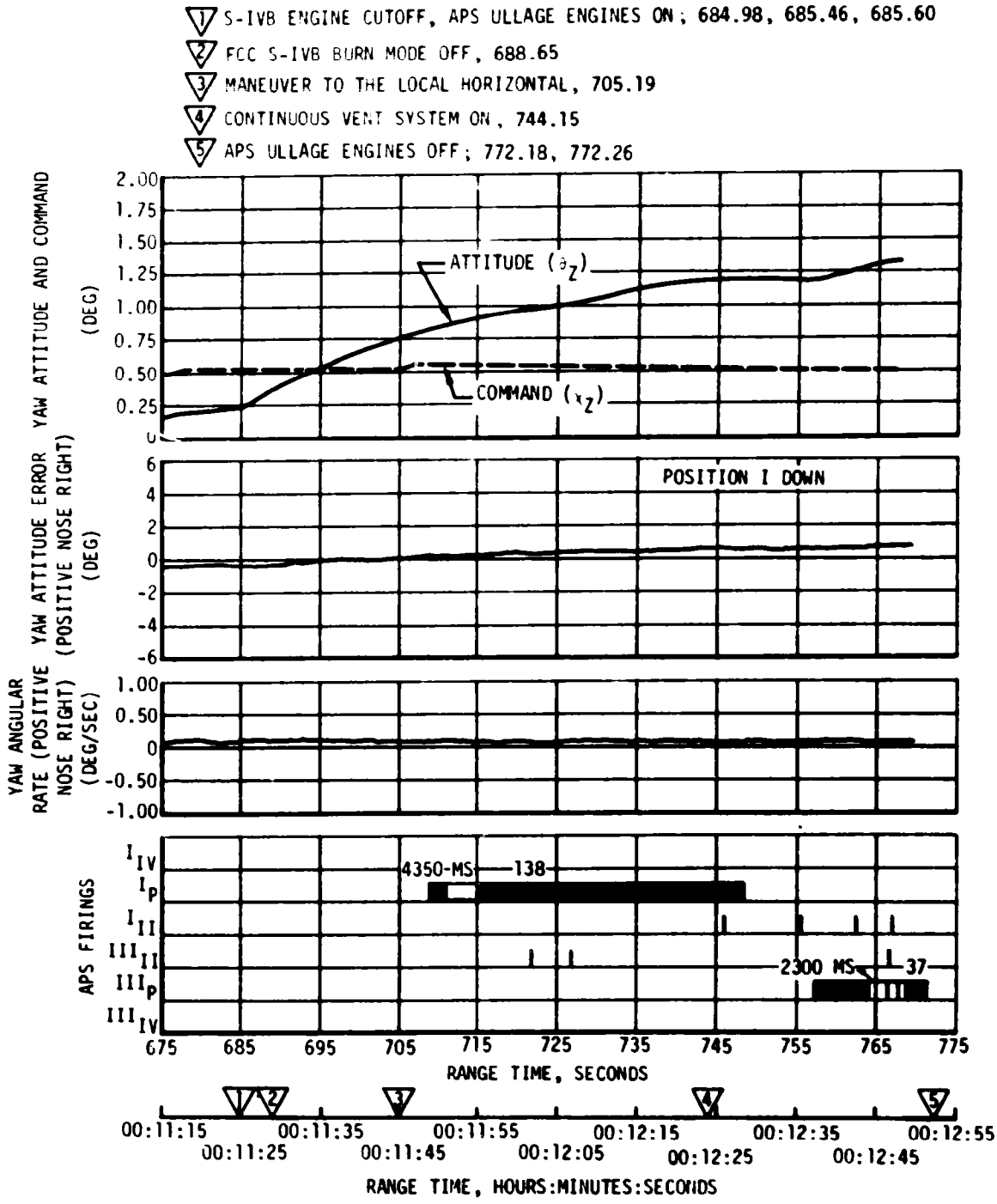

Figure 11-18. Yaw Attitude Control During Maneuver to Local Horizontal Following S-IVB First Burn

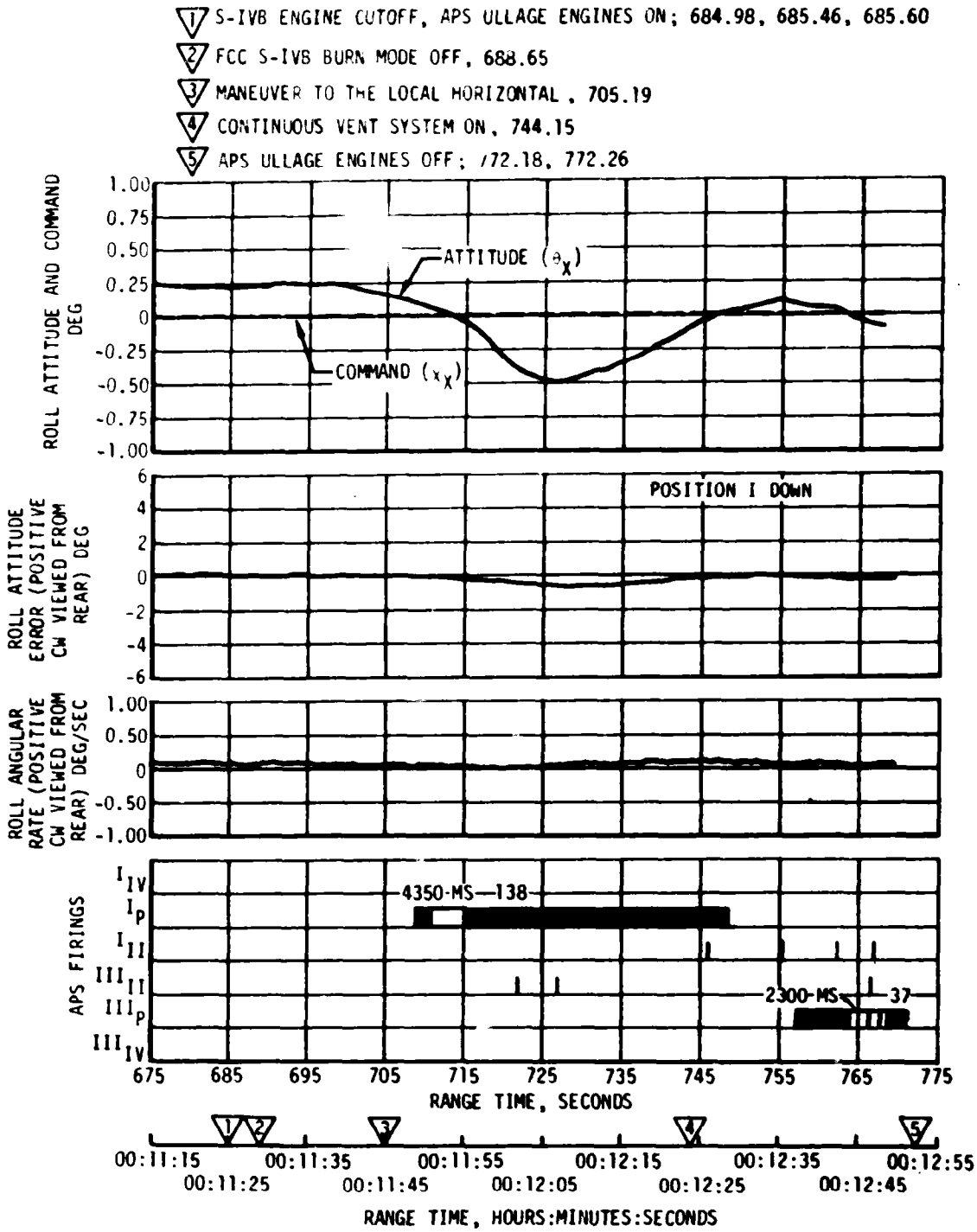

Figure 11-19. Roll Attitude Control During Maneuver to Local Horizontal Following S-IVB First Burn

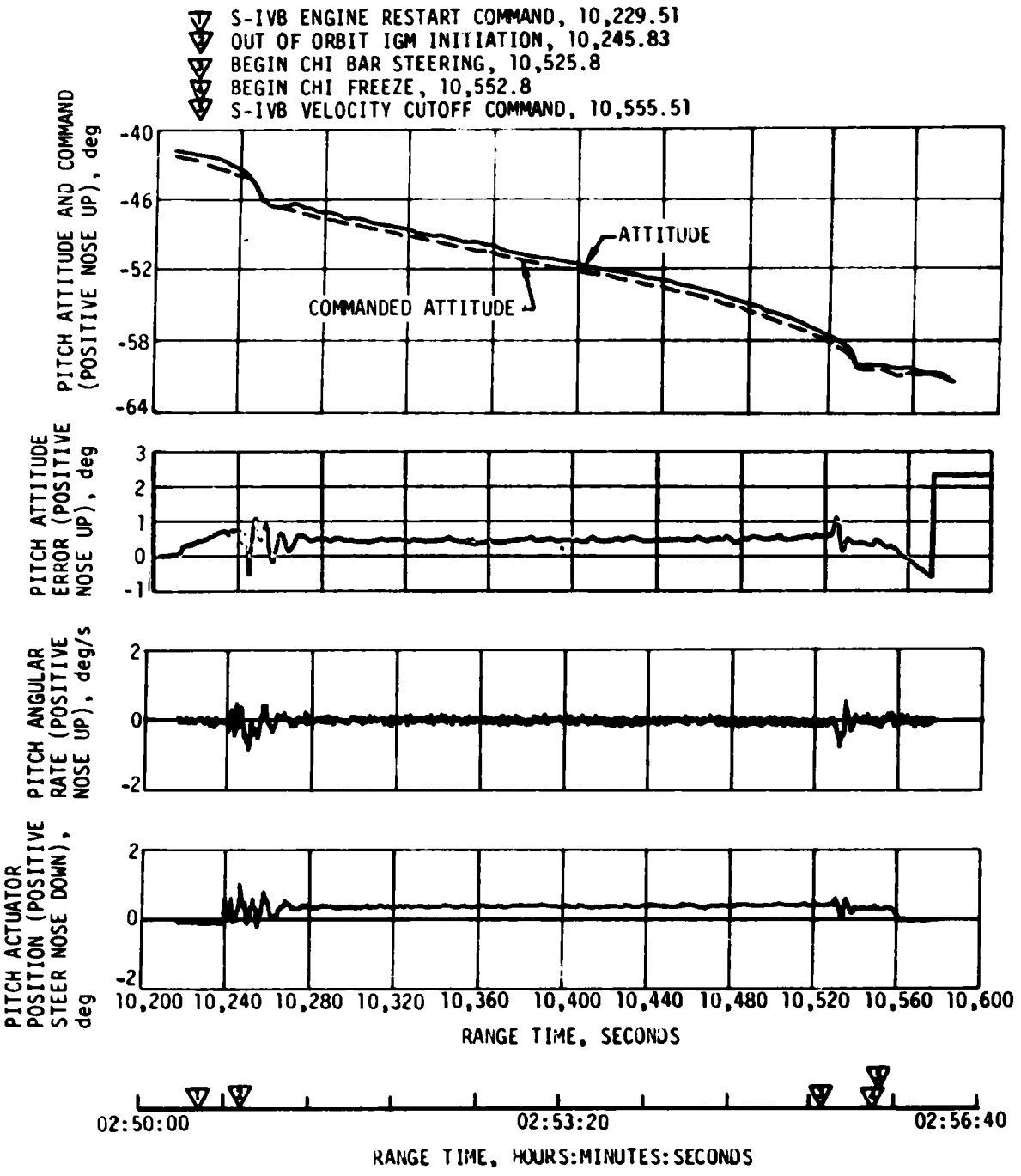

Figure 11-20. Pitch Plane Dynamics During S-IVB Second Burn

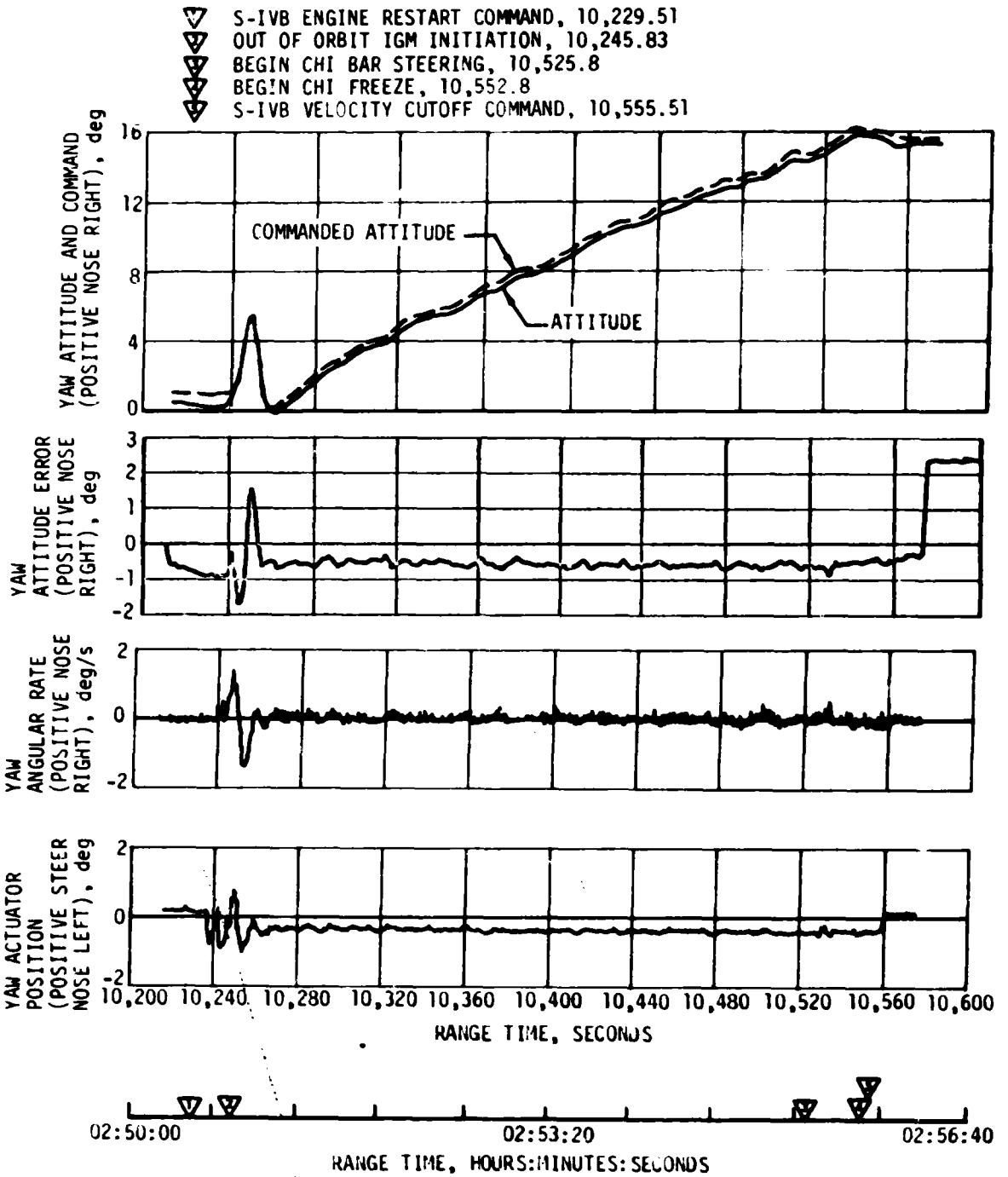

Figure 11-21. Yaw Plane Dynamics During S-IVB Second Burn

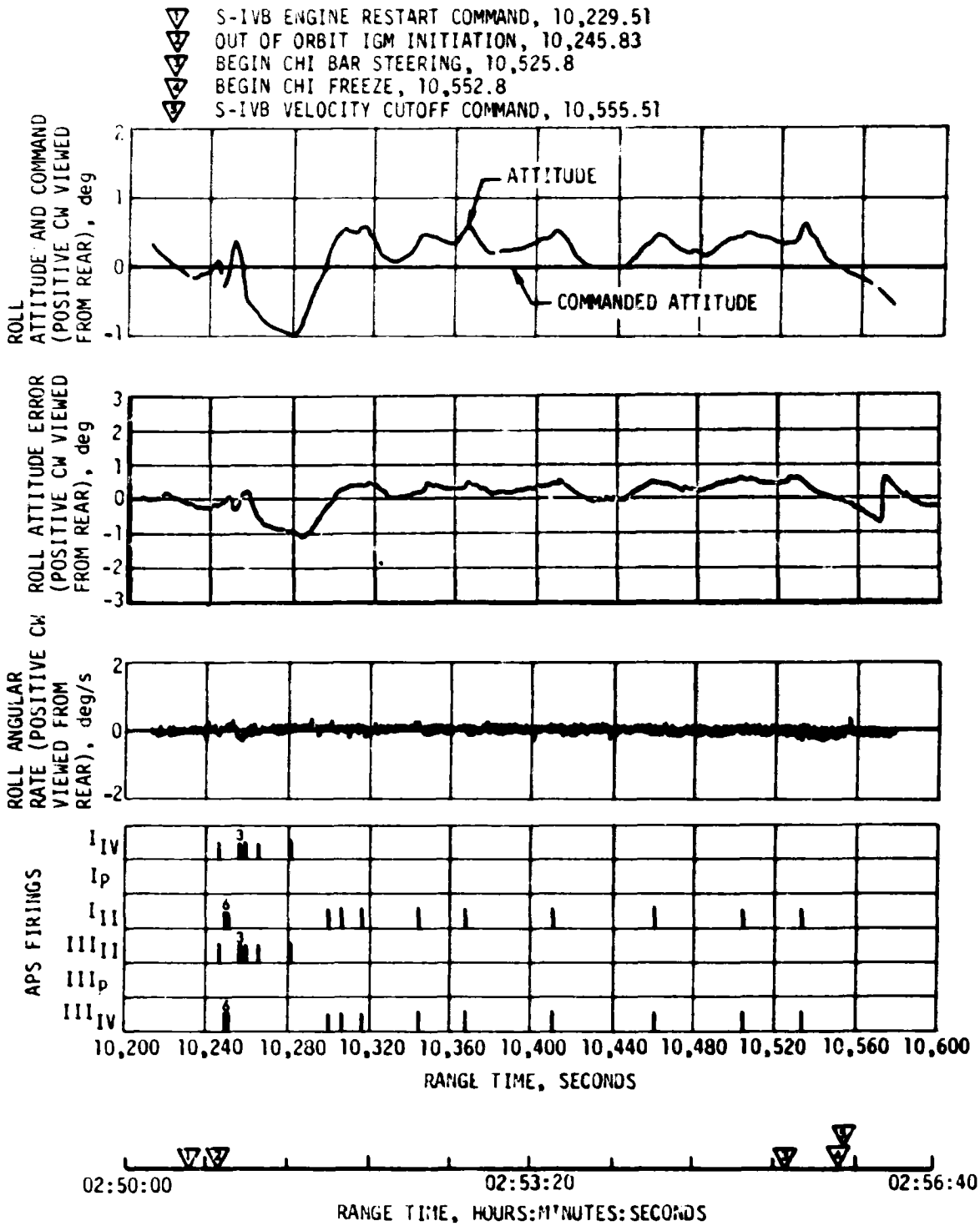

Figure II-22. Roll Plane Dynamics During S-IVB Second Burn

Table 11-6. Maximum Control Parameters During S-IVB Second Burn

PARAMETER	IGNITION AND GUIDANCE INITIATION	CHI BAR	CHI FREEZE	S-IVB CUTOFF
Pitch Attitude Error, deg	+1.1	+1.1	+0.4	+0.3
Yaw Attitude Error, deg	-1.7	-0.8	-0.4	-0.4
Roll Attitude Error, deg	-0.2	+0.6	-0.1	-0.2
Pitch Rate, deg/sec	-0.8	-0.7	+0.2	+0.1
Yaw Rate, deg/sec	±1.4	+0.4	-0.1	-0.2
Roll Rate, deg/sec	+0.2	Null	Null	+0.1
Pitch Actuator Position, deg	+1.0	+0.7	+0.4	+0.4
Yaw Actuator Position, deg	-1.0	-0.5	-0.4	-0.4

Propellant sloshing during second burn did not have an appreciable effect on control system operation. The maximum LOX slosh was about 4.4 centimeters (1.8 in.) peak-to-peak, and the maximum LH_2 slosh was about 6.9 centimeters (2.7 in.) peak-to-peak.

11.5.4 Control System Evaluation After Second Burn

The APS provided satisfactory orientation and stabilization during orbital coast. Each of the planned maneuvers was performed satisfactorily.

Significant periods of interest related to attitude control during orbital coast include maneuvers to align the vehicle with the local horizontal following second cutoff, the maneuver to spacecraft separation attitude, spacecraft separation, maneuver to slingshot attitude, LOX dump, and APS ullaging for slingshot. Each of the periods are discussed in the following paragraphs.

Following S-IVB second cutoff the vehicle was maneuvered to the local horizontal and an orbital pitch rate established and maintained until 11,458.40 seconds, at which time the vehicle was commanded to the separation attitude. Pitch, yaw, and roll control system responses during the maneuver to the local horizontal are shown in Figures 11-23, 11-24, and 11-25, respectively.

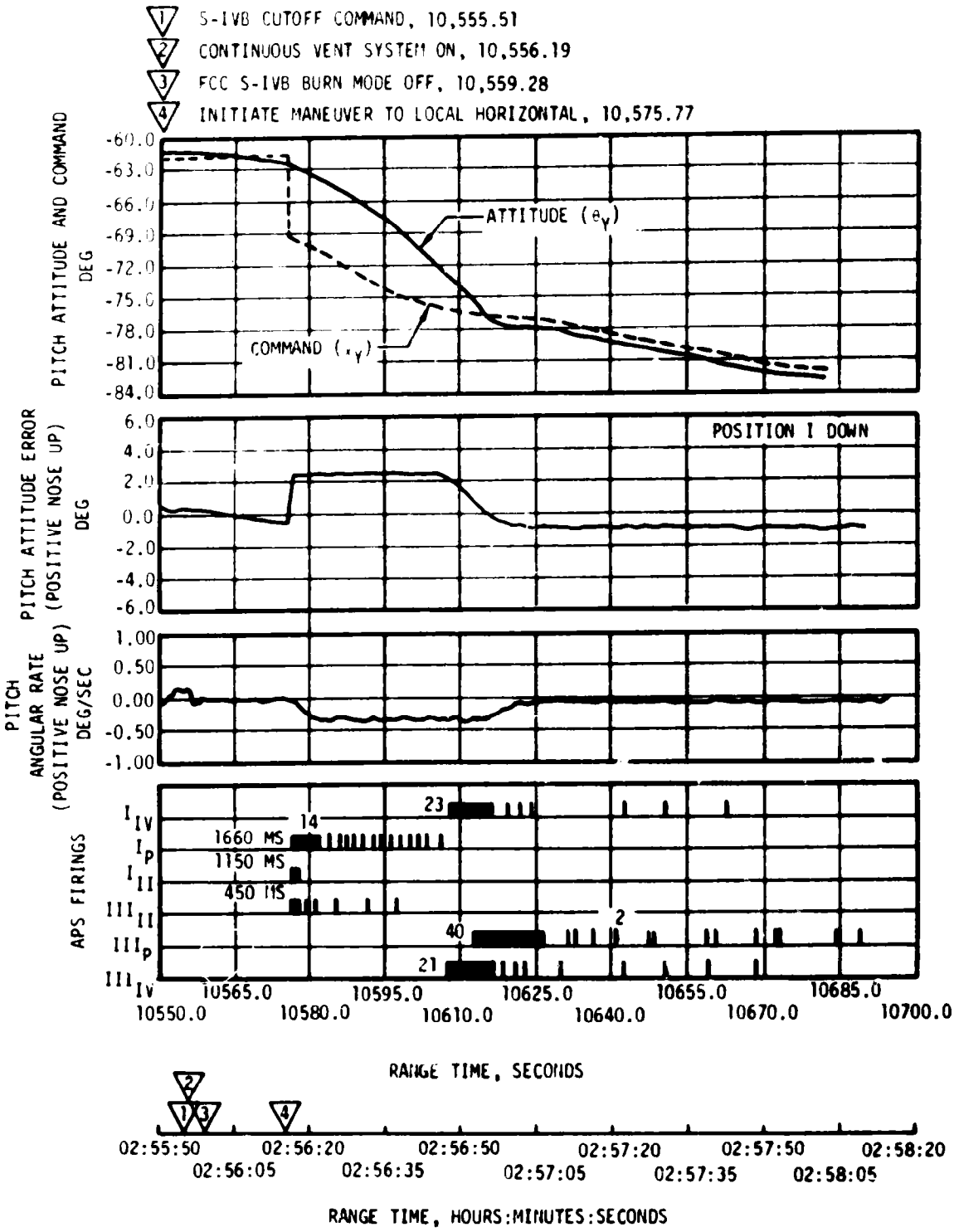

Figure 11-23. Pitch Attitude Control During Maneuver to Local Horizontal Following S-IVB Second Burn

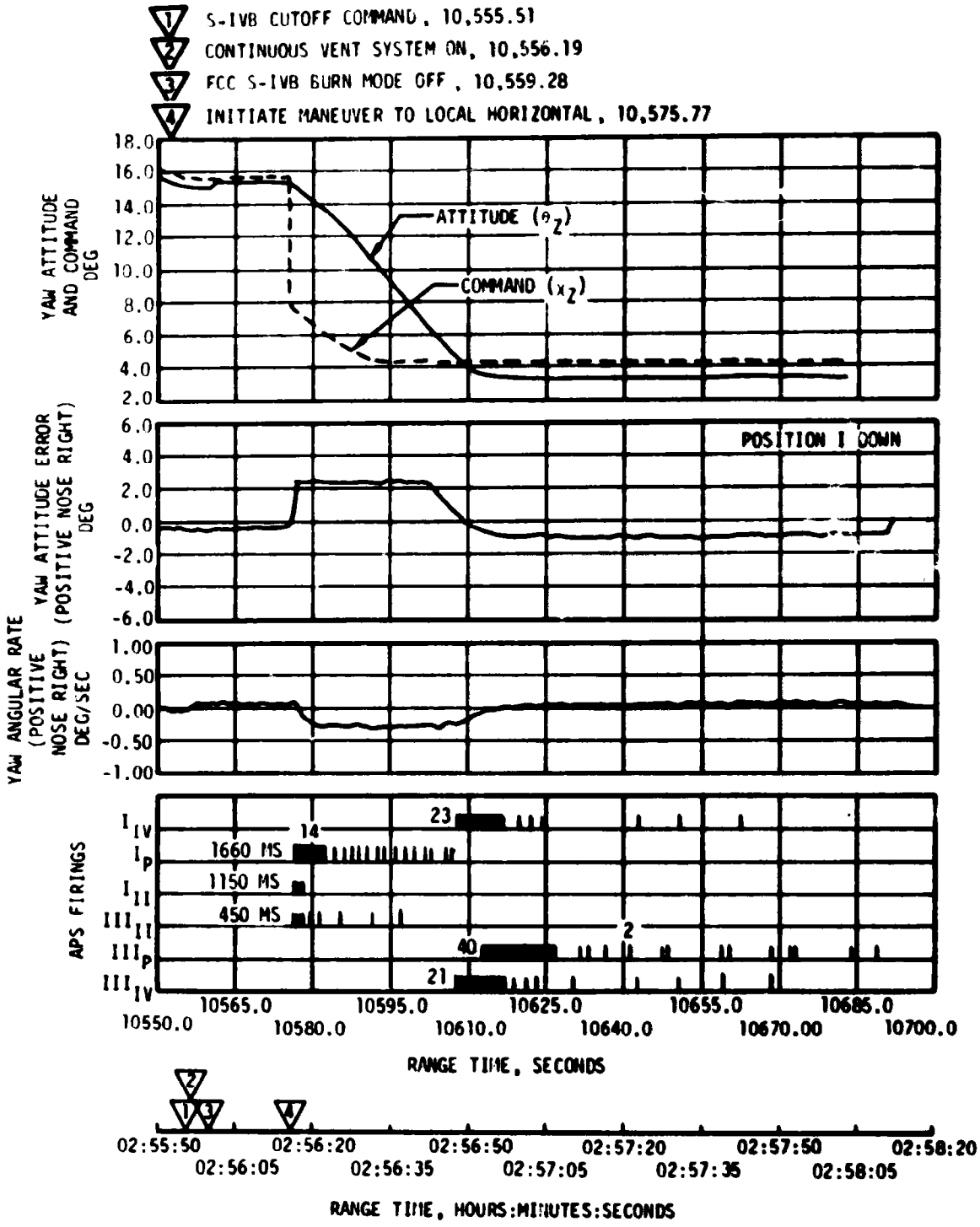

Figure 11-24. Yaw Attitude Control During Maneuver to Local Horizontal Following S-IVB Second Burn

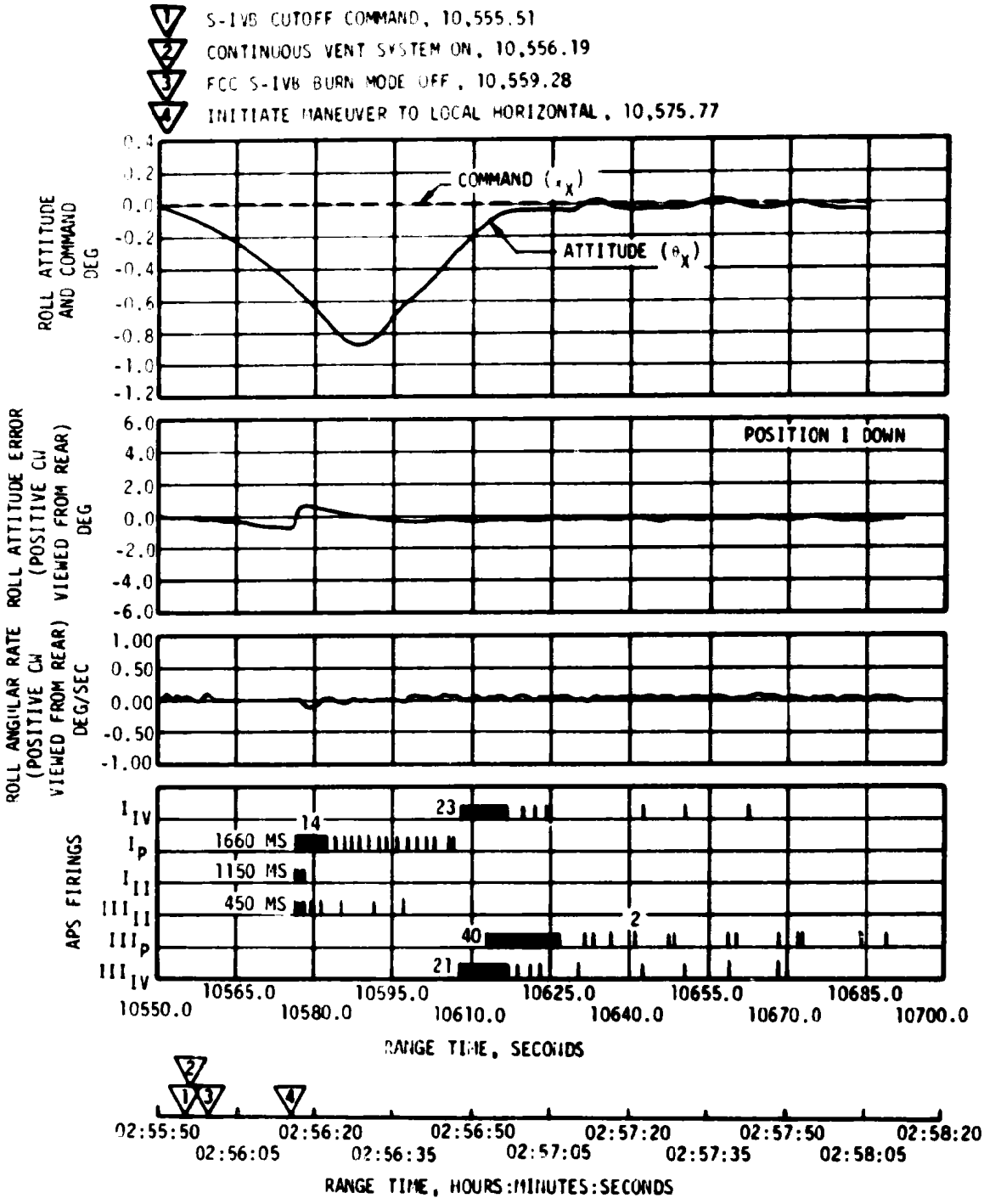

Figure 11-25. Roll Attitude Control During Maneuver to Local Horizontal Following S-IVB Second Burn

The spacecraft separation maneuver included a 120 degree pitch and 180 degree roll maneuver. The pitch, yaw, and roll control system responses during this maneuver are presented in Figures 11-26, 11-27, and 11-28, respectively.

Spacecraft separation appeared normal, as indicated by the relatively small disturbances induced on the S-IVB stage during separation. The pitch, yaw, and roll control system responses are shown in Figures 11-29, 11-30, and 11-31, respectively.

At 17,096.63 seconds the maneuver to slingshot attitude was begun. Once achieved, this attitude (180 degrees pitch relative to the local horizontal with position I down) was maintained throughout the LOX dump and APS ullage burn. Due to the initial alignment of the vehicle at the start of this maneuver, less than a 2-degree change in pitch attitude was required. LOX dump was initiated at 18,475.82 seconds to provide ΔV for the slingshot trajectory. Attitude control during the LOX dump was provided by the APS. The auxiliary hydraulic pump supplied hydraulic pressure to maintain the J-2 engine in a centered position and minimize disturbances during the LOX dump. APS impulse data converted from the APS high pressure helium supply spheres indicated the disturbances during the LOX dump were lower than expected. This is attributed primarily to the thrust vector being more closely aligned to the vehicle center of gravity than the mean thrust vector alignment determined through statistical studies. The pitch and yaw thrust vector misalignments during the LOX dump were 0.17 and -0.36 degree, respectively. These values of thrust misalignment are less than those experienced during the LOX dump on AS-205. Pitch, yaw, and roll attitude control during propellant removal is shown in Figures 11-32, 11-33, and 11-34, respectively.

Following completion of the LOX dump, the APS ullage engines were turned on at approximately 19,556 seconds and burned until depletion of APS propellants. The thrust provided by the ullage engines decreased the vehicle velocity for slingshot trajectory by approximately 20 m/s (67 ft/s), insuring that the S-IVB would not impact the moon. Module 2 depleted first (fuel depletion), after a burn of approximately 733 seconds, at 20,288.56 seconds. Module 1 depleted approximately 25 seconds after Module 2. Attitude control system data indicated the vehicle was controlled as expected following depletion of Module 2. Following depletion of Module 1, the vehicle attitude remained relatively constant for approximately 60 seconds; after which the rate of divergence was approximately 0.001, 0.01, and 0.0125 deg/s in pitch, yaw, and roll, respectively. Pitch, yaw, and roll attitude control during the APS ullage burn for the slingshot trajectory is shown in Figures 11-35, 11-36, and 11-37, respectively. After propellant depletion the LVDC continued to issue valid attitude commands until at least 21,214 seconds, by which time the outputs to the ladders had reached their 6-degree limits.

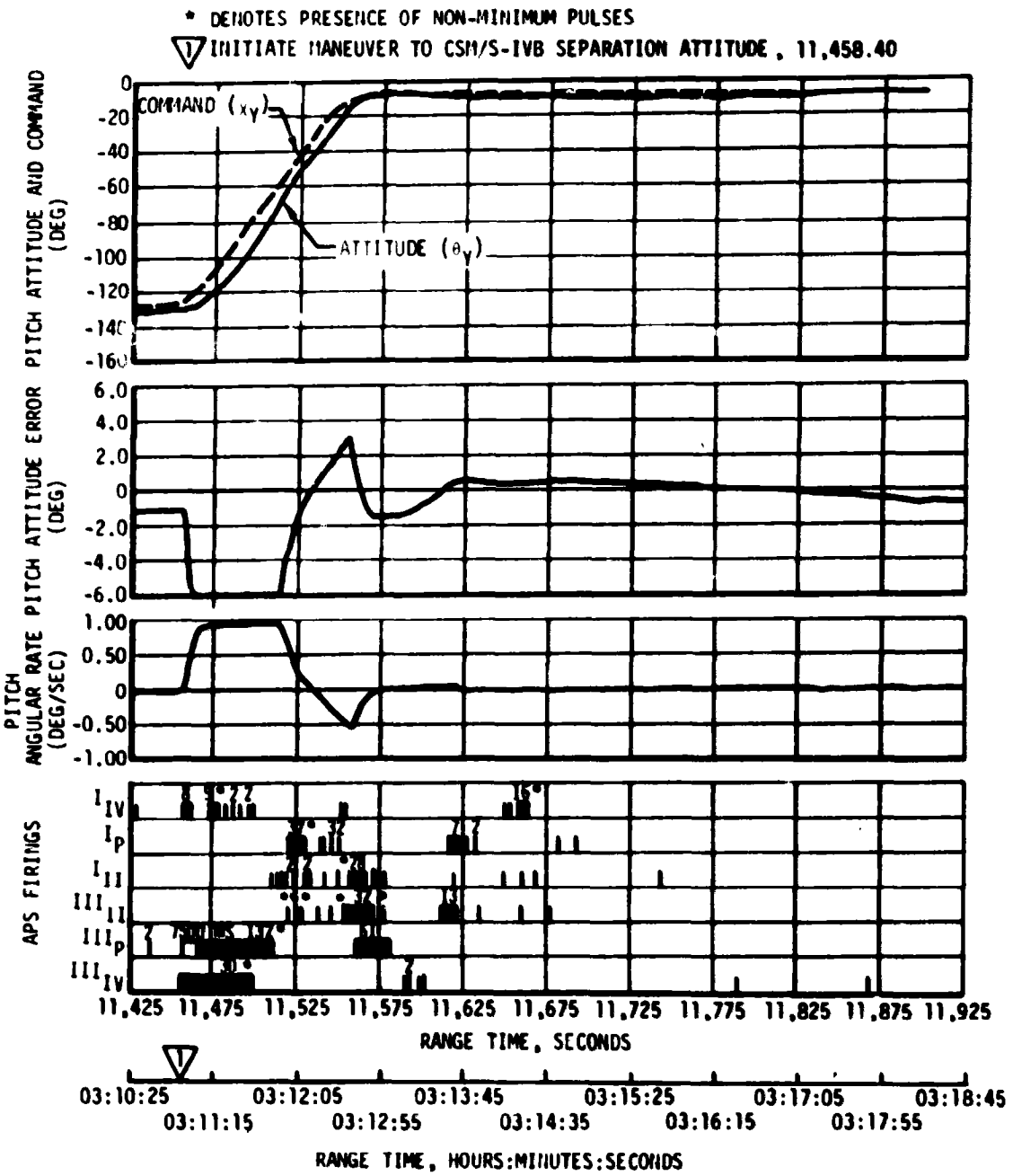

Figure 11-26. Pitch Attitude Control During Maneuver to CSM/S-IVB Separation Attitude

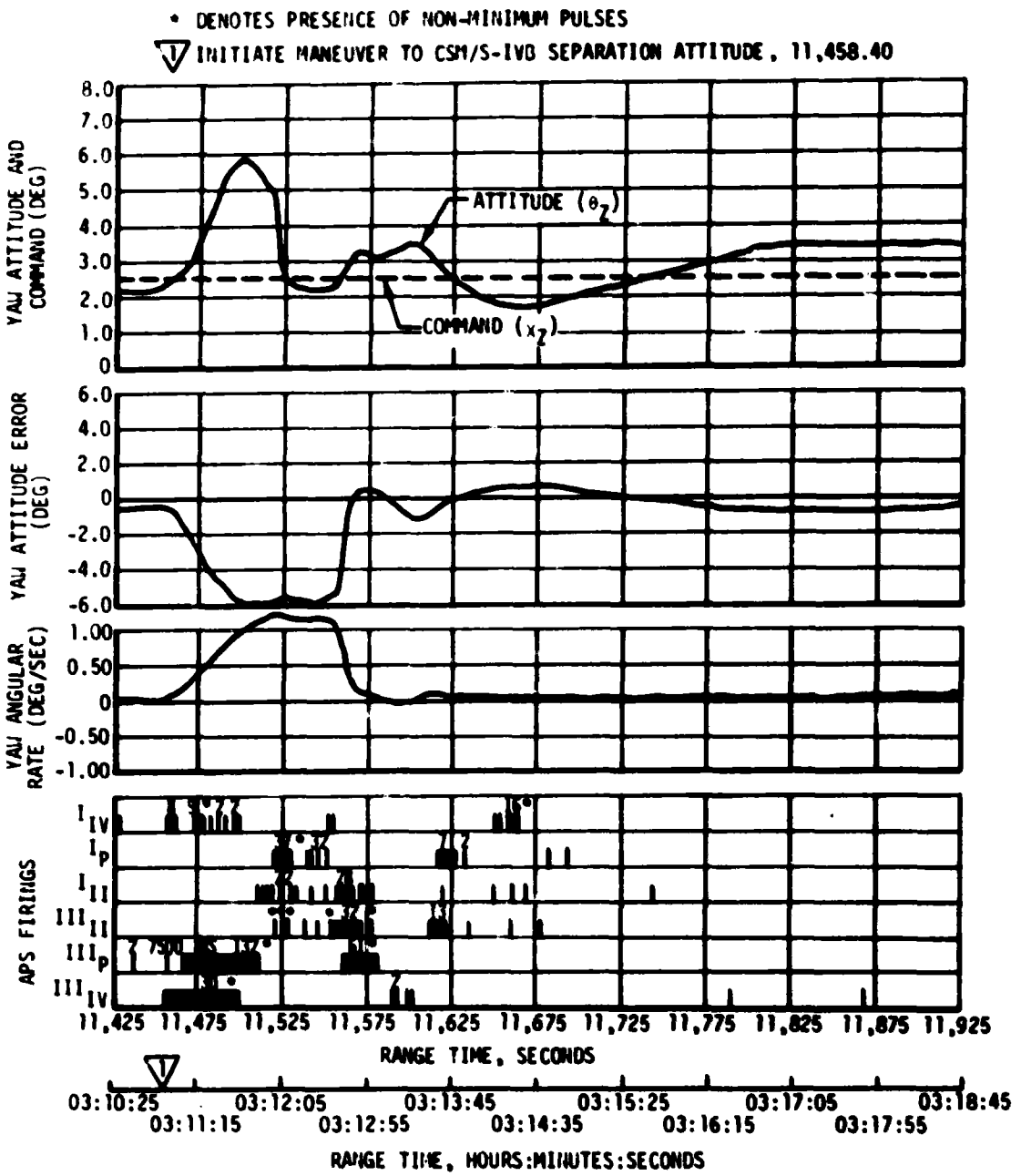

Figure 11-27. Yaw Attitude Control During Maneuver to CSM/S-IVB Separation Attitude

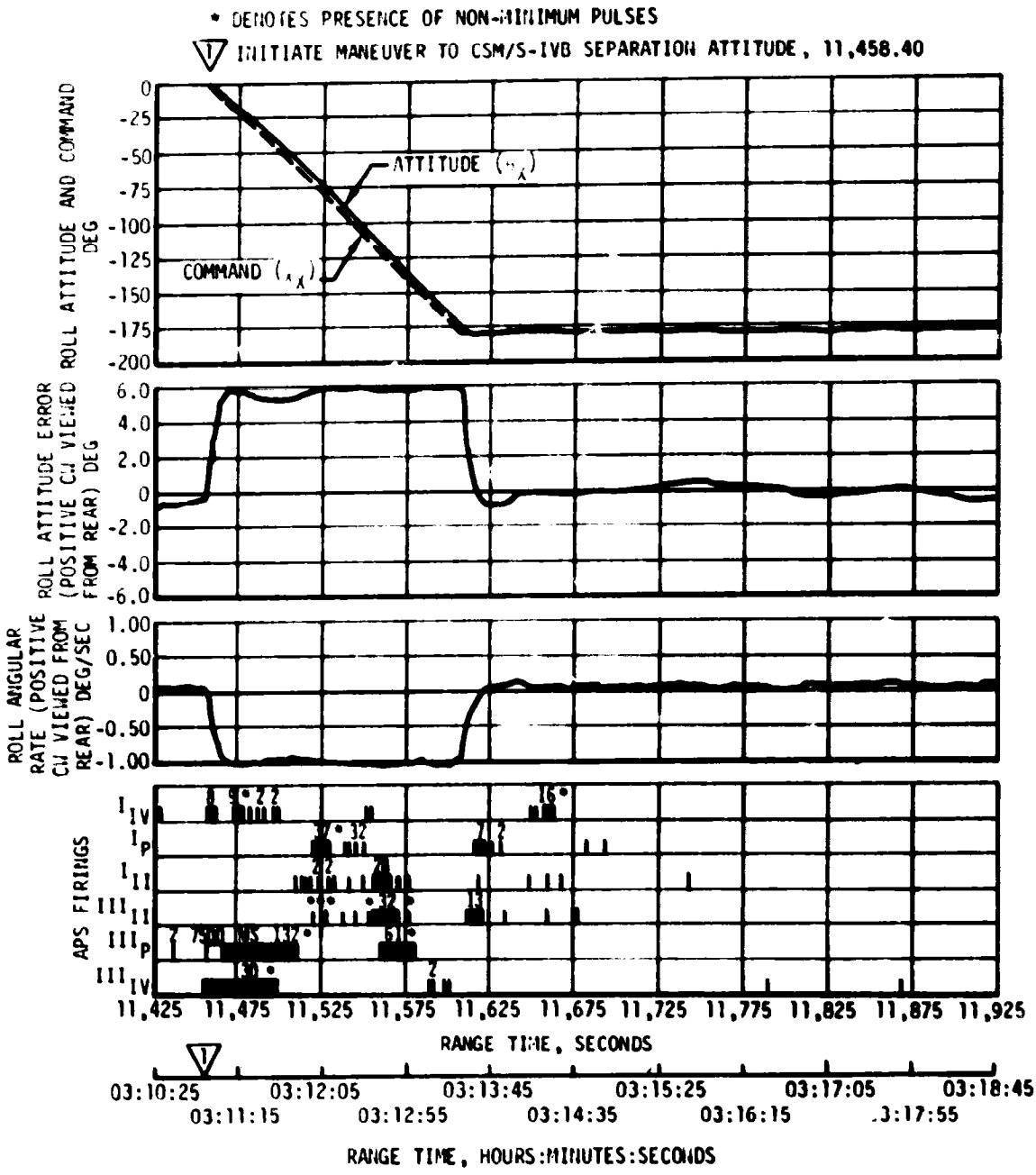

Figure 11-28. Roll Attitude Control During Maneuver to CSM/S-IVB Separation Attitude

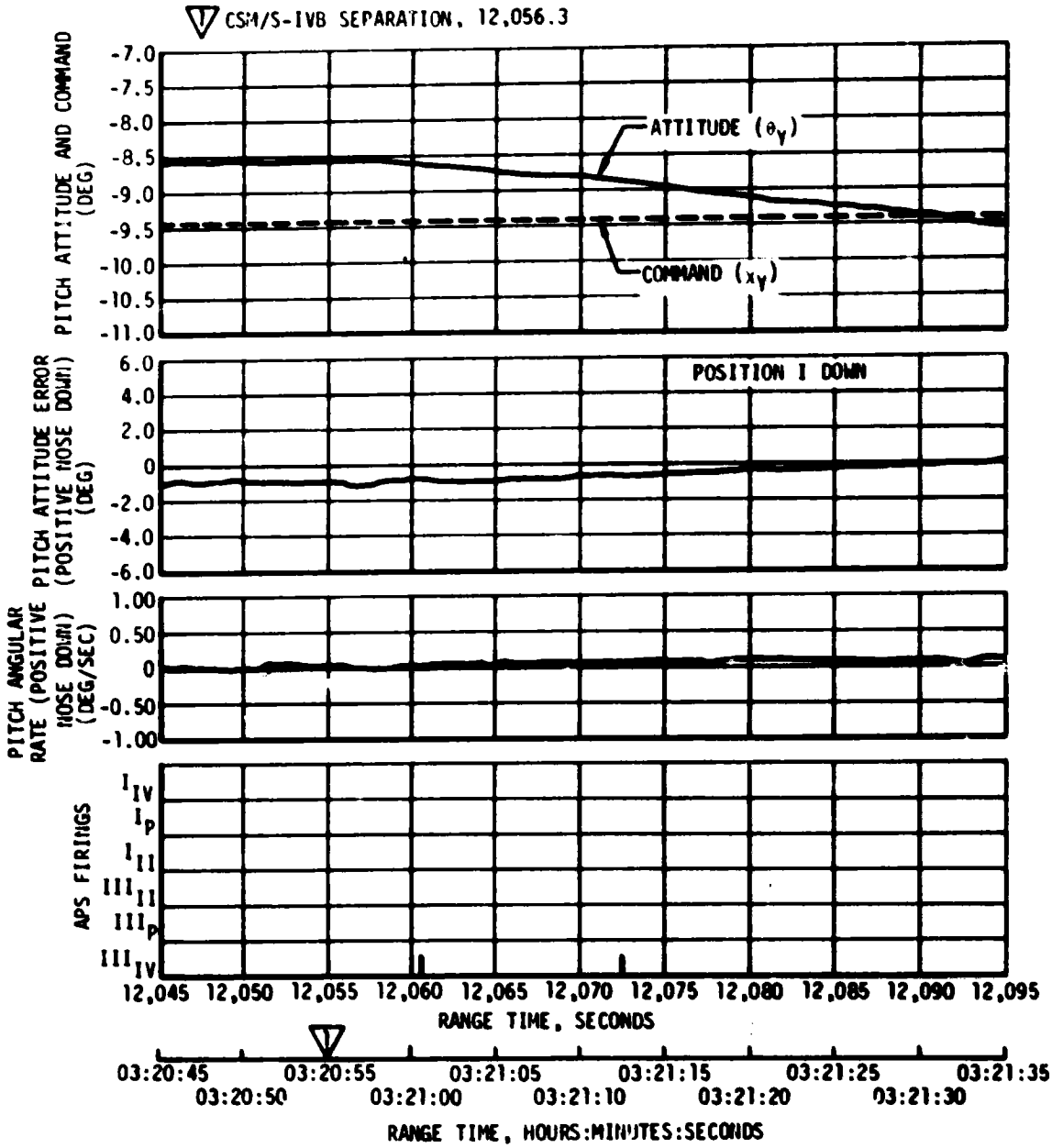

Figure 11-29. Pitch Attitude Control During CSM/S-IVB Separation

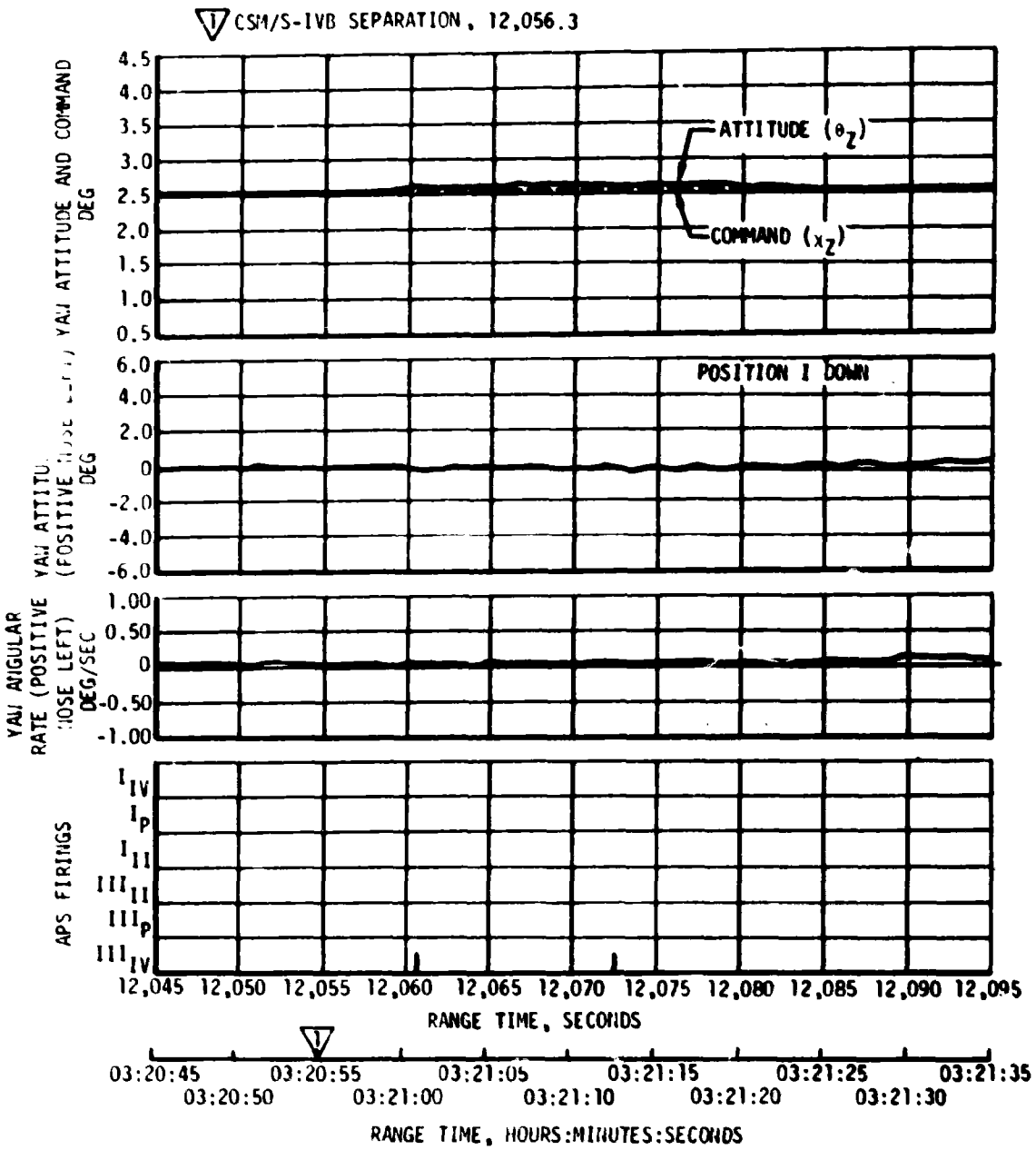

Figure 11-30. Yaw Attitude Control During CSM/S-IVB Separation

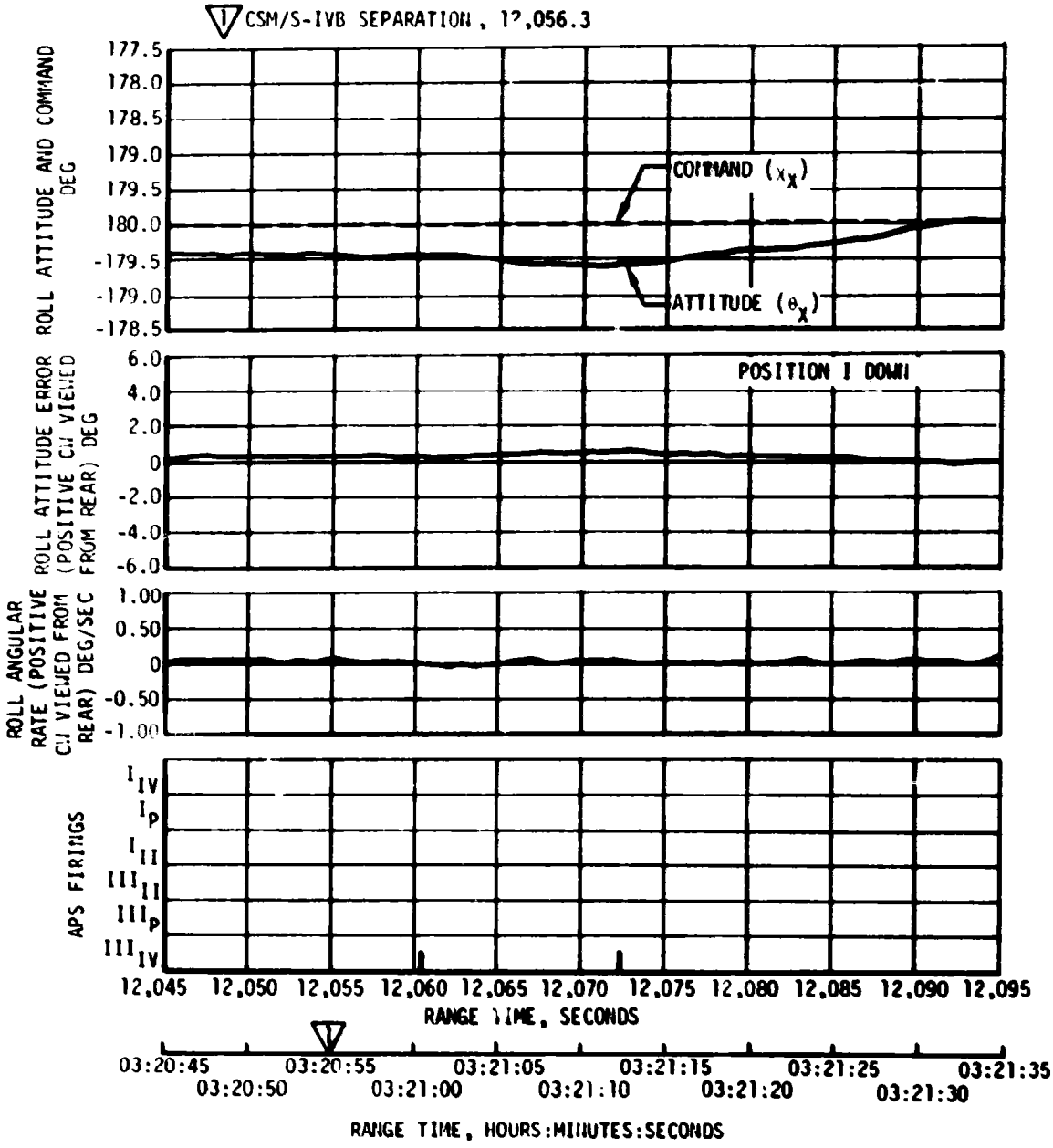

Figure 11-31. Roll Attitude Control During CSM/S-IVB Separation

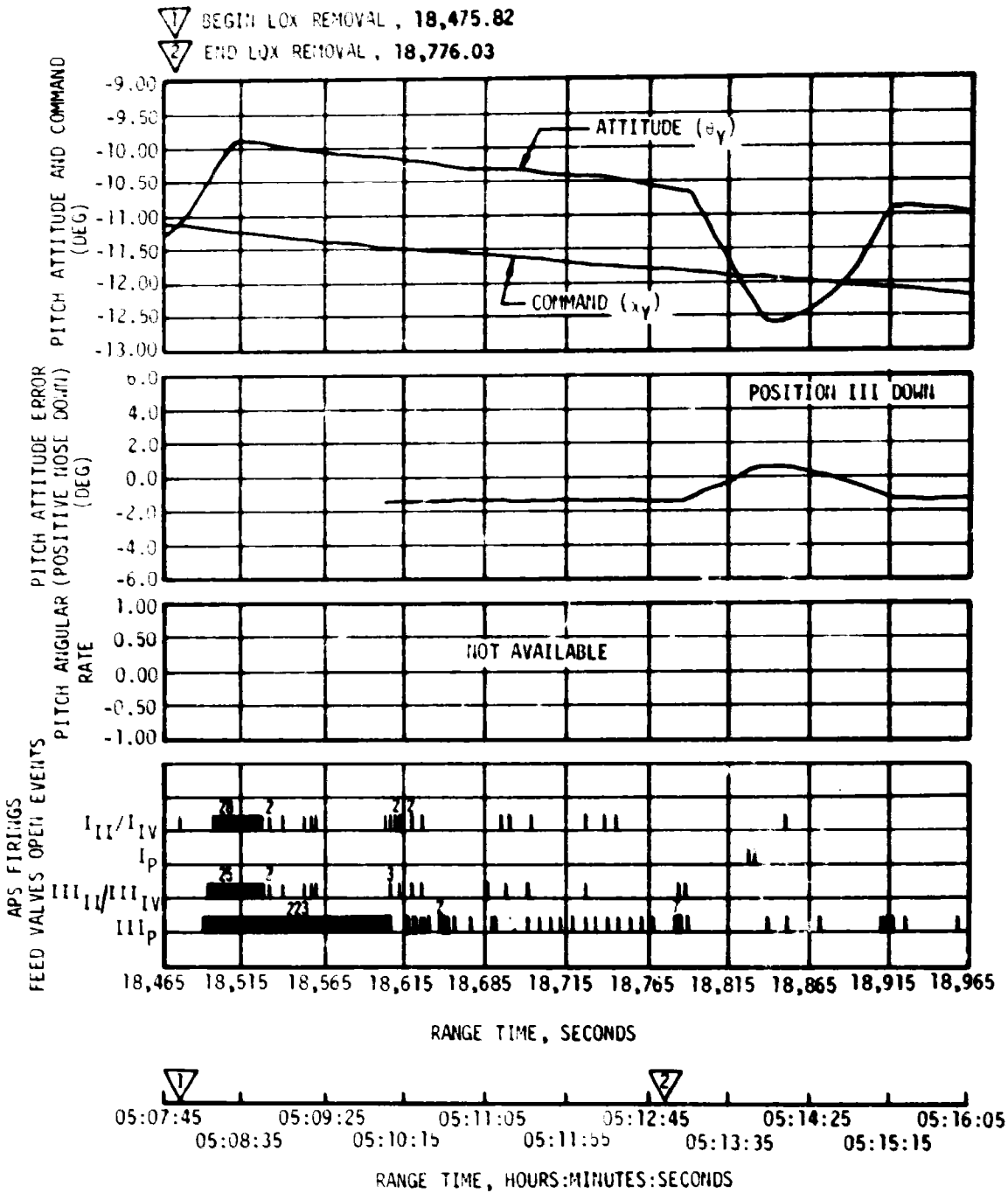

Figure 11-32. Pitch Attitude Control During Propellant Removal

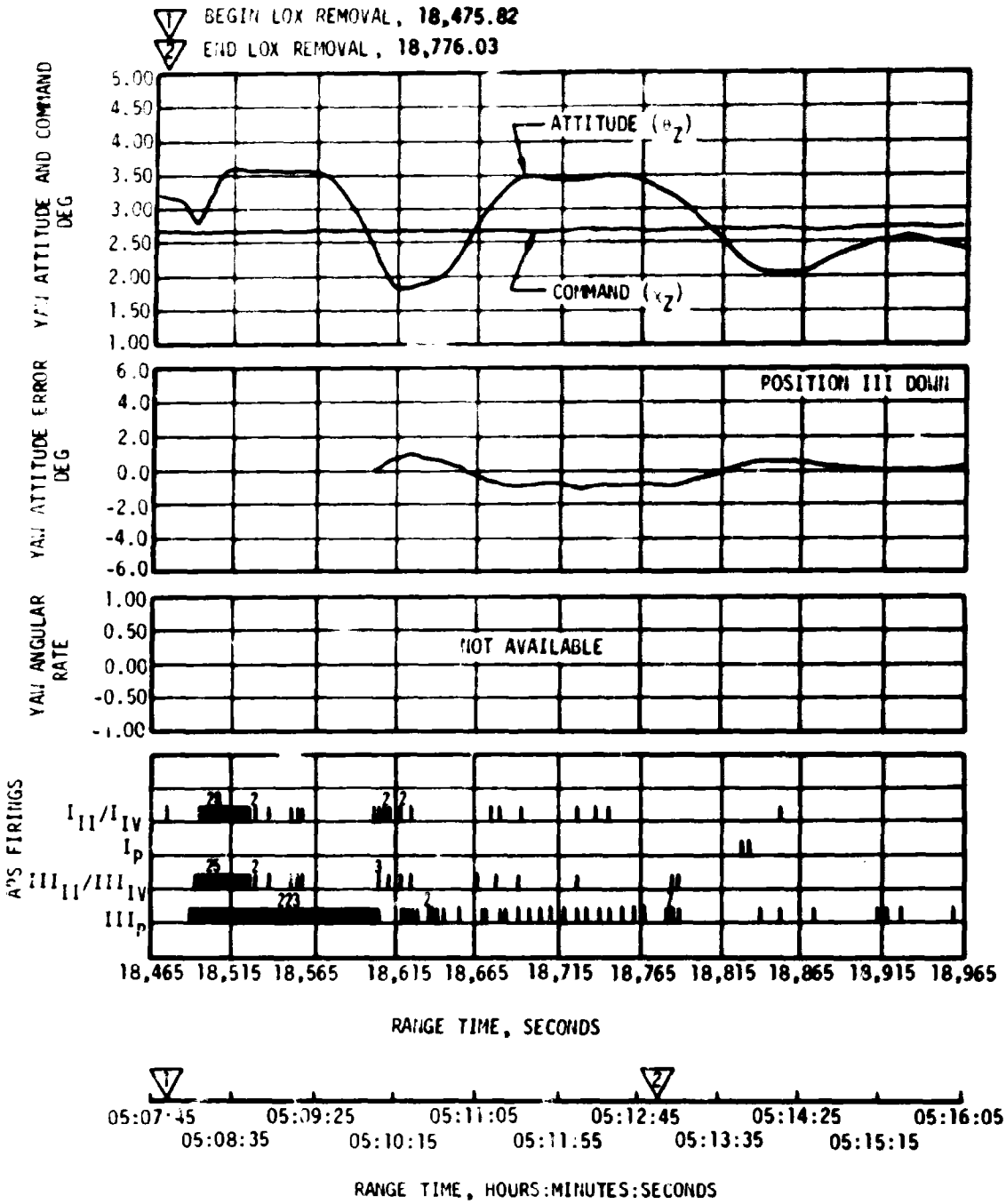

Figure 11-33. Yaw Attitude Control During Propellant Removal

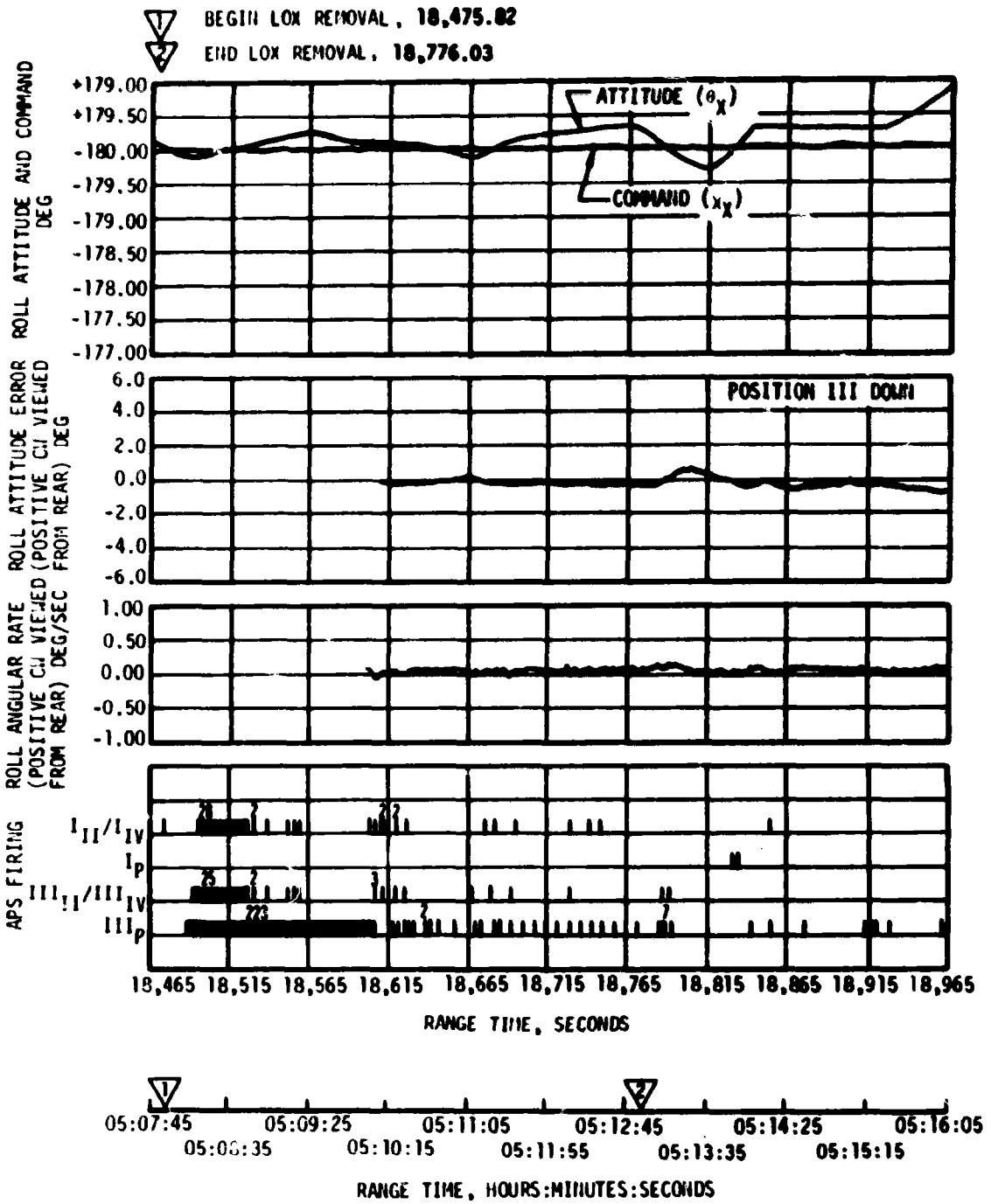

Figure 11-34. Roll Attitude Control During Propellant Removal

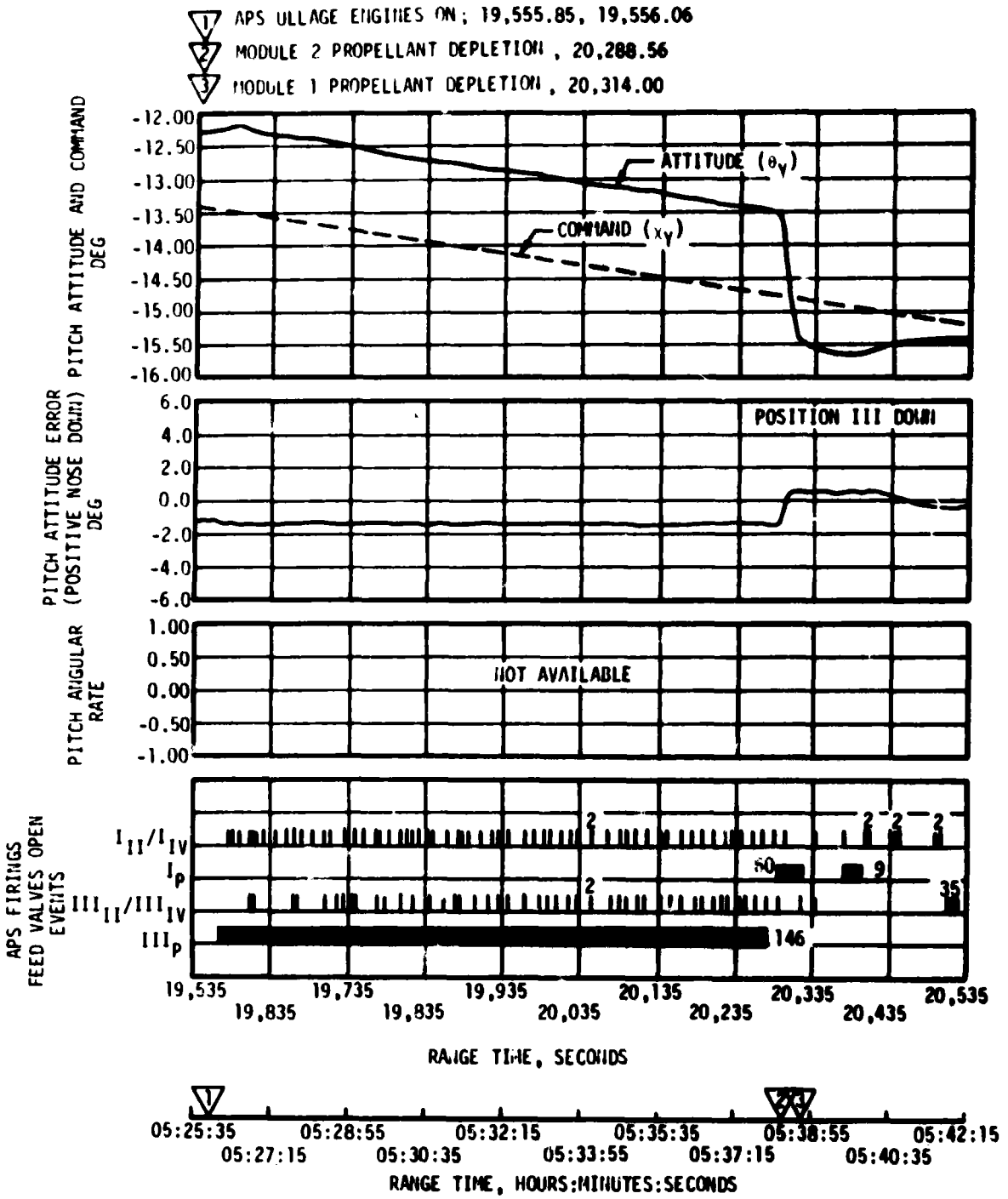

Figure 11-35. Pitch Attitude Control During APS Ullage Burn for Slingshot

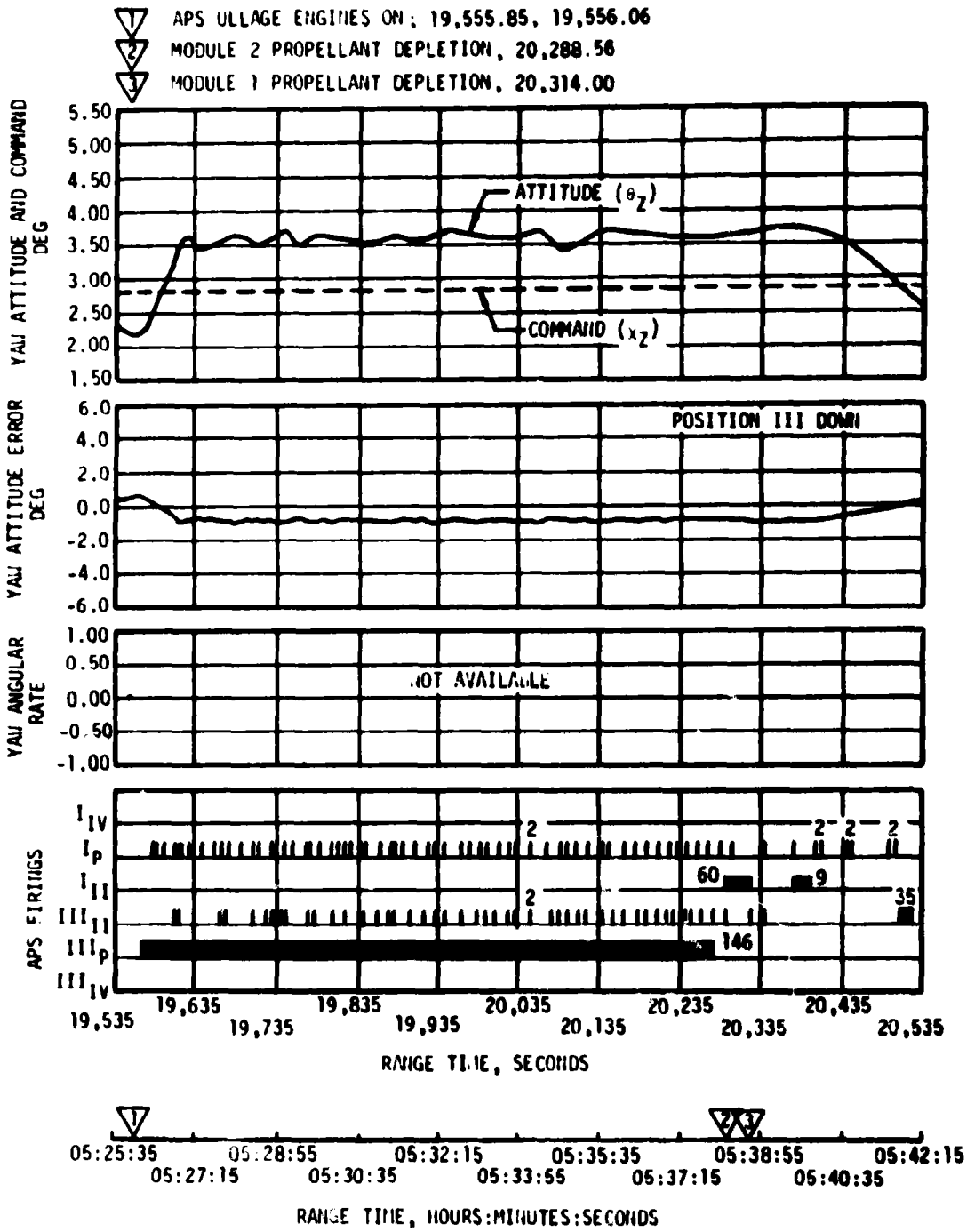

Figure 11-36. Yaw Attitude Control During APS Ullage Burn for Slingshot

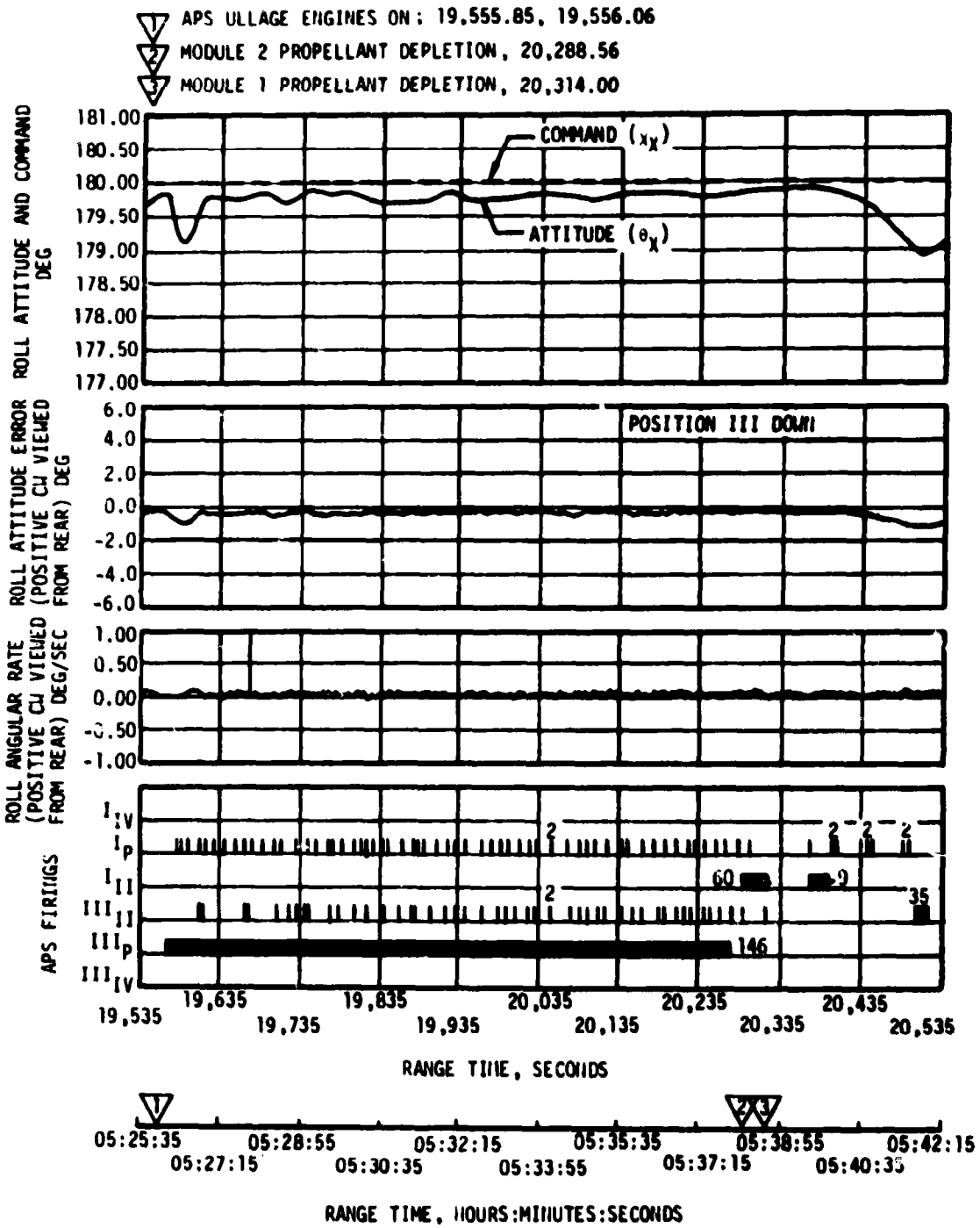

Figure 11-37. Roll Attitude Control During APS Ullage Burn for Slingshot

APS propellant requirements for attitude control during the AS-503 mission were generally lower than the mean predicted requirements. The total propellant (fuel and oxidizer) used prior to ullaging for slingshot ΔV was 40.4 kilograms (89 lbm) (Module 1) and 41.7 kilograms (92 lbm) (Module 2). The total propellant available in each module was approximately 145 kilograms (320 lbm), resulting in a total propellant usage for ullaging and attitude control (excluding slingshot) of approximately 30 percent of that available.

11.6 INSTRUMENT UNIT CONTROL COMPONENTS EVALUATION

11.6.1 Control-EDS Rate Gyros/Control Signal Processor Analysis

The analysis of the Control-EDS Rate Gyros/CSP indicates satisfactory performance.

11.6.2 Flight Control Computer Analysis

The FCC performed properly throughout the boost and coast phases of flight. Analyses of the angular velocity and attitude error signals indicate that these signals, as telemetered from the FCC, correlate well with the same signals telemetered from the originating components.

The outboard engine cant was accomplished in accordance with the design expectations.

SECTION 12

SEPARATION

12.1 SUMMARY

S-IC retro motor performance was satisfactory, with negligible thrust imbalance in the pitch and yaw planes. The data indicate 3 parameters out of 3 sigma tolerances, but this caused no problem. S-IC/S-II separation occurred nominally with adequate clearance between stages.

The S-II ullage motors performed as expected. There was no photographic coverage of the second plane separation, but there was no indication of any clearance problems. The simulation calculation indicated that the separation was nominal.

The S-II retro motors performed satisfactorily during S-II/S-IVB separation. The total impulse was greater than maximum for each of the four motors, but this had no detrimental effect on motor performance. S-IVB ullage motor performance was satisfactory. There was no chamber pressure instrumentation on this flight. S-II/S-IVB separation occurred nominally with no clearance problems.

Spacecraft separation after Translunar Injection (TLI) was nominal. The launch vehicle attitude errors were less than ±0.1 degree during the separation maneuver. The Spacecraft Lunar Module Adapter (SLA) panels were retracted and jettisoned from the launch vehicle on this flight and therefore caused no problems during separation.

A summary of separation events and times of occurrence is given in Table 12-1.

12.2 S-IC/S-II SEPARATION EVALUATION

12.2.1 S-IC Retro Motor Performance

Ignition signal to the retro motors occurred at 154.48 seconds. The retro motors performed satisfactorily and provided for a successful S-IC/S-II first plane separation. As was observed on previous flights, however, the telemetered chamber pressures were higher than expected. Since this has been attributed to instrumentation characteristics, the data were biased using a characteristic velocity and known propellant

Table 12-1. Separation Event Times

EVENT	ACTUAL TIME (SEC)		PREDICTED TIME (SEC)	
	RANGE TIME	TIME BASE +	RANGE TIME	TIME BASE +
LVDC Interrupt (S-IC OECO Sensed), Start of Time Base 3 (T_3)	153.82	--	151.37	--
S-II Ullage Motor Fire Signal	154.29	0.47	151.87	0.5
S-IC/S-II Separation Command	154.47	0.65	152.07	0.7
S-IC Retro Motor EBW Fire Signal	154.48	0.66	152.08	0.71
S-IC/S-II Physical Separation	154.64	0.82		
S-II Engine Start Command	155.19	1.37	152.77	1.4
S-II Second Plane Separation Command	184.47	30.65	182.07	30.7
LVDC Interrupt (S-II ECO Sensed), Start of Time Base 4 (T_4)	524.04	--	521.19	--
S-IVB Ullage Motor Ignition Command	524.78	0.74	521.89	0.7
S-II/S-IVB Separation Command	524.90	0.86	521.99	0.8
S-II Retro Motor EBW Fire Signal	524.93	0.89	522.02	0.83
90 Percent Retro Thrust	525.0			
S-IVB Engine Start Sequence Command	525.00	0.95	522.19	1.0
S-II/S-IVB Separation Complete	526.0	1.95		
S-IVB Second ECO Interrupt, Start of Time Base 7 (T_7)	10,555.73	--	10,552.48	--
Spacecraft Separation Command	12,056.3	1500.6	12,052.48	1500.0
S-IVB IU/CSM Physical Separation Complete	12,059.3	1503.6		
Spacecraft RCS Ignition Command	12,059.5	1503.8		

weights. Table 12-2 shows the performance of the retro motors. Even with the chamber pressure bias included, several of the parameters were out of the 3 sigma limit. This did not cause any problems. The chamber pressure measurement data for the motor on fin D, position I, was lost due to RF blackout, but the motor apparently performed nominally.

Thrust unbalance was negligible. Figure 12-1 shows the thrust versus time curves for the retro motor with the highest maximum thrust (fin B, position III), and the one with the lowest maximum thrust (fin A, position II).

Table 12-2. S-IC Retro Motor Performance

RETRO MOTOR	PARAMETER				
	EFFECTIVE BURN TIME (sec)[1]	AVG EFFECTIVE PRESSURE N/cm² (psia)[2]	TOTAL IMPULSE N-s (lbf-s)[3]	EFFECTIVE IMPULSE N-s (lbf-s)[4]	AVG EFFECTIVE THRUST N (lbf)[5]
Fin A - Pos I	0.656	1110 (1610)	273,521 (61,490)	247,757 (55,698)	377,676 (84,905)
Pos II	0.670	1069 (1551)	267,663 (60,173)	239,755 (53,899)	357,842 (80,446)
Fin B - Pos II	0.651	1111 (1611)	272,253 (61,205)	245,933 (55,288)	377,774 (84,927)
Pos III	0.668	1132 (1642)	276,057 (62,060)	256,876 (57,748)	384,544 (86,449)
Fin C - Pos III	0.655	1100 (1595)	270,981 (60,919)	244,363 (54,935)	373,072 (83,870)
Pos IV	0.659	1109 (1609)	272,187 (61,190)	248,362 (55,834)	376,875 (84,725)
Fin D - Pos IV	0.653	1116 (1619)	272,965 (61,365)	248,451 (55,854)	380.474 (85,534)
Pos I*	-- --	-- --	-- --	-- --	-- --
Average	0.658	1107 (1605)	272,231 (61,200)	247,357 (55,608)	375,470 (84,409)
Nominal 288.72°K (60°F) Motor	0.648	1114 (1616)	No Spec	247,156 (55,563)	386,564 (86,903)
-3σ Limit 288.72°K (60°F) Motor	0.610	1038 (1505)	No Spec	242,659 (54,552)	364,412 (81,923)
+3σ Limit 288.72°K (60°F) Motor	0.695	1190 (1726)	No Spec	251,654 (56,574)	408,716 (91,883)

*No data, measurement failure.

[1] Effective Burning Time - The effective burning time is the interval from attainment of the initial 75 percent of maximum pressure on the ascending portion of the pressure trace to the same level on the decay portion of the pressure trace.

[2] Average Effective Pressure - The average effective pressure is the pressure time integral between the limits of effective burning time divided by the effective burning time.

[3] Total Impulse - Total impulse is the area under the thrust-time trace from zero time until the thrust returns to zero.

[4] Effective Impulse - The effective impulse is the area under the thrust-time curve, between the limits of effective burning time.

[5] Average Effective Thrust - The average effective thrust is the effective impulse divided by the effective burning time.

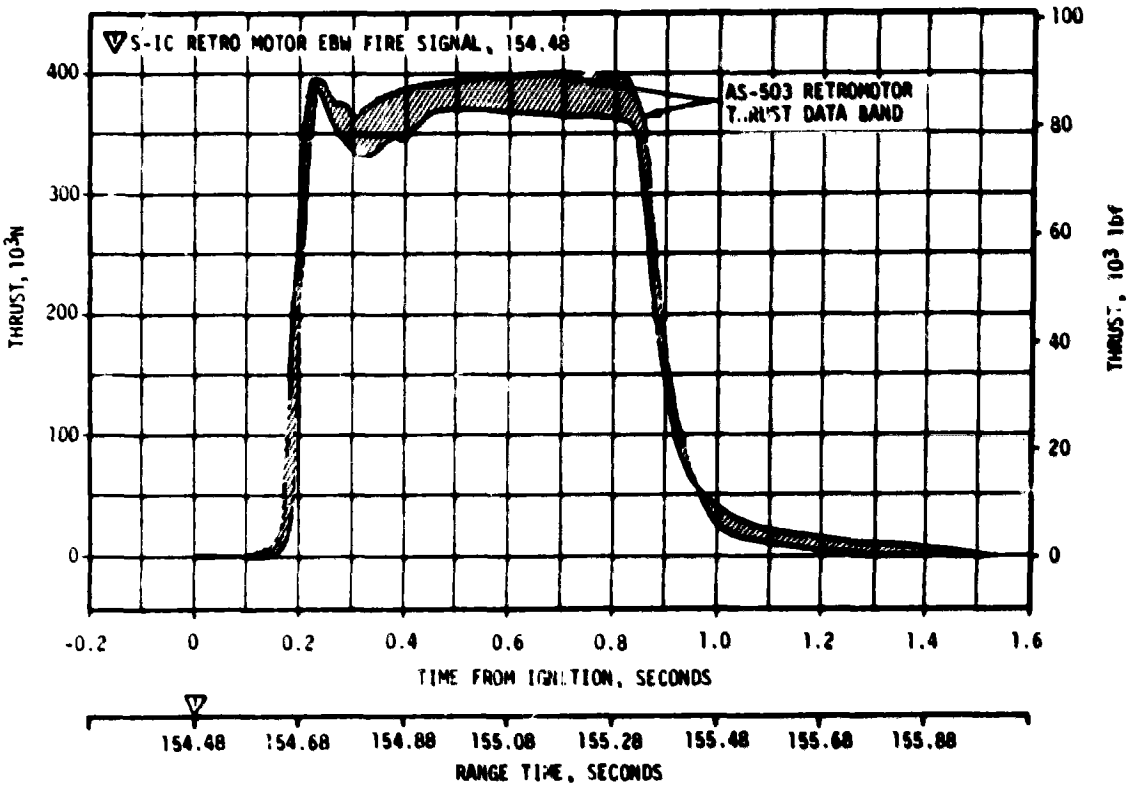

Figure 12-1. S-IC Retro Motor Thrust

12.2.2 S-II Ullage Motor Performance

The S-II ullage motors performed within the required limits. Performance parameters of the four ullage motors are summarized in Table 12-3. Ullage motor firing occurred at 154.29 seconds. The ullage motor composite thrust-time curve is shown in Figure 12-2. Chamber pressure measurements again indicated that motor web burn-through occurred as predicted.

12.2.3 S-IC/S-II Separation Dynamics

S-IC/S-II separation and associated sequencing was accomplished as planned. Subsequent S-IC and S-II dynamics provided adequate positive clearance between the stages. The predicted and measured dynamic pressures at separation were 0.0345 and 0.0397 N/cm^2 (7.2 and 8.3 lbf/ft^2), respectively. Dynamic conditions at separation fell within estimated end conditions and well within staging limits.

The first plane separation was monitored by accelerometers and rate gyros on each of the two stages. Separation rate transducers (extensometers) provided relative separation rate data. For evaluation purposes, first plane separation dynamics were calculated using a computer program which took into account F-1 thrust decay, S-IC retro motor thrust, S-II ullage motor thrust, initial trajectory conditions, engine gimbal

Table 12-3. S-II Ullage Motor Performance

PARAMETER	UNITS	ULLAGE MOTOR				PERFORMANCE LIMITS	
		1	2	3	4	MAXIMUM	MINIMUM
Effective Burn Time[1]	sec	3.914	3.918	3.95	3.88	4.75	3.25
Average Effective Pressure[2]	N/cm²	672	669	662	674	896	
	psi	975	970	960	978	1300	
Average Effective Thrust[3]	N	101,050	100,534	99,498	101,749		66,723
	lbf	22,717	22,601	22,368	22,874		15,000
Maximum Thrust[4]	N	109,133	107,994	105,921	109,342	129,666	
	lbf	24,534	24,278	23,812	24,581	29,150	
						NOMINAL	
Effective Burn Time Impulse[5]	N-s	368,833	366,947	363,166	371,382	373,206	
	lbf-s	82,917	82,493	81,643	83,490	83,900	

The above parameters correspond to parameters defined in the NR procurement specification ME-901-0089 as follows:

[1] Burn Time - The time interval beginning on the ignition pressure transient when the chamber pressure has risen to 75 percent of the maximum pressure, and ending when the pressure has dropped to 75 percent of the maximum chamber pressure.

[2] Burn Time Average Pressure - The average effective pressure is the integrated area under the pressure-time curve between the points defined by the burn time definition and divided by the effective burn time.

[3] Burn Time Average Thrust - The average effective thrust is the area under the thrust-time curve between the points defined in the burn time definition and divided by the effective burn time.

[4] Maximum Thrust - The maximum recorded thrust in the interval between the ignition phase and the beginning of final thrust decay.

[5] Burn Time Impulse - The integral of the thrust-time trace during burn time.

angles, and mass properties. The simulated first plane separation dynamics and separation distances agreed very well with the actual data.

Figure 12-3 shows separation distances and relative velocities of the two stages and their respective contributions to the total. These velocities are changes in velocity magnitudes from time of physical separation; whereas the distances are measured relative to the time from LVDC sensed S-IC OECO. The plot for separation distance also shows the point where the S-IC stage clears the J-2 engines, which extend beyond the separation plane by 0.41 meter (16 in.). Close agreement between the AS-502 and AS-503 flights is seen.

Lateral clearance and longitudinal accelerations for the separation were nominal. The minimum clearance was calculated to be 1.33 meters (52.4 in.) between engine No. 1 and the S-IC stage. The calculated longitudinal acceleration indicated that physical separation occurred approximately 0.1 second later than on AS-502. This was due to the retro motor thrust rising to full thrust approximately 0.1 second later than on AS-502.

S-IC pitch and yaw angular dynamics following separation are shown in Figure 12-4. Angular rates are S-IC rate gyro measurements. Attitude deviations following separation are the integrals of the rates, with

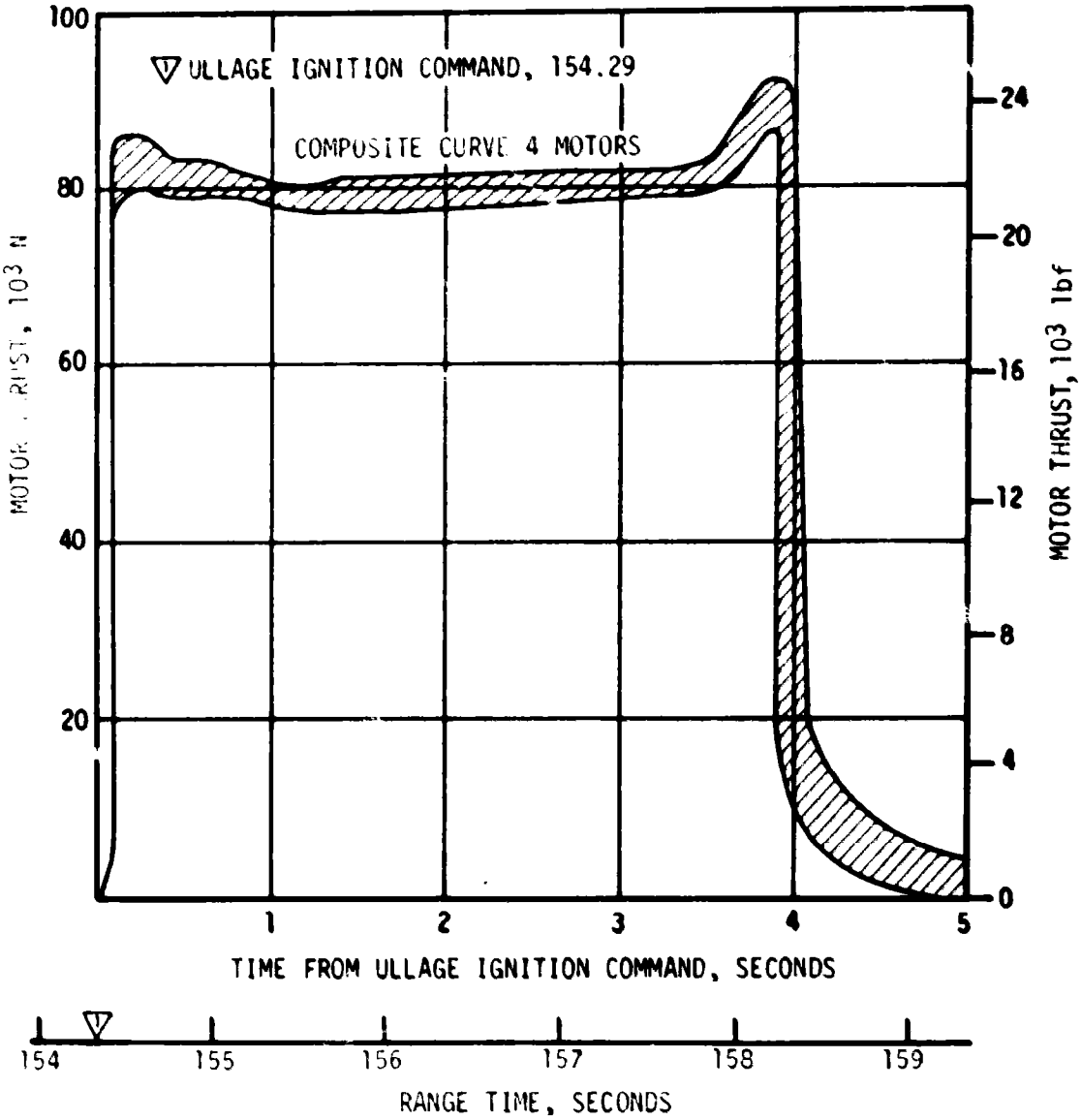

Figure 12-2. S-II Ullage Motor Thrust

initial values being the measured attitude errors at physical separation. The angular rate histories for the S-IC following separation are similar to those measured during AS-501 and AS-502 flights.

Figure 12-5 presents the angular dispersions of the S-II stage during separation. No significant difference existed between the AS-502 and AS-503 flights.

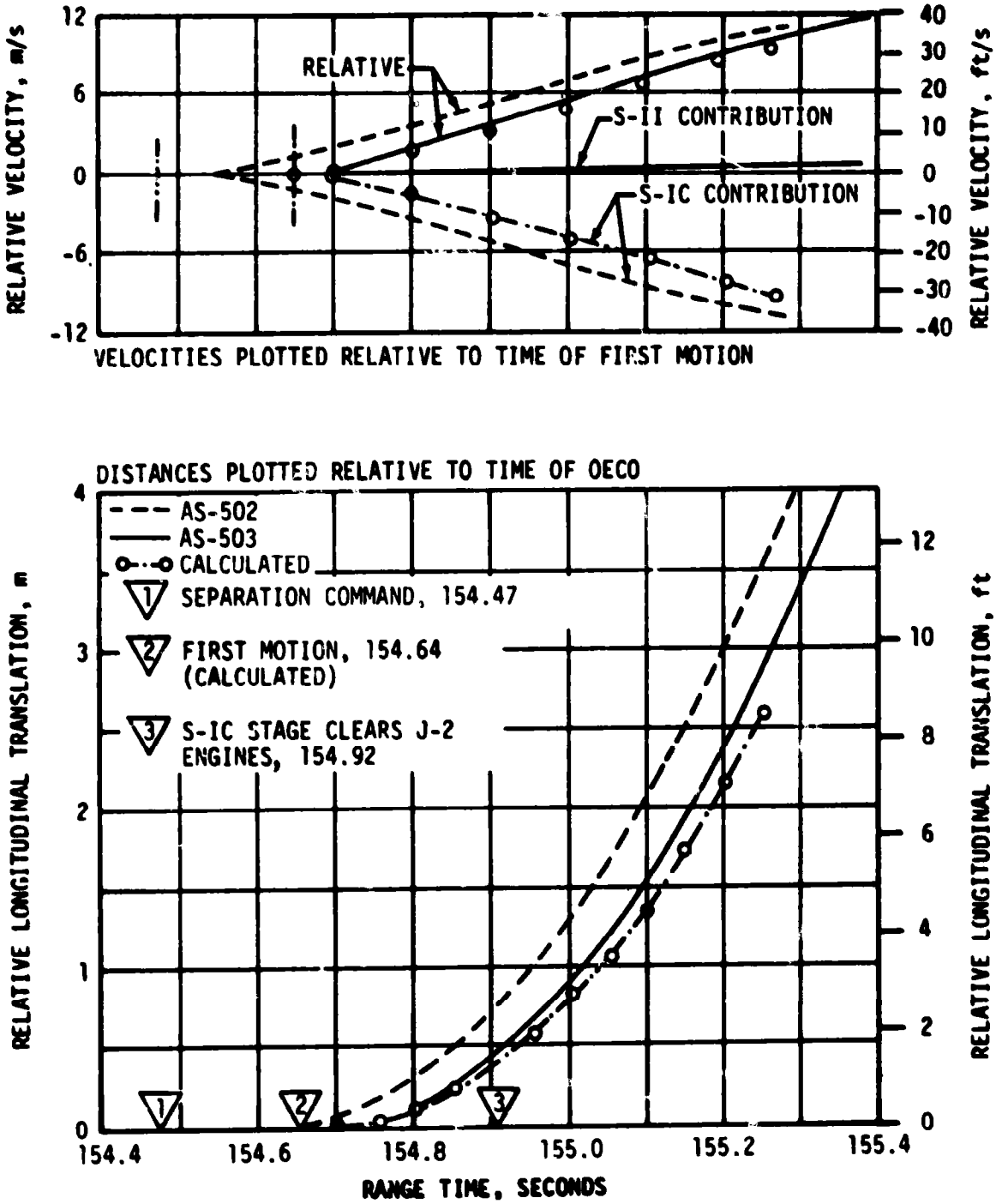

Figure 12-3. S-IC/S-II Relative Velocity and Separation Distance During First Plane Separation

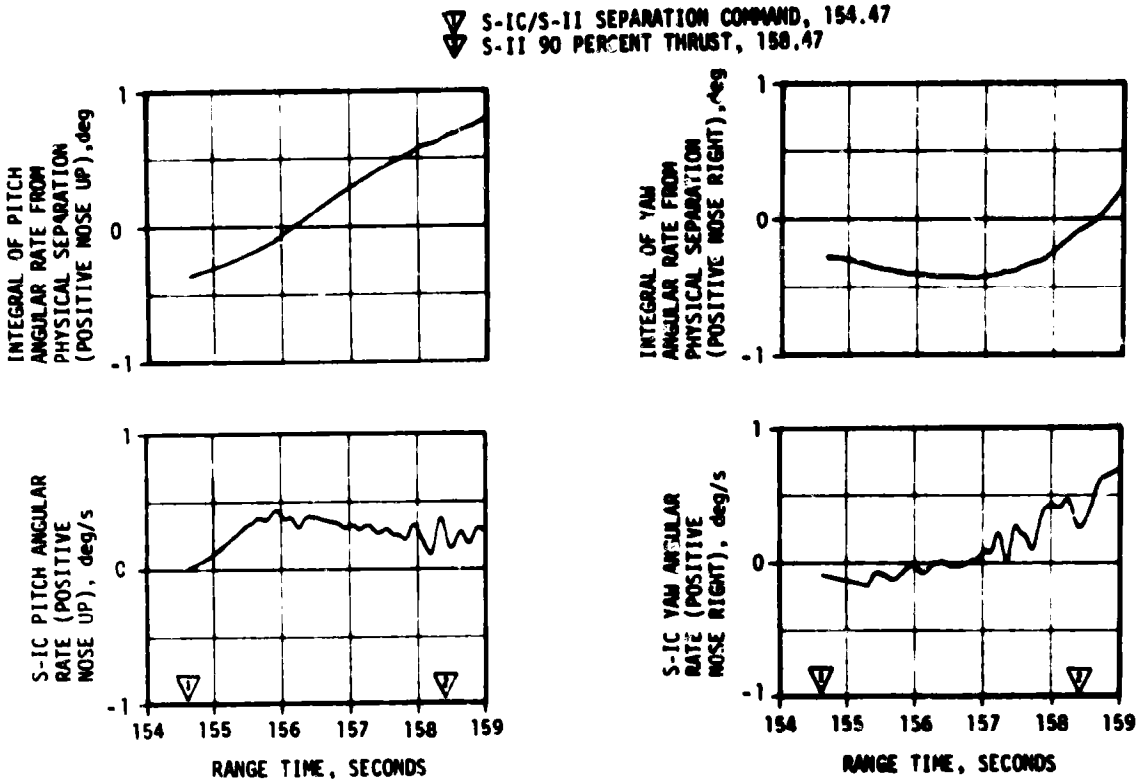

Figure 12-4. S-IC Pitch and Yaw Angular Dynamics Following S-IC/S-II Separation

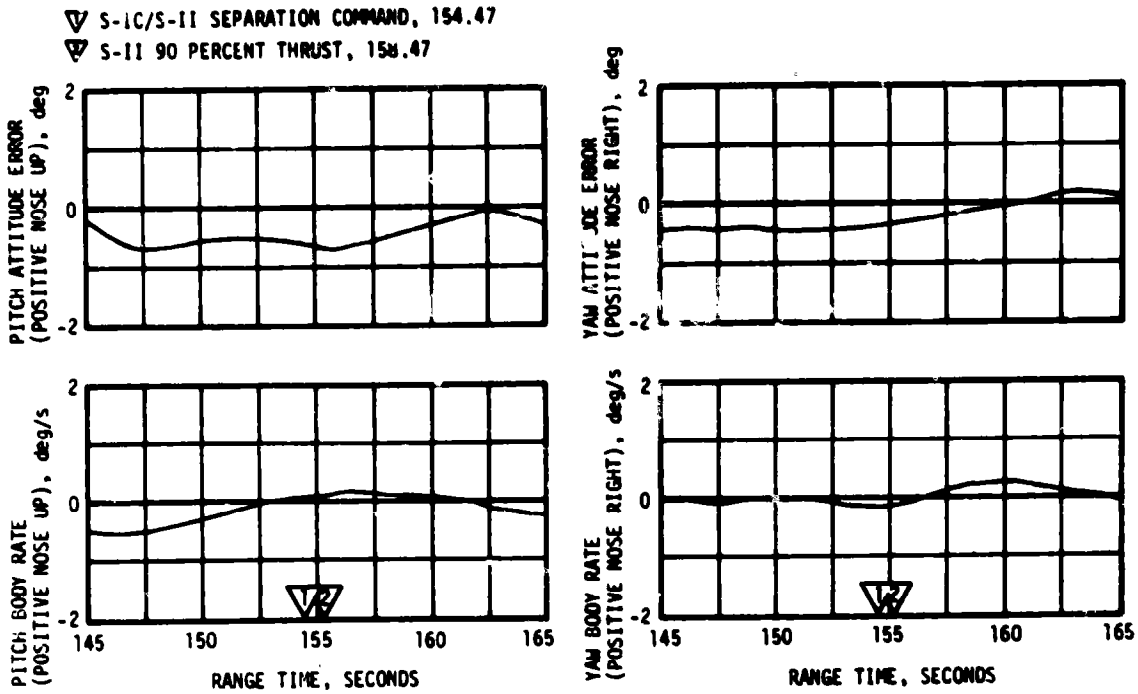

Figure 12-5. S-II Angular Dispersions During S-IC/S-II First Plane Separation

12.3 S-II SECOND PLANE SEPARATION EVALUATION

In the two previous flights, photographic coverage provided the only means of adequately monitoring second plane separation (this capability did not exist for AS-503 due to the lack of onboard cameras). Therefore, the dynamics of both the second stage and the separating interstage were calculated. These calculations utilized appropriate initial trajectory data, postflight mass characteristics, and J-2 engine plume characteristics obtained from flight data. The figures shown represent these calculated results.

The relative separation velocities, relative velocity contribution of each body to the total, and relative longitudinal separation distance between the two bodies are shown in Figure 12-6. Very good agreement is seen between AS-503 and AS-502 data. The velocities are the changes in velocities from time of physical separation. As was the case for the two previous flights, better agreement in relative velocity was obtained by using an electrical disconnect force of zero. The relative separation data also indicate very good agreement between AS-502 and AS-503 results. The separation was complete when the interstage passed the bottom of the J-2 engines and was calculated to have occurred at approximately 185.54 seconds. Attitude errors and rates remained near zero during second plane separation as they did on AS-502.

The body rates of the separating interstage, and the lateral clearances between the interstage and the engines were computed and were similar to the clearances on AS-502. There was a minimum clearance of 1.02 meters (40 in.) between engine No. 3 and the interstage ring at vehicle station 39.73 meters (1564 in.). The separation plane is located at vehicle station 44.70 meters (1760 in.).

12.4 S-II/S-IVB SEPARATION EVALUATION

12.4.1 S-II Retro Motor Performance

The four retro motors mounted on the S-II stage performed satisfactorily and separated the S-II stage from the S-IVB stage. The pressure buildup for all four retro motors began within 0.02 second of each other at 524.82 seconds. The thrust and chamber pressure profiles for the four motors were very similar, and the maximum difference in burn times was 0.10 second.

Table 12-4 presents the performance parameters for the individual motors. The total impulse for all four motors, and the burn time for motor No. 1 was greater than the maximum specified value. All other parameters were within the specified limits. The greater total impulses were due to burn times which were approximately 0.15 second longer than on AS-502. A large portion of the increase in burn times resulted from a slower thrust increase at motor ignition. The higher total impulses and longer burn times had no detrimental effect on motor performance. The retro motor thrusts are shown in Figure 12-7.

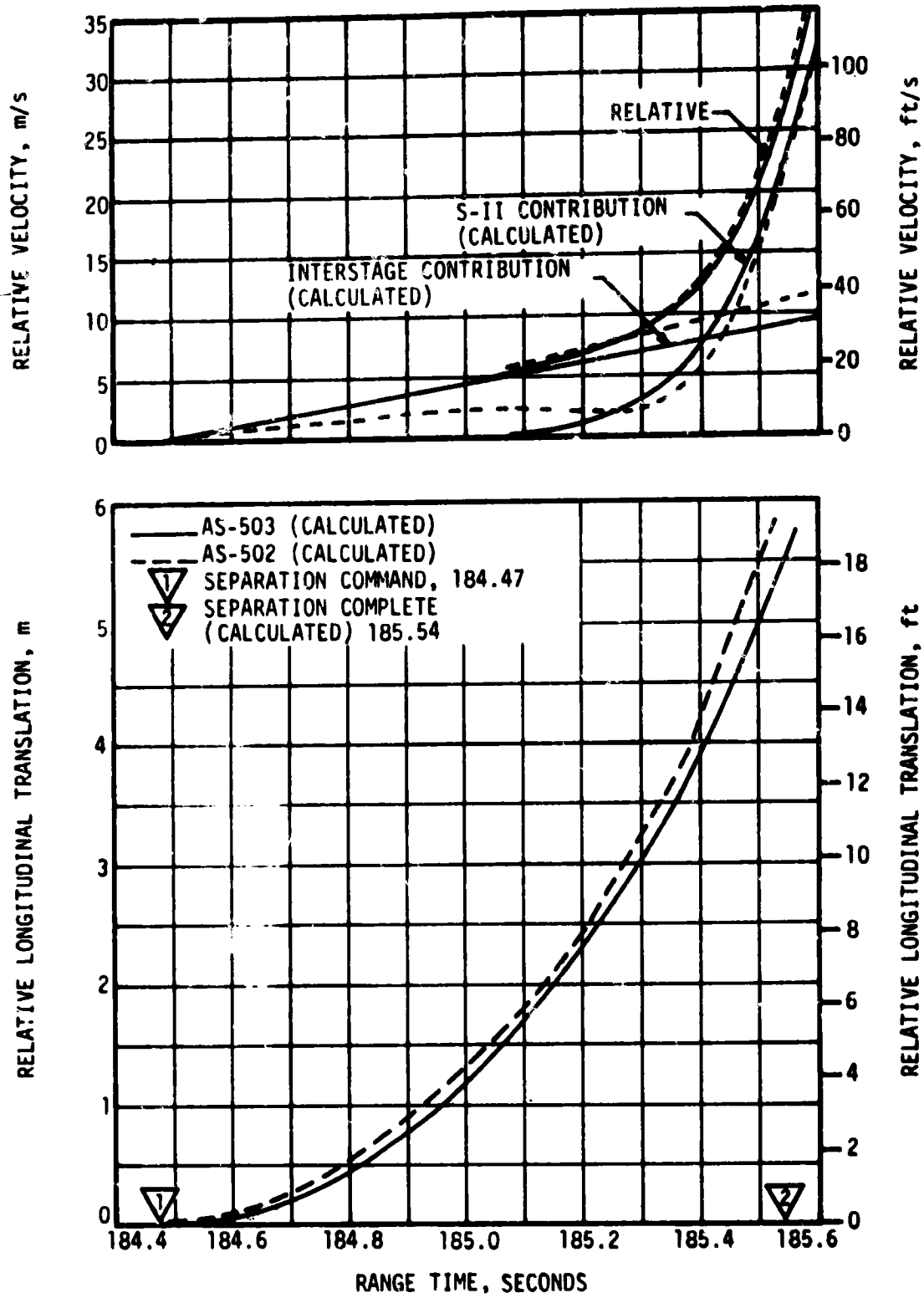

Figure 12-6. Interstage/S-II Relative Velocity and Separation Distance During Second Plane Separation

Table 12-4. AS-503 S-II Retro Motor Performance

PARAMETER	MOTOR					SPECIFICATION LIMITS AT 288.9 °K (60 °F)	
	1 POS IV-I	2 POS II-III	3 POS I-II	4 POS III-IV	AVERAGE	MAXIMUM	MINIMUM
Burn Time[1], sec	1.71	1.61	1.63	1.66	1.65	1.67	1.38
Average Burn Time Chamber Pressure[2], N/cm² (psia)	1149 (1667)	1180 (1711)	1205 (1747)	1167 (1693)	1176 (1705)	1293 (1875)	1065 (1545)
Maximum Thrust[3], N(lbf)	176,372 (39,650)	185,802 (41,770)	189,628 (42,630)	187,759 (42,210)	184,890 (41,565)	193,142 (43,420)	152,129 (34,200)
Average Burn Time Thrust[4], N (lbf)	155,772 (35,019)	159,709 (35,904)	163,832 (36,831)	158,486 (35,629)	159,451 (35,846)	175,416 (39,435)	134,292 (30,190)
Burn Time Total Impulse[5], N-s (lbf-s)	266,368 (59,882)	257,134 (57,806)	267,044 (60,034)	263,086 (59,144)	263,410 (59,217)	250,435 (56,300)	232,597 (52,290)

[1] Burn Time - Defined in Section 6.2.1.30 of Thiokol Model Specification TEMS-11.

[2] Burn Time Average Chamber Pressure - The average chamber pressure during burn time is the area under the pressure curve over the burn time, divided by the burn time.

[3] Maximum Thrust - The highest thrust developed by the retro motor under any normal operating condition excluding ignition.

[4] Burn Time Average Thrust - The average thrust during burn time is the burn time total impulse divided by the burn time.

[5] Burn Time Total Impulse - The area under the thrust-time curve over the burn time.

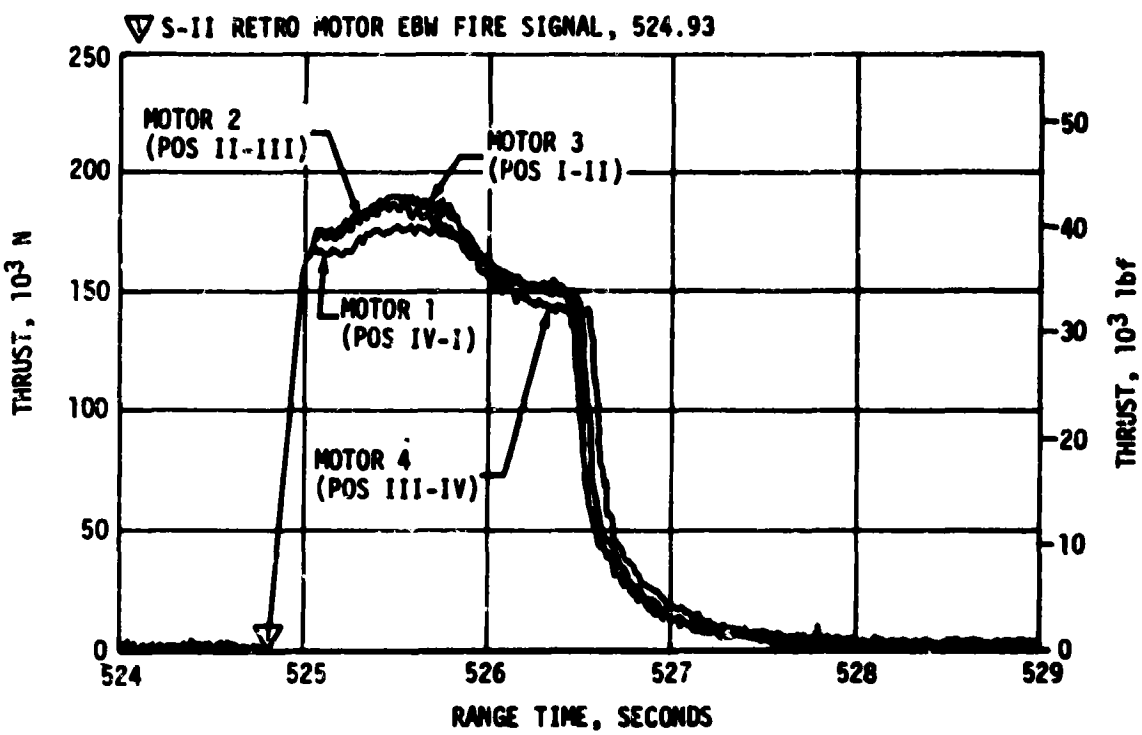

Figure 12-7. S-II Retro Motor Thrust

12.4.2 S-IVB Ullage Motor Performance

Ullage motor performance was satisfactory. The ullage motor ignition command was given at 524.78 seconds, with the jettison command at 536.80 seconds. These times were within 0.05 second of predicted times relative to engine start command. No instrumentation existed to measure the chamber pressure of the ullage motors.

12.4.3 S-II/S-IVB Separation Dynamics

The analysis of separation dynamics was done by comparing the data from the AS-503 flight to that of AS-501. Since the data compared very closely, detailed reconstruction was not performed to determine precisely the lateral clearance used and the separation completion time. From the comparative analysis performed it can be estimated that a detailed reconstruction would yield a separation completion time of approximately 1.0 second, and a lateral clearance utilization of less than 12.8 centimeters (5 in.).

Figure 12-8 shows the longitudinal accelerometer data for the S-II and S-IVB stages.

The angular rates for both the S-II and the S-IVB stages are presented in Figure 12-9. The S-IVB rates were small with pitch and yaw rates less than ±0.2 deg/s. The S-II rates reached 1.0 and 1.5 deg/s in pitch and yaw, respectively.

12.5 S-IVB-IU-LM TEST ARTICLE (LTA)/COMMAND SERVICE MODULE (CSM) SEPARATION EVALUATION

Spacecraft separation from the S-IVB-IU-LTA was performed while the vehicle was in an inertially frozen retrograde attitude to minimize separation transients. Separation was initiated by a command from the spacecraft at 12,056.3 seconds which was received by the LVDC at 12,056.48 seconds. At 12,059.3 seconds the separation devices were ignited and separation was detected by the CSM. The SLA panels were retracted and jettisoned by a spring-loaded piston device, completing the separation sequence. At about 12,059.5 seconds the first motion of the CSM was commanded through the use of the spacecraft translational hand controller. Launch vehicle and spacecraft attitudes during the separation indicated attitude changes of less than ±0.1 degree, and attitude rates were under ±0.1 deg/s. The separation was completed with no clearance or attitude problems. The S-IVB-IU-LTA after separation is shown in Figure 12-10.

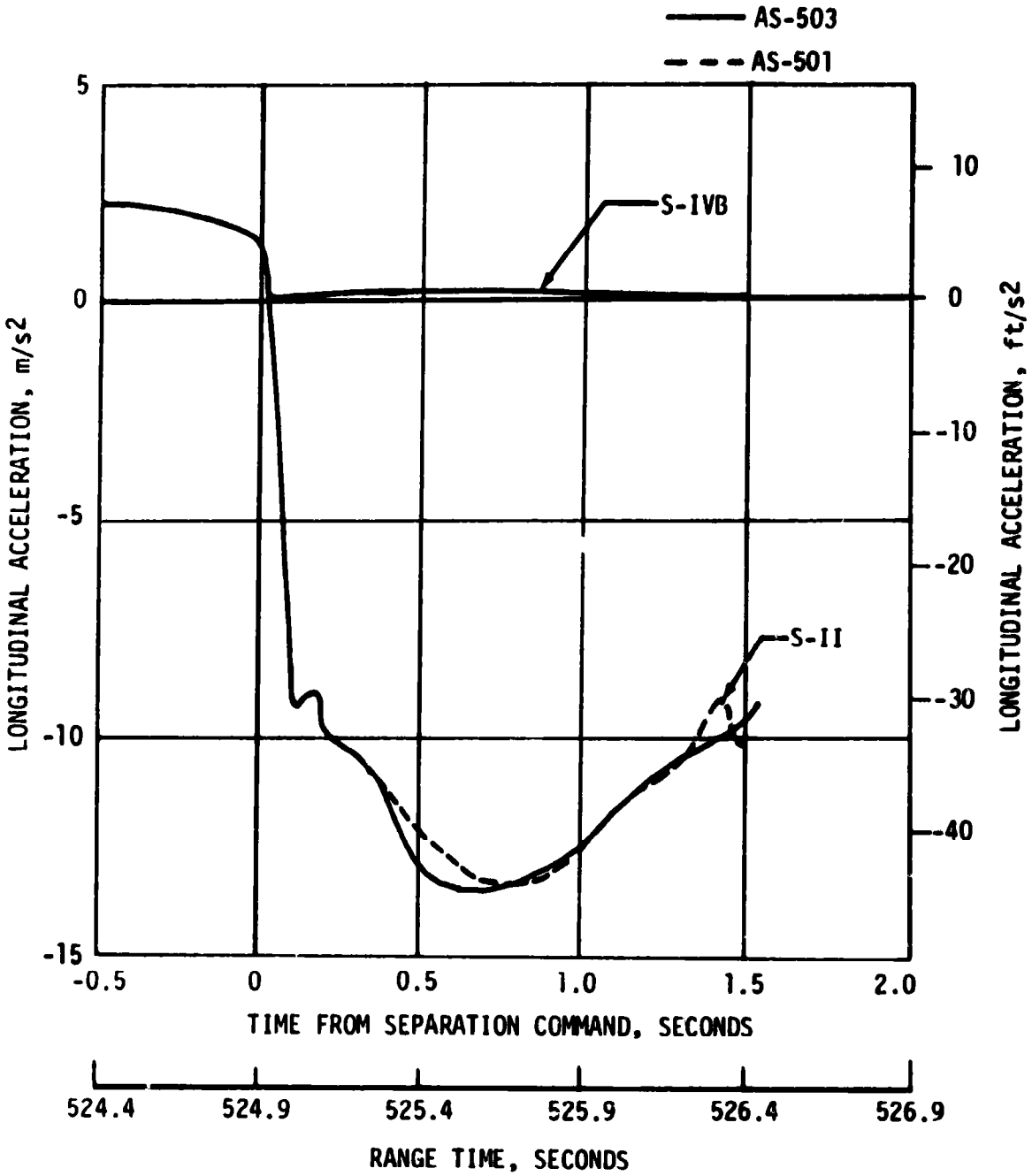

Figure 12-8. S-II/S-IVB Longitudinal Acceleration

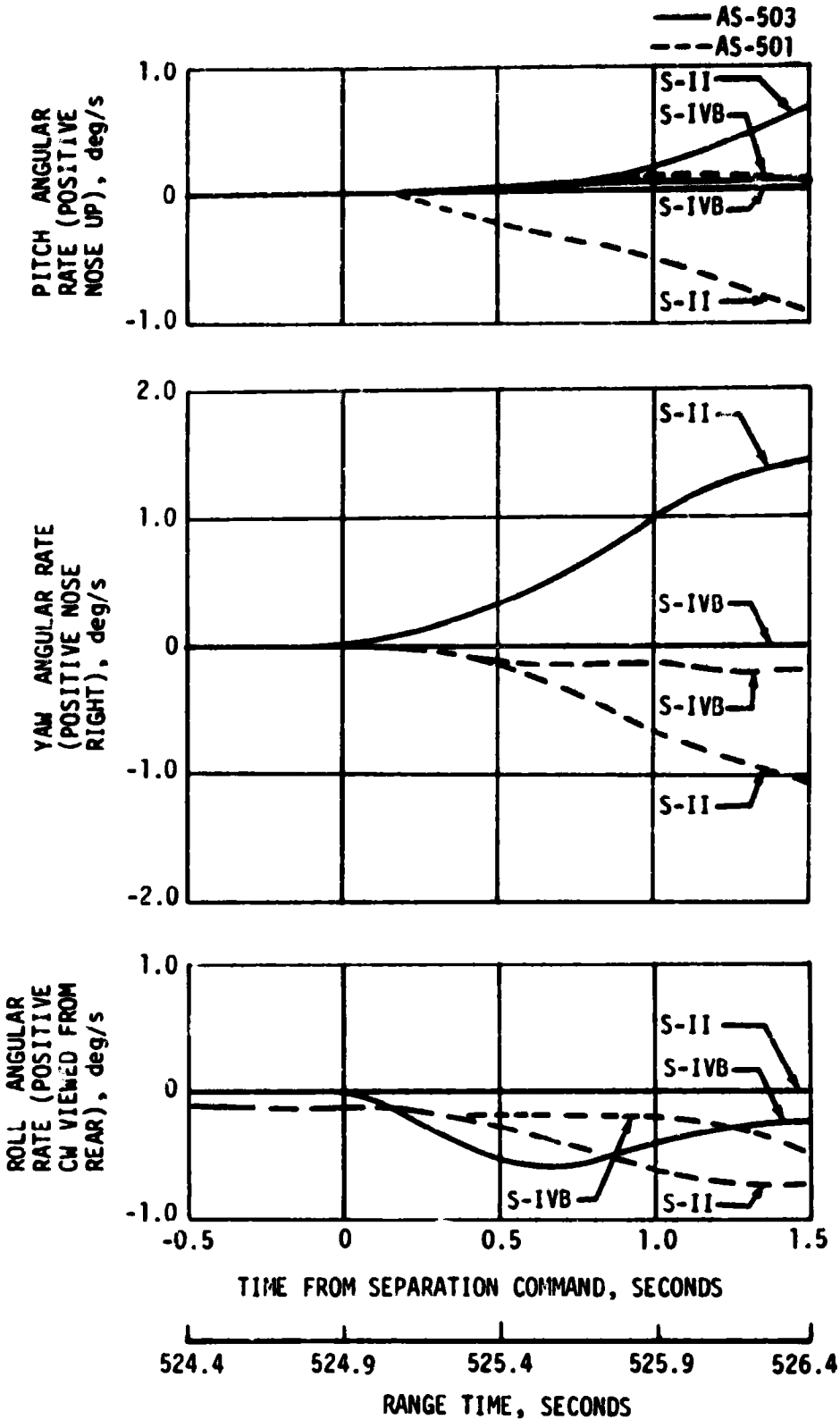

Figure 12-9. S-II and S-IVB Angular Dispersions During S-II/S-IVB Separation

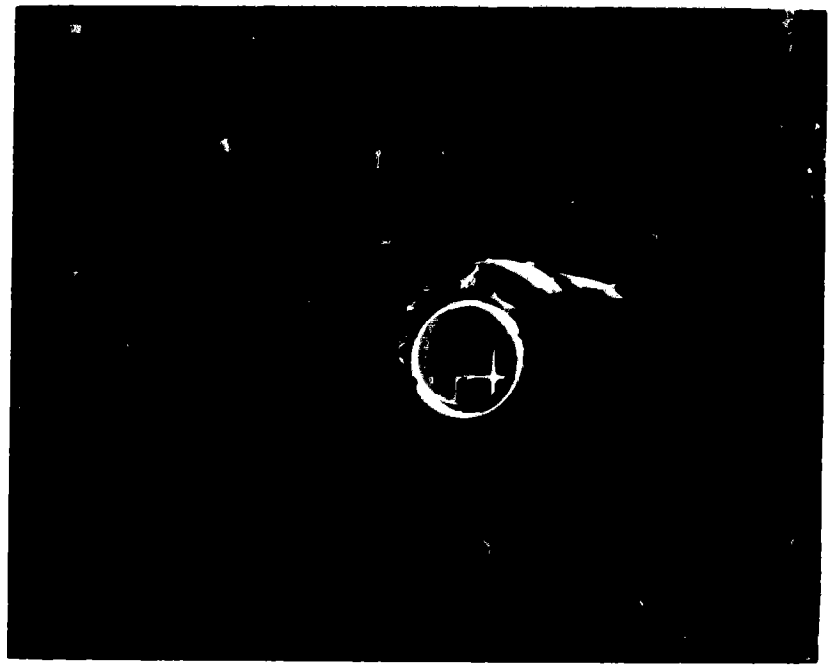

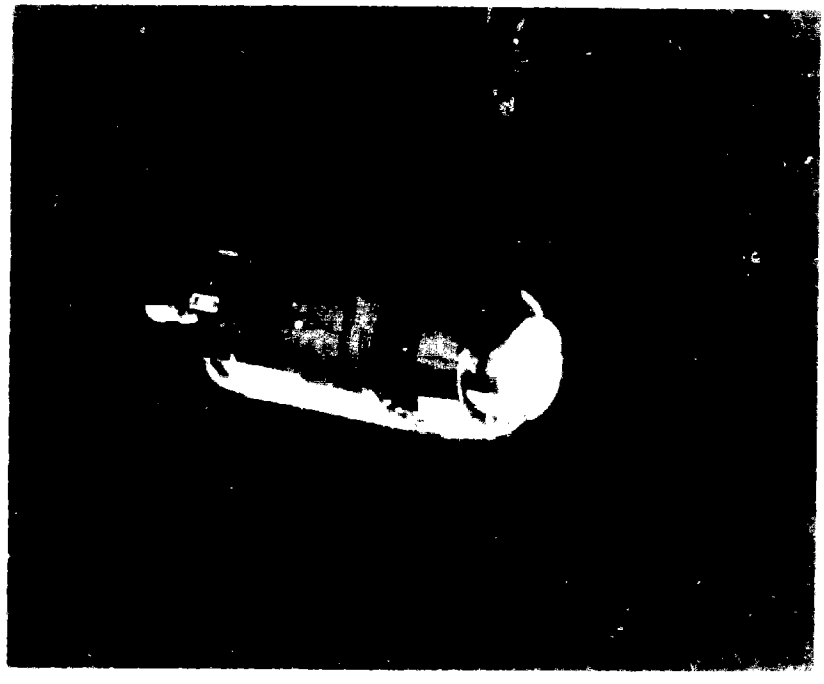

Figure 12-10. S-IVB-IU-LTA After Separation

SECTION 13

ELECTRICAL NETWORKS

13.1 SUMMARY

The launch vehicle electrical networks are comprised of independently battery-powered electrical systems for the four stages with interconnecting cabling to satisfy stage to stage electrical interface requirements. Each stage electrical system distributes power to continuous users, such as instrumentation and communications, and responds to commands initiated either by the stage or the Instrument Unit (IU) through the stage switch selector.

In general, all AS-503 launch vehicle electrical systems performed satisfactorily. The power profiles of all stages were normal and all stage and switch selector commands were properly executed. The only deviation or out-of-tolerance conditions noted during the flight were:

a. The intermittent operation of 3 temperature bridge power supplies on the S-II stage. Two of these supplies were affected for approximately 30 seconds through maximum dynamic pressure (Max Q) and the third for approximately 30 seconds starting at low Propellant Utilization (PU) step.

b. The S-IVB aft 5 volt excitation module dropped below the minimum of 4.975 vdc from approximately 9410 to 10,691 seconds.

13.2 S-IC STAGE ELECTRICAL SYSTEM

The S-IC stage electrical power is obtained from five 28-vdc batteries and is distributed to stage components through the power distribution system. Battery No. 1 furnishes operational power and battery No. 2, instrumentation power. Batteries No. 3, 4, and 5 furnish power for the optical instrumentation system all of which will be deleted from AS-504 and subsequent vehicles.

The electrical system performance during S-IC powered flight was excellent.

Batteries No. 1 and No. 2 performed near prediction. Both battery voltages remained well within the limits of 26.5 to 32 vdc and currents stayed below 45 percent of the limit of 64 amperes for battery No. 1 and below

80 percent of the limit of 125 amperes for battery No. 2, as shown in Figures 13-1 and 13-2, respectively. (See Section 2, Table 2-2 for Event Times reference). No battery current steps, such as those noted around S-IC/S-II separation on both AS-501 and AS-502, were experienced on this flight.

Batteries No. 1 and No. 2 usage was very close to predicted operation as shown in Table 13-1. These batteries were not instrumented to measure temperatures. The three optical instrumentation batteries were not instrumented to measure voltage and amperage and their performance could not be evaluated.

Seven 5-vdc power supplies provide closely regulated voltages for stage instrumentation. These power supply voltages stayed within design limits of 5 ±0.05 vdc. No power supply voltage drops were experienced as on AS-502.

There were 20 switch selector functions programmed for S-IC. All switch selector channels functioned correctly as commanded by the IU.

The separation and retro motor Explosive Bridge Wire (EBW) firing units were armed and triggered as programmed. Charging time and voltage characteristics of the EBW firing units were as predicted and within design specifications. Separation and retro motor ignition charging time and voltage characteristics were within predicted limits.

13.3 S-II STAGE ELECTRICAL SYSTEM

The S-II stage electrical system utilizies four 28-vdc batteries, the output of which is distributed to stage components through the power distribution system. Two of these batteries are connected in series to furnish 56 vdc to the five LH_2. recirculation pump inverters.

The S-II electrical system performed satisfactorily during all phases of the AS-503 flight.

Operation of the improved batteries, first used on this flight, were excellent. Battery bus voltages stayed well within specified limits during the flight, as shown in Figure 13-3 through 13-6. (See Section 2, Table 2-2 and Table 2-3 for Event Times reference). Main bus current averaged 38 amperes during S-IC boost and varied from 54 to 58 amperes during S-II boost. Instrumentation bus current varied from 54 to 58 amperes during S-IC and S-II boost. Recirculation bus current averaged 92 amperes during S-IC boost. Ignition bus current averaged 28 amperes during the S-II ignition sequence. No current spikes were experienced around J-2 engine No. 2 cutoff, as on AS-502.

Battery usages, in ampere-hours and as a percent of rated capacity, together with battery temperatures, are shown in Table 13-2. Battery power

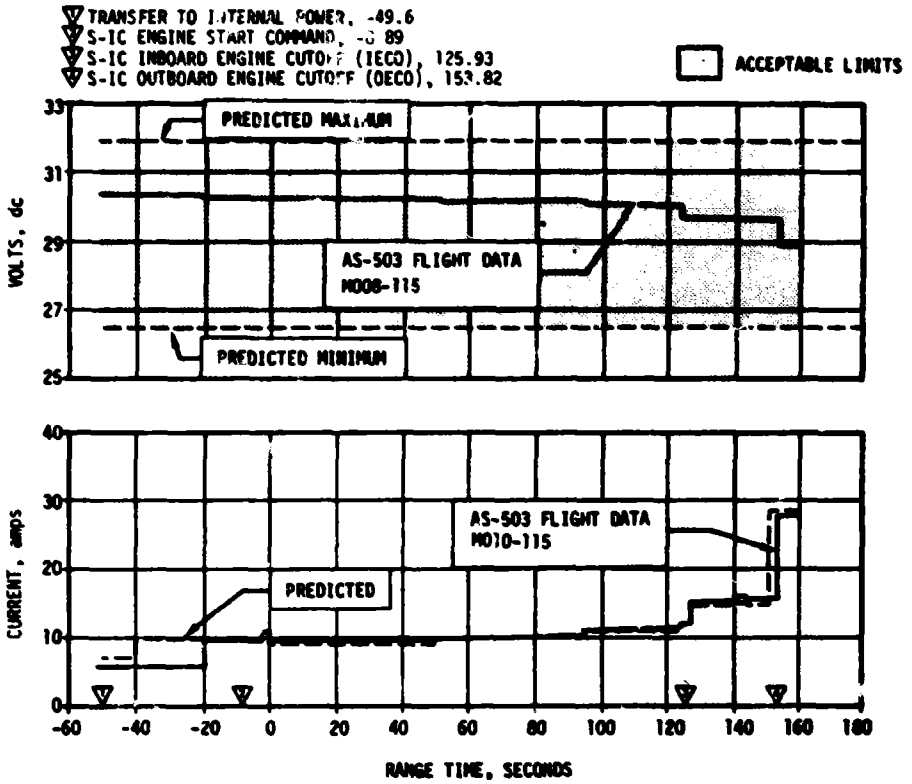

Figure 13-1. S-IC Stage Battery No. 1 Voltage and Current, Bus 1D10

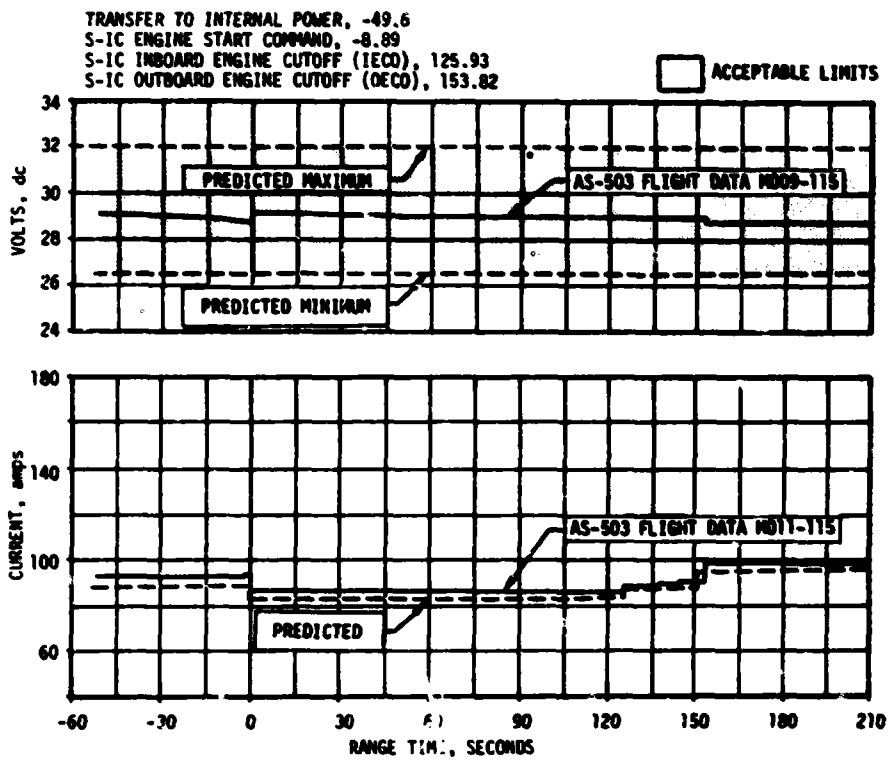

Figure 13-2. S-IC Stage Battery No. 2 Voltage and Current, Bus 1D20

Table 13-1. S-IC Stage Battery Power Consumption

BATTERY	BUS DESIGNATION	CAPACITY AMP/MIN	POWER CONSUMPTION AMP/MIN		PERCENT OF CAPACITY
			MAXIMUM EXPECTED	ACTUAL	
Operation No. 1	1D10	640	33.6	34.2	5.3
Instrumentation No. 2	1D20	1250	378.2	391.5	31.3
Optical Instrumentation No. 3	1D30	640	Not Instrumented		
Optical Instrumentation No. 4	1D40	1250	Not Instrumented		
Optical Instrumentation No. 5	1D50	1250	Not Instrumented		

NOTES:
1. Battery capacities are based on 10 minute discharge time.
2. Actual power consumption for Battery No. 1 was calculated from -50 seconds to S-IC/S-II stage separation.
3. Actual power consumption for Battery No. 2 was calculated from -50 to 210 seconds.

Table 13-2. S-II Stage Battery Power Consumption

BATTERY	BUS DESIGNATION	CAPACITY (AMP-HR)	*POWER CONSUMPTION			
			Sec AMP-HR	PERCENT OF CAPACITY	TEMPERATURE	
					MAX	MIN
Main	2D11	35	8.64	24.7	308°K (95°F)	304°K (87°F)
Instrumentation	2D21	35	11.1	31.7	312°K (101.5°F)	305°K (90°F)
Recirculation No. 1	2D51	30	5.21	17.4	302°K (84°F)	299°K (79°F)
Recirculation No. 2	2D51 and 2D61	30	5.25	17.5	301°K (83°F)	299°K (78.5°F)

* Power consumption calculated from -50 seconds (Power Transfer).

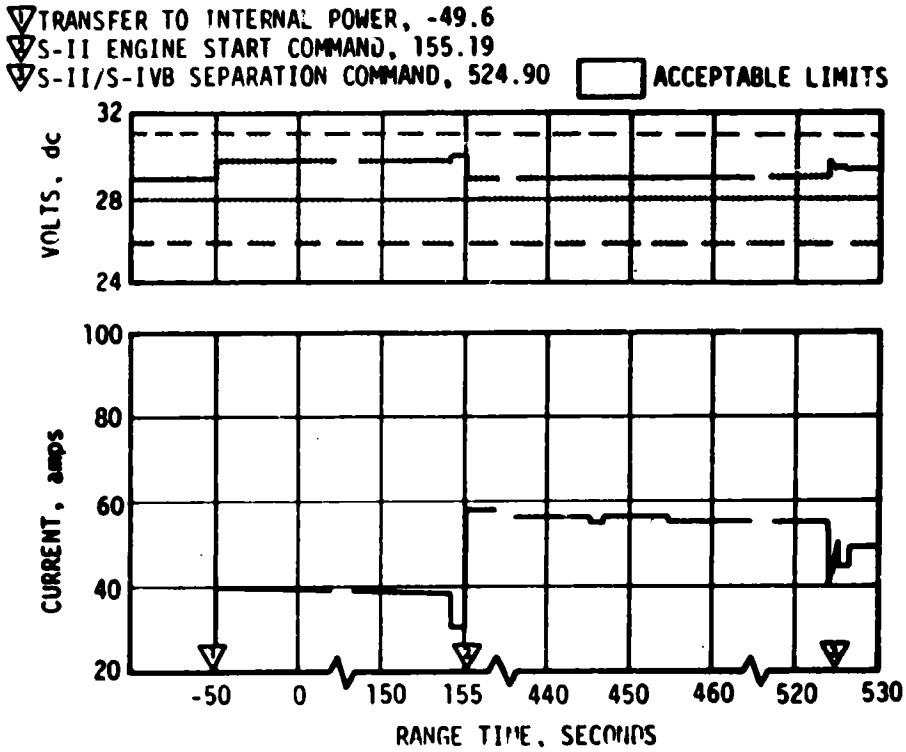

Figure 13-3. S-II Stage Main DC Bus Voltage and Current

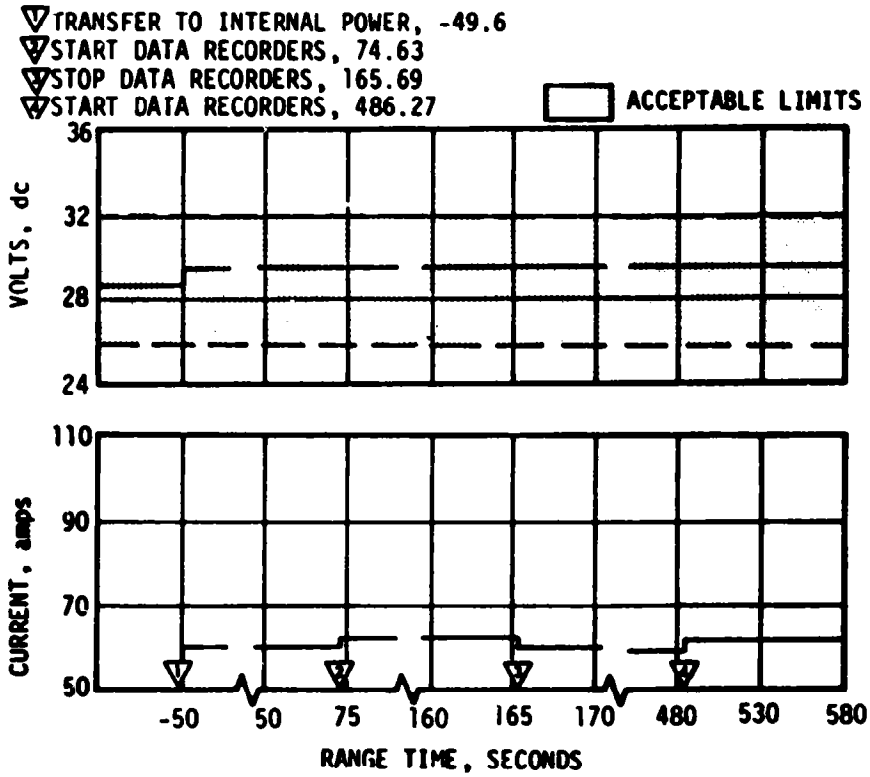

Figure 13-4. S-II Stage Instrumentation Bus Voltage and Current

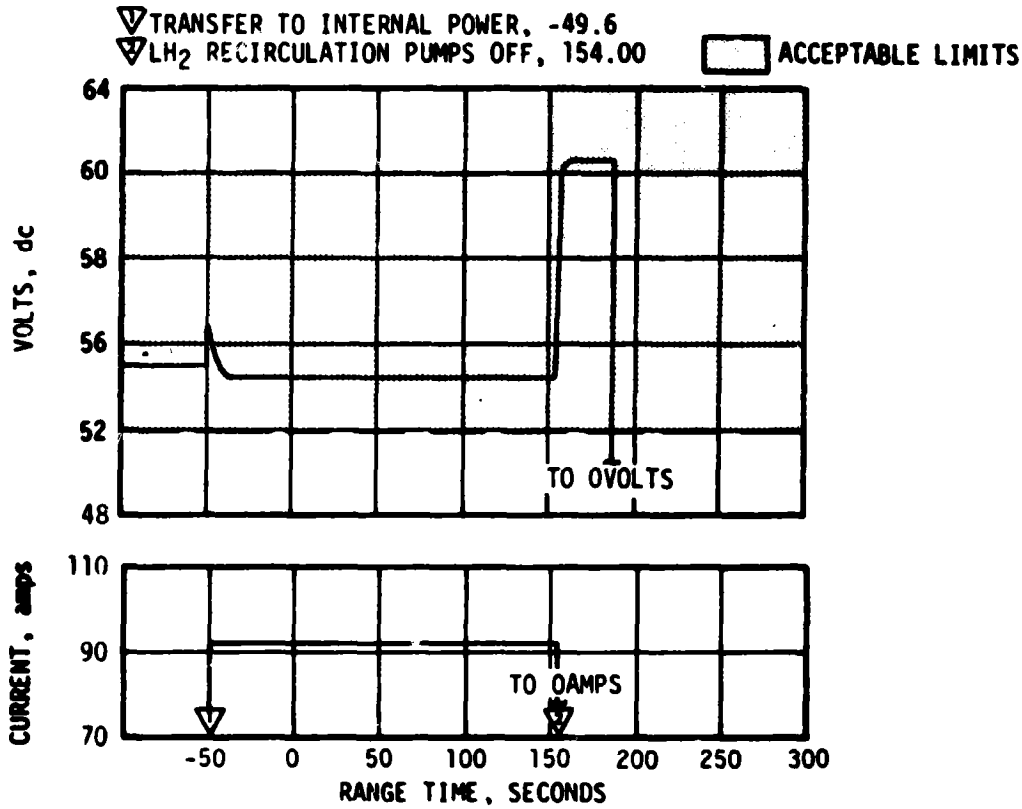

Figure 13-5. S-II Stage Recirculation DC Bus Voltage and Current

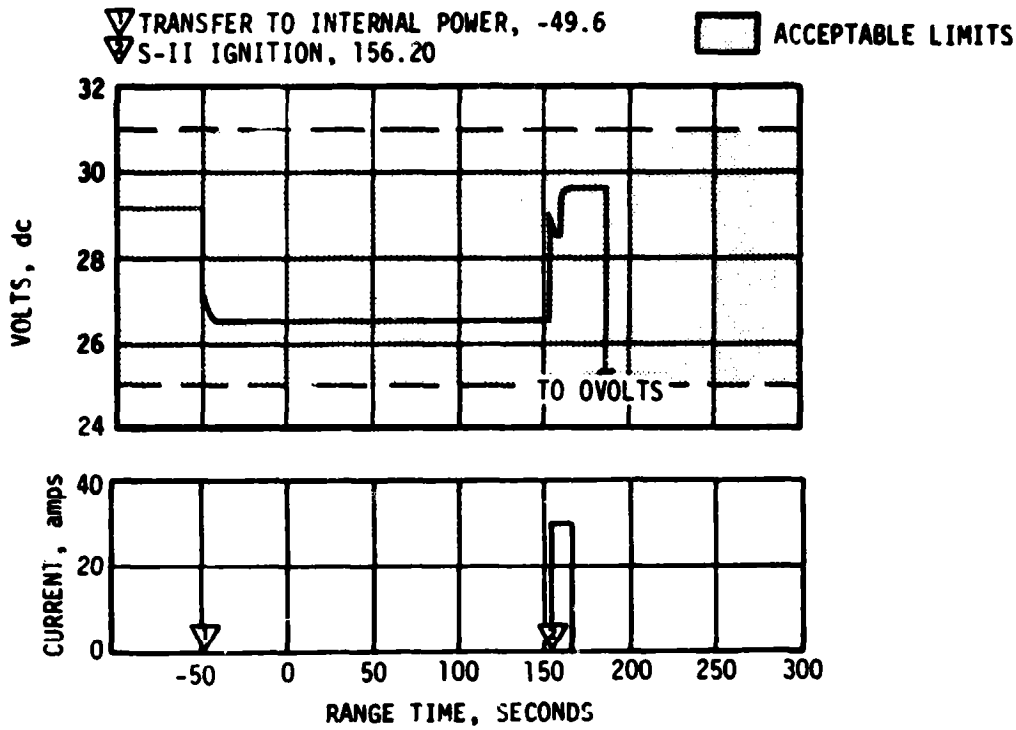

Figure 13-6. S-II Stage Ignition DC Voltage and Current

consumptions and temperatures were very close to those experienced on AS-502, except that percent usage of the two recirculation batteries was somewhat higher on AS-503.

Five 5-vdc power supplies furnish closely regulated voltages for stage instrumentation. The power supplies satisfactorily provided proper measuring voltage to the telemetry and other instrumentation.

Three of the 15 S-II temperature bridge power supplies operated intermittently for short periods, (see Figure 13-7) as follows:

BRIDGE POWER SUPPLY MEASUREMENT NO.	INTERMITTENT OPERATION, RANGE TIME, SECONDS	REMARKS
M046	71.5 to 95.0	During Max Q
M059	69.0 to 104.0	
M053	443.0 to 470.0	After low PU step

This deviation resulted in the temporary loss of various temperature measurements as detailed in paragraph 19.2.2. Indications are that the intermittent operation was caused by a dimensional tolerance buildup between the power supplies and the chassis, resulting in improper pin engagement of the mating connector (see Figure 13-8) during periods of higher than average vibration. Steps are being taken to correct this problem, but is is not considered a flight critical item.

The five LH_2 recirculation inverters which furnish power for the recirculation pumps operated properly during the J-2 engine chilldown period.

For the first time, two separate stage power supply sources (one on previous flights) were used to power the output section of the switch selector for increased reliability. Performance of the switch selector was excellent. Also for the first time, redundant power supply sources (one on previous flights) were used to electrically control the separation system relay circuitry for the two EBW firing units, which are associated with each separation system function. This redundancy was for increased reliability. The system is completely redundant except in the case of the all-engine-cutoff signals which are required for the trigger relay circuitry of S-II and S-IVB separation and retro motor ignition. These signals originate from either: (a) switch selector channel 18, all-engine cutoff, (b) LH_2 liquid level cutoff sensors dry (two out of five) or (c) LOX sensors dry (two out of five). On AS-503, these signals obtained power only from a single source, the main power bus. On subsequent flights, switch selector channel 18 all-engine cutoff relay circuitry will be powered from two separate power supply sources.

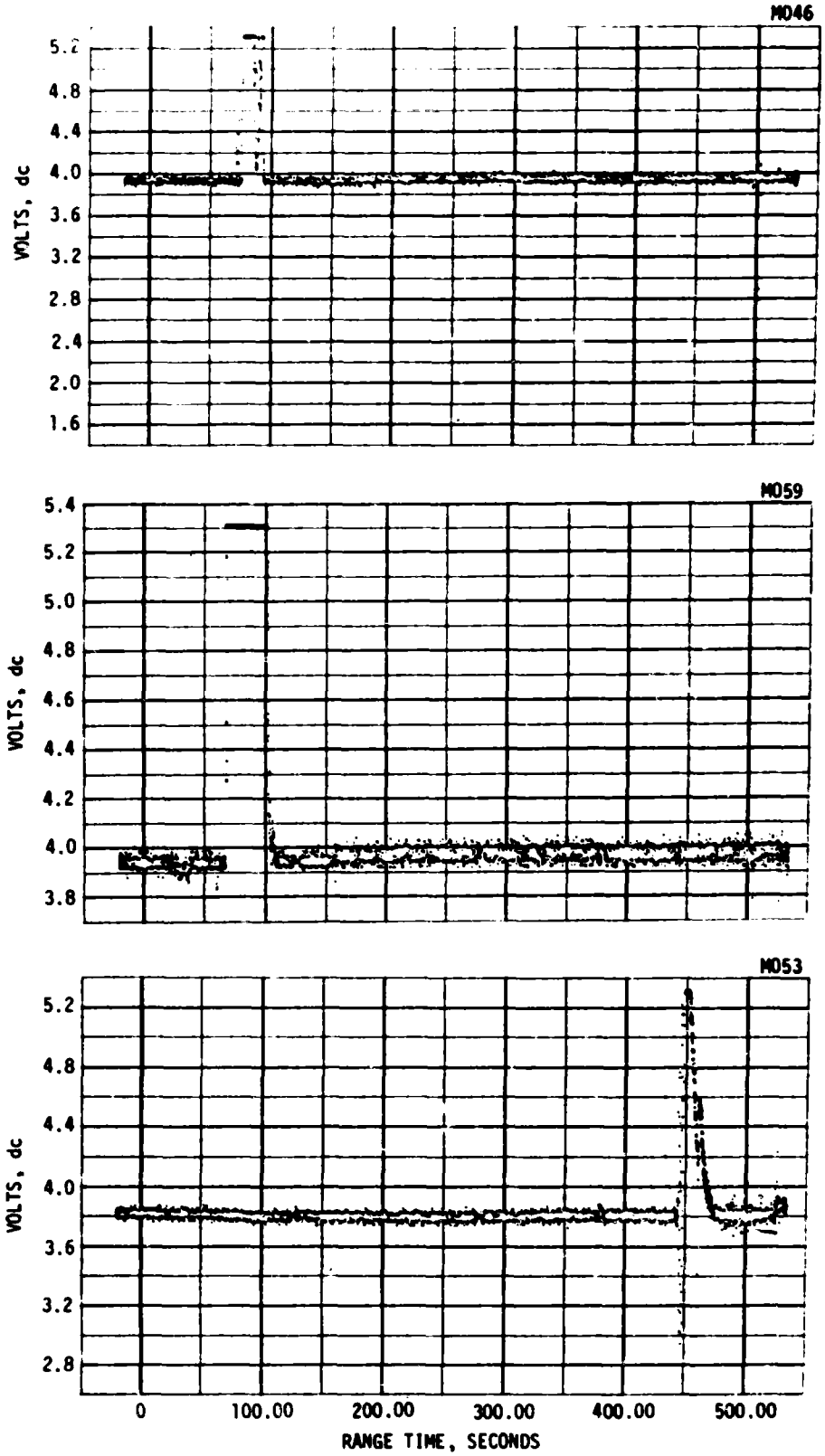

Figure 13-7. S-II Stage Temperature Bridge Power Supplies Voltage

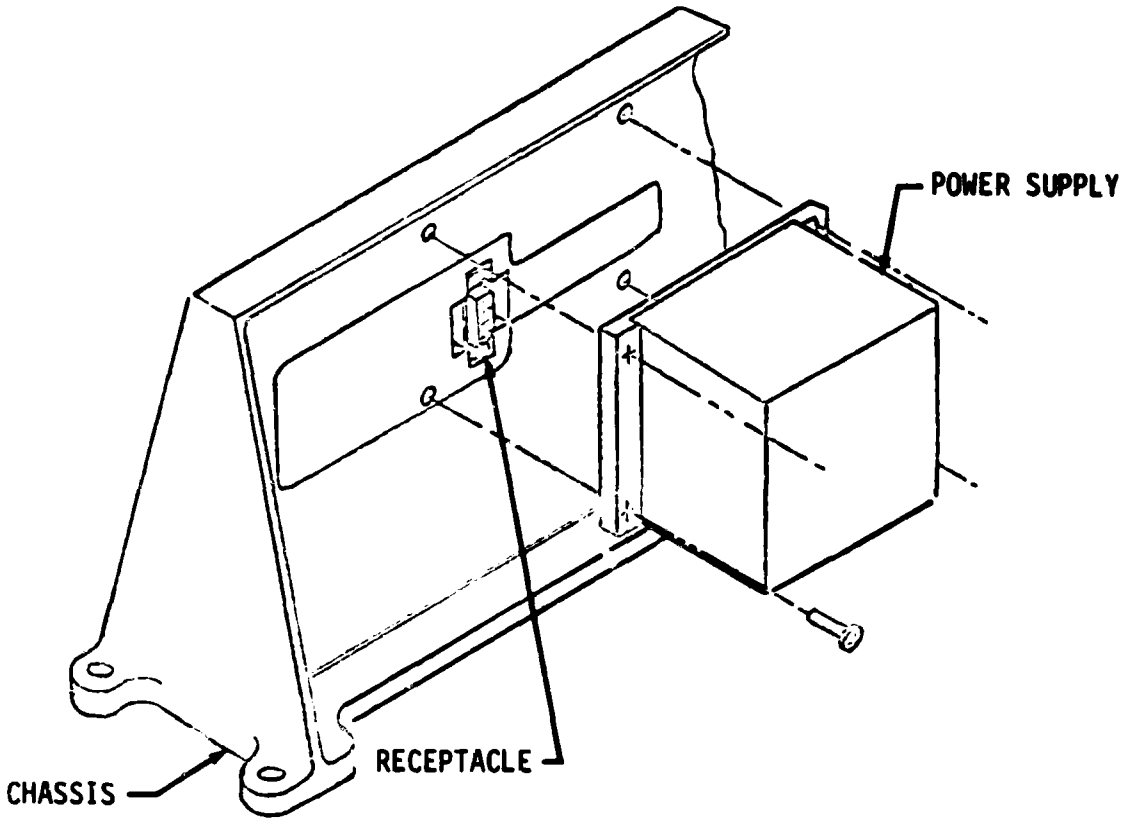

Figure 13-8. S-IVB Stage Bridge Power Supply Mounting and Chassis, Typical

Performance of the EBW circuitry for the separation system was satisfactory during the flight. EBW firing units charge and discharge responses were within predicted time and voltage limits.

13.4 S-IVB STAGE ELECTRICAL SYSTEM

The S-IVB stage electrical system includes three 28-vdc and one 56-vdc batteries to supply stage components through the power distribution system. The electrical system performed satisfactorily throughout all phases of flight and responded normally to IU commands.

In general, battery voltages, currents and temperatures stayed well within acceptable limits during boost and restart, as shown in Figures 13-9 through 13-12. Battery temperatures remained below the 322°K (120°F) limits for the powered portion of the flight (this limit does not apply after insertion into orbit). The highest temperature of 324°K (124°F) was reached on forward battery No. 2 during translunar coast (after injection).

S-IVB stage battery usage in ampere-hours and as a percent of rated capacity are given in Table 13-3. These parameters were within design limits. Forward battery No. 2 was expended at approximately 27,000 seconds, at which time the voltage was 24 vdc, one volt below minimum and falling rapidly.

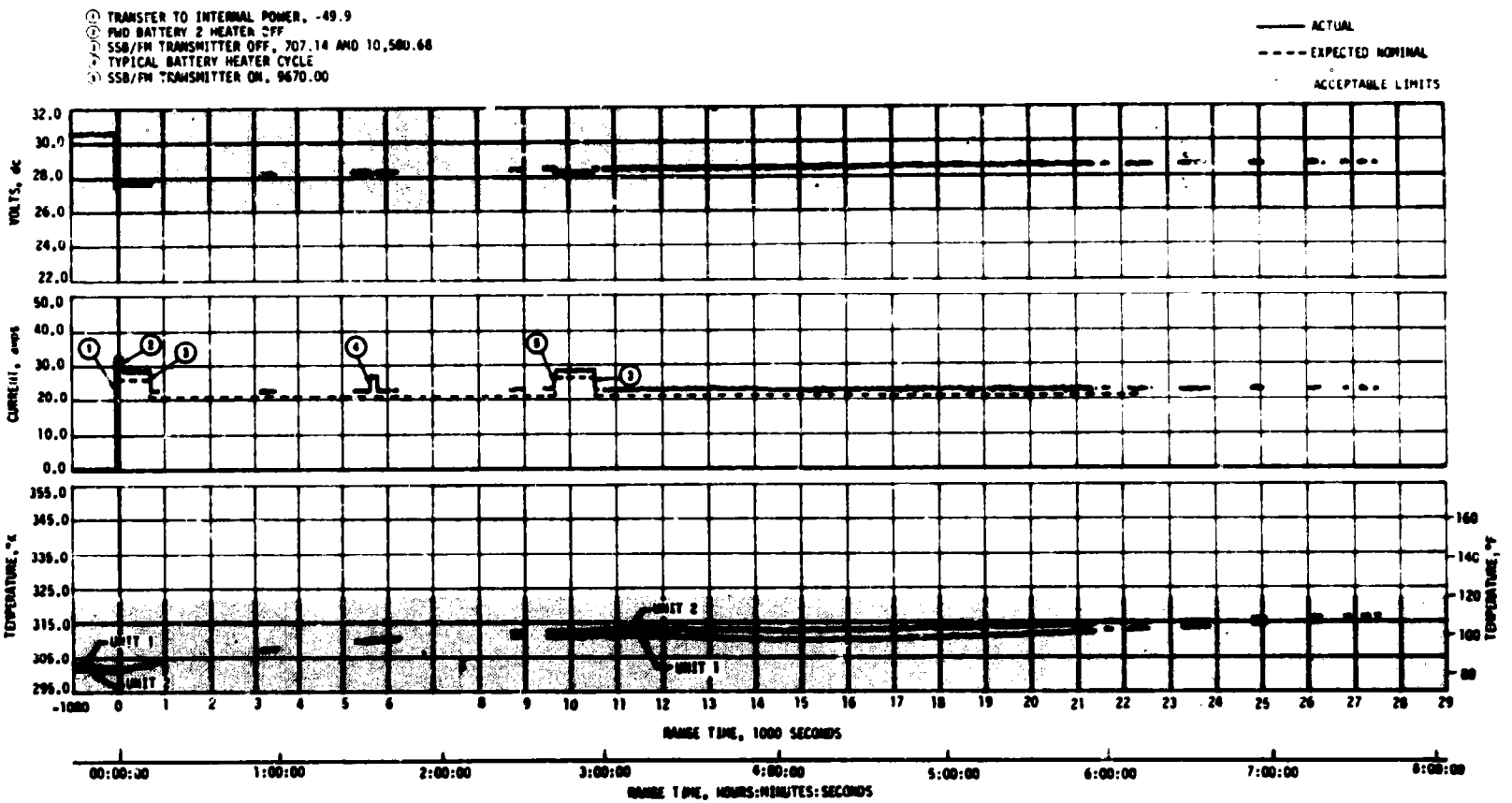

Figure 13-9. S-IVB Stage Fwd Battery No. 1 Voltage, Current, and Temperature

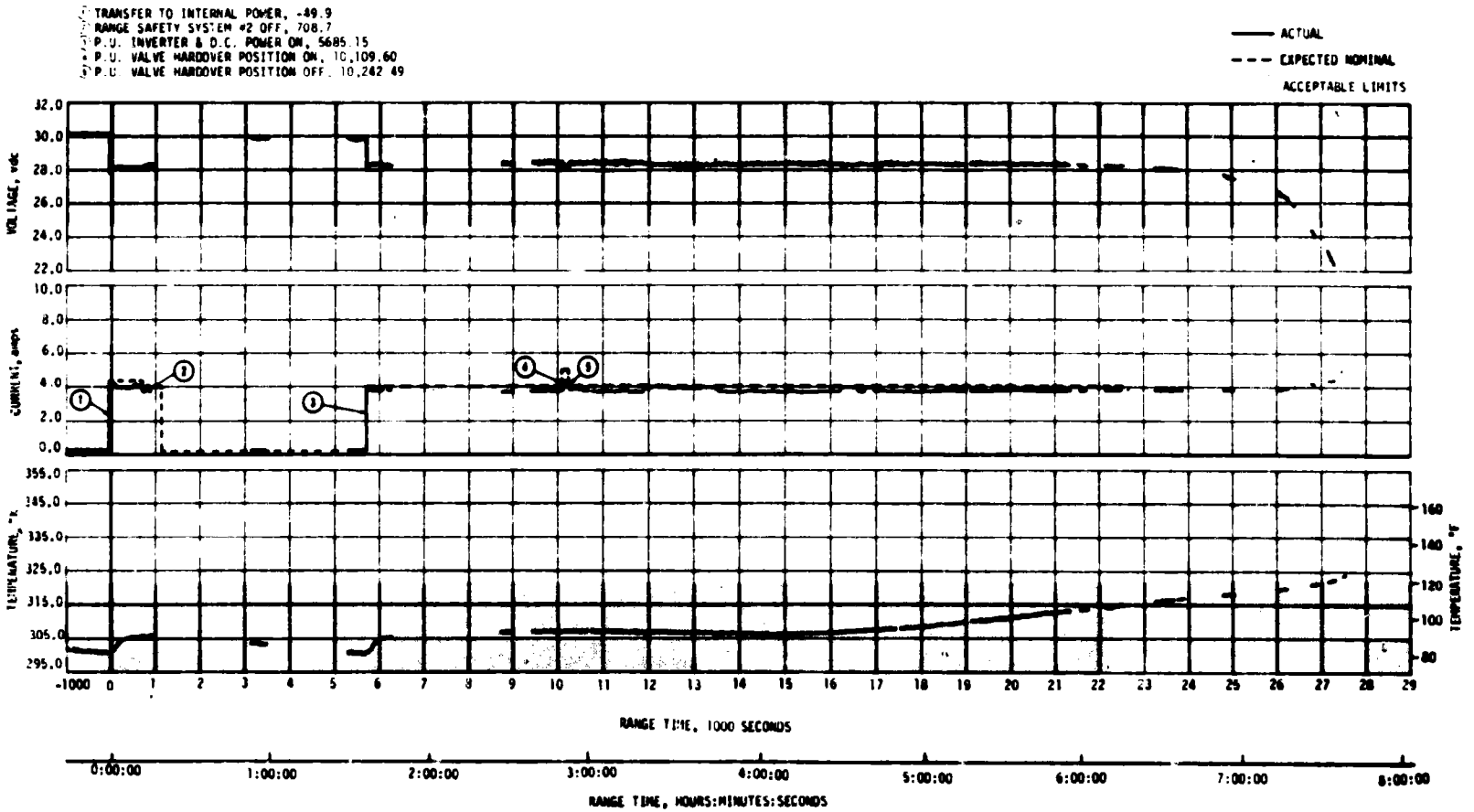

Figure 13-10. S-IVB Stage Fwd Battery No. 2 Voltage, Current, and Temperature

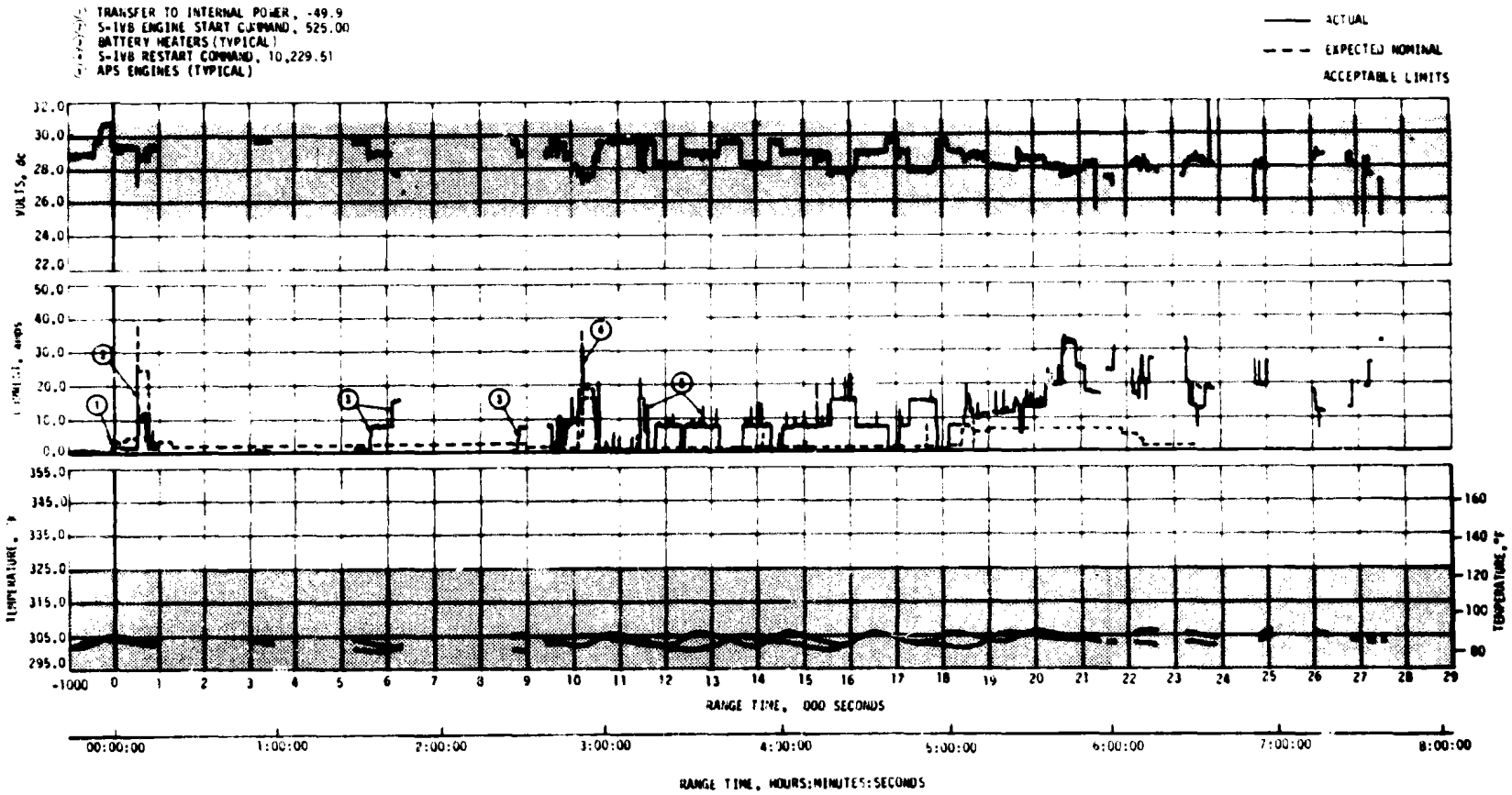

Figure 13-11. S-IVB Stage Aft Battery No. 1 Voltage, Current, and Temperature

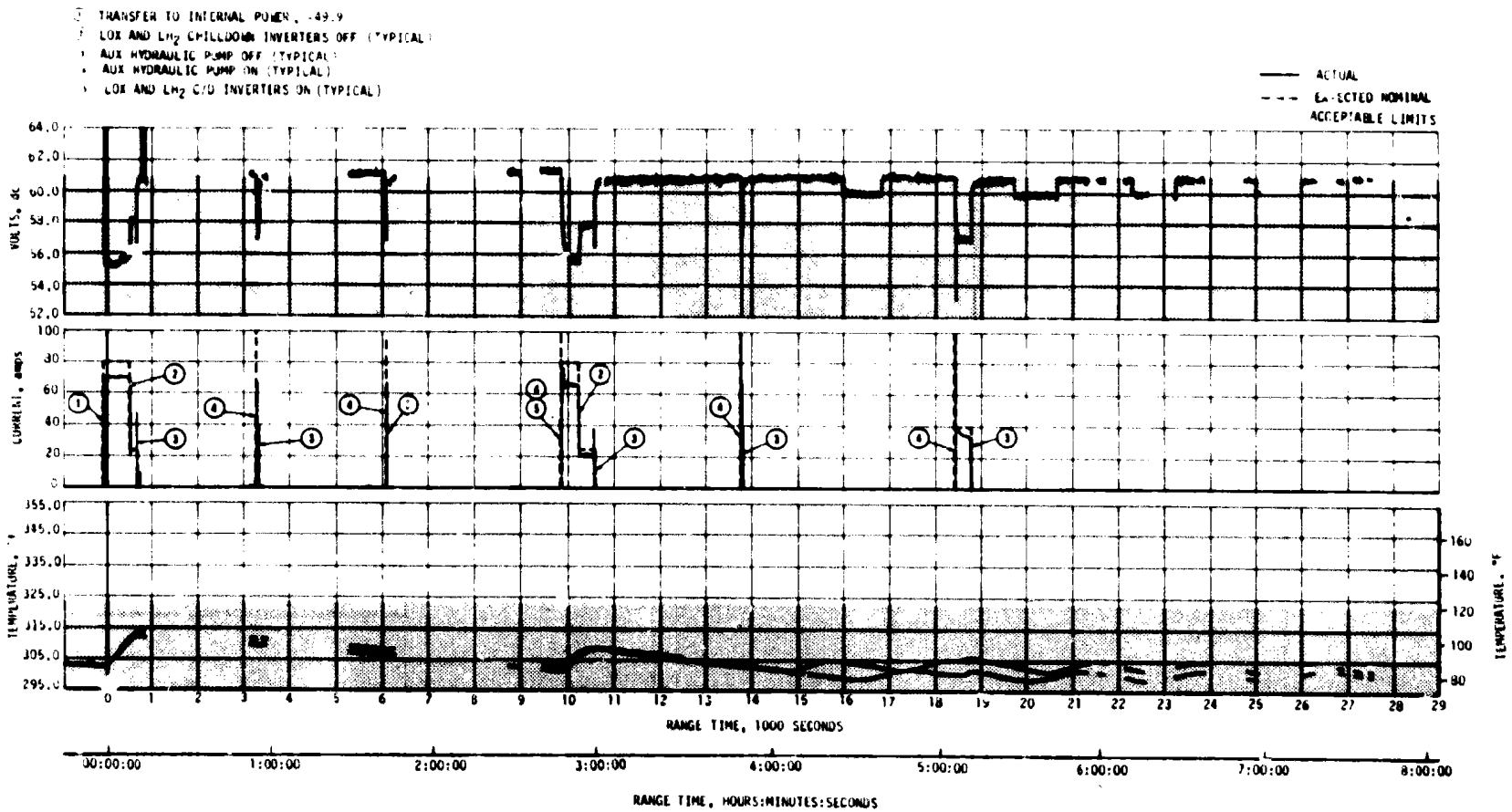

Figure 13-12. S-IVB Stage Aft Battery No. 2 Voltage, Current, and Temperature

Table 13-3. S-IVB Stage Battery Power Consumption

BATTERY	CAPACITY (AMP-HRS)	POWER CONSUMPTION		PERCENT OF CAPACITY
		MAXIMUM EXPECTED AMP-HRS	ACTUAL AMP-HRS	
Fwd No. 1	228	164	147	64
Fwd No. 2	25	25	24	96
Aft No. 1	228	58	46	20
Aft No. 2	67	40	33	49

NOTES:
1. Capacities are specification values.
2. Maximum expected power consumption based on maximum expected values for 6.5 hour flight.
3. Actual power consumption for Fwd 1, Aft 1 and Aft 2 based on 21,300 sec (5 hrs 55 min) of available flight data.
4. Actual power consumption for Fwd No. 2 based on 27,000 sec (7 hrs 30 min) of available flight data.

Three 5-volt excitation modules provide closely regulated measuring voltage to instrumentation measurement transducers and signal conditioners. Two of these modules are mounted forward and one aft. The two forward 5-volt excitation modules provided proper measuring voltage at 5 ±0.025 vdc. The aft 5-volt excitation module dropped below the minimum of 4.975 vdc to 4.970 vdc from approximately 9410 to 10,691 seconds. Since the 5 volt reference did not reflect the low voltage condition, it is likely that the 5-volt excitation module signal conditioning network experienced a slight degradation. The telemetry performance was not affected by the low voltage.

Eleven 20-vdc excitation modules provide signal conditioning power for event measurements, and excitation power for temperature and voltage measurements. The excitation modules performed satisfactorily. The LOX and LH_2 chilldown inverters which furnish power to the LOX and LH_2 recirculation pumps, performed in a satisfactory manner and met their load requirements.

In general, the PU system performed satisfactorily. However, during restart the PU static inverter/converter indicated positive level shifts (above its limits of 5 ±0.1 vdc and 400 ±6 Hz) during the PU hardover

mode of operation. Since the 117-vdc summing potentiometer loads are removed when the PU hardover command is initiated, the unregulated output of the oscillator module in the inverter/converter is affected, so that these shifts are to be expected and do not degrade PU system performance. The PU static inverter/converter also exhibited a positive out of level frequency shift for a short period during PU hardover operation on AS-501 and exceeded the upper voltage limit on AS-502 flight. Modifications to minimize the level shifts are being considered for AS-504 and subsequent vehicles.

The switch selector functioned correctly and all IU commands were properly executed.

All EBW firing units responded as predicted. The ullage motor ignition EBW firing units were charged at 484.99 seconds and fired at 524.78 seconds. The ullage motor jettison EBW firing units were charged at 533.80 seconds and fired at 536.80 seconds.

13.5 INSTRUMENT UNIT ELECTRICAL SYSTEM

The IU electrical system utilizes four 28-vdc batteries and a bus network to distribute power to the various IU components. The following configuration changes were made effective on S-IU-503 to enhance the reliability of the unit for manned flight.

a. A redundant power path was added to the Switch Selector stage verification circuitry.

b. Separate routing paths from primary power sources (batteries) to the Power Distributor were added.

c. All printed wiring boards that routed critical signals were redesigned by using a "double solder point" technique, to ensure greater reliability of solder connections.

d. A redundant power path was added to eliminate a single point failure possibility in the wiring of the Electrical Subsystem to the Control Signal Processor.

e. Addition of the O_2/H_2 burner malfunction signal from the S-IVB to the LVDA.

f. Addition of circuitry in the Control Distributor to provide spacecraft control of the IU Command Subsystem.

g. Addition of circuitry in the Control Distributor to provide commands to actuate bias currents in the Flight Control Computer.

IU electrical system data was available through approximately the first 5.9 hours (21,240 seconds) of flight. Based on this data, the electrical system as modified for AS-503 operated satisfactorily. Battery voltages, and currents remained well within predicted limits as shown in Figures 13-13 through 13-16. As expected, voltages increased in proportion to battery temperature increases, ranging from approximately 27.5 vdc during launch to 28.8 vdc and after 5.9 hours (21,240 seconds) of flight. Highest current drain (35 amperes) was on the 6D30 battery, which also registered the greatest temperature increase, from 291°K to 314.5°K (64.4°F to 105.7°F).

Battery usage, in ampere-hours and as a percent of rated capacity, was well within design limits, as shown in Table 13-4.

Table 13-4. IU Battery Power Consumption

BATTERY	BUS DESIG-NATION	CAPACITY (AMP-HRS)	POWER CONSUMPTION		AVERAGE CURRENT (AMPS)	PREDICTED LIFE (HRS)
			AMP-HRS	PERCENT OF CAPACITY		
No. 1	6D10	350	192.3	54.9	32.6	10.74
No. 2	6D20	350	200.6	57.3	34.0	10.29
No. 3	6D30	350	209.4	59.8	35.5	9.86
No. 4	6D40	350	177.0	50.6	30.0	11.67

NOTES:
1. Capacity based upon 10.0 hours operation at 35 amp discharge rate.
2. Actual power consumption based upon 5.9 hours operation from range zero.

Analysis of the voltage trace envelope indicates that the 56-volt power supply, which supplies voltage to the gyro, accelerometer servoloops and accelerometer signal conditioner, remained well within the limits of 56 ±2.5 vdc.

The 5-volt measuring reference voltage supply measurements indicated approximately 5.04 vdc output, which is above the design specifications of 5.000 ±0.005 vdc. However, the telemetry tolerance of 0.8 percent could account for the out of limits condition and telemetry data showed no detectable inaccuracies.

Available data indicates that the IU switch selector performed nominally throughout the flight.

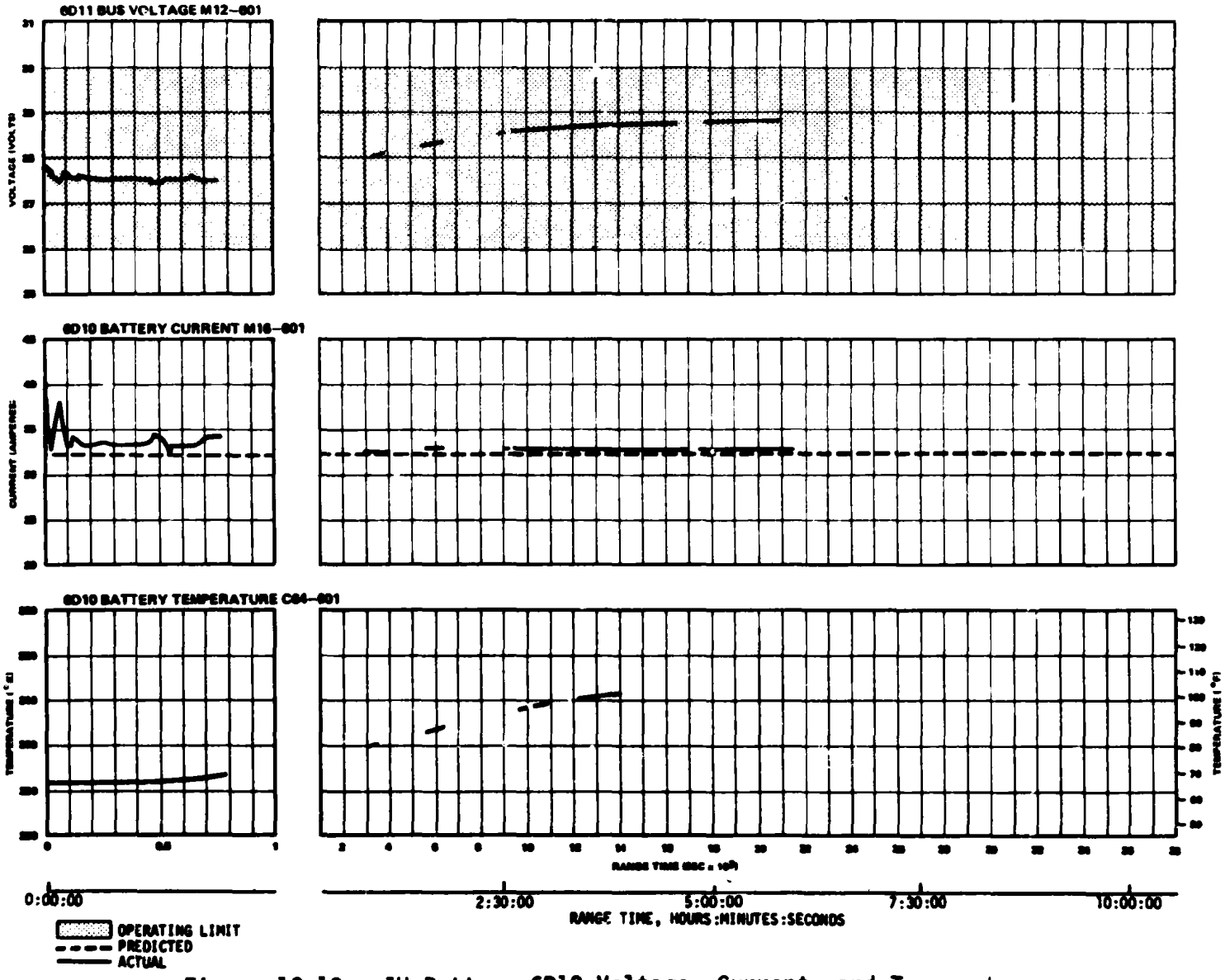

Figure 13-13. IU Battery 6D10 Voltage, Current, and Temperature

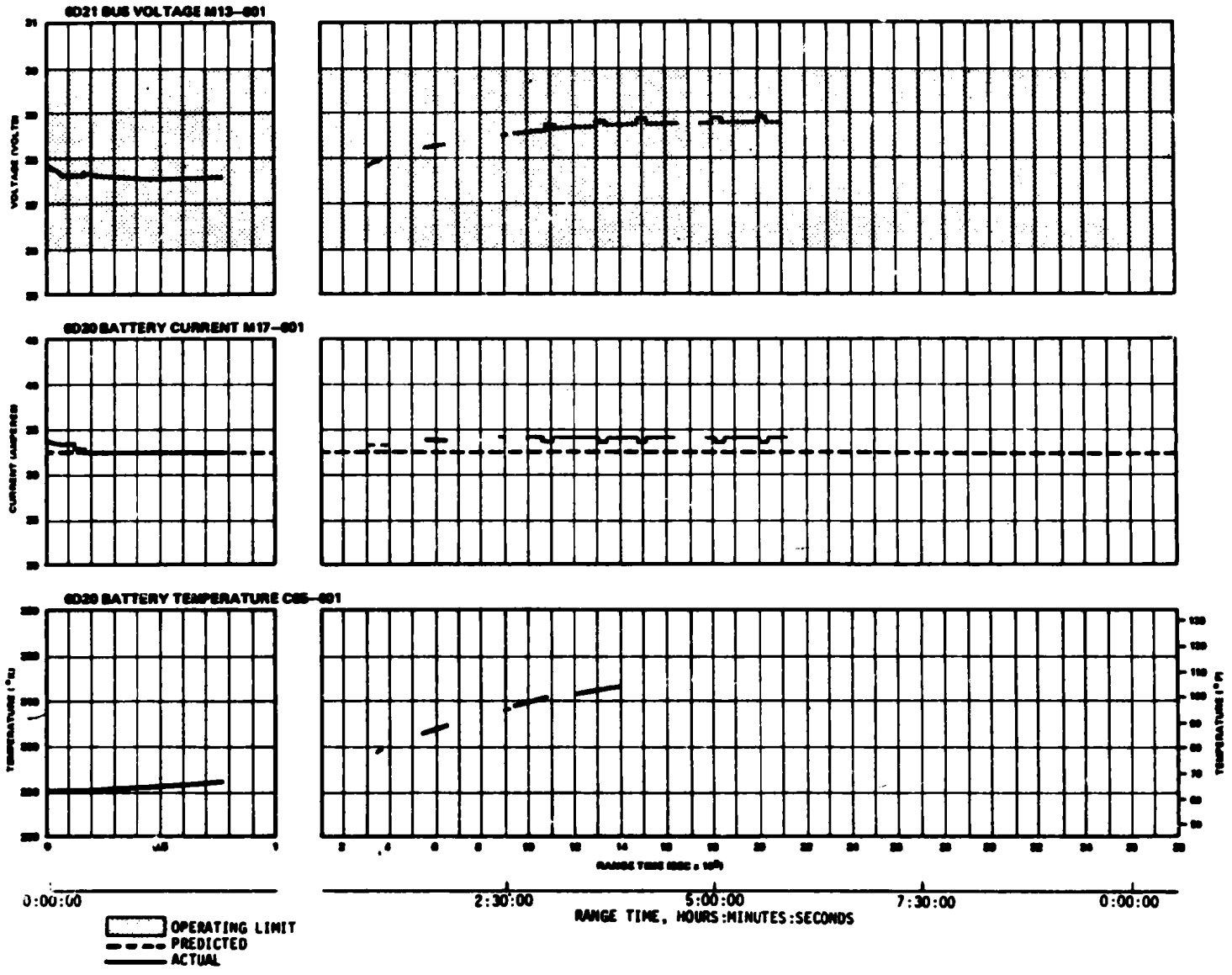

Figure 13-14. IU Battery 6D20 Voltage, Current, and Temperature

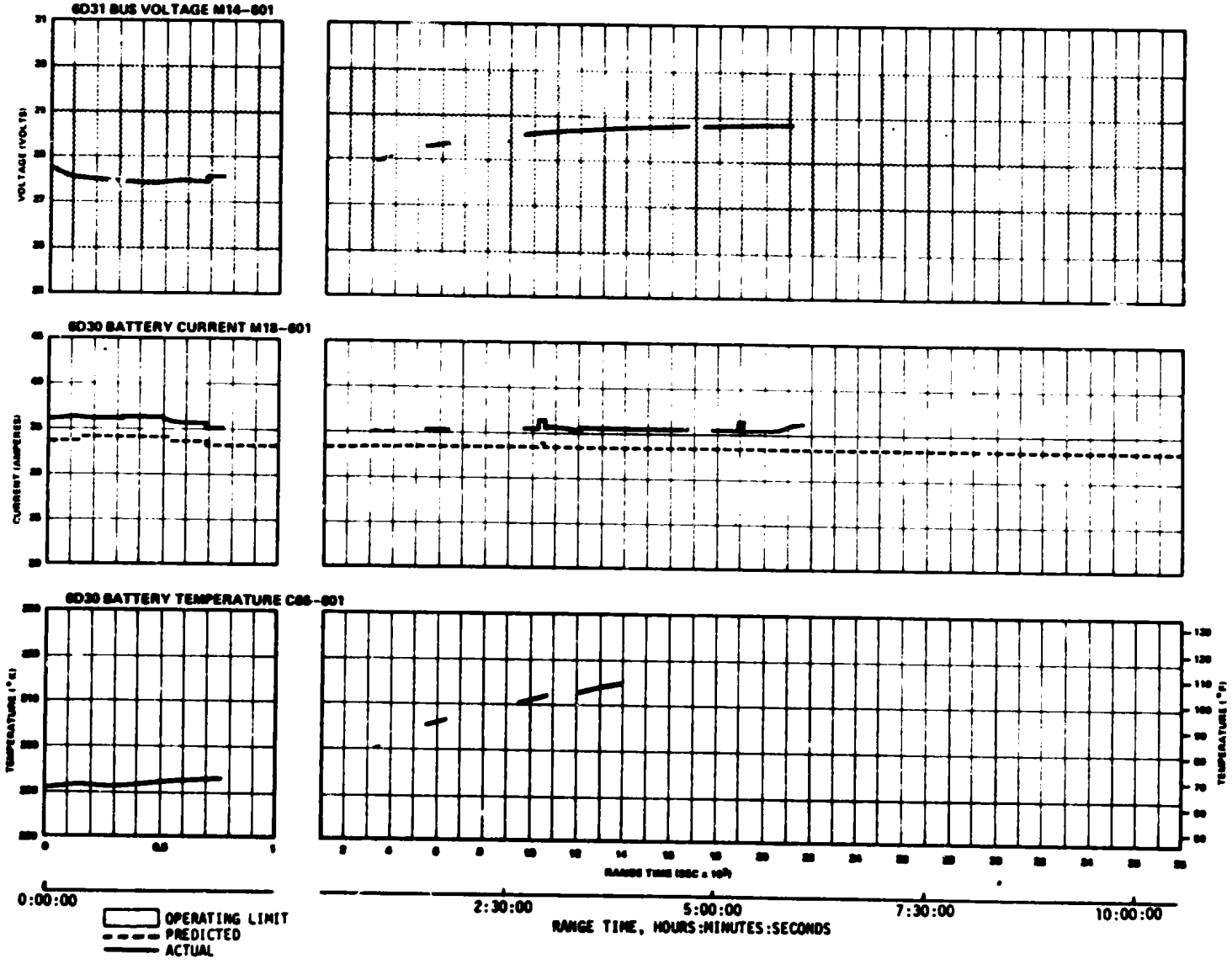

Figure 13-15. IU Battery 6D30 Voltage, Current, and Temperature

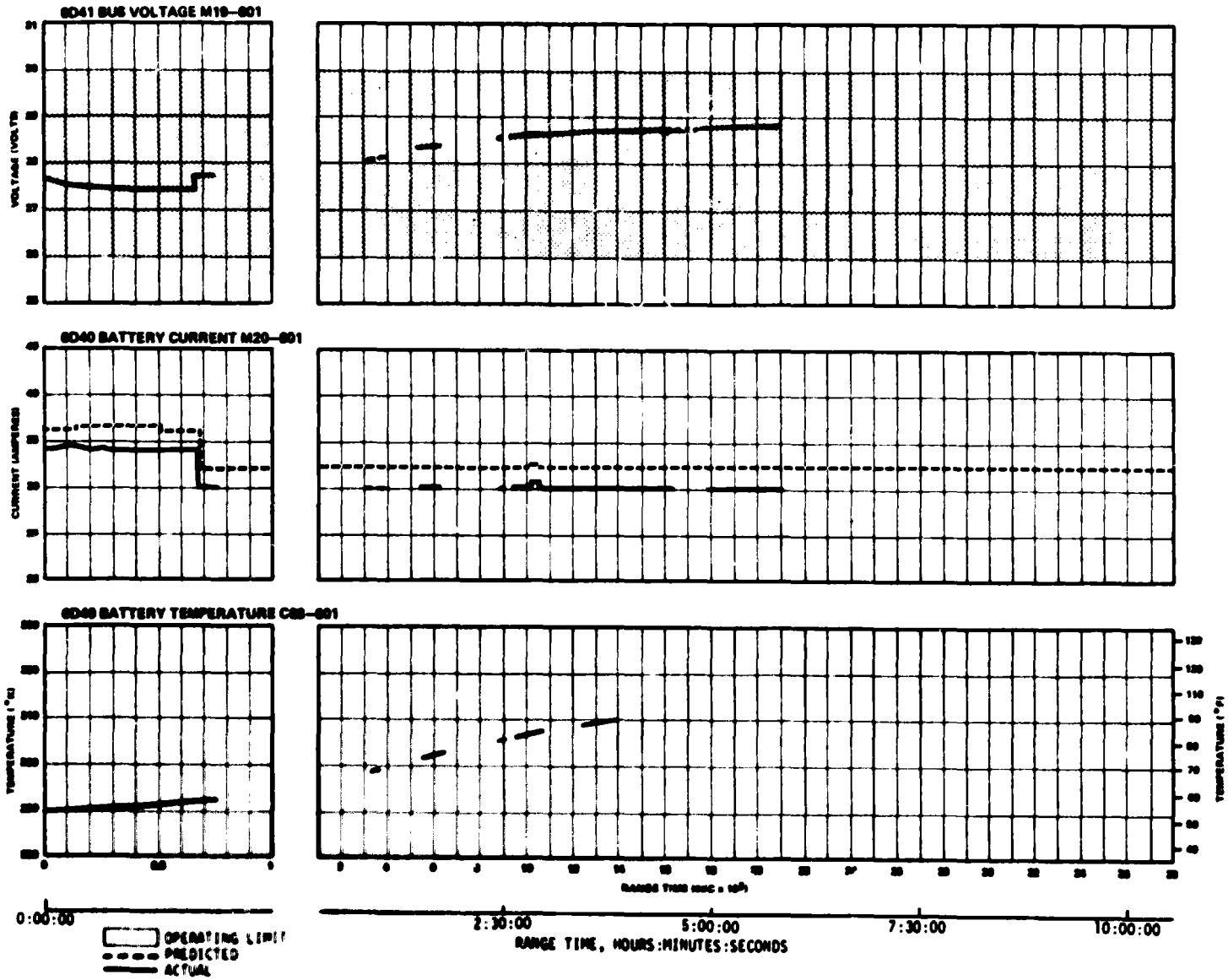

Figure 13-16. IU Battery 6D40 Voltage, Current, and Temperature

SECTION 14

RANGE SAFETY AND COMMAND SYSTEMS

14.1 SUMMARY

Data indicated that the redundant Secure Range Safety Command Systems (SRSCS) on the S-IC, S-II, and S-IVB stages were ready to perform their functions properly on command if flight conditions during the launch phase had required vehicle destruct. The system properly safed the S-IVB SRSCS on command from Kennedy Space Center (KSC). The performance of the Command and Communications System (CCS) in the Instrument Unit (IU) was satisfactory.

14.2 RANGE SAFETY COMMAND SYSTEMS

The SRSCS provides a means to terminate the flight of the vehicle by radio command from the ground in case of emergency situations in accordance with range safety requirements. After successful insertion into earth orbit, the system is deactivated (safed) by ground command. Each powered stage of the vehicle was equipped with two command receivers/decoders and necessary antennas. The SRSCS in each stage was completely independent of those in other stages.

Three types of SRSCS commands were programmed for this manned flight as follows:

a. Arm/fuel cutoff - Charging of the Exploding Bridge Wire (EBW) firing unit and thrust termination.

b. Destruct - Propellant dispersion by firing of the EBW.

c. Safe - Command system switched off.

During flight, telemetry indicated that the command antennas, receivers/decoders, and destruct controllers functioned properly and were in the required state of readiness if needed. Since no arm/cutoff or destruct commands were required, all data except receiver signal strength remained unchanged during the flight. At 708.7 seconds the safing command was initiated, deactivating the system. Both S-IVB stage systems, the only systems in operation at this time, responded properly to the safing command.

Radio Frequency (RF) performance aspects of the system are discussed in Section 19, paragraph 19.5.3.1.

14.3 COMMAND AND COMMUNICATIONS SYSTEM

Oral reports from Mission Control Center (MCC)/Houston indicate that the command section of the CCS performed satisfactorily. All commands transmitted during this mission were sent from Guaymas (GYM) after S-IVB second burn as indicated in Table 14-1. A total of 2626 known command words, all of which were in connection with the CCS test, were sent as follows:

a. Fourteen CCS antenna switching commands (one command word each) were transmitted by the ground station to select omnidirectional, low gain directional or high gain directional antennas. The CCS antenna switching commands also switched the Pulse Code Modulation (PCM) antennas.

b. Fifty-one Special Test Pattern (STP) sequences consisting of 51 identical words each (total 2601 words) were transmitted by the ground station.

c. Eleven terminate commands, consisting of one command word each, were transmitted by the ground station.

The CCS low gain directional antenna and the CCS high gain directional antenna were also selected by programmed switching at 11,756 seconds (3:15:56) and 19,636 seconds (5:27:16), respectively.

Unofficial sources in Houston have stated that several commands had to be retransmitted, as shown in Table 14-1, because of inability to establish down link lock, during times of low signal strength, on the UHF telemetry link used to verify commands during the translunar coast period. No attempts were made to transmit commands after 21,730 seconds (6:02:10) due to increasing difficulties experienced in obtaining verification pulses occasioned by UHF down link lock problems discussed above.

Good correlation cannot be made with the commanded switch selector events shown in Section 2, Table 2-4, due to the incomplete listing in Table 2-4. and the absence of some ground station command history.

RF performance of the system is discussed in Section 19, paragragh 19.5.3.1.

Table 14-1. Command and Communications System Command History, AS-503

RANGE TIME Seconds (HRS:MIN:SEC)		COMMAND	ANTENNA SELECTED
From	To		
13,500 (3:45:00)	13,830 (3:50:30)	STP every 30 seconds (12 patterns)	Low Gain
18,990 (5:16:30)		Terminate Command Uplink	Low Gain
19,025 (5:17:05)		Switch to Omni	Omni
19,080 (5:18:00)		Switch to Low Gain (3 Commands)	Low Gain
19,140 (5:19:00)	19,620 (5:27:00)	STP every 30 seconds (14 patterns)	Low Gain
19,680 (5:28:00)	19,650 (5:27:30)	STP every 30 seconds (9 patterns)	High Gain
19,942 (5:32:22)		Terminate Command Uplink	High Gain
20,430 (5:40:30	20,730 (5:45:30)	STP every 30 seconds (11 patterns)	High Gain
21,060 (5:51:00)		Terminate Command Uplink	High Gain
21,116 (5:51:56)		Switch to Low Gain (2 Commands)	Low Gain
21,300 (5:55:00)	21,480 (5:58:00)	STP every 30 seconds (5 patterns)	Low Gain
21,519 (5:58:39)		Terminate Command Uplink (4 Commands)	Low Gain
21,550 (5:59:10)		Switch to Omni (4 Commands)	Omni

Table 14-1. Command and Communications System Command History, AS-503 (Continued)

RANGE TIME Seconds (HRS:MIN:SEC)		COMMAND	ANTENNA SELECTED
From	To		
21,591 (5:59:51)		Terminate to clear (4 Commands)	
21,700 (6:01:40)		Terminate Command Uplink (4 Commands)	Omni
21,730* (6:02:10)		Switch to High Gain (4 Commands)	High Gain

* The CCS test was terminated at 21,730 seconds (6:02:10) due to loss of UHF lock and the subsequent loss of verification pulses. Corpus Christi (TEX) verified that the antenna was on high gain at 22,260 seconds (6:11:00).

SECTION 15

EMERGENCY DETECTION SYSTEM

15.1 SUMMARY

The AS-503 Emergency Detection System (EDS) configuration was essentially the same as AS-502 except that:

a. The presence of the crew provided the capability for EDS manual abort.

b. There was a display of launch vehicle tank pressures in the spacecraft.

The EDS performance was nominal; no abort limits were reached.

15.2 SYSTEM DESCRIPTION

The EDS provided for automatic abort during S-IC burn by monitoring two parameters: two or more S-IC engines out and excessive angular rates. In addition, the following parameters were displayed to the crew for manual abort cues:

a. Angle-of-attack (Q-Ball dynamic pressure).

b. S-IC engines status (Thrust OK pressure switch discretes).

c. S-II engines status (Thrust OK pressure switch discretes).

d. S-IVB engine status (Thrust OK pressure switch discretes).

e. Staging functions (Stage separation discretes).

f. Angular overrates (P, Y, R overrate discretes).

g. Launch vehicle attitude reference failure (Platform gimbal angle discrete).

h. S-IVB propellant tank pressures (orbital phase).

i. Vehicle attitudes, attitude rates, attitude errors (spacecraft sensed).

15.3 SYSTEM EVALUATION

15.3.1 General Performance

All parameters monitored by the EDS remained well within design limits for the proper time periods throughout flight and all discrete indications occurred as expected.

15.3.2 Propulsion System Sensors

Three thrust OK pressure switches are used on each F-1 engine and two on each J-2 engine. The F-1 thrust OK switches are voted two out of three for both thrust OK (switches closed) and thrust not OK (switches open) indications. The J-2 thrust OK switches are voted one out of two for thrust OK (switches closed) and two out of two for thrust not OK (switches open) indications.

All thrust OK pressure switches actuated within predicted times during engine startup and shutdown. There were no premature engine cutoffs as on AS-502 flight. Thrust switch operation times are shown in Table 15-1.

15.3.3 Angular Overrates

Angular rates are sensed by three rate gyros in each axis. Outputs of the gyros are fed through filters to rate switches. When two out of three rate switches in any one axis indicate an overrate, an indication is given to the spacecraft. Abort is automatic until just prior to S-IC Inboard Engine Cutoff (IECO), after which abort is initiated manually at the discretion of the crew.

Table 15-2 shows a tabulation of maximum angular rates reached on the AS-503 flight, with abort limits in parenthesis.

15.3.4 Angle-of-Attack

The angle-of-attack dynamic pressure is sensed by a Q-Ball with redundant outputs. One output is displayed in and telemetered from the spacecraft; the other is telemetered from the Instrument Unit (IU).

The angle-of-attack abort limit was 2.2 N/cm^2 (3.2 psid) on AS-503. The maximum delta pressure recorded on the flight was 0.48 N/cm^2 (0.7 psid) at approximately 75 seconds.

15.3.5 Tank Pressures

The S-IVB LOX hydrogen tank ullage pressures were displayed to the crew during orbital operations. The common bulkhead pressure differential abort limits are +24.8 and -17.9 N/cm^2 (+36 and -26 psid) ($P_{LOX}-P_{LH2}$). The AS-503 pressures remained within these limits.

Table 15-1. Performance Summary of Thrust OK Pressure Switches

STAGE	ENGINE	SWITCH	TIME CLOSED (RANGE TIME, SEC)	TIME OPENED (RANGE TIME, SEC)
S-IC	1	1	-1.85	153.99
	1	2	-1.86	153.99
	1	3	-1.84	153.99
	2	1	-1.48	153.99
	2	2	-1.48	153.99
	2	3	-1.44	153.99
	3	1	-1.88	153.99
	3	2	-1.81	153.99
	3	3	-1.85	153.99
	4	1	-1.41	153.97
	4	2	-1.40	153.97
	4	3	-1.40	153.97
	5	1	-2.21	126.14
	5	2	-2.24	126.14
	5	3	-2.24	126.14
S-II	1	1	157.94	524.24
	1	2	157.96	524.24
	2	1	158.02	524.24
	2	2	158.05	524.24
	3	1	157.94	524.23
	3	2	157.96	524.27
	4	1	157.94	524.24
	4	2	157.90	524.20
	5	1	157.94	524.24
	5	2	157.95	524.26
S-IVB 1ST BURN	1	1	529.78	685.18
	1	2	529.78	685.18
S-IVB 2ND BURN	1	1	10,239.34	10,555.73
	1	2	10,239.34	10,555.73

15.3.6 EDS Sequential Events

All EDS discrete events and indications occurred as expected. Table 15-3 shows significant EDS related event times.

Table 15-2. Maximum Angular Rates

PHASE	PITCH	YAW	ROLL
S-IC burn	-1.0 (4) deg/s	±0.6 (4) deg/s	+1.3 (20) deg/s
Upper stages	-1.3 (9.2) deg/s	+0.1 (9.2) deg/s	+1.4 (20) deg/s

Note: Abort limits are shown in parentheses.

Table 15-3. EDS Related Event Times

FUNCTION	STAGE	RANGE TIME (s)	TIMES FROM BASE
Launch Vehicle Engines EDS Cutoff Enable (Timer)	IU	30.44	T_1+29.77
Launch Vehicle Engines EDS Cutoff Enable (Switch Selector)	IU	30.62	T_1+29.95
S-IC Two Engines Out Auto-Abort Inhibit	IU	125.13	T_1+124.45
Excess Rate (P, Y, R) Auto-Abort Inhibit and Switch Rate Gyros SC Indication A	IU	125.53	T_1+124.85
Excess Rate (Roll) Auto-Abort Inhibit and Switch Rate Gyros SC Indication B	IU	126.84	T_2+0.96
Launch Escape Tower Jettison	Spacecraft	188.6	T_3+34.78

SECTION 16

VEHICLE PRESSURE AND ACOUSTIC ENVIRONMENT

16.1 SUMMARY

The vehicle internal, external, and base region pressure environments were monitored by a series of differential and absolute pressure gages. These measurements were used in confirming the vehicle external, internal, and base region design pressure environments. The flight data were generally in good agreement with the predictions and compared well with previous flight data. The pressure environment was well below design levels.

The vehicle internal and external acoustic environment was monitored by a series of microphones positioned to measure both the rocket engine and aerodynamically induced fluctuating pressure levels. The measured acoustic levels were generally in good agreement with the liftoff and inflight predictions, and with data from previous flights.

16.2 SURFACE PRESSURES AND COMPARTMENT VENTING

16.2.1 S-IC Stage

External and internal pressure environments on the S-IC stage were recorded by 43 measurements located on and inside the engine fairings, aft skirt, intertank, and forward skirt. Representative data from a portion of these instruments are compared with AS-501 and AS-502 data and with AS-503 predictions in Figures 16-1 through 16-4. Static pressure is presented as the difference between measurement pressure and free stream static pressure (Pint-Pamb). Pressure loading is the difference between structural internal and external pressures defined such that a positive loading is in the outward direction. The predictions are based on available wind tunnel data and values from the Observed Mass Point Trajectory (OMPT). The ambient pressure history of AS-503 is virtually the same as that for AS-502 and slightly greater, approximately 0.10 N/cm^2 (0.145 psid), than for AS-501.

The AS-503 S-IC engine fairing compartment pressure differentials are shown in Figure 16-1. The AS-503 data agree very well with AS-501 and AS-502 data and the trends are the same.

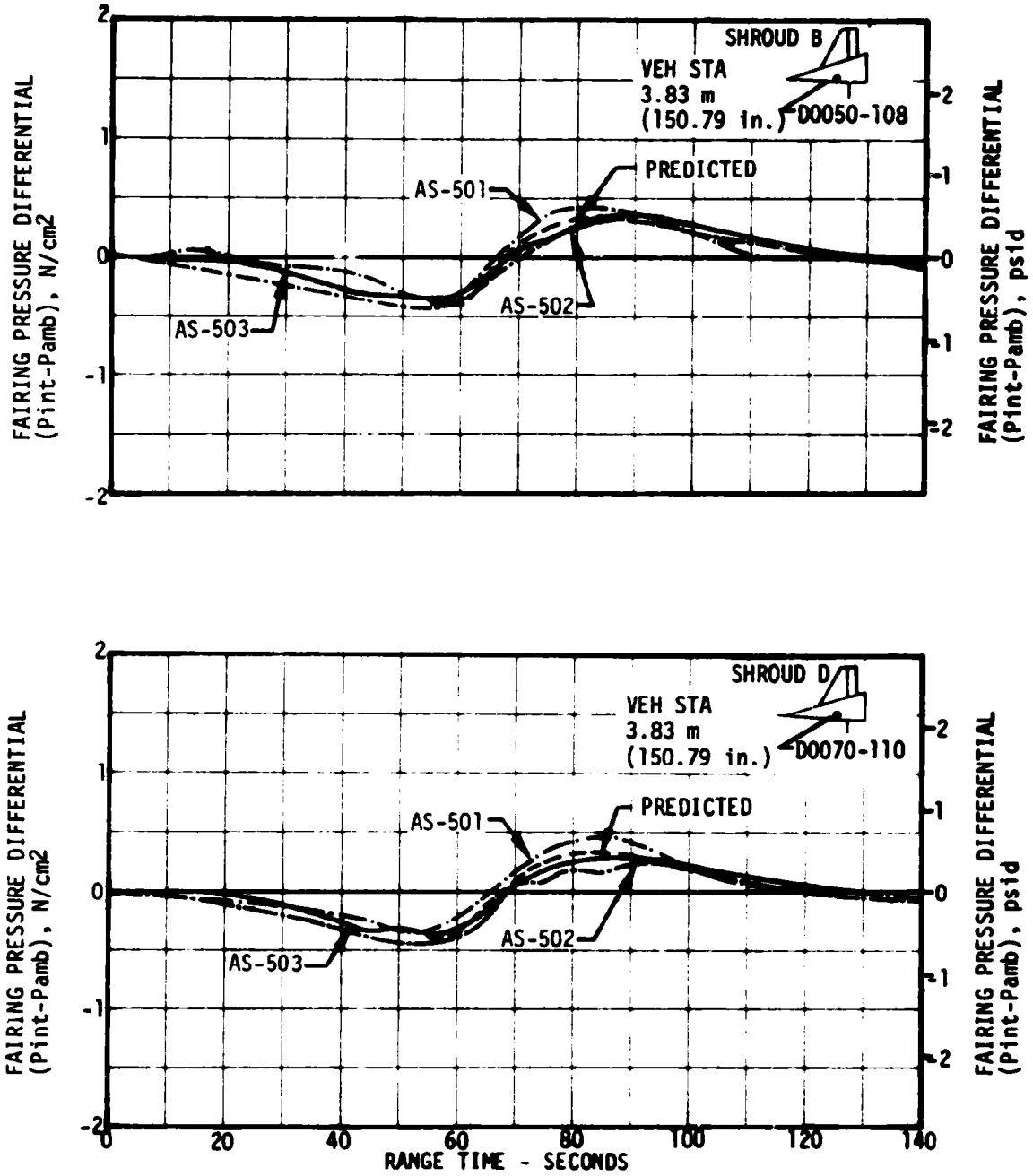

Figure 16-1. S-IC Engine Fairing Compartment Pressure Differential

The S-IC engine fairing pressure loading is shown in Figure 16-2. The AS-503, AS-502, and AS-501 data agree very well in magnitude and trend. The fairings experienced a crush loading over almost the entire flight. This is due to their geometry which deflected the air stream away from the S-IC engines.

The S-IC engine, intertank, and forward skirt compartment pressure differentials are shown in Figure 16-3 as a function of range time. The AS-503 engine compartment differential pressure levels were less than those on AS-501 and AS-502. Fuel line boots were omitted on AS-503 and the resulting increase in engine compartment leakage area probably accounted for the lower internal pressure. The intertank pressure differential agreed very well with AS-501 and AS-502 as a function of range time. The forward skirt compartment differential pressure levels were higher than those of AS-501 and AS-502 until Mach 1 was reached and were lower thereafter. However, these differences are close to the accuracy level of the instrumentation and as the trends are the same the agreement for the three flights are considered to be satisfactory. The predicted bands were derived analytically using the maximum expected leakage area, and minimum leakage area.

The intertank and forward skirt pressure differentials show an abrupt drop between 60 and 70 seconds on all three flights. This is associated with the vehicle passing through Mach 1 which occurred between 60 and 62 seconds.

The S-IC engine, intertank, and forward skirt compartment pressure loadings are shown in Figure 16-4. The AS-503 engine compartment experienced a greater crush pressure loading than the engine compartments on AS-501 and AS-502. This was caused by the lower engine compartment pressure on AS-503 as discussed in the preceding paragraph. The intertank compartment pressure loadings agreed well with AS-501 and AS-502 data. The forward skirt loading was generally greater on AS-503 throughout the first 90 seconds of flight. However, this presented no problem since the maximum value of approximately 0.27 N/cm^2 (0.39 psid) was well below the design value of 1.38 N/cm^2 (2.0 psid). The predictions were based on wind tunnel data and predicted internal pressures.

16.2.2 S-II Stage

Surface pressure and compartment venting analyses were conducted using the AS-503 OMPT with angle-of-attack data obtained from the S-IC Flight Control Conditioned Data Tape (Q-ball). Atmospheric data were obtained from the Preliminary Meteorological Data Tape (Met Tape).

The external flow field at a point on the S-II stage was analyzed by means of a digital computer flow field program. This program assumes a clean configuration, i.e., disturbances caused by protuberances are not accounted for. However, due to location the flight instruments are affected by these disturbances. Internal pressures for the forward

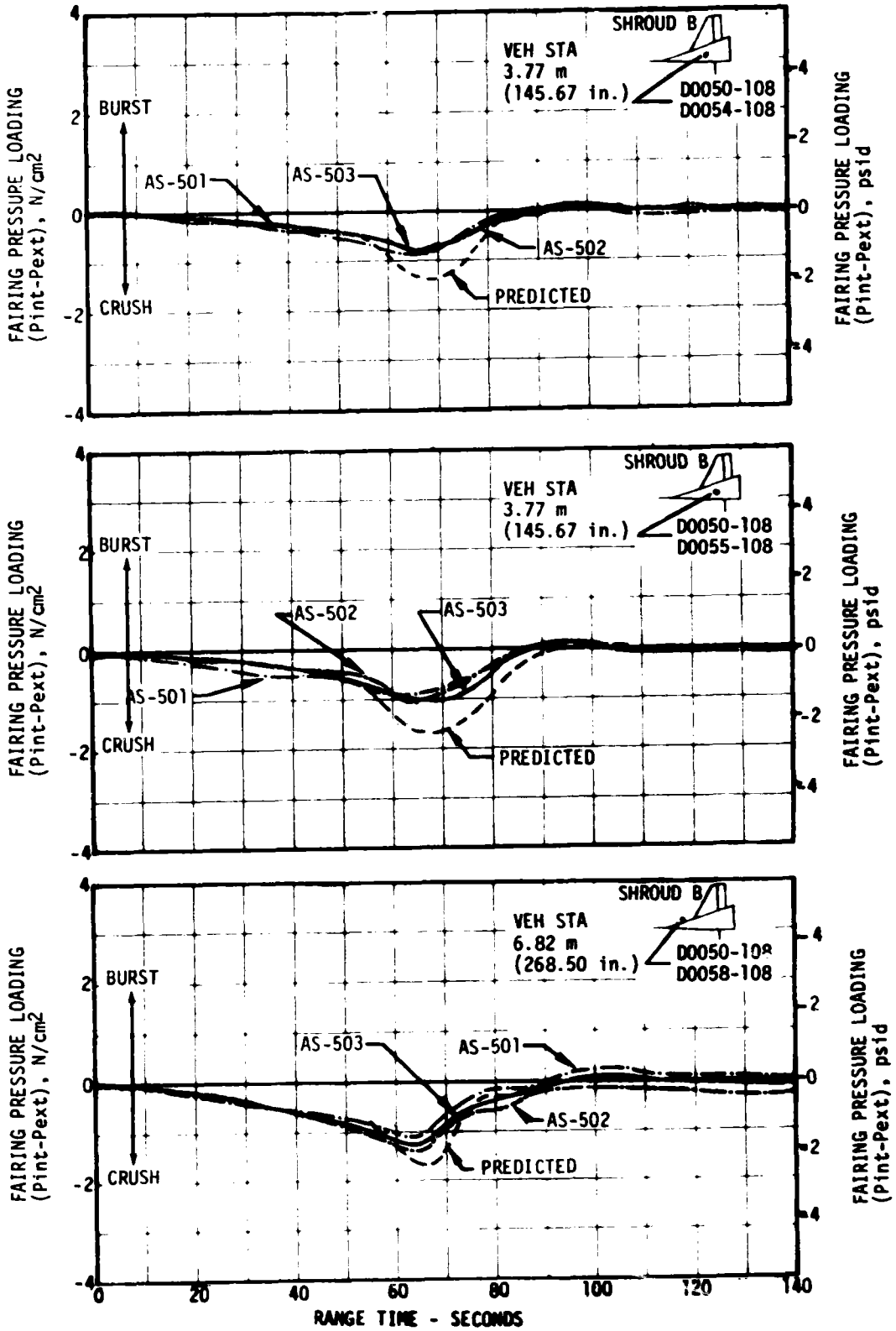

Figure 16-2. S-IC Engine Fairing Pressure Loading, Sheet 1 of 2

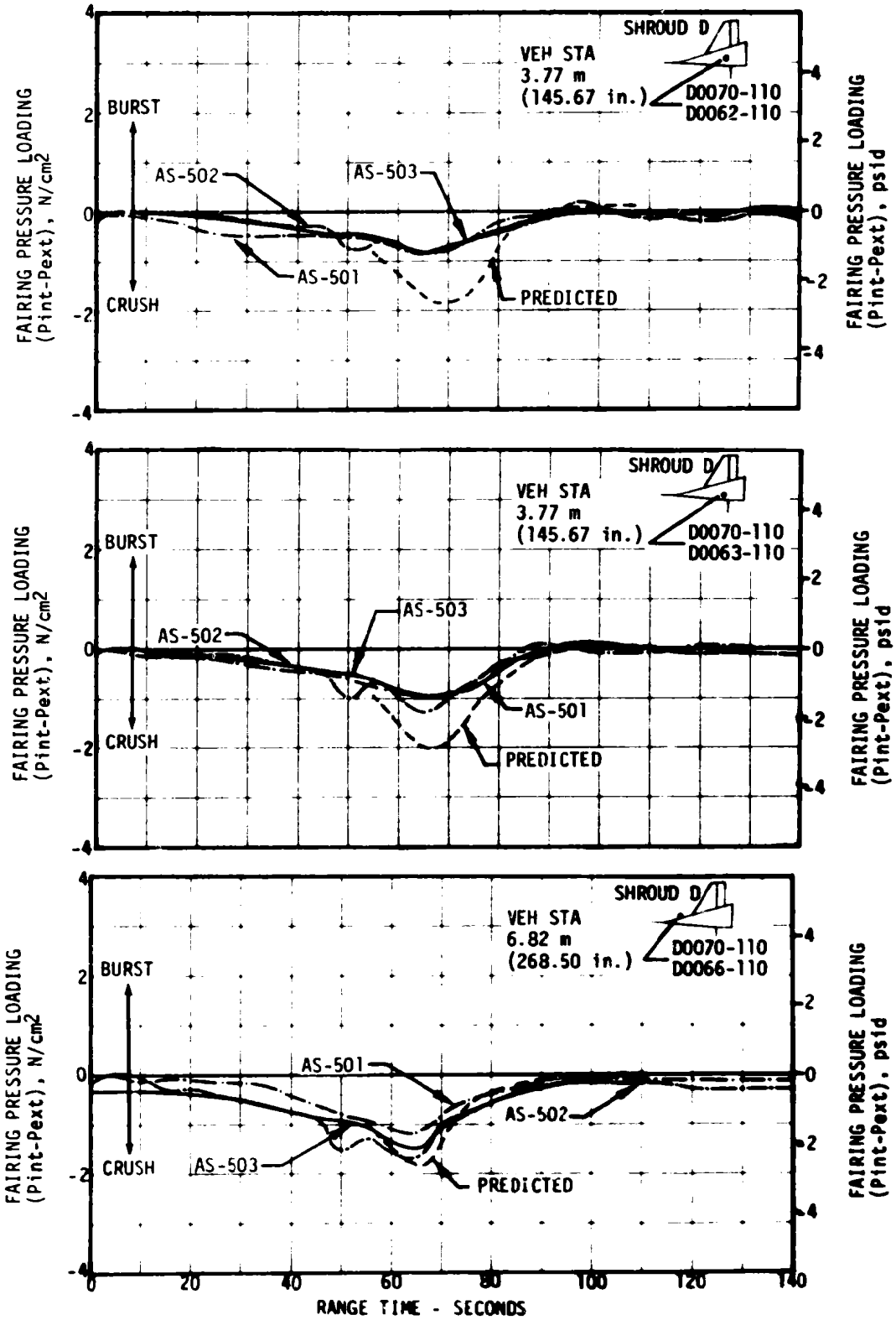

Figure 16-2. S-IC Engine Fairing Pressure Loading, Sheet 2 of 2

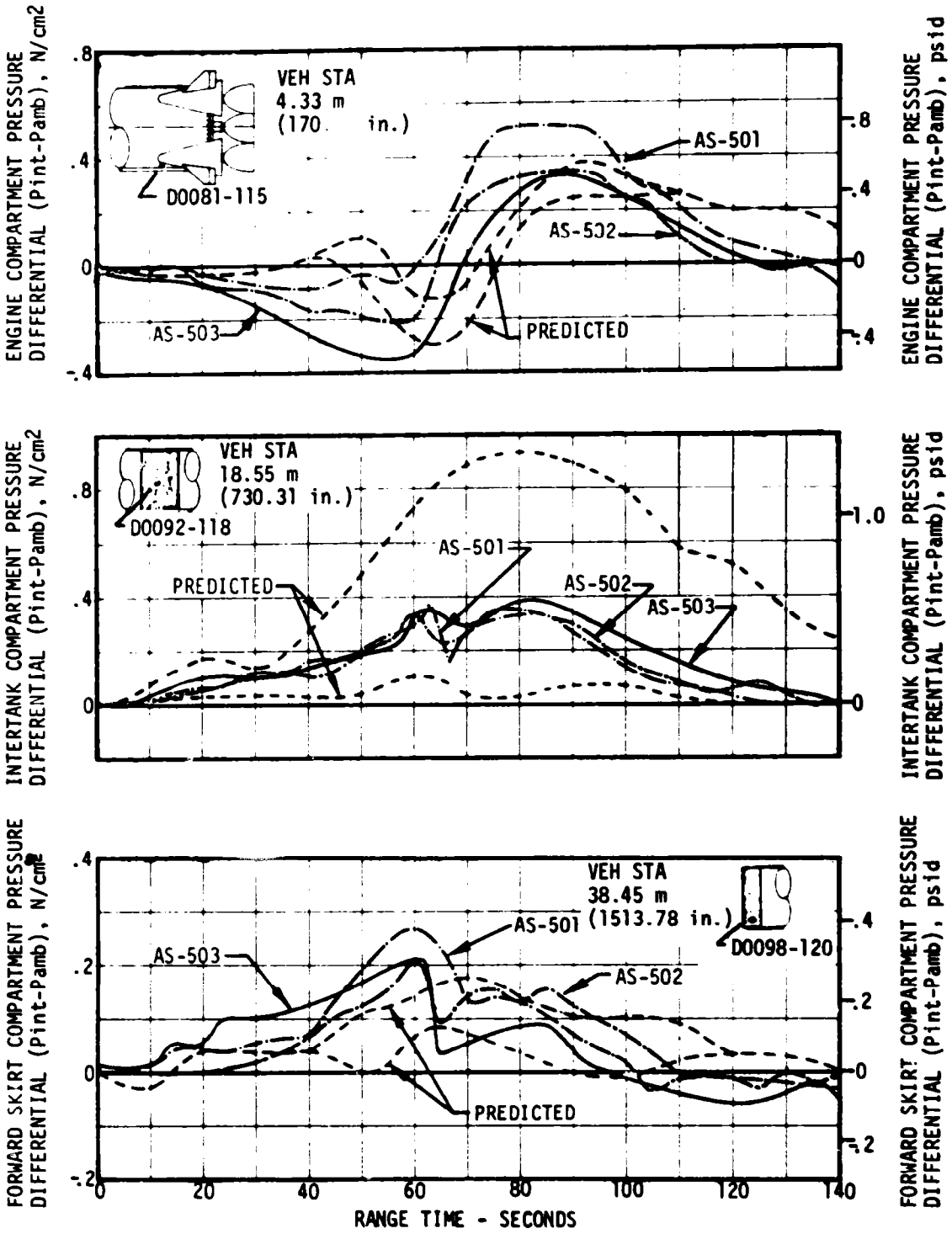

Figure 16-3. S-IC Compartment Pressure Differential

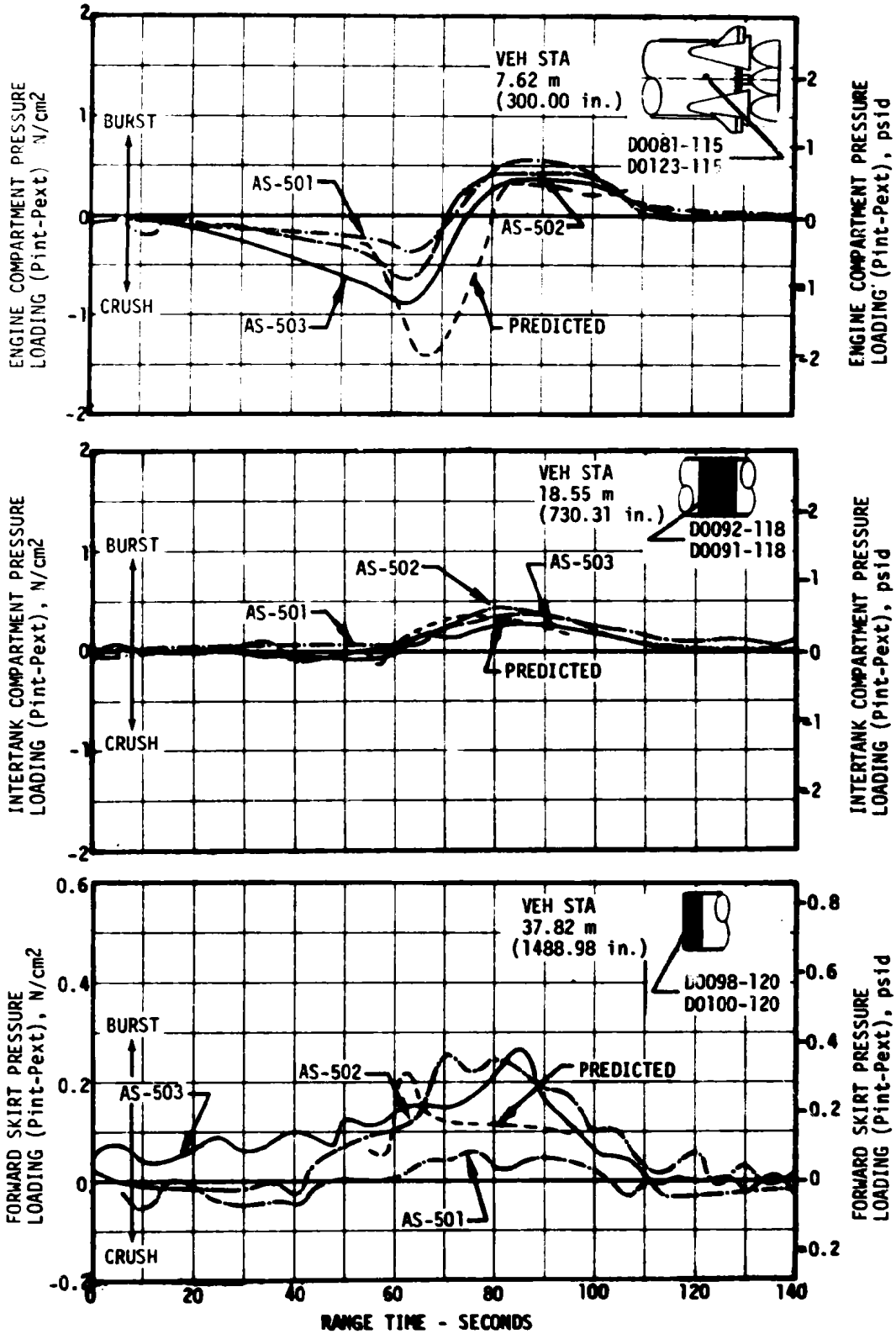

Figure 16-4. S-IC Compartment Pressure Loading

skirt, interstage, and insulation regions were analyzed by means of a digital computer multiple venting program. The validity of these methods of analysis was established by favorable comparison between predicted values for AS-501 and AS-502 flight data.

A plot of the pressure loading, acting across the forward skirt wall, is presented in the top graph of Figure 16-5. AS-503 flight data and post-flight predicted data are presented in the form of maximum-minimum data bands. AS-501 and AS-502 flight data bands are also shown for comparison.

Both flight and predicted pressure loads were obtained by taking the difference between the respective external pressure values and the assumed uniform internal pressure which was measured at vehicle longitudinal station 74.53 meters (2935 in.), and a peripheral angle of 191 degrees. The flight and predicted values show the same trends, are in good agreement, and well within the design limits.

Comparison of AS-503 flight data and postflight predicted pressure loading acting across the LH_2 sidewall insulation is presented in the lower graph of Figure 16-5. The time and magnitude of the peak bursting pressure agrees well with the postflight prediction. AS-501 and AS-502 data are also shown and compare well with AS-503 data.

16.2.3 S-IVB Stage

Pressures on the S-IVB stage were measured by one internal transducer in the forward compartment and one internal measurement for the aft compartment.

The top graph in Figure 16-6 shows the predicted design pressure differentials (Pint-Pamb) for the forward compartment together with f[illegible]t data for both AS-503 and AS-502. The AS-502 and AS-503 for[illegible]tments had identical vent areas of 0.097 meter^2 (150 in.^{2}). The [illegible] in general, was slightly lower than predicted up to about 60 sec[illegible] ich the agreement was good. However, this data is preliminar[illegible] s expected that the final data will give much closer agreement. The [illegible] graph in Figure 16-6 shows predicted and measured pressure different[illegible] r the aft compartment. The flight data for the aft compartment agreed very well with predicted values up to 85 seconds after which the data was slightly higher.

16.3 BASE PRESSURES

16.3.1 S-IC Base Pressures

Static pressures on the S-IC base heat shield were recorded by six measurements, two of which were heat shield differential pressures. Representative AS-503 data are compared with AS-501 and AS-502 data, and with AS-503 predictions based on previous flight data.

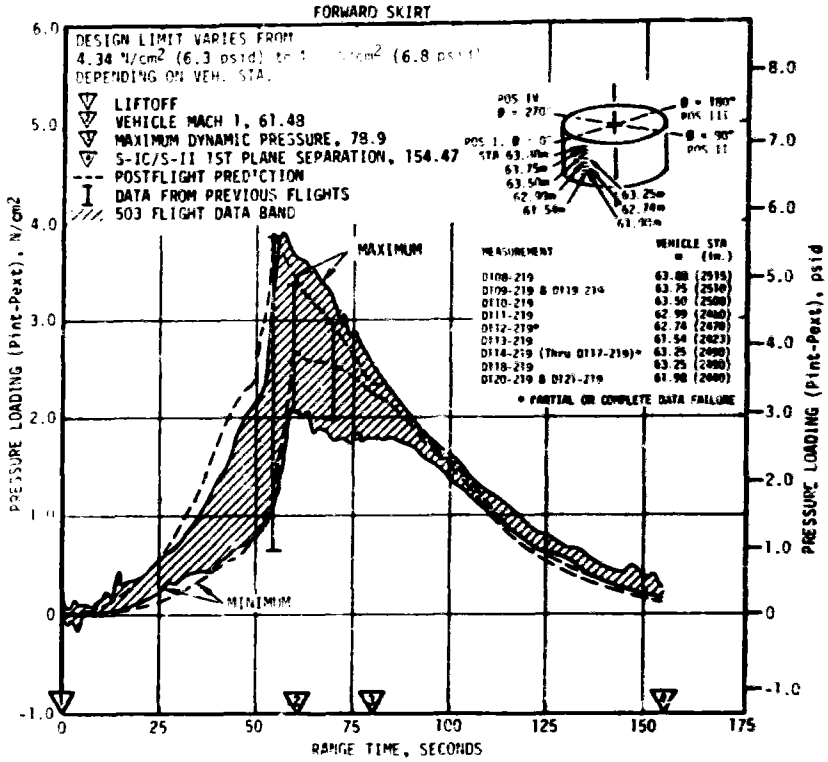

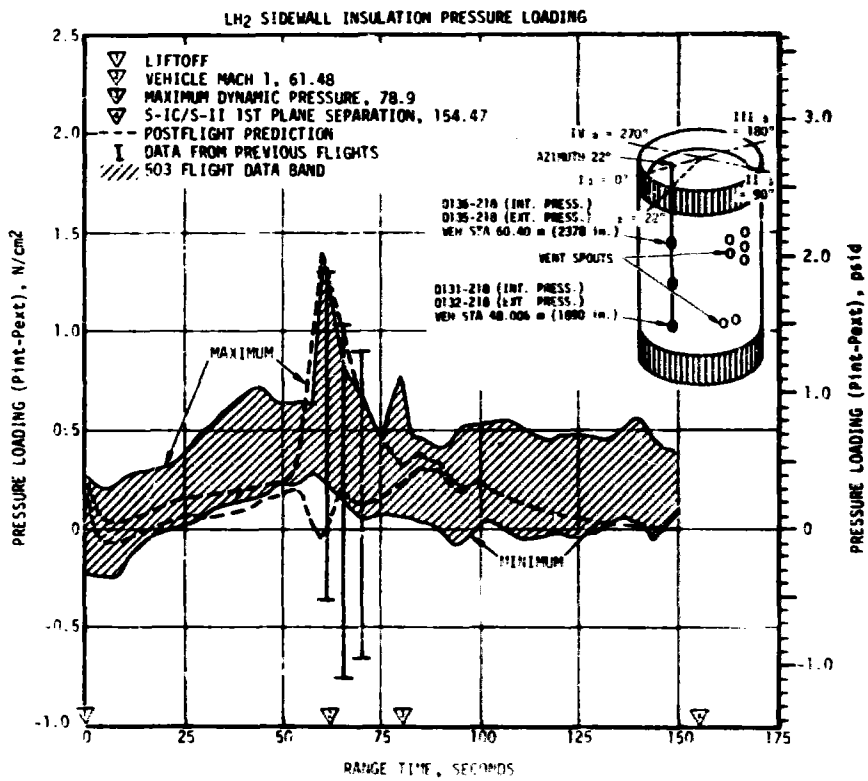

Figure 16-5. S-II Compartment Pressure Loading

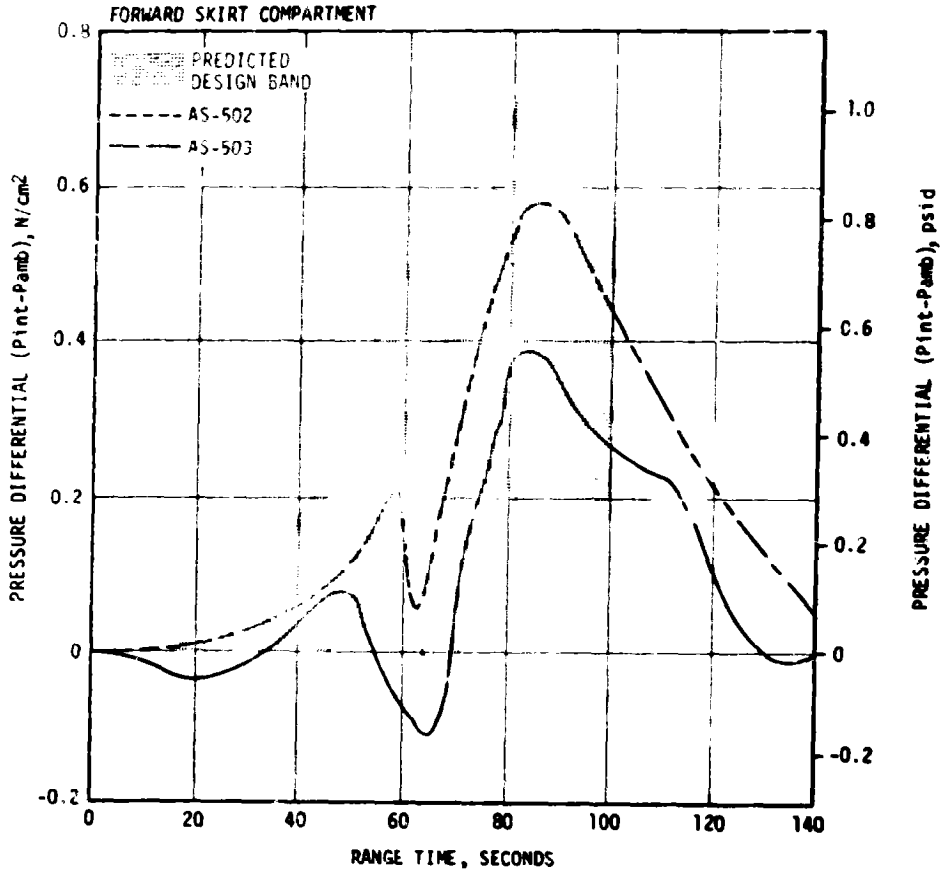

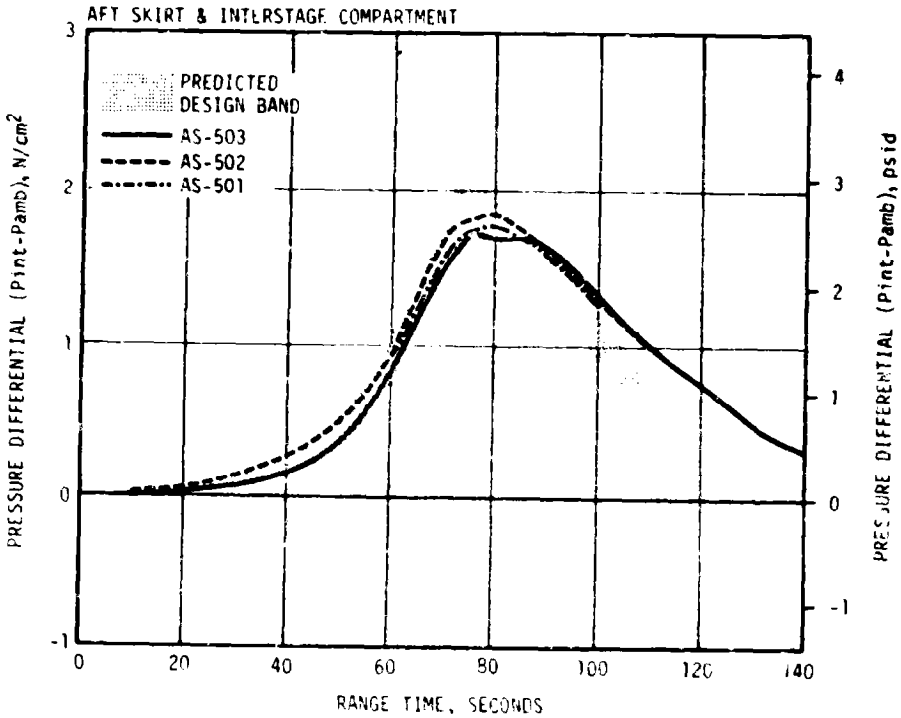

Figure 16-6 S-IVB Compartment Pressure Differential

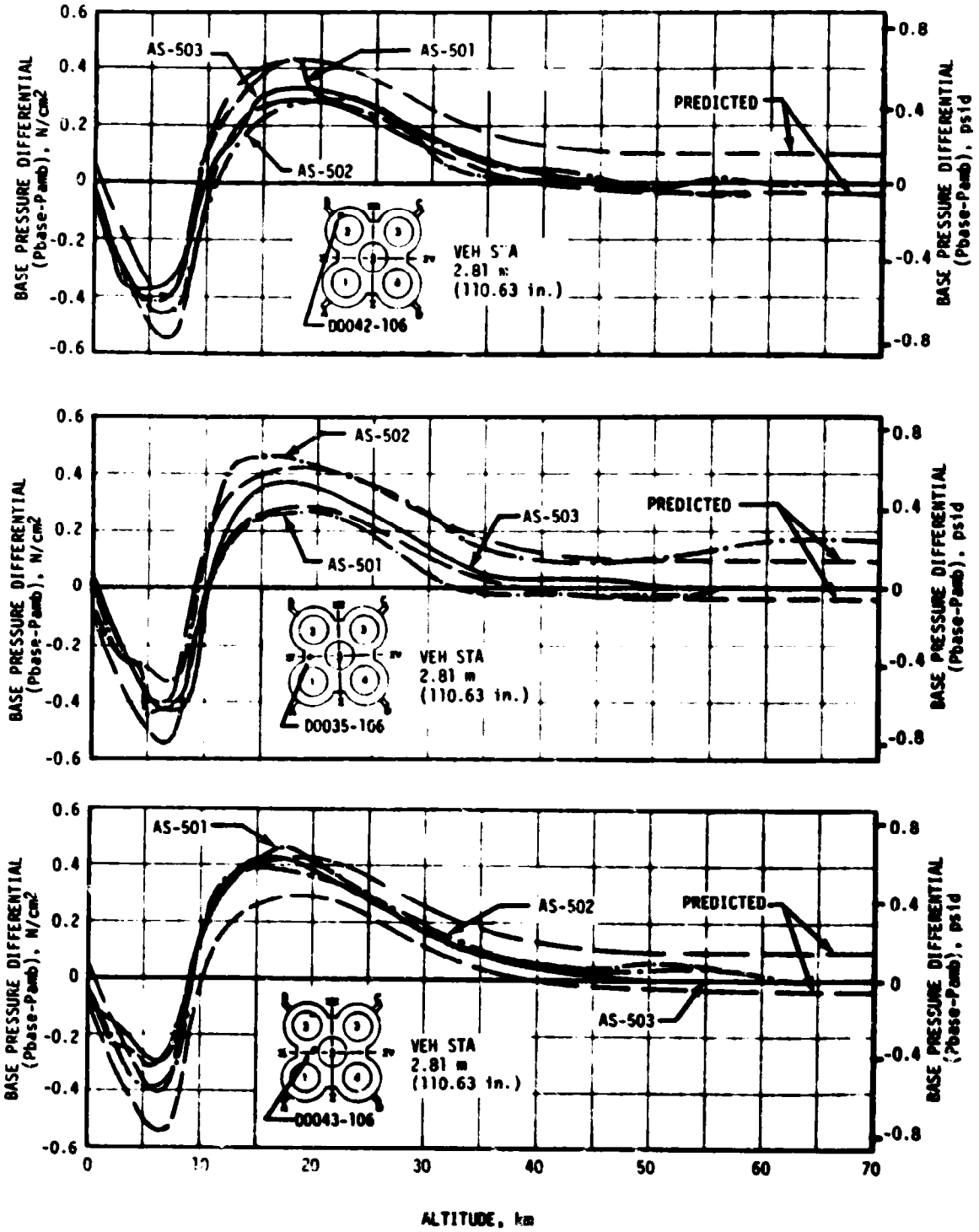

Figure 16-7. S-IC Base Pressure Differentials

Typical S-IC base pressure differentials are shown in Figure 16-7 as a function of altitude. In general, the agreement is good between the AS-503 base pressure data and the AS-502 data.

S-IC base heat shield pressure loading versus altitude is shown in Figure 16-8. The levels of AS-503 data were less than that for previous flight data because of a decrease in engine compartment pressure resulting from the increase in compartment venting, as discussed in paragraph 16.2.1. These heat shield loadings were well within the 1.38 N/cm^2 (2.0 psid) design values.

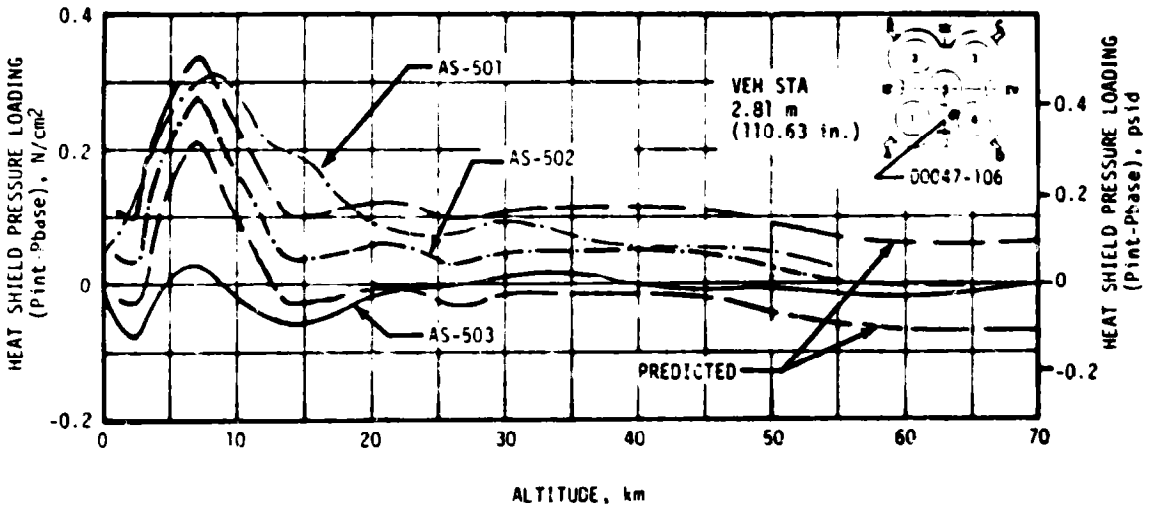

Figure 16-8. S-IC Base Heat Shield Pressure Loading

16.3.2 S-II Base Pressures

The postflight predictions of static pressures, on the aft face of the S-II base heat shield, were evaluated from a semi-empirical correlation of base pressure with heating rate derived from hot flow model test results, and AS-501 and AS-502 flight data. AS-501 and AS-502 flight data indicated that aft face heat shield pressure measurements, located away from the reverse flow stagnation point, would be reduced after interstage separation. The predictions of the heat shield forward face and thrust cone region static pressure were based on AS-501 and AS-502 flight data.

Figure 16-9 compares AS-503 measured static pressures, on the forward face of the heat shield and in the thrust cone region, with postflight predictions and with AS-501 and AS-502 flight data. The static pressure on the forward face of the heat shield and thrust cone region during the AS-503 flight was approximately equal to the static pressure in these areas during the AS-501 and AS-502 flights. The pressure peak which occurred on the forward face of the heat shield and in the thrust region during AS-503 interstage separation was observed in previous flight data.

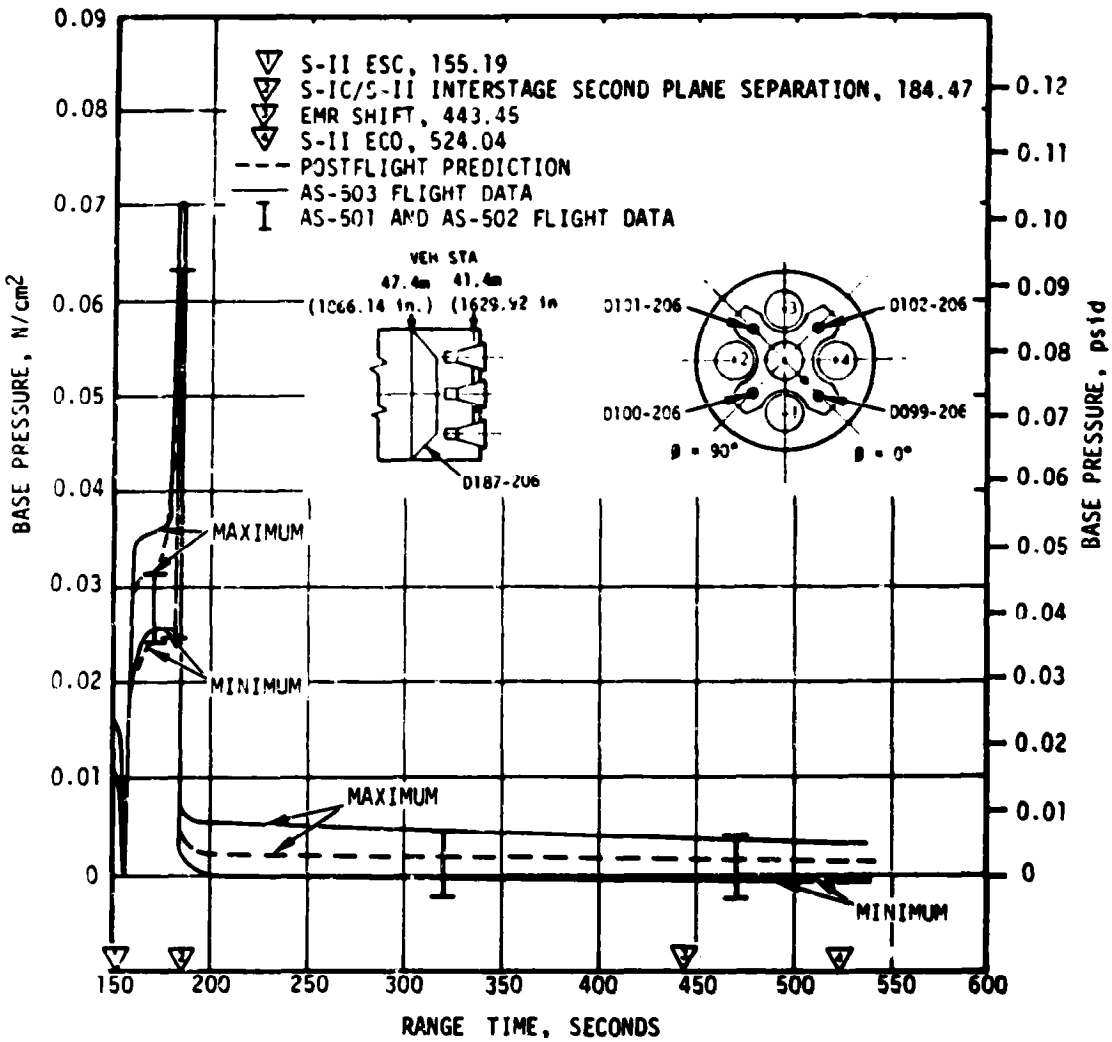

Figure 16-9. S-II Base Heat Shield Forward Face and Thrust Cone Pressures

Figure 16-10 presents both the postflight predicted and AS-503 measured static pressures on the aft face of the heat shield. Also superimposed on Figure 16-10 are bands of static pressure data from the AS-501 and AS-502 flights. In general, the analytical predictions were in good agreement with the flight data from S-II engine ignition (155 seconds) up to Programmed Mixture Ratio (PMR) stepdown at 443 seconds. After PMR stepdown the analytical predictions were approximately 50 percent higher than the flight data. This discrepancy is believed due to errors in the assumed engine positions caused by uncertainties in structural compliance during flight.

Figure 16-10 indicates that, except for a transient pressure peak, the static pressures near the stagnation point of the reverse flow were nearly independent of interstage separation, as observed in previous flight data. There was, however, a slow decay of static pressure with

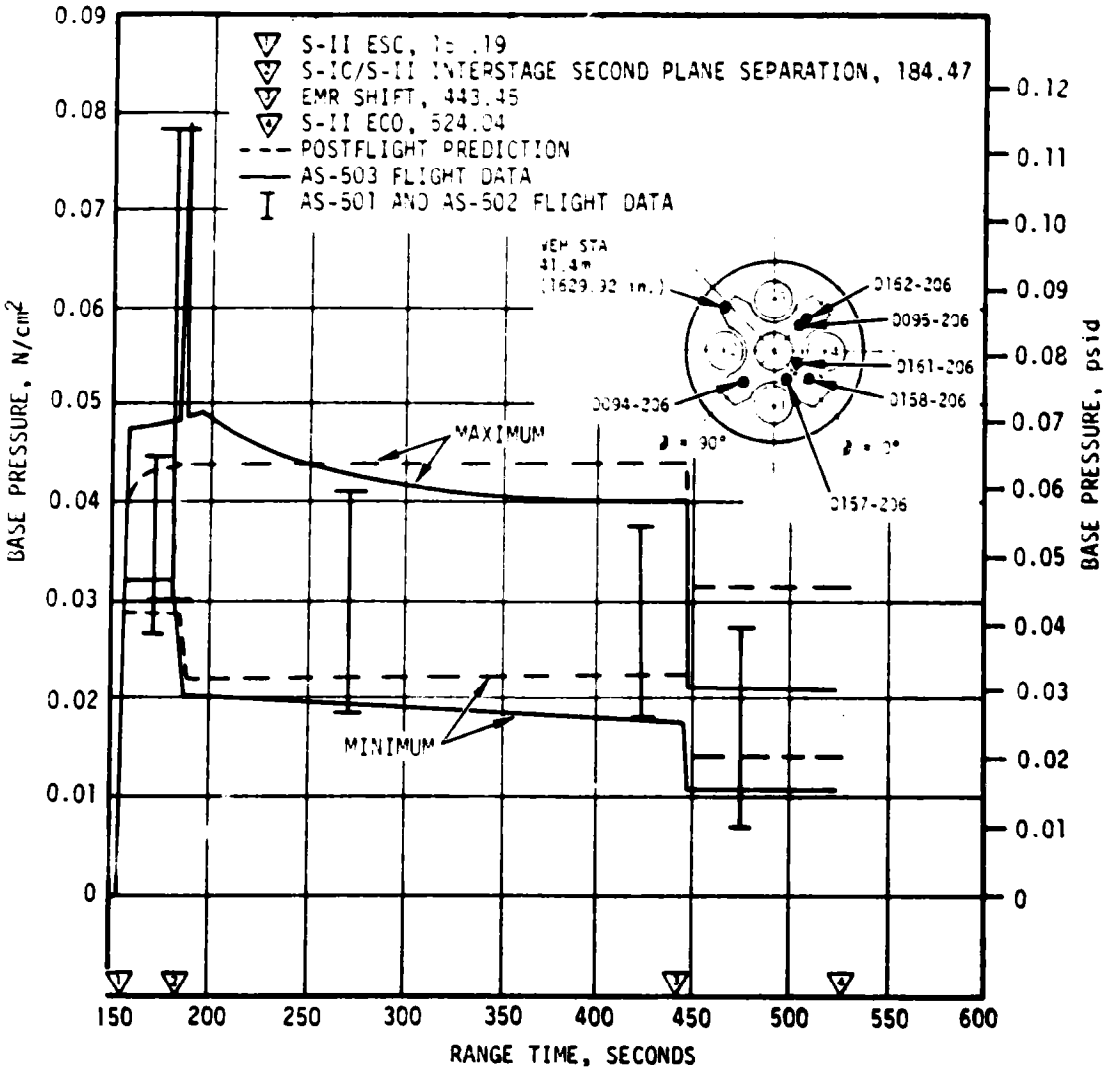

Figure 16-10. S-II Heat Shield Aft Face Pressures

time after interstage separation up to approximately 350 seconds. The decay vanished between 350 seconds and PMR stepdown at 443 seconds. The observed pressure decay during this period may be due to an incremental pressure caused by outgassing from within the base heat shield. The analytical predictions were based on the assumptions that the interstage has no effect on the base pressures near the stagnation point. Thus, the analytical predictions were constant from approximately 160 seconds up to PMR stepdown. For measurements located away from the stagnation point, the effect of interstage separation was to decrease the static pressure by about 27 percent.

The pressure peak observed during interstage separation is believed due to the sudden increase in velocity and temperature of exhaust gases due to the confinement of the engine exhaust plumes by the interstage as it separated from the S-II vehicle.

16.4 ACOUSTIC ENVIRONMENT

16.4.1 External Acoustics

The external fluctuating pressure environments for the AS-503 vehicle were recorded by nine instruments located on the instrument unit, S-IVB forward and aft skirts, S-II forward and aft skirts, S-IC Intertank, S-IC aft skirt and Fin D. Instrument B0004-114, located on Fin D, failed prior to launch and provided no valid data. Representative data for the remaining instruments, together with AS-501 and AS-502 data, are shown in Figures 16-11 through 16-14.

The AS-503 external environment at liftoff is shown in Figure 16-11. Instrument B0019-427, located on the S-IVB aft skirt, displayed a data dropout from -1 second to 2 seconds; AS-503 liftoff data is not shown for this instrument. Data before and after the dropout display expected levels. The spread, noted in the data of the S-II forward skirt and aft skirt, is caused by circumferential position changes at a fixed vehicle axial station. The data indicate that up to a 6 decibel circumferential variation existed at these vehicle stations. The lowest levels are from the measurement located on the Launch Umbilical Tower side of the vehicle. All S-IC instruments have been corrected by -3 decibels to account for a Remote Automatic Calibration System error. No other appreciable differences with previous flights have been noted.

Liftoff sound pressure spectral densities are compared with AS-501 and AS-502 data in Figure 16-12. Frequency characteristics generally appear similar for all flights. S-II instrument data from the AS-503 flight show some changes in spectrum shape, but these instruments have been moved 90 degrees from the corresponding AS-501 and AS-502 measurement.

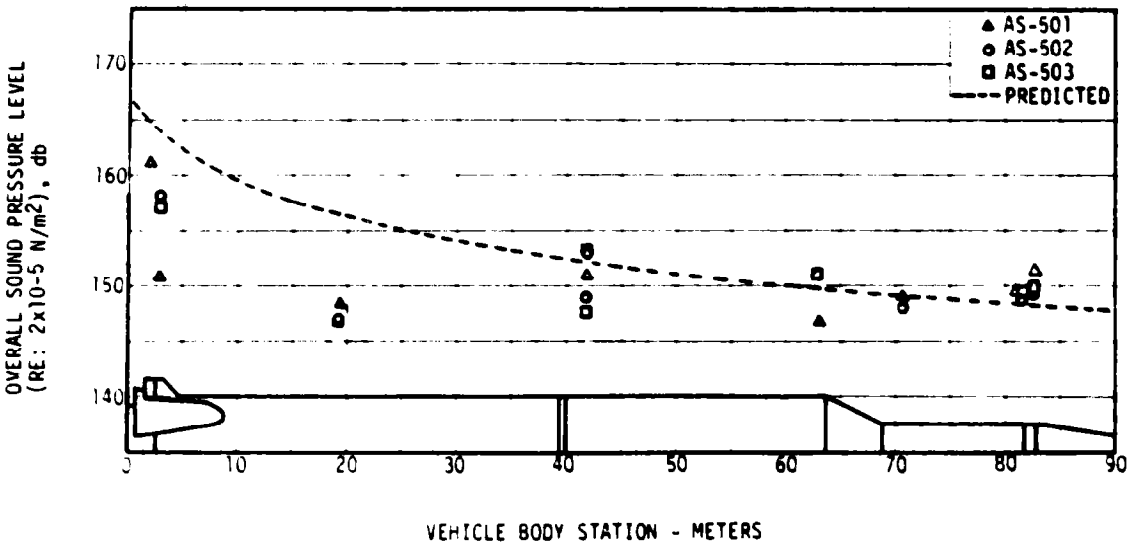

Figure 16-11. Vehicle External Overall Sound Pressure Level at Liftoff

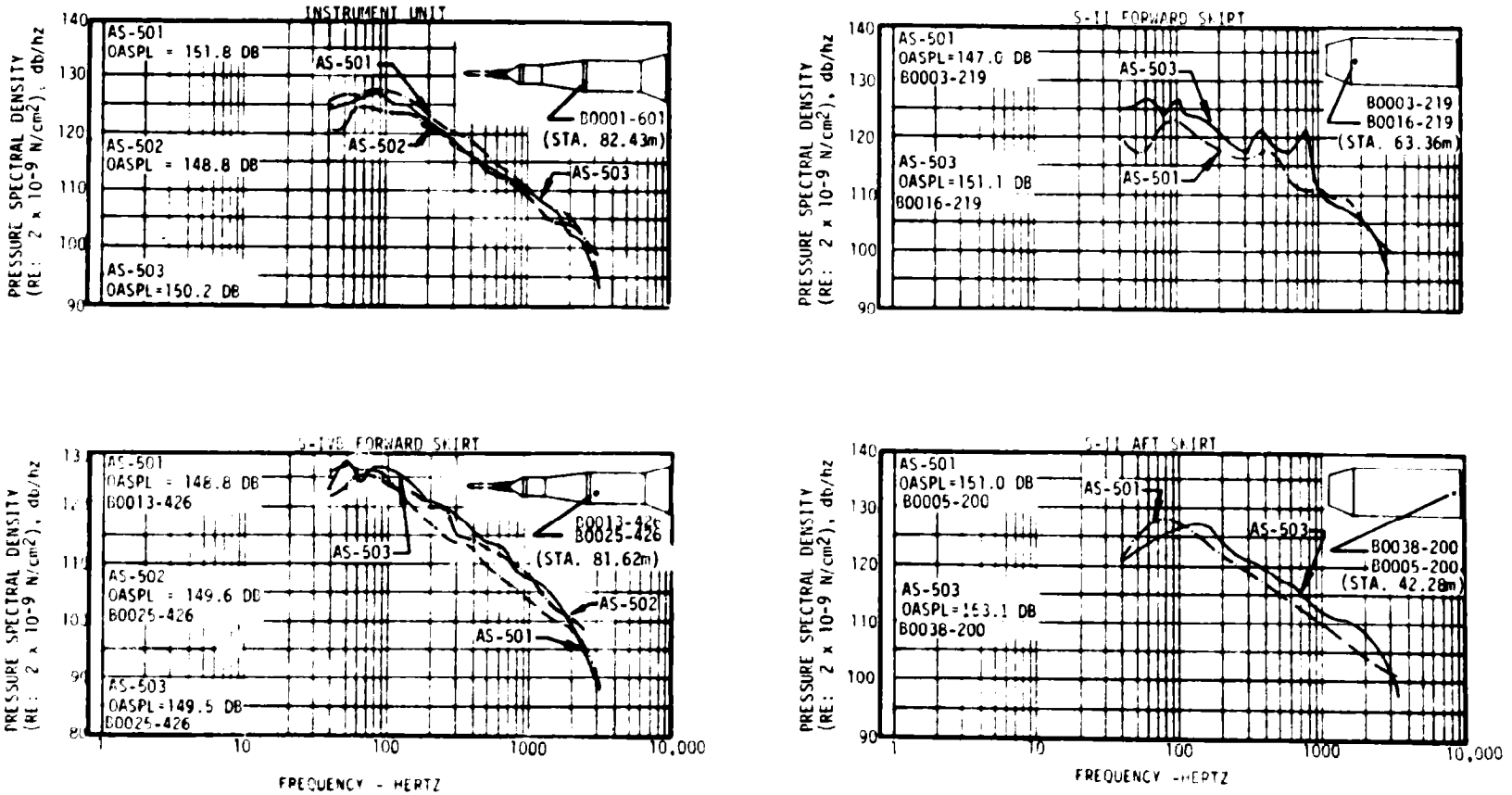

Figure 16-12. Vehicle External Sound Pressure Spectral Densities at Liftoff, Sheet 1 of 2

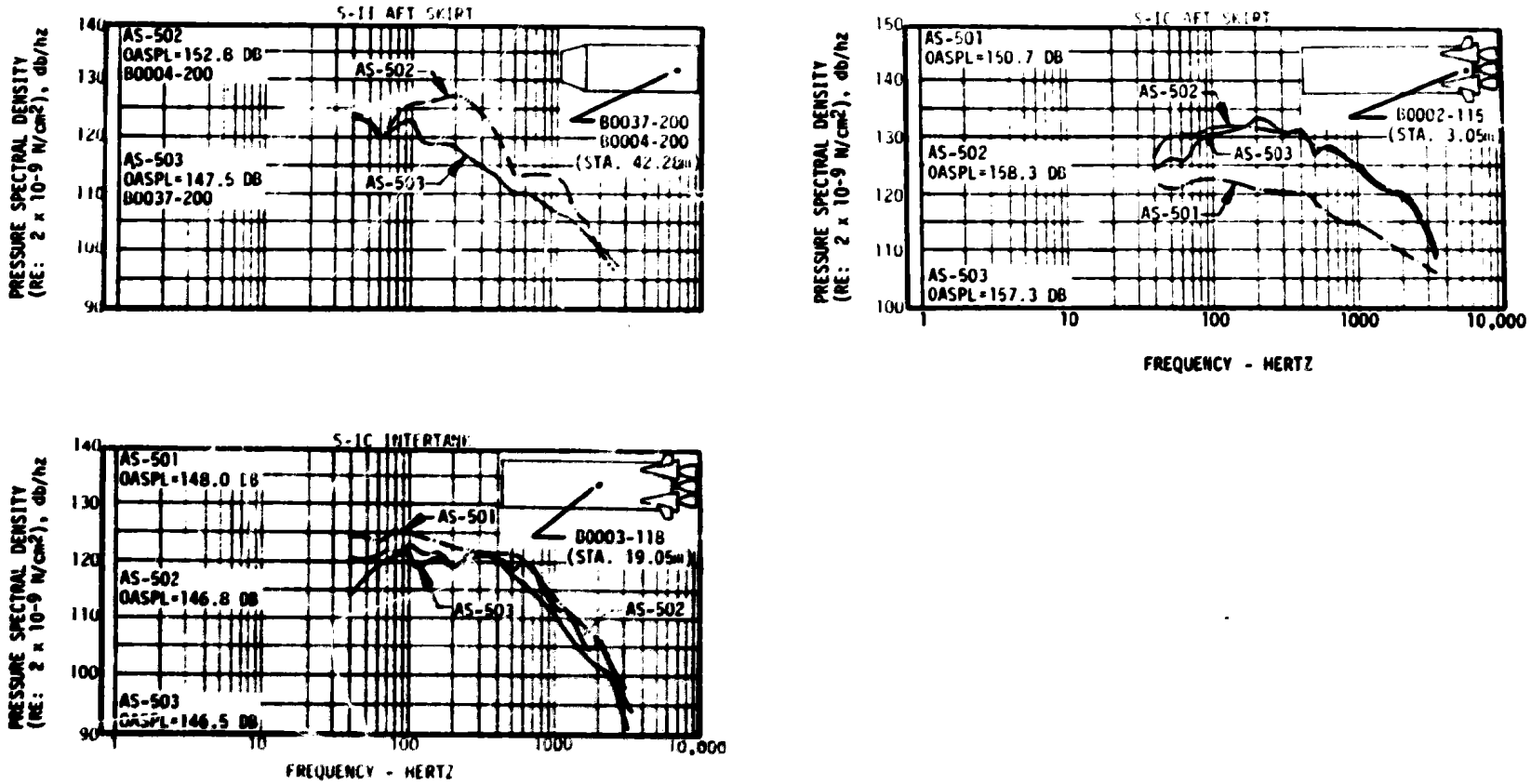

Figure 16-12. Vehicle External Sound Pressure Spectral Densities at Liftoff, Sheet 2 of 2

Overall fluctuating pressure time histories to 140 seconds are shown in Figure 16-13. The data peak in the S-IC intertank instrument, after 110 seconds, may be caused by flow separation and exhaust gas recirculation due to the expanded exhaust plume. The majority of time-histories show reasonable agreement between all three flights; however, B0037-200 (S-II aft skirt) shows consistently higher overall levels after 20 seconds than previous data. The cause appears to be a strong narrow band random, or possibly sinusoidal component in the 600 to 700 hertz frequency range. B0038-200 (S-II aft skirt) also shows this component at 80 seconds. B0019-427 displays intermittent data dropouts from 80 to 92 seconds, but the data otherwise appears to be valid.

Pressure spectral densities at maximum aerodynamic noise are shown in Figure 16-14. The 600 to 700 hertz peak is evident in the spectra for B0037-200 and B0038-200. All other spectra show reasonable agreement between flights.

16.4.2 Internal Acoustics

16.4.2.1 S-IC Stage. Internal acoustics were measured at two locations on the S-IC stage. One measurement, located above the heat shield in the thrust structure, was not taken on previous flights. The acoustic data at this location are shown in Figure 16-15. The level of this measurement at liftoff appears as expected when compared to static firing data, and the drop off of the curve immediately after liftoff compares closely with the drop off of the intertank measurement. Therefore, the data appears to be valid until it reaches the noise floor at approximately 100 seconds.

The intertank internal acoustic data are shown in Figure 16-16. Launch levels agreed with AS-501 and AS-502 levels. The levels during flight were slightly lower than on previous flights.

16.4.2.2 S-II Stage. Two internal microphones were located on the S-II stage as follows:

MEASUREMENT	S-II AREA	VEHICLE STATION (m)	(in.)	AZIMUTH (deg)	RADIUS (m)	(in.)
B017-219	Forward Skirt, Internal	63.3	2492.1	270	4.52	178
B039-206	Thrust Cone, Internal	42.6	1677.2	270	3.30	130

Figure 16-17 presents the measured overall acoustic internal levels versus range time for AS-503. AS-502 data is also shown for comparison purposes. AS-503 internal and external acoustics are shown in Table 16-1 and compared with data from previous flights.

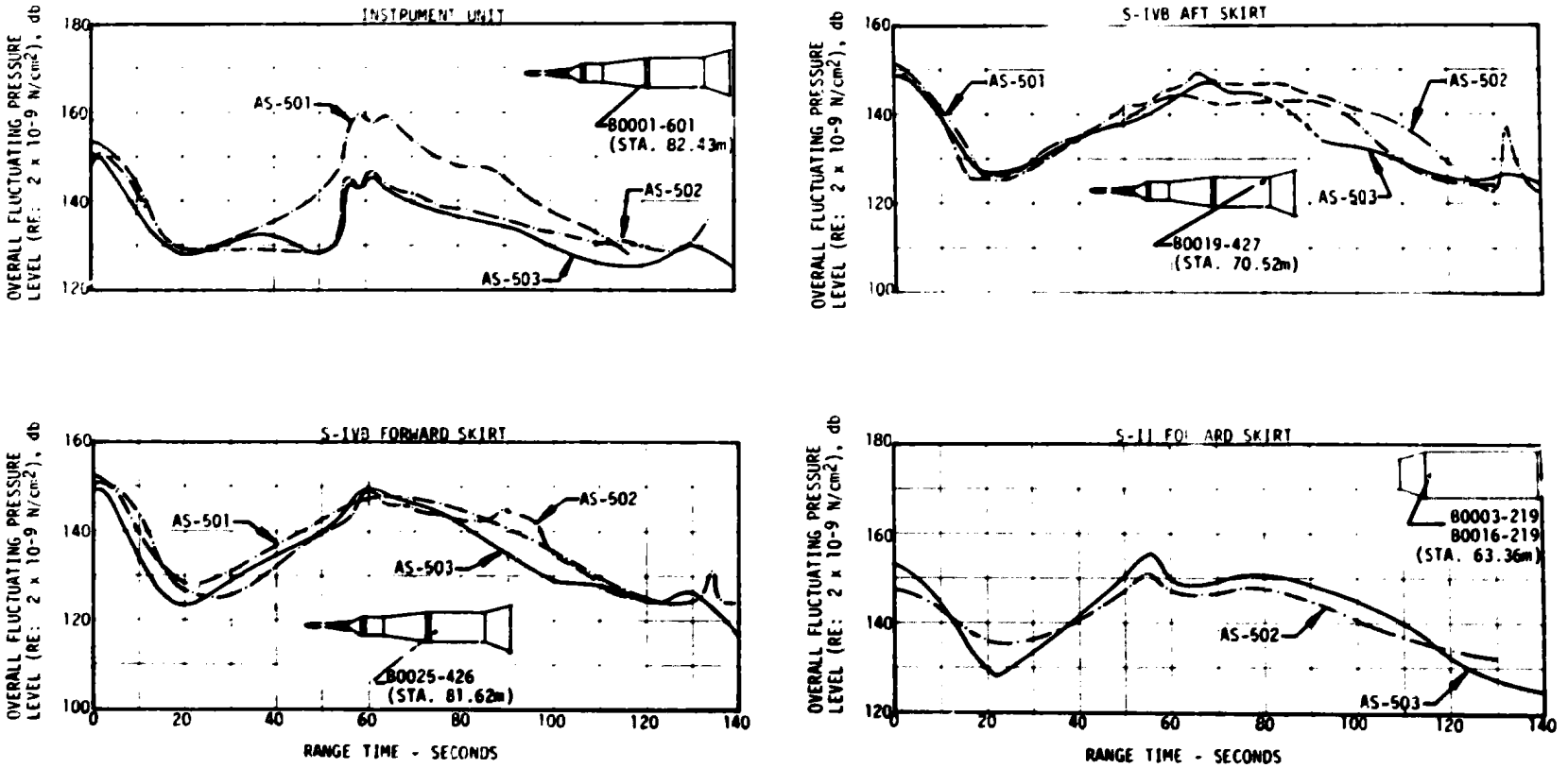

Figure 16-13. Vehicle External Overall Fluctuating Pressure Level, Sheet 1 of 2

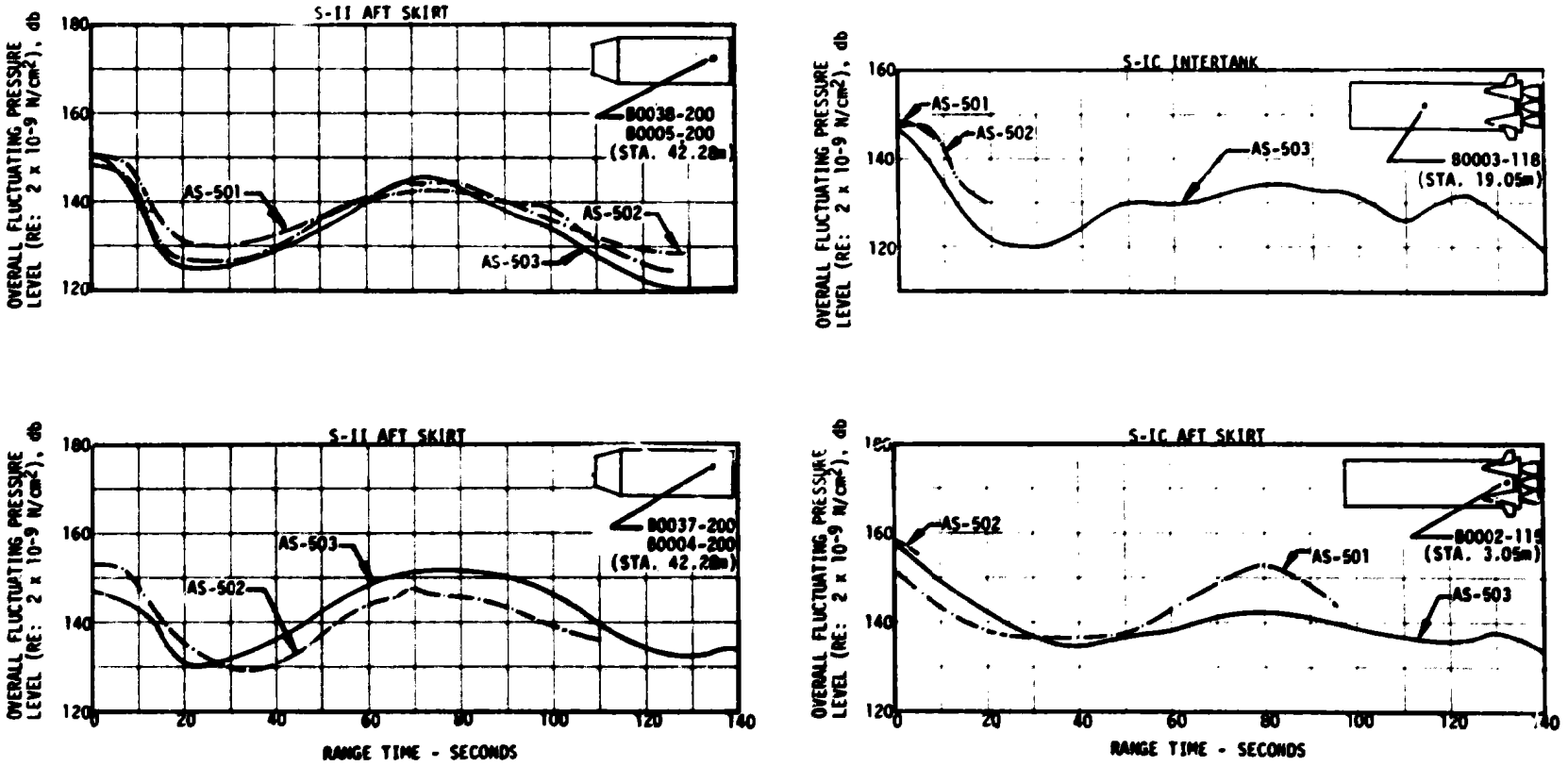

Figure 16-13. Vehicle External Overall Fluctuating Pressure Level, Sheet 2 of 2

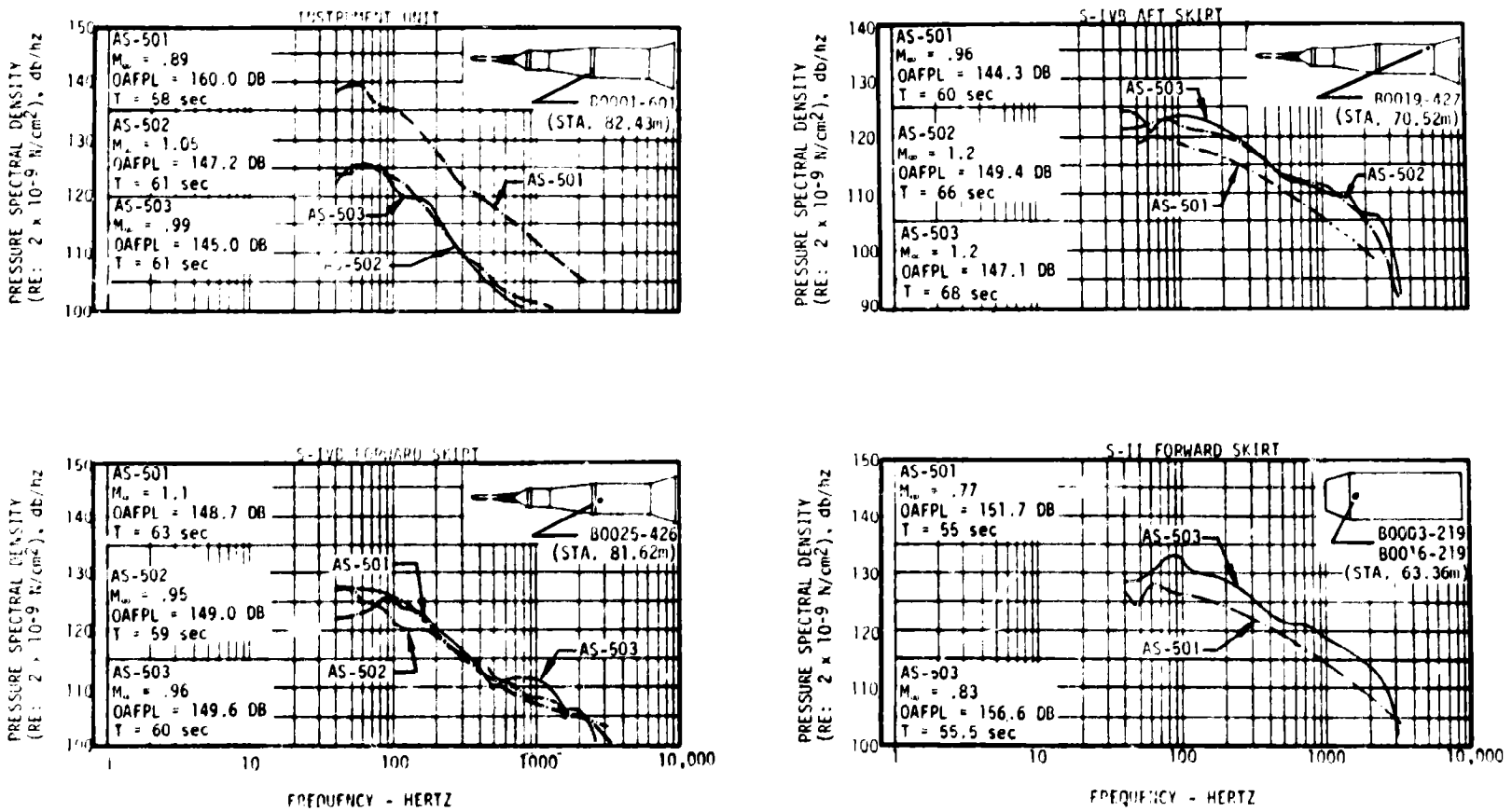

Figure 16-14. Vehicle External Fluctuating Pressure Spectral Densities at Maximum Aerodynamic Noise, Sheet 1 of 2

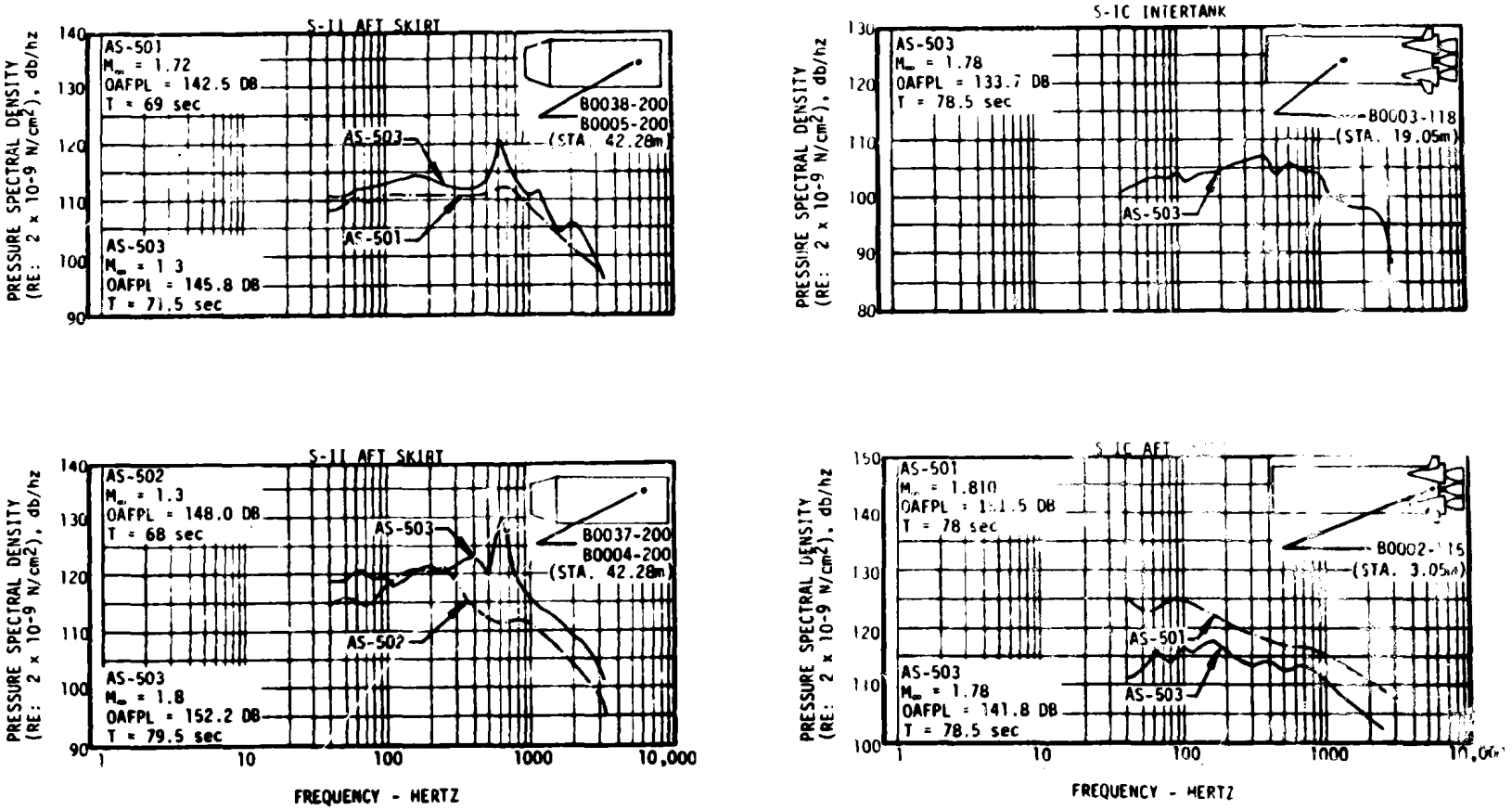

Figure 16-14. Vehicle External Fluctuating Pressure Spectral Densities at Maximum Aerodynamic Noise, Sheet 2 of 2

MEASUREMENT	MAXIMUM SPL		DESIGN OVERALL SPL	LEGEND
	PREVIOUS FLIGHT DATA	AS-503		
B005-106		144.6@T-1.0	169.0	STATIC FIRING DATA ENVELOPE AS-503 FLIGHT DATA

SPL in db referenced to 2×10^{-5} N/m^2

This measurement was not installed on previous flights

AS-503 data may be invalid; it is less than 5% of calibration level

Envelope of all static firing, internal thrust structure acoustic data

MACH 1, 61.48
MAX Q, 78.90
S-IC/S-II SEPARATION, 154.47

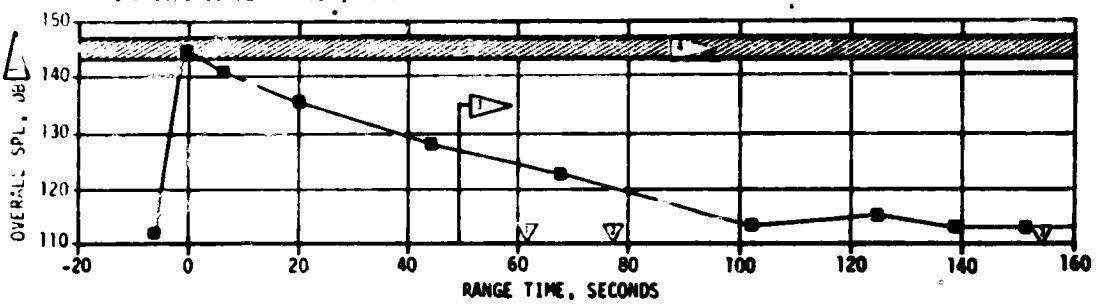

Figure 16-15. S-IC Heat Shield Panels Acoustic Environment

MEASUREMENT	MAXIMUM SPL		DESIGN OVERALL SPL	LEGEND
	PREVIOUS FLIGHT DATA	AS-503		
B001-118	142.3@T+0.5	139.2@T-1.0	157.0	PREVIOUS FLIGHT DATA ENVELOPE AS-503 FLIGHT DATA

SPL in db referenced to 2×10^{-5} N/m^2

Unexplained increase in data at 97 seconds for approximately one second duration

AS-503 data may be invalid; it is less than 5% of calibration level

MACH 1, 61.48
MAX Q, 78.90
S-IC/S-II SEPARATION, 154.47

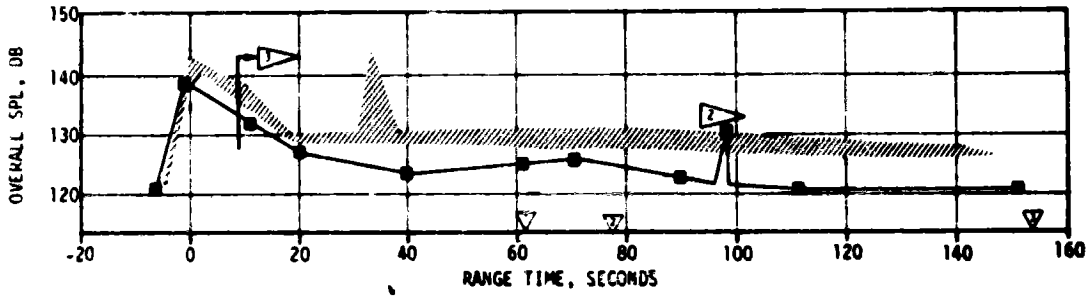

Figure 16-16. S-IC Internal Acoustic Environment

Table 16-1. S-II Acoustic Noise Levels Comparison of AS-503 with AS-501 and AS-502 Data

EVENT	MAXIMUM OVERALL db							
	FORWARD SKIRT				AFT INTERSTAGE/AFT SKIRT			
	EXTERNAL (8016-219)		INTERNAL (8017-219)		EXTERNAL (8037-200 & 8038-200)		INTERNAL (8039-206)	
	AS-503	AS-501	AS-503	AS-501/502	AS-503	AS-501	AS-503	AS-501/502
Liftoff	152.9	150	138.5	142	150.1	152.7	137.5	136
Transonic	156.5	149.3	133	131	147.8	144.5	126.0	129
Max Q	151.2	150.3	134.2	138	152.2	146.5	126.0	129
S-II Mainstage		140		126		145		141
Static Fire	131	no data	128	130	no data	no data	148.0	148

NOTE: AS-503 acoustic measurement locations were different from previous flights.

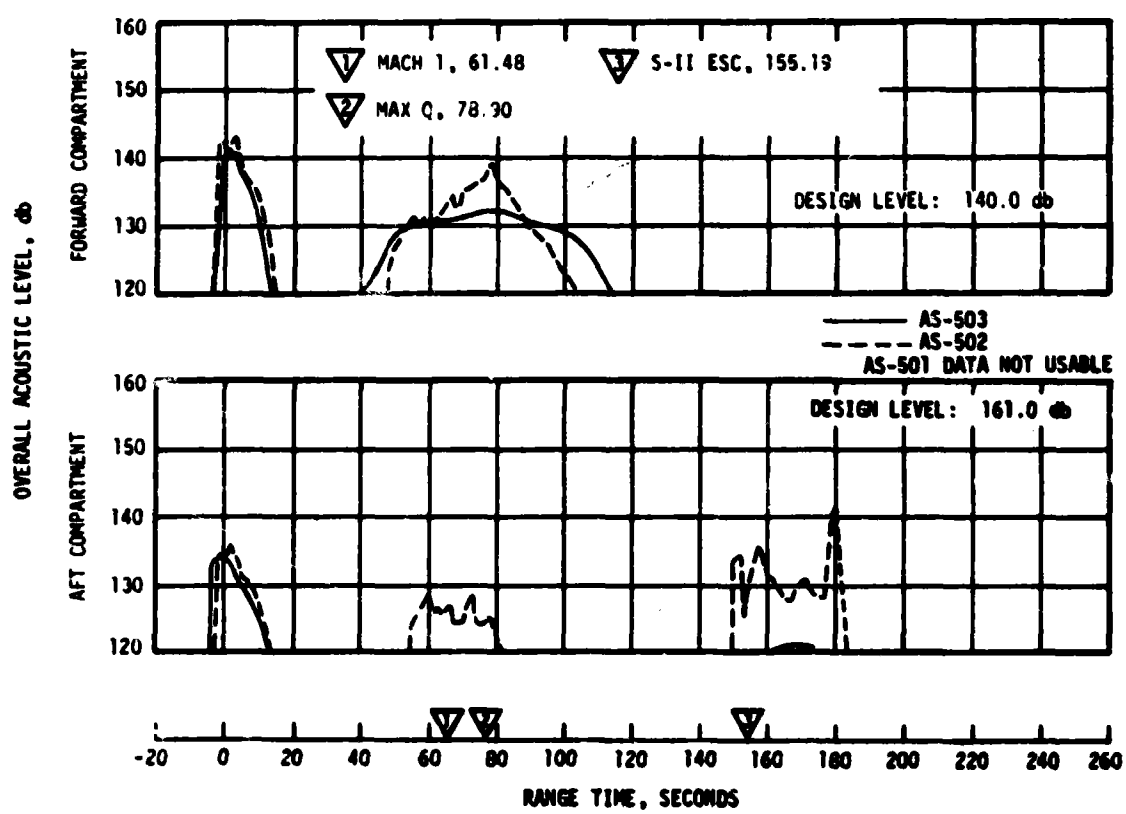

Figure 16-17. S-II Compartment Overall Acoustic Levels

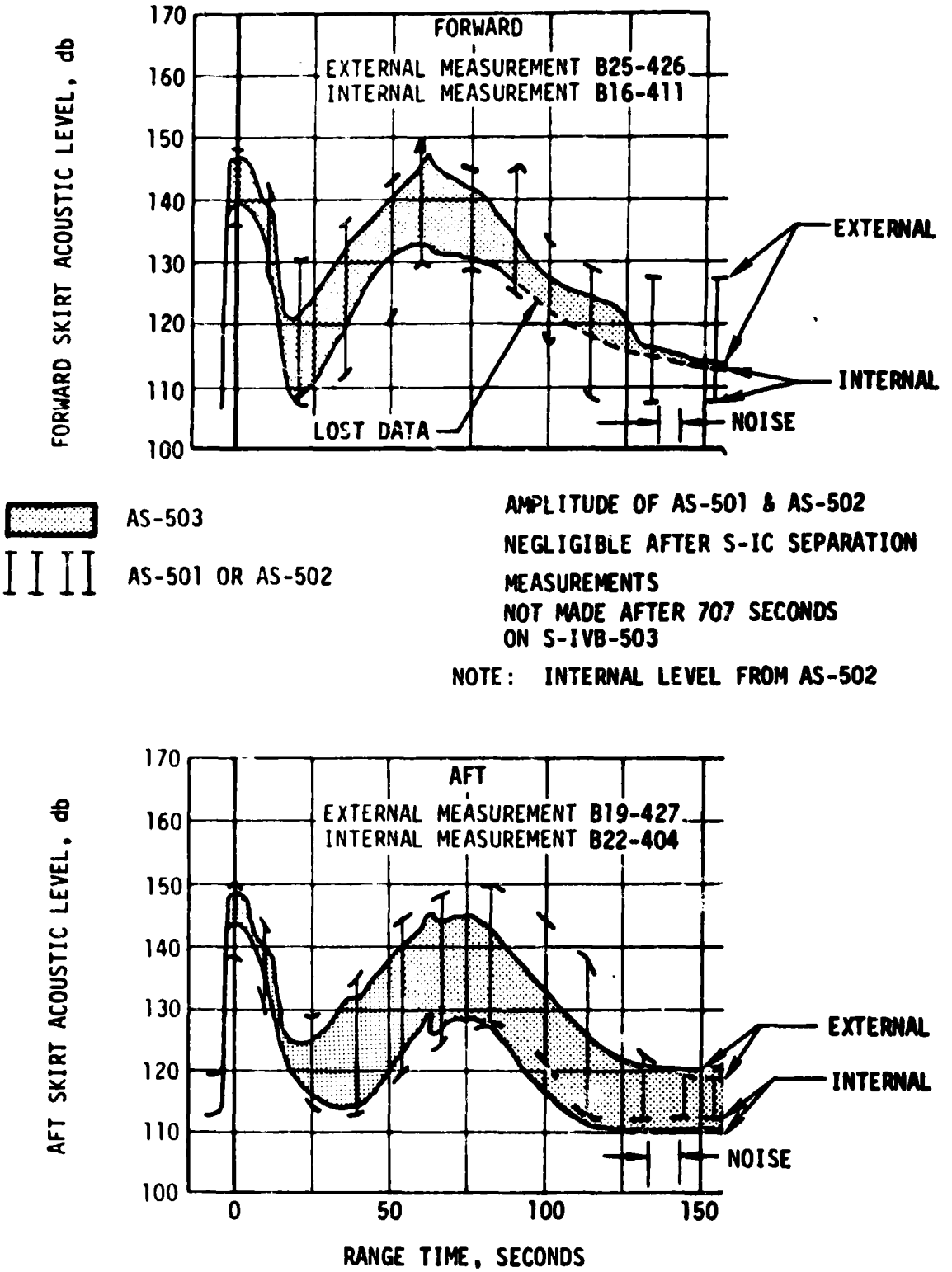

Figure 16-18. S-IVB Forward and Aft Skirt Acoustic Levels

Special prelaunch channelization and calibration checks were made on the AS-503 acoustic measurements to assure acquisition of valid acoustic data. Indications are that all acoustic measurements were valid.

The internal acoustic data shown in Figure 16-17 is in excellent agreement with AS-502 data during the liftoff period. This would indicate that both AS-502 and AS-503 internal acoustic levels were valid.

16.4.2.3 S-IVB Stage. The S-IVB acoustic environment was measured at four positions, internal and external on the forward skirt and internal and external on the aft skirt.

Composite levels, 50 to 3000 hertz, time histories for these locations are presented in Figure 16-18. The AS-503 structural transmittability for the sound pressure at liftoff, and for the boundary layer pressure fluctuations in the transonic portion of flight, is indicated by the difference (shaded band) between the external measurements and the internal measurements. The maximum external levels and the minimum internal levels measured during the AS-501 and AS-502 flights are also depicted, indicating that the AS-503 levels were nominal.

SECTION 17

VEHICLE THERMAL ENVIRONMENT

17.1 SUMMARY

The AS-503 S-IC base region thermal environment was similar to that experienced on earlier flights. The base region environment was not notably altered by the outboard engine cant. With the exception of a brief transient, the effects of early Inboard Engine Cutoff (IECO) on the base region thermal environment were minor. Again the radiation hump at the base heat shield was correlated with the hot recirculated exhaust gases, as shown by the base TV cameras. As on the previous flights, M-31 insulation was lost from the heat shield but caused no problems. Heating rates and structural temperatures forward of the heat shield were similar to those of earlier flights until IECO. Lower heat rates due to receding point of plume induced flow separation were then reflected in lower structural temperatures for the S-IC stage.

The S-IC forward skirt thermal environment after S-IC/S-II separation was similar to that measured on previous flights.

Base thermal environments on the AS-503 S-II stage were similar to those measured on AS-502 and were well below design. A reduction in heating rate was noted after Propellant Mixture Ratio (PMR) step down.

The aeroheating rates on the AS-503 S-II stage interstage, body structure, and fairings, though slightly lower, were similar to those on previous flights and no problems were noted.

The thermal environment in the S-IVB J-2 engine area appeared normal as evidenced by the skin temperatures on the Augmented Spark Igniter (ASI) lines.

Structural temperatures on the AS-503 IU stage were similar to those on previous flights and no problems were noted.

17.2 S-IC BASE HEATING AND SEPARATION ENVIRONMENT

17.2.1 S-IC Base Heating

Thermal environments in the base region of the S-IC stage were recorded by 39 measurements which were located on the heat shield, F-1 engines, and

base of Fin D. This instrumentation included 6 radiation calorimeters, 15 total calorimeters, and 14 gas temperature probes. Representative data from these instruments are compared with AS-501 and AS-502 flight data in Figures 17-1 through 17-3.

The radiation and total heating rates measured in the base region of the S-IC stage were approximately the same as those measured during the AS-502 flight. This similarity was expected since both AS-503 and AS-502 vehicles were flown without base flow deflectors. One instrument, C14-101 located on the lip of engine 101 facing the inboard engine, measured a total heating rate which was higher throughout flight than had been measured at this location during AS-501 and AS-502 flights. Data from the radiation calorimeter and gas temperature probe at the same engine location did not deviate significantly from the AS-502 flight data, indicating that instrument C14-101 gave questionable readings for AS-503.

Maximum base heating occurred at approximately 22 kilometers (11.9 n mi) on AS-503 and is principally radiation, as anticipated from previous Saturn V flight data. The initial rise in the AS-503 radiation heating rate correlates with the presence of hot recirculated gases near the heat shield as recorded by the S-IC base TV cameras. This is consistent with the conclusion, based upon AS-502 flight evaluation, that hot gas recirculation is the main cause of the radiation hump.

Comparisons of AS-502 and AS-503 flight data show that the 2-degree outboard engine cant on the AS-503 vehicle had a negligible effect on the base environment. IECO at 126 seconds on AS-503 produced a 2 to 10 watt/cm^2 (1.76 to 8.81 Btu/ft^2-s) spike in the base heat flux environment of approximately 4 seconds duration. The magnitude and duration of this spike was anticipated, based upon AS-501 and AS-502 flight data at IECO. The base environment for the stable four engine flow field after IECO, from 130 to 154 seconds, had approximately the same trend as the five engine environment prior to IECO.

No appreciable difference is noted in the convective heating measured on the heat shield or engines when comparing the AS-503 vehicle with previous Saturn V flight data. A convective cooling rate was measured at the base heat shield up to approximately 12 kilometers (6.5 n mi) altitude, after which a small convective heating rate was measured. A convective heating rate was present on the F-1 engine nozzle extension from liftoff and reached a maximum value at an altitude of 22 kilometers (11.9 n mi). Convective heating to the nozzle extension was negligible above 40 kilometers (21.6 n mi).

The total heating rate measured on the base of Fin D is compared with the AS-501 and AS-502 flight data in Figure 17-3. It is evident that fin total heating measurements for all three flights were approximately the same.

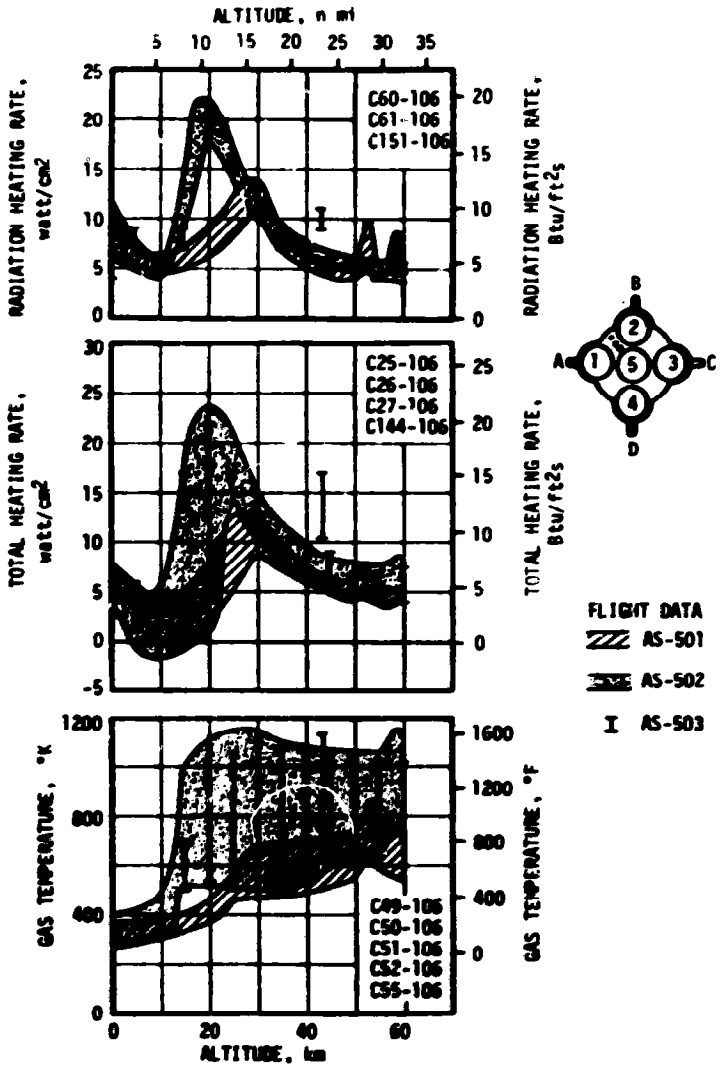

Figure 17-1. S-IC Base Heat Shield Thermal Environment

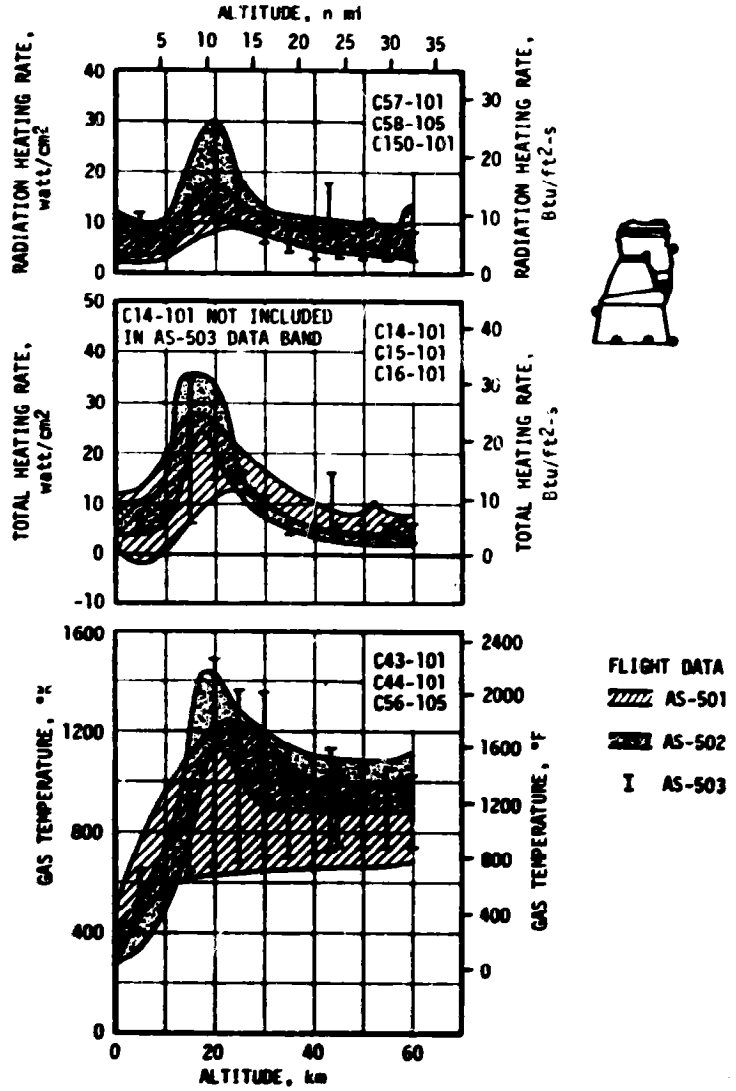

Figure 17-2. F-1 Engine Thermal Environment

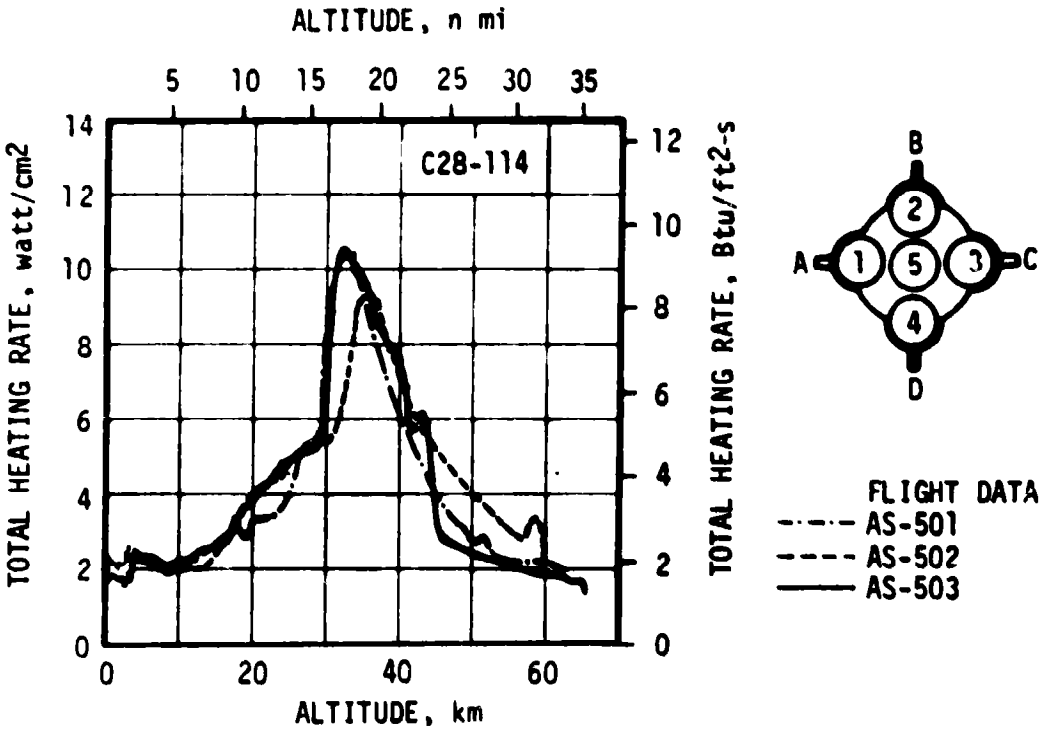

Figure 17-3. Base of Fin D Total Heating Rate

The initial rise in heating rate occurring at 15 kilometers (8.1 n mi) correlates with the recirculated exhaust gases reaching the heat shield as observed by TV cameras. The peak in the AS-503 data is coincident with the AS-501 data, and occurred at the time that flow separation was first observed.

The thermal response of the heat shield is delineated in Figures 17-4, 17-5, and 17-6 which show the forward surface, bondline, and M-31 internal temperatures, respectively. The upper edge of the data bands in all three figures is very clearly defined by measurements on the position lines where maximum heating occurred. Only 3 of the 14 thermocouples are located on the fin lines, as shown in Figure 17-7, and the traces from these give the lower edge of the data bands for the forward surface and bondline. As expected, fin line temperatures were low since the engines partially shield this area from the base environment.

Temperature histories of the heat exchanger bellows, exhaust manifold, and the nozzle are shown in Figure 17-8. The thermocouple on the engine nozzle did not experience the expected temperature rise during the latter half of flight and is suspect. The heat exchanger bellows thermocouple apparently failed at 100 seconds. In general, the valid data compares favorably with the expected temperatures on the engines.

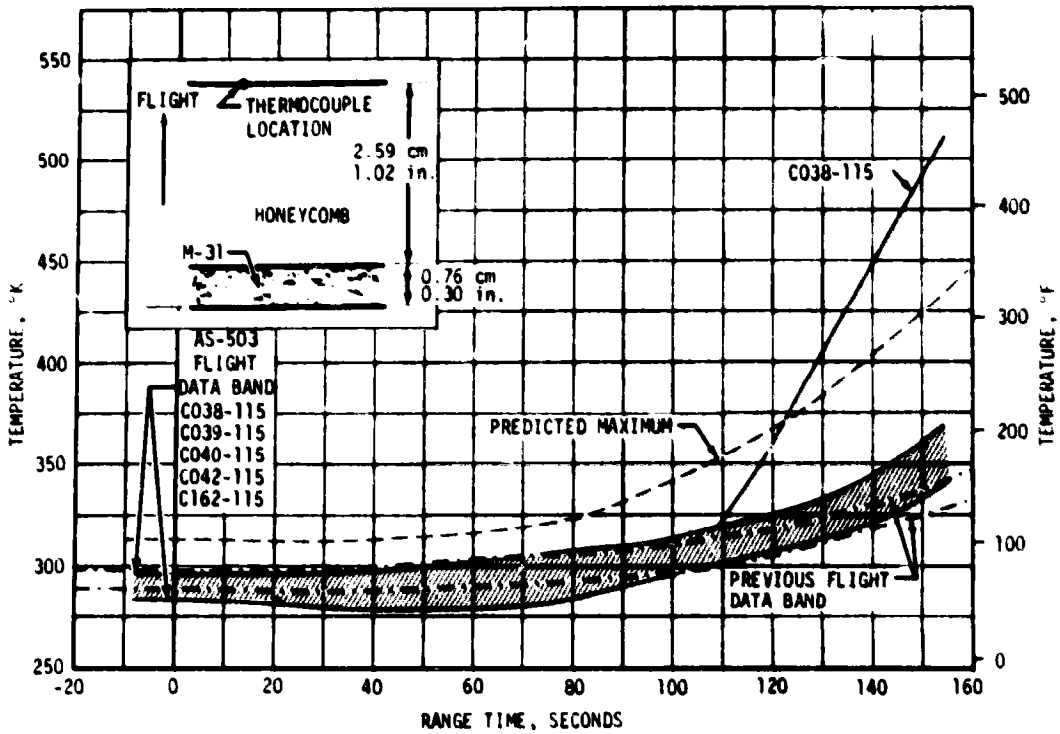

Figure 17-4. S-IC Heat Shield Forward Surface Temperature

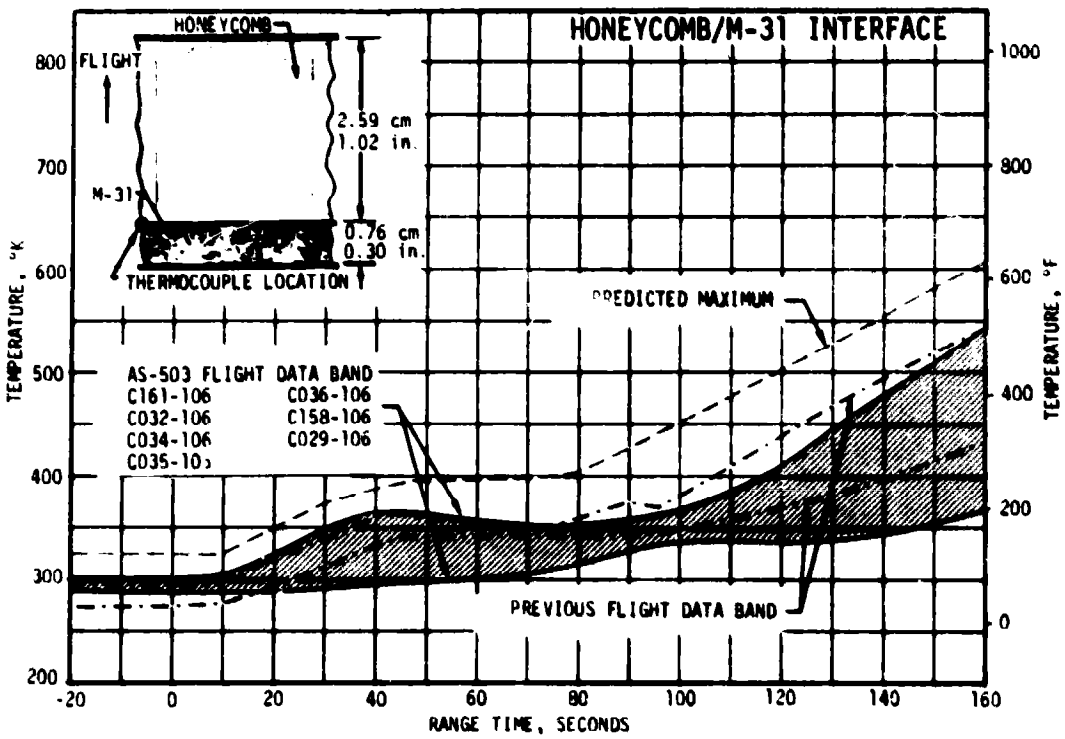

Figure 17-5. S-IC Heat Shield Bondline Temperature

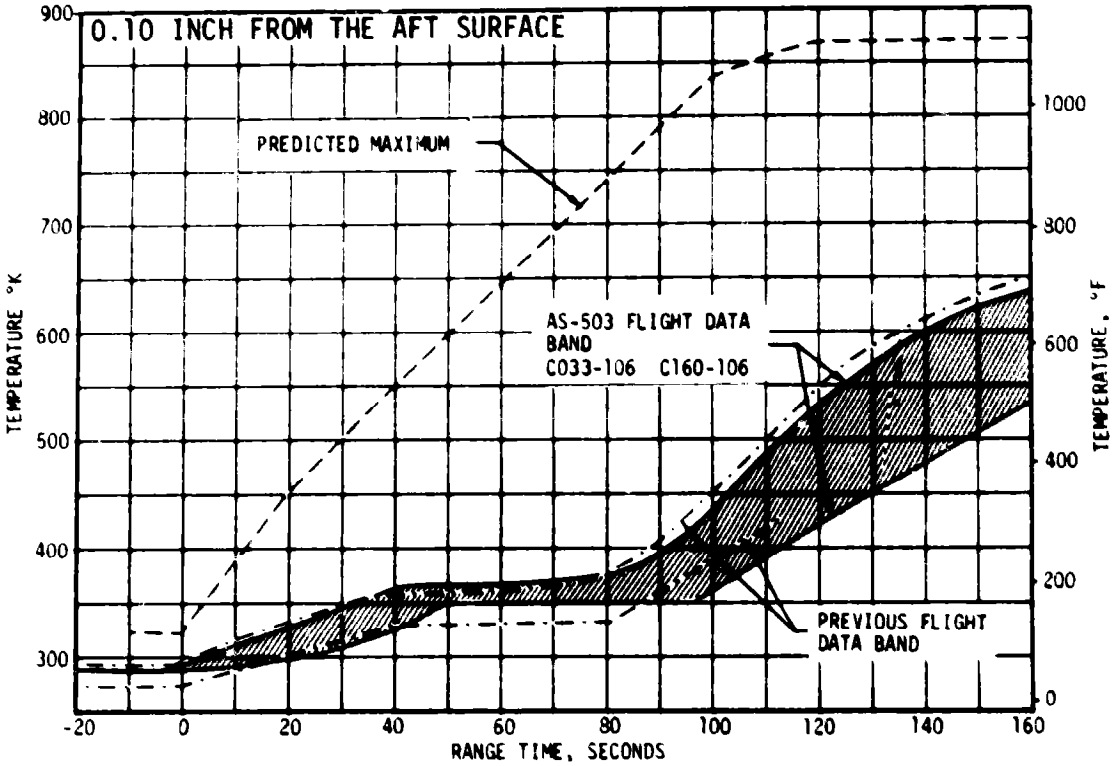

Figure 17-6. S-IC Heat Shield, M-31 Temperature

The M-31 loss to the crushed core level of the S-IC base heat shield, which means the 0.407 centimeter (0.16 in.) aft layer of M-31 broke away, was visually observed via the base region TV cameras. Losses were noted during initial flow reversal at approximately 70 to 90 seconds.

Figure 17-9 shows an area on the aft face of the S-IC base heat shield as recorded by the inflight TV monitor at 68 seconds and at 122 seconds. No loss of M-31 is shown in the 68-second frame; however, the frame taken at 122 seconds, which views the identical area, shows a single missing patch of M-31. The loss of this material seems to be less severe than on AS-502, based on TV observation for the two vehicles.

Although not in the same area of the heat shield as that viewed by the TV monitor, a similar missing patch of M-31 probably accounts for the divergence of measurement C038-115 from the nominal data band at 100 seconds, as shown in Figure 17-4. Based on the thermal environment at the heat shield and previous studies, the M-31 loss which caused this thermocouple response could have occurred as early as 50 seconds.

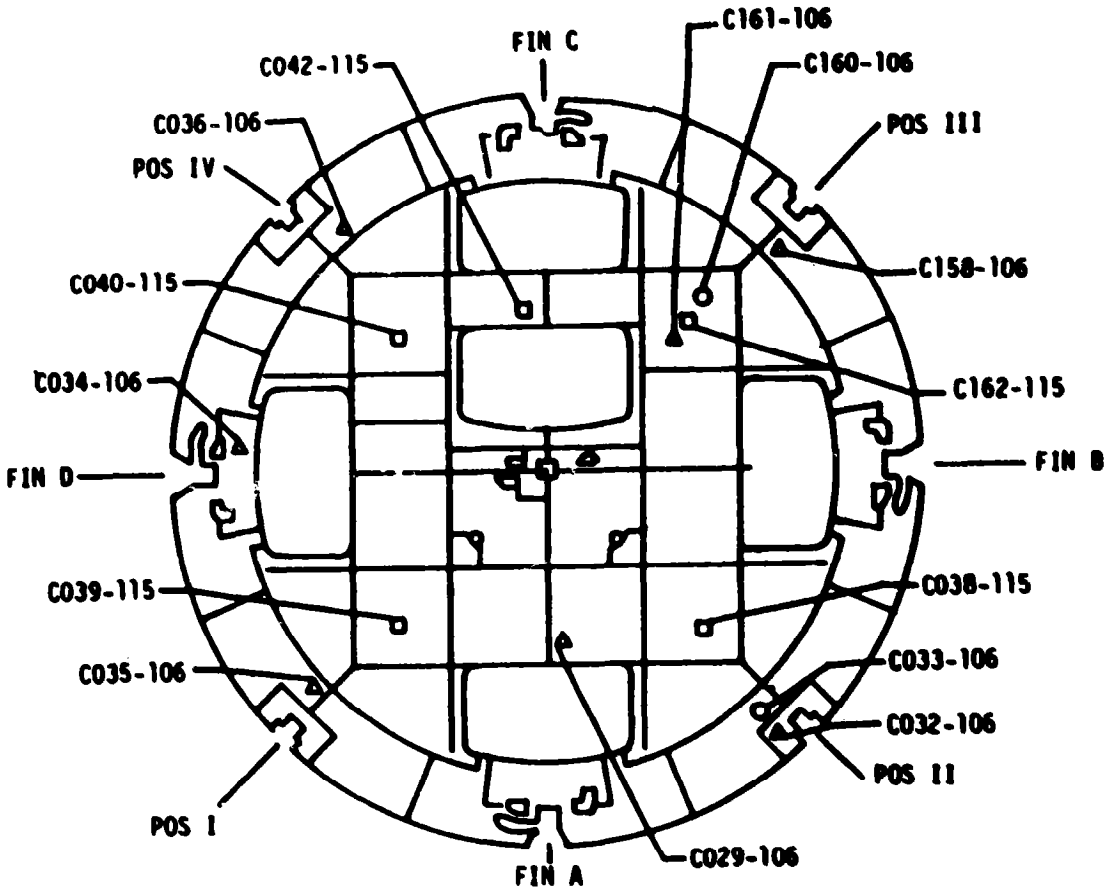

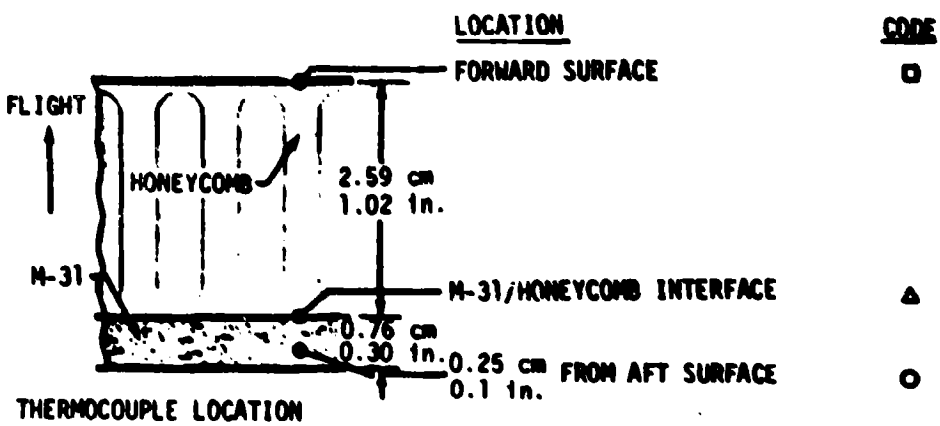

Figure 17-7. S-IC Base Heat Shield Measurement Locations

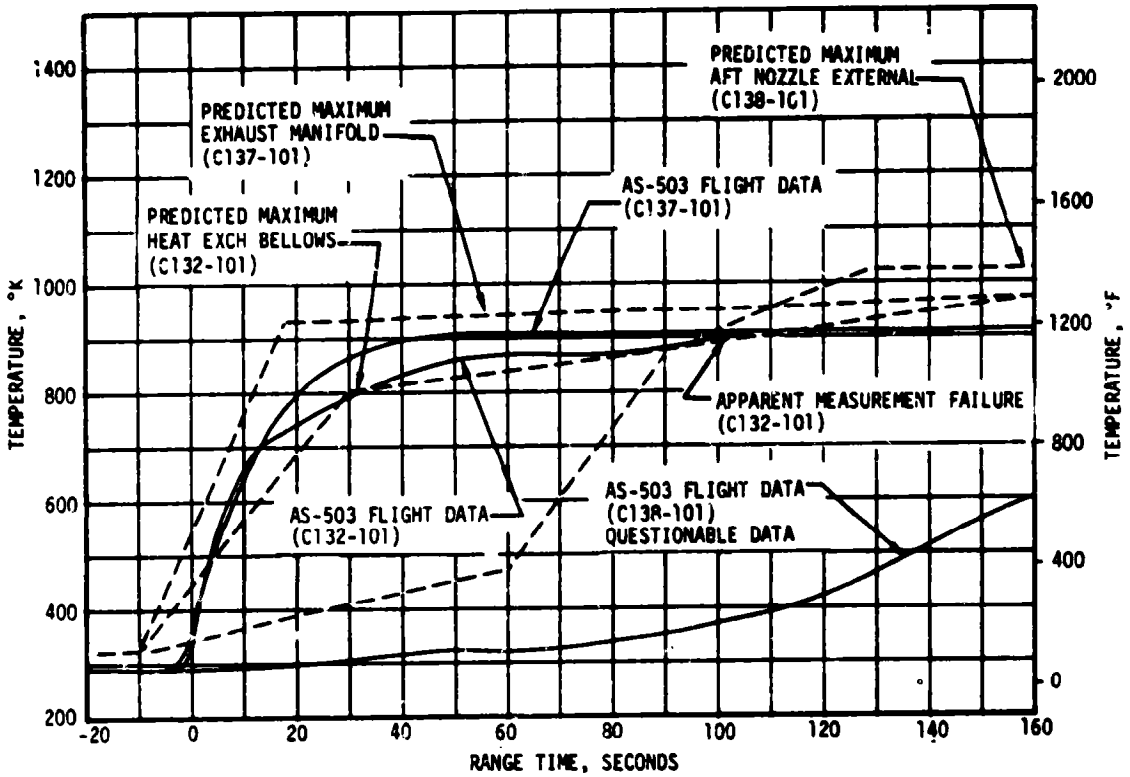

Figure 17-8. S-IC Temperature Under Insulation, Inboard Side Engine No. 1

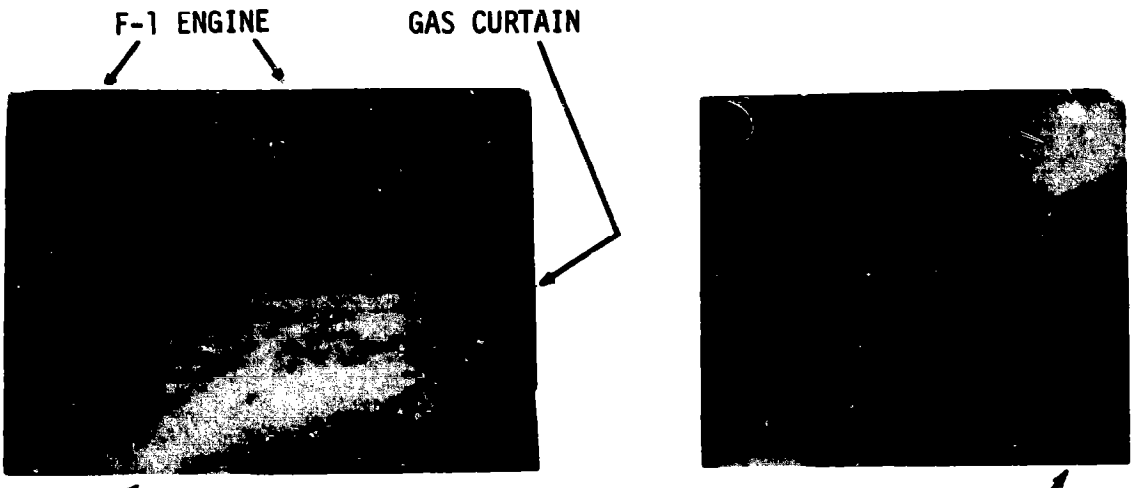

AFT FACE OF HEAT SHIELD SURFACE WITH M-31 INSULATION

FRAME AT 68 SECONDS RANGE TIME

MISSING PATCH OF M-31 INSULATION MATERIAL TO THE DEPTH OF THE CRUSHED CORE

FRAME AT 122 SECONDS RANGE TIME

Figure 17-9. S-IC AFT Face of Base Heat Shield Inflight TV Coverage

M-31 loss has been experienced on all S-IC boosters launched to date. On AS-501, the loss was noted at 110 seconds. On AS-502, M-31 was lost at 95 seconds in the vicinity of two measurements and at 108 seconds near another measurement as shown in Figure 17-4 of the AS-502 Evaluation Report (MPR-SAT-FE-68-3, dated June 25, 1968). The AS-502 TV camera film showed M-31 loss and substantiated the separation at the crushed core level, as did analytical reconstruction using gas temperature and radiometer data.

As reported in the AS-502 Evaluation Report, analysis conducted for AS-501 and AS-502 has indicated that loss of M-31, subsequent to flight times of 80 to 90 seconds, will not result in any detrimental effects on the S-IC stage aft thrust structure/engine compartment.

17.2.2 S-IC/S-II Separation Environment

As shown in Figure 17-10, gas temperatures during separation were similar to those measured on previous flights. Two spikes in gas temperature are evident; one immediately following separation and resulting from ullage motor gases entering the forward skirt area and the other corresponding to the S-II stage J-2 engine thrust buildup. Data from the separation transducers indicate separation rates and attitudes essentially the same as those experienced previously.

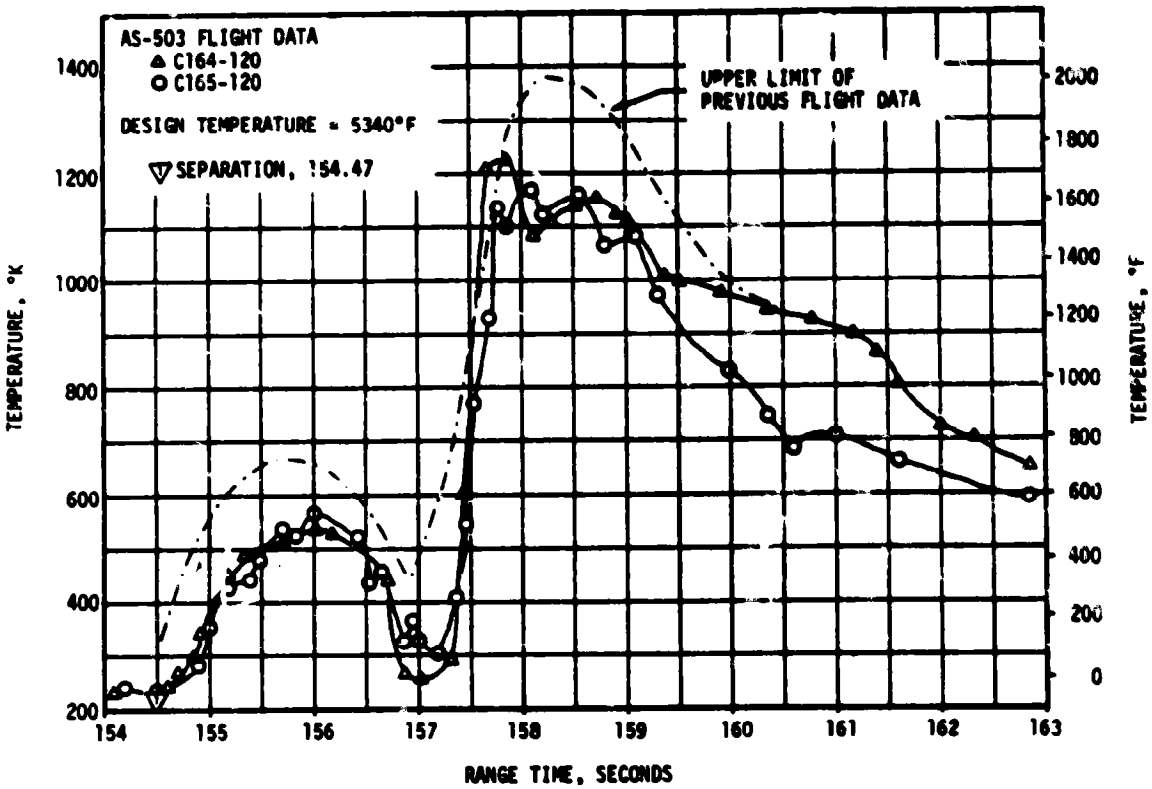

Figure 17-10. S-IC Upper Compartment Ambient Air Temperature During S-IC/S-II Stage Separation

The S-IC forward skirt skin temperatures measured during separation are shown in Figure 17-11. The maximum temperature reached was slightly higher than those previously experienced and occurred about 3 seconds later but presented no problem.

The S-IC LOX tank dome temperatures, Figure 17-12, show that no appreciable heating occurred during separation, and corresponding temperatures on previous flights were practically duplicated.

The maximum internal pressures, in the S-IC forward skirt area, were less than 1.0 N/cm^2 (1.45 psia) and occurred during S-II main engine start-up. Pressure spikes during ullage motor firing were small and did not reach magnitudes equal to AS-501.

17.3 S-II BASE HEATING AND SEPARATION ENVIRONMENT

The postflight predicted convective heating rates are based on hot flow model test data. The recovery temperature of the reverse flow gas was

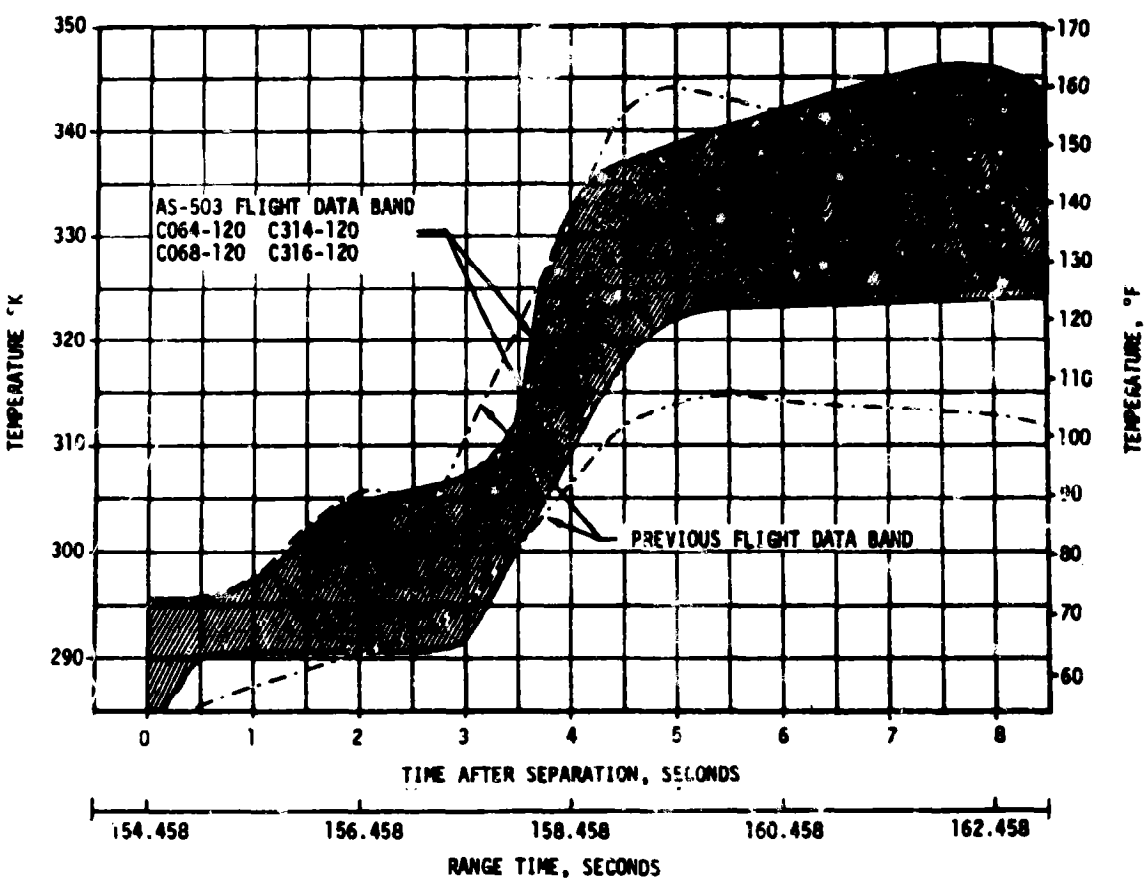

Figure 17-11. S-IC Forward Skirt Skin Temperature after S-IC/S-II Stage Separation

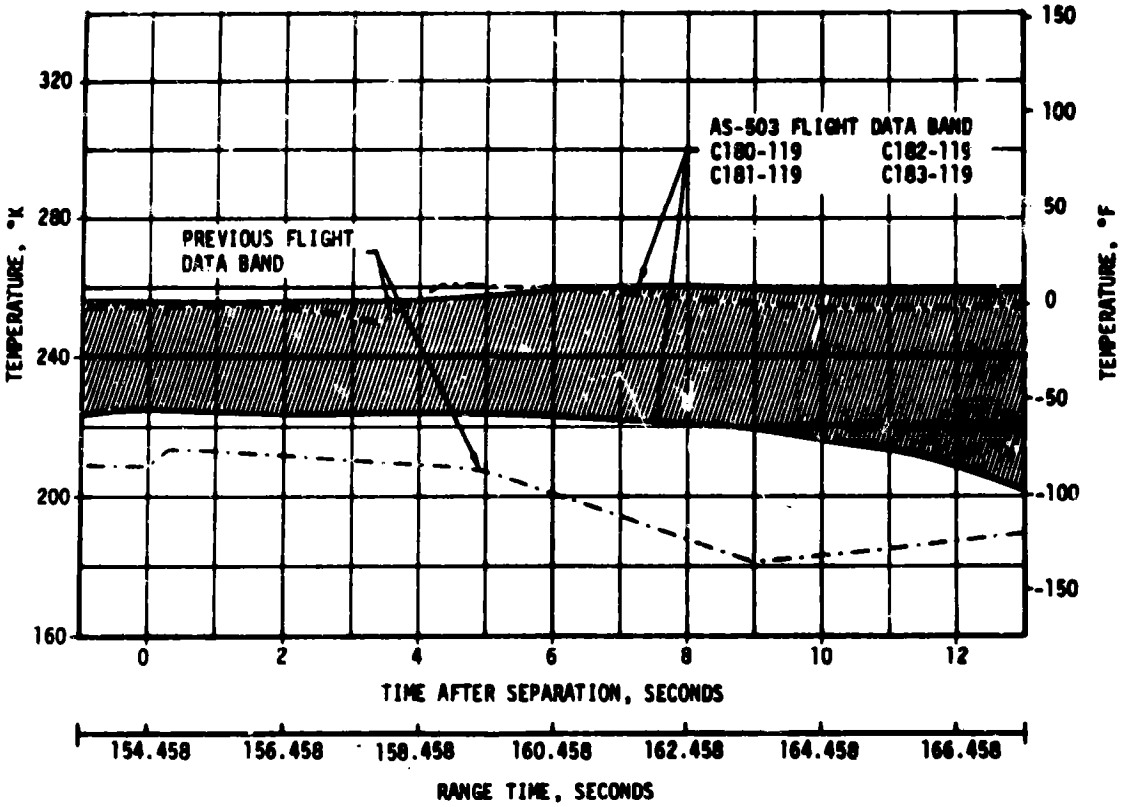

Figure 17-12. S-IC LOX Tank Forward Dome Temperature During S-IC/S-II Stage Separation

determined to be 978°K (1300°F) prior to PMR stepdown, and 894°K (1150°F) after PMR stepdown. The cold wall convective and radiation heat flux, and gas recovery temperatures were then used to establish the heat shield surface temperature and the corresponding postflight cold wall total heating rate predictions. Engine performance, i.e., mixture ratio, chamber pressure, temperature, and gimballing effects on convective heating rates were considered.

The AS-503 S-II measured base heating and separation environment was, in general, below design data and in good agreement with AS-501 and AS-502 flight data and AS-503 postflight predictions.

Figure 17-13 presents a band of total heating rates to the calorimeters on the aft face of the base heat shield for the S-II boost period. The AS-503 postflight predictions of these heating rates is shown together with AS-501 and AS-502 flight data for comparison. Figure 17-13 indicates that the analytical predictions are in good agreement with the flight data.

It is observed in Figure 17-13 that the maximum heating rate increased sharply after interstage separation. This change was noticed in data from a measurement located near the stagnation point of the reverse flow. Similar trends were observed on the previous flights but the increases were not as sharp as on AS-503.

The decrease in PMR at 443 seconds resulted in a 25 percent reduction in heating rate.

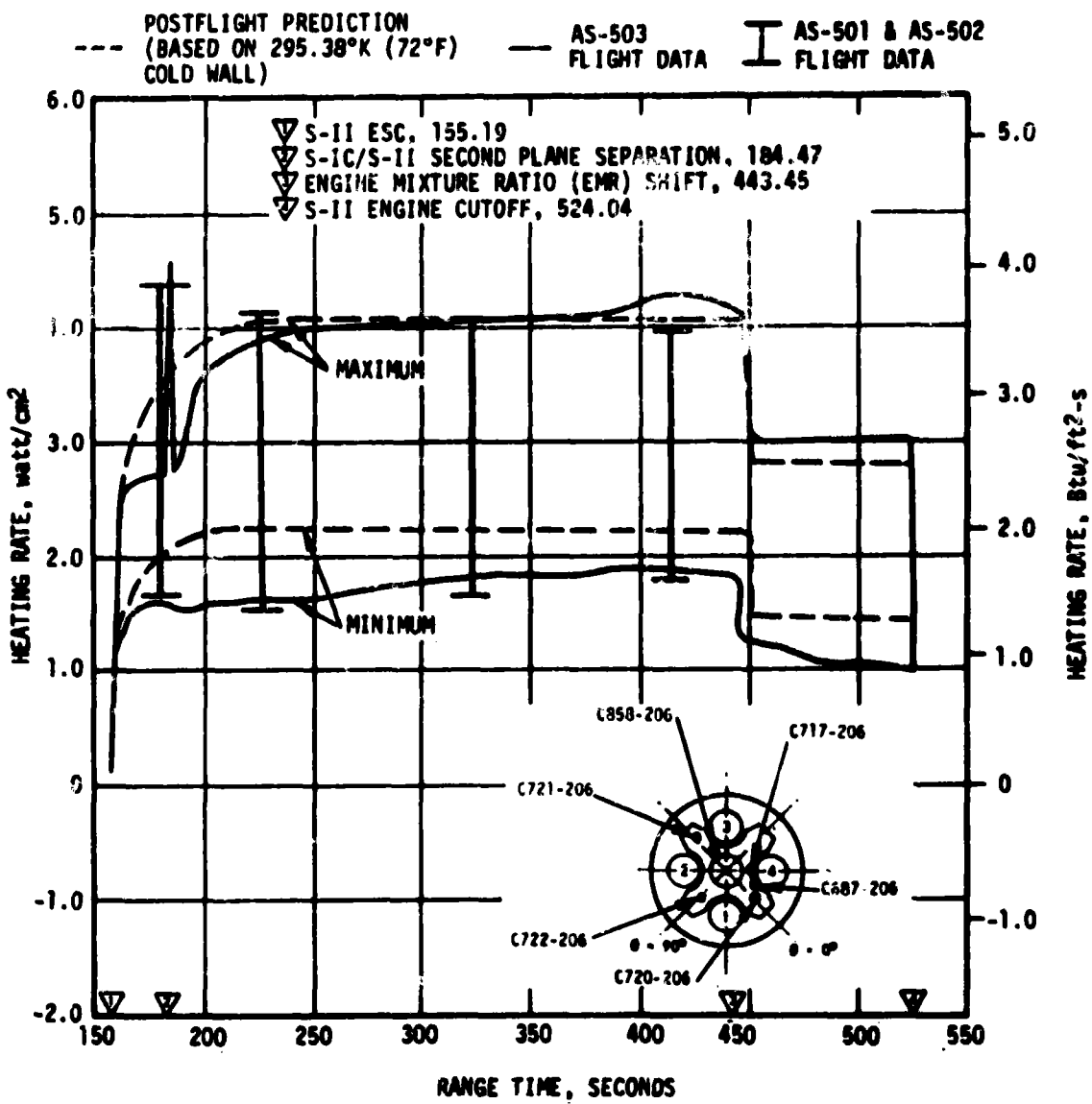

Figure 17-13. S-II Heat Shield Base Region Heating Rates

Postflight predicted and AS-503 measured thrust cone region total heating rates are presented in Figure 17-14. AS-501 and AS-502 flight data are also presented for comparison. The postflight predictions are in good agreement with the AS-503 flight data.

Figure 17-14 shows that the data band of total heating rates for AS-501 and AS-502 flights is wider prior to interstage separation when compared with the present flight data. This difference could be caused by a slight variation of the reversal flow phenomena and/or by variations in engine performance.

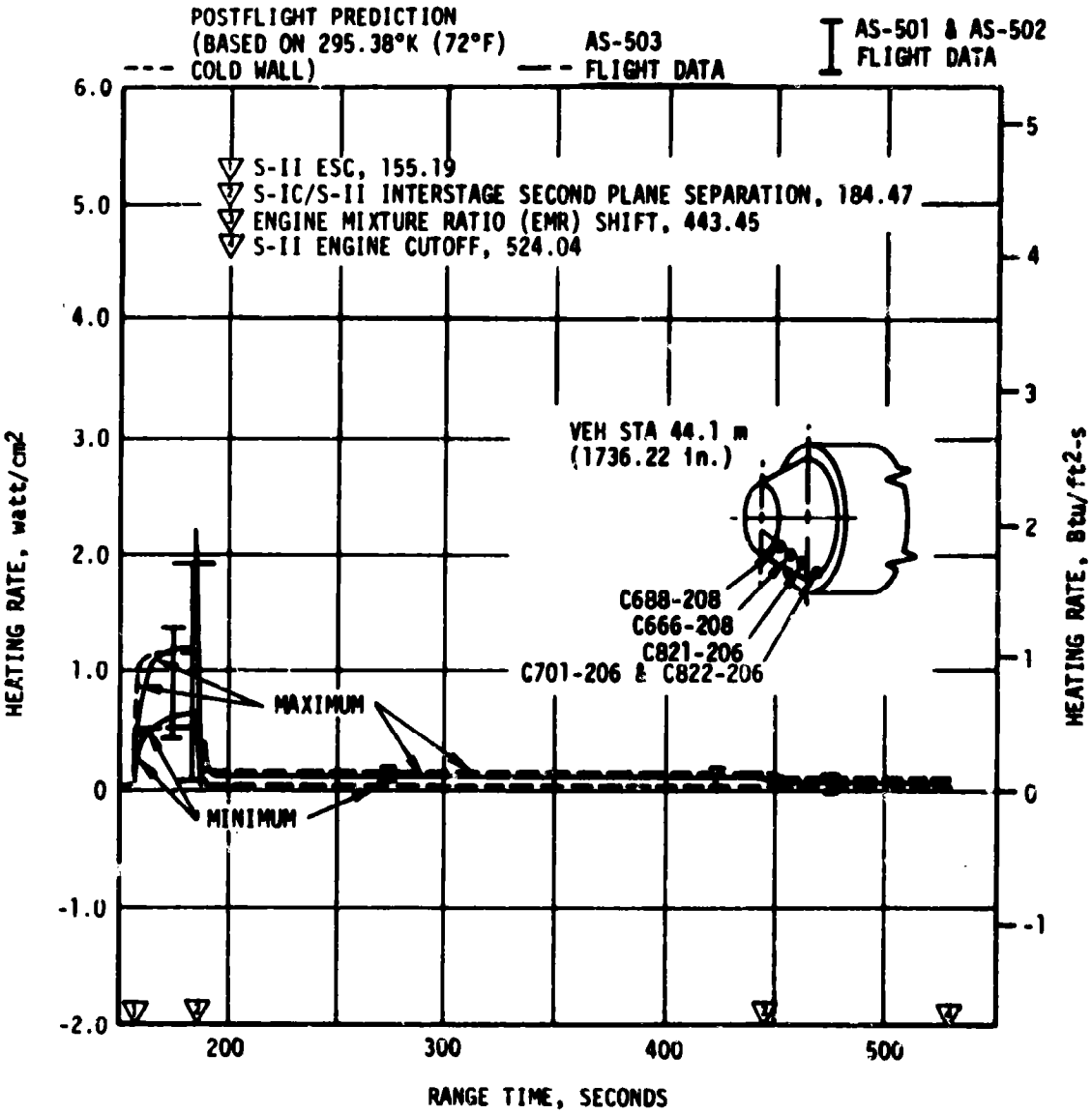

Figure 17-14. S-II Thrust Cone Heating Rate

Gas recovery temperature at the S-II stage base heat shield aft face is shown in Figure 17-15. The postflight predicted gas recovery temperature is based on model test data, and on AS-501 and AS-502 base heat shield heating rates. A gas recovery temperature was calculated from flight transducer temperature data, using a probe emissivity factor of 0.425, and is also shown in Figure 17-15.

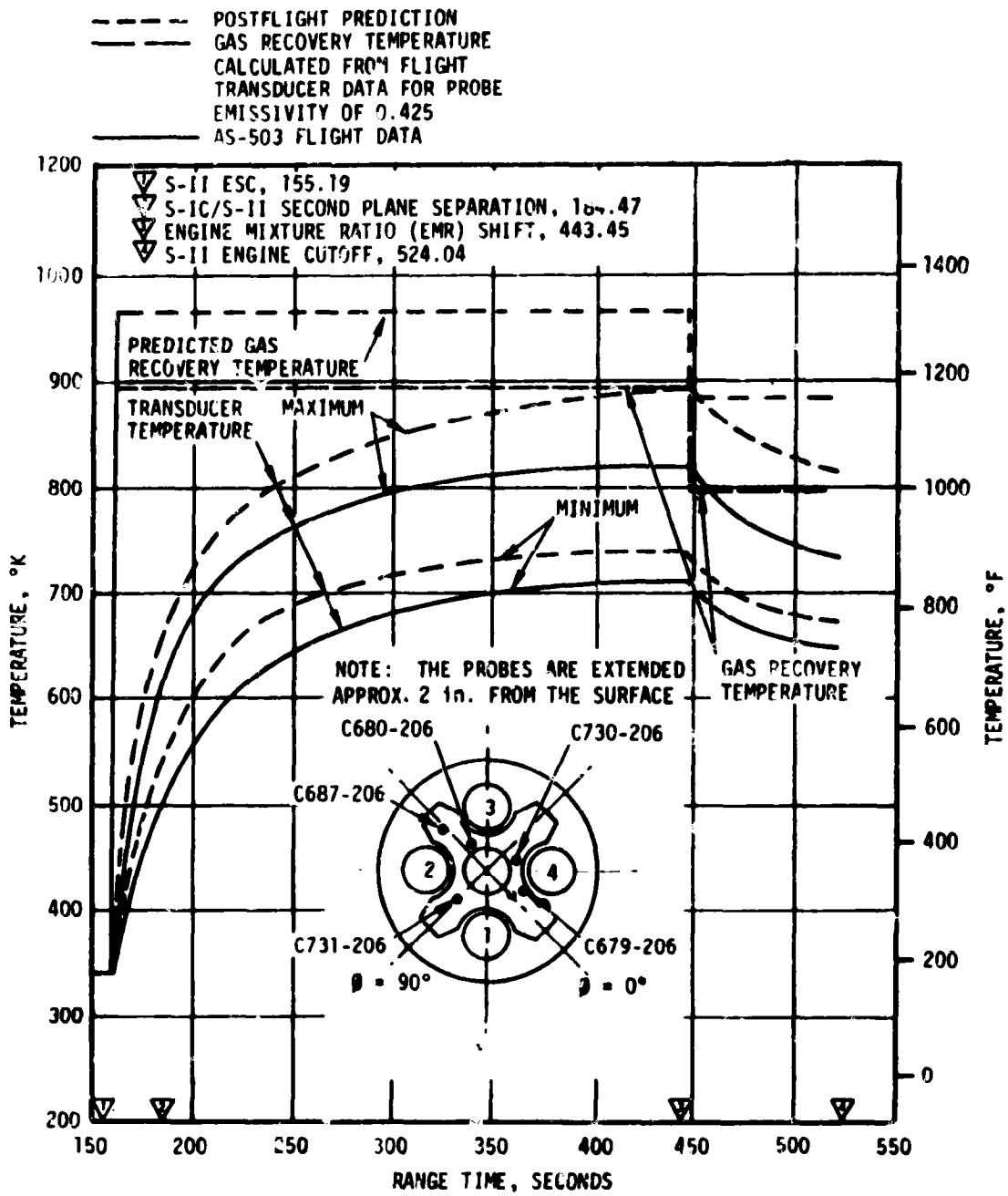

Figure 17-15. S-II Base Gas Temperature

Temperatures recorded during the AS-503 flight on the aft face of the base heat shield were well below design values, and compared favorably with previous flights. Figure 17-16 presents a comparison of AS-503 base heat shield aft face temperature data with AS-501 and AS-502 flight data and design temperatures. The lower temperatures in the AS-501 band were due to the added heat capacitance of special steel transducer mounts used for two of the AS-501 measurements. The extended flight time for the AS-502 was due to loss of two engines at 413 seconds. Thus, the AS-503 band is the first true indication of expected nominal flight data. The maximum recorded AS-503 temperature of 764°K (915°F) occurred at 443 seconds, immediately prior to the PMR shift which reduced the heating rate, and was slightly higher than the maximums of 742°K (875°F) and 735°K (865°F) recorded on AS-501 and AS-502, respectively. The design temperatures were calculated using the maximum design environment.

The effectiveness of the heat shield and flexible curtains as a thermal protection system was demonstrated by the relatively low temperatures of the heat shield forward surface, as shown in Figure 17-17, when compared to the high temperature on the heat shield aft face shown in Figure 17-16. The range of heat shield forward surface temperatures measured on AS-503, shown in Figure 17-17, was below design and similar to the range of temperatures measured on AS-501 and AS-502.

17.4 S-IVB ENGINE AREA THERMAL ENVIRONMENT

The S-IVB engine area thermal environment showed a normal response as evidenced by the J-2 engine ASI skin temperatures. These skin temperatures are discussed in paragraph 7.3 and are shown in Figure 7-10 of Section 7.

17.5 VEHICLE AEROHEATING THERMAL ENVIRONMENT

17.5.1 S-IC Stage Aeroheating Environment

The aerodynamic heating environments were measured using thermocouples attached to the backside of the structural skin on the S-IC forward skirt, intertank, engine fairings and fins. In addition, external skin temperature measurements were made on the forward skirt. Generally, the aerodynamic heating environments and skin temperatures were within prediction bands, below design limits, and were slightly lower than AS-501 and AS-502 flight data.

Comparisons of measured skin temperatures and heating rates derived from these temperatures for AS-501, AS-502, and AS-503 flights are presented in Figures 17-18 through 17-26. Postflight simulated skin temperatures are also included. The fin skin temperature simulation includes 0.284 watt/cm^2 (0.25 Btu/ft^2-s) for sea level plume radiation and a factor for variation with altitude. In addition, the flow separation environments were included in the fin temperature simulations.

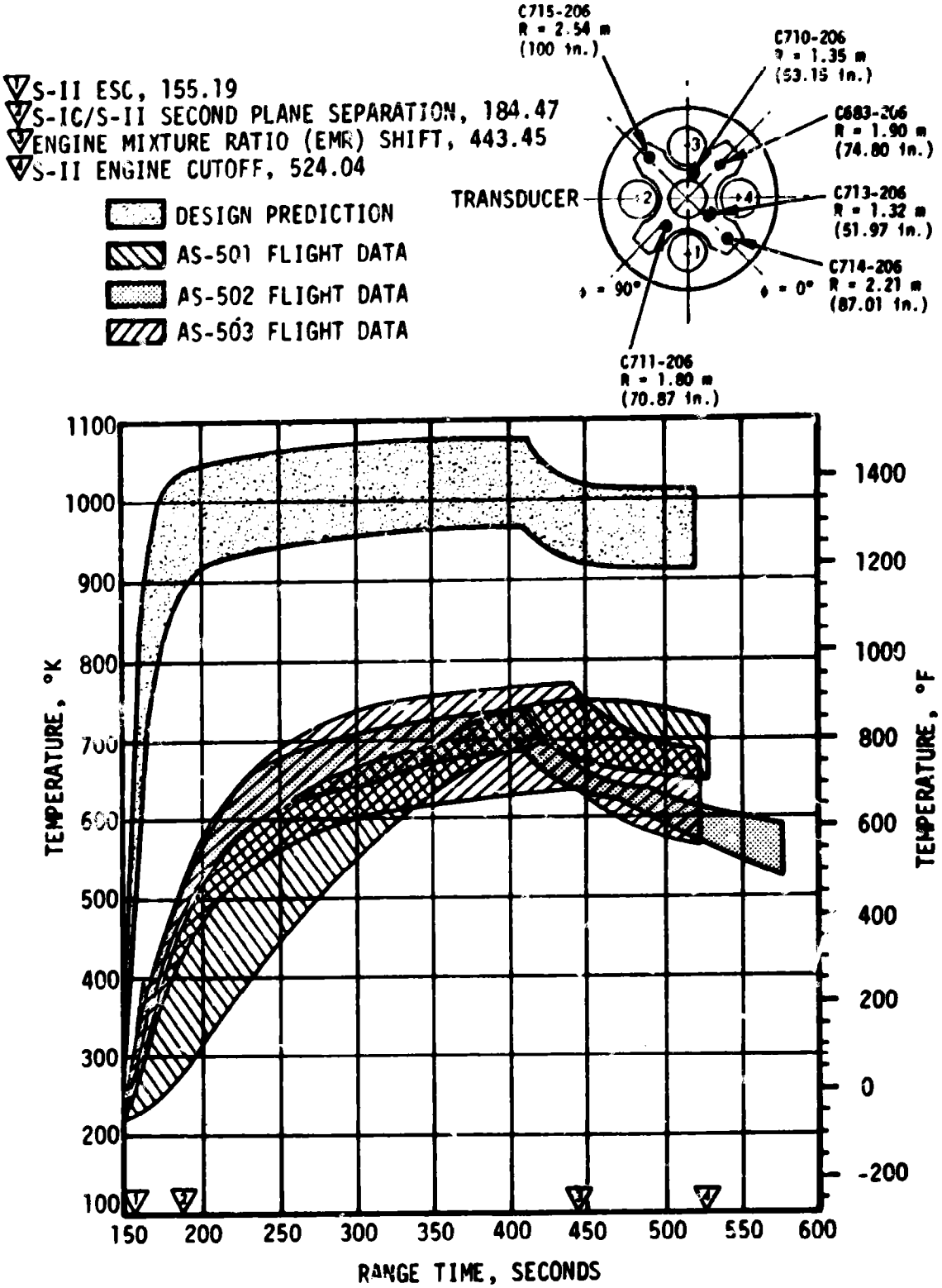

Figure 17-16. S-II Heat Shield Aft Face Temperatures

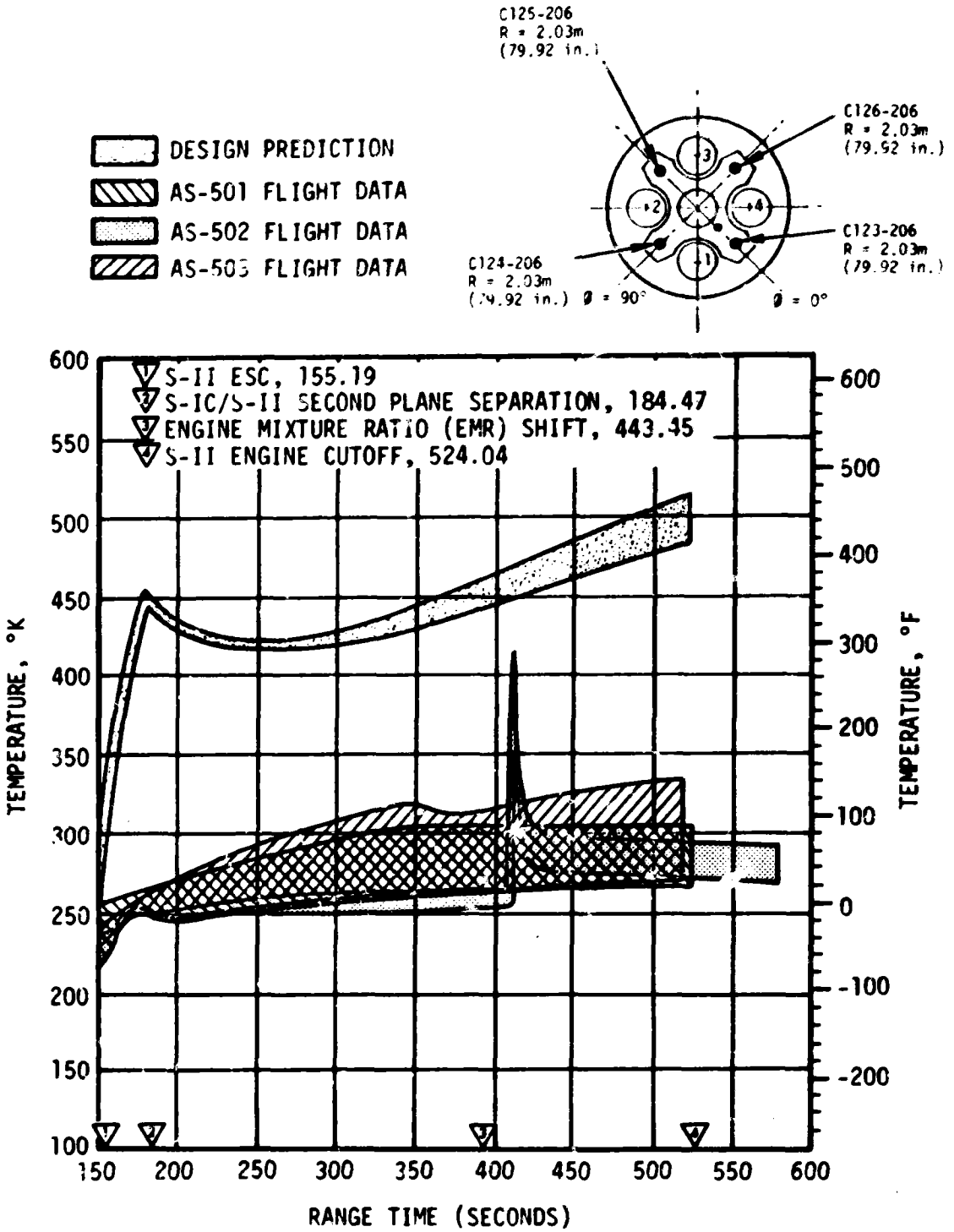

ALL FORWARD AND AFT FACE MEASUREMENTS ARE LOCATED ON THE DESIGNATED SURFACE OF THE HEAT SHIELD

Figure 17-17. S-II Heat Shield Forward Face Temperatures

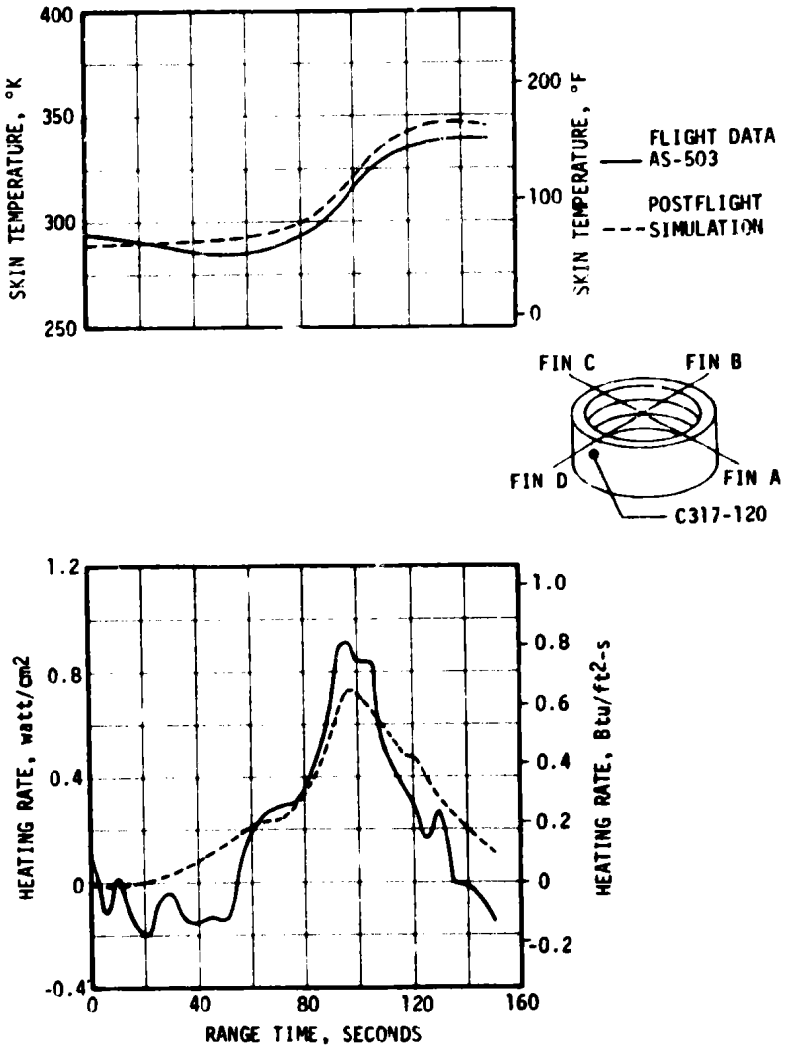

Figure 17-18. S-IC Forward Skirt Aerodynamic Heating Near Finline D

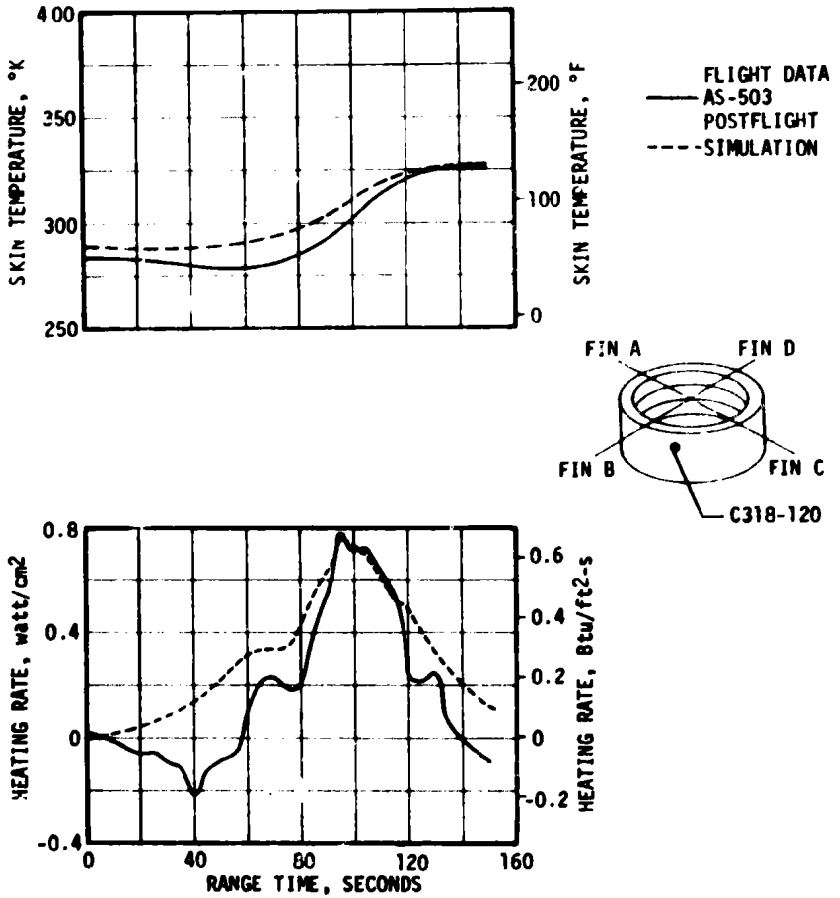

Figure 17-19. S-IC Forward Skirt Aerodynamic Heating Near Finline B

External skin temperatures and corresponding heating rates on the S-IC forward skirt are presented in Figures 17-18 and 17-19. The measurements shown in these figures were not installed on previous vehicles. Figure 17-18 shows a higher heating rate than Figure 17-19 due to one measurement being located in a protuberance wake interference area and the other being located in a clean skin area. A comparison of forward skirt skin temperatures for AS-501, AS-502, and AS-503 vehicles is shown in Figure 17-20. Measurement C316-120, located on the forward skirt inner skin and shown in the bottom graph of this figure, was not installed on previous vehicles but shows the same temperature response as adjacent measurements.

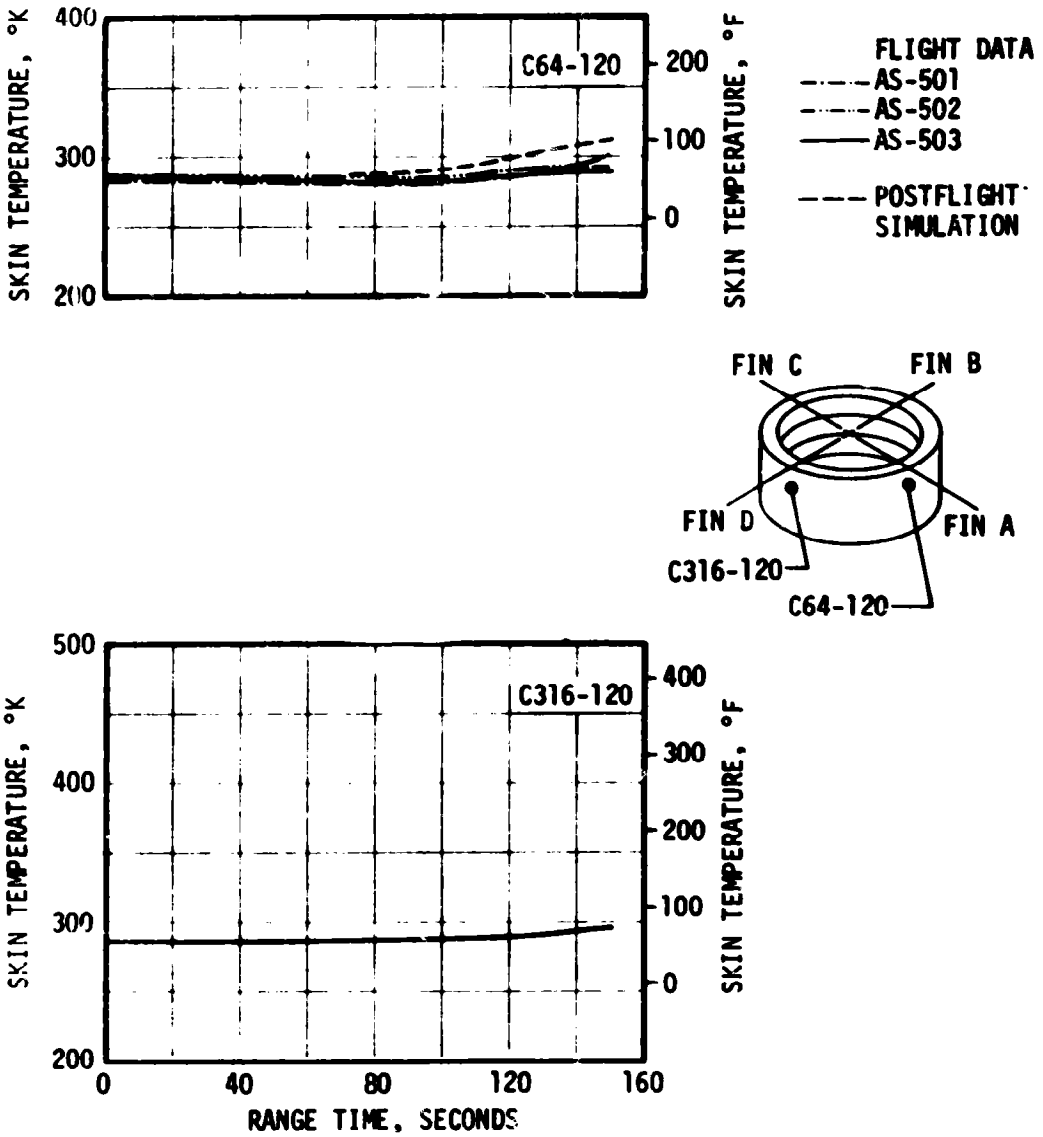

Figure 17-20. S-IC Forward Skirt Aerodynamic Heating Near Finlines A and D

Intertank skin temperatures are shown in Figures 17-21 and 17-22, along with heating rates derived from these temperatures. The AS-503 measured temperatures are below those of AS-501 and AS-502, thus reflecting a slightly less severe heating trajectory than that flown by AS-501 and AS-502 and a recession of the forward point of flow separation which was observed during AS-503 flight after IECO.

Measured skin temperatures and the corresponding heating rates for the engine fairings and fins are presented in Figures 17-23 through 17-26. These measurements indicate that flow separation reached the fins and engine fairings at approximately 110 seconds. The thermal environment during the period of flow separation was due to radiation. A sharp decrease in the flow separation environment is indicated at approximately 130 seconds, which represents a transition period of approximately 4 seconds after IECO. The temperature simulations include the predicted flow separation environment from 110 to 130 seconds and a reduced flow separation environment based on empirically established heating rates after 130 seconds.

Measurements made of the forward point of flow separation from flight optical data at various flight times are shown in Figure 17-27 for the AS-501, AS-502 and AS-503 flights. At IECO (125.93 seconds) this data indicates that separation receded rapidly and re-established at approximately 130 seconds at or near vehicle station 12.7 meters (500 in.). This recession in the forward point of flow separation was not confirmed by AS-501 optical data since IECO for AS-501 occurred at 135 seconds and optical data was not available beyond 135 seconds. Also, flow separation recession on AS-502 was not discernible due to IECO at 145 seconds and Outboard Engine Cutoff (OECO) a few seconds later. Fin and engine fairing temperatures did, however, show similar responses during AS-501 and AS-503 flights after IECO.

Skin temperatures on the forward skirt remained nearly constant until 90 seconds and then increased to a maximum of 303.16°K (86°F) just prior to S-IC/S-II separation, as shown in Figure 17-28. These temperatures closely resembled previous flight experience.

To assist in assessing the thermal environment that is actually present on the exterior of the forward skirt during flight, 0.1 inch-thick aluminum plates were installed on the outside of the silicone rubber insulation, on top of the hat sections at four locations. Figure 17-29 presents the preflight maximum plate temperature predictions, the measured temperature, and the postflight correlation for one of these plates.

Due to improved thermocouple installation techniques, the AS-503 flight is the first on which accurate LOX tank skin temperatures have been measured. The abbreviated previous flight data band shown in Figure 17-30

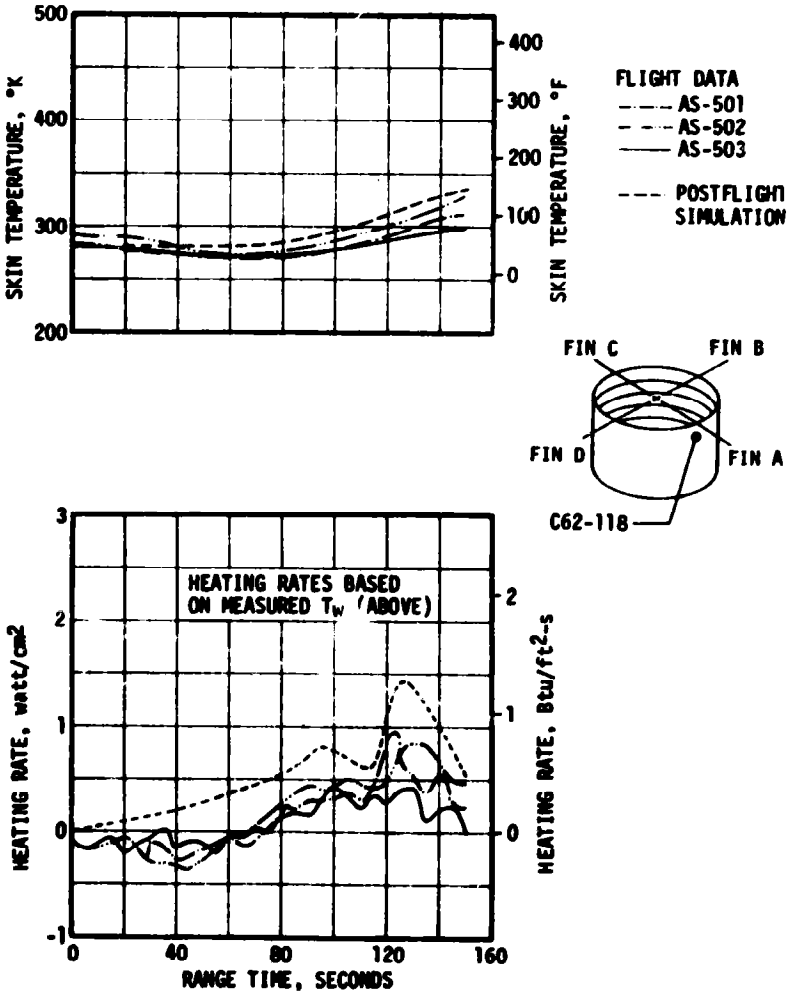

Figure 17-21. S-IC Intertank Aerodynamic Heating, Forward

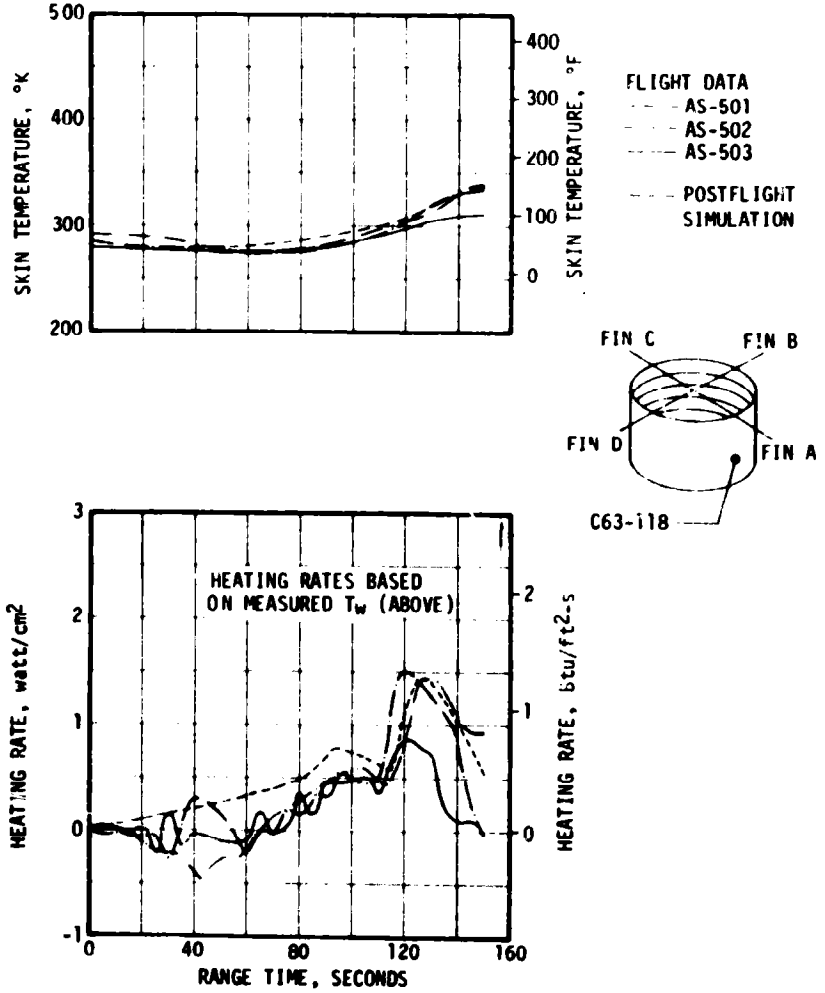

Figure 17-22. S-IC Intertank Aerodynamic Heating, Aft

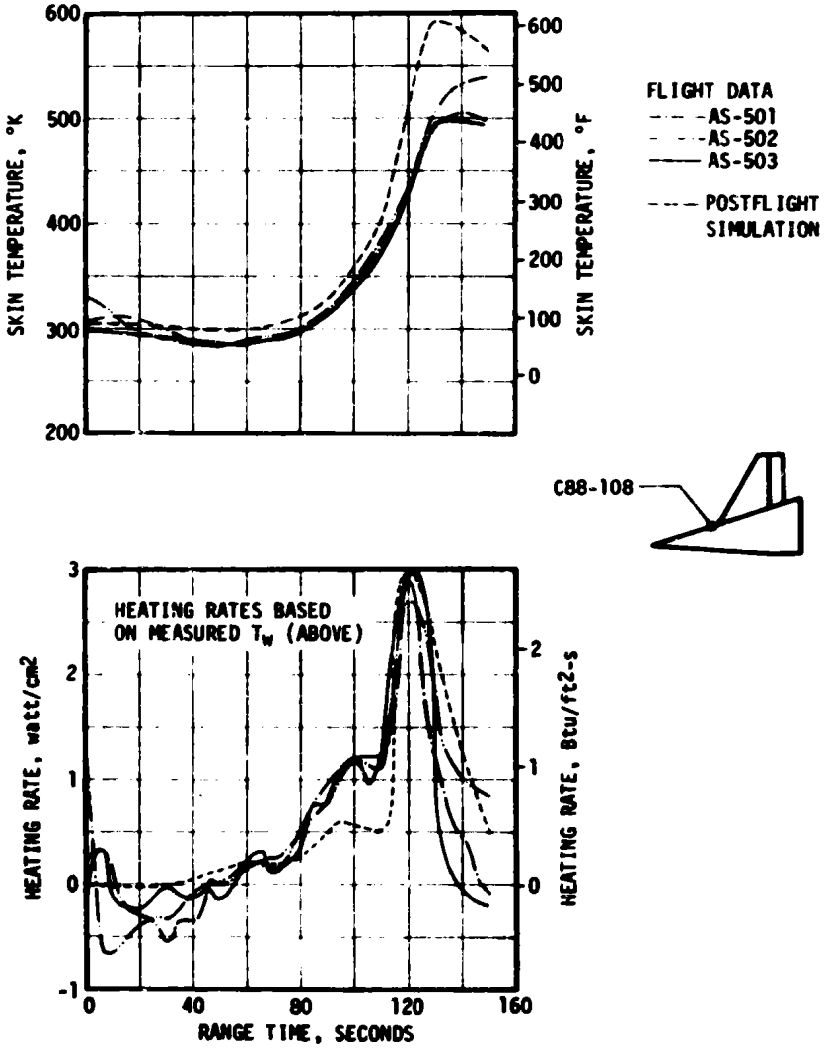

Figure 17-23. S-IC Engine Fairing (Fin B) Aerodynamic Heating

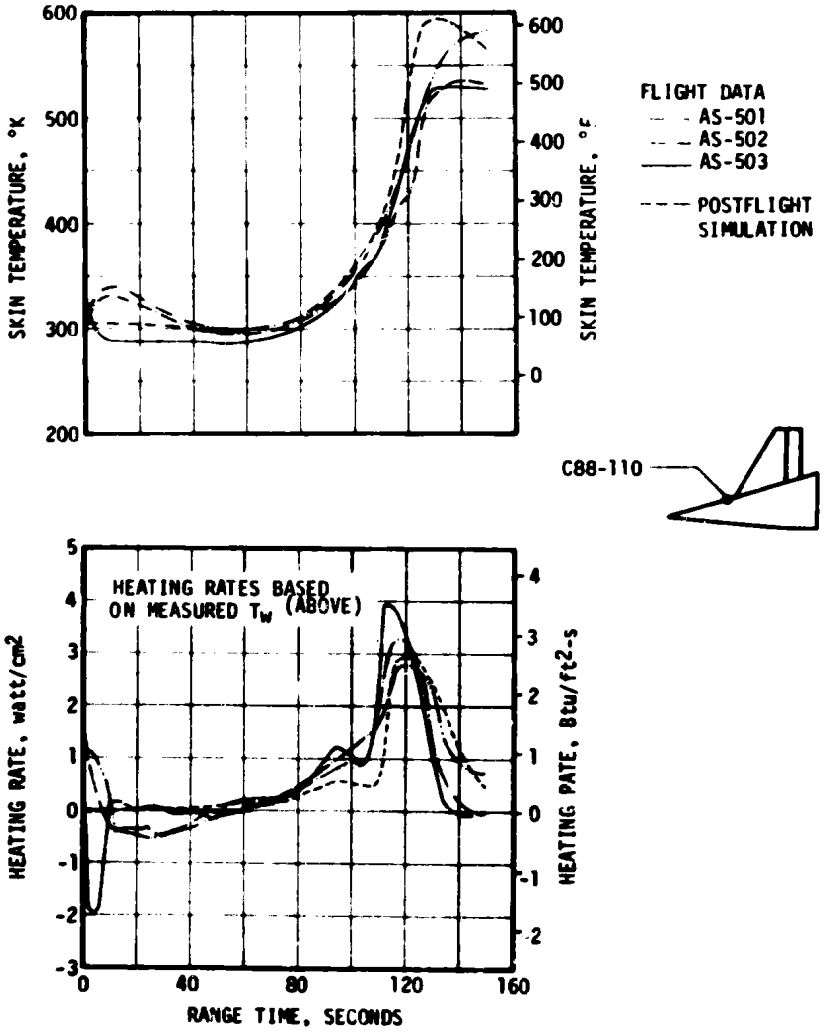

Figure 17-24. S-IC Engine Fairing (Fin D) Aerodynamic Heating

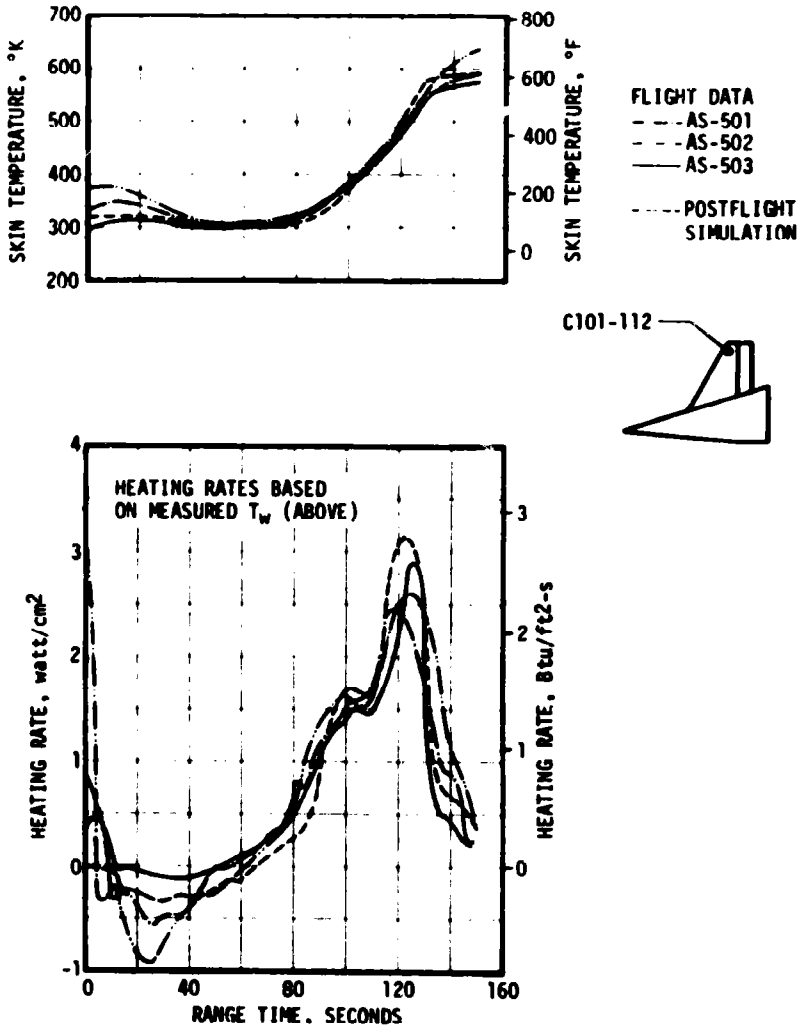

Figure 17-25. S-IC Fin B Aerodynamic Heating

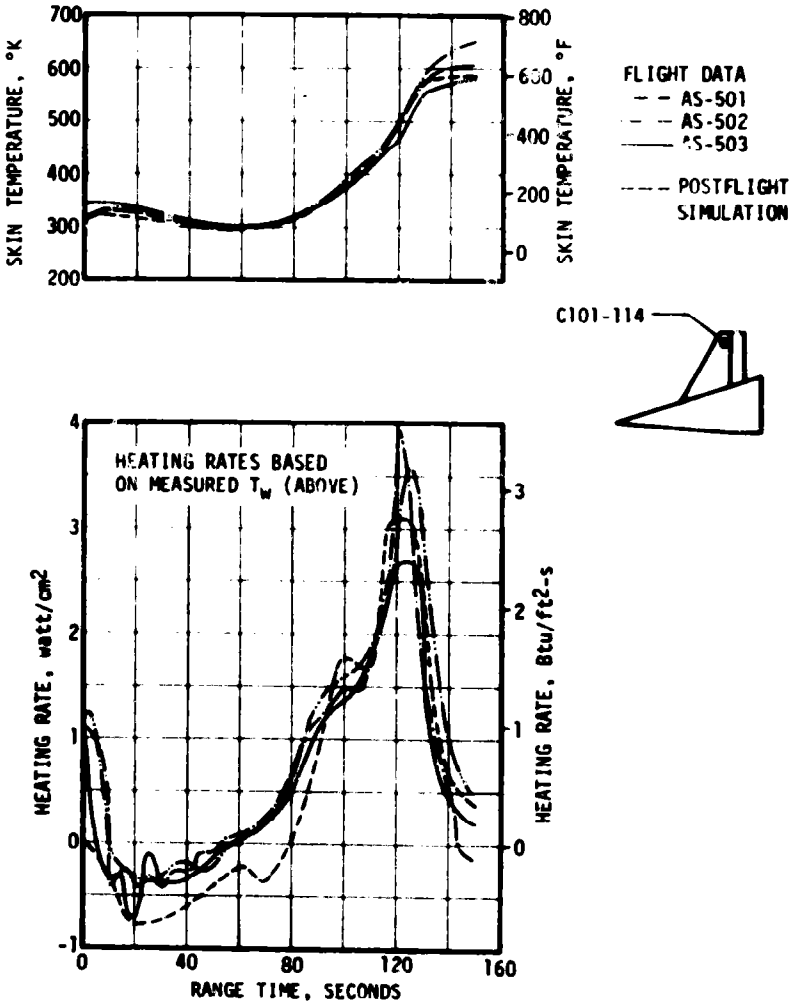

Figure 17-26. S-IC Fin D Aerodynamic Heating

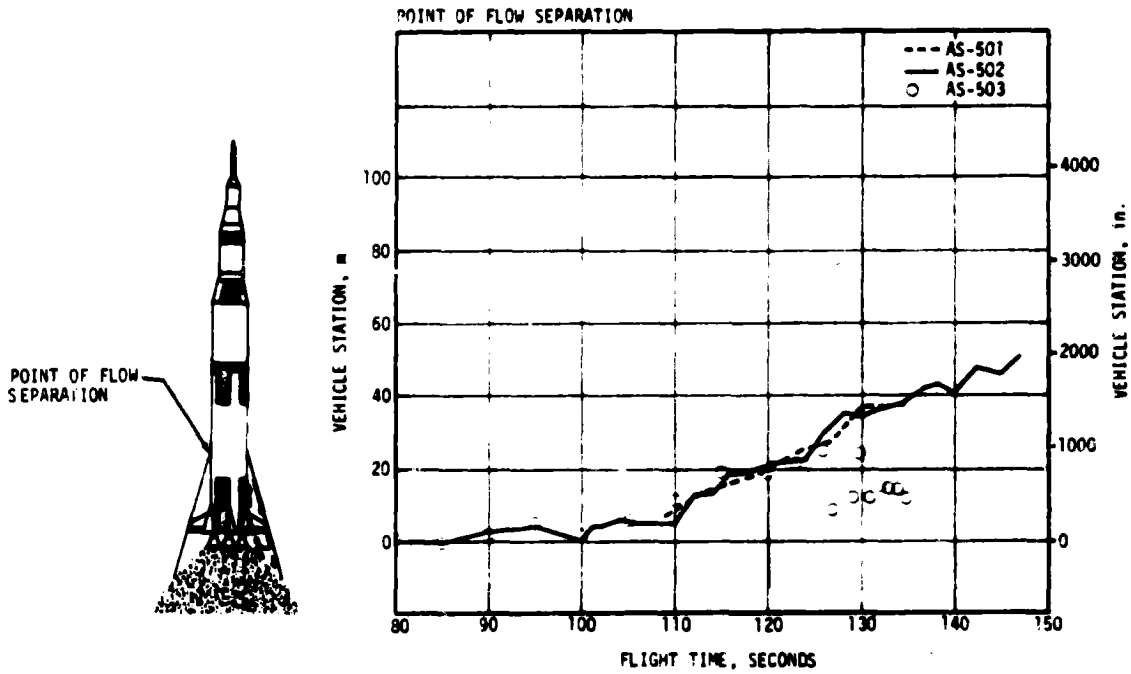

Figure 17-27. Forward Point of Separated Flow

represents the extent to which good data was received from the AS-501 and AS-502 flights. The AS-503 temperatures are well below the predicted maximum.

Intertank skin temperatures at liftoff were below those previously experienced, as seen in Figure 17-31. This is attributed to lower ambient temperatures and lower sea level wind velocities prior to liftoff. The temperatures at S-IC/S-II separation were well below those previously experienced which is attributed to the lack of plume-induced flow separation in this area for a significant period of time due to early IECO.

As was the case for the LOX tank, improved thermocouple installation techniques have permitted, for the first time, accurate fuel tank skin temperature measurements. These temperatures follow predicted trends, as seen in Figure 17-32.

As seen in Figure 17-33, the thrust structure skin temperature followed trends similar to those experienced on the first two flights. The sudden change of slope at 130 seconds, and failure to reach previously experienced temperatures is attributed to the sudden change in the extent and strength of the plume-induced flow separation region at IECO.

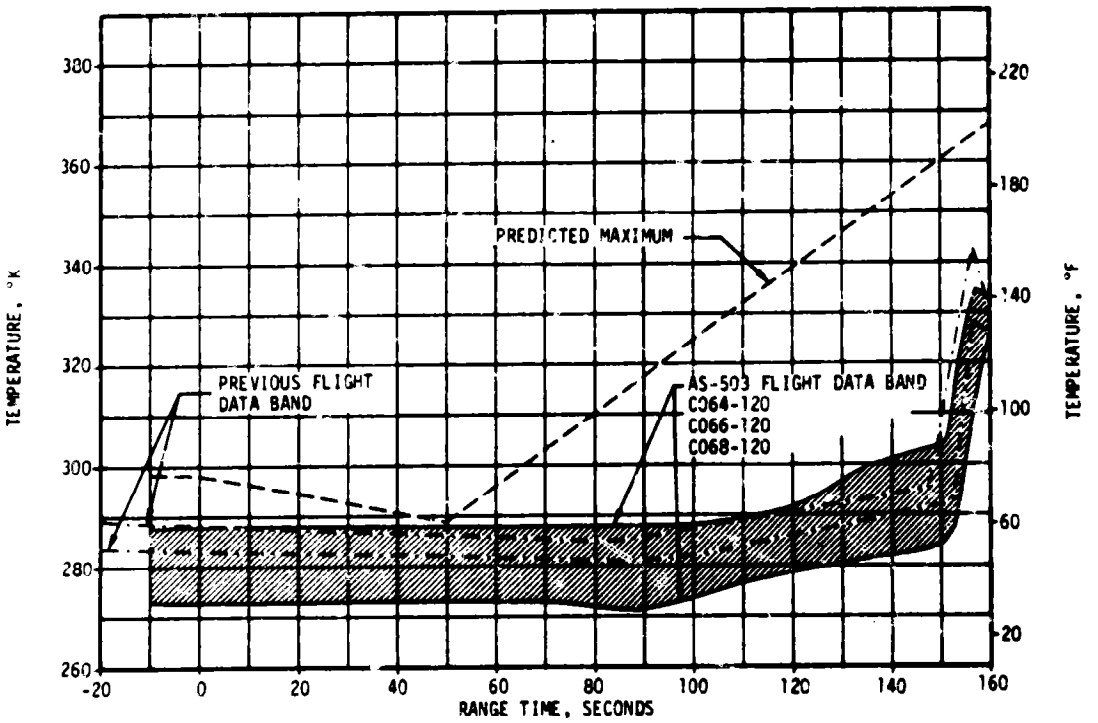

Figure 17-28. S-IC Forward Skirt Skin Temperature

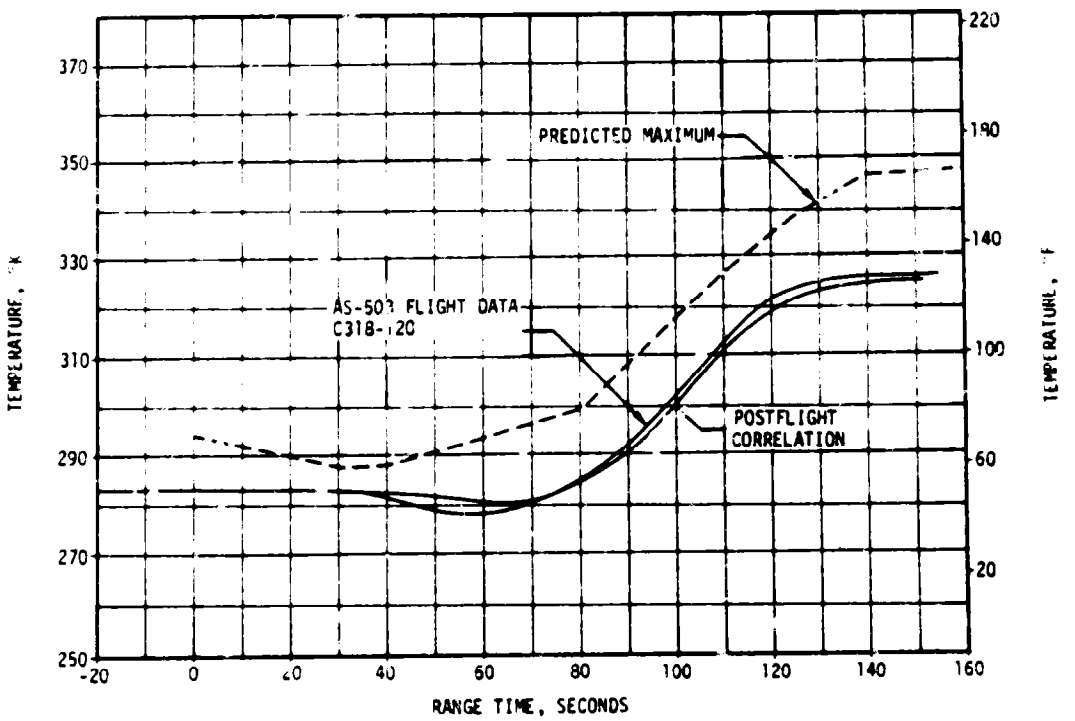

Figure 17-29. S-IC Forward Skirt Thermocouple Plate

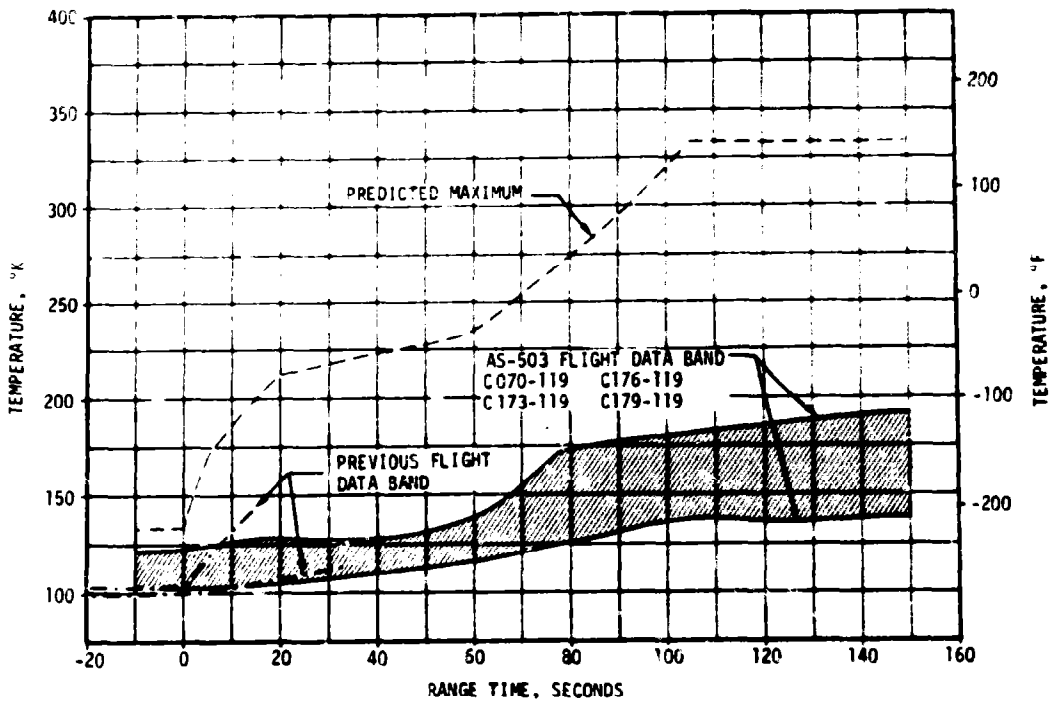

Figure 17-30. S-IC LOX Tank Skin Temperature

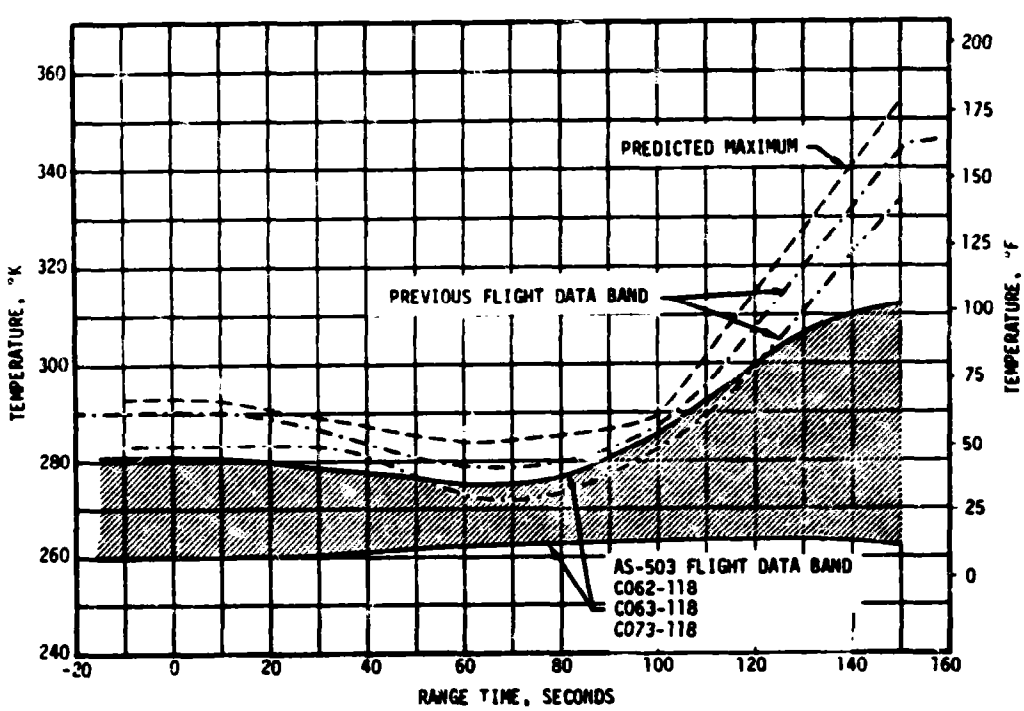

Figure 17-31. S-IC Intertank Skin Temperature

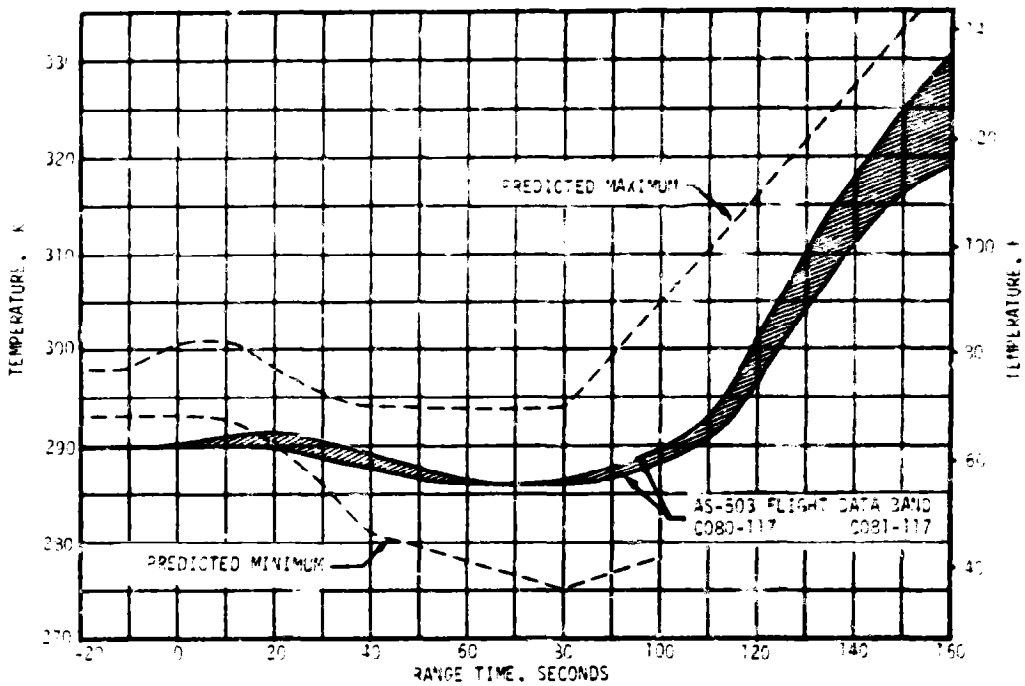

Figure 17-32. S-IC Fuel Tank Skin Temperature

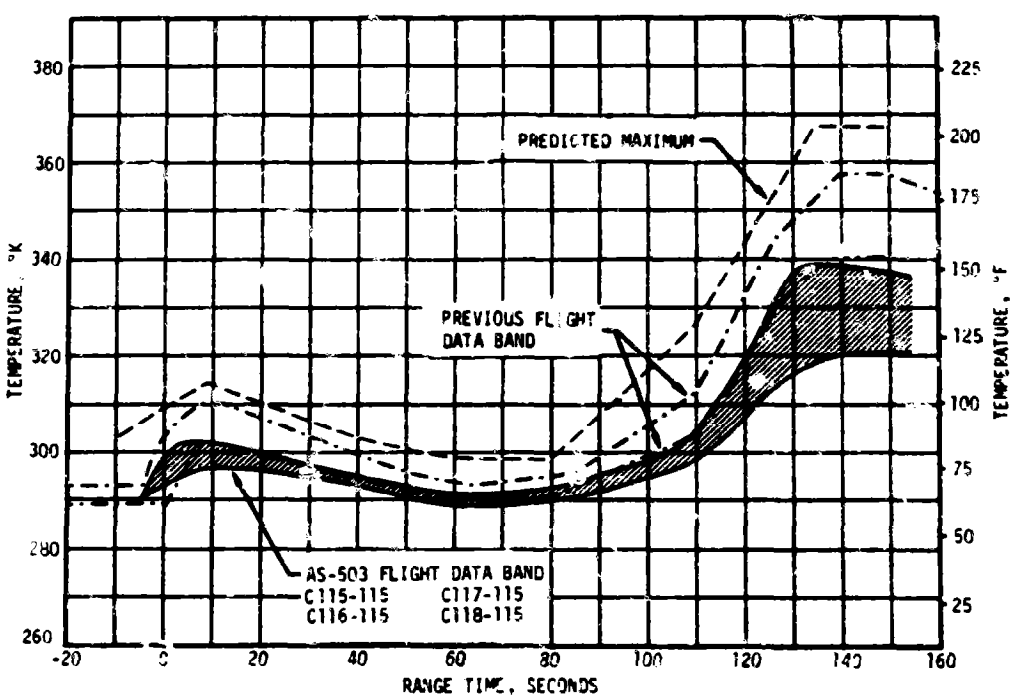

Figure 17-33. S-IC Thrust Structure Skin Temperature

Temperatures on the aluminum portion of the fairings (forward of the heat shield) closely resembled those previously experienced, as is evident in Figure 17-34. Once again, the sudden leveling off of temperatures at 130 seconds is attributed to IECO and the resultant changes in the plume-induced flow separation region.

Temperatures on the titanium portion of the fairings (aft of the heat shield) are similar to the temperatures from previous flights, as shown in Figure 17-35.

As seen in Figure 17-36, temperatures on the wedge or forward section of the fins closely resemble the data obtained from previous flights until 130 seconds, after which temperatures remain nearly constant until S-IC/S-II separation. This is due to the collapse of the region of plume-induced flow separation at IECO. Temperatures on the flat or aft portion of the fin are not shown for the sake of brevity, but are similar to those measured on the wedge portion.

Temperatures measured on the aft face of the fins were lower than those measured on earlier flights, as shown in Figure 17-37.

17.5.2 S-II Stage Aeroheating Environment

Aeroheating on the S-II stage was analyzed using the AS-503 preliminary Observed Mass Point Trajectory and angle-of-attack data from Q-ball measurements. Atmospheric data were obtained from the Meteorological Data Tape. The aeroheating rates were then calculated by means of a digital computer program. These predicted aeroheating rates were corrected to calorimeter conditions for purposes of direct comparison with flight data.

Postflight predicted heating rates to calorimeters on the S-II aft interstage are compared to AS-503 flight data in Figure 17-38. AS-501 and AS-502 flight data are also shown in Figure 17-38. These calorimeters are not affected by protuberances. The agreement of AS-503 data with postflight prediction and with previous flight data is good.

The heating rates to calorimeters on the forward conical fairings of ullage motors on the S-II aft interstage are compared with the postflight prediction in Figure 17-39. The agreement between the postflight prediction and AS-503 flight data is good.

The heating rate to a calorimeter on the aft boattail of an LH_2 feedline fairing is shown in Figure 17-40 together with a postflight prediction and AS-501 and AS-502 data.

A postflight heating rate prediction, together with the AS-503 heating rate to calorimeters located on the forward conical portion of the LH_2 feedline

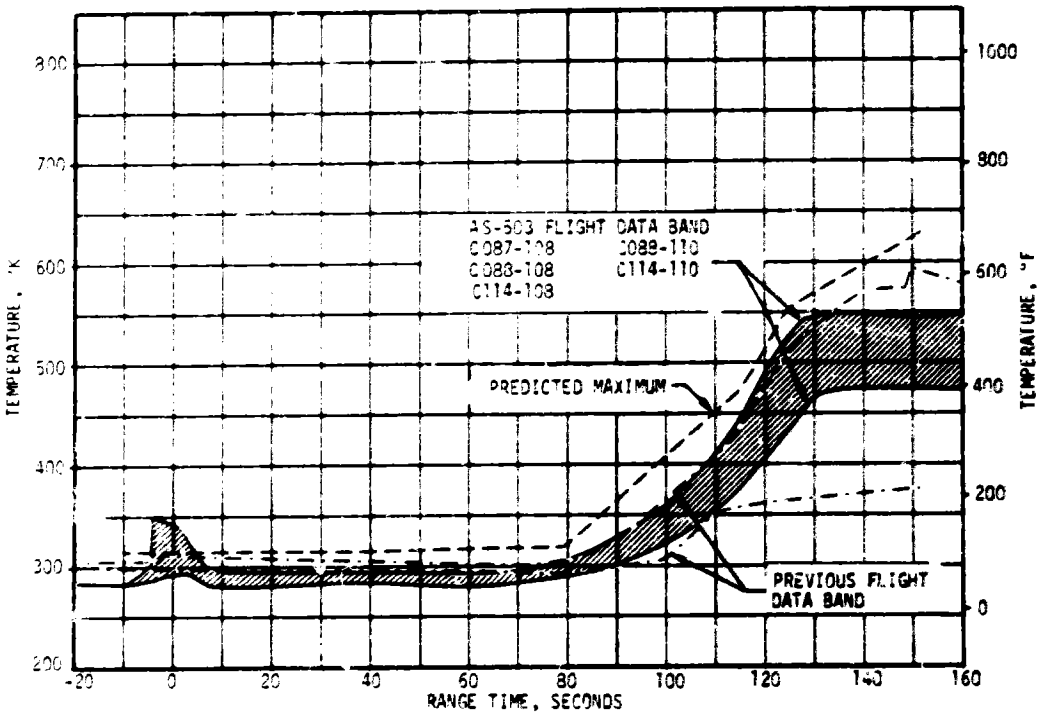

Figure 17-34. S-IC Forward Fairing Skin Temperature

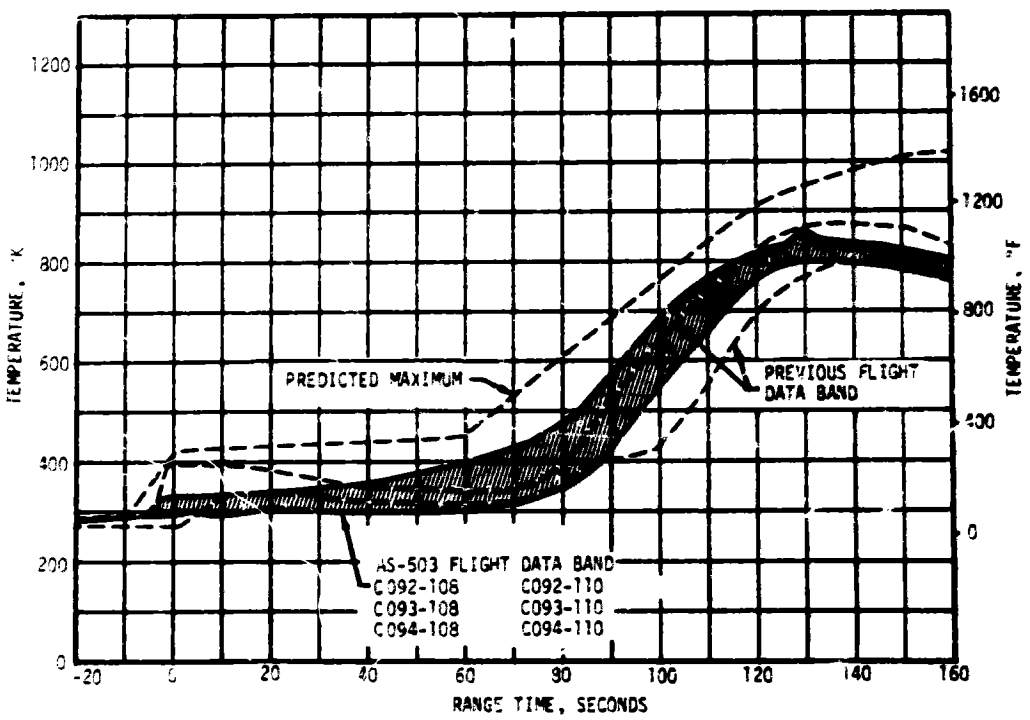

Figure 17-35. S-IC Aft Fairing Skin Temperature

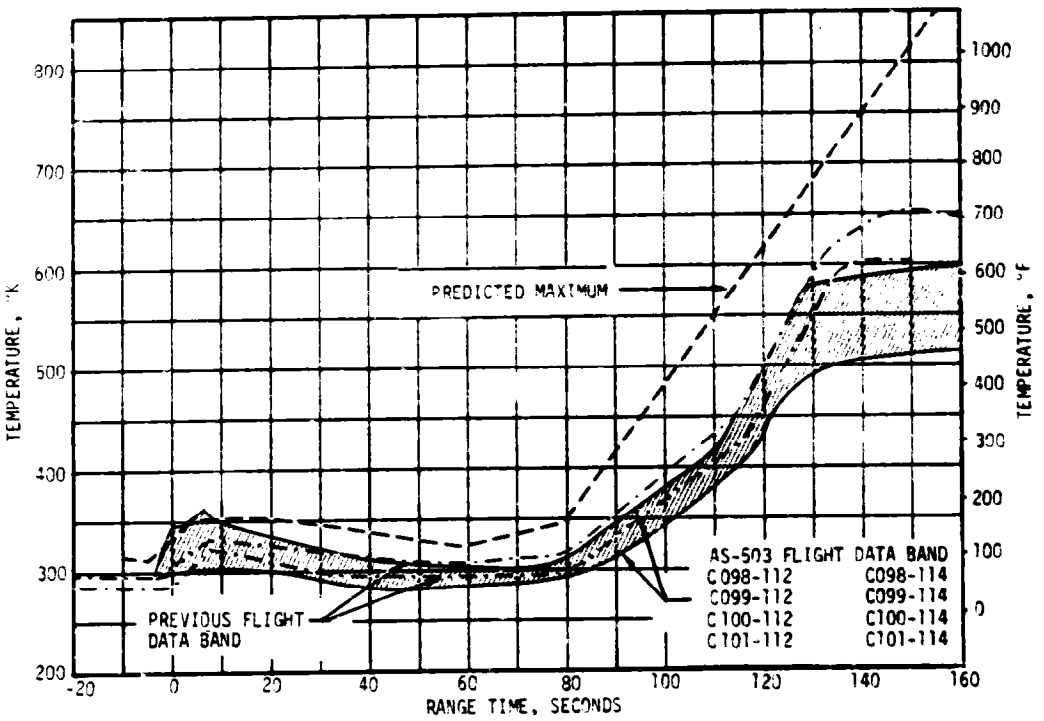

Figure 17-36. S-IC Fin Wedge Section Skin Temperature

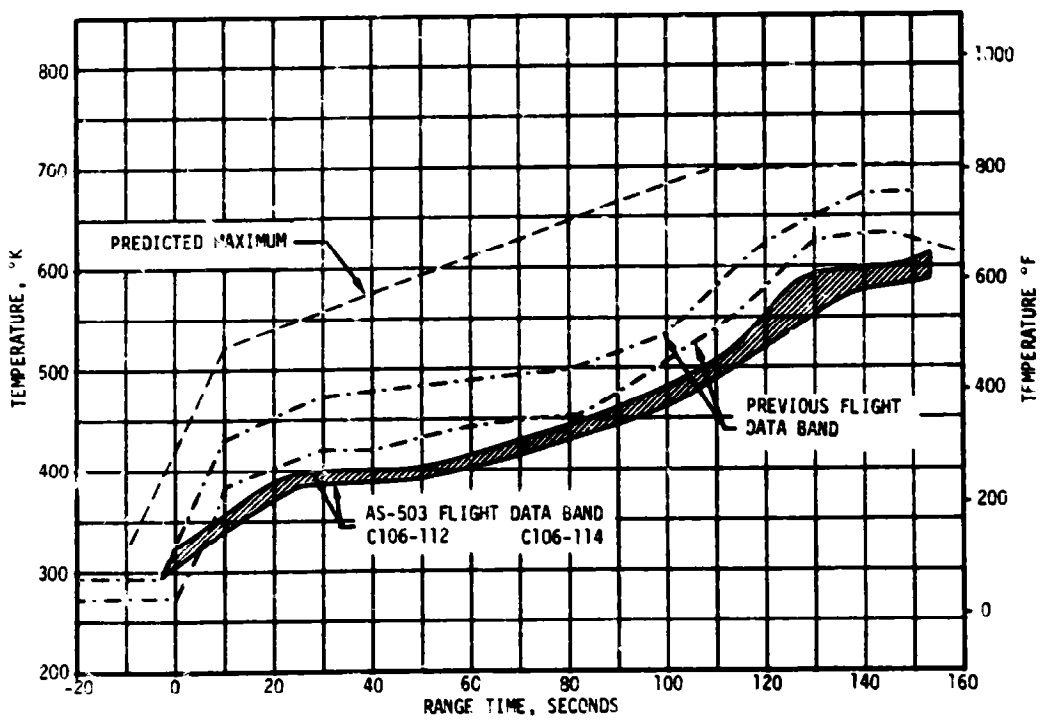

Figure 17-37. S-IC Fin Aft Face Structural Temperature

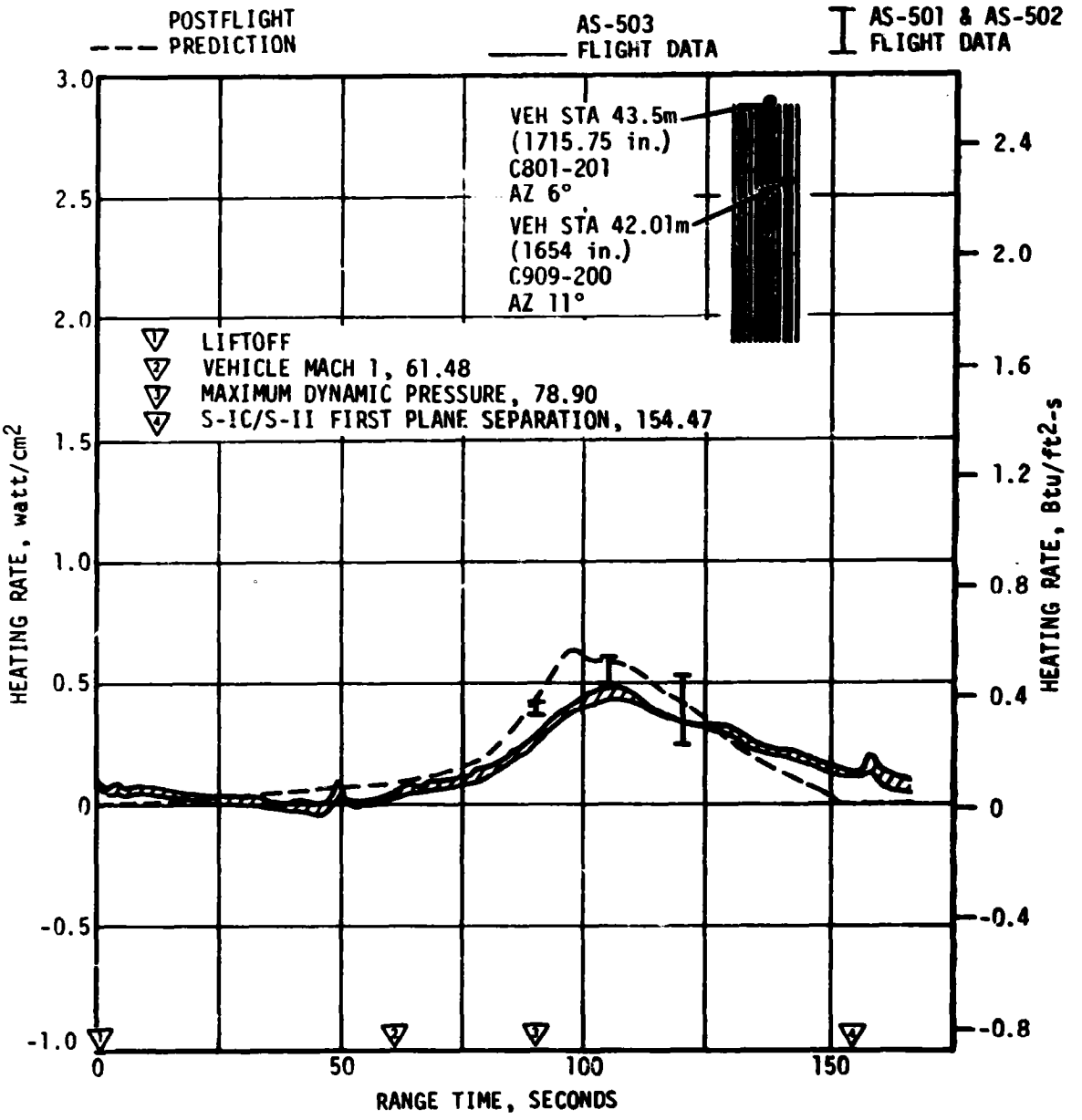

Figure 17-38. S-II Aft Interstage Aeroheating Environment

fairing, is shown in Figure 17-41. Also shown are AS-501 and AS-502 flight data. The AS-503 flight data agrees well with the postflight prediction, and with previous flight data.

The AS-503 flight aeroheating rates were considerably lower than the design values.

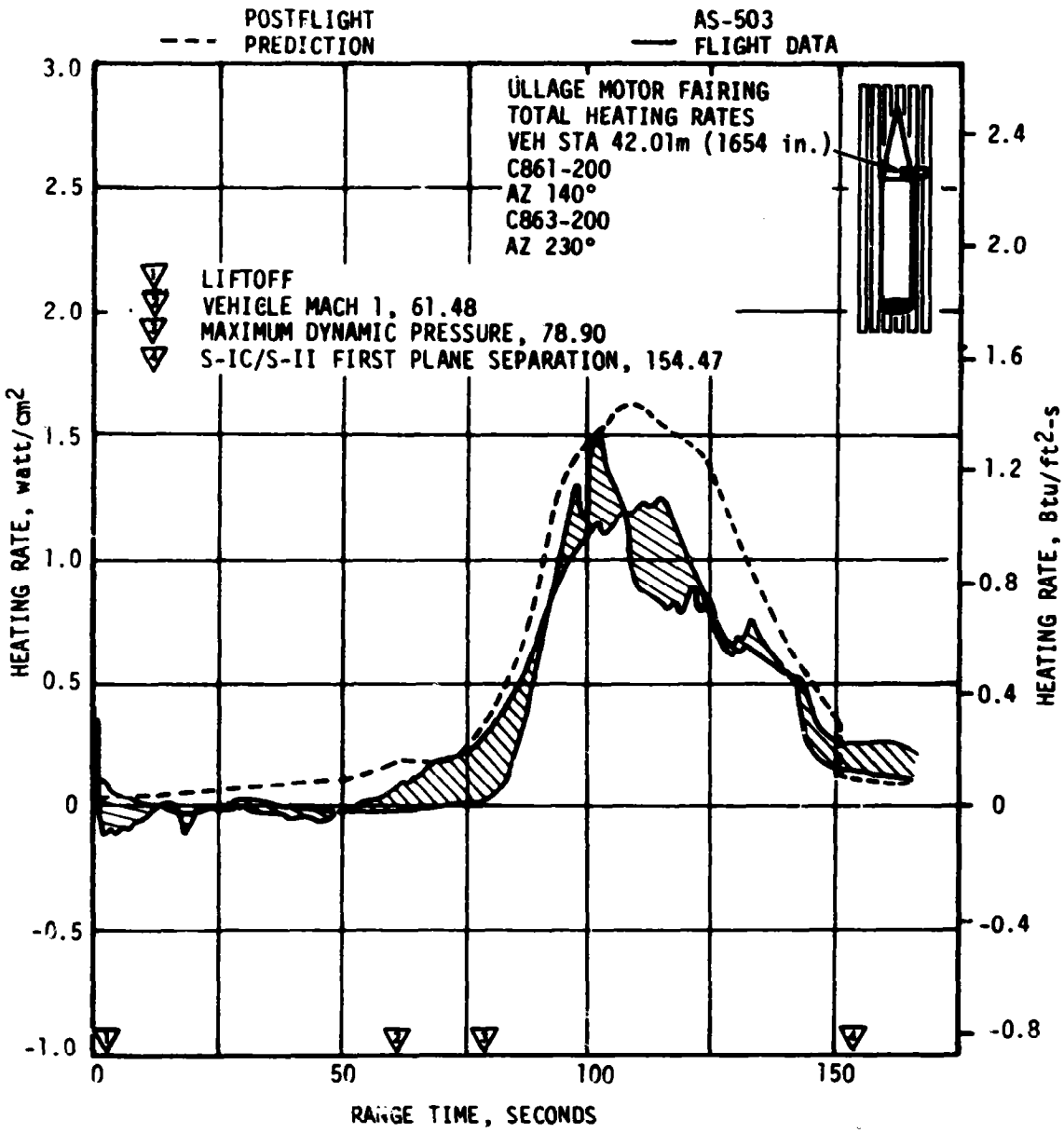

Figure 17-39. S-II Aft Interstage Aeroheating Environment, Ullage Motor Fairing

Representative AS-503 structural and fairing surface temperature data are shown in Figures 17-42 through 17-44. In general, temperatures based on postflight predicted heating rates are in good agreement with flight data. Flight data and prediction for forward skirt skin temperature are shown in Figure 17-42. The postflight prediction is only slightly higher than flight data. Figure 17-43 presents AS-503 aft interstage stringer cap temperature data. Predicted and flight values of temperature are in good

the CCS lost lock. These were the only stations tracking the CCS during this period. UHF telemetry link DP-1B, which is in parallel with links DP-1 and DP-1A, is transmitted through the CCS transponder and provided good data until 39,990 seconds (11:06:30). The data indicated that the IU batteries were decaying at this time. Projection of the decay rate indicated that the batteries would be depleted sufficiently at approximately 44,000 seconds (12:13:20) to materially affect the performance of the CCS transponder. There were no data received for unified S-Band (USB) telemetry link DP-1A to enable evaluation of the USB.

Approximately 20 minutes after TLI a programmed switch of antennas from OMNI to low gain was observed in the TEX and GYM data. This switch was recommended to maintain acceptable signal transmission during the final coast phase. Additional signal level changes were observed at these sites and fluctuations agree in time with antenna switching commands reported verbally as having been sent from GYM. These commands are listed in Table 14-1, Section 14 which discusses performance of the CCS. Ground Station Command Histories have not yet been received to confirm these commands.

A summary of CCS coverage showing AOS and LOS is presented in Table 19-12.

19.5.4 Television Propagation Evaluation

Ground signal strength data of the television station were not available in time for this report to permit evaluation of the television RF propagation. However, video tape data quality indicated satisfactory signal strength during S-IC powered flight.

19.6 OPTICAL INSTRUMENTATION

19.6.1 Onboard cameras

There was a total of four recoverable film camera capsules carried onboard the AS-503 vehicle, all on the S-IC stage. Two camera capsules were located on the S-IC forward interstage at positions I and III looking forward to view S-IC/S-II first plane separation and S-II engine start. The two remaining camera capsules were mounted on top of the S-IC stage LOX tank at positions II and IV, and contained pulse cameras which viewed aft into the LOX tank through fiber optics bundles.

There were also two television cameras located in the S-IC base region to view propulsion and control system components.

Only one camera capsule, the LOX camera located at position II, was recovered. It is not known whether the other three camera capsules were ejected. Radio acquisition of the recovered capsule was about 2 to 3 minutes before impact at about 15 to 20 miles from the recovery helicopter. The capsule was retrieved at 30 degrees 13 minutes north latitude, 73 degrees 58 minutes west longitude at approximately 8:15 AM EST. Inspection of the recovered capsule showed that 3 of the ground planes sheared off and 5 of the shroud lines on the drag skirt were broken.

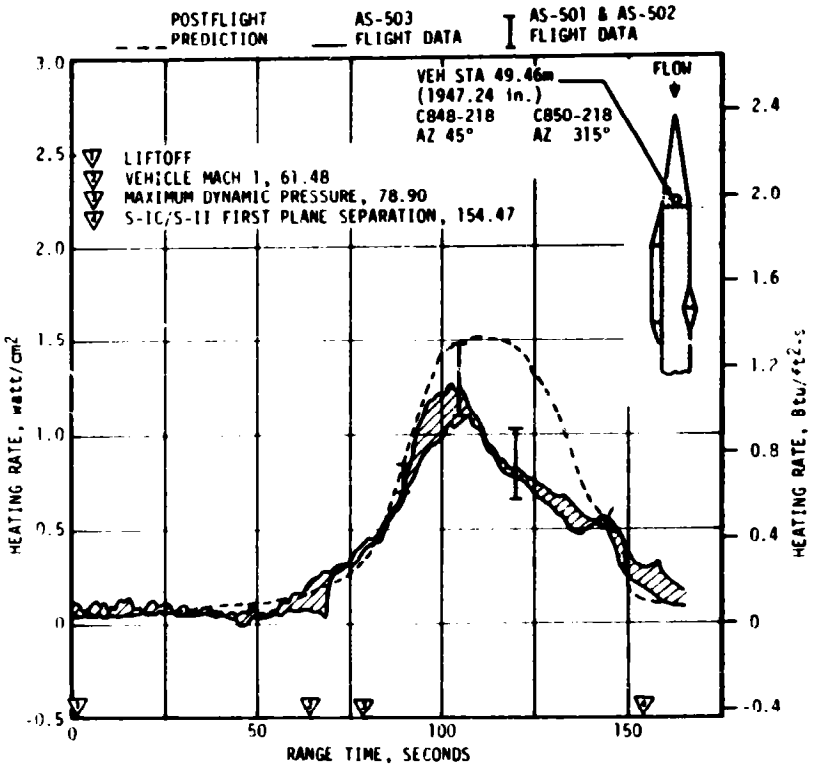

Figure 17-41. S-II LH_2 Feedline Forward Fairing Heating Rates

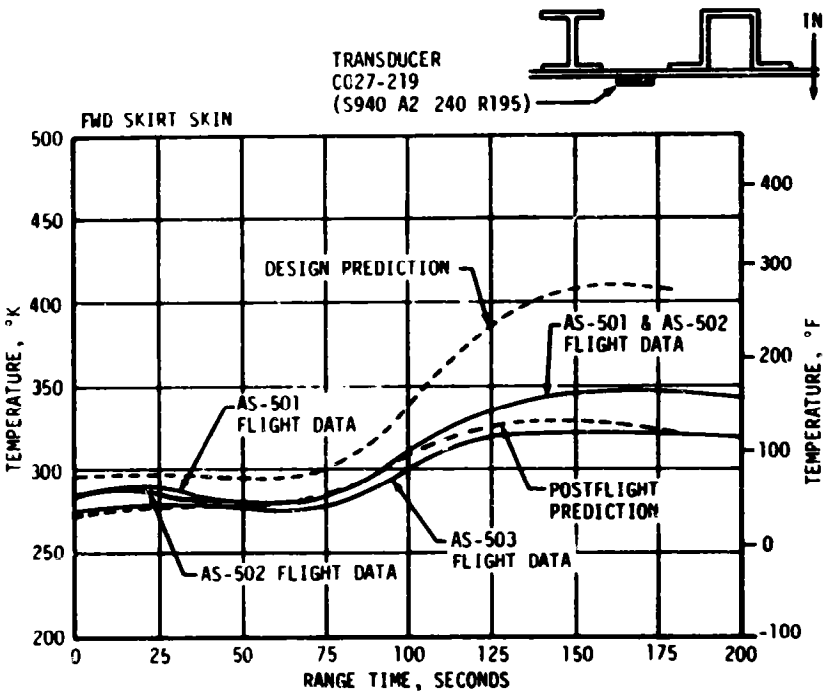

Figure 17-42. S-II Body Structural Temperature

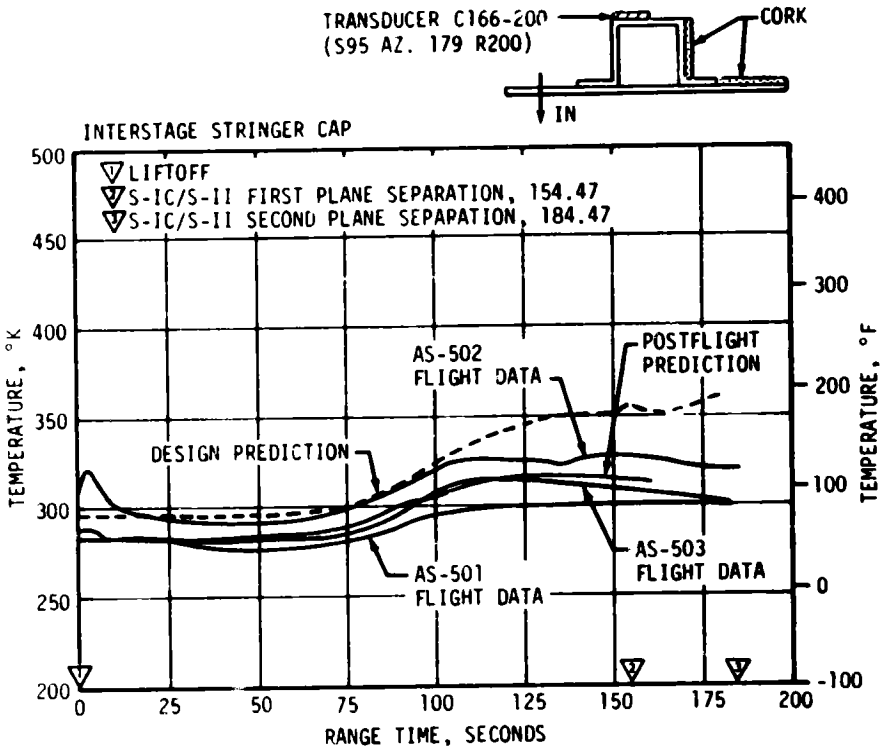

Figure 17-43. S-II Aft Interstage Structural Temperature

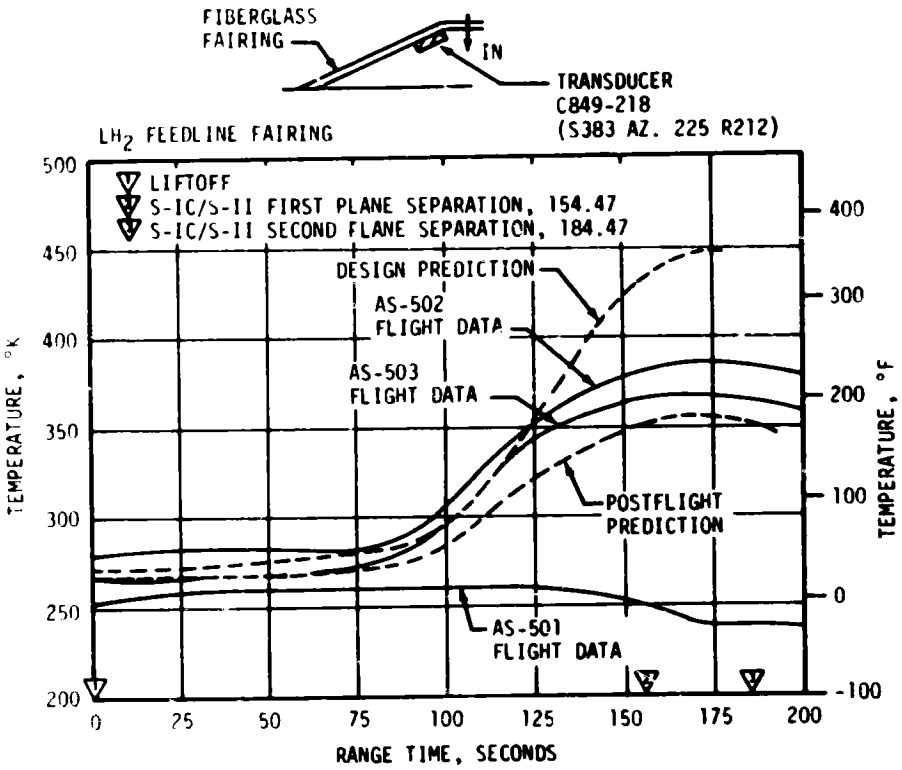

Figure 17-44. S-II LH_2 Feedline Fairing Structural Temperature

17.5.4 IU Aeroheating Environment

The IU inner skin temperatures from launch through the end of first burn at 685 seconds, are presented in Figure 17-45. These data, in general, show good agreement with AS-502 data and no problems were noted.

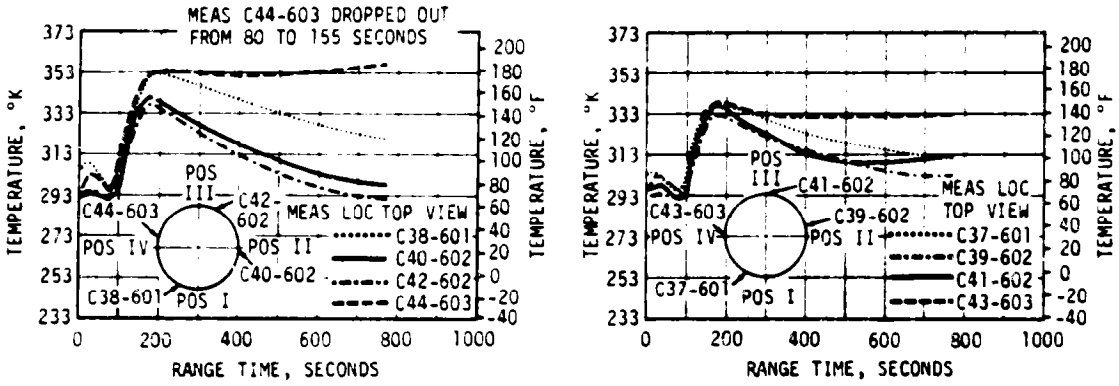

Figure 17-45. IU Inner Skin Temperatures for Ascent

17.6 VEHICLE ORBITAL HEATING ENVIRONMENT

The IU inner skin temperatures, for portions of the time in earth orbit, are shown in Figure 17-46. The temperatures are shown to be cycling between the same maximum and minimum values that were observed on the AS-502 flight, as the vehicle orbital path alternated between zones of earth shadow and solar heating.

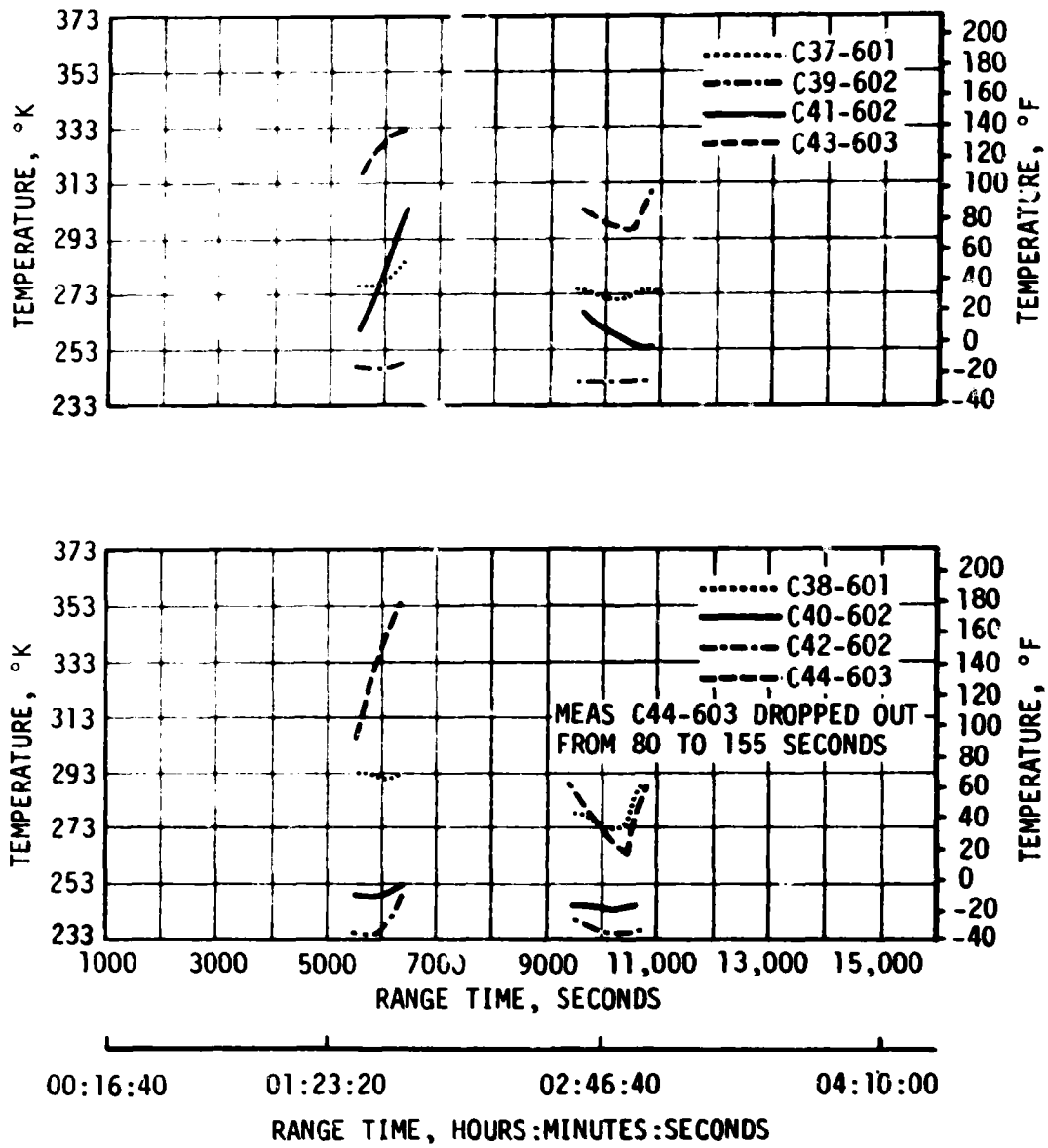

Figure 17-46. IU Inner Skin Temperature, Earth Orbit

SECTION 18

ENVIRONMENTAL CONTROL SYSTEM

18.1 SUMMARY

The S-IC canister conditioning system and the aft environmental conditioning system performed satisfactorily during the AS-503 countdown.

The S-II thermal control and compartment conditioning system maintained temperatures within the design limits throughout the prelaunch operations.

The IU Environmental Control System (ECS) performed well throughout the flight. Coolant temperatures, pressures, and flowrates remained within the predicted ranges and design limits for the first 3 hours of available flight data.

18.2 S-IC ENVIRONMENTAL CONTROL

The ambient temperature of the 18 canisters in the S-IC stage forward skirt compartment must be controlled at 299.8 ±11.1°K (80 ±20°F) during equipment operation prior to J-2 engine chilldown, and between 324.8 to 277.6°K (125 to 40°F) during J-2 engine chilldown. No canister conditioning is required after S-IC forward umbilical disconnect.

The canister temperatures remained within the required limits during the countdown, as shown in Figure 18-1. Canister No. 6 recorded the lowest temperature 285.9°K (55°F) during prelaunch. The lowest canister temperature measured in flight was 256.8°K (2.5°F) in canister No. 2, as shown in Figure 18-1.

During J-2 engine chilldown the thermal environment is at the most critical point. Within this period the ambient temperature in the forward skirt compartment dropped as shown in Figure 18-2. The lowest temperature, 173.2°K (-148°F), was recorded at instrument C207-120 which is located under a J-2 engine nozzle and receives the maximum effect of the cold helium. All other ambient temperatures were above the 205.4°K (-90°F) predicted minimum.

The design requirements for the aft compartment are that the prelaunch temperature be maintained at 299.7 ±8.3°K (80 ±15°F) near the batteries and the remainder of the compartment be maintained at 299.8 ±11.1°K (80 ±20°F).

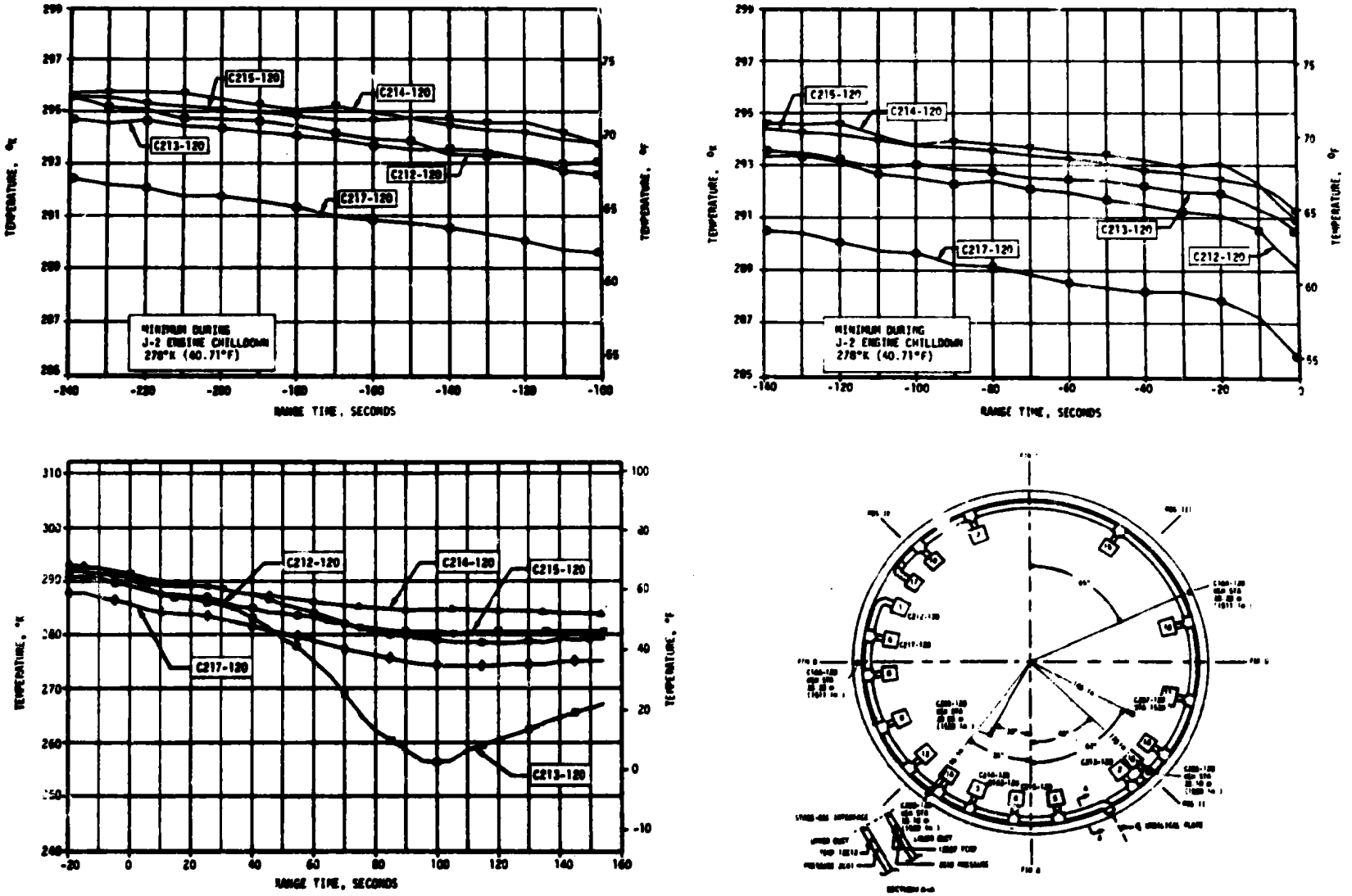

Figure 18-1. S-IC Forward Compartment Canister Temperature

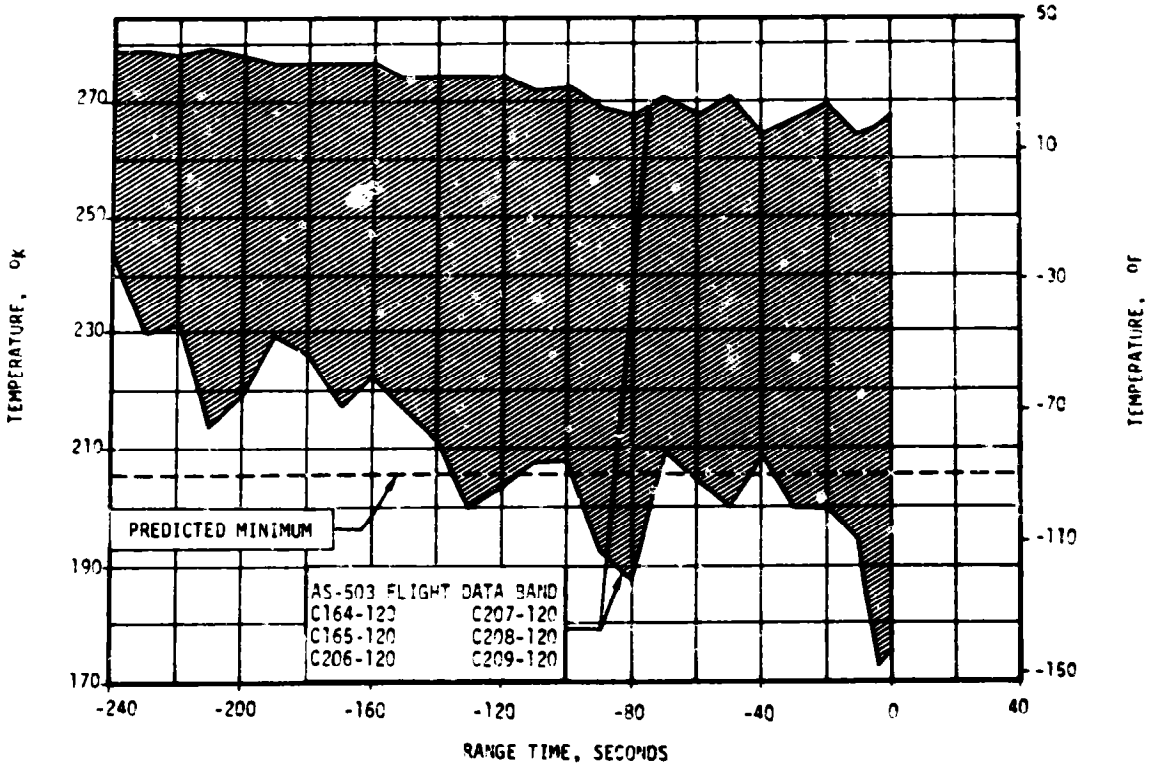

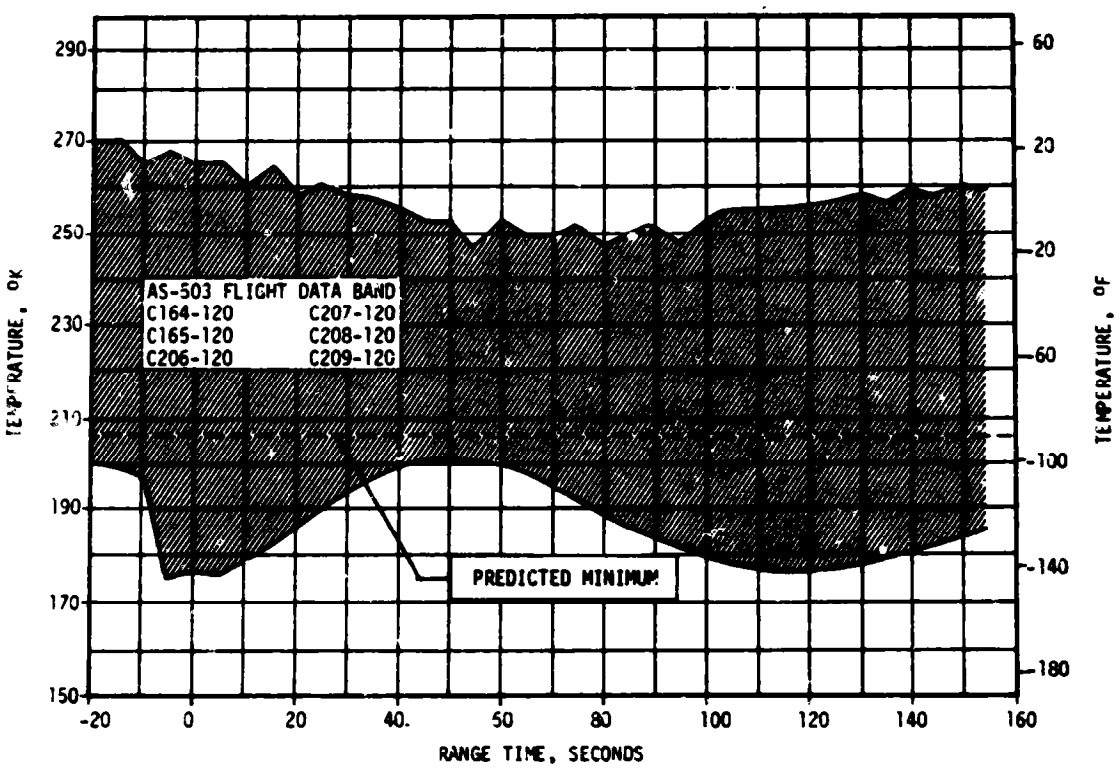

Figure 18-2. S-IC Forward Compartment Ambient Temperature

Aft compartment prelaunch temperatures were maintained within the design requirements, as shown in Figure 18-3. The lowest prelaunch temperature recorded was 293.2°K (68°F) at instrument number C203-115. During flight the lowest recorded temperature of 272.6°K (31°F) was also at instrument C203-115.

18.3 S-II ENVIRONMENTAL CONTROL

The S-II stage Environmental Control System consists of two parts.

a. The engine compartment conditioning system provides a means of purging the engine and aft interstage area of explosive mixtures during propellant loading operations, and maintaining proper temperature control for stage components. The compartment purge is effected by means of warm GN_2 and is operational only during the prelaunch period. The compartment vents have been designed to meet these objectives and to relieve internal pressure during S-IC boost.

b. The thermal control system is designed to provide both temperature control and an inert atmosphere for the electronic equipment containers in the aft compartment. Ground equipment provides conditioned air for cooling during ground checkout, and GN_2 for purging and heating during and after propellant loading. The conditioned gas is directed to the equipment containers through ducting, and exhausts to the interstage area. The flow is fixed by orifices and is continuous until terminated at umbilical disconnect. During flight, thermal inertia and container insulation will preclude out-of-tolerance equipment temperatures.

The engine compartment conditioning system maintained the compartment temperature within the design limit throughout the prelaunch operations. Engine compartment ambient temperature transducers, which were common to AS-502 and AS-503, generally indicated temperatures throughout the AS-503 countdown similar to those during AS-502 countdown.

AS-502 and AS-503 temperatures were generally lower than AS-501 because the purge temperature was adjusted to produce average compartment temperatures at the control thermistor (12K11) on the low side of the 275 to 280°K (35 to 45°F) tolerance. The new thrust cone aft ambient measurements and the new engine area ambient measurements indicated a relatively narrow temperature range in this zone of 283 to 294°K (50 to 70°F) prior to thrust chamber chilldown. However, a considerable temperature gradient relative to azimuth location was indicated by these measurements after thrust chamber chilldown. For example, the thrust cone ambient after chilldown was 213°K (-75°F) at position II, and was 255°K (0°F) at position I. The minimum engine area ambient was 194°K (-110°F) at position II, and the maximum was 241°K (-25°F) at position IV. It is suspected that the ambients in the vicinity of position I are lower than the others due to dissimilar helium flow rates

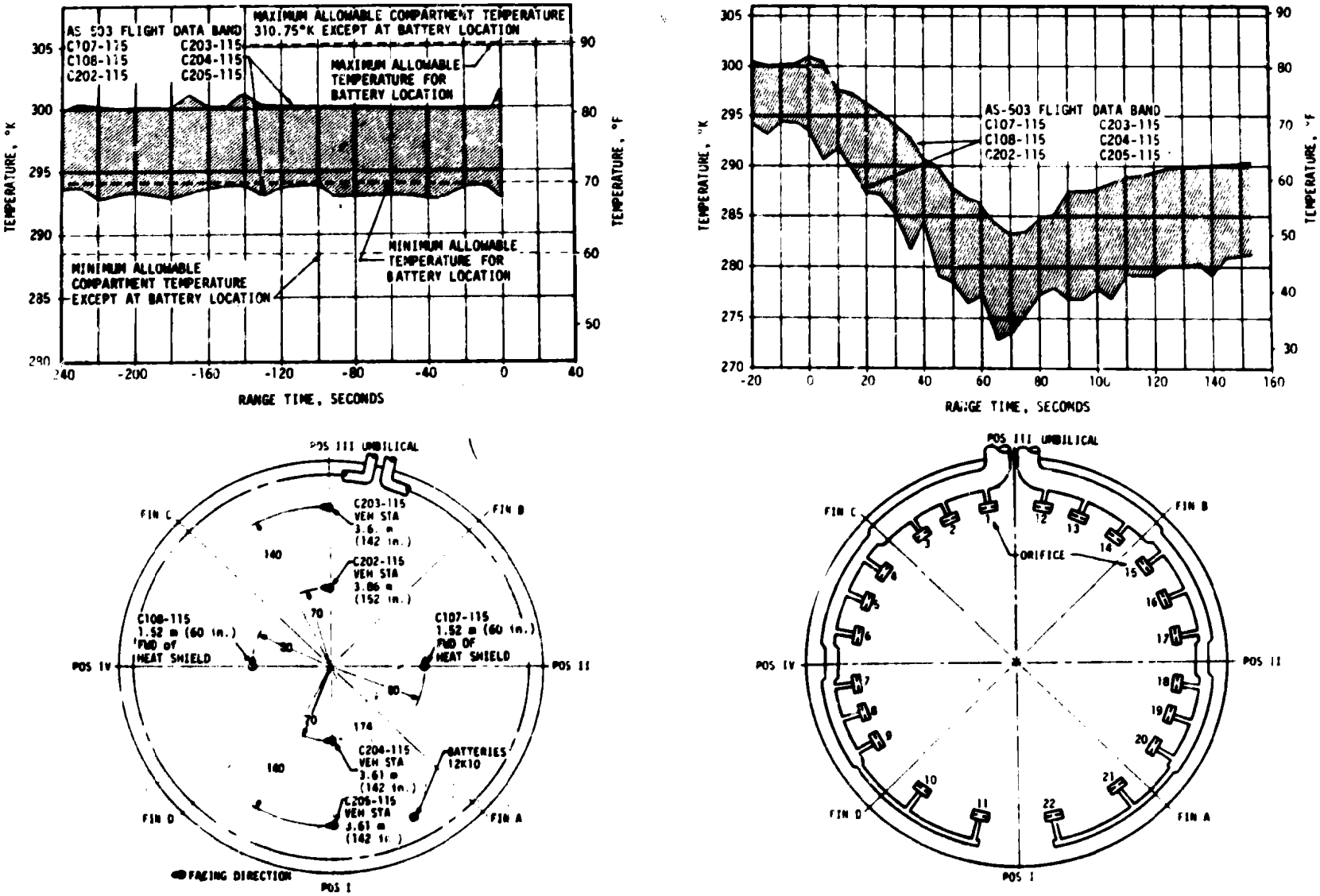

Figure 18-3. S-IC Aft Compartment Temperature Range

and/or temperatures issuing from the thrust chambers during chilldown. Supporting data for this theory are the thrust chamber jacket temperatures, and the fuel injection temperatures, which indicate that engines No. 1 and No. 2 (straddling position II) cooled faster and to lower temperatures than the other three engines.

Ambient temperature measurements, in the vicinity of the S-IC thermal control containers, indicated temperatures at liftoff of 243°K (-30°F) and 253°K (-4°F), respectively, indicating that the ambient temperature in this vicinity was above the minimum requirement of 205°K (-90°F).

Thrust cone temperature measurements indicated that the thrust cone structure was below the required 255°K (0°F) maximum design temperature at liftoff.

There were no indications of hydrogen or oxygen in the S-IC/S-II interstage throughout the countdown.

The forward thermal control system maintained the equipment mount temperatures in the middle of the design range throughout countdown and flight. The temperatures at liftoff were 4.5 to 9.5°K (8 to 17°F) colder than those of AS-501 and 0 to 4°K (0 to 7°F) colder than AS-502. Similar to AS-501, the greatest drop in equipment mount temperature during flight was 4.5°K (8°F) and the greatest rise was 1°K (2°F). These changes occurred in containers 221 and 225, respectively.

Container 214 was the only instrumented container in the aft thermal control system. The equipment mount temperature history in this container was within 2.75°K (5°F) of that recorded on AS-501 and AS-502. On the basis of this one measurement and the absence of any anomalies in equipment housed in the other containers, it is assumed that the aft thermal control system performed satisfactorily.

18.4 S-IVB ENVIRONMENTAL CONTROL

Temperature control for S-IVB forward skirt electronic components is provided by mounting the container on cold plates. A Methanol/Water (M/W) coolant, supplied by the IU Thermal Conditioning System (TCS), is circulated through these cold plates to carry away waste heat. The containers on AS-503 were not instrumented for temperature measurements, however, normal operation of the electronic components indicate that temperatures were maintained within proper limits.

The S-IVB Environmental Control System for the aft skirt and interstage provides the following:

a. Thermal conditioning of the atmosphere, during ground operations, around electrical equipment in the aft skirt.

b. Thermal conditioning of the Auxiliary Propulsion System (APS), hydraulic accumulator reservoir, and ambient helium bottle.

c. Purging of the aft skirt, aft interstage and thrust structure, and the S-II stage forward skirt of oxygen and combustible gases.

Temperature-controlled air or GN_2 is supplied at the rate of 3500 SCFM to accomplish the thermal conditioning. The GN_2 purge is initiated at LOX loading and is continued until umbilical disconnect. The system performance appeared to be satisfactory; however, a detailed analysis was not made.

18.5 IU ENVIRONMENTAL CONTROL

The ECS maintained acceptable operating conditions for components mounted within the Instrument Unit (IU) and the S-IVB stage forward skirt during preflight and flight operations. The ECS is composed of a Thermal Conditioning System (TCS) and a Gas Bearing Supply System (GBS). A Preflight Purge Subsystem provided compartment conditioning prior to launch.

18.5.1 Thermal Conditioning System

A conditioned environment in the IU/S-IVB stage compartment is maintained prior to launch by a temperature and flow regulated supply of air or GN_2. The environmental conditioning duct distributes the regulated ground supplied air throughout the compartment through orifices in the duct during the preflight checkout phases. During fueling operation, GN_2 is used to purge the IU compartment. Purging terminates with umbilical separation. Preflight data received from Kennedy Space Center indicate satisfactory operation. The required 290.2 to 295.8°K (63 to 73°F) compartment temperature was maintained.

The IU TCS, shown in Figure 18-4, maintained an acceptable M/W coolant temperature of 288 ±0.56°K (59 ±1°F) for the IU and S-IVB stage electrical components during prelaunch and 280.4 to 293.15°K (45 to 68°F) during flight operations. A coolant pump circulates the M/W fluid to the IU and S-IVB stage TCS. Flowrate distribution is controlled by fixed orifices. The IU flowrate is proportionally distributed to the 16 IU cold plates and the 4 internally cooled components. These components are: stabilized platform, Flight Control Computer (FCC), Launch Vehicle Data Adapter (LVDA), and Launch Vehicle Digital Computer (LVDC). The IU and S-IVB stage coolant is then returned to a heat exchanger assembly. This heat exchanger is cooled by a sublimation process. Water, supplied from a pressurized accumulator, passes through a porous plate in the sublimator where the pressure is reduced to compartment ambient. The water is then cooled to the frozen state and evaporates by sublimation at the near vacuum compartment pressure. This then serves as a heat sink. At 5 seconds after liftoff a switch selector command diverts 100 percent of the M/W coolant flow through the heat exchanger. At about 180 seconds, a switch selector command opens the

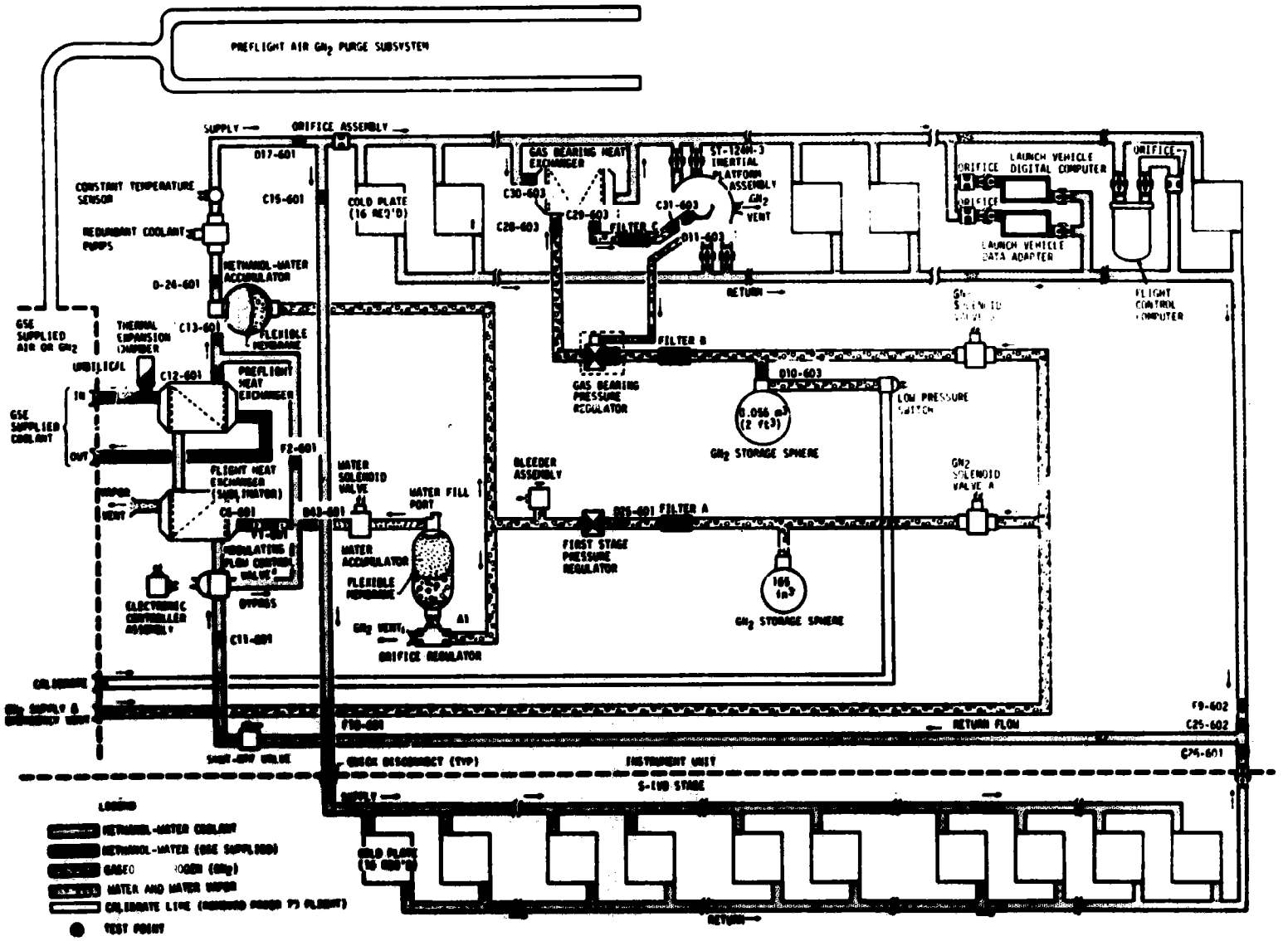

Figure 18-4. IU Environmental Control System Schematic Diagram

water solenoid valve and starts the sublimation cooling cycle. Starting at 480 seconds the LVDC senses the M/W coolant temperature once every 300 seconds. If the coolant temperature is above the thermal switch set point upper limit of 288.6°K (60°F) at this time, the water valve is commanded open to initiate a cooling cycle. If the coolant temperature is less than the thermal switch set point lower limit of 288.3°K (59.6°F), the water valve is commanded closed and sublimator cooling is terminated until the temperature is sampled again.

Figure 18-5 shows the M/W control temperature cycling within the required 280.2 to 293°K (45 to 68°F) temperature band during the period that data is available. Pressures and flowrates remained within the required ranges. Shortly after liftoff the MFCV went toward the full sublimator flow position. Figure 18-6 shows the sublimator performance during ascent. The water valve opened at 184.77 seconds and gradually increasing cooling was evident until approximately 500 seconds. At this time, the sublimator completed its fill cycle and a high level of cooling was apparent. The TCS GN_2 usage, shown in Figure 18-7, was slightly less than nominal. A 0.0322 kg/hr (0.07 lbm/hr) usage rate was within the allowable range of 0.03 to 0.044 kg/hr (0.066 to 0.097 lbm/hr).

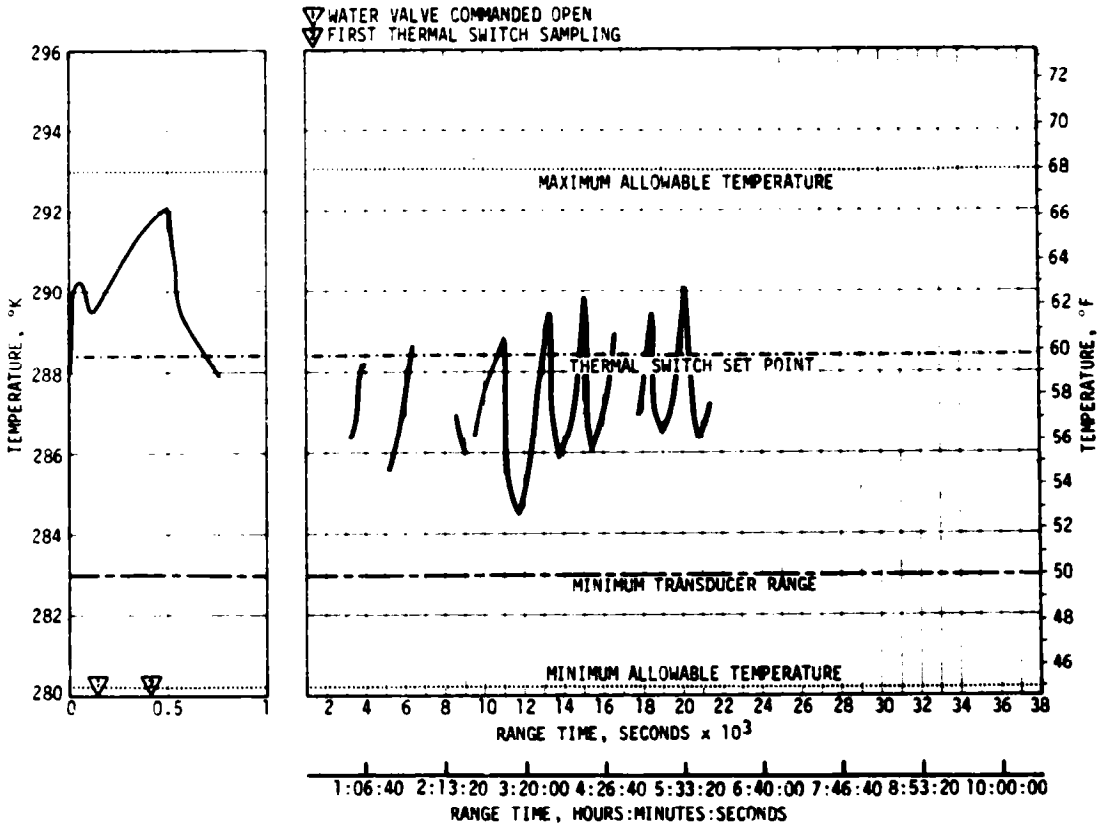

Figure 18-5. Thermal Conditioning System Metnanol/Water Control Temperature

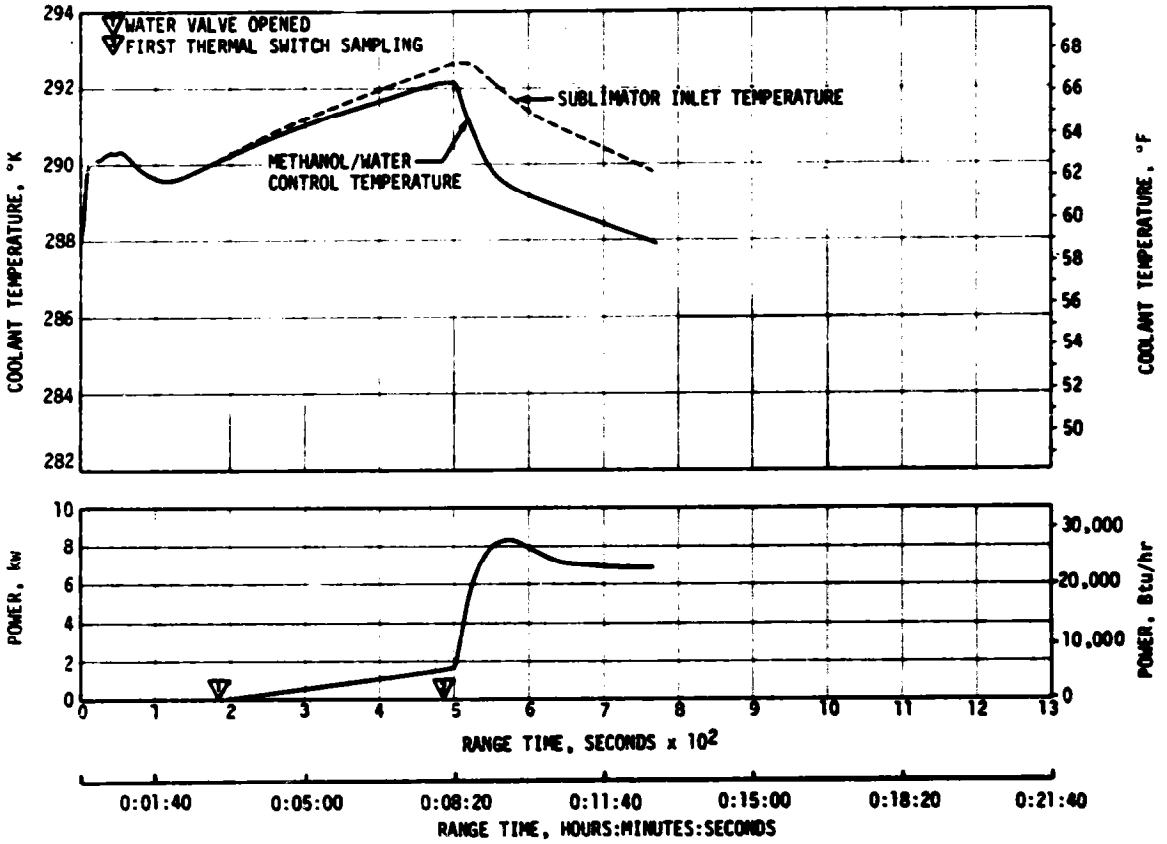

Figure 18-6. IU Sublimator Performance During Ascent

Selected component temperatures are shown in Figure 18-8.

18.5.2 Gas Bearing Supply System

The Gas Bearing System (GBS), shown in Figure 18-4, supplies GN_2 at a regulated pressure and temperature to the ST-124M Inertial Platform Assembly (Platform) for preflight and flight operation. The GBS consists of a storage sphere, heat exchanger, pressure regulator, low-pressure switch, two filters, a supply and emergency vent, solenoid valve, calibration line, and associated tubing.

During system operation, GN_2 flows from the storage sphere at an initial pressure of 2068 N/cm^2 (3000 psig). After the GN_2 is filtered, the pressure regulator drops the pressure to an acceptable value for the air bearing operation. The GN_2 flows through the heat exchanger and a second filter to the Platform gas bearing inlet. The heat exchanger thermally conditions the GN_2. A line from the Platform to the dome of the pressure regulator supplies the reference pressure required to control the pressure differential across the gas bearings.

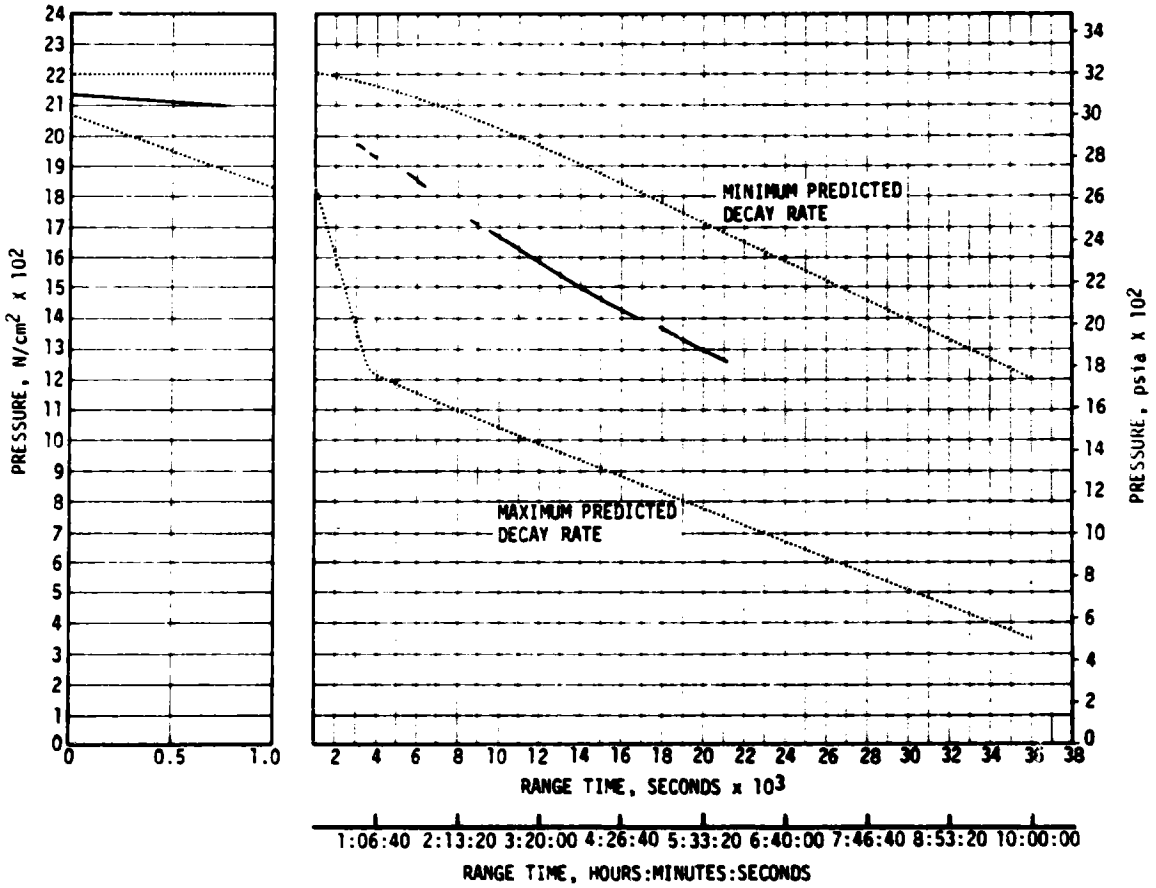

Figure 18-7. Thermal Conditioning System GN_2 Pressure

The gas bearing system performance is shown in Figure 18-9. A gradual increase in the inlet pressure differential can be seen starting during the second S-IVB stage burn, and a 0.31 N/cm^2 (0.45 psid) shift can be seen at spacecraft separation at 12,056.3 seconds after which the gradual increase continued. The 10.7 N/cm^2 (5.5 psid) specification maximum was exceeded when this shift occurred. The probable cause of this occurrence was a shift in spring displacement in the gas bearing pressure regulator. This shift has been seen during component testing and has been shown to be the result of low torque on the adjustment screw locknut. No problems occurred as a result of this shift in pressure differential. The GBS usage, as shown in Figure 18-10, was slightly less than that nominally expected. A 0.35 SCFM usage rate, which was within the 0.3 to 0.5 SCFM allowable range, is indicated.

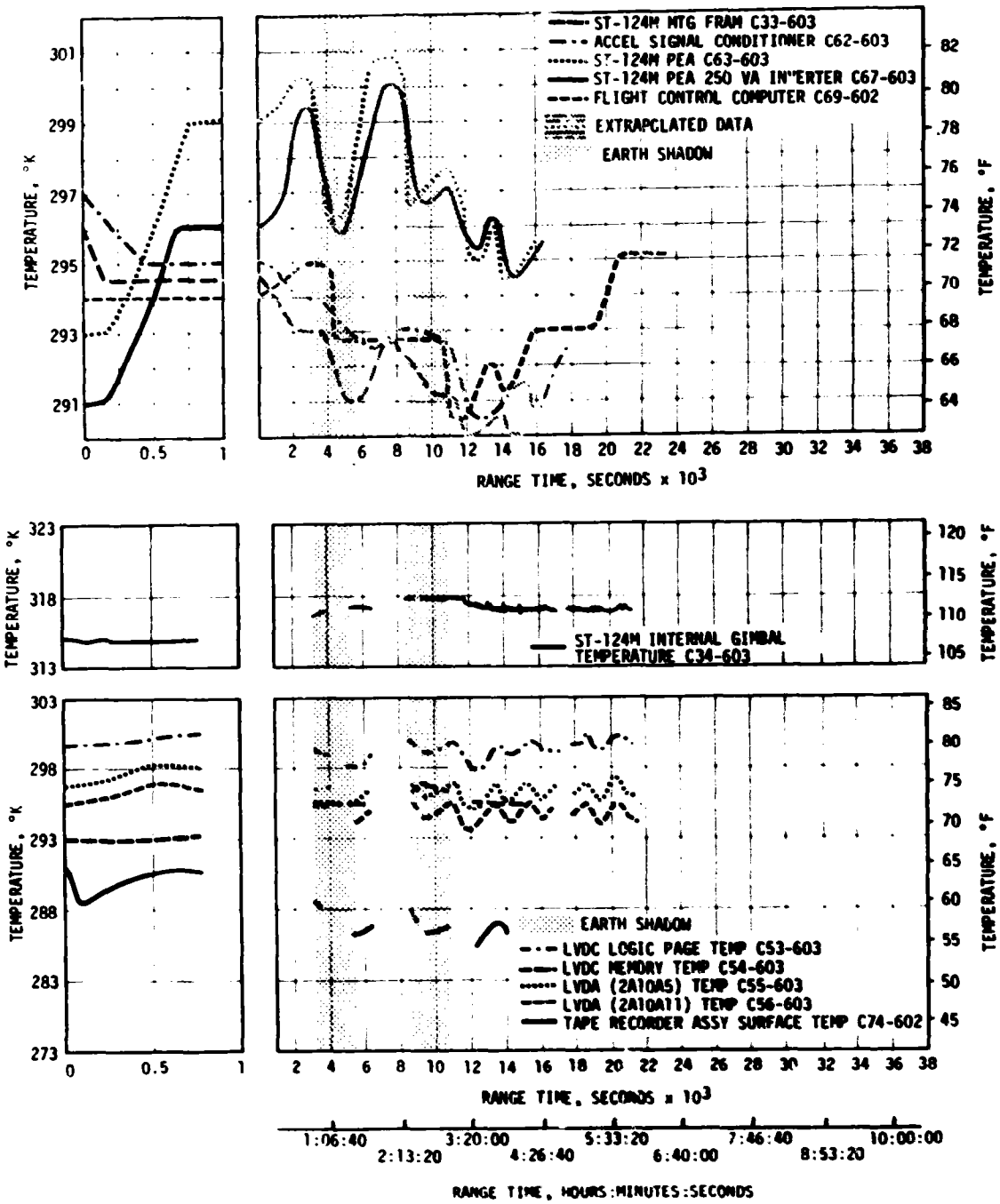

Figure 18-8. Selected Component Temperatures

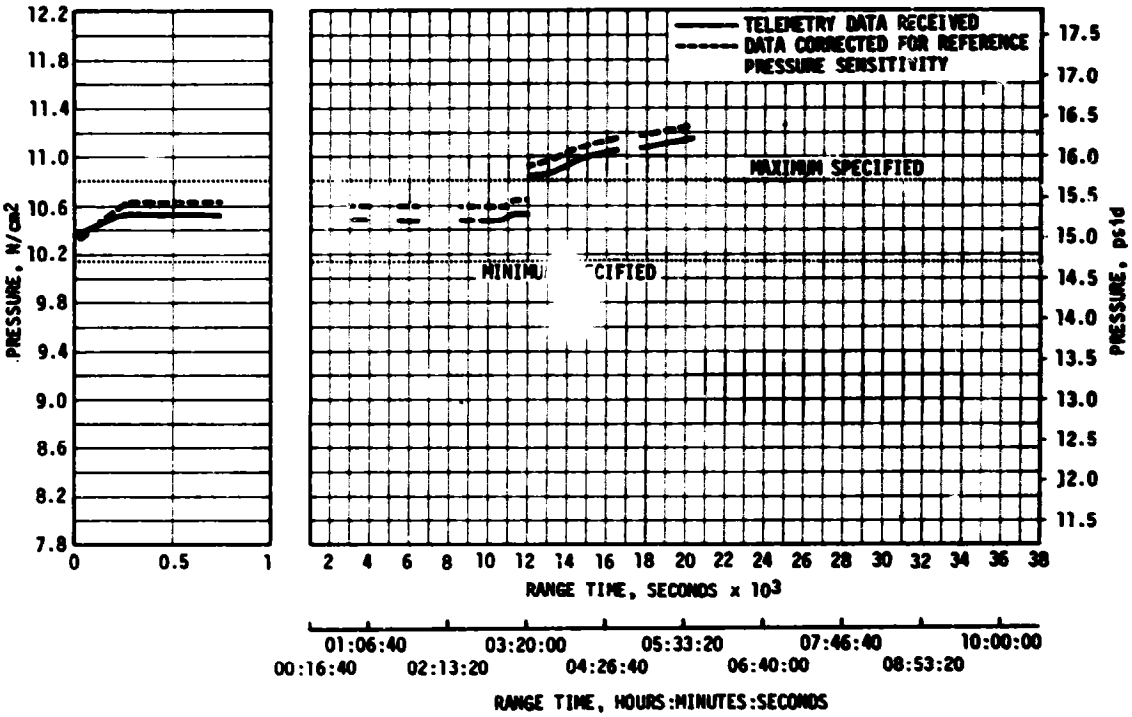

Figure 18-9. Pressure Differential Across Gas Bearings

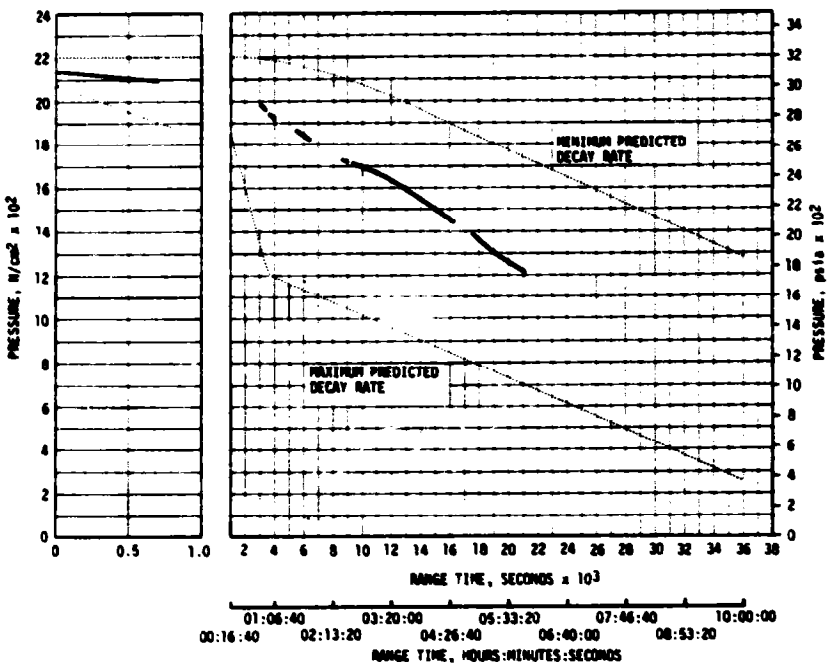

Figure 18-10. Gas Bearing System GN_2 Pressure

SECTION 19

DATA SYSTEMS

19.1 SUMMARY

The AS-503 launch vehicle data system consisted of 2670 active flight measurements, 21 telemetry links, onboard tape recorders, film and television cameras, and tracking. With the exception of the onboard film cameras, all data system elements performed very satisfactorily. As discussed in paragraph 19.6, only one of the four S-IC film cameras was recovered.

The performance of all vehicle telemetry systems was excellent. The last usable VHF data were received by the Guaymas and Texas stations from telemetry links CF-1 and CP-1 at 15,660 seconds (4:21:00).

Performance of the Radio Frequency (RF) systems was satisfactory. Measured flight data, with few exceptions, agreed favorably with expected trends. Final loss of RF carrier signals after translunar injection were as follows: VHF telemetry was last received by Guaymas at approximately 29,230 seconds (8:07:10), Command and Communication System (CCS) was lost by Guaymas at approximately 44,357 seconds (12:19:17), and the C-Band radar transmission was last received by Grand Turk Island (GTI) at approximately 21,325 seconds (5:55:25).

Ground camera coverage was good as evidenced by 81.5 percent system efficiency. The onboard television (TV) systems performed satisfactorily and provided useful data.

19.2 VEHICLE MEASUREMENTS EVALUATION

Flight measurements transmitted by the AS-503 instrumentation systems provided data for real time monitoring and postflight evaluation of the launch vehicle. The received data were reviewed and their respective measurements classified according to successfulness to achieve assigned flight requirements. This measurements evaluation provided an indication of the instrumentation system's performance and apprised data users of any limitations in the data for other vehicle systems analyses.

Definitions of the adopted flight measurement classifications follow as a guide for the interpretation of subsequent material:

Measurements, Scheduled	Those measurements listed in the Instrument Program and Components (IP&C) List for the particular flight and stage, which are wholly on the stage.
Measurements, Waived	Scheduled measurements which have been deleted as a flight requirement by NASA prior to start of automatic countdown sequence, but are not necessarily inoperative.
Measurements, Active	Scheduled flight measurements that have not been waived when automatic countdown sequence starts.
Measurements, Failed	Active flight measurements which, due to malfunction, fail to achieve their intended purpose.
Measurements, Partially Failed	Active flight measurements which successfully achieve their intended purpose despite a malfunction during flight.
Measurements, Successful	Measurements which achieve their intended purpose and include total successes and partial failures.
Measurement Reliability	The percentage of active flight measurements which achieve their intended purpose (including partial failures). Questionable measurements are excluded from assessment. The measurement reliability is determined as follows: $\% \text{ Reliability} = \frac{\text{No. of successful measurements} \times 100}{\text{No. of active flight measurements}}$
Measurements, Out of Range	Measurements which register above or below the assigned information bandwidth during any part of the flight are defined as being out of range. All out of range measurements, which are not also classified as failures or partial failures, are listed in the Out of Range Measurements table.
Measurements, Questionable	Any measurements that have not been judged as being successful, failed, or partially failed (at time of this report issuance) shall be referred to as questionable measurements.

There were 2675 scheduled flight measurements on the AS-503 launch vehicle of which only 5 were waived prior to automatic countdown. Of the remaining 2670 active measurements, 27 failed, resulting in a launch vehicle measurement reliability of 99.0 percent. A summary of the launch vehicle's measurements performance is presented in Table 19-1.

Measuring system performance for the AS-503 launch vehicle was excellent. The only abnormality of interest was the temporary loss of several S-II temperatures due to the intermittent operation of three power supplies. However, no critical operational parameters were affected and the data loss did not impair flight performance evaluation.

19.2.1 S-IC Stage Measurement Analysis

There were 893 flight measurements scheduled for the S-IC stage. Prior to the start of automatic countdown sequence, 3 measurements gave malfunction indications and were waived. (See Table 19-3 for a summary). However, two waived measurements did provide usable flight data. Of the remaining 890 active flight measurements, 6 failed, 23 partially failed, 5 were improperly ranged, and 2 were questionable. The failures and partial failures are summarized in Table 19-3. Table 19-4 gives a summary of the improperly ranged measurements and questionable measurements are presented in Table 19-5. Based upon the numbers of active and failed measurements, the S-IC stage flight measurement reliability was 99.3 percent.

Table 19-1. AS-503 Flight Measurement Summary

MEASUREMENTS CATEGORY	S-IC STAGE	S-II STAGE	S-IVB STAGE		INSTRUMENT UNIT	TOTAL VEHICLE
			PHASE I *	PHASE II*		
Scheduled	893	1001	404	404	377	2675
Waived	3	2	0	0	0	5
Failures	6	16	2	5	0	27
Partial Failures	23	49	0	0	3	75
Improper Range	5	0	0	1	0	6
Questionable	2	0	0	0	1	3
Reliability, %	99.3	98.4	99.5	98.8	100.0	99.0

*Notes: 1. S-IVB Phase I period of performance is from liftoff to parking orbit insertion.
2. S-IVB Phase II period of performance is fr[illegible] f until end of S-IVB stage flight period of performance.

Performance of the S-IC POGO suppression system measurements was satisfactory and a significant improvement was noted in the quality of acoustic and high frequency vibration data on this flight. Several of the latter category of measurements had increased ranges and low pass filters added. These modifications resulted in a 95.9 percent reliability in the acquisition of these measurements compared to 90.2 percent for AS-502.

19.2.2 S-II Stage Measurement Analysis

There were 1001 flight measurements scheduled for the S-II stage. Prior to the start of automatic countdown sequence, 2 measurements gave malfunction indications and were waived. The waived measurements, summarized in Table 19-2, provided no useful flight data The remaining 999 active flight measurements, 16 failed, and 49 partially failed (44 of which were associated with the intermittent performance of three temperature bridge power supplies). The failed and partially failed measurements are summarized in Table 19-3. Based upon the number of active and failed measurements, the S-II stage flight measurement reliability was 98.4 percent.

Twice during the flight, power supplies for temperature measurement bridges intermittently open-circuited. As discussed in paragraph 13.3, output voltages M046 and M059 were intermittent for approximately 30 seconds through the period of Max Q. During this time, all 25 temperature measurements connected to these power supplies similarly went off scale. All affected measurements returned to normal following the return of correct power supply voltage. At approximately 443 seconds, power supply voltage M053 became intermittent and caused 19 temperature measurements to go off scale for approximately 30 seconds and then return to normal when correct power was reapplied. All 44 measurements provided satisfactory

Table 19-2. AS-503 Flight Measurements Waived Prior to Launch

MEASUREMENT NUMBER	MEASUREMENT TITLE	NATURE OF FAILURE	REMARKS
		S-IC STAGE	
C041-115	Temperature, Helium Inlet Manifold	Remained at Maximum	Waiver L1A-1-47; No Valid Data.
D027-101	Pressure, Surface, Outboard Engine	Inoperative Before Flight	Waiver L1A-1-46; Valid Data During Flight.
N020-115	Film Camera Timer Operation Indicator	Time Code Not Per Specification	Waiver L1A-1-48; Partially Valid Data.
		S-II STAGE	
C063-218	Temperature, LH_2 Dome External Insulation Surface	Indicated Maximum Temperature Before And During Flight	No Valid Data.
D030-201	Pressure, El LH_2 Recirculation Pump Discharge	Abnormally Low Indication Before And During Flight	No Valid Data.

Table 19-3. AS-503 Flight Measurement Malfunctions

MEASUREMENT NUMBER	MEASUREMENT TITLE	NATURE OF FAILURE	TIME OF FAILURE (RANGE TIME)	DURATION SATISFACTORY OPERATION	REMARKS
TOTAL MEASUREMENT FAILURES, S-IC STAGE					
B004-114	Acoustic Rear Fin D	High amplitude, low frequency noise	-5 seconds	None	Saturation of system due to high vibration level
N001-120	Telemetry Antenna Reflected Power Link F-1	No data	-5 seconds	None	Failure of VSWR monitor
D046-106	Pressure, Diff, Heat Shield	Data high throughout most of flight	Entire Flight	None	Port cap probably left on
D015-103	Pressure Engine Gimbal System Pitch Actuator Return	Data reads 40 psi low but shows normal trend throughout flight	-5 seconds	None	Reason unknown
E039-101	Vibration, Fuel Pump Inlet	Data does not agree with previous flight data	-5 seconds	None	System saturation due to high vibration level
E042-104	Vibration, Fuel Pump Flange	Data does not agree with previous flight data	-5 seconds	None	System saturation due to high vibration level
TOTAL MEASUREMENT FAILURES, S-II STAGE					
C852-218	E1 LH_2 Feedline Q FWD	Offscale, Low	33 seconds	None	Apparent open transducer circuit
C895-218	LH_2 Tank Insulation Surface T	Erratic Signature	-90 seconds	None	Apparent transducer failure
D030-202	E2 LH_2 Recirc Pump Disch P	Offscale, Low	-300 seconds	None	Transducer installation incompatible with thermal environment
D030-203	E3 LH_2 Recirc Pump Disch P	Offscale, Low	-300 seconds	None	Transducer installation incompatible with thermal environment
D030-204	E4 LH_2 Recirc Pump Disch P	Abnormal pressure indication	-300 seconds	None	Transducer installation incompatible with thermal environment
D030-205	E5 LH_2 Recirc Pump Disch P	Offscale, Low	-300 seconds	None	Transducer installation incompatible with thermal environment
D112-219	Forward Skirt Static P	Slow Pressure Decay	60 seconds	None	Possible moisture or ice in sensing tube
D115-219	Forward Skirt Static P	Slow Pressure Decay	60 seconds	None	Possible moisture or ice in sensing tube
D116-219	Forward Skirt Static P	Slow Pressure Decay	Entire flight	None	Possible moisture or ice in sensing tube
D117-219	Forward Skirt Static P	Slow Pressure Decay	Entire flight	None	Possible moisture or ice in sensing tube
D131-218	LH_2 Tank Insulation Ext P	No Pressure Decay Until 20 Seconds	0 seconds	None	Possible moisture or ice in sensing tube
D134-218	LH_2 Tank Insulation Ext P	Incomplete Pressure Decay	90 seconds	None	Possible moisture or ice in sensing tube
D152-202	LH_2 Recirc Pump Inlet P	Remained at Atmospheric Pressure	0 seconds	None	Transducer installation incompatible with thermal environment
D158-206	Heat Shield Aft Face P	No increase at ignition	40 seconds	None	Transducer failure
E002-203	E3 Radial Vib LOX Pump	Data transients	Entire flight	None	Transducer failure
G001-205	E5 Turbine Bypass Vlv Pos	Data intermittent	Prior to liftoff	None	Transducer failure
TOTAL MEASUREMENT FAILURES, S-IVB STAGE, PHASE I					
D0020-403	Press - Fuel Tank He Bottle Repress	Only data trends useful	0 seconds	None	Cause unknown
E0209-401	Vib - Combustion Chamber Dome - Long	No useable data	0 seconds	None	Loose cable connector suspected
TOTAL MEASUREMENT FAILURES, S-IVB STAGE, PHASE II					
C0149-401	Temp - GG Oxid Bleed Valve Wall	Erratic data	18600 seconds	17229 seconds	Sensor open circuited
C0208-405	Temp - Cold He Sphere No. 1 Gas	Large data shift	9700 seconds	9700 seconds	Possible calibration error
C2041-403	Temp - Cold He Fill Line	Erratic data NOTE: Phase I failures not relisted.	9793 seconds	9793 seconds and 11630 to LOS	Sensor open circuited

Table 19-3. AS-503 Flight Measurement Malfunctions (Continued)

MEASUREMENT NUMBER	MEASUREMENT TITLE	NATURE OF FAILURE	TIME OF FAILURE (RANGE TIME)	DURATION SATISFACTORY OPERATION	REMARKS
PARTIAL MEASUREMENT FAILURES, S-IC STAGE					
A001-118	Acceleration, Longitudinal	Measurement shows -4gs at 5 seconds	-1 to 11 seconds	144 seconds	Data satisfactory after T+11 seconds
C003-102	Temperature, Turbine Manifold	Measurement failed at 18 seconds	18 seconds	23 seconds	Failed transducer
C020-105	Temperature, Engine, Total Calorimeter	Data erratic between 80 and 105 seconds	80 seconds	135 seconds	Apparent electrical connector chatter
C087-110	Temperature, Skin Shroud, Internal	Loss of data from 125 to 130 seconds	125 seconds	155 seconds	Transducer failure
C093-110	Temperature, Skin Shroud, Inner Surface	Data erratic until 130 seconds	-5 seconds	25 seconds	Transducer failure
C132-101	Temperature, Heat Exchanger Bellows	Data erratic after 105 seconds	105 seconds	110 seconds	Installation problem. Weld broken.
C228-105	Temperature, Calorimeter Body	Data erratic from 80 to 105 seconds	80 seconds	135 seconds	Apparent electrical connector chatter
C342-115	Temperature, LOX Prevalve 1, Engine No. 5	Measurement failed at 70 seconds	70 seconds	75 seconds	Apparent transducer failure
D008-101	Pressure, Combustion Chamber	Measurement did not respond correctly at OECO	158 seconds	160 seconds	Apparent clogged sensing port
D038-106	Pressure, Base Heat Shield	Data noisy and erratic from ignition until 80 seconds	-5 seconds	60 seconds	Apparent connector chatter
D089-115	Pressure, Differential Skin	Measurement did not respond correctly	80 seconds	15 seconds	Clogged sensing port. Measurements D089-115 and D120-115 connected to same port
D120-115	Pressure, Surface, Aft Skirt	Data does not track from 70 to 105 seconds	70 seconds	125 seconds	Clogged sensing port. Measurements D089-115 and D120-115 connected to same port
D151-115	Pressure, LOX Pump Inlet	Measurement failed at 30 seconds	30 seconds	35 seconds	Transducer failed due to excessive environment
E042-102	Vibration, Fuel Pump Flange, Radial	Measurements contained high amplitude, low frequency noise	0 to 20 seconds	130 seconds	Saturation of system due to high vibration level
E042-103	Vibration, Fuel Pump Flange, Radial	Measurements contained high amplitude, low frequency noise	0 to 20 seconds	130 seconds	Saturation of system due to high vibration level
K014-118	LOX Level Cutoff 4	Measurement switched throughout flight	-5 seconds	Inter-mittent	Apparently triggered by strobe light
K043-115	Thrust OK Pressure Switch 2, Engine No. 4	Measurement switched throughout flight	-5 seconds	Inter-mittent	Pressure switch chatter
K047-115	Thrust OK Pressure Switch 3, Engine No. 5	Measurement switched throughout flight	-5 seconds	Inter-mittent	Pressure switch chatter
L011-119	Segment Identification, Fuel Discrete	Measurement did not lock on until 0.3 seconds	Prior to 0.35 seconds	After 0.3 seconds	Cause unknown
L020-119	Segment Identification, Position III	Indicated incorrect segment throughout flight		Segments 11, 10, 9, 3, 2	Probable cable failure
S009-120	Strain, Forward Skirt, Longitudinal	Data shifted throughout flight	Prior to flight	Shifted	Strain gage installation failure
S011-120	Strain, Forward Skirt, Longitudinal	Data shifted throughout flight	Prior to flight	Shifted	Strain gage installation failure
S046-115	Strain, Lower Skirt, Longitudinal	Data shifted throughout flight	Prior to flight	Shifted	Improper adjustment

Table 19-3. AS-503 Flight Measurement Malfunctions (Continued)

MEASUREMENT NUMBER	MEASUREMENT TITLE	NATURE OF FAILURE	TIME OF FAILURE (RANGE TIME)	DURATION SATISFACTORY OPERATION	REMARKS
PARTIAL MEASUREMENT FAILURES, S-II STAGE					
C043-202	E2 ASI Fuel Line Skin T	Loss of data, indicated max temp	299 seconds	299 seconds	Transducer opens
D256-203	E3 Fuel Pump Interstage P	Loss of data, indicated min press	298 seconds	298 seconds	Transducer failure
E001-204	E4 Long Vib Combstn Dome	Noise spikes	349 seconds	349 seconds	Intermittent
E002-204	E4 Radial Vib LOX Pump	Noise spikes	353 seconds	353 seconds	Intermittent
E003-204	E4 Radial Vib Fuel Pump	Noise spikes	345 seconds	345 seconds	Intermittent
*C018-219	Forward Skirt Internal Amb T	Data out of range for approximately 30 seconds	69 seconds	732 seconds	Intermittent operation of bridge power supplies M046 and M059
*C021-219	Forward Skirt Internal Amb T				
*C024-219	Forward Skirt Internal Surf T				
*C045-218	LH_2 Dome Internal Amb T				
*C051-218	LH_2 Dome Internal Surf T				
*C054-218	LH_2 Dome Internal Surf T				
*C063-218	LH_2 Dome Ext Insul Surf T				
*C066-218	LH_2 Dome Ext Insul Surf T				
*C076-219	Forward Skirt Internal Surf T				
*C115-218	LH_2 Tank Insulation Surf T				
*C121-218	LH_2 Tank Insulation Surf T				
*C122-218	LH_2 Tank Insulation Surf T				
*C195-216	Systems Tunnel Int Wall T				
*C355-220	PM Contr Equip Mt T				
*C361-222	Instr Contr Equip Mt T				
*C516-225	Tlm Contr Wall Surf T				
*C763-218	LH_2 Tank Liquid T				
*C764-218	LH_2 Tank Liquid T				
*C807-219	Temperature at C805				
*C889-218	LH_2 Tank Insulation Surf T				
*C891-218	LH_2 Tank Insulation Surf T				
*C892-218	LH_2 Tank Insulation Surf T				
*C893-218	LH_2 Tank Insulation Surf T				
*C894-218	LH_2 Tank Insulation Surf T				
*C895-218	LH_2 Tank Insulation Surf T		69 seconds		Intermittent operation of bridge power supplies M046 and M059
*C001-204	E4 Fuel Pump Discharge T		443 seconds		Intermittent operation of temperature bridge power supply M053
*C001-205	E5 Fuel Pump Discharge T				
*C002-204	E4 LOX Pump Discharge T				
*C002-205	E5 LOX Pump Discharge T				
*C004-204	E4 LOX Turbine Inlet T				
*C004-205	E5 LOX Turbine Inlet T				
*C005-204	E4 Electric Control Box T				
*C005-205	E5 Electric Control Box T				
*C006-204	E4 Primary Instr Pkg T				
*C006-205	E5 Primary Instr Pkg T				
*C008-204	E4 GG Fuel Valve Inlet T				
*C008-205	E5 GG Fuel Valve Inlet T				
*C009-204	E4 GG LOX Valve Inlet T				
*C009-205	E5 GG LOX Valve Inlet T	Data out of range for approximately 30 seconds	443 seconds	732 seconds	Intermittent operation of temperature bridge power supply M053

*Considered successful measurements by stage contractor.

Table 19-3. AS-503 Flight Measurement Malfunctions (Continued)

MEASUREMENT NUMBER	MEASUREMENT TITLE	NATURE OF FAILURE	TIME OF FAILURE (RANGE TIME)	DURATION SATISFACTORY OPERATION	REMARKS
PARTIAL MEASUREMENT FAILURES, S-II STAGE					
*C180-206	O2 Vent Ln Surf T at Exit	Data out of range for approximately 30 seconds	443 seconds	732 seconds	Intermittent operation of temperature bridge power supply M053
*C191-206	Thrust Cone Fwd Amb T				
*C236-206	Thrust Cone Fwd Amb T				
*C515-208	Instr Contr Cover Surf T				
*C672-206	Engine Compartment Gas T	Data out of range for approximately 30 seconds	443 seconds	732 seconds	Intermittent operation of temperature bridge power supply M053
PARTIAL MEASUREMENT FAILURES, S-IV STAGE					
C19-601	Cold Plate Exit Coolant Temp (Loc 5)	Instantly dropped off-scale low and remained there throughout data reviewed	75 seconds	75 seconds	
C30-603	Heat Exchanger, Meth/Water Inlet Temp	Instantly dropped off-scale low and remained there until S/C separation	83 seconds	83 seconds	Recovered at S/C separation; provided useable data thereafter
C44-603	IU Inner Skin No. 8 (Loc 20) Temp	Went off-scale low between 87 and 157 seconds, then normal indication returned	87 seconds	97 seconds and 157 seconds to end of data reviewed (10,700) seconds	

*Considered successful measurements by stage contractor.

Table 19-4. AS-503 Flight Measurements With Improper Range

MEASUREMENT NUMBER	MEASUREMENT TITLE	NATURE OF OUTPUT	TIME	REMARKS
S-IC STAGE				
E059-118	Vibration Bending, Pitch	Offscale high	T-3 to T+15 seconds	Valid data except between noted time
E061-118	Vibration Bending, Pitch	Offscale high	T-3 to T+15 seconds	Valid data except between noted time
E094-120	Vibration Destruct System Mounting Panel	Low throughout flight	Duration of flight	Valid data; vibration environment low
F049-115	Flowrate, Joint Leakage	Offscale high	Duration of flight	Measurement saturated full scale because of flange leak
L003-119	Lox Level, Position 3	Exceeded full scale	55.3 to 56.3 seconds 79.3 to 80.0 seconds	Electronics out of alignment Data useable at other times
S-IVB STAGE				
*C0391-403	Temp - He Heater Support 2	Offscale low	During He heater operation	Measurement ranged for longer burner times than occurred

*Stage contractor considers measurement correctly ranged.

data except for the short time periods mentioned and none of these measurements, nor measurements powered by twelve other similar temperature bridge power supplies, were associated with operational functions of the stage. Their intermittent operation, therefore, did not constitute a hazard to the flight.

The quality of vibration data showed considerable improvement compared with that from AS-502. Modifications were incorporated that increased measurement ranges and added low pass filters to several of these measurement channels. As a result, the acquisition of vibrational data was 98.4 percent successful on AS-503 compared with 70.0 percent on AS-502.

19.2.3 S-IVB Stage Measurement Analysis

The S-IVB stage had 404 flight measurements scheduled for AS-503, all of which were active at the start of automatic countdown. There were only 2 measurement failures in Phase I, which begins at liftoff and ends at parking orbit insertion. Three other measurements failed during the latter part of Phase II, which also starts at liftoff but continues until the end of S-IVB stage flight period of performance. These failures are summarized in Table 19-3. Measurement C0391-403, Table 19-4, was considered improperly ranged because it remained offscale low during the short O_2/H_2 burner operation. The measurement was ranged for much longer burner times and was therefore not expected to read onscale on AS-503. Based upon the number of active and failed measurements, the S-IVB stage flight measurement reliability was 99.5 percent for Phase I and 98.8 percent for Phase II. Thirty eight other measurements were handled by the S-IVB stage though not wholly on the stage and therefore excluded from the reliability assessment. An evaluation of these measurements, however, indicated that they were all successful.

Table 19-5. AS-503 Questionable Flight Measurements

MEASUREMENT NUMBER	MEASUREMENT TITLE	REASON QUESTIONED	REMARKS
		S-IC STAGE	
C014-101	Temp Eng T Cal	Abnormally high throughout flight.	Measurement appears valid but does not correlate with related measurements nor with previous flight data.
C138-101	Temp Aft Nozzle External	Expected temperature rise not indicated.	Data after 100 seconds indicates the possibility of thermocouple failure.
		S-IU STAGE	
J032-602	RF Reflect Power, S1 Telemeter	Abnormally high reading.	Measurement appears valid but related measurements and telemetry performance do not substantiate validity.

19.2.4 S-IU Stage Measurement Analysis

There were 377 flight measurements scheduled for the S-IU stage. None of the measurements were waived prior to the start of automatic countdown and all measurements provided usable data. Only 3 measurements partially failed and they are summarized in Table 19-3. Measurement J032-602, S1 Telemeter RF Reflected Power, indicated abnormally high throughout the flight while the RF output power indicated normal performance, and data from the link were satisfactory. This measurement problem has not been resolved and is listed in Table 19-5 as questionable. The flight measurement reliability of the S-IU stage was 100.0 percent based upon zero totally failed measurements.

19.3 AIRBORNE TELEMETRY SYSTEMS

The AS-503 launch vehicle contained 21 telemetry links: 6 on the S-IC stage, 6 on the S-II stage, 3 on the S-IVB stage, and 6 on the S-IU stage. Table 19-6 presents a listing of the vehicle's telemetry links and summarizes their performances by stage. The 19 VHF and 1 of the 2 UHF telemetry links performed very satisfactorily; however, lack of data precluded an evaluation of UHF link DP-1. Predicted real time data losses occurred during S-IC/S-II separation, S-II main engines ignition, and S-II second plane separation. However, onboard tape recorders stored pertinent data during these blackout periods and later successfully transmitted the data to ground stations. Four unpredicted data dropouts were experienced, all of which were of short duration. Three of the data losses pertained to the S-II stage, and one affected both the S-IVB stage and IU stage links for approximately 3 seconds over Hawaii at 10,375 seconds.

19.3.1 S-IC Stage Telemetry System

The S-IC stage telemetry system for AS-503 consisted of six data links and all performed very satisfactorily. Data were lost only during S-IC retro motor firing at approximately 154.4 seconds, and S-II engine ignition at approximately 157.9 seconds for periods of 1.4 and 1.2 seconds, respectively. The real time data lost on the AF-1 and AF-2 links were later recovered from playback of the onboard tape recorder as planned. Inflight calibrations were initiated at 24.6 and 115.8 seconds. Data show that the inflight calibrator and multiplexer calibrator performed within specified flight requirements.

The three PAM/FM/FM telemetry links performed well within established flight criteria. Noise figures for the multiplexers were well within tolerance and the systems' accuracy, linearity and noise figures were very acceptable.

The single PCM/FM link, AP-1, performed as predicted. System noise was very low with no synchronization errors occurring for 99.2 percent of the flight. Only during separation and S-II main engine ignition were synchronization errors large enough to make the data not usable.

Table 19-6. AS-503 Launch Vehicle Telemetry Links

LINK	FREQUENCY (MHz)	MODULATION	STAGE	FLIGHT PERIOD (RANGE TIME, SEC)	PERFORMANCE SUMMARY
AF-1 AF-2 AF-3 AP-1 AS-1 AS-2	240.2 252.4 231.9 244.3 235.0 256.2	PAM/FM/FM PAM/FM/FM PAM/FM/FM PCM/FM SS/FM SS/FM	S-IC S-IC S-IC S-IC S-IC S-IC	0-408 0-408 0-408 0-408 0-408 0-408	Satisfactory Data Dropouts Range Time (sec) — Duration (sec) 154.4 — 1.4 157.9 — 1.2
BF-1 BF-2 BF-3 BP-1 BS-1 BS-2	241.5 234.0 229.9 248.6 227.2 236.2	PAM/FM/FM PAM/FM/FM PAM/FM/FM PCM/FM SS/FM SS/FM	S-II S-II S-II S-II S-II S-II	0-762 0-762 0-762 0-762 0-762 0-762	Satisfactory Data Dropouts Range Time (sec) — Duration (sec) 78.5 — BP-1 only 2.3 135 — BP-1 only 3.5 154 — 2.8 185 — 2.0 200 — BP-1 only 1.7
CF-1 CP-1 CS-1	253.8 258.5 246.3	FM/FM PCM/FM SS/FM	S-IVB S-IVB S-IVB	Flight Duration Flight Duration 0-707; 9670-10580	Satisfactory Data Dropouts Range Time (sec) — Duration (sec) 154 — 1.0 10375 (Intermittent) 3.0
DF-1 DF-2 DS-1 DP-1 DP-1A DP-1B	250.7 245.3 259.7 255.1 2277.5 2282.5	FM/FM/FM PAM/FM/FM SS/FM PCM/FM PCM/FM PCM/FM	S-IU S-IU S-IU S-IU S-IU S-IU	Flight Duration Flight Duration 0-695 Flight Duration Flight Duration Flight Duration	Satisfactory Data Dropouts Range Time (sec) — Duration (sec) 154 — 1.1 10375 (DF-2 only) 3.0

Data requiring a frequency response between 30 and 3000 hertz are acquired and transmitted by single side band telemetry links AS-1 and AS-2. All performance requirements for these links were met. Except for the data loss at separation and S-II mainstage, data quality was excellent.

19.3.2 S-II Stage Telemetry System

The telemetry system for the S-II stage consisted of six data links, three of which were PAM/FM/FM, two SS/FM, and one PCM/FM. All telemetry links performed exceptionally well throughout the flight. Three short data dropouts occurred during the 762 seconds of telemetry operation which had not been predicted. Further discussion of these data losses is presented in paragraph 19.5. Predictable data dropouts due to S-IC retro motor firing, at approximately 154 seconds, and S-II second plane separation, at about 185 seconds, did occur and lasted for approximately 3 seconds and 2 seconds, respectively. Inflight calibrations of the S-II telemetry links were initiated at approximately 126.2, 278.8, 378.8 and 542.3 seconds. Analyses indicated that all systems operated within required specification limits. All Time Division Multiplexers (TDM) and Inter Range Instrumentation Group (IRIG) calibration levels were within

3 percent of required values. Judged by the quality of data received and evaluated to assess vehicle flight performance, all 6 telemetry links of the S-II stage performed satisfactorily.

19.3.3 S-IVB Stage Telemetry System

The S-IVB stage telemetry system for AS-503 consisted of three data links all of which performed satisfactorily. Two data dropouts were experienced during the flight; the first occurred at S-IC/S-II separation (154 seconds) of 1-second duration, and the second was a 3-second intermittent dropout over Hawaii at 10,375 seconds (see paragraph 19.5.1 for discussion). Inflight calibrations were conducted four times and the data revealed a possible malfunction in the DP180 model 270 multiplexer. The abnormality consisted in a negative level being produced when the zero level of the five step calibration sequence was expected. This condition has not been displayed on previous flights and its cause has not yet been identified. However, flight data quality were not affected and no data reduction difficulties were experienced due to this multiplexer abnormality.

Performance of the PCM/FM system was excellent except for the minor calibration difficulty previously discussed. Data reveal that all multiplexers were properly synchronized.

Performance of the FM system was excellent. The center and band edge frequencies of all voltage controlled oscillators remained well within their specified tolerances.

Analysis of data taken from the single side band telemetry link verified its proper operation. The model 245 multiplexer properly sampled the measurements assigned to the subchannels and the 1700 hertz calibration signal was within the tolerance limits. The system was commanded ON prior to launch and OFF at 707 seconds for S-IVB first burn. It was turned ON for second burn at 9670 seconds and OFF at 10,580 seconds.

19.3.4 S-IU Stage Telemetry System

The S-IU stage telemetry system consisted of six data links. Evaluations of received data indicate that the FM/FM/FM and PAM/FM/FM telemetry links performed satisfactorily, had very little system noise and produced high quality information. Only two data dropouts occurred; the first occurred at S-IC/S-II separation (154 seconds) of 1.1 second duration, and the second was a 3-second intermittent dropout of DF-2 at 10,375 seconds over Hawaii (see paragraph 19.5.1 for discussion).

Two of the 3 PCM/FM links performed nominally. There were insufficient data to evaluate DP-1A. All received data were of good quality. Very little loss of synchronization was seen or reported. No redundant UHF data from DP-1A were available for comparison with the CCS PCM data.

The performance of the one SS/FM link was satisfactory. The reflected power for this link was above the specification of 9 percent of the forward power. However, this power level was also out of specification prior to launch. This discrepancy is thought to be a measurement problem.

19.4 AIRBORNE TAPE RECORDERS

Airborne tape recorders were installed on the S-IC, S-II and S-IU stages of the AS-503 launch vehicle to store necessary real time data during predicted transmission blackouts. All tape recorders operated as expected. Data stored during the predicted S-IC/S-II separation, S-II main engines ignition, and S-II second plane separation blackout periods were successfully transmitted to ground stations with little degradation.

.4.1 S-IC Stage Recorder

rformance of the 2-track tape recorder on the S-IC stage was very satisfactory. The recording and playback of telemetry links AF-1 and AF-2 was accomplished successfully.

Record and playback commands were initiated on schedule as shown in Table 19-7. Data was recorded for approximately 129.2 seconds. The duration of the airborne timer which initiates playback was 24.9 seconds and was within design limits of 24 ± 1.5 seconds. Airborne recorder playback amplifier gain was within specification limits of ±3 db of the corresponding real time data.

19.4.2 S-II Stage Recorders

There were two tape recorders on the S-II stage to record the BF-1, BF-2, and BF-3 PAM/FM telemetry links and the output of the BT-1 time division multiplexer during anticipated RF blackout periods (S-IC/S-II and S-II/S-IVB separations).

The S-II airborne tape recorders and associated hardware performed as required during this flight. Table 19-7 summarizes the S-II tape recorder subsystem operation. Operation of the timers used to provide the necessary tape recorder sequence after S-II/S-IVB separation was satisfactory. Calibration accuracy of the BT-1 multiplexer recorder on track 2 of the No. 2 tape recorder was reviewed and determined to be within 3 percent of the desired nominal calibration levels.

19.4.3 S-IU Stage Recorder

The AS-503 Instrument Unit (IU) had one magnetic tape recorder which recorded the outputs of links DF1 and DF2 during retro firings to insure that no data were lost. Two record periods were programmed during the mission. A summary of tape recorder operation is given in Table 19-7.

Table 19-7. Tape Recorder Summary

RECORDER	LINK RECORDED	RECORD TIME (RANGE TIME)		PLAYBACK TIME (RANGE TIME)	
		START	STOP	START	STOP
LAUNCH PHASE					
S-IC Recorder	AF-1,AF-2	50.2	179.5	179.5	309.3
S-II Recorder No. 1	BF-1,BF-2	74.6 486.3	165.7 547.3	547.3	700.0
S-II Recorder No. 2	BF-3,BT-1	74.6 486.3	165.7 547.3	547.3	699.6
S-IU Recorder	DF-1,DF-2	124.4 486.1	165.5 538.4	696.4	767.2

The switch selector program did not allow enough time for playback. There were 93.4 seconds of data recorded and only 70.8 seconds allowed for playback. However, all the data lost due to retro firings were played back.

19.5 RF SYSTEMS EVALUATION

The launch vehicle RF systems provide telemetry, tracking, command system and television transmission and reception. Not all of the data required to perform a detailed RF analysis were available for this evaluation. Based on available data, the overall performance of launch vehicle RF systems was satisfactory and measured flight data, with few exceptions, agreed favorably with expected trends. Telemetry propagation was good, as was tracking performance. Preliminary data indicate that the Command and Communications System (CCS) performance was satisfactory. Insufficient data were received to evaluate the video RF propagation, however, video tape quality indicates that signal levels were adequate.

Final loss of VHF telemetry signals was at approximately 29,230 seconds (8:07:10) at Guaymas (GYM), loss of CCS signals at approximately 44,357 seconds (12:19:17) at GYM and C-Band radar signals at approximately 21,325 seconds (5:55:25) at Grand Turk Island (GTI). Other stations viewing the vehicle during these time periods lost signal at earlier times.

19.5.1 Telemetry Systems RF Propagation Evaluation

The RF propagation of all 19 VHF telemetry links was excellent. The systems performance with the few exceptions noted agreed with predicted data. Gross main engine effects, causing 18-20 db attenuation were observed between 110 and 150 seconds at Cape Telemetry 4 (TEL 4) and Central Instrumentation Facility (CIF). Main engine effects were not noted at Grand Bahama Island (GBI).

The 2-second period of RF signal dropout which occurred shortly after Inboard Engine Cutoff (IECO) for the AS-501 and AS-502 flights did not recur on AS-503 probably due to the earlier IECO on AS-503, with the result that the flow separation field did not reach the S-IC antennas as on previous flights.

Staging effects at approximately 154 seconds were as expected with all telemetry links dropping to threshold, resulting in VHF telemetry data loss to all sites except for that which could be recovered by tape recorder playback. The S-IC stage blackout period was approximately 1.4 seconds duration, S-II approximately 2.8 seconds duration, S-IVB approximately 1.0 second duration, and IU approximately 1.1 seconds duration.

S-II stage ignition effects on the VHF telemetry system were observed at 158 seconds. The S-IC VHF telemetry signal strength dropped to threshold resulting in 1.2 seconds of data loss. The upper stages experienced 20 to 25 db drop during this period; however, signal levels remained sufficiently high to transmit usable data. The AF-1, AF-2, and AF-3 links continued to experience short periods of low RF signal level due to a partial antenna breakdown occasioned by the S-II engine flame effects until approximately 167 seconds at which time the antennas recovered. These short periods of low RF signal strength did not cause any loss of data since recovery occurred prior to S-IC tape recorder playback.

S-II telemetry signal strength level at TEL 4, CIF, and Bermuda (BDA) dropped to threshold at approximately 185 seconds during S-II second plane separation resulting in approximately 2 seconds of data dropout. The S-IVB stage and the IU experienced a 20 to 22 db drop in signal level at this time. These effects were not noted at GBI during this period. Antenna recovery of 15 db occurred at 187 seconds.

The S-II stage telemetry experienced 3 additional dropout periods on the BP-1 link which were not expected: at 78.5 seconds for approximately 2.3 seconds duration, at 135 seconds for approximately 3.5 seconds duration, and at 200 seconds for approximately 1.7 seconds duration. High resolution signal strength data indicated that a number of momentary RF transients were experienced during these time periods. These phenomena were noted on the BP-1 link only, and were observed on signal strength data from all sites. The BP-1 RF assembly is of an earlier configuration than that used for the other five links. The suspected cause of these transients is

intermittent operation of the BP-1 RF assembly. On AS-504 and subsequent vehicles the later configuration will be used on all links; and it is expected that this problem will not recur.

The performance of the S-IVB and IU telemetry systems during orbit, Translunar Injection (TLI) burn, and final coast was satisfactory. The telemetry signal received at Hawaii (HAW) showed an unexpected drop in signal level from 10,370 to 10,380 seconds with a 3-second intermittent data dropout at approximately 10,375 seconds on all S-IVB telemetry links and link DF-2 on the IU telemetry. This intermittent dropout can be partially related to S-IVB and IU onboard antenna pattern nulls.

VHF coverage was provided during the final coast phase by BDA, GYM, and Corpus Christi (TEX). Final loss of signal (LOS) from these sites, for all telemetry links active during this period, as shown in Table 19-8, were derived from PLIM summaries.

Table 19-8. Final RF LOS, VHF Telemetry

STATION	RANGE TIME (SECONDS)	RANGE TIME (HRS:MIN:SEC)
BDA	21,614	6:00:14
GYM	29,230	8:07:10
TEX	26,490	7:21:30

The times to which usable data were acquired for all VHF telemetry links active during the final coast phase are shown in Table 19-9.

Table 19-9. Last Usable VHF Telemetry Data

TELEMETRY LINK	STATION	RANGE TIME (SECONDS)	RANGE TIME (HRS:MIN:SEC)
CF-1	GYM, TEX	15,660	4:21:00
CP-1	GYM, TEX	15,660	4:21:00
DF-1	GYM	13,640	3:47:20
DF-2	GYM	12,980	3:36:20
DF-3	GYM	12,600	3:30:00

During the time period between last usable data and final LOS, data were so degraded that in effect only the RF carriers were tracked.

A summary of telemetry coverage showing acquisition of signal (AOS) and LOS is presented in Table 19-10.

19.5.2 Tracking Systems RF Propagation Evaluation

Sufficient data were not received to provide a complete assessment of the ODOP and C-Band tracking systems. Based upon the limited data available, however, RF performance of these systems appears to have been satisfactory.

19.5.2.1 ODOP. The Offset Doppler (ODOP) transponder was carried on the S-IC stage of the vehicle; therefore, ODOP tracking was limited to the flight of first stage only. Signal strength data for the ODOP ground stations were not available for analysis, so evaluation was limited to performance as indicated by the onboard data from the MARGO interrogating station.

S-IC main engine flame attenuation on the ODOP transponder uplink signal strength seen onboard occurred from 80 seconds to S-IC/S-II separation. Valid PCM data used for evaluating the ODOP immediately after IECO were available for the first time on this flight permitting evaluation during this time period. Signal strength to the ODOP transponder dropped approximately 40 db immediately after IECO and remained low for 2.9 seconds. Static phase error was abnormal indicating that the transponder lost phase lock during this period; however, the ODOP phase lock measurement did not confirm this. Phase lock between the ground interrogating station and transponder was lost at S-IC/S-II separation due to the staging blackout but was recovered shortly thereafter at approximately 159.8 seconds.

19.5.2.2 C-Band Radar. Insufficient data were received to compile a comprehensive analysis of the C-Band radar system throughout the mission in time for this report. Available data, however, indicate that the C-Band radar functioned satisfactorily during flight although several ground stations experienced tracking problems because of antenna nulls, main engine flame attenuation, and malfunctions of ground equipment.

Two data dropouts were reported at 60 to 84 seconds and 135 to 153 seconds by station operators at the Patrick Air Force Base (PAFB) and MILA radar stations, respectively. The PAFB dropout (60 to 84 seconds) was caused by a balance point shift (sudden drop in signal or distorted beacon return) which produced antenna pointing errors. The MILA dropout (135 to 153 seconds) was caused by a series of balance point shifts and flame attenuation. Automatic track was reacquired by MILA skin tracking for 10 seconds before switching back to automatic beacon tracking at 163 seconds. At 300 seconds MILA switched from beacon to skin track due to a weak beacon return signal and remained on skin track through the remainder of the pass. Cape Kennedy Air Force Site (CKAFS) also switched to skin track at 252 seconds because of a weak beacon return signal and remained on skin track until the ground transmitter was turned off. The GBI radar station reported modulation of 30 to 50 percent on the beacon returns. The cause of the modulation has not been determined due to unavailability of signal strength data.

Table 19-10. VHF Telemetry Systems RF Summary

STATION	STAGE	LAUNCH		1ST ORBIT		2ND ORBIT		TLC		REMARKS
		AOS	LOS	AOS	LOS	AOS	LOS	AOS	LOS	
CTF	S-IC	00:00:00	00:06:50 (B)							
	S-II	"	" "							
	S-IVB	"	" "							
	S-IU	"	" "							
WIL	S-IU	00:00:00	00:09:00 (D)			01:35:00	01:42:36 (D)	03:01:18	03:21:00 (D)	
								03:01:18	07:39:16 (D)	
CT4	S-IC	00:00:00	00:09:55 (E)							
	S-II	"	" "							
	S-IVB	"	" "							
	S-IU	"	" "							
GBI	S-IC	00:00:40	00:10:00 (E)							
	S-II	"	" "							
	S-IVB	"	" "							
	S-IU	"	" "							
GBM	S-IU	00:00:56	00:09:20 (D)			01:35:29	01:42:42 (D)			
BDA	S-II	00:03:40	00:12:40 (A,B)							
	S-IVB	00:03:40	00:12:58 (A,B)			01:38:00	01:46:03 (A)	03:03:14	04:59:00 (A)	
	S-IU	"	" "			"	" (A)	03:03:14	06:00:00 (A)	
ANT	S-IVB							03:57:20	05:58:00 (D)	
	S-IU							03:04:51	03:57:19 (D)	
HAW	S-IVB			00:09:03	00:15:59 (B,D)					
	S-IU			"	" "	01:42:14	01:49:43 (D)			
CYI	S-IVB			00:16:13	00:24:10 (D)	01:49:35	01:56:08 (D)			
	S-IU			"	" "	"	"			
TRN	S-IU			00:36:31	00:42:55 (D)	02:08:57	02:16:25 (D)			
CRO	S-IVB			00:51:21	00:58:47 (A,B)	02:25:01	02:32:18 (A)			
	S-IU			"	" (A,B)	"	" (A)			
	S-IU			"	" (D)	"	" (D)			
MER	S-IVB					02:44:11	02:51:31 (A)			
	S-IU					"	(A)			
	S-IU					"	(D)			
HAW	S-IVB					02:49:55	02:58:15 (A,B,D)			
	S-IU					"	"			
GYM	S-IVB			01:26:45	01:35:42 (B)			02:55:45	08:07:10 (D)	
	S-IU			"	" "			"	" "	
TEX	S-IVB			01:30:54	01:38:40 (B,D)			02:59:08	07:21:30 (D)	
	S-IU			"	" "			"	" "	

A - STRIPCHART
B - 4020 PLOT
C - OPERATORS LOG
D - PLIW SUMMARY
E - ALL OF ABOVE

The California (CAL) radar station tracked on a side lobe for the first 27 seconds during the first revolution. The main lobe signal was then acquired and good signal was received for the remainder of the pass. Recorded data from CAL during the first pass was from 5358 to 5577 seconds. Four data dropouts were recorded by CAL during the final coast phase occurring at 11,687 to 11,706 seconds (3:14:47 to 3:15:06), 13,110 to 14,297 seconds (3:38:30 to 3:58:17), 16,992 to 17,016 seconds (4:43:12 to 4:43:36), and 17,050 to 17,101 seconds (4:44:10 to 4:45:01). The cause of these dropouts, as verified by telecon with the ground station, was site oriented. Final loss of signal for the C-Band radar was reported from GTI as occurring at 21,325 seconds (5:55:25).

A summary of C-Band tracking coverage showing AOS and LOS is presented in Table 19-11.

19.5.2.3 CCS Tracking. There is no mandatory tracking requirement of the CCS; however, the CCS transponder has turnaround ranging capabilities and provides a backup to the Command and Service Module (CSM) transponder used for tracking in case of failure or desire for a cross check. Ranging data for AS-503 were provided by MILA, Vanguard (VAN), HAW, and GYM. All ranging data, with the minor exceptions discussed below, looked good and did not affect other CCS functions indicating satisfactory performance of the system.

Both MILA and VAN lost lock during the RF blackout period experienced from 155 to 161 seconds due to S-IC/S-II staging.

During the second revolution, range modulation was turned on and off 3 times at VAN because of problems experienced due to lock on to a spurious signal from the CCS transponder.

During the S-IVB second burn period, HAW experienced no problems. During the translunar coast period there were several intervals of special test pattern commands at GYM when ranging data were not available. There were no problems experienced until 21,293 to 21,361 seconds (5:54:53 to 5:56:01) during which period down link was lost. The system was on low gain antenna at that time and the lock angles on low gain were poor during this period. No further ranging data were obtained after this time.

19.5.3 Command Systems RF Evaluation

The AS-503 Command Systems consisted of the Secure Range Safety Command System (SRSCS) and the CCS. All indications were that these systems performed satisfactorily.

19.5.3.1 Secure Range Safety Command System. VHF telemetry measurements received by the ground stations from the S-IC, S-II and S-IVB stages indicated that the SRSCS RF subsystems functioned properly. Canaveral (CNV) and BDA were the only command stations used for this flight.

Table 19-11. C-Band Tracking System RF Summary

STATION	STAGE	LAUNCH		1ST ORBIT		2ND ORBIT		TLC		REMARKS
		AOS	LOS	AOS	LOS	AOS	LOS	AOS	LOS	
CNV	S-IU	00:00:00	00:04:59 (A)							
MIL	S-IU	00:00:00	00:08:52 (A)(C)			01:35:15	01:24:21 (A)(C)			
PAT	S-IU	00:00:24	00:09:10 (A)(C)			01:35:12	01:42:00 (A)(C)	03:06:01	05:55:12 (A)(C)	
GBI	S-IU	00:01:37	00:08:46 (C)			01:36:09	01:41:59 (C)			
GTK	S-IU	00:03:20	00:10:07 (A)(C)			01:38:33	01:43:18 (A)(C)	03:06:03	05:55:25 (A)(C)	
BDA (FPS-16)	S-IU	00:04:02	00:12:59 (C)(D)							
BDA (FPQ-6)	S-IU	00:04:00	00:13:08 (C)(D)			01:38:15	01:46:10 (C)(D)	03:03:54	05:54:06 (C)(D)	
VAN	S-IU	00:11:18	00:15:56 (C)(D)			01:24:22	01:49:45 (C)(D)			
CYI	S-IU			00:16:25	00:23:52 (D)	01:50:10	01:56:01 (D)			
TAN	S-IU			00:37:40	00:42:29 (C)(D)	02:09:37	02:16:14 (C)(D)			
CRO	S-IU			00:52:00	00:58:18 (A)(C)(D)	02:25:00	02:32:06 (A)(C)(D)			
RED	S-IU							02:44:39	02:44:43 (C)(D)	
MER	S-IU							02:44:40	02:51:38 (A)(C)(D)	
HAW	S-IU							02:51:04	02:57:24 (C)(D)	
CAL	S-IU			01:29:18	01:32:57 (A)(C)(D)			03:12:56	05:50:40 (A)(C)(D)	
ANS	S-IU			01:30:28	01:35:04 (D)			03:01:02	05:53:28 (D)	

A = STRIPCHART
B = 4020 PLOT
C = OPERATOR LOG
D = PLIN SUMMARY
E = ALL OF ABOVE

CNV used an omni antenna until approximately 116.3 seconds when a switch was made to a high power helical antenna. A signal loss for approximately 0.5 second on the S-IC, S-II and S-IVB receivers occurred at this time due to the mechanical switching arrangements. This dropout is normal during this period. At approximately 136 seconds a data spike was observed on the S-IVB Range Safety System No. 2 low level signal strength. Review of data indicates a loss of data synchronization during this period. At S-IVB first burn engine start and cutoff, the Range Safety System No. 2 low level signal strength exhibited level perturbations of approximately 0.18 volt and 0.1 volt maximum, respectively. This is believed to be due to S-II retro motor firing at engine start and S-IVB ullage motor firing after cutoff. Handover from CNV to BDA occurred at 409 seconds. Evaluation of the SRSCS is discussed in paragraph 14.2.

19.5.3.2 Command and Communications System. Preliminary assessment based on the limited data available for this report indicate that there were no onboard equipment malfunctions.

Downlink dropouts occurred at MILA from 155 to 161 seconds, 163.5 to 176 seconds, 186 to 191.5 seconds, and 300 to 332 seconds. The first dropout was due to S-IC/S-II staging, the second dropout was probably the result of faulty acquisition procedures, and the third dropout was caused by signal interference during the time the S-II interstage was passing through the S-II stage flame after second plane separation.

The last dropout occurred during handover from MILA to BDA. This dropout was longer than is normally experienced during handover periods; however, the cause of this dropout cannot be determined at this time since data received from MILA are incomplete and no data have been received from BDA.

Acquisition problems apparently occurred at VAN during launch phase. An uplink dropout from 630.5 to 634 seconds indicates that handover to VAN occurred at this time. The exciter sweep voltage was ON at VAN from 631 to 641 seconds, and downlink phase lock was established at 634.5 seconds; however, the continued exciter sweep after acquisition caused large static phase errors and phase lock was lost at 643 seconds when range modulation was turned on. The exciter sweep voltage was ON again from 646 to 661.5 seconds, and down link phase lock reestablished at 647.5 seconds. Another downlink phase lock dropout occurred at VAN from 680 to 684.5 seconds, the reason for which is unknown at this time.

During the second revolution VAN experienced additional problems due to lock on to a spurious signal from the CCS transponder.

Sufficient data have not been received to make any additional assessment of the CCS performance during the launch and orbital flight phases.

Performance during the TLI burn, and final coast phase was satisfactory. Signal transmission to GYM was lost at approximately 44,357 seconds (12:19:17) and to TEX approximately 600 seconds earlier, at which time

the CCS lost lock. These were the only stations tracking the CCS during this period. UHF telemetry link DP-1B, which is in parallel with links DP-1 and DP-1A, is transmitted through the CCS transponder and provided good data until 39,990 seconds (11:06:30). The data indicated that the IU batteries were decaying at this time. Projection of the decay rate indicated that the batteries would be depleted sufficiently at approximately 44,000 seconds (12:13:20) to materially affect the performance of the CCS transponder. There were no data received for unified S-Band (USB) telemetry link DP-1A to enable evaluation of the USB.

Approximately 20 minutes after TLI a programmed switch of antennas from OMNI to low gain was observed in the TEX and GYM data. This switch was recommended to maintain acceptable signal transmission during the final coast phase. Additional signal level changes were observed at these sites and fluctuations agree in time with antenna switching commands reported verbally as having been sent from GYM. These commands are listed in Table 14-1, Section 14 which discusses performance of the CCS. Ground Station Command Histories have not yet been received to confirm these commands.

A summary of CCS coverage showing AOS and LOS is presented in Table 19-12.

19.5.4 Television Propagation Evaluation

Ground signal strength data of the television station were not available in time for this report to permit evaluation of the television RF propagation. However, video tape data quality indicated satisfactory signal strength during S-IC powered flight.

19.6 OPTICAL INSTRUMENTATION

19.6.1 Onboard cameras

There was a total of four recoverable film camera capsules carried onboard the AS-503 vehicle, all on the S-IC stage. Two camera capsules were located on the S-IC forward interstage at positions I and III looking forward to view S-IC/S-II first plane separation and S-II engine start. The two remaining camera capsules were mounted on top of the S-IC stage LOX tank at positions II and IV, and contained pulse cameras which viewed aft into the LOX tank through fiber optics bundles.

There were also two television cameras located in the S-IC base region to view propulsion and control system components.

Only one camera capsule, the LOX camera located at position II, was recovered. It is not known whether the other three camera capsules were ejected. Radio acquisition of the recovered capsule was about 2 to 3 minutes before impact at about 15 to 20 miles from the recovery helicopter. The capsule was retrieved at 30 degrees 13 minutes north latitude, 73 degrees 58 minutes west longitude at approximately 8:15 AM EST. Inspection of the recovered capsule showed that 3 of the ground planes sheared off and 5 of the shroud lines on the drag skirt were broken.

Table 19-12. CCS RF Summary

STATION	STAGE	LAUNCH		1ST ORBIT		2ND ORBIT		TLC		REMARKS
		AOS	LOS	AOS	LOS	AOS	LOS	AOS	LOS	
MIL	S-IU	00:00:00	00:10:40.1 (A)(C)(D)			01:35:00	01:42:35.1 (A)(D)			*DATA REQ'D
GBM	S-IU					01:35:40	01:42:29 (B)(D)			
BDA	S-IU	00:03:48	00:13:12 (C)(D)			01:38:12	01:46:12 (D)			
VAN	S-IU	00:09:12	00:15:45 (C)(D)			01:42:23	01:49:46 (C)(D)			
CYI	S-IU									NO DATA
CRO	S-IU			00:51:49	00:58:24 (C)(D)	02:15:09	02:22:18 (C)(D)			
HSK	S-IU			01:00:34	01:04:38 (C)(D)					
HAW	S-IU					02:50:23	02:57:40 (D)	07:18:43	12:14:45 (C)(D)	
GYM	S-IU			01:28:03	01:35:45 (C)(D)			02:57:45	12:27:00 (A)(C)(D)	
GDS	S-IU			01:29:37	01:31:52 (C)(D)					
TEX	S-IU							2:59:10	12:17:00 (A)(C)(D)	
GWM	S-IU							11:30:00	12:18:30 (D)	
ACN	S-IU									
ANS	S-IU									
MAD	S-IU									
MER	S-IU					02:44:17	02:51:36 (C)(D)			

A - STRIPCHART
B - 4020 PLOT
C - OPERATORS LOG
D - PLIM SUMMARY
E - ALL OF ABOVE

Dye marker operation was satisfactory on the recovered capsule. Significant quantities of water and dye marker leaked into the camera compartment through the electrical connector causing film damage; however, the film provided usable data.

The TV cameras provided good quality data.

19.6.2 Ground Engineering Cameras

In general, ground camera coverage was good. Eighty one items were received from KSC and evaluated. Eight cameras had unusable data due to bad timing, five cameras did not provide film due to film jamming, one film had no image, and one film was extremely underexposed providing no usable data. As a result of the 15 failures listed above, system efficiency was 81.5 percent.

SECTION 20

VEHICLE AERODYNAMIC CHARACTERISTICS

20.1 SUMMARY

The AS-503 vehicle, as with prior Saturn flights, flew at very low angles-of-attack that did not exceed 2.5 degrees during the period of interest. Because of this a reliable stability and fin load analysis could not be made.

The AS-503 average base differential pressure fell within a predicted band based on AS-502 data even though AS-503 had a 2-degree outboard engine cant and only six valid base pressure measurements whereas AS-502 had eight measurements.

20.2 VEHICLE AXIAL FORCE CHARACTERISTICS

The vehicle axial force characteristics are shown in Figures 20-1 and 20-2. Experience with AS-501, AS-502, and AS-503 flight data has shown that the base differential pressure is a function of altitude and is insensitive to slight Mach number variations. An average base differential pressure which can be used to calculate the base axial force is shown in Figure 20-1. This average was calculated using the six valid base pressure measurements on the AS-503 vehicle whereas eight pressure measurements were used on AS-502. The data for AS-502 and AS-503 show fair agreement. The AS-503 S-IC engines were canted outboard 2 degrees from 20 seconds throughout first stage boost. The small differences that exist are probably a combination of outboard engine cant on AS-503 and the number of base measurements on each flight. Therefore, the effects of engine cant on AS-503 are not readily discernible. The predictions shown are based on AS-502 data. The AS-501 data is also shown, but it should be noted that this vehicle flew with S-IC base flow deflectors installed. A drop off of the data occurred after inboard engine cutoff on each flight.

The forebody axial force coefficient remains a function of Mach number as shown in Figure 20-2. The AS-501 coefficient is greater because of the base flow deflectors. These coefficients are predictions based on wind tunnel data.

The total aerodynamic axial force is then the sum of the base axial force calculated from the base differential pressure and the forebody axial force, as calculated from the forebody coefficient.

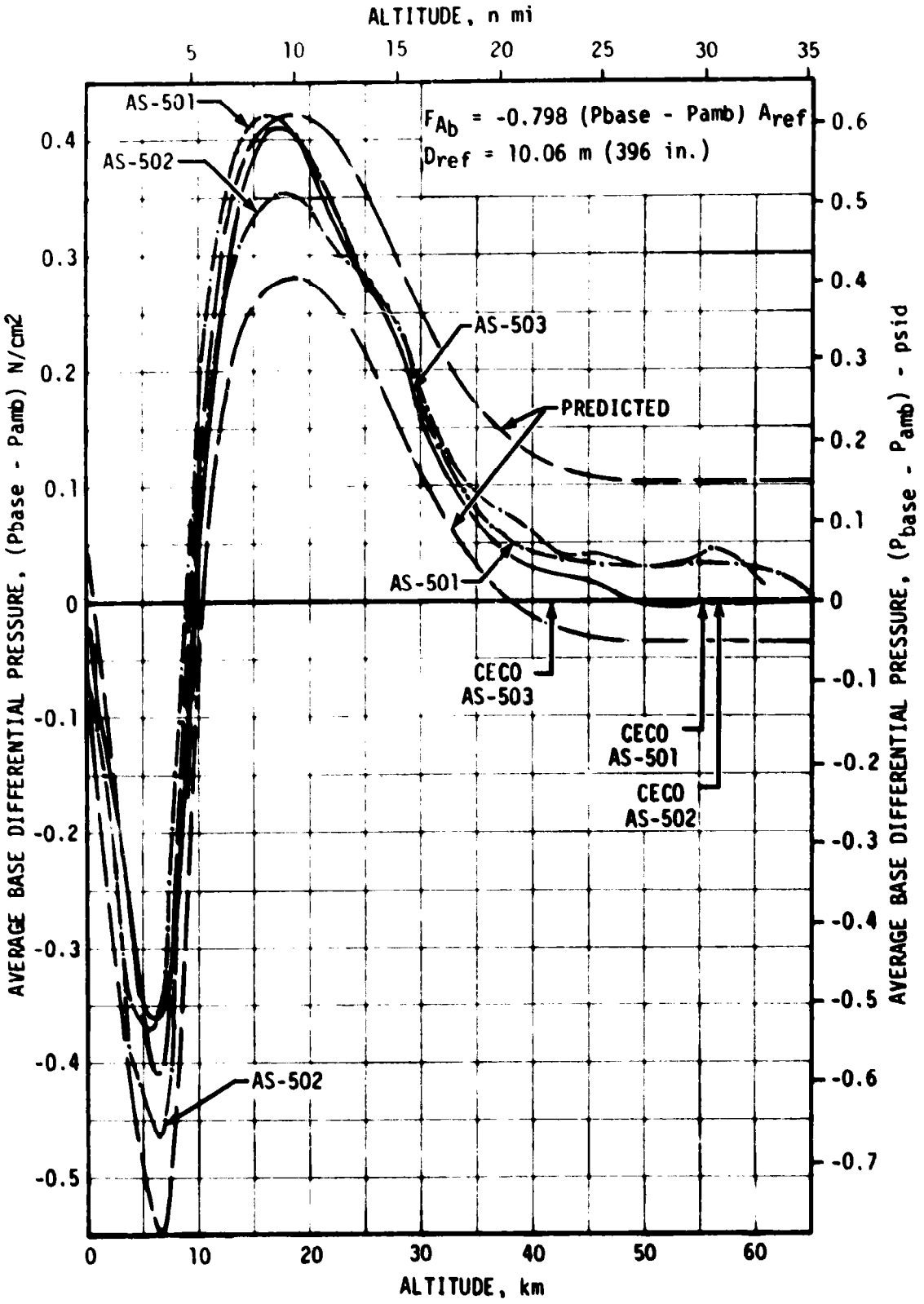

Figure 20-1. Average Base Differential Pressure

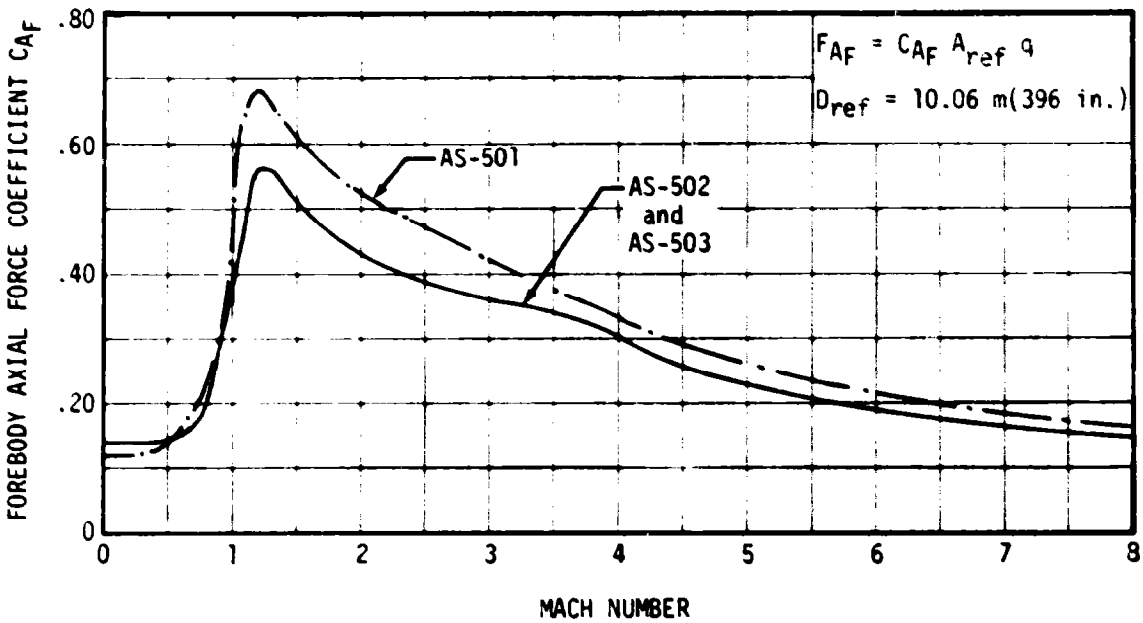

Figure 20-2. Forebody Axial Force Coefficient

20.3 VEHICLE STATIC STABILITY

A reliable evaluation of the static aerodynamic stability characteristics of the AS-503 flight was not possible due to the small vehicle angle-of-attack and resulting small engine deflections.

20.4 FIN PRESSURE LOADING

External static pressures on the S-IC fins were recorded by 16 measurements. Each surface of fins B and D had four measurements located in the same relative position.

Comparisons with predictions or with previous flight data would be misleading because the vehicles flew different angle-of-attack time histories and insufficient low angle-of-attack wind tunnel data are available for accurate predictions. The AS-503 flight angle-of-attack was well below the 10-degree design angle, hence the fin differential pressures were well below design values. Typical fin pressure differentials are shown in Figure 20-3.

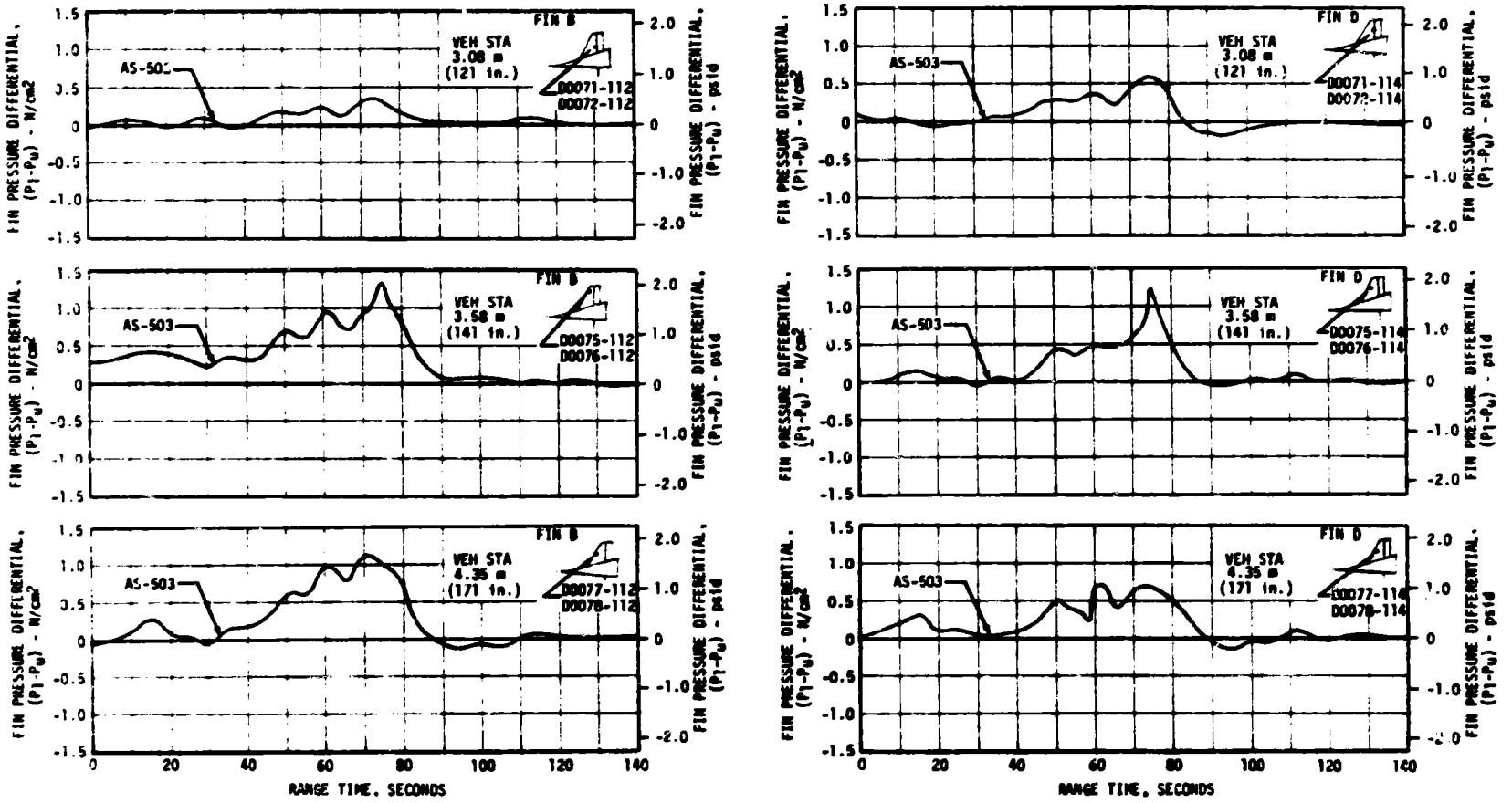

Figure 20-3. S-IC Fin Pressure Differential

SECTION 21

MASS CHARACTERISTICS

21.1 SUMMARY

Postflight analysis indicates that vehicle mass from S-IC stage ignition through spacecraft separation deviated less than 0.8 percent from predicted with the exception of the mass at spacecraft separation. This value was 1.8 percent greater and was due to a higher than expected S-IVB LOX residual. Center of gravity and moment of inertia deviations throughout flight were negligible except at the beginning and end of flight. The larger deviations at these times were due primarily to inexact S-IC propellant loading (less LOX, more fuel) and excess S-IVB residuals.

21.2 MASS EVALUATION

Postflight mass characteristics are compared with the final predicted mass characteristics (R-P&VE-VAW-69-2) which were used in the determination of the final operational trajectory (SSR-237/ Memorandum Number 5-9600-H-181).

The postflight mass characteristics were determined from an analysis of all available actual and reconstructed data from S-IC stage ignition through S-IVB stage/spacecraft separation. Dry weights of the launch vehicle were based on actual stage weighings and evaluation of the weight and balance log books (MSFC Form 998). Propellant loading and utilization was evaluated from propulsion system performance reconstructions. Spacecraft data was obtained from the Manned Spacecraft Center (MSC).

Deviations in dry weights of the inert stages and the loaded spacecraft were all less than 1.4 percent which is well within the predicted 3 sigma deviation limits. Major items that contributed to these small deviations were as follows:

a. Actual weight of some vehicle components were slightly different from predicted weight.

b. S-IC stage engine changeout at Kennedy Space Center (KSC).

c. Removal of S-IC/S-II interstage ullage motor fairings.

d. Deletion of the Azusa transponder and filter from the Instrument Unit (IU).

e. Engineering Change Proposals (ECP) listed below were not incorporated.

1. ECP 0219 - Proposed modification to protect engine interface connectors from excess moisture.

2. ECP 0252 - Proposed modification to eliminate possible hydraulic actuator support interference with engine fairings during flight.

3. ECP 0299 - Proposed modification for sealing of S-IC stage structure to prevent equipment damage from precipitation.

4. ECP 0442 - Proposed installation of LOX duct helium injection system for POGO suppression.

During S-IC stage powered flight, mass of the total vehicle was determined to be 0.03 percent higher than predicted at ignition and 0.10 percent higher at S-IC/S-II separation. These very small deviations are attributed to a slightly higher than predicted total vehicle propellant loading. The vehicle pitch and yaw moment of inertias at liftoff were about 4.5 percent higher than expected due primarily to the S-IC fuel mass being greater and the LOX mass being less than predicted. S-IC burn phase total vehicle mass is shown in Table 21-1 and Table 21-2.

During S-II burn deviations from predicted of vehicle mass, center of gravity, and moment of inertia were insignificant except near the end of flight. Vehicle mass and pitch and yaw moment of inertia were 0.29 percent and 0.74 percent, respectively, below predicted at S-II/S-IVB separation. Total vehicle mass for the S-II burn phase is shown in Table 21-3 and Table 21-4.

The largest deviations during the two S-IVB burns occurred at second burn engine cutoff and are attributed to excess S-IVB LOX residual. The vehicle mass at second cutoff was 0.78 percent higher than predicted, longitudinal Center of Gravity (CG) was 0.19 meter (7.61 in.) aft of predicted, and moment of inertia was 2.58 percent (pitch) and 2.62 percent (yaw) higher than predicted. Total vehicle mass at S-IVB/spacecraft separation was 2.08 percent greater than predicted. Tables 21-5 through 21-8 show total vehicle mass from first S-IVB ignition through spacecraft separation.

A summary of mass utilization and loss, actual and predicted, from S-IC stage ignition to spacecraft separation is presented in Table 21-9. A comparison of actual and predicted mass, center of gravity, and moment of inertia, is shown in Table 21-10. Figures 21-1 through 21-3 present the mass, center of gravity, and moment of inertia for each stage burn.

Table 21-1. Total Vehicle Mass, S-IC Burn Phase, Kilograms

EVENTS	S-IC GROUND IGNITION		HOLDDOWN ARM RELEASE		S-IC INBOARD ENGINE CUTOFF		S-IC OUTBOARD ENGINE CUTOFF		S-IC/S-II SEPARATION	
	PRED	ACT	PRED	ACT	PRED	ACT	PRED	ACT	PRED	ACT
RANGE TIME--SEC	-6.51	-6.59	0.33	0.27	125.92	125.95	151.37	153.79	152.07	[illegible]
S-IC STAGE.DRY	138641.	138451.	138641.	138451.	138641.	138451.	138641.	138451.	138641.	138451.
LOX IN TANK	1399769.	1397925.	1368536.	1365103.	190240.	207118.	1041.	1990.	953.	1990
LOX BELOW TANK	20824.	20928.	21584.	21688.	21583.	21617.	16615.	13904.	14509.	[illegible]
LOX ULLAGE GAS	502.	498.	532.	541.	2829.	2921.	3338.	3515.	2344.	3521.
FUEL IN TANK	608669.	611441.	598474.	601300.	91280.	56260.	8262.	6056.	7158.	4929.
FUEL BELOW TANK	6313.	6372.	5996.	6055.	5996.	6055.	5958.	6017.	5958.	6017.
FUEL ULLAGE GAS	86.	99.	90.	104.	259.	298.	293.	341.	293.	342.
N2 PURGE GAS	36.	36.	36.	36.	20.	20.	20.	20.	20.	[illegible]
HELIUM IN BOTTLE	288.	288.	284.	284.	115.	90.	81.	47.	80.	46.
FROST	635.	635.	635.	635.	340.	340.	340.	340.	340.	340.
RETROMOTOR PROP	1027.	1027.	1027.	1027.	1027.	1027.	1027.	1027.	1027.	1027.
OTHER	239.	239.	239.	239.	239.	239.	239.	239.	239.	239.
TOTAL S-IC STAGE	2175031.	2175940.	2136074.	2135462.	452568.	474436.	179855.	176947.	172564.	173510.
S-IC/S-II IS-SMALL	658.	654.	658.	654.	658.	654.	658.	654.	658.	654.
S-IC/S-II IS-LARGE	4445.	4376.	4445.	4376.	4445.	4376.	4445.	4376.	4445.	4376.
S-IC/S-II IS-PROP	617.	611.	617.	611.	617.	611.	617.	611.	58[illegible].	578.
TOTAL S-IC/S-II IS	5720.	5641.	5720.	5641.	5720.	5641.	5720.	5641.	5667.	5608.
TOTAL S-II STAGE	471003.	471114.	471003.	471114.	470744.	470855.	470744.	470855.	470744.	470855.
TOTAL S-II/S-IVB	3973.	3960.	3973.	3960.	3973.	3960.	3973.	3960.	3973.	3960.
TOTAL S-IVB STAGE	119634.	119652.	119634.	119652.	119589.	119561.	119589.	119561.	119589.	119561.
TOTAL IU	2214.	2196.	2214.	2196.	2214.	2196.	2214.	2196.	2214.	2196.
TOTAL S/C	43806.	43668.	43806.	43668.	43806.	43665.	43806.	43665.	43806.	43665.
TOTAL UPPER STAGE	640629.	640590.	640629.	640590.	640325.	640241.	640325.	640241.	640325.	640241.
TOTAL LAUNCH VEH	2821380.	2822171.	2782424.	2781694.	1098613.	1120319.	821901.	822829.	816576.	819359.

Table 21-2. Total Vehicle Mass, S-IC Burn Phase, Pounds Mass

EVENTS	S-IC GROUND IGNITION		HOLDDOWN ARM RELEASE		S-IC INBOARD ENGINE CUTOFF		S-IC OUTBOARD ENGINE CUTOFF		S-IC/S-II SEPARATION	
	PRED	ACT	PRED	ACT	PRED	ACT	PRED	ACT	PRED	ACT
RANGE TIME--SEC	-6.51	-6.59	0.33	0.27	125.92	125.95	151.37	153.79	152.07	154.47
S-IC STAGE,DRY	305650.	305232.	305650.	305232.	305650.	305232.	305650.	305232.	305650.	305232.
LOX IN TANK	3085963.	3081696.	3017105.	3009536.	419407.	456618.	2294.	4388.	2101.	4388.
LOX BELOW TANK	45910.	46138.	47585.	47813.	47503.	47658.	36630.	41677.	31986.	36570.
LOX ULLAGE GAS	1106.	1099.	1172.	1193.	6236.	6439.	7358.	7749.	7372.	7762.
FUEL IN TANK	1341886.	1347996.	1319410.	1325639.	201237.	212218.	18214.	13351.	15781.	10867.
FUEL BELOW TANK	9509.	9638.	13219.	13348.	13219.	13346.	13136.	13265.	13136.	13265.
FUEL ULLAGE GAS	189.	219.	199.	229.	572.	657.	646.	752.	647.	753.
N2 PURGE GAS	80.	80.	80.	80.	43.	43.	43.	43.	43.	43.
HELIUM IN BOTTLE	636.	636.	526.	526.	253.	198.	179.	103.	177.	102.
FROST	1400.	1400.	1400.	1400.	750.	750.	750.	750.	750.	750.
RETROMOTOR PROP	2264.	2264.	2264.	2264.	2264.	2264.	2264.	2264.	2264.	2264.
OTHER	528.	528.	528.	528.	528.	528.	528.	528.	526.	528.
TOTAL S-IC STAGE	4795123.	4797126.	4709238.	4707888.	997742.	1045953.	387694.	390102.	380438.	382524.
S-IC/S-II IS-SMALL	1450.	1441.	1450.	1441.	1450.	1441.	1450.	1441.	1450.	1441.
S-IC/S-II IS-LARGE	9800.	9648.	9800.	9648.	9800.	9648.	9800.	9648.	9800.	9648.
S-IC/S-II IS-PROP	1360.	1347.	1360.	1347.	1360.	1347.	1360.	1347.	1287.	1274.
TOTAL S-IC/S-II IS	12610.	12436.	12610.	12436.	12610.	12436.	12610.	12436.	12537.	12363.
TOTAL S-II STAGE	1038393.	1038629.	1038383.	1038628.	1037813.	1038058.	1037813.	1038058.	1037813.	1038058.
TOTAL S-II/S-IVB	8760.	8731.	8760.	8731.	8760.	8731.	8760.	8731.	8760.	8731.
TOTAL S-IVB STAGE	263768.	263787.	263768.	263787.	263648.	263587.	263648.	263587.	263648.	263587.
TOTAL IU	4880.	4842.	4880.	4842.	4880.	4842.	4880.	4842.	4880.	4842.
TOTAL S/C	96575.	96272.	96575.	96272.	96575.	96272.	96575.	96272.	96575.	96272.
TOTAL UPPER STAGE	1412346.	1412260.	1412346.	1412260.	1411676.	1411490.	1411676.	1411490.	1411676.	1411490.
TOTAL LAUNCH VEH	6220079.	6221823.	6134195.	6132585.	2422028.	2469879.	1811981.	1814028.	1804651.	1806377.

Table 21-3. Total Vehicle Mass, S-II Burn Phase, Kilograms

EVENTS	S-IC IGNITION		S-II IGNITION COMMAND		90 O/O THRUST		ENGINE CUTOFF COMMAND		S-II/S-IVB SEPARATION	
	PRED	ACT	PRED	ACT	PRED	ACT	PRED	ACT	PRED	ACT
RANGE TIME-SEC			152.77	159.19	155.77	158.47	521.19	524.04	521.99	524.90
S-IC/S-II IS-SMALL	658.	654.								
S-IC/S-II IS-LARGE	4445.	4376.	4445.	4376.	4445.	4376.				
S-IC/S-II IS-PROP	617.	611.	306.	300.						
TOTAL S-IC/S-II IS	5720.	5641.	4751.	4677.	4445.	4376.				
S-II STAGE DRY	40188.	40143.	40188.	40143.	40188.	40143.	40188.	40143.	40188.	40143.
LOX IN TANK	358832.	359322.	358832.	359322.	358515.	359006.	1905.	1544.	1756.	1396.
LOX BELOW TANK	737.	737.	737.	737.	800.	800.	800.	800.	800.	800.
LOX ULLAGE GAS	250.	240.	250.	240.	254.	244.	1778.	1882.	1783.	1882.
LH2 IN TANKS	70682.	70160.	70682.	70160.	70284.	69761.	1961.	1960.	1895.	1894.
LH2 BELOW TANK	105.	105.	105.	105.	128.	128.	128.	128.	129.	129.
LH2 ULLAGE GAS	101.	100.	101.	100.	103.	102.	699.	576.	701.	576.
INSULATION PURGE	54.	54.								
FROST	204.	204.								
START TANK GAS	14.	14.	14.	14.	2.	2.	14.	2.	14.	2.
CAMERAS	0.	0.								
OTHER	34.	34.	34.	34.	34.	34.	34.	34.	34.	34.
TOTAL S-II STAGE	471003.	471114.	470744.	470855.	470308.	470420.	47508.	47071.	47299.	46856.
TOT S-II/S-IVB IS	3973.	3960.	3973.	3960.	3973.	3960.	3973.	3960.	3973.	3960.
TOTAL S-IVB STAGE	119634.	119652.	119589.	119561.	119589.	119561.	119589.	119561.	119586.	119559.
TOTAL IU	2214.	2196.	2214.	2196.	2214.	2196.	2214.	2196.	2214.	2196.
TOTAL S/C	43806.	43668.	43806.	43668.	43806.	43668.	39780.	39636.	39780.	39636.
TOTAL UPPER STAGES	169627.	169477.	169581.	169386.	169581.	169386.	165556.	165353.	165554.	165351.
TOTAL LAUNCH VEH	646349.	645231.	645077.	644918.	644335.	644182.	213064.	212429.	212852.	212207.

Table 21-4. Total Vehicle Mass, S-II Burn Phase, Pounds Mass

EVENTS	S-IC IGNITION		S-II IGNITION COMMAND		90 % THRUST		ENGINE CUTOFF COMMAND		S-II/S-IVB SEPARATION	
	PRED	ACT	PRED	ACT	PRED	ACT	PRED	ACT	PRED	ACT
RANGE TIME-SEC			152.77	158.18	155.77	158.47	521.19	524.04	521.99	524.90
S-IC/S-II IS-SMALL	1450.	1441.								
S-IC/S-II IS-LARGE	9800.	9648.	9800.	9648.	9800.	9648.				
S-IC/S-II IS-PROP	1360.	1347.	675.	662.						
TOTAL S-IC/S-II IS	12610.	12436.	10475.	10310.	9800.	9648.				
S-II STAGE,DRY	88600.	88500.	88600.	88500.	88600.	88500.	88600.	88500.	88600.	88500.
LOX IN TANK	791089.	792170.	791089.	792170.	790391.	791473.	4200.	3405.	3872.	3077.
LOX BELOW TANK	1625.	1625.	1625.	1625.	1764.	1764.	1764.	1764.	1764.	1764.
LOX ULLAGE GAS	552.	530.	552.	530.	559.	537.	3920.	4150.	3930.	4150.
LH2 IN TANKS	155387.	154676.	155387.	154676.	154049.	154237.	4324.	4322.	4177.	4175.
LH2 BELOW TANK	231.	231.	231.	231.	282.	282.	282.	282.	282.	282.
LH2 ULLAGE GAS	222.	220.	222.	220.	226.	224.	1541.	1270.	1545.	1270.
INSULATION PURGE	120.	120.								
FROST	450.	450.								
START TANK GAS	30.	30.	30.	30.	5.	5.	30.	5.	30.	5.
CAMERAS	2.	2.								
OTHER	76.	76.	76.	76.	76.	76.	76.	76.	76.	76.
TOTAL S-II STAGE	1038383.	1038620.	1037813.	1038058.	1036852.	1037098.	104738.	103774.	104276.	103299.
TOT S-II/S-IVB IS	8760.	8731.	8760.	8731.	8760.	8731.	8760.	8731.	8760.	8731.
TOTAL S-IVB STAGE	263742.	263797.	263640.	263597.	263648.	263597.	263648.	263597.	263648.	263597.
TOTAL IU	4850.	4842.	4850.	4842.	4850.	4842.	4850.	4842.	4850.	4842.
TOTAL S/C	96575.	96272.	96575.	96272.	96575.	96272.	87700.	87382.	87700.	87382.
TOTAL UPPER STAGES	373863.	373632.	373863.	373632.	373863.	373632.	364938.	364642.	364983.	364537.
TOTAL LAUNCH VEH	1424956.	1424696.	1422151.	1421890.	1420515.	1420178.	469726.	469316.	469259.	467836.

Table 21-5. Total Vehicle Mass, S-IVB First Burn Phase, Kilograms

EVENTS	S-IC IGNITION		S-IVB IGNITION COMMAND		90 0/0 THRUST		ENGINE CUTOFF COMMAND		END THRUST DECAY	
	PRED	ACT	PRED	ACT	PRED	ACT	PRED	ACT	PRED	ACT
RANGE TIME--SEC			522.19	525.00	527.69	530.53	683.99	684.98	685.69	686.67
S-IVB STAGE,DRY	11793.	11760.	11770.	11736.	11770.	11736.	11709.	11673.	11709.	11673.
LOX IN TANK	87342.	87304.	87342.	87304.	87195.	87170.	59171.	59794.	59124.	59732.
LOX BELOW TANK	166.	166.	166.	166.	180.	180.	180.	180.	180.	180.
LOX ULLAGE GAS	19.	19.	19.	19.	20.	20.	66.	108.	67.	108.
LH2 IN TANK	19643.	19642.	19638.	19657.	19596.	19607.	13904.	13889.	13896.	13877.
LH2 BELOW TANK	22.	22.	26.	26.	26.	26.	26.	26.	26.	26.
LH2 ULLAGE GAS	26.	7.	26.	7.	26.	8.	70.	50.	70.	50.
ULLAGE VOTOR PROP	54.	54.	10.	9.						
APS PROPELLANT	286.	289.	286.	289.	286.	289.	285.	288.	285.	288.
HELIUM IN BOTTLES	202.	203.	202.	203.	202.	202.	179.	177.	179.	177.
START TANK GAS	2.	2.	2.	2.						
FROST	45.	136.	0.	45.	0.	45.	0.	45.	0.	45.
OTHER	33.	28.	33.	28.	33.	28.	33.	28.	33.	28.
TOTAL S-IVB STAGE	119634.	119652.	119522.	119492.	119327.	119311.	85627.	86263.	85573.	86189.
TOTAL INSTRU UNIT	2214.	2196.	2214.	2196.	2214.	2196.	2214.	2196.	2214.	2196.
TOTAL SPACECRAFT	43806.	43668.	39780.	39636.	39780.	39636.	39780.	39636.	39780.	39636.
TOTAL UPPER STAGE	46019.	45865.	41994.	41832.	41994.	41832.	41994.	41832.	41994.	41832.
TOTAL VEHICLE	165653.	165516.	161516.	161324.	161321.	161143.	127620.	128095.	127567.	128021.

Table 21-6. Total Vehicle Mass, S-IVB First Burn Phase, Pounds Mass

EVENTS	S-IC IGNITION		S-IVB IGNITION COMMAND		90 0/0 THRUST		ENGINE CUTOFF COMMAND		END THRUST DECAY	
	PRED	ACT	PRED	ACT	PRED	ACT	PRED	ACT	PRED	ACT
RANGE TIME--SEC			528.19	528.00	527.69	530.53	683.99	684.98	685.69	686.67
S-IVB STAGE,DRY	26000.	25926.	25949.	25873.	25949.	25873.	25814.	25735.	25814.	25735.
LOX IN TANK	192556.	192473.	192556.	192473.	192231.	192176.	130449.	131823.	130345.	131686.
LOX BELOW TANK	367.	367.	367.	367.	397.	397.	397.	397.	397.	397.
LOX ULLAGE GAS	41.	42.	41.	42.	43.	45.	146.	239.	147.	239.
LH2 IN TANK	43305.	43347.	43295.	43337.	43184.	43225.	30654.	30620.	30636.	30593.
LH2 BELOW TANK	48.	48.	58.	58.	58.	58.	58.	58.	58.	58.
LH2 ULLAGE GAS	58.	15.	58.	15.	58.	17.	154.	111.	154.	111.
ULLAGE MOTOR PROP	118.	118.	22.	19.						
APS PROPELLANT	630.	637.	630.	637.	630.	637.	628.	635.	628.	635.
HELIUM IN BOTTLES	446.	448.	446.	448.	445.	446.	395.	391.	395.	391.
START TANK GAS	5.	5.	5.	5.	1.	1.	7.	7.	7.	7.
FROST	100.	300.	0.	100.	0.	100.	0.	100.	0.	100.
OTHER	73.	61.	73.	61.	73.	61.	73.	61.	73.	61.
TOTAL S-IVB STAGE	263748.	263787.	263501.	263439.	263071.	263036.	188775.	190177.	188696.	190013.
TOTAL INSTRU UNIT	4880.	4842.	4880.	4842.	4880.	4842.	4880.	4842.	4880.	4842.
TOTAL SPACECRAFT	96575.	96272.	87700.	87382.	87700.	87382.	87700.	87382.	87700.	87382.
TOTAL UPPER STAGE	101455.	101114.	92580.	92224.	92580.	92224.	92580.	92224.	92580.	92224.
TOTAL VEHICLE	365203.	364901.	356081.	355659.	355651.	355260.	281355.	282401.	281236.	282237.

Table 21-7. Total Vehicle Mass, S-IVB Second Burn Phase, Kilograms

EVENTS	IGNITION COMMAND		90 O/O THRUST		ENGINE CUTOFF COMMAND		END THRUST DECAY		SPACECRAFT SEPARATION	
	PRED	ACT	PRED	ACT	PRED	ACT	PRED	ACT	PRED	ACT
RANGE TIME--SEC	10228.03	10229.51	10239.13	10240.02	10552.26	10555.51	10553.98	10557.21	12055.48	12059.30
S-IVB STAGE,DRY	11709.	11673.	11709.	11673.	11709.	11673.	11709.	11673.	11709.	11673.
LOX IN TANK	59035.	59696.	58891.	59562.	2903.	3479.	2862.	3416.	2862.	3416.
LOX BELOW TANK	166.	166.	180.	180.	180.	180.	180.	180.	166.	166.
LOX ULLAGE GAS	131.	140.	132.	141.	203.	255.	203.	256.	203.	256.
LH2 IN TANK	12716.	12837.	12665.	12784.	1245.	1225.	1238.	1213.	1238.	1213.
LH2 BELOW TANK	26.	26.	26.	26.	26.	26.	26.	26.	22.	22.
LH2 ULLAGE GAS	151.	107.	151.	109.	245.	195.	245.	195.	245.	195.
ULLAGE MOTOR PROP	0.	0.								
APS PROPELLANT	183.	235.	183.	235.	179.	235.	179.	235.	144.	220.
HELIUM IN BOTTLES	158.	165.	158.	164.	108.	110.	108.	110.	108.	110.
START TANK GAS	2.	2.								
FROST	0.	45.	0.	45.	0.	45.	0.	45.	0.	45.
OTHER	33.	28.	33.	28.	33.	28.	33.	28.	33.	28.
TOTAL S-IVB STAGE	84311.	85121.	84131.	84948.	16835.	17453.	16787.	17379.	16734.	17346.
TOTAL INSTRU UNIT	2214.	2196.	2214.	2196.	2214.	2196.	2214.	2196.	2214.	2196.
TOTAL SPACECRAFT	39780.	39636.	39780.	39636.	39780.	39636.	39780.	39636.	9667.	9667.
TOTAL UPPER STAGE	41994.	41832.	41994.	41832.	41994.	41832.	41994.	41832.	11880.	11863.
TOTAL VEHICLE	126305.	126953.	126124.	126780.	58829.	59285.	58781.	59212.	28614.	29210.

Table 21-8. Total Vehicle Mass, S-IVB Second Burn Phase, Pounds Mass

EVENTS	IGNITION COMMAND		90 0/0 THRUST		ENGINE CUTOFF COMMAND		END THRUST DECAY		SPACECRAFT SEPARATION	
	PRED	ACT	PRED	ACT	PRED	ACT	PRED	ACT	PRED	ACT
RANGE TIME--SEC	102[illegible]	102[illegible]	10239.13	10240.02	10552.28	10555.51	10553.98	10557.21	12055.48	12059.30
S-IVB STAGE,DRY	25814.	25735.	25814.	25735.	25814.	25735.	25814.	25735.	25814.	25735.
LOX IN TANK	130149.	131608.	129833.	131311.	6401.	7667.	6309.	7530.	6309.	7530.
LOX BELOW TANK	367.	367.	397.	397.	397.	397.	397.	397.	367.	367.
LOX ULLAGE GAS	289.	309.	290.	310.	447.	563.	447.	564.	447.	564.
LH2 IN TANK	28033.	28300.	27922.	28184.	2744.	2701.	2730.	2674.	2730.	2674.
LH2 BELOW TANK	58.	58.	58.	58.	58.	58.	58.	58.	48.	48.
LH2 ULLAGE GAS	333.	235.	334.	240.	541.	430.	541.	430.	541.	430.
ULLAGE MOTOR PROP	0.	0.								
APS PROPELLANT	403.	519.	403.	519.	395.	517.	395.	517.	318.	484.
HELIUM IN BOTTLES	349.	363.	348.	362.	237.	243.	237.	243.	237.	243.
START TANK GAS	5.	5.	1.	1.	6.	6.	6.	6.	5.	6.
FROST	0.	100.	0.	100.	0.	100.	0.	100.	0.	100.
OTHER	73.	61.	73.	61.	73.	61.	73.	61.	73.	61.
TOTAL S-IVB STAGE	185874.	187660.	185476.	187278.	37115.	38478.	37009.	38315.	36892.	38242.
TOTAL INSTRU UNIT	4880.	4842.	4880.	4842.	4880.	4842.	4880.	4842.	4880.	4842.
TOTAL SPACECRAFT	87700.	87382.	87700.	87382.	87700.	87382.	87700.	87382.	21312.	21312.
TOTAL UPPER STAGE	92580.	92224.	92580.	92224.	92580.	92224.	92580.	92224.	26192.	26154.
TOTAL VEHICLE	278454.	279884.	278056.	279502.	129695.	130702.	129589.	130539.	63084.	64396.

Table 21-9. Flight Sequence Mass Summary

MASS HISTORY	ACTUAL KG	ACTUAL LBM	PREDICTED KG	PREDICTED LBM
S-IC STAGE, TOTAL	2175940.	4797126.	2175030.	4799120.
S-IC/S-II INTERSTAGE-SMALL	654.	1441.	658.	1450.
S-IC/S-II INTERSTAGE-LARGE	4987.	10995.	5062.	11160.
S-II STAGE, TOTAL	471114.	1038628.	471009.	1038389.
S-II/SIIVB INTERSTAGE	3960.	8731.	3973.	8760.
S-IVB STAGE, TOTAL	119652.	263787.	119634.	263749.
VEHICLE INSTRUMENT UNIT	2196.	4842.	2214.	4880.
SPACECRAFT INCLUDING LES	43668.	96272.	43906.	96575.
1ST FLT STG AT IGN	2822171.	6221823.	2821380.	6220078.
S-IC THRUST BUILDUP	-40476.	-89237.	-38955.	-85884.
1ST FLT STG HOLDDOWN ARM REL	2781694.	6132585.	2782424.	6134194.
S-IC FROST	-294.	-650.	-294.	-650.
S-IC MAINSTAGE PROPELLANT	-1957147.	-4314773.	-1958894.	-4318624.
S-IC N2 PURGE	-16.	-37.	-16.	-37.
S-IC INBD ENGINE T.D. PROP	-864.	-1907.	-822.	-1814.
S-IC INBD ENG EXPENDED PROP	-189.	-418.	-189.	-418.
S-II INSULATION PURGE GAS	-53.	-120.	-53.	-120.
S-II FROST	-203.	-450.	-203.	-450.
S-IVB FROST	-90.	-200.	-44.	-100.
1ST FLT STAGE AT S-IC OECOS	822829.	1814028.	821901.	1811981.
S-IC OTBD ENGINE T.D. PROP	-3436.	-7578.	-3290.	-7256.
S-IC/S-II ULLAGE RKT PROP	-32.	-73.	-32.	-73.
1ST FLT STAGE AT SIC/SII SEP	819359.	1806377.	818577.	1804653.
S-IC STAGE AT SEPARATION	-173509.	-382524.	-172563.	-380439.
S-IC/S-II INTERSTAGE SMALL	-653.	-1441.	-657.	-1450.
S-IC/S-II ULLAGE RKT PROP	-277.	-612.	-277.	-612.
2ND FLT STAGE AT S-II IGN	644918.	1421800.	645077.	1422151.
S-II THRUST BUILDUP	-423.	-935.	-423.	-935.
S-II START TANK	-10.	-25.	-10.	-25.
S-IC/S-II ULLAGE RKT PROP	-299.	-662.	-305.	-675.
2ND FLT STAGE 90 PC THRUST	644182.	1420178.	644335.	1420515.
LAUNCH ESCAPE TOWER	-4031.	-8890.	-4025.	-8875.
S-IC/S-II INTERSTAGE LARGE	-4375.	-9648.	-4444.	-9800.
S-II MAINSTAGE & VENTING	-423347.	-933323.	-422799.	-932114.
2ND FLT STAGE AT S-II C.O.S.	212425.	468316.	213064.	469726.
S-II T.D. PROPELLANT	-214.	-474.	-210.	-465.
S-IVB ULLAGE PROPELLANT	-1.	-5.	-1.	-5.
2ND FLT STG AT SII/SIVB SEP	212207.	467836.	212853.	469259.

Table 21-9. Flight Sequence Mass Summary (Continued)

MASS HISTORY	ACTUAL KG	ACTUAL LBM	PREDICTED KG	PREDICTED LBM
2ND FLT STG AT S11/S1VB SEP	212207.	467836.	212853.	469259.
S-II STAGE AT SEPARATION	-46855.	-103299.	-47298.	-104276.
S-II/S-IVB INTERSTAGE-DRY	-3477.	-7667.	-3492.	-7700.
S II/S IVB INTESTG PROP	-482.	-1064.	-480.	-1060.
S-IVB AFT FRAME	-21.	-48.	-21.	-48.
S-IVB ULLAGE ROCKET PROP	0.	-1.	-0.	-3.
S-IVB DET PACKAGE	-1.	-5.	-0.	-3.
3RD FLT STG AT 1ST SSC	161366.	355752.	161556.	356169.
S-IVB ULLAGE ROCKET PROP	-41.	-93.	-39.	-88.
S-IVB FUEL LEAD LOSS	0.	0.	0.	0.
3RD FLT STG AT 1ST S1VB IGN	161324.	355659.	161516.	356081.
S-IVB ULLAGE ROCKET PROP	-8.	-19.	-9.	-22.
S-IVB H2 IN START TANK	-1.	-4.	-1.	-4.
S-IVB T.B. PROPELLANT	-169.	-375.	-182.	-403.
3RD FLT STG AT 90 PC THRUST	161143.	355260.	161321.	355651.
S-IVB ULLAGE ROCKET CASES	-62.	-138.	-60.	-135.
S-IVB MAINSTAGE PROP	-32984.	-72719.	-33637.	-74159.
S-IVB APS PROPELLANT	-0.	-2.	-0.	-2.
3RD FLT STG AT 1ST S1VB COS	128095.	282401.	127620.	281355.
S-IVB T.D. PROPELLANT	-73.	-163.	-54.	-121.
3RD FLT STG AT ST OF COAST	128021.	282237.	127567.	281236.
S-IVB ENG PROP EXPENDED	-17.	-40.	-17.	-40.
S-IVB FUL TK VNT--1-1/2 ORB	-976.	-2153.	-1094.	-2415.
S-IVB LOX TK VNT--1-1/2 ORB	0.	0.	-28.	-65.
S-IVB APS PROPELLANT	-52.	-116.	-101.	-225.
S-IVB H2 IN START TANK	-0.	-2.	-0.	-2.
S-IVB O2/H2 BURNER	-6.	-16.	-6.	-16.
3RD FLT STG AT 2ND SSC	126965.	279909.	126312.	278471.
S-IVB FUEL LEAD LOSS	-10.	-24.	-7.	-17.
3RD FLT STG AT 2ND S1VB IGN	126953.	279884.	126305.	278454.
S-IVB H2 IN START TANK	-1.	-4.	-1.	-4.
S-IVB T.B. PROPELLANT	-170.	-378.	-177.	-393.
3RD FLT STG AT 90 PC THRUST	126780.	279502.	126124.	278056.
3RD FLT STG AT 90 PC THRUST	126780.	279502.	126124.	278056.
S-IVB MAINSTAGE PROP	-67493.	-148798.	-67291.	-148353.
S-IVB APS PROPELLANT	-0.	-2.	-3.	-8.
3RD FLT STG AT 2ND S1VB COS	59285.	130702.	58829.	129695.
S-IVB T.D. PROPELLANT	-73.	-163.	-47.	-105.
3RD FLT STG AT END 2ND T.D.	59211.	130539.	58781.	129589.
S-IVB ENG PROP EXPENDED	-17.	-40.	-17.	-40.
S-IVB APS PROPELLANT	-14.	-33.	-34.	-77.
JETTISON SLA	-1151.	-2539.	-1200.	-2647.
S/C LESS LEM AND SLA	-28816.	-63531.	-28911.	-63741.
LAUNCH VEH AT S/C SEP	29210.	64396.	28615.	63084.
LUNAR MODULE	-9025.	-19900.	-9025.	-19900.
SLA--NOT JETTISONED	-639.	-1412.	-639.	-1412.
INSTRUMENT UNIT	-2195.	-4842.	-2213.	-4880.
S-IVB STAGE AT SEP	-17345.	-38242.	-16733.	-36892.

Table 21-10. Mass Characteristics Comparison

EVENT		MASS KILO POUNDS	D/C DEV.	LONGITUDINAL C.G. (X STA.) METERS INCHES	DELTA	RADIAL C.G. METERS INCHES	DELTA	ROLL MOMENT OF INERTIA KG-M2 X10-6	D/C DEV.	PITCH MOMENT OF INERTIA KG-M2 X10-6	D/C DEV.	YAW MOMENT OF INERTIA KG-M2 X10-6	D/C DEV.
		139641.		9.862		0.0916							
	PRED	305650.		388.2		3.2140		2.786		18.866		18.776	
S-IC STAGE DRY													
		138451.		9.850	-0.012	0.0916	0.0000						
	ACTUAL	305232.	-0.13	387.8	-0.50	3.2140	0.0000	2.782	-0.13	18.840	-0.13	18.750	-0.13
		5720.		41.615		0.1239							
S-IC/S-II INTER-	PRED	12610.		1638.4		4.8795		0.145		0.087		0.087	
STAGE, TOTAL													
		5641.		41.615	0.000	0.1275	0.0035						
	ACTUAL	12436.	-1.37	1638.4	0.00	5.0209	0.1414	0.143	-1.37	0.085	-1.24	0.086	-1.37
		40189.		48.262		0.1025							
	PRED	88600.		1900.1		4.0360		0.677		2.279		2.286	
S-II STAGE,DRY													
		40143.		48.254	-0.007	0.1023	-0.0001						
	ACTUAL	88500.	-0.10	1899.8	-0.30	4.0311	-0.0049	0.675	-0.23	2.271	-0.17	2.282	-0.17
		3973.		66.481		0.0577							
S-II/S-IVB INTER-	PRED	8760.		2617.4		2.6683		0.066		0.043		0.044	
STAGE,TOTAL													
		3960.		66.481	0.000	0.0677	0.0000						
	ACTUAL	8731.	-0.32	2617.4	0.00	2.6683	0.0000	0.066	-0.32	0.043	-0.32	0.043	-0.32
		11793.		72.628		0.1912							
	PRED	26000.		2859.4		7.5286		0.085		0.311		0.311	
S-IVB STAGE,DRY													
		11760.		72.628	0.000	0.1912	0.0000						
	ACTUAL	25926.	-0.27	2859.4	0.00	7.5286	0.0000	0.084	-0.27	0.311	-0.27	0.311	-0.27
		2214.		82.410		0.2588							
VEHICLE INSTRUMENTED	PRED	4880.		3246.5		10.1921		0.021		0.012		0.010	
UNIT													
		2196.		82.407	-0.002	0.2490	-0.0098						
	ACTUAL	4842.	-0.77	3244.4	-0.10	9.8061	-0.3860	0.021	-0.77	0.012	-0.77	0.010	-0.77
		43806.		92.428		0.1911							
	PRED	96575.		3638.9		5.1623		0.093		1.286		1.286	
SPACECRAFT,TOTAL													
		43668.		92.422	-0.005	0.1911	0.0000						
	ACTUAL	96272.	-0.30	3638.7	-0.20	5.1623	0.0000	0.092	-1.00	1.278	-0.68	1.280	-0.49

Table 21-10. Mass Characteristics Comparison (Continued)

EVENT		MASS KILO POUNDS	MASS O/O DEV.	LONGITUDINAL C.G. (X STA.) METERS INCHES	LONGITUDINAL C.G. DELTA	RADIAL C.G. METERS INCHES	RADIAL C.G. DELTA	ROLL MOMENT OF INERTIA KG-M2 X10-6	ROLL MOMENT OF INERTIA O/O DEV.	PITCH MOMENT OF INERTIA KG-M2 X10-6	PITCH MOMENT OF INERTIA O/O DEV.	YAW MOMENT OF INERTIA KG-M2 X10-6	YAW MOMENT OF INERTIA O/O DEV.
1ST FLIGHT STAGE AT IGNITION	PRED	2021380.		30.105		0.0048							
		6220078.		1185.2		0.1910		3.996		896.669		896.572	
		2022171.		30.071	-0.033	0.0048	0.0000						
	ACTUAL	6221923.	0.03	1183.9	-1.30	0.1910	0.0000	3.989	-0.17	895.290	4.51	895.240	4.51
1ST FLIGHT STAGE AT HOLDDOWN ARM RELEASE	PRED	2782424.		30.058		0.0050							
		6134194.		1183.4		0.1984		3.999		857.604		857.508	
		2781694.		30.021	-0.037	0.0050	0.0000						
	ACTUAL	6132585.	-0.02	1181.9	-1.46	0.1984	0.0000	3.991	-0.17	894.099	4.26	894.040	4.26
1ST FLIGHT STAGE AT OUTBOARD ENGINE CUTOFF SIGNAL	PRED	821901.		45.886		0.0166							
		1811981.		1806.5		0.6543		3.984		441.311		441.219	
		822829.		45.849	-0.037	0.0162	-0.0003						
	ACTUAL	1814028.	0.11	1805.0	-1.46	0.6403	-0.0140	3.977	-0.17	440.806	-0.10	440.761	-0.09
1ST FLIGHT STAGE AT SEPARATION	PRED	818577.		46.031		0.0166							
		1804653.		1812.2		0.6543		3.982		437.008		436.916	
		819359.		46.001	-0.030	0.0164	-0.0001						
	ACTUAL	1806377.	0.10	1811.0	-1.18	0.6466	-0.0077	3.975	-0.17	436.276	-0.16	436.231	-0.15
2ND FLIGHT STAGE AT IGNITION	PRED	645077.		55.695		0.0139							
		1422151.		2192.7		0.5500		1.080		130.794		130.796	
		644918.		55.679	-0.016	0.0139	0.0000						
	ACTUAL	1421800.	-0.01	2192.1	-0.63	0.5503	0.0002	1.076	-0.37	130.549	-0.17	130.561	-0.17
2ND FLIGHT STAGE AT 90 O/O THRUST	PRED	644935.		55.702		0.0139							
		1420515.		2193.0		0.5500		1.073		130.713		130.726	
		644192.		55.685	-0.017	0.0139	0.0000						
	ACTUAL	1420178.	-0.01	2192.3	-0.67	0.5503	0.0002	1.069	-0.34	130.481	-0.17	130.494	-0.17
2ND FLIGHT STAGE AT CUTOFF SIGNAL	PRED	213064.		70.228		0.0408							
		469726.		2764.9		1.6079		0.960		45.987		45.995	
		212425.		70.258	0.029	0.0402	-0.0005						
	ACTUAL	468316.	-0.29	2766.0	1.14	1.5861	-0.0217	0.958	-0.21	45.645	-0.73	45.656	-0.73

Table 21-10. Mass Characteristics Comparison (Continued)

EVENT		MASS KILO POUNDS	O/C DEV.	LONGITUDINAL C.G. (X STA.) METERS INCHES	DELTA	RADIAL C.G. METERS INCHES	DELTA	ROLL MOMENT OF INERTIA KG-M2 X10-6	O/C DEV.	PITCH MOMENT OF INERTIA KG-M2 X10-6	O/C DEV.	YAW MOMENT OF INERTIA KG-M2 X10-6	O/C DEV.
		212853.		70.253		0.0408							
2ND FLIGHT STAGE	PRED	469259.		2765.8		1.6079		0.960		45.957		45.968	
AT SEPARATION													
		212207.		70.293	0.039	0.0405	-0.0003						
	ACTUAL	467836.	-0.29	2767.0	1.18	1.5961	-0.0118	0.958	-0.21	45.511	-0.74	45.523	-0.74
		151556.		76.839		0.0407							
3RD FLIGHT STAGE	PRED	356185.		3025.1		1.6031		0.204		13.090		13.076	
AT 1ST START SEQ-													
UENCE COMMAND		161356.		76.824	-0.015	0.0404	-0.0002						
	ACTUAL	355752.	-0.11	3024.5	-0.59	1.5922	-0.0108	0.204	-0.42	13.025	-0.41	13.024	-0.39
		161314.		76.837		0.0407							
3RD FLIGHT STAGE	PRED	356081.		3025.1		1.6031		0.204		13.078		13.074	
AT 1ST IGNITION													
		161324.		76.822	-0.015	0.0404	-0.0002						
	ACTUAL	355659.	-0.11	3024.5	-0.59	1.5922	-0.0108	0.203	-0.42	13.023	-0.41	13.022	-0.39
		161321.		76.838		0.0407							
3RD FLIGHT STAGE	PRED	355651.		3025.1		1.6031		0.204		13.078		13.074	
AT 1ST 90 C/O													
THRUST		161143.		76.823	-0.015	0.0404	-0.0002						
	ACTUAL	355240.	-0.10	3024.5	-0.59	1.5922	-0.0108	0.203	-0.42	13.023	-0.41	13.022	-0.39
		127420.		77.829		0.0512							
3RD FLIGHT STAGE	PRED	281355.		3064.1		2.0191		0.204		12.262		12.258	
AT 1ST CUTOFF SIG-													
NAL		129095.		77.776	-0.052	0.0504	-0.0008						
	ACTUAL	282401.	0.37	3062.0	-2.08	1.9859	-0.0332	0.203	-0.44	12.240	-0.17	12.239	-0.15
		127567.		77.831		0.0512							
3RD FLIGHT STAGE	PRED	281236.		3064.2		2.0191		0.204		12.260		12.256	
AT 1ST END THRUST													
DECAY, START COAST		128021.		77.779	-0.052	0.0504	-0.0008						
	ACTUAL	282237.	0.36	3062.1	-2.05	1.9858	-0.0332	0.203	-0.44	12.237	-0.17	12.236	-0.15
		126912.		77.844		0.0515							
3RD FLIGHT STAGE	PRED	278471.		3064.7		2.0302		0.202		12.254		12.251	
AT 2ND START SEQ-													
UENCE COMMAND		126965.		77.787	-0.056	0.0507	-0.0007						
	ACTUAL	279909.	0.52	3062.5	-2.23	1.9997	-0.0305	0.202	-0.10	12.235	-0.15	12.234	-0.13

Table 21-10. Mass Characteristics Comparison (Continued)

EVENT		MASS KILO POUNDS	MASS O/O DEV.	LONGITUDINAL C.G. (X STA.) METERS INCHES	LONGITUDINAL C.G. DELTA	RADIAL C.G. METERS INCHES	RADIAL C.G. DELTA	ROLL MOMENT OF INERTIA KG-M2 X10-6	ROLL MOMENT OF INERTIA O/O DEV.	PITCH MOMENT OF INERTIA KG-M2 X10-6	PITCH MOMENT OF INERTIA O/O DEV.	YAW MOMENT OF INERTIA KG-M2 X10-6	YAW MOMENT OF INERTIA O/O DEV.
3RD FLIGHT STAGE AT 2ND IGNITION	PRED	126305.		77.941		0.0515							
		278454.		3064.6		2.0302		0.202		12.256		12.253	
		126955.		77.784	-0.056	0.0507	-0.0007						
	ACTUAL	279884.	0.51	3062.3	-2.23	1.9997	-0.0305	0.202	-0.10	12.237	-0.15	12.236	-0.13
3RD FLIGHT STAGE AT 2ND 90 O/O THRUST	PRED	126124.		77.947		0.0515							
		278056.		3064.8		2.0302		0.202		12.253		12.250	
		126790.		77.799	-0.057	0.0507	-0.0007						
	ACTUAL	279502.	0.52	3062.5	-2.26	1.9997	-0.0305	0.202	-0.10	12.234	-0.14	12.233	-0.12
3RD FLIGHT STAGE AT 2ND CUTOFF SIGNAL	PRED	58829.		85.472		0.1093							
		129695.		3365.0		4.3059		0.201		5.611		5.608	
		59285.		85.279	-0.193	0.1070	-0.0022						
	ACTUAL	130702.	0.78	3357.4	-7.61	4.2160	-0.0898	0.201	-0.09	5.756	2.59	5.754	2.62
3RD FLIGHT STAGE AT 2ND END THRUST DECAY	PRED	58781.		85.485		0.1093							
		129589.		3365.5		4.3059		0.201		5.599		5.595	
		59211.		85.298	-0.186	0.1074	-0.0019						
	ACTUAL	130539.	0.73	3358.2	-7.33	4.2299	-0.0759	0.201	-0.09	5.737	2.46	5.736	2.52
3RD FLIGHT STAGE AT SPACECRAFT SEPARATION	PRED	29614.		77.056		0.0919							
		63084.		3034.8		3.6209		0.145		1.466		1.464	
		29210.		76.913	-0.172	0.0914	-0.0005						
	ACTUAL	64396.	2.08	3028.1	-6.78	3.6011	-0.0197	0.146	0.71	1.504	2.57	1.500	2.52
SPACECRAFT AT SEPARATION	PRED	28912.		93.747		0.1970							
		63741.		3690.8		7.7574		0.046		0.107		0.110	
		28817.		93.730	-0.017	0.1907	-0.0063						
	ACTUAL	63531.	-0.32	3690.1	-0.67	7.5091	-0.2482	0.046	-0.13	0.105	-1.85	0.109	-1.04

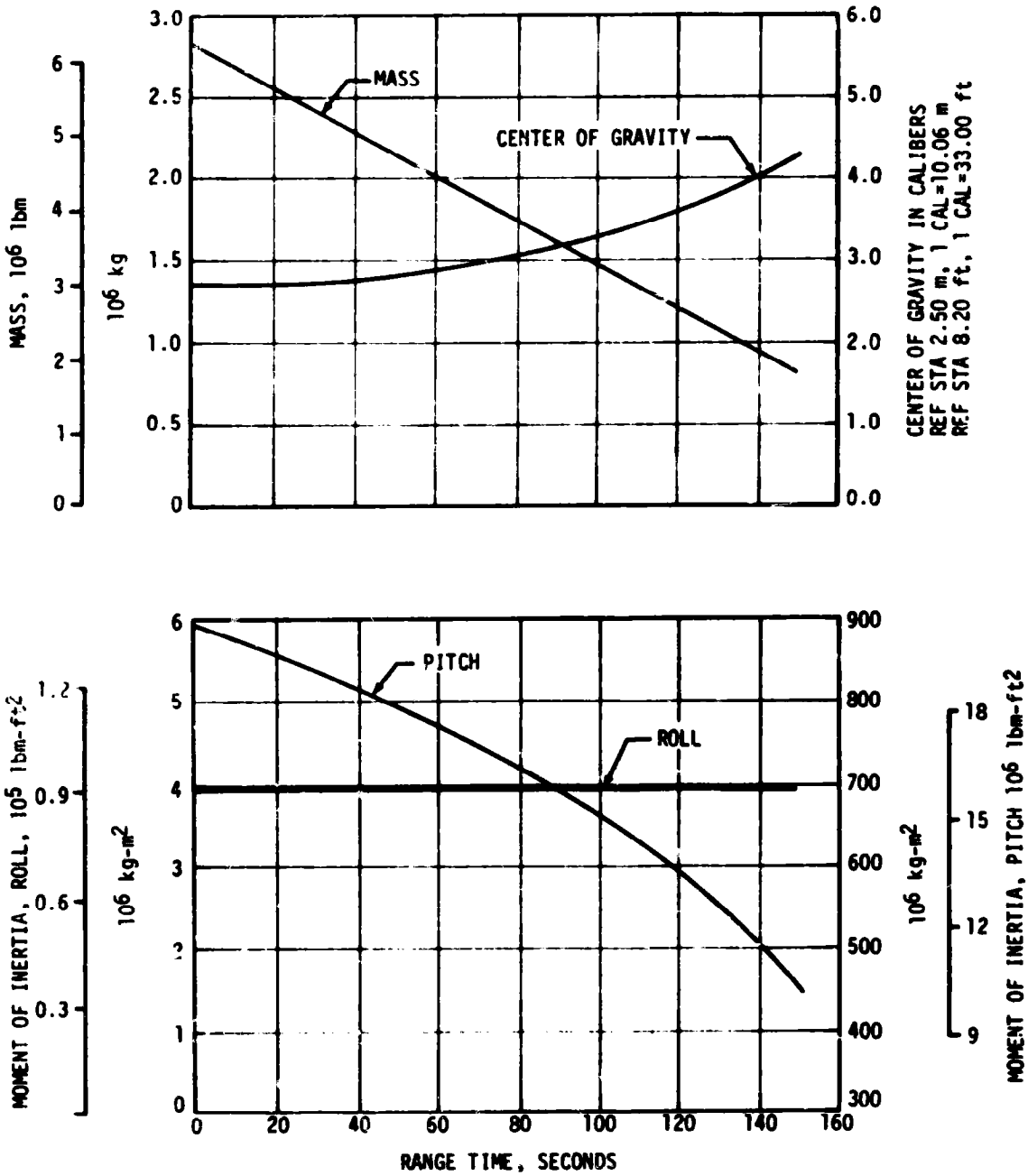

Figure 21-1. Total Vehicle Mass, Center of Gravity, and Mass Moment of Inertia During S-IC Stage Powered Flight

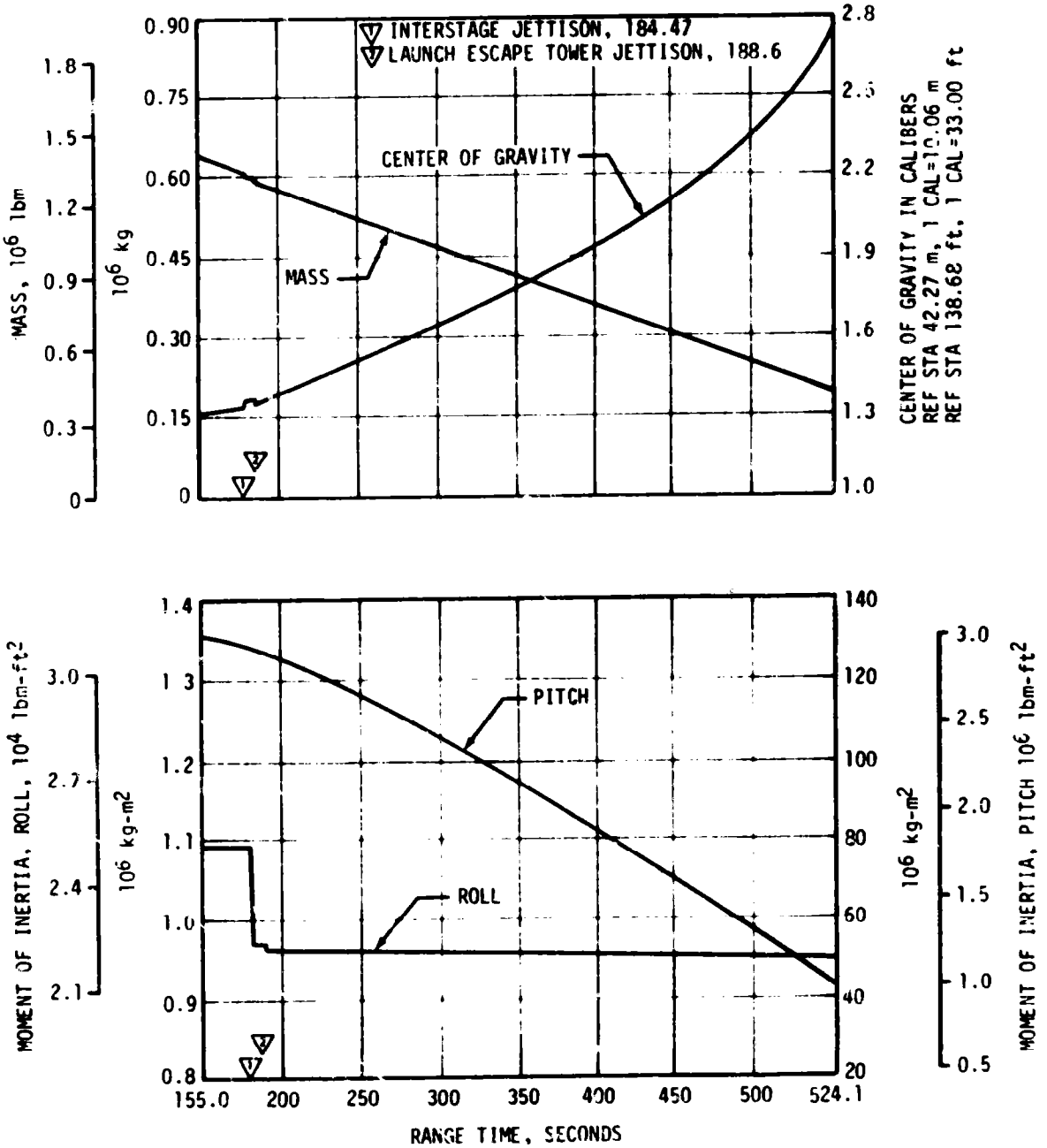

Figure 21-2. Total Vehicle Mass, Center of Gravity, and Mass Moment Of Inertia During S-II Stage Powered Flight

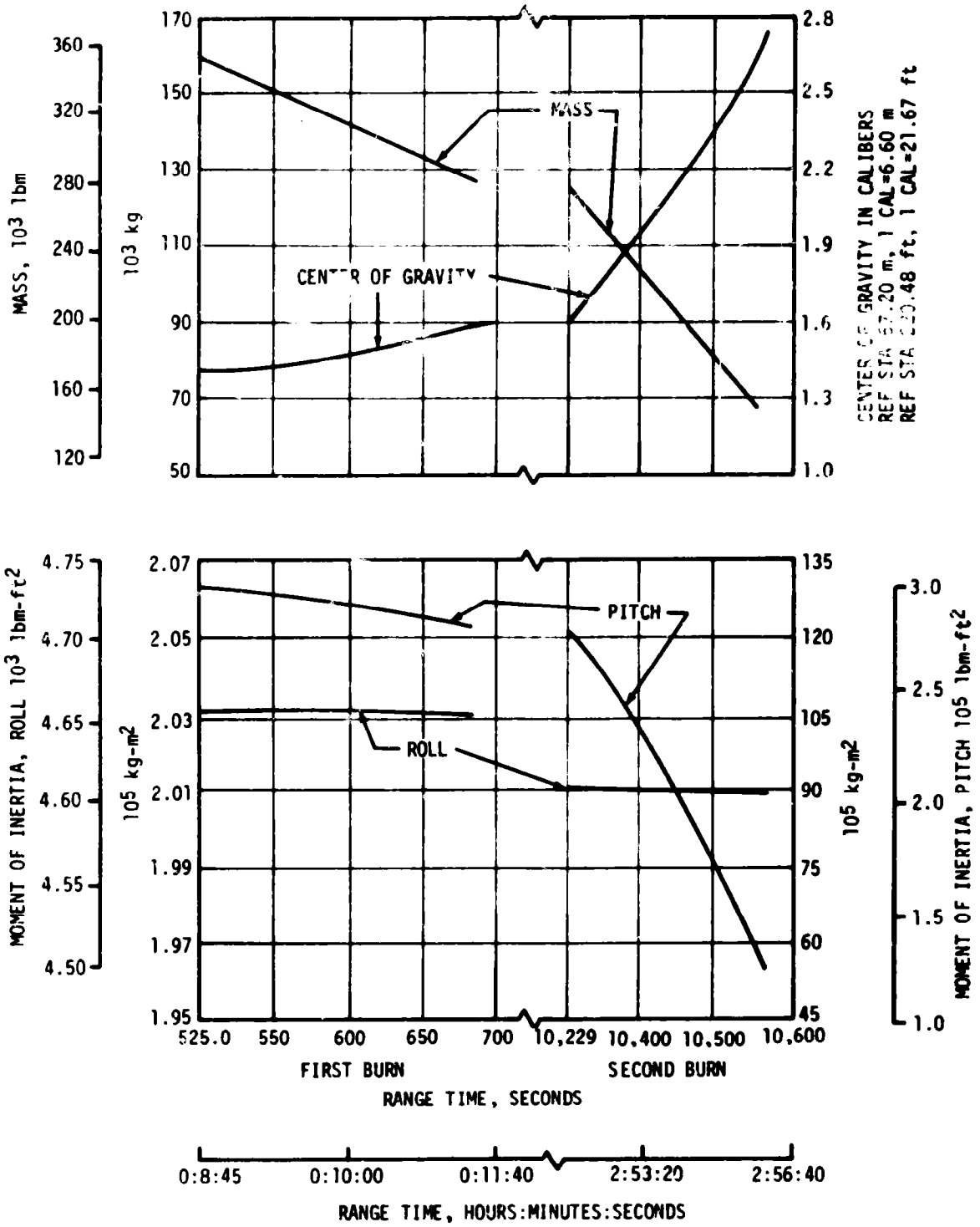

Figure 21-3. Total Vehicle Mass, Center of Gravity, and Mass Moment of Inertia During S-IVB Stage Powered Flight

SECTION 22

MISSION OBJECTIVES ACCOMPLISHMENT

Table 22-1 presents the MSFC AS-503 detailed test objectives as defined in the Saturn V Mission Implementation Plan, Mission C Prime. An assessment of the degree of accomplishment of each objective is shown. Discussion supporting the assessment can be found in the indicated sections of the Saturn V Launch Vehicle Flight Evaluation Report - AS-503, Apollo 8 Mission.

The nine principal and one secondary detailed test objectives were completely accomplished.

Table 22-1. Mission Objectives Accomplishment Summary

NO.	DETAILED TEST OBJECTIVES PRINCIPAL (P) SECONDARY (S)	DEGREE OF ACCOMPLISHMENT	DISCREPANCIES	SECTION IN WHICH DISCUSSED
1.	Verify that modifications incorporated in the S-IC stage suppress low frequency longitudinal oscillations. (P)	Complete	None	9.2.3.1, 5.9
2.	Confirm launch vehicle longitudinal oscillation environment during S-IC stage burn period. (P)	Complete	None	9.2.3.1
3.	Verify J-2 engine modifications. (P)	Complete	None	9.3.2, 9.3.3, 7.3
4.	Confirm J-2 engine environment in S-II and S-IVB stages. (P)	Complete	None	9.3.2, 9.3.3
5.	Demonstrate the S-IVB stage restart capability. (P)	Complete	None	7.5
6.	Demonstrate helium heater (O_2H_2 burner) repressurization system operation. (P)	Complete	None	7.5
7.	Demonstrate capability to safe S-IVB stage. (P)	Complete	None	7.13
8.	Verify capability to inject S-IVB/IU/LTA-B into a lunar "slingshot" trajectory. (P)	Complete	None	7.13.2
9.	Verify launch vehicle capability for free return, Translunar Injection (TLI). (P)	Complete	None	4.3.3
10.	Verify the onboard Command and Communications System (CCS)/ground system interface and operation in the deep space environment. (S)	Complete	None	14.3, 19.5.3.2

SECTION 23

FAILURES, ANOMALIES AND DEVIATIONS

23.1 SUMMARY

Evaluation of the launch vehicle performance during the AS-503 flight test revealed two areas of concern with a mission criticality category of three. Modifications are planned to improve these problem areas on future flights.

23.2 SYSTEM FAILURES AND ANOMALIES

Since all studies and corrective actions (ECPs) pertinent to these anomalies are not complete, Table 23-1 represents the action status of each item as of the release date of this report. This table complies with Apollo Program Directive No. 19. Reference paragraph numbers are given for sections in which the specific problem area is discussed in more detail. Table 23-2 defines the criticality categories assigned to the failures and anomalies listed in Table 23-1.

23.3 SYSTEM DEVIATIONS

Five system deviations occurred without any significant effects on the flight or operation of that particular system. Table 23-3 presents these deviations with the recommended corrective actions and a reference to the paragraphs containing further discussion of the deviation. These deviations are of no major concern, but are presented in order to complete the summary of deviations experienced on AS-503.

Table 23-1. Summary of Failures and Anomalies

FAILURE/ANOMALY IDENTIFICATION							RECOMMENDED CORRECTIVE ACTION			
ITEM	VEHCLE SYSTEM	DESCRIPTION (CAUSE)	EFFECT ON MISSION	AS-503 MISSION CRITI-CALITY	EFFECT ON NEXT MISSION	TIME OF OCCURRENCE (RANGE TIME)	DESCRIPTION	ACTION STATUS	VEHICLE EFFEC-TIVITY	PARAGRAPH REFERENCE
1	S-II Propulsion/ Structural	Engine No. 5 parameters oscillating at 17 to 18 hertz and structure oscillations at 9 to 11 hertz. (Lateral and longitudinal accelera-ation buildup starting after PU step and damping out before engine cutoff.)	None	3	AS-503 oscil-lation anom-aly will not compromise AS-504 mission or performance.	Starting at T+443.45 Maximum at T+483 Damped at T+521	As a result of evalu-ation and testing to date, ECP 6237 has been approved for AS-504 and subs to increase LOX tank ullage press. during later portion of S-II burn; thereby allevi-ating the condition which contributed to the oscillation. This pressure increase will raise LOX NPSH which will reduce cavitation tendencies of the LOX pump.	ECP 6237 Approved	AS-504 and subs	Section 6, 6A, 8.3
							To provide better data the following action was taken; Establish higher sample rates.	ECP 6208 Approved	AS-504 and AS-505	
							Provide lower freq. range data.	ECP 6230 Approved	AS-504 and AS-505	
							Although essential progress has been made in isolating and effecting a solution to this problem, the nature of it does not permit termination of further consideration at this time. *	Open		

* Oscillations found to be an engine generated phenomenon amplified by structural interaction during flight.
Mechanics of this interaction and amplification are not understood at present.
Testing presently underway at MSFC and Rocketdyne.
Analysis of testing will continue past AS-504 launch.
Apollo Program Director will be informed of significant findings throughout the investigation.

Table 23-2. Hardware Criticality Categories For Flight Hardware

CATEGORY	DESCRIPTION
1	Hardware, failure of which results in loss of life of any crew member. This includes normally passive systems such as the Emergency Detection System (EDS), Launch Escape System (LES), etc.
2	Hardware, failure of which results in abort of mission but does not cause loss of life.
3	Hardware, failure of which will not result in abort of mission nor cause loss of life.

Table 23-3. Summary of Deviations

VEHICLE SYSTEM	DEVIATIONS	PROBABLE CAUSE	CORRECTIVE ACTION BEING CONSIDERED	PARAGRAPH REFERENCE
S-IC Propellant System	Engine No. 5 LOX suction duct pressure decayed after Inboard Engine Cutoff (IECO).	Leak below prevalve of ≈ 6 cu. in./s. Cause or location of leak still under investigation.	None anticipated	5.6.2
S-IC Hydraulics	Engine No. 3 pitch actuator hydraulic fluid return temperature was higher than expected after 117 seconds but within maximum specification limit.	Still under investigation	None anticipated	8.2
S-IC Visual Instrumentation	Loss of photographic data:		None. This camera system is deleted on future vehicles.	19.6
	a. Failure to recover 3 of 4 onboard film cameras. (Recovery failure unknown).	Unknown		
	b. The camera recovered had film damage from sea water and dye marking. (Film damage - loose jam nut on camera power umbilical connector).	Loose jam nut on camera power umbilical connector.		
	c. Both LOX tank cameras and one strobe light stopped at T+79 seconds.	Unknown		
S-IC Heat Shield	Some localized partial loss of M-31 at T+70 to T+90 seconds.	Still under investigation	None - Loss of M-31 was apparently less than on AS-502.	9.3.1.3 7.2
S-II Propulsion	Engine No. 5 c/o transient appears abnormal. Thrust chamber pressure and GG pressure decay durations are longer than normal to 5 percent thrust.	Under investigation	None anticipated	6.4
S-II Data System	Bridge Power Supplies M046 (P/N V227A3) and M059 (P/N V227A5) were intermittent during Max Q and M053 (P/N V212A11) was intermittent after PU step.	Improper connector pin engagement during periods of high vibration.	None on AS-504. AS-505 and Subsequent Flights: Inspection of power supply connectors. Conduct of verification tests. Shimming of connectors as required. ECP 6021 (Closed)	13.3

SECTION 24

SPACECRAFT SUMMARY

Following a nominal boost phase, the spacecraft and S-IVB combination was inserted into a parking orbit of 185 kilometers (100 n mi). After a post insertion checkout of spacecraft systems, the nominal translunar injection maneuver was initiated at 2:50:38 by reignition of the S-IVB engine and lasted for 5 minutes 18 seconds.

The spacecraft separated from the S-IVB at 3:20:59, followed by two separation maneuvers using the service module reaction control system. The first midcourse correction, made with a velocity change of 7.56 m/s (24.8 ft/s), was conducted at 11:00:00. The translunar coast phase was devoted to navigation sightings, two television transmissions, and various systems checks. The second midcourse correction of 0.43 m/s (1.4 ft/s) was conducted at 60:59:55.

The 246.9-second lunar orbit insertion maneuver was performed at 69:08:20, and the initial lunar orbit was 312.1 by 111.1 kilometers (168.5 by 60.0 n mi). A maneuver to circularize the orbit was conducted at 73:35:07 and resulted in a lunar orbit of 110.6 by 112.4 kilometers (59.7 by 60.7 n mi). The coast phase between maneuvers was devoted to orbit navigation and ground track determination. A total of ten revolutions were completed during the 20 hours 11 minutes spent in lunar orbit.

The lunar orbit coast phase involved numerous landing site/landmark sightings, lunar photography, and preparation for transearth injection. The transearth injection maneuver, 204 seconds in duration, was conducted at 89:19:17 using the Service Propulsion System (SPS).

When possible during both the translunar and transearth coast phases, passive thermal control maneuvers of about one revolution per hour were effected to maintain temperatures within nominal limits. The transearth coast period involved a number of star/horizon navigation sightings using both the earth and moon horizons. The only transearth midcourse correction was a 1.5 m/s (4.8 ft/s) maneuver made at 103:59:54.

Command module/service module separation was at 146:28:48, and the command module reached the entry interface of 122 kilometers (400,000 ft) altitude at 146:46:14. Following normal deployment of all parachutes

the spacecraft landed in the Pacific Ocean at 8 degrees 8 minutes north latitude and 165 degrees 2 minutes west longitude, as determined by the primary recovery ship USS Yorktown. The total flight duration was 147 hours 42 seconds.

Almost without exception, spacecraft systems operated as intended. All temperatures varied in a predictable manner within acceptable limits, and consumables usage was always maintained at safe levels. Communications quality was exceptionally good, and live television was transmitted on six occasions. The crew satisfactorily performed all flight plan functions and achieved all photographic objectives.

APPENDIX A

ATMOSPHERE

A.1 SUMMARY

This appendix presents a summary of the atmospheric environment at launch time of the AS-503. The format of these data is similar to that presented in previous launches of Saturn vehicles to permit comparisons. Surface and upper winds and thermodynamic data near the launch time are given.

A.2 GENERAL ATMOSPHERIC CONDITIONS AT LAUNCH TIME

A cold front passed through the launch area the afternoon before launch and became a stationary front about launch time, laying through the Miami area. Surface winds were from the north.

A.3 SURFACE OBSERVATIONS AT LAUNCH TIME

At launch time, the only cloudiness was 4/10 cirrus of unknown height. Table A-1 summarizes the surface observations at launch time. The solar radiation data is given in Table A-2.

A.4 UPPER AIR MEASUREMENTS

Data was used from four of the upper air wind systems to compile the final meteorological tape. Table A-3 summarizes the data systems used.

A.4.1 Wind Speed

Wind speed increased with altitude, reaching a speed of 34.8 m/s (67.6 knots) at 15.2 kilometers (49,900 ft). There was a second peak in the wind speed curve of 46.0 m/s (89.4 knots) at 33.0 kilometers (108,300 ft). See Figure A-1 for more information of the wind speeds.

A.4.2 Wind Direction

The surface wind was from the north, but changed to westerly about 1.5 kilometers (4,900 ft). Above 1.5 kilometers (4,900 ft) winds remained generally from the west as shown in Figure A-2.

A.4.3 Pitch Wind Component

The pitch wind speed component was very close to the bias wind used for the vehicle (50-percentile wind). The maximum pitch wind speed component was a tail wind component of 31.2 m/s (60.6 knots) at 15.1 kilometers (49,500 ft). See Figure A-3.

A.4.4 Yaw Wind Component

The yaw wind speed component increased with altitude to a maximum value from the left of 22.6 m/s (43.9 knots) at 15.8 kilometers (51,800 ft). See Figure A-4.

A.4.5 Component Wind Shears

Component wind shears (Δh = 1000 m) were of low magnitude at all altitudes. The largest wind shear was a yaw shear of 0.0157 s^{-1} at 15.8 kilometers (51,800 ft). See Figure A-5.

A.4.6 Extreme Wind Data in the High Dynamic Pressure Region

A summary of the maximum wind speeds, wind components, and shears are given in Tables A-4, A-5, and A-6; A-7, A-8, and A-9.

A.5 THERMODYNAMIC DATA

Comparisons of the thermodynamic data taken at AS-503 launch time with the Patrick Reference Atmosphere (PRA) (1963) for temperature, density, pressure, and Optical Index of Refraction (OIR) are shown in Figures A-6 and A-7, and discussed in the following paragraphs.

A.5.1 Temperature

Above 11 kilometers (36,100 ft), temperatures were lower than the PRA temperatures reaching a maximum deviation of -5.3 percent (-11.0°K) at 18.5 kilometers (60,700 ft). This was an actual air temperature of -77.6°C at this altitude.

A.5.2 Atmospheric Pressure

There were little deviations (less than 1 percent) of the atmospheric pressure from the PRA pressures below 15 kilometers (49,200 ft). Above 15 kilometers (49,200 ft), atmospheric pressures were less than the PRA pressures reaching a maximum deviation of -6.8 percent at 34.25 kilometers (112,400 ft).

A.5.3 Atmospheric Density

Atmospheric density deviations were small, being less than 5 percent deviations from the PRA.

A.5.4 Optical Index of Refraction

At the surface, the OIR was 5.02 (n-1) x 10^{-6} units higher than the corresponding value of the PRA. The deviation decreased with altitude becoming less than 1 (n-1) x 10^{-6} at 4 kilometers (13, 100 ft).

A.6 COMPARISON OF SELECTED ATMOSPHERIC DATA FOR ALL SATURN LAUNCHES

Tables A-10, A-11, and A-12 show a summary of the atmospheric data for each Saturn launch.

Table A-1. Surface Observations at AS-503 Launch Time

LOCATION	TIME AFTER T-0 (MIN)	PRESSURE N/cm2 (psia)	TEMPERATURE °K (°F)	DEW POINT °K (°F)	VISIBILITY km (STAT MI)	SKY COVER AMOUNT (TENTHS)	SKY COVER TYPE	SKY COVER HEIGHT OF BASE	WIND SPEED m/s (KNOTS)	WIND DIR (DEG)
Kennedy Space Center, Station B, Florida	0	10.207 (14.80)	288.15 (59.0)	286.45 (56.0)	16 (10)	4	Cirrus	Unknown	1.0 (2.0)	360
Cape Kennedy Rawinsonde Measurements	10	10.202 (14.80)	287.95 (58.6)	286.05 (55.2)	--	--	--	--	1.0 (2.0)	360
Pad 39A Lightpole NW (20.4 m)*	0	--	--	--	--	--	--	--	5.1 (10.0)	360
Pad 39A Service Structure Top (112.5 m)*	0	--	--	--	--	--	--	--	9.3 (18.0)	345

* Above Natural Grade

Table A-2. Solar Radiation at AS-503 Launch Time Launch Pad 39A

DATE	HOUR ENDING EST	TOTAL HORIZONTAL g-cal/cm2 (MIN)	NORMAL INCIDENT g-cal/cm2 (MIN)	DIFFUSE SKY g-cal/cm2 (MIN)
12/20/68	0800	0.04	0	0.04
	0900	0.16	0.02	0.16
	1000	0.30	0	0.30
	1100	0.45	0.01	0.45
	1200	0.30	0	0.30
	1300	0.30	0	0.30
	1400	0.54	0.14	0.46
	1500	0.63	0.40	0.46
	1600	0.42	0.24	0.36
	1700	0.16	0.09	0.15
	1800	0.03	0	0.03
12/21/68	0800	0.06	0.20	0.03
	0900	0.23	0.65	0.02

Table A-3. Systems Used to Measure Upper Air Wind Data

TYPE OF DATA	RELEASE TIME		PORTION OF DATA USED			
			START		END	
	TIME (UT)	TIME AFTER T-0 (MIN)	ALTITUDE M (ft)	TIME AFTER T-0 (MIN)	ALTITUDE M (ft)	TIME AFTER T-0 (MIN)
FPS-16 Jimsphere	1401	70	0	70	16,500 (54,100)	125
Rawinsonde	1301	10	16,750 (54,900)	65	34,000 (111,500)	122
Arcasonde	1515	144	51,250 (168,100)	150	34,250 (112,400)	157
Viper Dart	1807	316	89,750 (294,400)	326	51,500 (169,000)	328

Table A-4. Maximum Wind Speed in High Dynamic Pressure Region for Saturn 1 through Saturn 10 Vehicles

VEHICLE NUMBER	MAXIMUM WIND			MAXIMUM WIND COMPONENTS			
	SPEED m/s (KNOTS)	DIR (DEG)	ALT km (ft)	PITCH (W_x) m/s (KNOTS)	ALT km (ft)	YAW (W_z) m/s (KNOTS)	ALT km (ft)
SA-1	47.0 (91.4)	242	12.25 (40,200)	36.8 (71.5)	13.00 (42,600)	-29.2 (-55.8)	12.25 (40,200)
SA-2	33.6 (65.3)	216	13.50 (44,300)	31.8 (61.8)	13.50 (44,300)	-13.3 (-25.9)	12.25 (40,200)
SA-3	31.3 (60.8)	269	13.75 (45,100)	30.7 (59.7)	13.75 (45,100)	11.2 (21.8)	12.00 (39,400)
SA-4	51.8 (100.7)	253	13.00 (42,600)	46.2 (89.8)	13.00 (42,600)	-23.4 (-45.5)	13.00 (42,600)
SA-5	42.1 (81.8)	268	10.75 (35,300)	41.1 (79.9)	10.75 (35,300)	-11.5 (-22.4)	11.25 (36,900)
SA-6	15.0 (29.2)	96	12.50 (41,000)	-14.8 (-28.8)	12.50 (41,000)	12.2 (23.7)	17.00 (55,800)
SA-7	17.3 (33.6)	47	11.75 (38,500)	-11.1 (-21.6)	12.75 (41,800)	14.8 (28.8)	12.00 (39,400)
SA-9	34.3 (66.7)	243	13.00 (42,600)	27.5 (53.5)	10.75 (35,300)	23.6 (45.9)	13.25 (43,500)
SA-8	16.0 (31.1)	351	15.25 (50,000)	12.0 (23.3)	11.00 (36,100)	14.6 (28.4)	15.25 (50,000)
SA-10	15.0 (29.2)	306	14.75 (48,400)	12.9 (25.1)	14.75 (48,400)	10.8 (21.0)	15.45 (50,700)

Table A-5. Maximum Wind Speed in High Dynamic Pressure Region for Apollo/Saturn 201 through Apollo/Saturn 205 Vehicles

VEHICLE NUMBER	MAXIMUM WIND			MAXIMUM WIND COMPONENTS			
	SPEED m/s (KNOTS)	DIR (DEG)	ALT km (ft)	PITCH (W_x) m/s (KNOTS)	ALT km (ft)	YAW (W_z) m/s (KNOTS)	ALT km (ft)
AS-201	70.0 (136.1)	250	13.75 (45,100)	57.3 (111.4)	13.75 (45,100)	-43.3 (-84.2)	13.25 (43,500)
AS-203	18.0 (35.0)	312	13.00 (42,600)	11.1 (21.6)	12.50 (41,000)	16.6 (32.3)	13.25 (43,500)
AS-202	16.0 (31.1)	231	12.00 (39,400)	10.7 (20.8)	12.50 (41,000)	-15.4 (-29.9)	10.25 (33,600)
AS-204	35.0 (68.0)	288	12.00 (39,400)	32.7 (63.6)	15.25 (50,000)	20.6 (40.0)	12.00 (39,400)
AS-205	15.6 (30.3)	309	14.60 (44,500)	15.8 (30.7)	12.08 (36,800)	15.7 (30.5)	15.78 (47,500)

Table A-6. Maximum Wind Speed in High Dynamic Pressure Region for Apollo/Saturn 501 through Apollo/Saturn 503 Vehicles

VEHICLE NUMBER	MAXIMUM WIND			MAXIMUM WIND COMPONENTS			
	SPEED m/s (KNOTS)	DIR (DEG)	ALT km (ft)	PITCH (W_x) m/s (KNOTS)	ALT km (ft)	YAW (W_z) m/s (KNOTS)	ALT km (ft)
AS-501	26.0 (50.5)	273	11.50 (37,700)	24.3 (47.2)	11.50 (37,700)	12.9 (25.1)	9.00 (29,500)
AS-502	27.1 (52.7)	255	12.00 (42,600)	27.1 (52.7)	12.00 (42,600)	12.9 (25.1)	15.75 (51,700)
AS-503	34.8 (67.6)	284	15.22 (49,900)	31.2 (60.6)	15.10 (49,500)	22.6 (43.9)	15.80 (51,800)

Table A-7. Extreme Wind Shear Values in the High Dynamic Pressure Region for Saturn 1 through Saturn 10 Vehicles

(Δh = 1000 m)				
VEHICLE NUMBER	PITCH PLANE		YAW PLANE	
	SHEAR (SEC^{-1})	ALTITUDE km (ft)	SHEAR (SEC^{-1})	ALTITUDE km (ft)
SA-1	0.0145	14.75 (48,400)	0.0168	16.00 (52,500)
SA-2	0.0144	15.00 (49,200)	0.0083	16.00 (52,500)
SA-3	0.0105	13.75 (45,100)	0.0157	13.25 (43,500)
SA-4	0.0155	13.00 (42,600)	0.0144	11.00 (36,100)
SA-5	0.0162	17.00 (55,800)	0.0086	10.00 (32,800)
SA-6	0.0121	12.25 (40,200)	0.0113	12.50 (41,000)
SA-7	0.0078	14.25 (46,800)	0.0068	11.25 (36,900)
SA-9	0.0096	10.50 (34,500)	0.0184	10.75 (35,300)
SA-8	0.0065	10.00 (32,800)	0.0073	17.00 (55,800)
SA-10	0.0130	14.75 (48,400)	0.0090	15.00 (49,200)

Table A-8. Extreme Wind Shear Values in the High Dynamic Pressure Region for Apollo/Saturn 201 through Apollo/Saturn 205 Vehicles

(Δh = 1000 m)				
VEHICLE NUMBER	PITCH PLANE		YAW PLANE	
	SHEAR (SEC^{-1})	ALTITUDE km (ft)	SHEAR (SEC^{-1})	ALTITUDE km (ft)
AS-201	0.0206	16.00 (52,500)	0.0205	12.00 (39,400)
AS-203	0.0104	14.75 (48,400)	0.0079	14.25 (46,800)
AS-202	0.0083	13.50 (44,300)	0.0054	13.25 (43,500)
AS-204	0.0118	16.75 (55,000)	0.0116	14.00 (45,900)
AS-205	0.0113	15.78 (48,100)	0.0085	15.25 (46,500)

Table A-9. Extreme Wind Shear Values in the High Dynamic Pressure Region for Apollo/Saturn 501 through Apollo/Saturn 503 Vehicles

(Δh = 1000 m)				
VEHICLE NUMBER	PITCH PLANE		YAW PLANE	
	SHEAR (SEC^{-1})	ALTITUDE km (ft)	SHEAR (SEC^{-1})	ALTITUDE km (ft)
AS-501	0.0066	10.00 (32,800)	0.0067	10.00 (32,800)
AS-502	0.0125	14.90 (48,900)	0.0084	13.28 (43,500)
AS-503	0.0103	16.00 (52,500)	0.0157	15.78 (51,800)

Table A-10. Selected Atmospheric Observations for Saturn 1 Through Saturn 10 Vehicle Launches at Kennedy Space Center, Florida

VEHICLE NUMBER	VEHICLE DATA			SURFACE DATA						INFLIGHT CONDITIONS		
	DATE	TIME (EST) NEAREST MINUTE	LAUNCH COMPLEX	PRESSURE N/cm²	TEMPERATURE °C	RELATIVE HUMIDITY PERCENT	WIND* SPEED m/s	WIND* DIRECTION deg	CLOUDS	MAXIMUM WIND IN 8-16 km LAYER ALTITUDE m	SPEED m/s	DIRECTION deg
SA-1	27 Oct 61	1006	34	10.222	26.2	64	6.4	65	8/10 cumulus	12.25	47.0	242
SA-2	25 Apr 62	0900	34	10.205	24.6	59	3.5	180	1/10 cumulus, 3/10 cirrostratus	13.50	33.6	261
SA-3	16 Nov 62	1245	34	10.193	23.9	54	4.0	250	2/10 cumulus, 4/10 cirrus	13.75	31.3	259
SA-4	28 Mar 63	1512	34	10.176	23.9	71	6.0	40	1/10 stratocumulus, 1/10 cirrus	13.00	51.8	253
SA-5	29 Jan 64	1125	37B	10.278	17.8	59	9.0	38	4/10 stratocumulus, 2/10 cirrus	10.75	42.1	268
SA-6	28 May 64	1207	37B	10.142	28.7	64	7.0	150	1/10 cumulus, 1/10 cirrus	12.50	15.0	96
SA-7	18 Sep 64	1123	37B	10.173	29.5	55	5.0	70	1/10 cumulus, 5/10 altocumulus, 1/10 cirrus	11.75	17.3	47
SA-9	16 Feb 65	0937	37B	10.244	23.3	74	6.0	125	1/10 stratocumulus	13.00	34.3	243
SA-8	25 May 65	0235	37B	10.186	22.8	93	4.4	140	1/10 cumulus	15.25	16.0	351
SA-10	30 Jul 65	0800	37B	10.163	24.7	86	10.7	185	1/10 cumulonimbus, 2/10 altostratus, 5/10 cirrus	14.75	15.0	306

* Instantaneous readings from charts at T-0 from anemometers on poles at 19.5 m (59.4 ft) on launch complex 34, 20.7 m (63.1 ft) on launch complex 37B. Heights of anemometers are above natural grade.

Table A-11. Selected Atmospheric Observations for Apollo-Saturn 201 Through Apollo-Saturn 205 Launches at Kennedy Space Center, Florida

VEHICLE NUMBER	VEHICLE DATA			SURFACE DATA						INFLIGHT CONDITIONS		
	DATE	TIME (EST) NEAREST MINUTE	LAUNCH COMPLEX	PRESSURE N/cm²	TEMPERATURE °C	RELATIVE HUMIDITY PERCENT	WIND* SPEED m/s	WIND* DIRECTION deg	CLOUDS	MAXIMUM WIND IN 8-16 km LAYER ALTITUDE m	SPEED m/s	DIRECTION deg
AS-201	26 Feb 66	1112	34	10.217	16.1	48	6.5	330	Clear	13.75	70.0	250
AS-203	5 Jul 66	0953	37B	10.173	30.2	70	6.3	242	8/10 cumulus, 1/10 cirrus	13.00	18.0	312
AS-202	25 Aug 66	1216	34	10.166	30.2	69	4.1	160	1/10 cumulus, 1/10 altocumulus, 1/10 cirrus	12.00	16.0	231
AS-204	23 Jan 68	1748	37B	10.186	16.1	93	4.2	45	3/10 cumulus	12.00	35.0	288
AS-205	11 Oct 68	1003	34	10.180	28.3	65	11.5	90	3/10 cumulonimbus	15.60	14.6	309

* Instantaneous readings from charts at T-0 from anemometers on poles at 19.5 m (59.4 ft) on launch complex 34, 20.7 m (63.1 ft) on launch complex 37B. Heights of anemometers are above natural grade.

Table A-12. Selected Atmospheric Observations for Apollo-Saturn 501 Through Apollo-Saturn 503 Launches at Kennedy Space Center, Florida

VEHICLE NUMBER	VEHICLE DATA			SURFACE DATA						INFLIGHT CONDITIONS		
	DATE	TIME (EST) NEAREST MINUTE	LAUNCH COMPLEX	PRESSURE N/cm²	TEMPERATURE °C	RELATIVE HUMIDITY PERCENT	WIND* SPEED m/s	WIND* DIRECTION deg	CLOUDS	MAXIMUM WIND IN 8-16 km LAYER ALTITUDE m	SPEED m/s	DIRECTION deg
AS-501	9 Nov 67	0700	39A	10.261	17.6	55	8.0	70	1/10 cumulus	11.50	26.0	273
AS-502	4 Apr 68	0600	39A	10.200	20.9	83	5.4	132	5/10 strato-cumulus	13.00	27.1	255
AS-503	21 Dec 68	0751	39A	10.207	15.0	88	1.0	360	4/10 cirrus	15.22	34.8	284

* Instantaneous readings from charts at T-0 from anemometers on poles on launch pad at 18.3 m (60.0 ft) on launch complex 39A. Heights of anemometers are above natural grade.

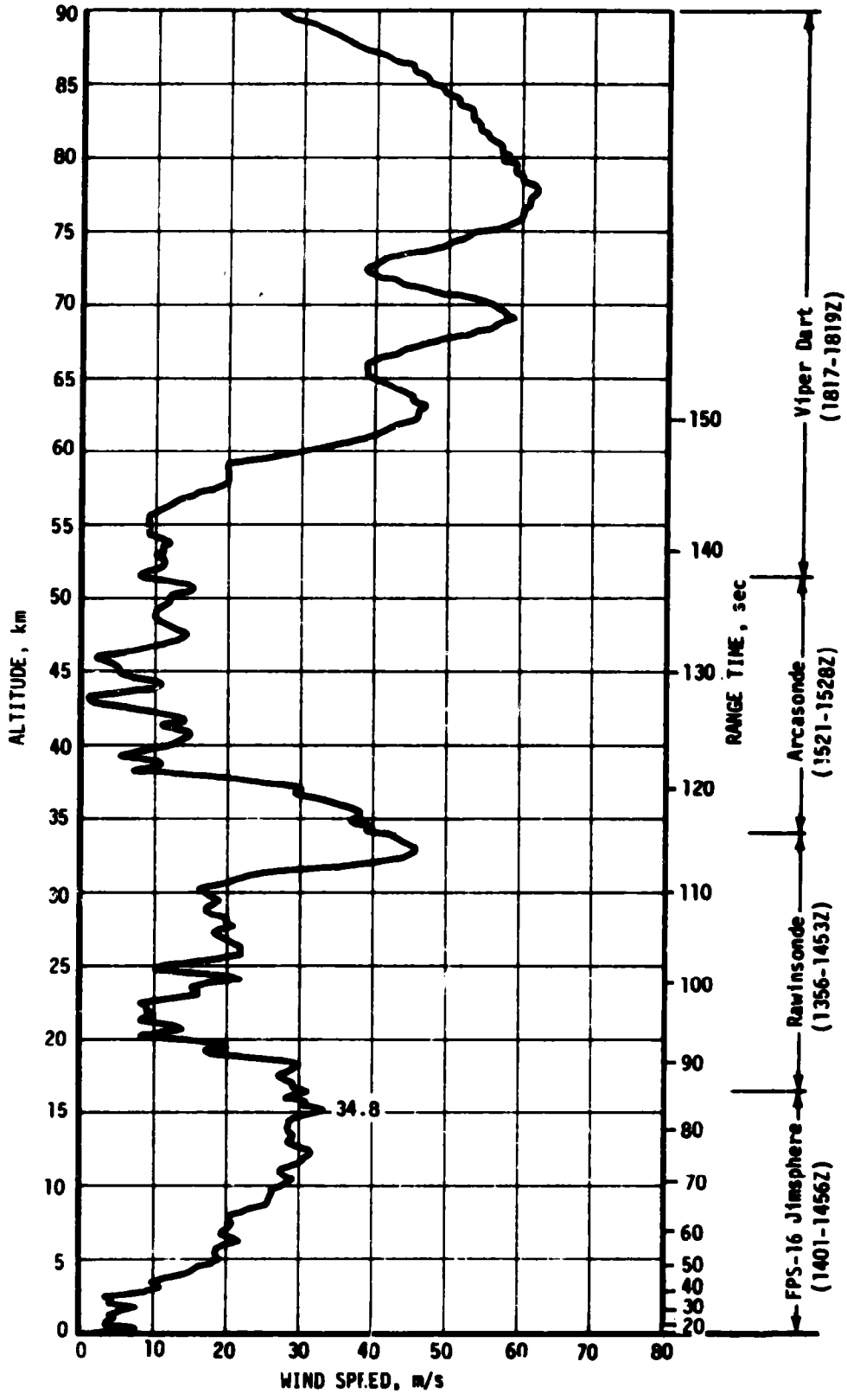

Figure A-1. Scalar Wind Speed at Launch Time of AS-503

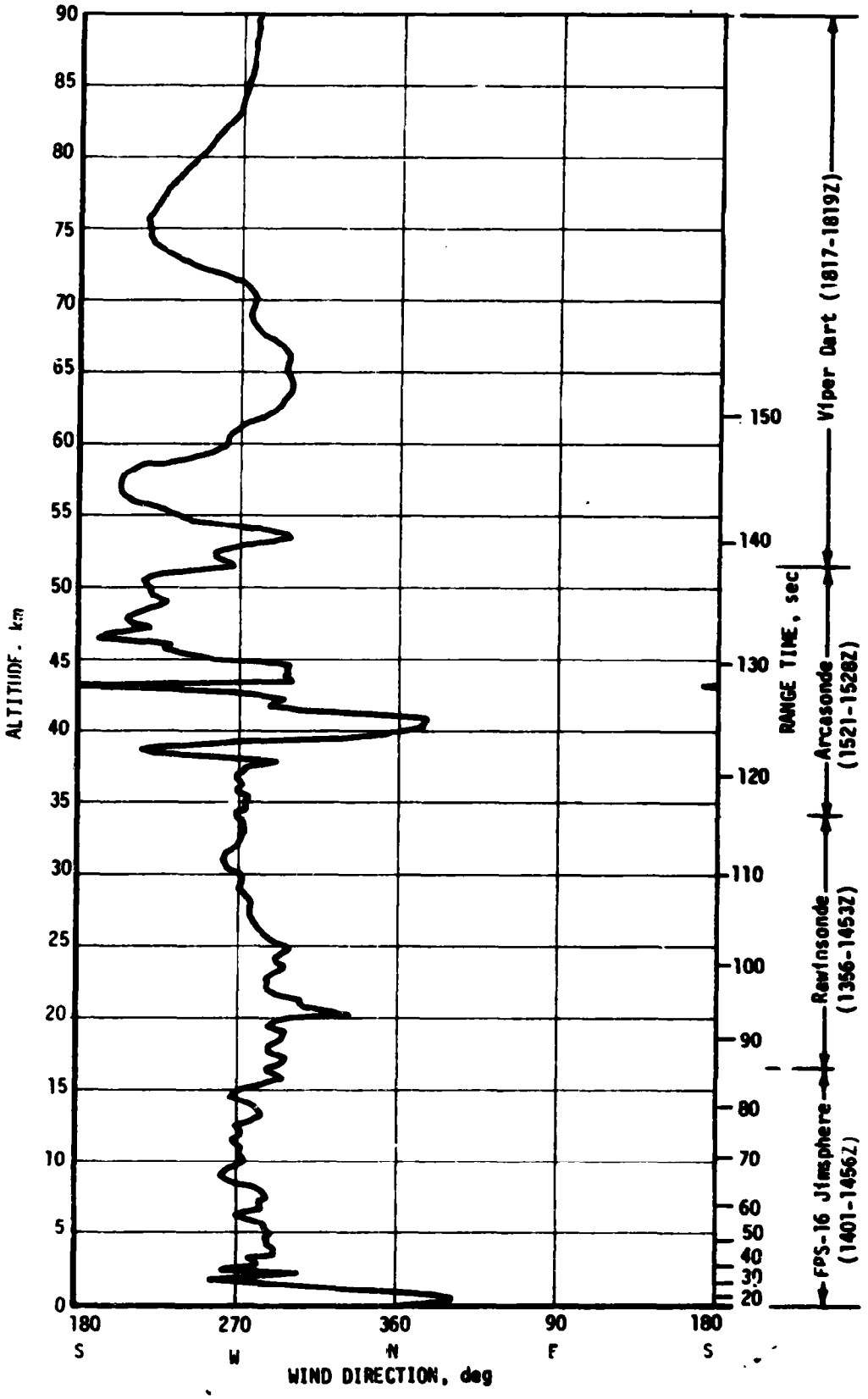

Figure A-2. Wind Direction at Launch Time of AS-503

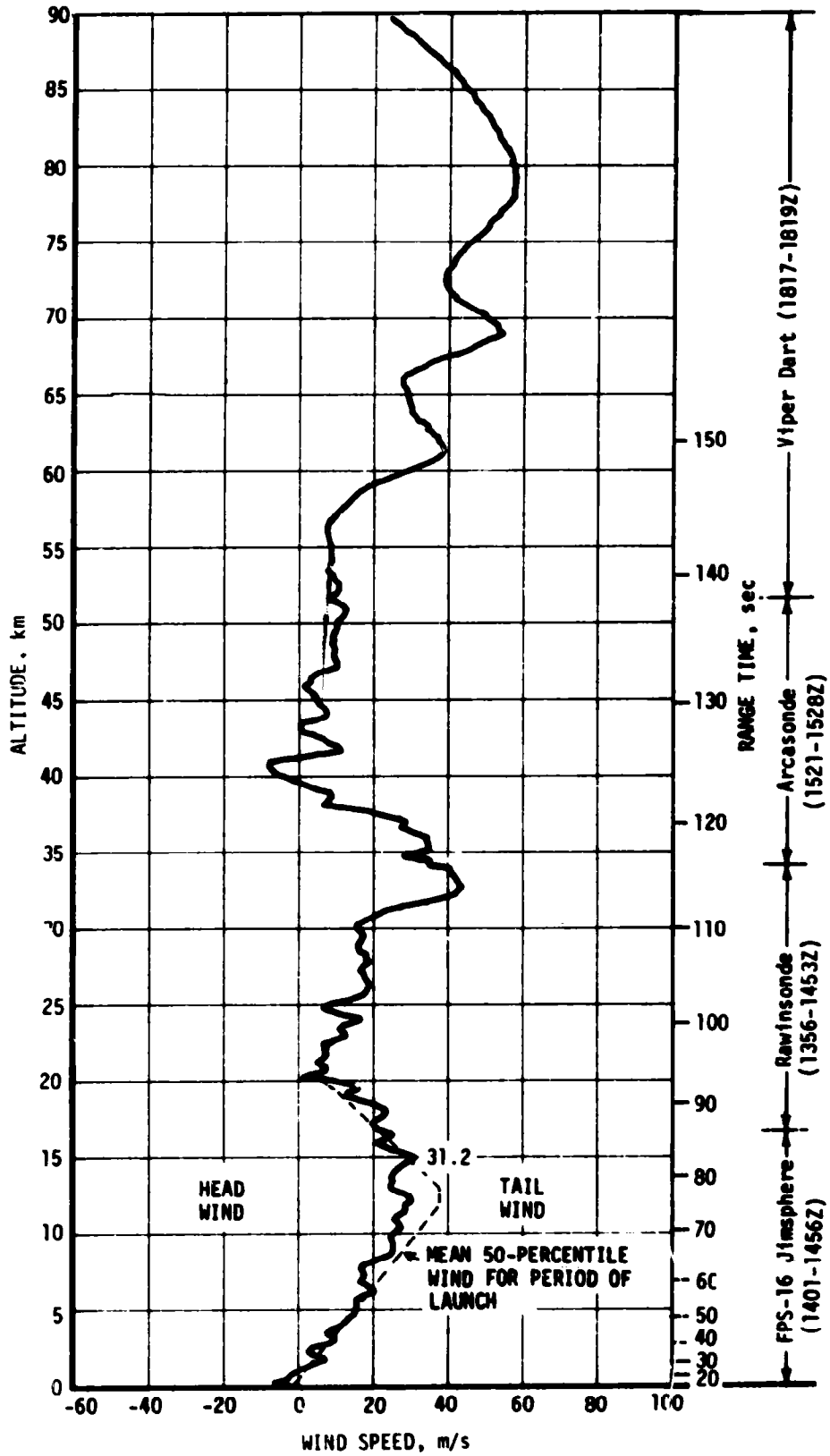

Figure A-3. Pitch Wind Speed Component (W_x) at Launch Time of AS-503

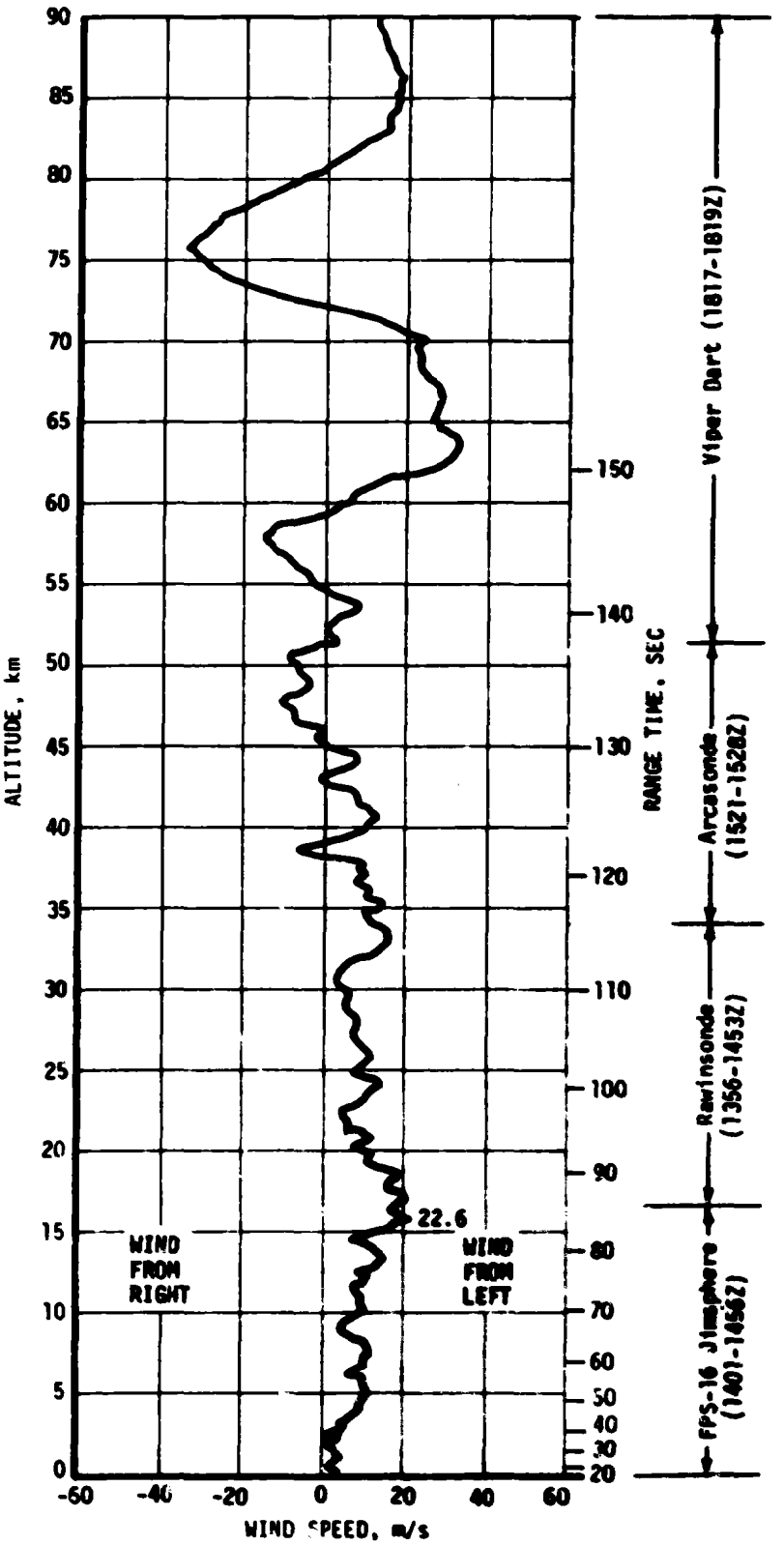

Figure A-4. Yaw Wind Speed Component at Launch Time of AS-503

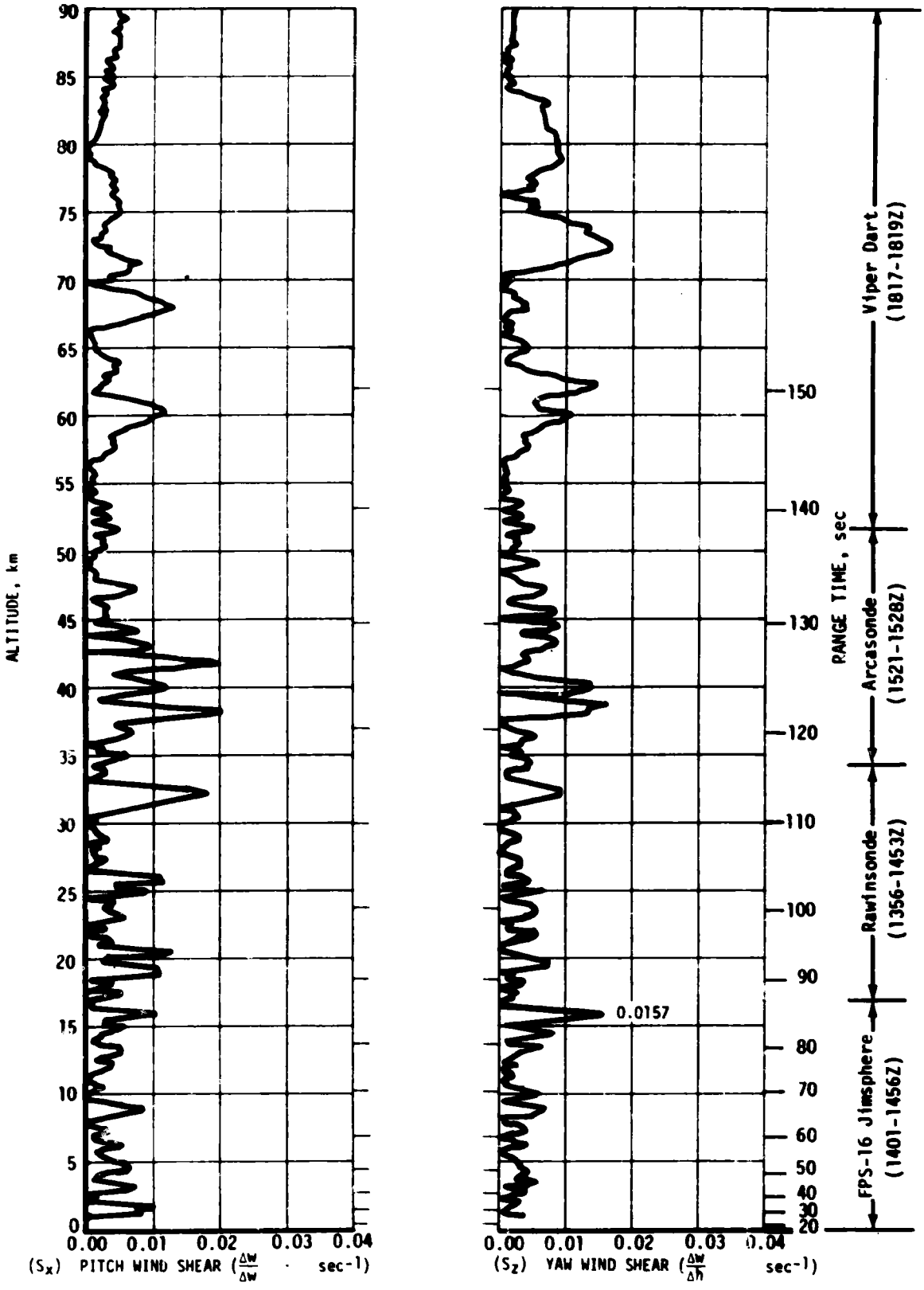

Figure A-5. Pitch (S_x) and Yaw (S_z) Component Wind Shears at Launch Time of AS-503

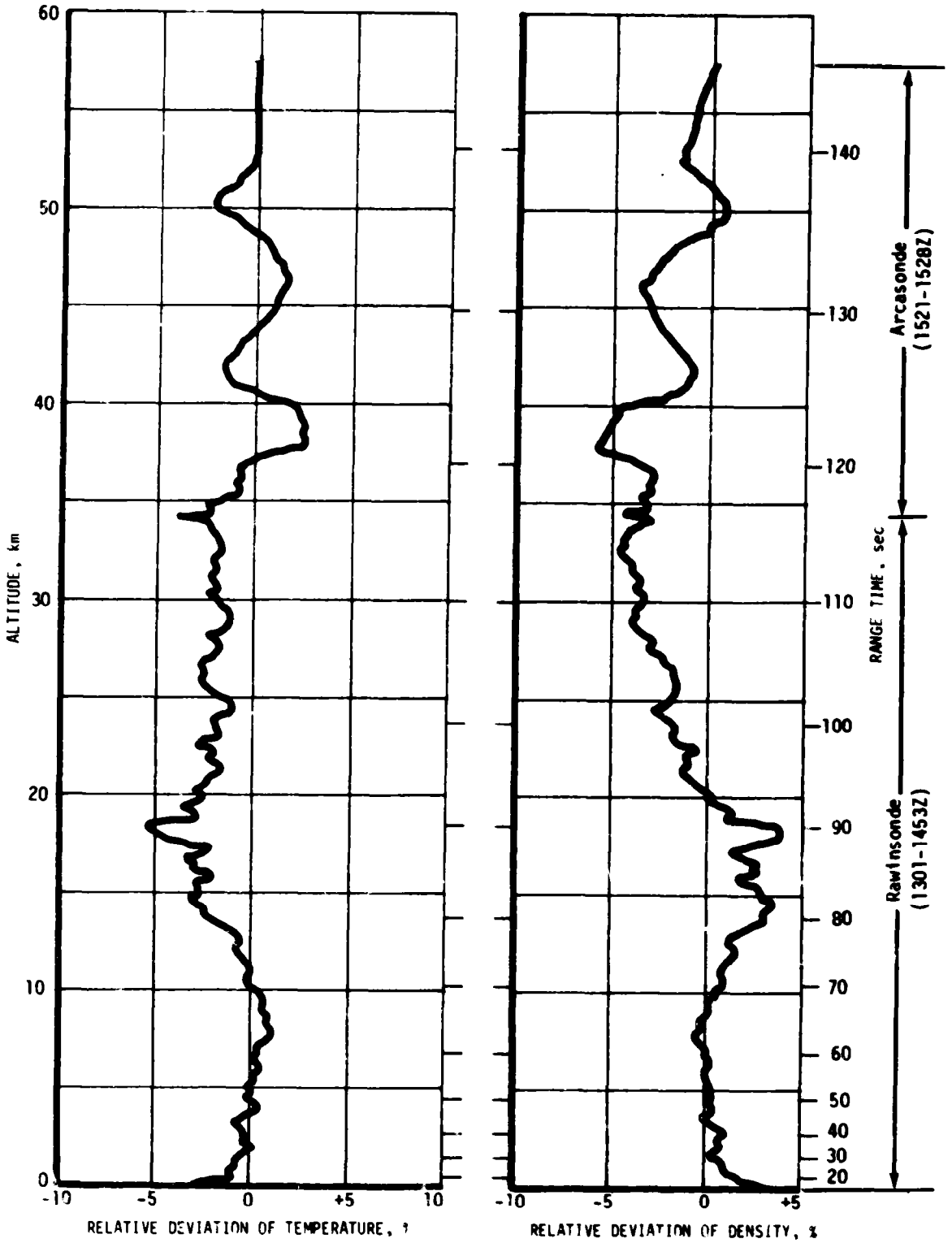

Figure A-6. Relative Deviation of AS-503 Temperature and Density from PAFB (63) Reference Atmosphere

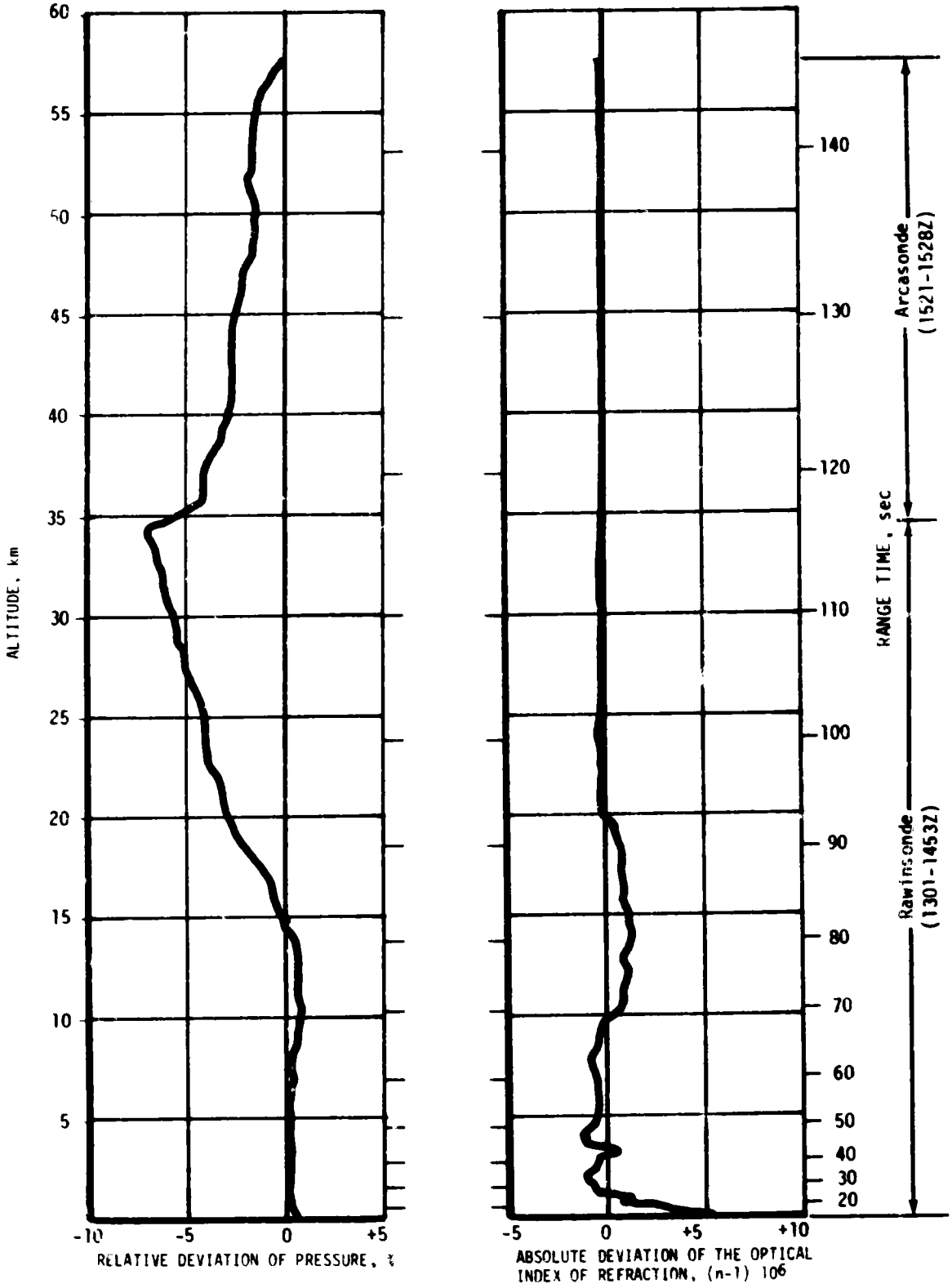

Figure A-7. Relative Deviation of Pressure and Absolute Deviation of the Index of Refraction from the PAFB (63) Reference Atmosphere, AS-503

APPENDIX B

AS-503 VEHICLE DESCRIPTION

B.1 SUMMARY

AS-503, third flight of the Saturn V series, was the first to test a manned Saturn V Apollo space vehicle. The vehicle consists of five major units. From bottom to top they are: S-IC stage, S-II stage, S-IVB stage, Instrument Unit (IU), and the Spacecraft. The Saturn V Apollo vehicle is approximately 110.6 meters (363 ft) in length. See Figure B-1 for a pictorial description of the vehicle.

B.2 S-IC STAGE

B.2.1 S-IC Configuration

The S-IC stage, as shown in Figure B-2, is a cylindrical structure designed to provide the initial boost for the Saturn V Apollo vehicle. This booster is 42.1 meters (138 ft) long and has a diameter of 10.1 meters (33 ft). The basic structures of the S-IC are the thrust structure, fuel (RP-1) tank, intertank section, LOX tank, and the forward skirt. Attached to the thrust structure are the five F-1 engines which produce a combined nominal sea level thrust of 33,850,000 Newtons (7,610,000 lbf). Four of these engines are spaced equidistantly about a 9.243 meters (30.33 ft) diameter circle. The four outboard engines are attached so they have a gimbaling capability. Each outboard engine can move in a 5 degree, 9 minute square pattern to provide pitch, yaw, and roll control. The fifth engine is fixed mounted at the stage centerline. In addition to supporting the engines, the thrust structure also provides support for the base heat shield, engine accessories, engine fairings and fins, propellant lines, retro motors, and environmental control ducts. The intertank structure provides structural continuity between the LOX and fuel tanks, which provide propellant storage; and the forward skirt provides structural continuity with the S-II stage.

Propellants are supplied to the engine turbopumps by 15 suction ducts: 5 from the LOX tank, and 10 from the fuel tank. The fuel tank is a semimonocoque cylindrical structure closed at each end by an ellipsoidal bulkhead. Antislosh ring baffles are located on the inside wall of the tank, and an antivortex cruciform baffle is located in the lower bulkhead area. The configuration of the LOX tank is basically the same with the exception of capacity. The LOX tank will provide storage for 1342 m^3 (47,405 ft^3) including ullage. The fuel tank will hold approximately 827 m^3 (29,221 ft^3) including ullage. The mixture ratio between LOX and RP-1 is approximately 2.27:1 (LOX to RP-1).

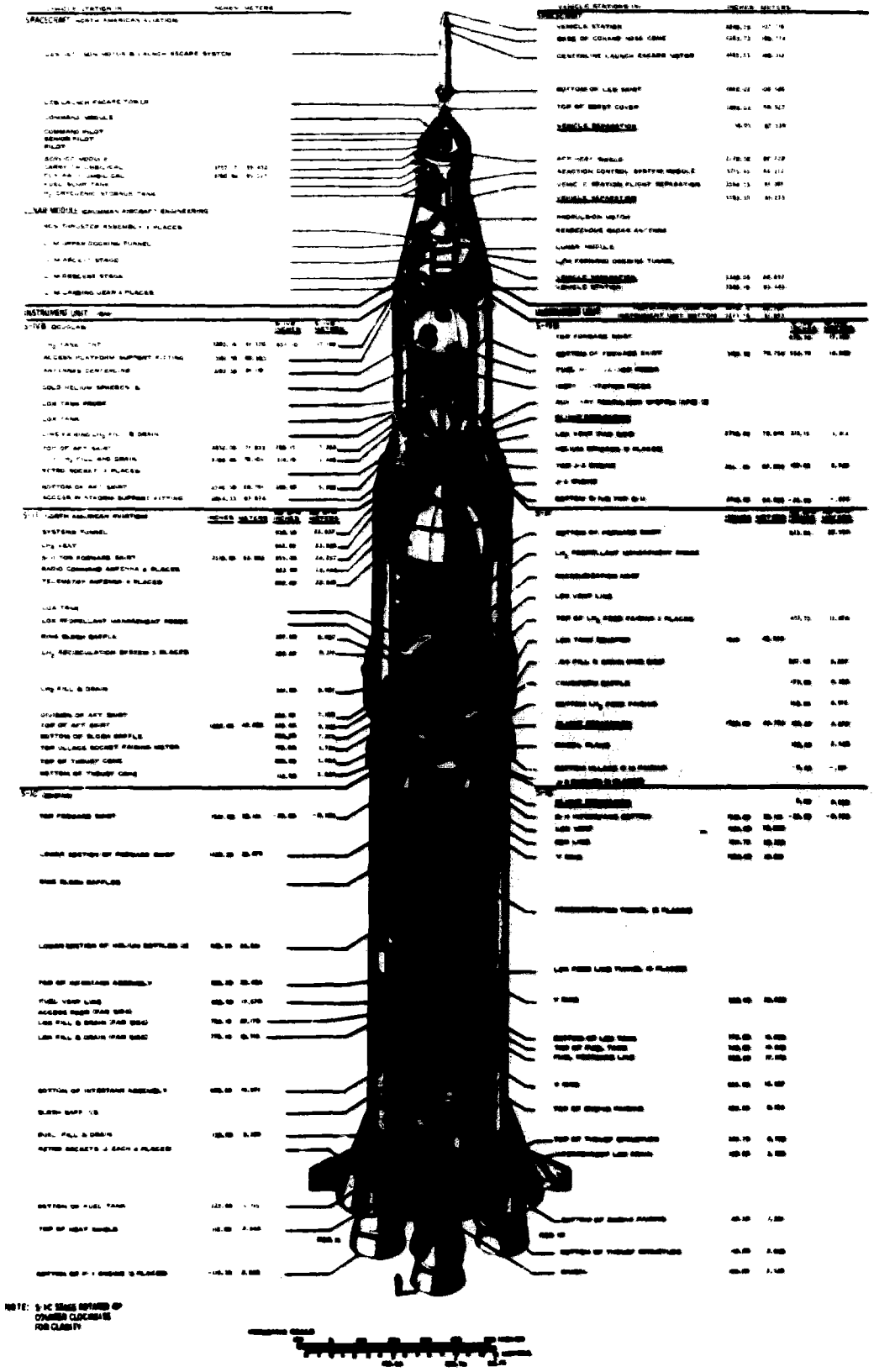

Figure B-1. Saturn V Apollo Configuration

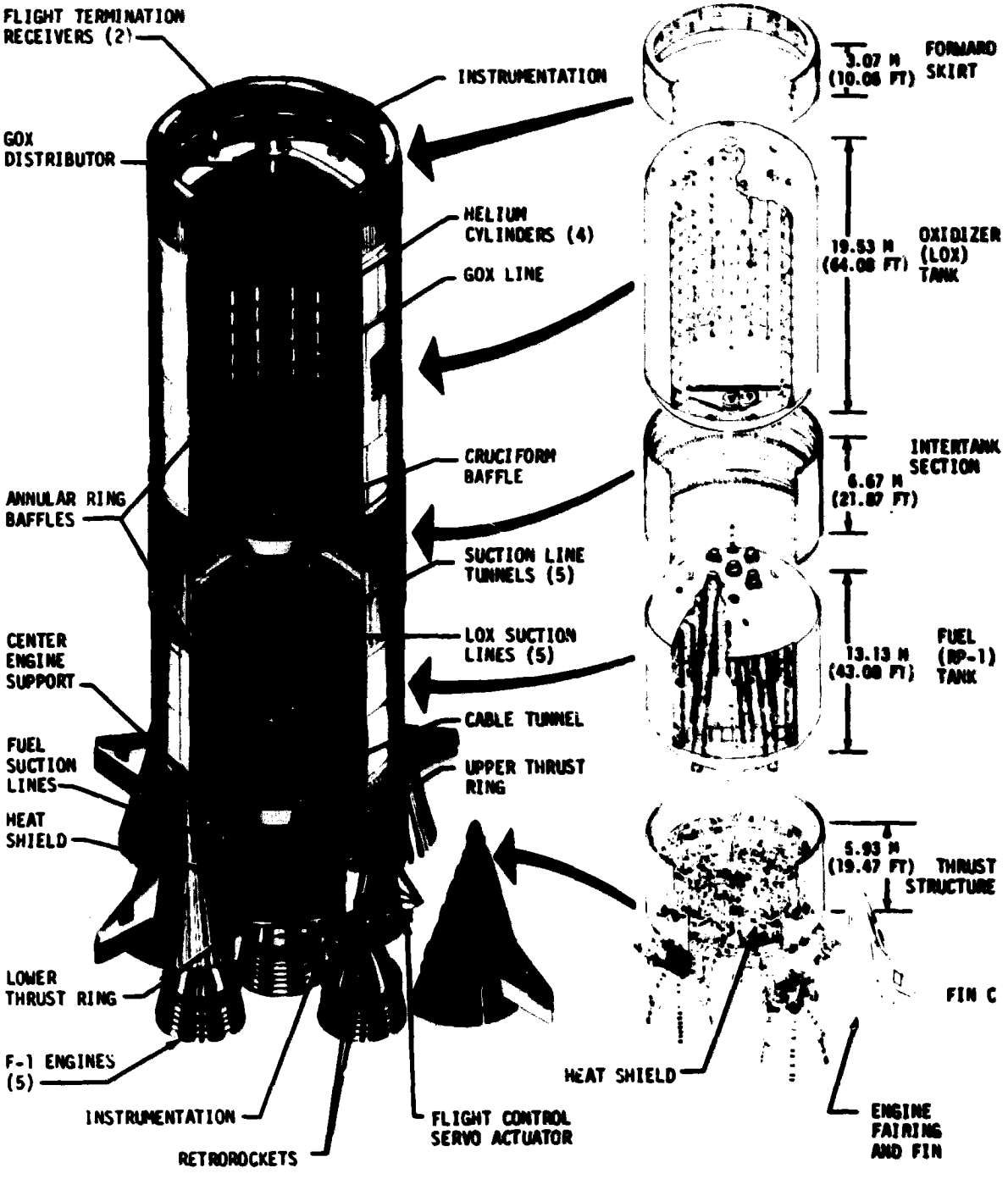

Figure B-2. S-IC Stage Configuration

The LOX and fuel pressurization systems provide and maintain the Net Positive Suction Pressure (NPSP) required for the LOX and fuel turbopumps during engine start and flight. These systems also provide protection from high pressures which might occur in the LOX and fuel tanks. Before engine ignition, the LOX and fuel tanks are pressurized from a ground helium supply. During flight, LOX pressurization is accomplished by gaseous oxygen obtained by using F-1 engine heat exchangers to convert oxygen from liquid to gas. The fuel tank is pressurized by gaseous helium supplied by helium bottles located in the LOX tank. The LOX and fuel feed systems contain LOX and fuel depletion sensors for purposes of outboard engine cutoff during flight. The inboard engine was cutoff by an IU signal on AS-503.

Eight solid propellant retro motors provide separation thrust after S-IC burnout. They are located inside the four outboard engine fairings and are attached externally to the thrust structure. The S-IC and S-II stages are severed by linear shaped charges, and the retro motors supply the necessary acceleration force to provide separation. Each retro motor is pinned securely to the vehicle support and pivot support fittings at an angle of 7.5 degrees from stage centerline.

Additional systems on the S-IC include:

a. The Environmental Control System (ECS) which protects the S-IC stage from temperature extremes, excessive humidity, and hazardous gas concentrations.

b. The hydraulic system which distributes power to operate the engine valves and thrust vector control system.

c. The pneumatic control pressure system which provides a pressurized nitrogen supply for command operations of various pneumatic valves, and a purge for TV camera lenses.

d. The electrical system which distributes and controls the stage electrical power.

e. The instrumentation system which monitors functional operation of the stage systems and provides signals for vehicle tracking during S-IC burn.

f. The film camera system.

g. The POGO suppression system. This system provides gaseous helium to a cavity in each of the LOX prevalves of the four outboard engine suction lines. These gas filled cavities act as a "spring" and serve to lower the natural frequency of the feed system and thereby prevent coupling between engine thrust oscillations and the first longitudinal mode of the vehicle structure.

The more significant configuration changes between AS-502 S-IC and AS-503 S-IC are shown in Table B-1.

Table B-1. S-IC Significant Configuration Changes

SYSTEM	CHANGE	REASON
Propulsion	Addition of POGO suppression system.	To eliminate the POGO problem which occurred on the AS-502 flight.
	Inboard engine cutoff commanded by IU at 125 seconds. AS-502 inboard engine cutoff was by LOX depletion at 145 seconds.	To prevent vehicle maximum acceleration from exceeding 4.0 g's.
	Planned outboard engines cutoff by LOX depletion. Fuel depletion cutoff was used for AS-502.	LOX depletion cutoff is the normal mode. Fuel depletion cutoff was used on AS-502 only to demonstrate the backup mode.
	Outboard engines canted 2 degrees outboard at 20 seconds.	To reduce the effect of thrust imbalance in the event an outboard engine prematurely shuts down.
Electrical	Incorporated revisions to provide redundancy in critical electrical circuitry.	To eliminate 53 critical single point failure modes.
Instrumentation	Additional and improved instrumentation.	To determine systems performance, to verify and establish corrective action for S-IC AS-502 flight anomalies, and to further define flight environment.
Forward Skirt	Hardware changes and additional thermal-insulation protection for control pressure, camera ejection and purge, system and data components vulnerable to damage due to the S-IC/S-II separation environment.	To minimize probability of recurrence of S-IC AS-502 flight anomalies during separation.

B.3 S-II STAGE

B.3.1 S-II Configuration

The S-II stage shown in Figure B-3 provides second stage boost for the Saturn V launch vehicle. The S-II stage has a cylindrical structure, 24.8 meters (81.5 ft) long and 10.1 meters (33 ft) in diameter. Propulsive power is provided by five J-2 engines with a combined nominal thrust of 5,004,249 Newtons (1,125,000 lbf) at an oxidizer to fuel ratio of 5.5:1. The approximate weight of the stage is 40,098 kilograms (88,400) lbm) dry and 469,423 kilograms (1,034,900 lbm) fully loaded.

The S-II airframe consists of a body shell structure, (forward and aft skirt and interstage), a propellant tank structure, and a thrust structure.

Each of the shell structure units are of basically the same construction consisting of a semimonocoque cylindrical shell fabricated from 7075 aluminum alloy material. These units are stiffened by external hat-section stringers and internal ring frames. These units provide structural continuity between adjacent stages.

The thrust structure is a semimonoque conical shell which tapers from the stage diameter down to a 5.49 meter (18 ft) diameter. It is constructed in the same manner as the skirt section and is fabricated from 7075 aluminum alloy material. Four pairs of thrust longerons (two at each outboard engine location) and a center engine support beam distribute the thrust loads of the five J-2 engines. A fiberglas honeycomb heat shield, supported from the lower portion of the thrust structure, protects the stage base area from excessive temperatures during S-II boost.

Propellants are supplied to the J-2 engines from the LH_2 and LOX tanks. The LH_2 tank is a cylindrical shell with the ends closed by a forward elliptical bulkhead and an aft reversed elliptical bulkhead. The tank, 17 meters (56 ft) long and 10.1 meters (33 ft) in diameter, has a capacity of 1069 m^3 (37,737 ft^3). The tank wall is composed of six cylindrical sections which incorporate longitudinal and circumferential stiffeners. Wall sections and bulkheads are fabricated from 2014 aluminum alloy joined by fusion welding. The LOX tank is of ellipsoidal shape. It has a volume of 361 m^3 (12,745 ft^3). The tank is 7 meters (22 ft) long and 10.1 meters (33 ft) in diameter. The bottom of the fuel tank is common to both tanks and serves as the forward half of the LOX tank. This common bulkhead is a sandwich structure composed of aluminum facing sheets and a fiberglass/phenolic honeycomb core. The fore and aft halves of the LOX tank are formed from waffle-stiffened gore segments fabricated from 2014 aluminum alloy.

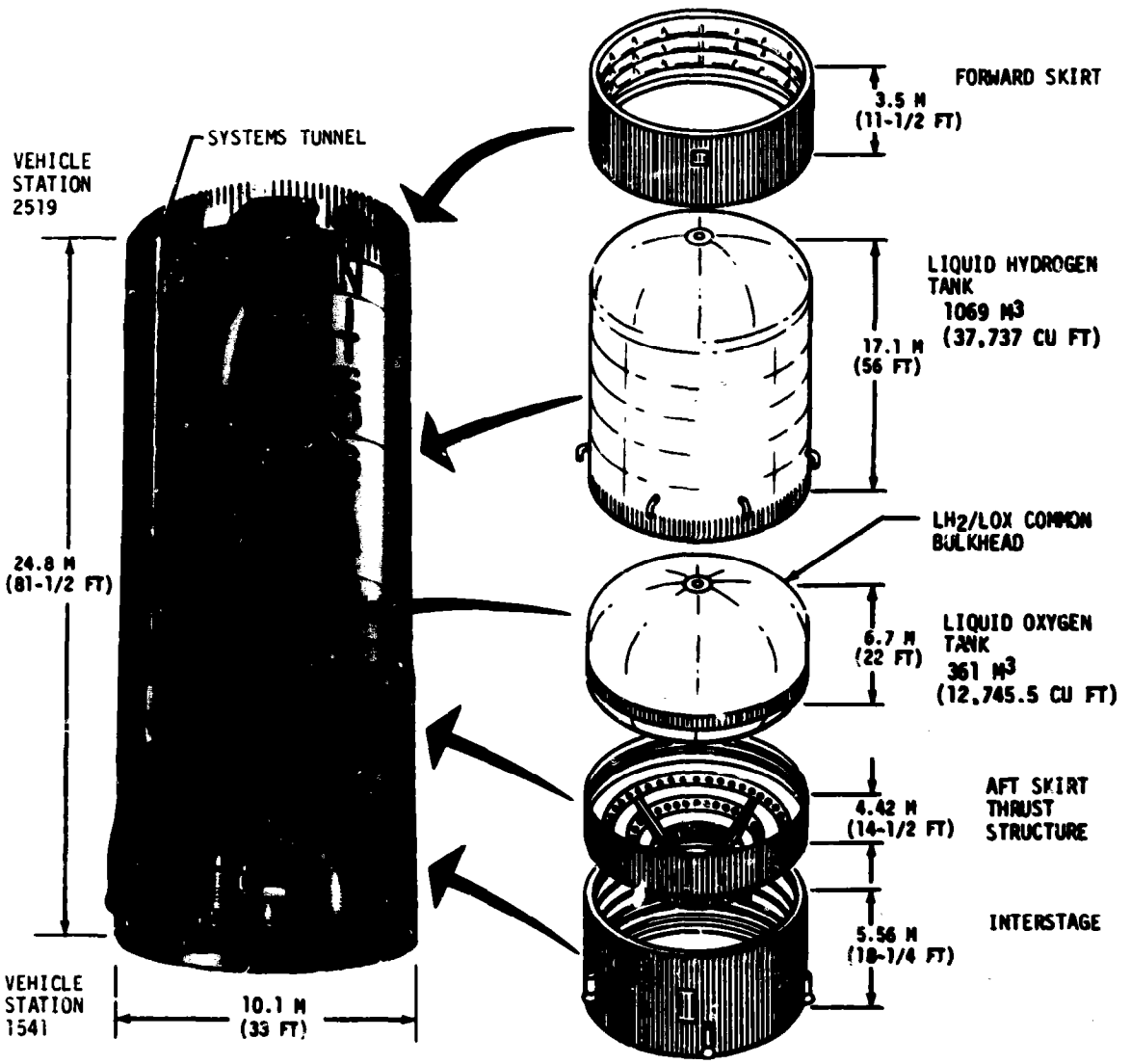

Figure B-3. S-II Stage Configuration

The stage propulsion system consists of five single start J-2 engines utilizing LOX and LH_2 for propellants. Each engine attains a nominal thrust of 1,000,851 Newtons (225,000 lbf) at an oxidizer to fuel ratio of 5.5:1. The four outboard J-2 engines are mounted with gimbal bearings and hydraulic powered actuator rods to provide thrust vector control. The fifth engine is mounted on stage centerline and is not gimbaled.

The J-2 engine is a high performance, high altitude engine employing a tubular walled, one-and-a-half pass, regeneratively cooled thrust chamber. Propellants are fed through two independently driven turbopumps. The ratio of fuel to oxidizer is controlled by bypassing LOX from the discharge side of the oxidizer turbopump back to the inlet side through a Propellant Utilization (PU) valve.

The propellant tanks are prepressurized from a ground regulated helium source prior to liftoff to provide the turbopump inlet pressure required for engine start. Prepressurization is terminated 30 seconds prior to liftoff for both tanks. During the engine burn period, the LOX tank is pressurized by flowing LOX through the heat exchanger in the oxidizer turbine exhaust duct and the LH_2 tank is pressurized by GH_2 from the thrust chamber fuel manifold. Both the LOX and LH_2 propellant tanks have vent valves for over-pressure protection.

Inflight separation of the S-IC/S-II stages is accomplished by a dual-plane separation system. Both separation events are controlled by the flight program stored in the Launch Vehicle Digital Computer (LVDC) which is located in the IU stage. First plane separation, occurring at vehicle station 39.73 meters (1564 in.), is initiated by an ordnance train. This train consists of an Explosive Bridge Wire (EBW) firing unit, an EBW detonator, and a linear shaped charge which severs the tension plates around the periphery of the stage at the separation plane. Four ullage motors on the S-II stage are fired to provide a propellant settling force and retro motors on the S-IC stage are fired to provide positive separation of the two stages. Second plane separation occurs about 30 seconds later at vehicle station 44.7 meters (1760 in.) using the same type of ordnance train.

Additional systems on the S-II stage include:

a. The leak detection and insulation purge system detects hydrogen, oxygen, or nitrogen leaking into the LH_2 tank insulation or LH_2 feedline elbows and provides a means for purging and diluting any leakage into the insulation prior to liftoff.

b. The Environmental Control System (ECS) provides protection against hazardous gas concentrations and also provides temperature control in the engine compartment and equipment containers prior to liftoff.

c. The pneumatic control pressure system provides the actuating force for the prevalves, recirculation valves, and propellant fill and drain valves.

d. The propellant utilization system is used for propellant management during propellant loading operations and S-II boost (flown open-loop on AS-503).

e. The engine actuation system provides engine gimbaling. The actuators, which are part of the engine actuation system, receive the gimbaling commands from the flight control system in the IU.

f. The electrical system is used for supplying and distributing electrical power to the various systems.

g. The Emergency Detection System (EDS) supplies engine mainstage thrust OK and LH_2 ullage pressure signals to the IU and spacecraft, respectively.

h. The engine preconditioning (recirculation) system which recirculates LOX and LH_2 and provides LOX helium injection prior to S-II engine start.

i. The data system is used for obtaining and transmitting data for stage performance evaluations.

j. The propellant dispersion system is provided for range safety.

k. The propellant feed system supplies propellants to the engines.

l. The propellant level monitoring system uses liquid level monitoring devices to provide propellant depletion cutoff signals to the engines and also provides backup propellant loading information.

The recoverable separation camera system, which was used on AS-501 and AS-502 to provide visual data for second plane separation, has been deleted for AS-503 and subsequent vehicles.

A structural change between this and previous S-II stages is the use of a "light weight" forward bulkhead for the LH_2 tank.

No new systems were added for AS-503. The significant S-II stage configuration changes within systems are listed in Table B-2.

B.4 S-IVB STAGE

B.4.1 S-IVB Configuration

The S-IVB stage, as shown in Figure B-4, is a bi-propellant tank structure designed to withstand the loads and stresses incurred on the ground and during launch, preignition boost, ignition, and all flight phases. The S-IVB stage has nominal dimensions of 18.0 meters (59 ft) in length and 6.6 meters (21.6 ft) in diameter. The basic airframe consists of the aft interstage, thrust structure, aft skirt, propellant tanks, and forward skirt. The aft interstage assembly provides the load supporting

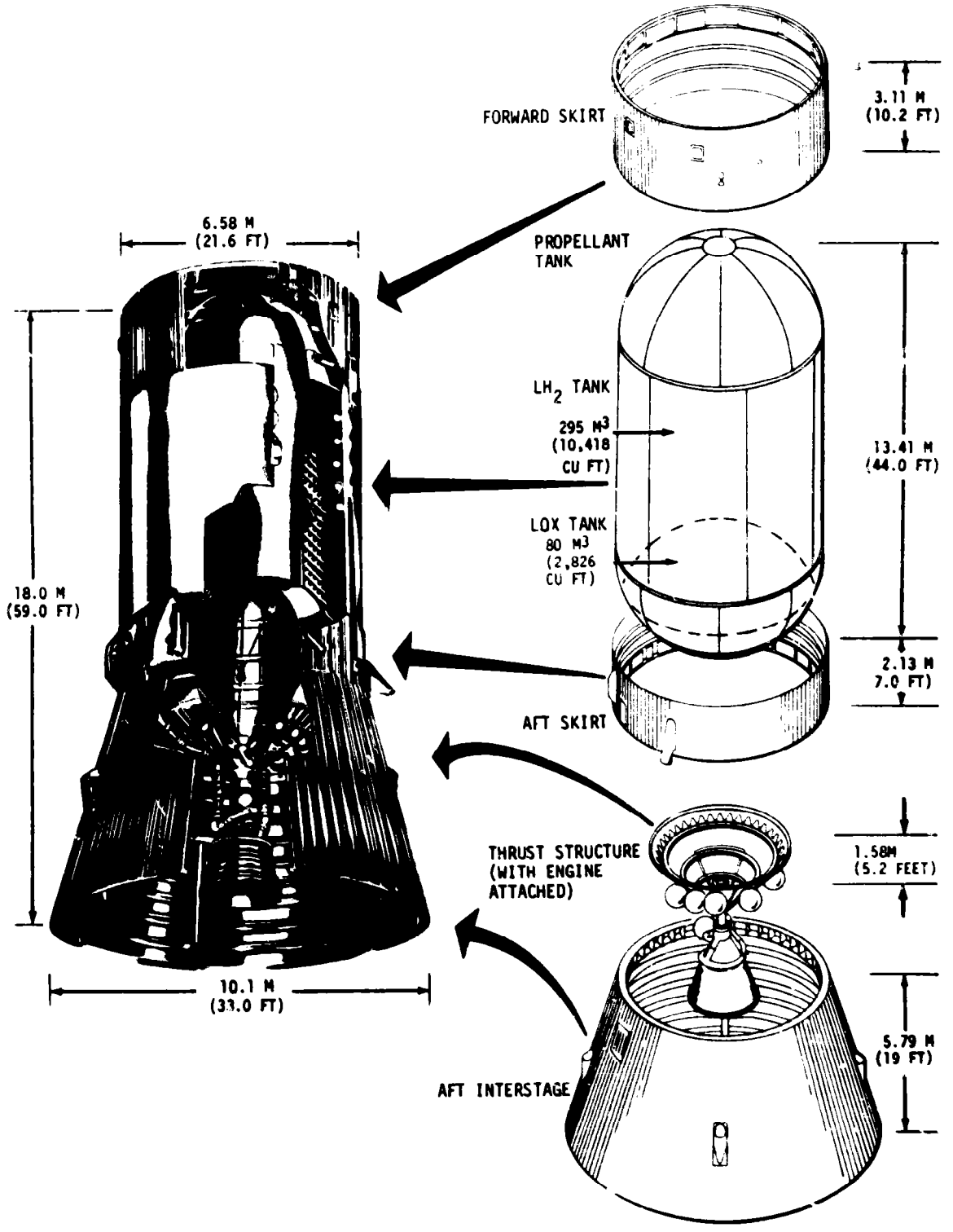

Figure B-4. S-IVB Stage Configuration

Table B-2. S-II Significant Configuration Changes

SYSTEM	CHANGE	REASON
Propulsion	Replaced flexible hose sections in J-2 Augmented Spark Igniter (ASI) fuel and LOX lines with rigid, tubular lines.	Eliminated failure due to flow-induced vibrations in a vacuum environment.
	LH_2 tank vent valves replaced by dual-setting vent valves.	Reduce structural pressure loads during S-IC and S-II boost.
	Propellant Utilization (PU) system to be operated "open loop." Timed mixture ratio shifts will be commanded by the LVDC.	To minimize the effect on vehicle performance in case of a PU malfunction.
	Engine and prevalve control circuits modified; engine electrical power removed when an emergency engine cutoff command is received and prevalves are inhibited from premature closure until thrust chamber pressure drops below 90 percent level.	Insure proper response to an emergency engine cutoff command.
	LOX sump baffle deleted and sump screen replaced with an inverted conical screen configuration of finer mesh.	Eliminates potential baffle failure and LOX fill contamination will be more effectively filtered by the finer mesh modification.
Separation	Separation cameras deleted from engine compartment.	Separation clearances on previous flights were adequate.
Instrumentation	Timer No. 3, which limits playback time, for onboard data tape recorder disconnected.	Insure that all data recorded during S-II separation, engine start, and engine cutoff will be played back.
Structures	LH_2 forward bulkhead changed to light weight configuration.	Weight saving.

structure between the S-IVB stage and the S-II stage. The thrust structure assembly is an inverted truncated cone attached at its large end to the aft dome of the LOX tank and at its small end to the engine mount. This structure provides support for engine piping, wiring and interface panels, ambient helium spheres, and some of the LOX tank and engine instrumentation. The aft skirt assembly is the load bearing structure between the LH_2 tank and aft interstage. The propellant tank assembly consists of a cylindrical tank with a hemispherical shaped dome at each end. Contained within this assembly is a common bulkhead which separates the LOX and LH_2.

The forward skirt assembly extends forward from the intersection of the LH_2 tank sidewall and the forward dome providing a hard attach point for the IU.

The S-IVB is powered by one J-2 engine similar to those on the S-II stage with the exceptions that the nominal thrust is 1,023,092 Newtons (230,000 lbf) at a 5.5 mixture ratio and the S-IVB J-2 engine has a restart capability. LOX is supplied to the engine by a 6 inch low pressure duct from the LOX tank. LH_2 is supplied by a vacuum jacketed low pressure 10 inch duct emanating from the LH_2 tank. Prior to liftoff LH_2 tank pressurization is provided by ground supplied helium. After S-IVB engine start, for both first and second burns, GH_2 for LH_2 tank pressurization is bled from the thrust chamber hydrogen injector manifold. During orbital coast (parking orbit), LOX and LH_2 tank repressurization GHe storage spheres, attached to the thrust structure, and/or the O_2/H_2 burner using a cold helium supply are used to supply engine restart pressure requirements for second burn. This dual repressurization mode was first incorporated on the AS-503 flight. Prior to launch LOX tank pressurization is also accomplished by a ground helium supply. During first and second burns GHe from storage spheres, located in the LH_2 tank, is warmed by a heat exchanger to supply tank pressurization.

Pitch and yaw control of the S-IVB is accomplished during powered flight by gimbaling the J-2 engine and roll control is provided by operating the Auxiliary Propulsion System (APS).

The APS provides three axis stage attitude control and main stage propellant control during coast flight. The ullage engines are necessary for the propellant seating which is required for engine restart. The APS modules are located on opposite sides of the S-IVB aft skirt at positions I and III. Each module contains its own oxidizer system, fuel system, and pressurization system. Nitrogen Tetroxide (N_2O_4) is used as the oxidizer and Monomethyl Hydrazine (MMH) is the fuel for these engines.

Additional systems on the S-IVB are:

a. The hydraulic system which gimbals the J-2 engine.

b. Electrical system which supplies and distributes power to the various electrical components.

c. Thermoconditioning system which thermally conditions the electrical/electronic modules in the forward skirt area.

d. Data acquisition and telemetry system which acquires and transmits data for stage evaluation.

e. A set of ordnance systems used for rocket ignition, stage separation, ullage motor jettison and range safety.

The more significant configuration changes between AS-502 S-IVB and AS-503 S-IVB are shown in Table B-3.

Table B-3. S-IVB Significant Configuration Changes

SYSTEM	CHANGE	REASON
Propulsion	Dual repressurization system using: a. Cryogenic mode for repressurization of both the LOX and LH_2 tank using the O_2/H_2 burner and cold helium. b. Ambient mode for repressurization using the ambient repress bottle.	Provide repressurization system redundancy and checkout of cryogenic mode.
	J-2 engine ASI line assemblies redesigned and replaced with rigid tubing.	Reduce the probability of failures due to flow induced vibration in a vacuum environment.
	Cold helium system conoseals changed to 7075 aluminum/teflon.	Prevent S-IVB cold helium leakage.
	LH_2 and LOX repressurization bottles and engine control bottle are manifolded together with check valves to limit the flow path.	Assure adequate pressuring gas to the LH_2 tank to satisfy NPSP requirements for second burn, and to provide additional pneumatic power to the engine valves for orbital safing.
	PU system to be operated "open loop".	To minimize the effect of any PU malfunction.
	Addition of LOX tank nonpropulsive vent system.	Improved attitude control during coast mode.

B.5 Instrument Unit (IU)

B.5.1 IU Configuration

The IU, as shown in Figure B-5, is basically a short cylinder fabricated from an aluminum alloy honeycomb sandwich material. The IU has a diameter of 6.6 meters (21.6 ft) and a length of 0.9 meter (3 ft). The cylinder is manufactured in three 120 degree segments which are joined by splice plates into an integral load bearing unit. The top and bottom edges of the cylinder are made from extruded aluminum channels bonded to the honeycomb sandwich material. Cold plates are attached to the interior of the cylinder which serve both as mounting structure and thermal conditioning units for the electrical/electronic equipment.

Other systems included in the IU are:

a. The Environmental Control System (ECS) which maintains an acceptable environment for the IU equipment.

b. The electrical system which supplies and distributes electrical power to the various systems.

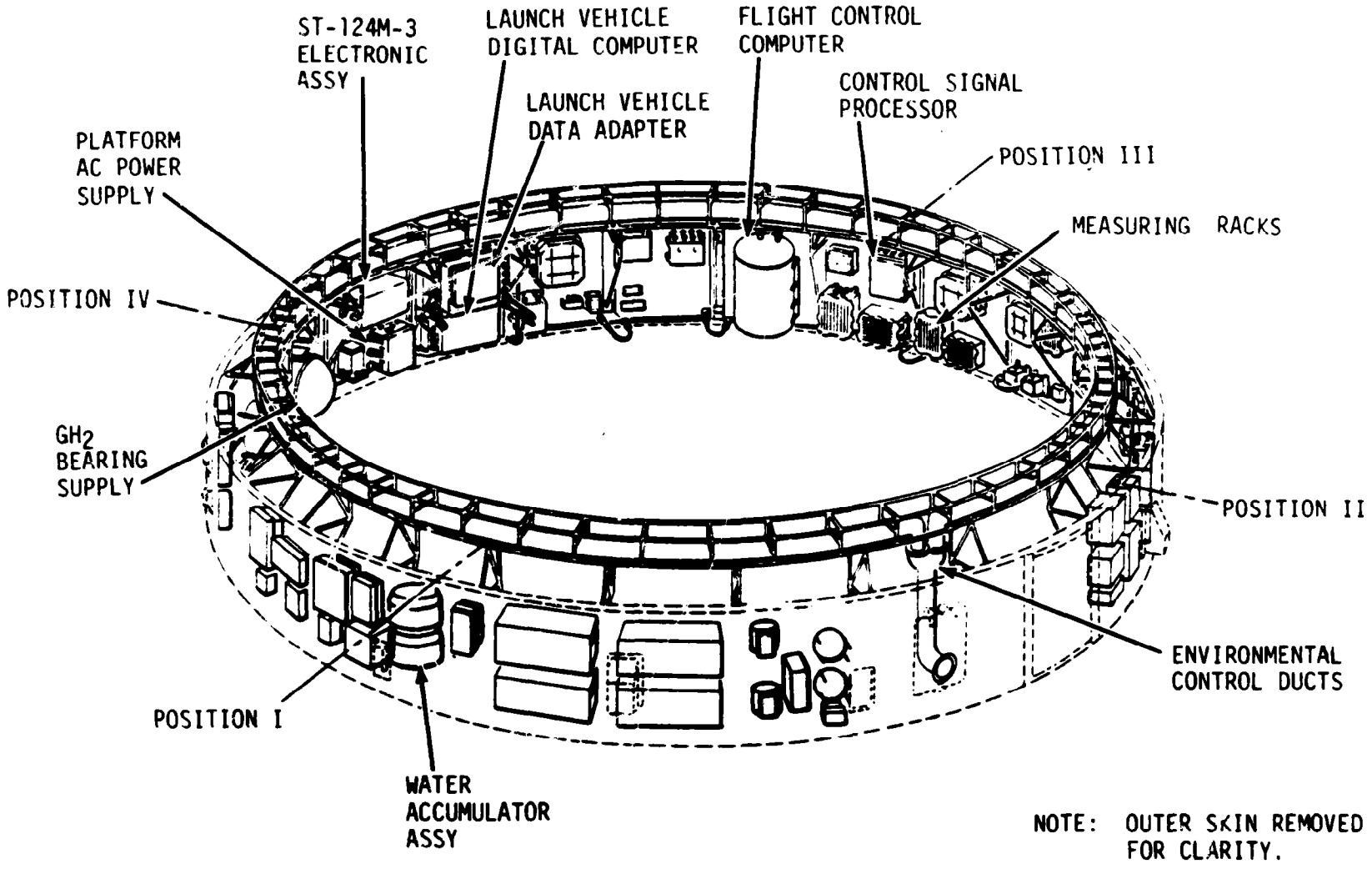

Figure B-5. Instrument Unit Configuration

c. The EDS which senses onboard emergency situations.

d. The navigation, guidance, and control system.

e. The measurements and telemetry system which monitors and transmits signals to ground monitoring stations.

f. The flight program which controls the LVDC from seconds before liftoff until the end of the launch vehicle mission.

The more significant configuration changes between AS-502 IU and AS-503 IU are shown in Table B-4.

Table B-4. IU Significant Configuration Changes

SYSTEM	CHANGE	REASON
Flight Program	Variable targeting calculations in boost initialization added.	
	Propellant Utilization system will be operated "open loop".	
	Incorporated spacecraft commands for S-IVB early staging and S-IVB cutoff.	
	Translunar injection burn can be inhibited by spacecraft command.	
	Logic incorporated to provide two restart opportunities.	
	Capability for a second S-IVB burn without the spacecraft included.	
	All simplex computer operations were deleted.	
	A redundant indication of guidance failure was added.	
	Acquisition and loss of telemetry stations will be done on navigation calculations.	
Flight Control Subsystem	Flight Control Computer modified to cant S-IC outboard engines 2 degrees outward from liftoff plus 20 seconds to OECO.	To reduce the probability of structural damage resulting from outboard engine malfunctions during S-IC burn phase.
	Filters added to the flight control computer attitude rate spatial channels.	To filter vehicle shell vibration modes resulting in reduced attitude error sensitivity.
Electrical Systems	Addition of circuitry in the EDS distributor.	Provide two out of three voting logic to eliminate S-IC stage engine failure due to relay contact failure.
Tracking	Azusa System deleted.	No longer required.
Electrical System	Several wiring changes to the EDS distributor.	Added reliability for manned flight.

B.6 SPACECRAFT

B.6.1 Spacecraft Configuration

The Apollo 8 spacecraft and launch vehicle adapter, as shown in Figure B-6, includes a Launch Escape System (LES), a Command Module (CM), a Service Module (SM), a Spacecraft Lunar Module Adapter (SLA), and a Lunar Module Test Article (LTA). From the bottom of the SLA to the top of the LES, the spacecraft measures approximately 24.9 meters (81.8 ft).

The LES is the forward most part of the Saturn V Apollo space vehicle. Basic configuration of the LES consists of an integral nose cone Q-ball, three rocket motors, a canard assembly, a structural skirt, a titanium-tube tower, and a boost protective cover. The purpose of the three rocket motors is tower jettison, escape, and pitch control. The LES is jettisoned shortly after S-II stage ignition in a normal flight.

The CM is designed to accommodate the three astronauts. The CM is a conically shaped structure consisting of an inner pressure vessel (crew compartment) and an outer heat shield. The CM is approximately 3.39 meters (11.15 ft) long. Aluminum honeycomb panels and aluminum longerons are used to form the pressure tight crew compartment. Stainless steel honeycomb covered with an ablative material is used to construct the outer heat shield. The unified side hatch is hinged to the vehicle and provides quick opening and improved egress/ingress capabilities.

The SM is a cylindrical aluminum honeycomb shell with fore and aft aluminum honeycomb bulkheads. Six aluminum radial beams divide the SM into sectors. These beams have a triangular truss between the CM and SM with pads at the apex to support the CM. The SM also houses the Service Propulsion System (SPS) which includes an engine and propellant tanks.

The SLA is a simple truncated cone measuring approximately 8.5 meters (28.0 ft) long and having forward and aft diameters of 3.9 meters (12.83 ft) and 6.6 meters (21.6 ft), respectively. There are four attachment points in the aft section of the SLA for the LTA. The SLA is constructed in two sets of four panels, the panels being made from aluminum honeycomb At CSM/S-IVB separation the forward section panels are jettisoned by a mild detonating explosive train.

The Lunar Test Article (LTA-B) simulated the mass of the lunar module as stowed in the adapter. This LTA weighed 9026 kilograms (19,900 lbm) and was instrumented about all axes for boost loads.

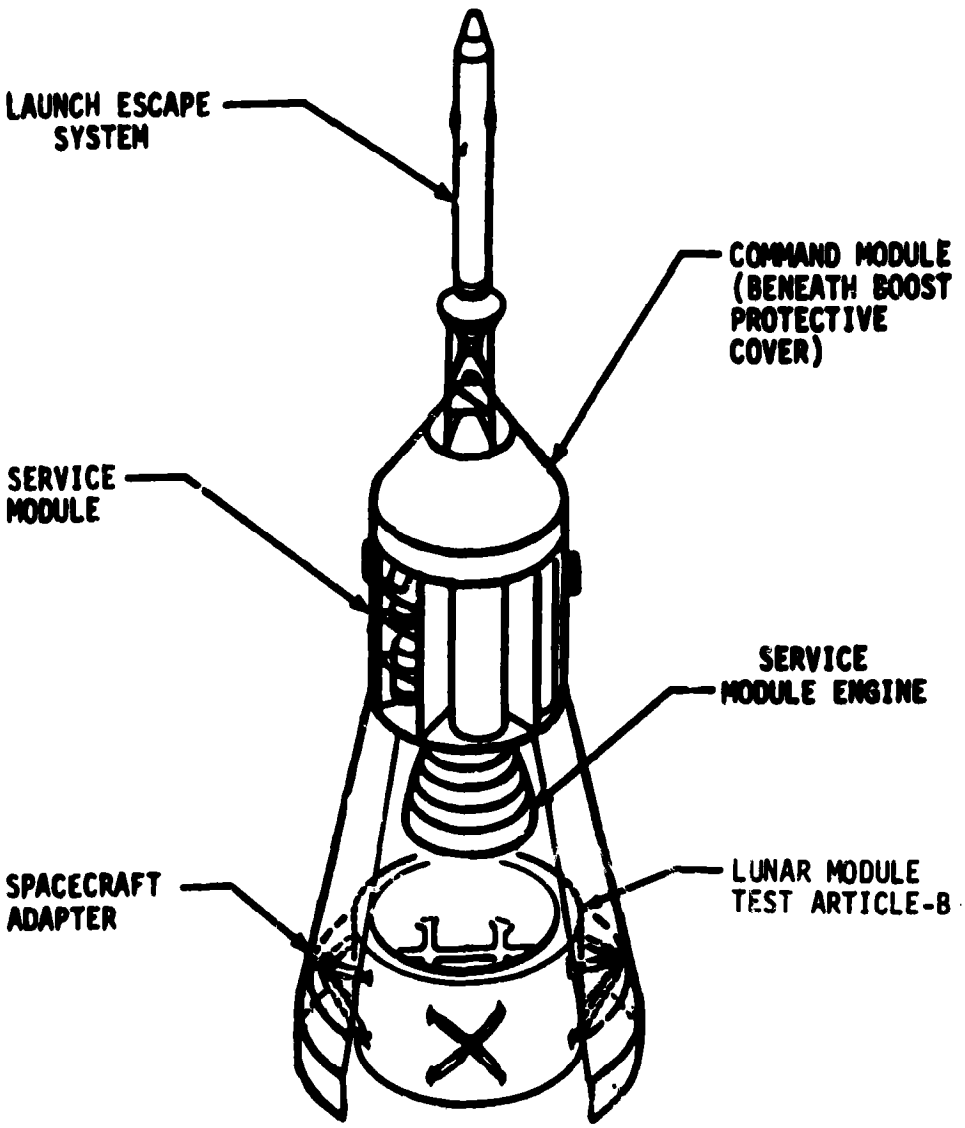

Figure B-6. Apollo Space Vehicle

APPROVAL

SATURN V LAUNCH VEHICLE FLIGHT EVALUATION REPORT

AS-503, APOLLO 8 MISSION

By Saturn Flight Evaluation Working Group

The information in this report has been reviewed for security classification. Review of any information concerning Department of Defense or Atomic Energy Commission programs has been made by the MSFC Security Classification Officer. The highest classification has been determined to be Unclassified.

for Clyde L. Bunch

Stanley L. Fragge
Security Classification Officer

This report has been reviewed and approved for technical accuracy.

J. P. Lindberg
Chairman, Saturn Flight Evaluation Working Group

Hermann K. Weidner
Director, Research and Development Operations

for L. James
Saturn Program Manager